

INFORMATION TO USERS

This manuscript has been reproduced from the microfilm master. UMI films the text directly from the original or copy submitted. Thus, some thesis and dissertation copies are in typewriter face, while others may be from any type of computer printer.

The quality of this reproduction is dependent upon the quality of the copy submitted. Broken or indistinct print, colored or poor quality illustrations and photographs, print bleedthrough, substandard margins, and improper alignment can adversely affect reproduction.

In the unlikely event that the author did not send UMI a complete manuscript and there are missing pages, these will be noted. Also, if unauthorized copyright material had to be removed, a note will indicate the deletion.

Oversize materials (e.g., maps, drawings, charts) are reproduced by sectioning the original, beginning at the upper left-hand corner and continuing from left to right in equal sections with small overlaps. Each original is also photographed in one exposure and is included in reduced form at the back of the book.

Photographs included in the original manuscript have been reproduced xerographically in this copy. Higher quality 6" x 9" black and white photographic prints are available for any photographs or illustrations appearing in this copy for an additional charge. Contact UMI directly to order.

UMI

A Bell & Howell Information Company
300 North Zeeb Road, Ann Arbor MI 48106-1346 USA
313/761-4700 800/521-0600



**STRUCTURE, METAMORPHISM, AND U-Pb AND $^{40}\text{Ar}/^{39}\text{Ar}$
GEOCHRONOLOGY OF THE MING'S BIGHT GROUP, AND THE
PALEOZOIC TECTONIC EVOLUTION OF THE BAIE VERTE PENINSULA,
NEWFOUNDLAND**

by

Scott D. Anderson

Submitted in partial fulfillment of the requirements

for the degree of Doctor of Philosophy

at

Dalhousie University

Halifax, Nova Scotia

August, 1998

© Copyright by Scott D. Anderson, 1998



National Library
of Canada

Acquisitions and
Bibliographic Services

395 Wellington Street
Ottawa ON K1A 0N4
Canada

Bibliothèque nationale
du Canada

Acquisitions et
services bibliographiques

395, rue Wellington
Ottawa ON K1A 0N4
Canada

Your file Votre référence

Our file Notre référence

The author has granted a non-exclusive licence allowing the National Library of Canada to reproduce, loan, distribute or sell copies of this thesis in microform, paper or electronic formats.

The author retains ownership of the copyright in this thesis. Neither the thesis nor substantial extracts from it may be printed or otherwise reproduced without the author's permission.

L'auteur a accordé une licence non exclusive permettant à la Bibliothèque nationale du Canada de reproduire, prêter, distribuer ou vendre des copies de cette thèse sous la forme de microfiche/film, de reproduction sur papier ou sur format électronique.

L'auteur conserve la propriété du droit d'auteur qui protège cette thèse. Ni la thèse ni des extraits substantiels de celle-ci ne doivent être imprimés ou autrement reproduits sans son autorisation.

0-612-36566-2

Canada

DALHOUSIE UNIVERSITY

FACULTY OF GRADUATE STUDIES

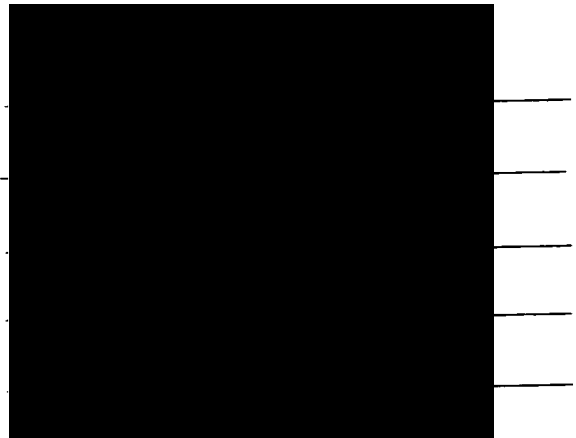
The undersigned hereby certify that they have read and recommend to the Faculty of Graduate Studies for acceptance a thesis entitled "Structure, Metamorphism, and U-Pb and ⁴⁰Ar/³⁹Ar Geochronology of the Ming's Right Group and the Paleozoic Tectonic Evolution of the Baie Verte Peninsula, Newfoundland"

by Scott Douglas Anderson

in partial fulfillment of the requirements for the degree of Doctor of Philosophy.

Dated: April 7, 1998

External Examiner
Research Supervisor
Examining Committee



DALHOUSIE UNIVERSITY

DATE: September 8, 1998

AUTHOR: Scott D. Anderson

TITLE: "Structure, Metamorphism, and U-Pb and $^{40}\text{Ar}/^{39}\text{Ar}$
Geochronology of the Ming's Bight Group, and the Paleozoic
Tectonic Evolution of the Baie Verte Peninsula, Newfoundland"

Permission is herewith granted to Dalhousie University to circulate and to have copied for non-commercial purposes, at its discretion, the above title upon the request of individuals or institutions.



Signature of Author

The author reserves other publication rights, and neither the thesis nor extensive extracts from it may be printed or otherwise reproduced without the author's written permission.

The author attests that permission has been obtained for the use of any copyrighted material in this thesis (other than brief excerpts requiring only proper acknowledgement in scholarly writing), and that all such use is clearly acknowledged.

TABLE OF CONTENTS

	Page
Table of contents	iv
List of Figures	ix
List of Tables	xii
Abstract	xiii
Acknowledgements.....	xv
Chapter 1 Introduction	1
1.1 BACKGROUND.....	1
1.2 PURPOSE AND SIGNIFICANCE.....	8
Chapter 2 Regional Setting and General Geology	11
2.1 INTRODUCTION	11
2.2 REGIONAL SETTING AND PREVIOUS WORK	12
2.2.1 Newfoundland Appalachians	12
2.2.2 Baie Verte Peninsula.....	19
<u>2.2.2.1 Humber Zone.....</u>	<u>19</u>
<u>2.2.2.2 Dunnage Zone</u>	<u>22</u>
<u>2.2.2.3 Early Silurian volcano-plutonic rocks</u>	<u>27</u>
<u>2.2.2.4 The Baie Verte Line and the Ming’s Bight Group.....</u>	<u>29</u>
2.3 GENERAL GEOLOGY - MING’S BIGHT-PACQUET	30
HARBOUR AREAS	
2.3.1 Ming’s Bight Group	34
<u>2.3.1.1 General characteristics</u>	<u>34</u>
<i>Description of the MBG pegmatites.....</i>	<i>37</i>
<u>2.3.1.2 Age and Correlation.....</u>	<u>39</u>
<u>2.3.1.3 Contact Relations.....</u>	<u>40</u>
2.3.2 Pacquet Harbour Group	42
<u>2.3.2.1 General Characteristics</u>	<u>42</u>
<u>2.3.2.2 Age and Correlation.....</u>	<u>49</u>
<u>2.3.2.3 Contact Relations.....</u>	<u>50</u>
2.3.3 Dunamagon Granite	50
<u>2.3.3.1 General Characteristics</u>	<u>50</u>
<u>2.3.3.2 Age and Correlation.....</u>	<u>54</u>
<u>2.3.3.3 Contact Relations.....</u>	<u>54</u>
2.3.4 Cape Brule Porphyry.....	55
<u>2.3.4.1 General Characteristics</u>	<u>55</u>
<u>2.3.4.2 Age and Correlation.....</u>	<u>57</u>
<u>2.3.4.3 Contact Relations.....</u>	<u>57</u>

2.3.5 <i>Point Rousse Ophiolite Complex</i>	58
2.3.5.1 <u>General Characteristics</u>	58
2.3.5.2 <u>Age and Correlation</u>	64
2.3.5.3 <u>Contact Relations</u>	65
2.3.6 <i>Eastern Shore of Ming's Bight</i>	65
2.3.6.1 <u>Background</u>	65
2.3.6.2 <u>General Characteristics</u>	66
<i>Ming's Bight Group</i>	66
<i>PROC ultramafic rocks</i>	66
<i>PROC cover sequence</i>	69
2.3.6.3 <u>Age and Correlation</u>	74
2.3.6.4 <u>Contact Relations</u>	77
2.4 CONCLUSION	77
 Chapter 3 Structural Geology - Pacquet Harbour area	 78
3.1 INTRODUCTION - CHAPTERS 3 AND 4	78
3.1.1 <i>Structural setting and previous work</i>	80
3.1.2 <i>Methodology and terminology</i>	86
3.2 PACQUET HARBOUR AREA - INTRODUCTION	89
3.2.1 <i>Background</i>	89
3.2.2 <i>Previous structural studies</i>	90
3.3 DETAILED STRUCTURAL ANALYSIS	91
3.3.1 <i>Primary Structures</i>	96
3.3.2 <i>D₁ deformation - the Pelee Point Shear Zone</i>	97
3.3.3 <i>D₂ deformation</i>	103
3.3.3.1 <u>Ming's Bight Group</u>	104
3.3.3.2 <u>Pacquet Harbour Group</u>	106
3.3.3.3 <u>Cape Brule Porphyry</u>	122
3.3.4 <i>D₃ deformation - the Big Brook Shear Zone</i>	123
3.3.4.1 <u>D₁-D₂ structures in the BBSZ</u>	124
3.3.4.2 <u>D₃ structures in the BBSZ</u>	125
3.3.5 <i>Late Faulting</i>	129
3.3.6 <i>Dunamagon Granite</i>	129
3.3.6.1 <u>Group 1 structures</u>	130
3.3.6.2 <u>Group 2 structures</u>	132
3.3.6.3 <u>Relative chronology of Group 1 and 2 structures</u>	134
3.3.7 <i>Quartz veins and pegmatite dykes</i>	136
3.3.7.1 <u>Quartz veins - general characteristics and timing</u>	136
3.3.7.2 <u>Pegmatites - general characteristics and timing</u>	141
3.3.7.3 <u>Structural significance - pegmatites and Group 3 & 4 veins</u> .	142
3.4 CONCLUSIONS - PACQUET HARBOUR AREA	143

Chapter 4 Structural Geology - Ming's Bight area	145
4.1 MING'S BIGHT AREA - INTRODUCTION	145
4.1.1 Background	145
4.1.2 Previous structural studies	146
4.1.2.1 Point Rouse Ophiolite Complex	146
4.1.2.2 Pacquet Harbour Group	147
4.2 DETAILED STRUCTURAL ANALYSIS	150
4.2.1 D₁ deformation	150
4.2.2 D₂ deformation	158
<i>Relative timing of D₁ and D₂ structures - microstructural evidence</i>	166
4.2.3 D₃ deformation	170
4.2.4 D₄ deformation	173
4.2.5 D₅ deformation	180
4.2.5.1 Northerly-dipping D₅ shear zones	180
4.2.5.2 Southerly-dipping D₅ shear zones	188
4.2.6 Point Rouse Ophiolite Complex	194
4.2.6.1 D₁ deformation	196
4.2.6.2 D₂ deformation	197
4.2.6.3 D₃ deformation	198
4.2.7 Kinematic analysis of D₃, D₄, and D₅ shear zones and faults	199
4.2.7.1 Introduction	199
4.2.7.2 Assumptions	200
4.2.7.3 Kinematic analysis - Ming's Bight area	202
4.2.7.4 Discussion	203
4.3 CONCLUSIONS - MING'S BIGHT AREA	206
4.4 DISCUSSION - CHAPTERS 3 AND 4	209
4.4.1 Timing of deformation	209
4.4.2 Correlation of deformation - Ming's Bight and Pacquet Harbour areas	210
 Chapter 5 Metamorphic Petrology and Thermobarometry	 217
5.1 INTRODUCTION	217
5.1.1 Background	217
5.1.2 Regional metamorphic setting and previous work	218
5.2 MINERAL GROWTH, RECRYSTALLIZATION, AND DEFORMATION	220
5.2.1 Pacquet Harbour area	220
5.2.1.1 Microstructural relationships	223
<i>Staurolite S_r-S_e relationships</i>	223
<i>Hornblende S_r-S_e relationships</i>	225
<i>Garnet S_r-S_e relationships</i>	227
5.2.1.2 Pre-peak metamorphic assemblages	231

5.2.1.3 Peak metamorphic assemblages	232
5.2.1.4 Post-peak metamorphic assemblages	242
5.2.2 <i>Ming's Bight area</i>	244
5.2.2.1 D ₁ metamorphic assemblages	245
5.2.2.2 D ₂ metamorphic assemblages	246
5.2.2.3 D ₃ metamorphic assemblages	250
5.2.2.4 D ₄ metamorphic assemblages	251
5.2.2.5 D ₅ metamorphic assemblages	251
5.3 THERMOBAROMETRY	252
5.3.1 <i>Rationale, sample selection, and approach</i>	252
5.3.2 <i>P-T results</i>	256
5.3.2.1 TWO calculations	256
5.3.2.2 Semi-quantitative estimates of P-T conditions	257
5.4 DISCUSSION.....	259
5.4.1 <i>Generalized P-T paths of the MBG in Pacquet Harbour and Ming's Bight</i>	259
5.4.2 <i>Metamorphic gradient - Ming's Bight</i>	262
5.5 CONCLUSIONS	264
5.5.1 <i>Pacquet Harbour area</i>	264
5.5.2 <i>Ming's Bight area</i>	264
 Chapter 6 Geochronology	 266
6.1 INTRODUCTION	266
6.1.1 <i>Background</i>	266
6.1.2 <i>Previous geochronology</i>	267
6.1.2.1 <i>West of the BVL</i>	268
6.1.2.2 <i>East of the BVL</i>	269
6.2 SAMPLE SELECTION AND ANALYTICAL TECHNIQUES	270
6.2.1 <i>U-Pb samples</i>	270
6.2.2 <i>⁴⁰Ar / ³⁹Ar samples</i>	272
6.2.3 <i>Closure temperatures</i>	274
6.3 RESULTS.....	275
6.3.1 <i>⁴⁰Ar / ³⁹Ar incremental release analyses</i>	275
6.3.1.1 <i>Muscovite</i>	275
<i>Ming's Bight Group - schist</i>	276
<i>Ming's Bight Group - pegmatite</i>	279
6.3.1.2 <i>Hornblende</i>	280
<i>Pacquet Harbour Group - amphibolite</i>	280
<i>Dunamagon Granite - mafic dyke</i>	283
<i>Big Brook Shear Zone - mafic dyke</i>	285
<i>Eastern Shore of Ming's Bight - amphibolite</i>	286
6.3.2 <i>U-Pb analyses</i>	290
6.3.2.1 <i>MBG pegmatite sample - Pelee Point, Pacquet Harbour</i>	290

6.3.2.2 Rutile-titanite bearing chlorite schist -	296
NMTSZ, Ming's Bight	
6.4 DISCUSSION AND CONCLUSIONS	298
6.4.1 <i>Pacquet Harbour area</i>	298
6.4.1.1 Significance of the microlite U-Pb date.....	298
6.4.1.2 Overview of U-Pb and ⁴⁰ Ar/ ³⁹ Ar data.....	301
6.4.1.3 Timing of deformation and metamorphism	302
6.4.2 <i>Ming's Bight area</i>	302
6.4.2.1 Overview of U-Pb and ⁴⁰ Ar/ ³⁹ Ar data.....	302
6.4.2.2 Age of the sequences on the eastern shore of Ming's Bight .	305
6.4.2.3 Timing of deformation and metamorphism	305
6.4.3 <i>Thermal history: Ming's Bight and Pacquet Harbour</i>	307
 Chapter 7 Tectonic Synthesis and Discussion	 312
7.1 INTRODUCTION	312
7.2 TECTONIC EVOLUTION AND REGIONAL IMPLICATIONS	313
7.2.1 <i>Late Proterozoic to Early Silurian (ca. 600-440 Ma)</i>	313
7.2.2 <i>Early Silurian to Early Devonian (ca. 440-400 Ma)</i>	317
7.2.2.1 <u>Sinistral transpression and deformation</u>	319
<u>partitioning along the BVL</u>	
7.2.2.2 <u>D₁-D₂ deformation in the Ming's Bight area</u>	326
7.2.2.3 <u>Extensional collapse in the northern Appalachians</u>	328
7.2.3 <i>Early Devonian to Early Carboniferous (ca. 400-360 Ma)</i>	331
7.2.3.1 <u>Early Devonian to Early Carboniferous dextral shear</u>	332
7.2.3.2 <u>Late orogenic extension and metamorphic core complexes</u> ..	335
7.2.3.3 <u>The MBG symmetrical metamorphic core complex</u>	337
7.2.3.4 <u>Regional implications</u>	341
7.3 IMPLICATIONS FOR GOLD AND VMS EXPLORATION	342
7.3.1 <i>Mesothermal gold mineralization</i>	342
7.3.2 <i>Volcanogenic massive sulphide mineralization</i>	344
 Appendix A ⁴⁰ Ar / ³⁹ Ar analytical data for muscovite and hornblende.....	 346
 References	 355

LIST OF FIGURES

Chapter 1

- Figure 1.1 Simplified tectonostratigraphic map of the Newfoundland..... 3
Appalachians.
- Figure 1.2 Simplified geological map of the Baie Verte Peninsula. 7

Chapter 2

- Figure 2.1 Simplified geological map of the island of Newfoundland. 14
- Figure 2.2 Simplified geological map of the thesis area. 32
- Figure 2.3 Field photographs of the Ming's Bight Group and..... 36
granitic pegmatites.
- Figure 2.4 Field photographs of the Pacquet Harbour Group. 46
- Figure 2.5 Field photographs of the Dunamagon Granite. 53
- Figure 2.6 Field photographs of the Point Rouse Ophiolite Complex..... 62
cover sequence on the western shore of Ming's Bight.
- Figure 2.7 Field photographs of the sequences exposed on the eastern..... 68
shore of Ming's Bight.
- Figure 2.8 Geochemical characteristics of gabbro from the eastern shore 76
of Ming's Bight.

Chapter 3

- Figure 3.1 Simplified geology of the thesis area illustrating the 84
locations of Maps 1, 3, 4, 7, and 9.
- Figure 3.2 Lower hemisphere, equal area, stereographic projections of..... 94
structural data in the Pacquet Harbour area.
- Figure 3.3 Field photographs of D_1 and D_2 structures in the Pelee Point..... 99
Shear Zone, Ming's Bight Group, and Pacquet Harbour Group.
- Figure 3.4 Field photographs of D_2 structures in the Pacquet Harbour Group... 110
- Figure 3.5 Schematic sketches of D_2 - D_3 structures, and a graph of the..... 114
angular relationship between F_2 axes and L_2 in Pacquet Harbour.
- Figure 3.6 Structural relationships in the Big Brook Shear Zone and..... 127
Dunamagon Granite in the Pacquet Harbour area.
- Figure 3.7 Lower hemisphere, equal area, stereographic projections of the 138
orientation of quartz veins and granitic pegmatites.
- Figure 3.8 Field photographs of quartz veins and granitic pegmatites 139
in the Pacquet Harbour area.

Chapter 4	
Figure 4.1	Lower hemisphere, equal area, stereographic projections of..... 152 structural data in the Ming's Bight area.
Figure 4.2	Field photographs of D ₁ - D ₂ structures in the Ming's Bight area. ... 155
Figure 4.3	Photographs of D ₂ and D ₃ structures and syn-D ₁ -D ₂ 165 porphyroblasts along the south shore of Ming's Bight.
Figure 4.4	Schematic, composite, sketch illustrating S ₁ -S _e relationships..... 167 in garnet porphyroblastic Ming's Bight Group schist.
Figure 4.5	Photographs of D ₄ structures in the Grappling Point area. 175
Figure 4.6	Lower hemisphere, equal area, stereographic projections of..... 176 structural data from the Grand Toss Cove Shear Zone.
Figure 4.7	Lower hemisphere, equal area, stereographic projections of..... 181 structural data from northerly-dipping D ₅ shear zones.
Figure 4.8	Field photographs of D ₅ structures in the Ming's Tickle area..... 186 and structures in the Point Rousse Ophiolite Complex.
Figure 4.9	Lower hemisphere, equal area, stereographic projections of..... 190 structural data from southerly-dipping D ₅ shear zones.
Figure 4.10	Lower hemisphere, equal area, stereographic projections of..... 195 structural data from the Point Rousse Ophiolite Complex.
Figure 4.11	Lower hemisphere, equal area, stereographic projections of the 205 results of the fault kinematic analysis in the Ming's Bight area.
Figure 4.12	Simplified geological and structural map illustrating structures..... 214 attributed to Silurian compressional deformation.
Figure 4.13	Simplified geological and structural map illustrating structures..... 216 attributed to Devonian extensional deformation.
 Chapter 5	
Figure 5.1	Simplified map showing the distribution of greenschist and 222 upper greenschist to amphibolite facies metamorphic rocks.
Figure 5.2	Microstructural relationships of staurolite, hornblende, and..... 224 garnet porphyroblasts in the Pacquet Harbour area.
Figure 5.3	Schematic, composite, sketches of S ₁ -S _e relationships in the 226 Pacquet Harbour area.
Figure 5.4	Line drawings of S ₁ -S _e relationships in garnet porphyroblastic 230 Ming's Bight Group schist.
Figure 5.5	Textures and mineral assemblages in Ming's Bight Group 236 schist and Pacquet Harbour Group amphibolite.
Figure 5.6	Compositional variations across garnet porphyroblasts from 237 Pacquet Harbour Group amphibolite at Pelee Point.
Figure 5.7	Compositional variations across garnet porphyroblasts..... 239 from Ming's Bight Group schist in the Big Brook Shear Zone.
Figure 5.8	Schematic, generalized, P-T paths for the Ming's Bight Group. 261

Chapter 6	
Figure 6.1	Simplified geological map of the thesis area showing the location of $^{40}\text{Ar}/^{39}\text{Ar}$ and U-Pb samples. 277
Figure 6.2	$^{40}\text{Ar}/^{39}\text{Ar}$ age spectra for muscovite samples. 278
Figure 6.3	$^{40}\text{Ar}/^{39}\text{Ar}$ age spectra and measured $^{37}\text{Ar}/^{39}\text{Ar}$ ratios for hornblende samples. 282
Figure 6.4	Isotope correlation plot for sample 94-17. 284
Figure 6.5	Photographs of the U-Pb geochronology samples. 291
Figure 6.6	U-Pb concordia diagrams. 297
Figure 6.7	Plot of temperature-time data for the thesis area. 308
Chapter 7	
Figure 7.1	Schematic diagram illustrating the Early to Middle Ordovician tectonic evolution of western Newfoundland. 314
Figure 7.2	Schematic diagram illustrating the Early Silurian to Middle Devonian tectonic evolution of Newfoundland. 320
Figure 7.3	Correlation chart of regional deformation events in the northern Appalachians. 322
Figure 7.4	Schematic diagram illustrating the structural evolution of the north-central portion of the BVP in Early to Late Silurian time. 325
Figure 7.5	Schematic diagram illustrating the structural evolution of the north-central portion of the BVP in Early to Late Devonian time. 334
Back pocket	
Map 1	Geological and structural map: Pacquet Harbour - Handy Harbour area.
Map 2	Detailed geological and structural map: Pacquet Harbour and Pelee Point.
Map 3	Geological and structural map: Pacquet Harbour Group southwest of Pacquet Harbour.
Map 4	Geological and structural map: Ming's South Brook - Deep Cove Brook.
Map 5	Detailed geological and structural map: south shore of Ming's Bight.
Map 6	Detailed geological and structural map: Ming's South Brook area.
Map 7	Geological and structural map: northeastern shore of Ming's Bight.
Map 8	Detailed geological and structural map: Ming's Tickle - Caplin Cove area.
Map 9	Detailed geological and structural map: Point Rouse Ophiolite Complex.
Cross-section 1	Pacquet Harbour (Map 2).
Cross-section 2	Pacquet Harbour Group southwest of Pacquet Harbour (Map 3).
Cross-section 3	South shore of Ming's Bight (Map 5).
Cross-section 4	Actinolite Bay on the south shore of Pacquet Harbour (Map 5).
Cross-section 5	Northeast shore of Ming's Bight (Map 7).
Cross-section 6	Ming's Tickle - Caplin Cove (Map 8).
Cross-section 7	Caplin Cove amphibolites (Map 8).

LIST OF TABLES

Chapter 3

Table 3.1	Deformation structures: Pacquet Harbour area.....	92
-----------	---	----

Chapter 4

Table 4.1	Deformation structures: Ming's Bight area.....	151
Table 4.2	Correlation and regional significance of deformation - Pacquet Harbour and Ming's Bight	211

Chapter 6

Table 6.1	U-Pb analytical data.....	273
-----------	---------------------------	-----

Appendix A

Table A1	$^{40}\text{Ar}/^{39}\text{Ar}$ analytical data for muscovite and hornblende.	346
----------	--	-----

ABSTRACT

The Ming's Bight Group (MBG) comprises a sequence of Late Proterozoic to Early Ordovician continental margin siliciclastic rocks of Humber Zone tectonostratigraphic affinity which is surrounded by Early Ordovician volcanic arc and ophiolitic rocks of Dunnage Zone affinity on the eastern side of a major terrane boundary (the Baie Verte-Brompton Line; BVL) on the Baie Verte Peninsula (BVP) in northwest Newfoundland. The apparently anomalous tectonostratigraphic setting of the MBG reflects the protracted Ordovician to Carboniferous tectonic history of the BVP, and the tectonic evolution of the Newfoundland Appalachians. The deformation history of the MBG, as constrained by overprinting relationships and geochronologic data, indicates a progressive transition from sinistral transpressional deformation, to dextral transpression, to dextral transtension from Late Silurian to Carboniferous time. Sinistral transpressional structures comprise a thick, south-verging zone of sinistral-reverse, oblique-slip shear that is bounded to the east by a wide zone of contemporaneous sinistral wrench shear that dips steeply east and west. These structures are constrained to late-Early Silurian to early-Early Devonian time by a previously published U-Pb date of 420 ± 5 Ma from hydrothermal zircon in syntectonic quartz veins and a $^{40}\text{Ar}/^{39}\text{Ar}$ date of 405 ± 4 Ma from hornblende porphyroblasts that post-date the earliest extensional structures in the MBG, respectively. $^{40}\text{Ar}/^{39}\text{Ar}$ ages of 386 and 388 ± 2 Ma from syntectonic hornblende in the zone of sinistral wrench shear are interpreted to record cooling subsequent to an amphibolite facies metamorphic peak, and provide a younger age limit for maximum subsidence during sinistral transpression along the BVL. These relationships indicate that, in contrast to the correlative Fleur de Lys Supergroup (FdLS), the MBG occupied a relatively high structural level of the Taconian (Early Ordovician) thrust stack, and remained at this level until it was overthrust by high grade metamorphic rocks of the FdLS that were rapidly exhumed in the hangingwall of the BVL through Early Silurian time. Dextral transpressional structures were observed in a single shear zone in the thesis area, and are overgrown by titanite porphyroblasts with a U-Pb age of 388 ± 4 Ma. This shearing is tentatively correlated with a dextral transpressional shear zone exposed further west along

the main trace of the BVL. Dextral transtensional structures are symmetrically developed about the MBG. To the southeast, the MBG is bounded by a thick zone of penetrative, southeast-directed, normal-sense, non-coaxial shear which initiated during peak amphibolite facies metamorphism ($T \geq 600^\circ\text{C}$; $P \geq 6$ kbar), and continued to greenschist facies conditions. $^{40}\text{Ar}/^{39}\text{Ar}$ cooling ages of $377\text{-}382 \pm 3$ Ma from syntectonic hornblende in the footwall of this zone indicate extensional shearing through Middle to Late Devonian time. To the northwest, a series of narrow, high-angle, brittle-ductile, greenschist facies, dextral-normal, oblique-slip shear zones bound the MBG. $^{40}\text{Ar}/^{39}\text{Ar}$ muscovite cooling ages throughout the MBG cluster between 360 ± 3 and 368 ± 4 Ma, indicating that this deformation, and coeval rapid post-metamorphic cooling through the muscovite closure temperature, continued through to Early Carboniferous time. Based on the geometry of these extensional structures and the spatial patterns of cooling ages and cooling rates, the MBG is interpreted to be a symmetrical metamorphic core complex. These relationships indicate that the recently proposed models for Silurian extensional collapse of the Newfoundland Appalachians cannot account for rapid post-metamorphic cooling in either the MBG or FdLS. The regional transition from a deformation regime of sinistral transpression to a regime of dextral transtension is interpreted to result from a regional-scale counterclockwise rotation of the kinematic axes from northwest-southeast in the late-Early to Late Silurian, to east-west in the Late Silurian to late-Early Devonian, to southwest-northeast in the late-Early to Late Devonian, similar to that documented in other portions of the northern Appalachians. This study indicates that transpressional shear zones controlling gold mineralization on the BVP are far more widespread than previously recognized, and provides a new model which may assist future volcanogenic massive sulphide (VMS) exploration in the vicinity of the Rambler VMS deposits.

ACKNOWLEDGMENTS

I would particularly like to thank my supervisor, Becky Jamieson, for her advice, financial support, time, constructive criticism, and encouragement throughout my studies. Nick Culshaw and John Waldron are thanked for reading various drafts of the thesis, and providing constructive criticism which greatly improved the final version.

I thank Peter Reynolds and Keith Taylor for their technical assistance and advice in the $^{40}\text{Ar}/^{39}\text{Ar}$ geochronology laboratory at Dalhousie University, Gordon Brown for thin-section preparation, and Bob McKay for technical assistance with the microprobe. Greg Dunning and Rod Churchill provided advice and technical assistance in the U-Pb geochronology laboratory at Memorial University of Newfoundland (MUN), and I thank Scott Swinden (Newfoundland Department of Mines and Energy) and George Jenner (MUN) for analyzing the whole-rock geochemistry samples.

I extend my thanks to Laurel McDonald, Brad McCallum, and Neil Banerjee for their cheerful and entertaining field assistance, Peter Dimmell for putting us up at the Chateaux Ming for a summer, and Gill, Kim, and Maisie Regular of Ming's Bight for their Newfoundland hospitality, boatmanship, and the evenings spent jigging a few fish. The people of Ming's Bight and Pacquet Harbour are thanked for the lively conversations, and for inviting us in for tea and toast on cold wet days too numerous to mention.

The research was funded by two Natural Sciences and Engineering Research Council of Canada (NSERC) postgraduate scholarships and a Geological Society of America research grant to the author, and a Lithoprobe supporting geoscience grant and NSERC operating grant to Dr. R.A. Jamieson.

I would especially like to thank my extended family of graduate students at Dalhousie University (what can I say?) and, of course, Tracy for her support, love, tolerance, and companionship through it all.

Chapter 1 Introduction

1.1 BACKGROUND

The Paleozoic Appalachian orogen is one of the best exposed and most thoroughly studied orogenic belts in the world. Along the eastern seaboard of North America, the Appalachian orogen is nearly continuously exposed from the southeastern United States to the northern shores of Newfoundland, and can be traced through the British Isles, eastern Greenland, and northern Norway as the Caledonide orogen (e.g., Dewey 1969). The present study however, refers mainly to the Newfoundland Appalachians.

With the advent of plate tectonic theory, much early progress was made in understanding the nature and evolution of the Newfoundland Appalachians (e.g., Wilson 1966; Church 1969; Dewey 1969; Bird and Dewey 1970; Stevens 1970; Church and Stevens 1971; Dewey and Bird 1971; Kennedy 1975; Dewey et al. 1983). A contribution of particular significance was made by Williams (1979) who, based on the distribution of pre-Late Ordovician lithologies in northern Newfoundland, proposed a tectono-stratigraphic framework that, from west to east, comprises the Humber, Dunnage, Gander, and Avalon Zones. Within this 'first order' framework (Fig. 1.1), the Newfoundland Appalachians are now widely regarded as a broadly symmetrical orogen formed through collisional interaction of the Laurentian margin (Humber Zone), oceanic terranes of the Iapetus ocean (Dunnage Zone), and elements of the Gondwanan margin (Gander and

Figure 1.1 Simplified map illustrating the principal tectonostratigraphic divisions and major tectonic boundaries of the Newfoundland Appalachians (Colman-Sadd et al. 1990). Segments of the Humber-Dunnage boundary zone which have been the focus of recent detailed structural and geochronologic studies are outlined. The inset map illustrates the principal tectonostratigraphic zones of the northern Appalachians (Williams et al. 1988; van Staal and de Roo 1995).

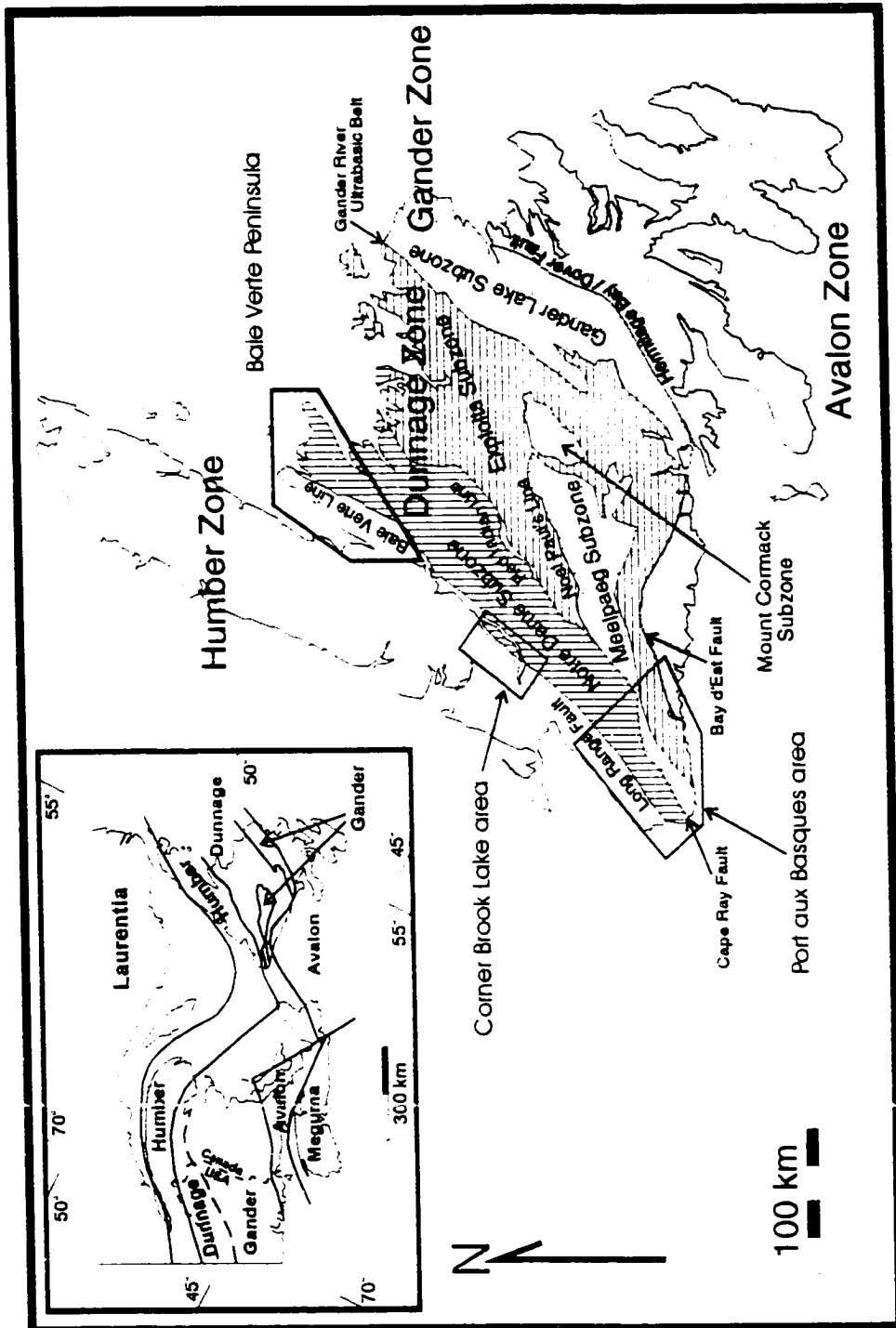


Figure 1.1

Avalon Zones: e.g., Williams 1964, 1979; Williams and Hatcher 1982; Dewey et al. 1983; Dewey and Shackleton 1984; Keen et al. 1986; Stockmal et al. 1987, 1990; van der Pluijm 1987; van der Pluijm and van Staal 1988).

The 'second order' framework, or tectonic evolution, of the Newfoundland Appalachians is the focus of continuing research. In the past, conceptual models focused primarily on arc-continent collision and west-directed ophiolite obduction during the Middle Ordovician Taconian orogeny, and post-Taconian tectonism was typically attributed to a poorly constrained and defined middle Paleozoic 'Acadian' orogeny (e.g., Kennedy 1975; Bursnall and de Wit 1975; Williams 1979; Dewey et al. 1983; Stockmal et al. 1987; Cawood and Williams 1988; Stockmal and Waldron 1990). However, recent regional mapping and detailed structural and metamorphic studies, coupled with modern U-Pb and $^{40}\text{Ar}/^{39}\text{Ar}$ geochronology techniques, have resulted in considerable progress towards refining second-order tectonic models and, in particular, the post-Ordovician tectonic evolution of Newfoundland (e.g., Dunning et al. 1990; Elliott et al. 1991; O'Brien et al. 1991, 1993; Colman-Sadd et al. 1992; Cawood 1992; Cawood et al. 1994, 1995; Lin et al. 1994; Burgess et al. 1995; Dubé and Lauzière 1996; Dubé et al. 1996). For example, the peak of orogenic activity in western Newfoundland, traditionally ascribed to the Taconian orogeny, is now widely interpreted in terms of a climactic Silurian (i.e., Salinian; Dunning et al. 1990) orogenic event associated with oblique convergence of the Laurentian and Gondwanan margins, high-grade metamorphism, and ductile deformation in a regime of bulk sinistral transpression (e.g., Currie and Piasecki 1989; Dunning et al. 1990; Soper et al. 1990; Cawood et al. 1994; Holdsworth 1994; Lin et al. 1994; Burgess

et al. 1995; Dubé et al. 1996). In addition, several authors have noted that the Early Silurian metamorphic peak was generally followed by rapid regional cooling through the muscovite $^{40}\text{Ar}/^{39}\text{Ar}$ closure temperature, leading Cawood et al. (1994, 1995) to propose that the orogen underwent extensional collapse subsequent to Silurian orogenesis.

The Baie Verte Peninsula (BVP) in northwestern Newfoundland (Fig. 1.2) figured prominently in early models for the tectonic evolution of Newfoundland and the Appalachian orogen (e.g., Dewey 1969; Bird and Dewey 1970; Church and Stevens 1971; Kennedy 1975; Williams 1979; Dewey et al. 1983), due to its key exposures of the Humber-Dunnage boundary (i.e., the Baie Verte Line; Williams and St. Julien 1982). Accordingly, the tectonic evolution of the BVP was thought to reflect Taconian westward transport of Dunnage Zone ophiolites over the Humber Zone, and local 'Acadian' modification of the resultant zone boundary (e.g., Bursnall and de Wit 1975; Kennedy 1975; Williams 1977, 1979; Kidd et al. 1978; Hibbard 1983; Dallmeyer and Hibbard 1984). However, several aspects of BVP geology point toward a significantly more complex tectonic evolution. In particular, the Ming's Bight Group (MBG) is correlative with Humber Zone successions (Hibbard 1983; Fryer et al. 1992) but it outcrops amid Dunnage Zone sequences on the eastern side of the Baie Verte Line (BVL), and thus apparently represents a significant anomaly in the tectonostratigraphic framework of western Newfoundland (Hibbard 1982, 1983; Fig. 1.2). In addition, it has recently been proposed that correlative Humber Zone rocks on the western side of the BVL record intense ductile deformation coeval with an Early Silurian amphibolite-facies metamorphic peak, similar to areas affected by the climactic Silurian orogenic event elsewhere in

Figure 1.2 Simplified geological map of the Baie Verte Peninsula (modified after Hibbard 1983). The generalized trace of the Baie Verte Line, as proposed in the present study, is indicated by the thick long-dashed line. The trace of the Baie Verte Line around the Baie Verte Flexure, as proposed by Hibbard (1982, 1983), is indicated by the thin short-dashed line (see Chapter 2). The white triangles mark the locations of the significant structurally-controlled mesothermal gold deposits and showings situated along the proposed trace of the Baie Verte Line. 1, East Pond Metamorphic Suite; 2, Fleur de Lys Supergroup; 3, Ming's Bight Group; 4, Betts Cove ophiolite complex and Snooks Arm Group; 5, Pacquet Harbour Group; 6, Point Rousse ophiolite complex; 7, Advocate ophiolite complex; 8, Flat Water Pond Group; 9, Burlington Granodiorite; 10, Cape Brule Porphyry; 11, King's Point complex; 12, Dunamagon Granite; 13, Wild Cove Pond igneous suite; 14, La Scie intrusive complex; 15, Cape St. John Group; 16, MicMac Lake Group; VMS, volcanogenic massive sulphide deposits of the Rambler camp.

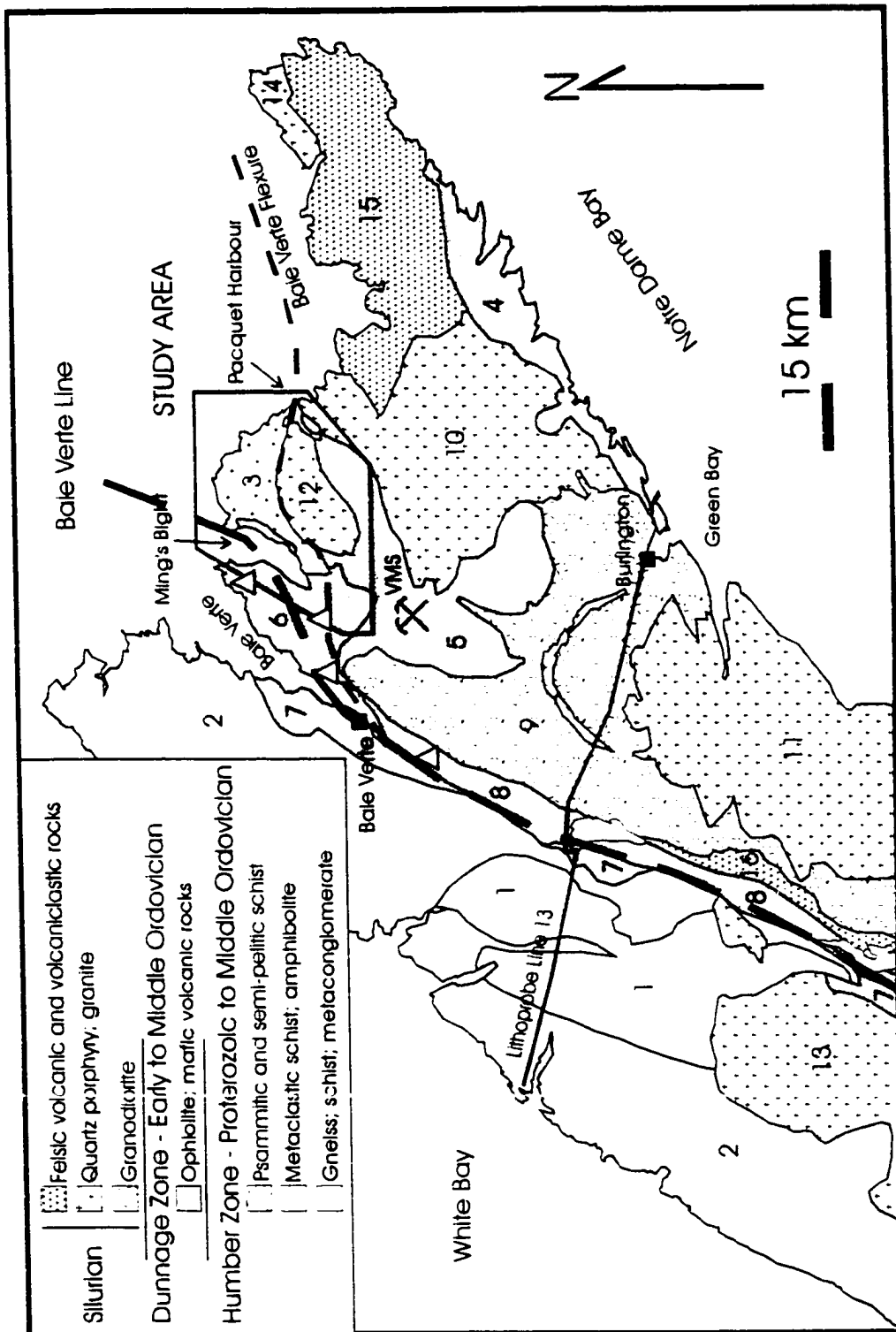


Figure 1.2

Newfoundland (Cawood and Dunning 1993; Cawood et al. 1994). Moreover, $^{40}\text{Ar}/^{39}\text{Ar}$ cooling ages (Dallmeyer 1977; Dallmeyer and Hibbard 1984) indicate that an Early Silurian metamorphic peak in the Humber Zone rocks was followed by rapid cooling (e.g., Cawood et al. 1995).

These observations raise important questions regarding the previously proposed models for the tectonic evolution of the BVP, and serve to highlight some of the current outstanding problems in Newfoundland geology. How widespread were the effects of the recently defined Early Silurian orogenic event? What are the nature, timing and significance of Silurian deformation structures, and how do they relate to the distribution of litho-tectonic units (e.g., the MBG) and timing of metamorphism? What process(es) could account for the rapid post-metamorphic cooling paths recorded in Humber Zone rocks on the BVP, and is there any structural evidence for extensional collapse? Does the post-Taconian tectonism reflect one progressive orogenic phase, or can it be subdivided into a coherent series of distinct orogenic events (i.e., Salinian, Acadian, and/or Alleghanian)?

1.2 PURPOSE AND SIGNIFICANCE

In the present study, the lithological, geochemical, structural, metamorphic, and geochronologic aspects of the MBG and environs (i.e., essentially the Ming's Bight and Pacquet Harbour areas; Fig. 1.2) were examined in detail. The specific goals of this thesis are as follows:

- (1) to map and sample the MBG and adjacent units [Pacquet Harbour Group (PHG), Dunamagon Granite, and eastern part of the Point Rouse ophiolite complex

(PROC)] in order to constrain the lithological and geochemical characteristics, contact relationships, and regional correlations.

(2) to examine the deformation structures in these units, and establish detailed deformation histories for each unit through the use of well constrained overprinting relations and U-Pb and $^{40}\text{Ar}/^{39}\text{Ar}$ geochronology.

(3) to examine the metamorphic assemblages and textures, and determine P-T conditions for each unit.

(4) to collect well constrained samples of hornblende and muscovite for $^{40}\text{Ar}/^{39}\text{Ar}$ thermochronology and, where possible, define P-T-t histories for the units.

(5) to incorporate the structural, metamorphic, and thermochronologic data into a tectonic history of the MBG, and to compare this history to that of the correlative Fleur de Lys Supergroup on the western side of the BVL.

(6) to incorporate the results of this comparison into a comprehensive model for the tectonic evolution of the BVP, and compare this model to previous models from the BVP and western Newfoundland.

(7) to evaluate potential mechanisms for rapid post-metamorphic cooling on the BVP, and the hypotheses for extension of the Newfoundland Appalachians.

The present study was undertaken primarily in order to address the problem of the anomalous tectonostratigraphic location of the MBG; however, the conclusions reached have important implications for the broader understanding of the tectonic evolution of the western Newfoundland Appalachians. In particular, the thesis provides a basis for future

comparisons of the tectonic evolution of the Humber - Dunnage boundary-zone on the BVP, to that of the Corner Brook (e.g., Bosworth 1985; Waldron and Milne 1991; Waldron and Stockmal 1994; Cawood et al. 1994, 1995, 1996) and Port aux Basques areas (e.g., O'Brien et al. 1991; Lin et al. 1994; Burgess et al. 1995; Dubé and Lauzière 1996; Dubé et al. 1996; Fig. 1.1), and may also assist in the interpretation of seismic reflectors imaged in Lithoprobe East Line 13, which transects the BVP from west to east (Quinlan et al. 1992; Fig. 1.2).

This study also documents the structural evolution of one of the most significant and prospective gold-bearing deformation zones and volcanogenic massive sulphide districts in the Canadian Appalachians (e.g., Tuach and Kennedy 1978; Hibbard 1983; Tuach et al. 1988; Dubé et al. 1992; Ritcey and Ramezani 1993; Fig. 1.2), and thus the structural data presented in this thesis may significantly assist in future gold and volcanogenic massive sulphide exploration on the BVP.

Chapter 2 Regional Setting and General Geology

2.1 INTRODUCTION

Complex orogenic systems typically comprise several distinct tectonostratigraphic terranes that often contain diverse assemblages of lithological units. Reconstructing the tectonic evolution of an orogenic belt requires a detailed analysis of the lithological character, geochemistry, contact relationships, depositional setting, paleotectonic significance, and age of individual lithological units, and correlation of these units into tectonically significant terranes.

In the Newfoundland Appalachians, much research effort has focused on establishing a coherent stratigraphic and tectonostratigraphic framework in which to address the tectonic evolution of the orogen (e.g., Williams 1964, 1979; Williams and Hatcher 1982; Williams et al. 1988). The purpose of the present chapter is twofold: 1) to summarize current theories regarding the geology, tectonostratigraphic framework and tectonic evolution of the Newfoundland Appalachians and the BVP; and 2) to provide a detailed description of the geology of the Ming's Bight - Pacquet Harbour area on the BVP. In the present study, the time scale of Tucker and McKerrow (1995) is employed for Cambrian through Early Devonian time, whereas the time scale of Harland et al. (1989) is employed for post-Early Devonian time.

2.2 REGIONAL SETTING AND PREVIOUS WORK

2.2.1 *Newfoundland Appalachians*

The Newfoundland Appalachians are subdivided, from west to east, into four tectonostratigraphic zones: the Humber, Dunnage, Gander, and Avalon (Williams 1979; Williams and Hatcher 1982; Figs. 1.1 and 2.1).

The Humber Zone comprises three essential tectonic elements: 1) pre-Late Proterozoic gneissic basement complexes of the rifted Laurentian margin (e.g., Owen and Erdmer 1989); 2) an unconformably overlying wedge of Late Proterozoic to Middle Ordovician rift-facies, passive-margin, and foreland basin carbonate and siliciclastic rocks (e.g., Stevens 1970); and 3) a structurally overlying allochthonous succession of passive margin sedimentary rocks and Early Ordovician ophiolites (e.g., Church and Stevens 1971; Dewey and Bird 1971; Dunning and Krogh 1985). These elements collectively record Late Proterozoic rifting of Laurentia to form the Iapetus ocean (e.g., Stukas and Reynolds 1974; Kamo et al. 1989), development of a passive continental margin, and destruction of the passive margin through arc-continent collision and westward emplacement of ophiolites during the Middle Ordovician Taconian orogeny (e.g., Stevens 1970; Bird and Dewey 1970; Church and Stevens 1971; Dewey and Bird 1971; Williams 1979; Stockmal et al. 1987; van der Pluijm 1987; Cawood and Williams 1988; Suhr and Cawood 1993). The Humber Zone is tectonically separated from the Dunnage Zone to the east by a major ductile deformation zone termed the BVL (Williams and St. Julien 1982). In general, the metamorphic grade and intensity of deformation in the Humber Zone increase from west to east toward the BVL (e.g., Cawood et al. 1995).

Figure 2.1 Simplified geological map of the island of Newfoundland, illustrating the main tectonostratigraphic units and terrane boundaries (Colman-Sadd et al. 1990). The Hermitage Flexure is the proposed site of the promontory-promontory collision between the Laurentian and Gondwanan continental margins in Early Silurian time (e.g., Lin et al. 1994; Dubé et al. 1996).

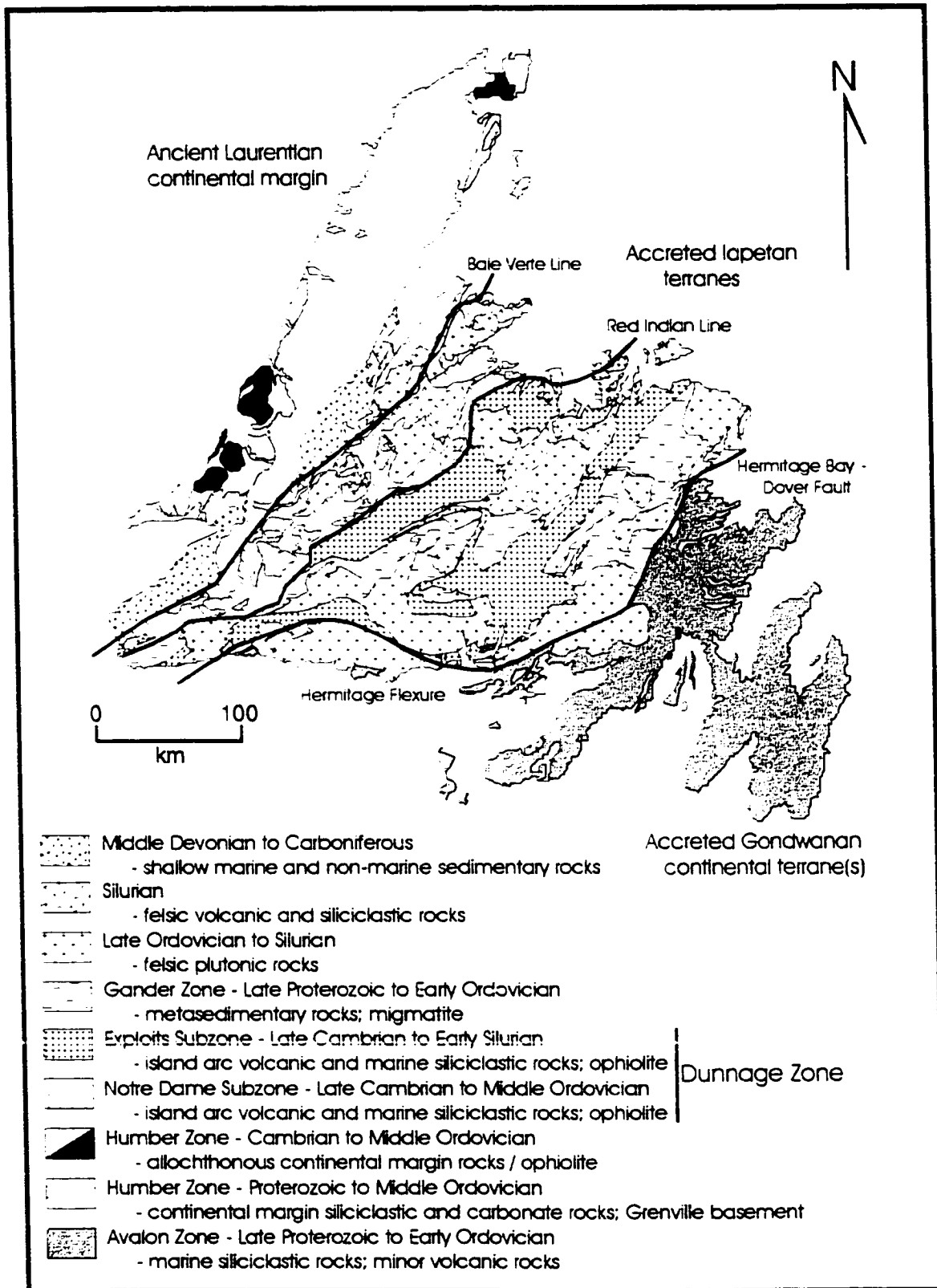


Figure 2.1

The Dunnage Zone comprises Cambrian to Middle Ordovician island-arc and back-arc basin successions that conformably overlie oceanic crust and consist of mafic to felsic volcanic and marine siliciclastic rocks that collectively represent the vestiges of the Early Paleozoic Iapetus ocean basin (e.g., Williams 1979; Arnott et al. 1985; Dunning and Krogh 1985; Dunning et al. 1987; Williams et al. 1988; Swinden et al. 1990; Fyffe and Swinden 1991; Dec et al. 1997; O'Brien et al. 1997). The Dunnage Zone is subdivided on the basis of stratigraphy, paleomagnetic signatures and biogeographic affinities into the Notre Dame and Exploits Subzones to the west and east, respectively, of the Red Indian Line (Williams et al. 1988; Fig. 2.1). Notre Dame Subzone rocks apparently formed in an island-arc setting above a subduction zone proximal to the Laurentian margin (van der Pluijm et al. 1993; Dec et al. 1997), and contain faunas of Laurentian affinity (e.g., Williams et al. 1992). These rocks were accreted to Laurentia in the Middle Ordovician Taconian orogeny (e.g., Williams 1979; van der Pluijm 1987; Johnson et al. 1991; van der Pluijm et al. 1993). In contrast, the Exploits Subzone rocks probably evolved in a peri-Gondwanan setting, as indicated by faunas of Gondwanan (Celtic) affinity (e.g., Williams et al. 1992; O'Brien et al. 1997), and were, at least in part, accreted to the Gander Zone in the Middle Ordovician Penobscotian orogeny (Colman-Sadd et al. 1992). The ocean basin that separated the Notre Dame and Exploits Subzones probably closed in the Early Silurian, as indicated by overlap successions of the same age on either side of the Red Indian Line (Williams et al. 1988; van der Pluijm et al. 1993).

The Gander Zone comprises thick successions of continentally-derived siliciclastic rocks which are separated on the basis of geographic location into the Meelpaeg, Mount

Cormack, and Gander Lake Subzones (Williams et al. 1988; Fig. 1.1). The Gander Zone rocks were probably deposited near the eastern margin of Iapetus adjacent to the Gondwanan margin sometime prior to the Middle Ordovician Penobscotian orogeny (Colman-Sadd et al. 1992), though the nature of the Gander Zone basement remains uncertain (Williams et al. 1988). The subzones are everywhere in tectonic contact with the adjacent Dunnage Zone rocks along major northeast-trending ductile deformation zones such as the Gander River Ultrabasic Belt and Noel Paul's Line (Fig. 1.1). The Mount Cormack Subzone may represent a structural window through the overlying Exploits Subzone (e.g., Colman-Sadd and Swinden 1984; Williams et al. 1988; Colman-Sadd et al. 1992). To the east, the Gander Zone is separated from the Avalon Zone by the Hermitage Bay and Dover Faults which record complex Siluro-Devonian movement (e.g., Hanmer 1981; Holdsworth 1994; Fig. 1.1).

The Avalon Zone lies outboard of the Gander Zone, and comprises a thick succession of Late Proterozoic to Early Ordovician marine to terrestrial clastic and bimodal volcanic rocks which have a Gondwanan biogeographic affinity (e.g., Williams 1979; O'Brien et al. 1983; Williams et al. 1992). The Avalon Zone is thus interpreted as a continental terrane of Gondwanan affinity which was accreted to the Gander Zone along the Hermitage Bay and Dover Faults sometime prior to the Late Devonian (e.g., Williams 1979; Williams and Hatcher 1982; O'Brien et al. 1983). The Avalon Zone is relatively undeformed and unmetamorphosed compared to the adjacent Gander Zone, indicating that it was not strongly affected by the Paleozoic orogenic activity (Williams and Hatcher 1982).

The tectonic evolution of the Newfoundland Appalachians involved a protracted series of Paleozoic orogenic events. The Taconian and Penobscotian orogenies involved Middle Ordovician subduction and ophiolite obduction along the western and eastern margins, respectively, of the Iapetus ocean basin (e.g., Williams 1979; Colman-Sadd et al. 1992). These orogenic events resulted in burial of the Iapetus passive margins to >20km depth, as recorded by pre-Late Silurian eclogite to amphibolite facies metamorphism in Humber Zone rocks (e.g., Jamieson 1990; Williams 1993; Cawood et al. 1994, 1995), and by late-Middle Ordovician migmatites in the Mount Cormack Subzone (Colman-Sadd et al. 1992). In the Early Silurian, the Iapetus ocean basin between the Notre Dame and Exploits Subzones apparently closed, owing to continued subduction, orogen-scale sinistral oblique convergence of the Laurentian and Gondwanan continental margins (e.g., Doig et al. 1990; Soper et al. 1992), and promontory-promontory collision within the Hermitage Flexure (Lin et al. 1994; Fig. 2.1). This collisional event resulted in penetrative ductile deformation and high-grade metamorphism along the Gander-Dunnage and Humber-Dunnage zone boundaries (e.g., Hanmer 1981; Currie and Piasecki 1989; Dunning et al. 1990; O'Brien et al. 1991; Cawood and Dunning 1993; Williams 1993; Cawood et al. 1994, 1995, 1996; Holdsworth 1994; Lin et al. 1994; Burgess et al. 1995; Dubé et al. 1996), and widespread, less intense ductile deformation and low-grade metamorphism in north-central Newfoundland (e.g., Karlstrom et al. 1982; Kusky et al. 1987; LaFrance 1989; Elliot et al. 1991; LaFrance and Williams 1992; Williams 1993). This orogenic activity also coincided with a general emergence of the orogen, as indicated by the transition from marine to non-marine and subaerial sedimentation between the Late

Ordovician and Early Silurian (e.g., Williams 1979; Arnott et al. 1985; Williams 1993). In addition, the Early Silurian was marked by widespread felsic plutonism and subaerial to shallow-marine felsic volcanism throughout what is now central Newfoundland (e.g., Coyle and Strong 1987; Bevier and Whalen 1990; Dunning et al. 1990; Fig. 2.1).

The Silurian orogenesis was followed by a protracted episode of latest Silurian to Carboniferous deformation which was spatially and temporally heterogeneous on the scale of the Newfoundland and northern Appalachians. In western Newfoundland, this deformation is mainly characterized by post-Taconian, west-directed, primarily thin-skinned thrusting (e.g., Bosworth 1985; Cawood and Williams 1988; Stockmal and Waldron 1990; Waldron and Milne 1991; Waldron and Stockmal 1991, 1994; Cawood et al. 1995). In the remainder of the northern Appalachians, this deformation is characterized by distributed ductile to brittle-ductile dextral shear and reactivation of earlier structural zones (e.g., Kusky et al. 1987; Ferrill and Thomas 1988; Currie and Piasecki 1989; Stockmal et al. 1990; LaFrance and Williams 1992; Malo et al. 1992; Kirkwood and Malo 1993; O'Brien et al. 1993; de Roo and van Staal 1994; Hibbard 1994; Holdsworth 1994; Langdon and Hall 1994; Lin 1995; Malo and Kirkwood 1995; van Staal and de Roo 1995; Williams et al. 1995; Dubé and Lauzière 1996; Dubé et al. 1996). In many locations, these structures are spatially associated with fault-bounded basins of Middle Devonian to Carboniferous non-marine siliciclastic rocks which, at least locally, unconformably overlie all tectonostratigraphic zones in Newfoundland and collectively point toward a widespread transtensional deformation regime by Middle to Late Devonian time, with local evidence for dextral transpression (e.g., Bradley 1982; Hyde et al. 1988; Miller et al. 1990;

Langdon and Hall 1994; Hamblin et al. 1995).

It is within this presently-accepted tectonostratigraphic and regional-tectonic framework that the geology and the tectonic evolution of the BVP are addressed below.

2.2.2 Baie Verte Peninsula

The geology of the BVP is broadly divided into rocks of Humber and Dunnage affinity to the west and east, respectively, of the BVL (Fig. 1.2). The one exception to this simplified division, the 'problematic' MBG, is addressed in Sections 2.2.2.4 and 2.3.1.

2.2.2.1 Humber Zone

The Humber Zone rocks to the west of the BVL are divided into two main lithological units which are both intruded by the Early Silurian, syn to late-tectonic, Wild Cove Pond felsic igneous suite (Hibbard 1983; Cawood et al. 1994; Fig. 1.2).

The East Pond Metamorphic Suite primarily comprises psammitic and semi-pelitic schist and metaconglomerate, with minor migmatite, ortho- and paragneiss, and amphibolite (e.g., de Wit 1972, 1974, 1980; Hibbard 1983). These rocks are disposed in two elliptical outcrop areas which are interpreted to form the core of a regional scale antiformal structure that plunges north (de Wit 1974, 1980; Fig. 1.2). In the East Pond Metamorphic Suite, the thinly layered psammitic and semi-pelitic schist is conformably interlayered with metaconglomerate (de Wit 1972, 1974; Hibbard 1983), consistent with a primary depositional relationship (Hibbard 1983). The migmatite comprises a quartzofeldspathic leucosome, pelitic to amphibolitic paleosome, and is locally found as boulders in the metaconglomerate, prompting de Wit (1972, 1974, 1980) and Hibbard (1983) to propose that the metaconglomerate unconformably overlies a basement complex

comprised of migmatite and gneiss. Thus, the metaclastic rocks are widely regarded as Late Proterozoic to Early Cambrian sedimentary rocks deposited on Grenvillian basement during the early stages of rifting along the Laurentian margin, and the amphibolite, which locally occurs in cross-cutting dyke-like bodies, is thought to represent rift-related mafic dykes (Church 1969; Bursnall and de Wit 1975; Hibbard 1983).

The East Pond Metamorphic Suite is structurally overlain by the Fleur de Lys Supergroup along a series of high-angle ductile shear zones which may have reactivated a primary depositional contact (de Wit 1974, 1980; Hibbard 1983). The Fleur de Lys Supergroup comprises a thick, generally upright (de Wit 1980), succession of siliciclastic rocks, with minor amphibolite, calc-silicate, and marble. The siliciclastic rocks consist of layered psammitic to semi-pelitic schist, with minor pelite and metaconglomerate. The amphibolite occurs within the siliciclastics as numerous tholeiitic cross-cutting dyke-like bodies, and concordant sill-like bodies (de Wit 1980). Collectively, these rocks are widely regarded as Laurentian rift-related continental margin sediments and mafic intrusions of probable Cambrian to Middle Ordovician age (e.g., Church 1969; Bird and Dewey 1970; de Wit 1972, 1974, 1980; Bursnall and de Wit 1975; Kennedy 1975; Williams 1979; de Wit 1980; Hibbard 1983). The calc-silicate and carbonate rocks typically occur in 5 to 50m thick layers or pods which are concordant to the layered siliciclastic rocks. Internally, they vary from massive to thinly-layered to conglomeratic (de Wit 1972; Bursnall and de Wit 1975; Hibbard 1983). The conglomerates comprise very coarse (up to ~1m), angular (tabular) carbonate clasts in a fine-grained carbonate to siliciclastic matrix, and resemble the Cow Head conglomerates of the external Humber Zone, leading to the proposition

that the Fleur de Lys Supergroup may be partly correlative with the Middle Cambrian to Middle Ordovician Cow Head Group (Bursnall and de Wit 1975; Hibbard 1983).

Alternatively, Jamieson (pers. comm., 1996) noted that the conglomerates along the coast of White Bay are confined to fault bounded slivers, and therefore might not be a primary part of the Fleur de Lys Supergroup.

Towards the BVL, the Fleur de Lys Supergroup is imbricated with mafic volcanic and ultramafic rocks of the Advocate ophiolite complex, prompting several authors to propose a primary depositional contact between these units (e.g., Kennedy 1973, 1975; Bursnall and de Wit 1975). However, given that the ophiolitic rocks only occur immediately adjacent to the BVL (Williams 1977; Hibbard 1982, 1983, 1987) and are associated with early high strain zones (Bursnall 1975; Hibbard 1983, 1987), it seems more probable that they represent tectonic inclusions in the Fleur de Lys Supergroup which are related to the obduction of ophiolites during the Taconian orogeny (Williams 1977), or to the protracted post-Taconian movement history along the BVL (e.g., Goodwin and Williams 1990).

In general, the deformation and metamorphic history of East Pond Metamorphic Suite and Fleur de Lys Supergroup, excluding the possible Grenvillian basement, is thought to involve three phases (e.g., Kennedy 1975; Bursnall and de Wit 1975; de Wit 1980; Hibbard 1983). The main phase of deformation (D_M) was contemporaneous with peak amphibolite facies metamorphism in the Fleur de Lys Supergroup (Jamieson and Vernon 1987), and was previously attributed to the Middle Ordovician Taconian orogeny (e.g., Church 1969; Bursnall and de Wit 1975; Kennedy 1975; Williams 1977, 1979;

Hibbard 1983). However, on the basis of a U-Pb monazite date from migmatitic schist in the Fleur de Lys Supergroup, Cawood et al. (1994) assigned an Early Silurian age to the metamorphic peak, and thus the main phase of deformation, in the East Pond Metamorphic Suite and Fleur de Lys Supergroup.

The deformation and metamorphism of the Humber Zone rocks is treated in greater detail in Chapters 3 and 5, respectively. However, these data illustrate that the tectonic evolution of the Humber Zone rocks on the BVP probably involved the combined effects of Late Proterozoic to Middle Ordovician development of the Laurentian passive margin, destruction and burial of the passive margin to >20km depth during the Middle Ordovician Taconian orogeny, and intense deformation and peak metamorphism coincident with the Early Silurian orogenic event (e.g., Jamieson 1990; Vance and O'Nions 1990; Cawood and Dunning 1993; Cawood et al. 1994).

2.2.2.2 Dunnage Zone

On the BVP, Dunnage Zone rocks consist of several variably dismembered Early Ordovician ophiolite complexes that occur in fault-bounded sections along the BVL, and in tectonic, intrusive, and/or unconformable contact with Early Silurian felsic volcanic-plutonic successions to the east of the BVL (Fig. 1.2).

Much has been written regarding the geology, geochemistry, correlation, relative age, and tectonic significance of the ophiolite complexes on the BVP (e.g., Neale and Kennedy 1967; Church 1969; Dewey 1969; Church and Stevens 1971; Dewey and Bird 1971; Gale 1971, 1973; Kennedy 1973, 1975; Upadhyay 1973; Kidd 1974; Bursnall 1975; Bursnall and de Wit 1975; Neale et al. 1975; Norman and Strong 1975; Kidd 1977;

Williams 1977; Kidd et al. 1978; Jenner and Fryer 1980; Hibbard 1982; Dunning and Krogh 1985). In the present study, the ophiolite complexes are considered in the context of the stratigraphic framework for the BVP proposed by Hibbard (1983). In this framework, the ophiolite complexes are interpreted to comprise at least one of two components: 1) ophiolitic basement; and 2) ophiolitic cover sequence. The ophiolitic basement comprises a generally dismembered succession of massive to cumulate ultramafic rock and gabbro, sheeted dykes, and pillowed basalt. In contrast, the ophiolitic cover sequence typically comprises the following: 1) units of pillowed basalt, with minor pillow breccia, mafic intrusions, and mafic volcanoclastic rock; 2) generally subordinate sections of felsic volcanic and volcanoclastic rock; and 3) sedimentary sections comprising boulder to pebble conglomerate, greywacke, siltstone, and iron formation, with variable amounts of mafic and/or felsic volcanic and volcanoclastic material. The sedimentary sections are quite distinctive because of abundant, ~1cm diameter, detrital pyroxene crystals, and the locally immense (>100m) clasts of ophiolitic basement lithologies in conglomerate (e.g., Kidd 1974, 1977; Kidd et al. 1978; Hibbard 1983). All of these units are intruded by synvolcanic mafic dykes and sills.

Significantly, the major-element geochemistry of pillowed basalt in the ophiolitic basement tends to be boninitic, whereas that of pillowed basalt in the cover sequence tends to be tholeiitic, with a highly variable trace-element geochemistry indicative of back-arc, oceanic-island, and/or island-arc paleotectonic environments (Gale 1971, 1973; Norman and Strong 1975; Kidd 1977; Jenner and Fryer 1980; Hibbard 1983; Swinden et al. 1989; Fyffe and Swinden 1991). Collectively, these relationships are interpreted to reflect ocean

crust development and cover sequence deposition in a rifted arc and/or back-arc paleotectonic setting in the Early Paleozoic Iapetus ocean (Kidd 1977; Kidd et al. 1978; Swinden et al. 1989; Fyffe and Swinden 1991).

In the context of this framework, the Point Rouse and Advocate ophiolite complexes are interpreted to comprise dismembered ophiolitic basement that is overlain conformably and unconformably, respectively, by ophiolitic cover (Bursnell 1975; Norman and Strong 1975; Kidd et al. 1978; Hibbard 1983). Aeromagnetic data clearly indicate that these successions continue under the waters of Baie Verte (Kidd et al. 1978; Miller and Wiseman 1994), and in the present study they are interpreted as heterogeneously deformed portions of a single ophiolite complex (e.g., Norman and Strong 1975; Fig. 1.2). The Betts Cove ophiolite comprises partially dismembered ophiolitic basement that is conformably overlain by the Snooks Arm Group cover sequence (Upadhyay 1973), whereas the PHG probably comprises both the uppermost section of ophiolitic basement (pillowed basalts), and a thick, possibly conformable, cover sequence (Hibbard 1983).

Based on lithological and geochemical constraints, all of the ophiolite complexes on the BVP are considered to represent a single generation of Early Ordovician ocean crust, and are thus mutually correlative (Hibbard 1983). This correlation is supported by the 488.6 ± 1.8 Ma U-Pb zircon age of the gabbro in the Betts Cove ophiolite (Dunning and Krogh 1985), the 483 ± 2 Ma U-Pb zircon age from a synvolcanic gabbro sill in the cover sequence of the PROC (Ramezani 1992), the Arenig-Llanvirn (ca. 470 Ma) graptolites in the Snooks Arm Group (Williams 1992), and by regional geologic and geochronologic constraints (e.g., Dunning and Krogh 1985).

The nature of the Flat Water Pond Group, however, is somewhat more ambiguous. The Flat Water Pond Group outcrops in a thin succession along the trace of the BVL (Fig. 1.2), and comprises unseparated mafic volcanic and volcanoclastic rocks, with subordinate pillowed basalt, felsic volcanic and volcanoclastic rocks, conglomerate, sandstone, siltstone, and iron formation (e.g., Kidd 1974, 1977; Hibbard 1983). The sedimentary and volcanoclastic sections contain abundant detrital pyroxene crystals and immense clasts (locally in excess of 100m) of ophiolitic basement lithologies in conglomerate, and all of these lithologies are intruded by synvolcanic mafic dykes and sills (Kidd 1974, 1977). Thus, the lithology of the Flat Water Pond Group is essentially identical to that of the Early Ordovician ophiolitic cover sequence, and in the past these sequences have been correlated (e.g., Kidd 1977; Kidd et al. 1978; Hibbard 1983). Indeed, the Flat Water Pond Group contains pillowed basalts with trace-element geochemical signatures resembling ocean-ridge basalts (Kidd 1977), and is associated with sections of ophiolitic basement along its entire outcrop length. Moreover, the Flat Water Pond Group can be traced northward with apparently continuity into the cover sequence of the Point Rouse - Advocate ophiolite complex near Baie Verte (Hibbard 1983). To the south it is unconformably overlain by the Early Silurian MicMac Lake Group, consistent with a pre-Late Silurian depositional age (Kidd 1974, 1977; Hibbard 1983; Coyle and Strong 1987; Fig. 1.2).

However, conglomerates that are widely regarded as conformable basal members of the Flat Water Pond Group contain clasts that superficially resemble the Early Silurian Burlington Granodiorite (e.g., Kidd 1974, 1977; Hibbard 1983), and this relationship has

been used as evidence in support of an Early Silurian age for the Flat Water Pond Group (e.g., Hibbard 1983; Cawood and Dunning 1993; Jamieson et al. 1993a, 1993b; Bélanger et al. 1996). However, based on the established field relationships, this interpretation requires: 1) intrusion of the Burlington Granodiorite (432 ± 2 Ma; U-Pb zircon; Cawood and Dunning 1993); 2) subaqueous deposition of the Flat Water Pond Group and associated ocean-ridge-type pillowed basalts proximal to exposed ophiolite and granodiorite (Kidd 1977; Hibbard 1983); and 3) subaerial deposition of the MicMac Lake Group felsic volcanic and volcanoclastic rocks, which lack ophiolitic detritus, over the Burlington Granodiorite and Flat Water Pond Group (Hibbard 1983). The marked contrast in lithology and clast-provenance in the Flat Water Pond Group and MicMac Lake Group implies a rather significant change in tectonic and/or depositional setting in the time interval between deposition of these units. However, the MicMac Lake Group is widely considered to be correlative with several nearby Early Silurian (ca. 430-425 Ma.) felsic volcano-plutonic successions (e.g., DeGrace et al. 1976; Hibbard 1983; Coyle and Strong 1987; Cawood and Dunning 1993). Thus, the timing constraints require intrusion of the granodiorite (ca. 430 Ma), exposure of the granodiorite, deposition of the Flat Water Pond Group, a significant change in depositional setting, and deposition of the MicMac Lake Group (ca. 430-425 Ma) within, at the very most, 10 million years, and probably significantly less.

In light of the rather tight timing constraints, the author considers it much more reasonable to correlate the Flat Water Pond Group with the lithologically and geochemically similar Early Ordovician ophiolite cover sequence, and attribute the

granodiorite clasts in the Flat Water Pond Group to erosion of an arc-related felsic pluton of pre-Early Ordovician age, such as those that are known to exist in other segments of the Notre Dame Subzone (e.g., the Twillingate pluton; Elliott et al. 1991). Significantly, granodioritic clasts noted in conformable conglomerate layers in the lower portions of the Snooks Arm Group were also formerly interpreted as having Burlington Granodiorite affinity (Church 1969), although this interpretation is now stratigraphically untenable (e.g., Williams 1992). Alternatively, it is conceivable that only some portions of the Flat Water Pond Group are Silurian (e.g., Cawood and Dunning 1993); however, this would have to be reconciled with the abundance of ophiolitic detritus in the Flat Water Pond Group conglomerate, and the lack of such detritus in the MicMac Lake Group. Thus, the Flat Water Pond Group is interpreted to be correlative with the ophiolitic cover sequence.

In general, the deformation and metamorphism of the ophiolite complexes is highly variable, but in most cases demonstrably post-dates the Early Silurian felsic plutons. Along the BVL, the ophiolites typically contain multiple penetrative ductile fabrics, and record greenschist to (locally) amphibolite facies metamorphism. The Betts Cove ophiolite, Snooks Arm Group, and the southern portions of the PHG, typically contain a single penetrative fabric, and record greenschist facies metamorphism, except where contact-metamorphosed to amphibolite facies. In contrast, the northern portion of the PHG contains multiple penetrative ductile fabrics, and records middle amphibolite facies metamorphism. The significance of these relationships is discussed in Chapters 3, 4, and 5.

2.2.2.3 Early Silurian volcano-plutonic rocks

The Humber and Dunnage Zone rocks on the BVP are intruded by numerous Early

Silurian felsic plutons (Fig. 1.2), including: the Burlington Granodiorite (432 ± 2 Ma.; Cawood and Dunning 1993); the Dunamagon Granite (429 ± 4 Ma.; Cawood and Dunning 1993); and the Wild Cove Pond igneous suite (427 ± 2 to 423 ± 3 Ma.; Cawood and Dunning 1993). Based on field and regional relationships, the Cape Brule Porphyry, La Scie intrusive complex, and King's Point complex are also considered to be Early Silurian (e.g., Hibbard 1983; Coyle and Strong 1987; Cawood and Dunning 1993). In addition, the Dunnage Zone rocks and Silurian plutons are unconformably overlain by the Cape St. John Group and MicMac Lake Group volcanic successions comprising rhyolitic to dacitic flows, domes and agglomerates, as well as pyroclastic breccias and tuffs (Kidd 1974, 1977; Neale et al. 1975; DeGrace et al. 1976). These successions also contain abundant epiclastic volcanic conglomerate and sandstone, and locally significant amounts of mafic flows. The general characteristics of these rocks are consistent with a shallow marine to subaerial depositional setting, proximal to a large, primarily felsic, volcanic centre (Kidd 1974; DeGrace et al. 1976; Hibbard 1983). This hypothesis is supported by the well documented syn-volcanic relationship between the Cape Brule Porphyry and the overlying Cape St. John Group (Neale et al. 1975; DeGrace et al. 1976; Hibbard 1983).

These rocks are collectively interpreted in terms of an extensive, high-level, epicontinental caldera complex and volcanic field which formed throughout western Newfoundland during the final closure of the Iapetus ocean in the Early Silurian (e.g., Coyle and Strong 1987; Dunning et al. 1990; Fryer et al. 1992). In the area of the BVP, three such caldera complexes have been proposed (Coyle and Strong 1987), comprising: 1) the Wild Cove Pond igneous suite, MicMac Lake Group, and Sops Arm Group; 2) the

King's Point complex; and 3) the Cape Brule Porphyry, Cape St. John Group, and Springdale Group.

For the most part, the Early Silurian volcano-plutonic successions were deformed and metamorphosed together with the pre-Silurian rocks on the BVP, and are particularly significant because: 1) the disposition of the subaerial volcanic and epiclastic rocks, as well as their relationships to regional deformation and metamorphism, indicates that the present erosional surface of the eastern BVP was near-surface in the Early Silurian, whereas that of the western BVP was at considerable depth; and 2) the plutons provide important age constraints on deformation structures that record the subsequent relative movement of the Humber and Dunnage Zone rocks.

2.2.2.4 The Baie Verte Line and the 'problematic' Ming's Bight Group

The BVL (Williams and St. Julien 1982) is a fundamental tectonic boundary in the Newfoundland Appalachians, and has figured prominently in geological interpretations of the BVP (e.g., Baird 1951; Neale and Kennedy 1967; Church 1969; Kennedy 1973, 1975; Kidd 1977; Bursnall and de Wit 1975; Williams 1977, 1979; Hibbard 1982, 1983; Dallmeyer and Hibbard 1984; Cawood and Dunning 1993; Jamieson et al. 1993a, 1993b; Cawood et al. 1994, 1995; Anderson 1995). In spite of this attention, remarkably little is actually known about the timing and kinematics of movement along the BVL, and the role it has played in the arrangement of the litho-tectonic units on the BVP. This is particularly evident in the case of the MBG.

The BVL is a narrow structural zone that strikes northeast, and dips steeply. The BVL is marked by a series of highly dismembered ophiolite complexes, and is widely

regarded as the 'root zone' for the westward obduction of ophiolitic allochthons during the Taconian orogeny (Williams and St. Julien 1982; Williams 1979; Fig. 1.2). However, recent examination of the deformation structures associated with the BVL reveals a complex post-Ordovician movement history (e.g., Goodwin and Williams 1990); a detailed description is provided in Chapter 3.

With regard to the 'MBG problem', Hibbard (1982) proposed that the BVL turns sharply to the east near the town of Baie Verte and can be traced eastward along the northern contact of the Dunamagon Granite, thereby tectonically separating the MBG from Dunnage Zone rocks to the south (Fig. 1.2), and apparently solving the problem of the anomalous tectonostratigraphic location of the MBG. This change in orientation of the BVL was termed the Baie Verte Flexure, and was thought to reflect the original geometry of the rifted Laurentian margin (i.e., the Baie Verte area as a re-entrant in the Laurentian margin; Hibbard 1982, 1983). However, this model was not reconciled with the apparent timing and kinematics of deformation structures associated with the flexure, and was proposed at a time when the significance of post-Taconian tectonism along the BVL was not fully appreciated. Indeed, detailed structural mapping conducted in the present study reveals that the structural trends used by Hibbard (1982) to define the flexure formed during two spatially, temporally, and kinematically distinct deformation events (Chapters 3 and 4). In light of these limitations, an alternative model is presented in Chapter 7.

2.3 GENERAL GEOLOGY - MING'S BIGHT-PACQUET HARBOUR AREAS

The geology of the Ming's Bight and Pacquet Harbour areas (Fig. 2.2) has been extensively scrutinized over the past four decades, resulting in often conflicting

Figure 2.2 Simplified geological map of the thesis area (modified after Hibbard 1983). All contacts are tectonic, except the western contact between the PHG and Cape Brule Porphyry. Small black squares denote fishing outports. The principal contribution of the present study, in terms of the distribution of lithological units, is the recognition of: 1) a sequence of PROC rocks on the eastern shore of Ming's Bight; 2) PHG mafic volcanic rocks at Pelee Point; and 3) the thick sequence of felsic volcanic and volcaniclastic rocks in the north central portion of the PHG.

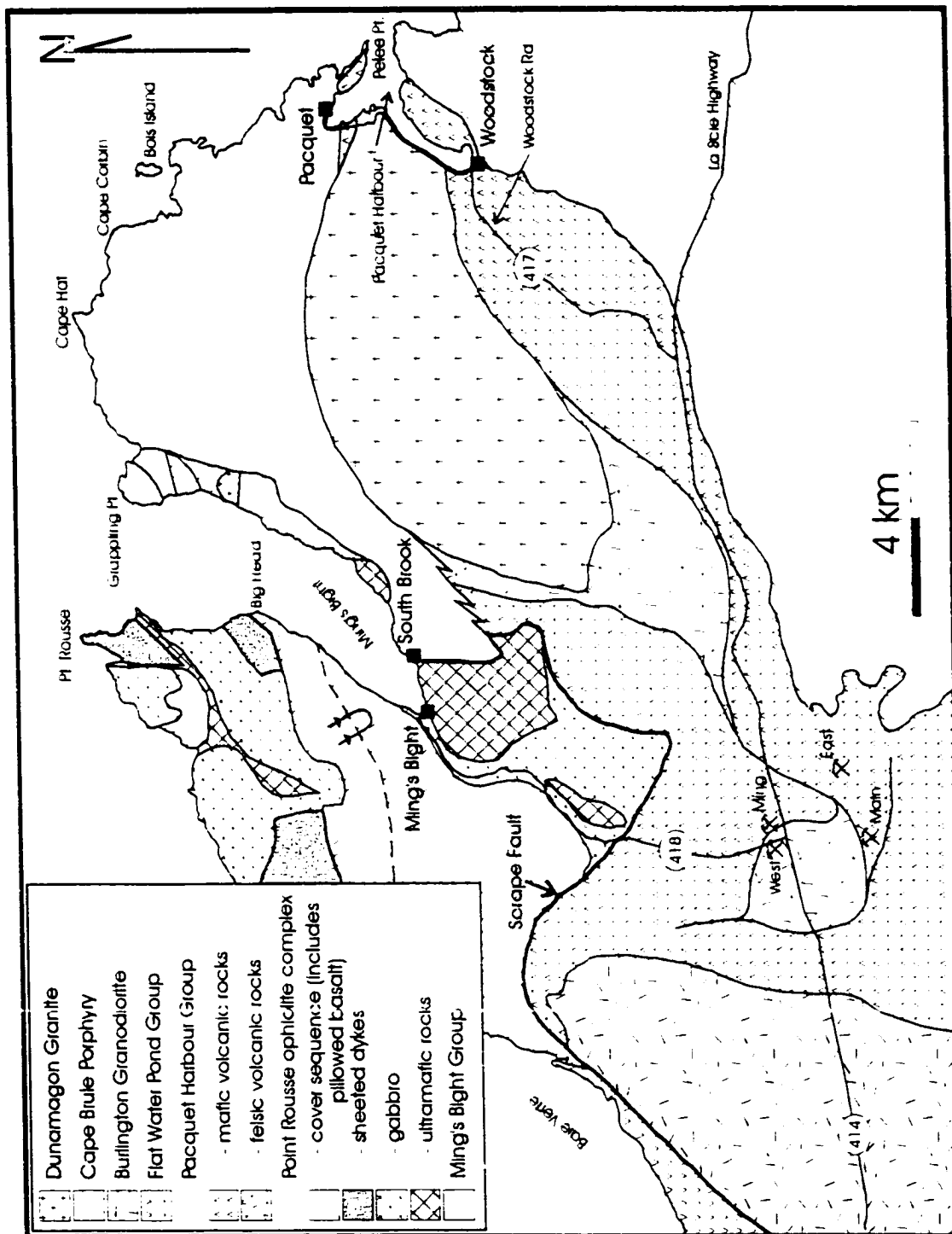


Figure 2.2

interpretations concerning the age, correlation, and tectonic significance of the lithological units (e.g., Hibbard 1983, and references therein). Although much of this controversy stemmed from a lack of age constraints, the correlation of units solely on the basis of their structural and/or metamorphic character has also been a detrimental factor. This problem has been particularly acute in the Pacquet Harbour area, where the MBG and PHG were considered to be partly correlative on the basis of structural and metamorphic similarities (e.g., Neale and Kennedy 1967; Church 1969; Coates 1970; Dewey and Bird 1971; Kennedy 1973, 1975; Bursnall and DeWit 1975; Dallmeyer 1977; Kidd 1977; Tuach and Kennedy 1978). This interpretation had several implications which collectively served to greatly complicate geological interpretations of the BVP (e.g., Neale et al. 1975; DeGrace et al. 1976; Williams 1977; Hibbard 1983).

In light of the past contention, the purpose of the remainder of this chapter is to provide a detailed summary of the geological and geochemical characteristics and contact relations of the main lithological units in the thesis area, and to summarize current theories regarding their age, depositional setting, and tectonostratigraphic affinity. Information related to the geological characteristics, depositional setting, contact relations, and deformation / metamorphism of particular units is based primarily on fieldwork conducted by the author. Observations concerning the regional correlation, tectonostratigraphic affinity, and age of particular units are based primarily on the work of others, with references provided accordingly.

2.3.1 Ming's Bight Group

2.3.1.1 General characteristics

The MBG (Baird 1951) comprises the strongly deformed succession of psammitic and semi-pelitic schist that crops out on the wide peninsula between Pacquet Harbour and Ming's Bight (Fig. 2.2). The MBG is bounded to the south by the Dunamagon Granite and PHG, and to the west by the PROC.

The MBG is characterized by monotonously layered psammitic and semi-pelitic schist (Fig. 2.3a). The psammities are grey-brown, medium- to coarse-grained, and comprise 50-80% quartz, 5-30% plagioclase, and <15% weakly foliated biotite and/or muscovite. The semi-pelites are dark brown-grey, medium- to coarse-grained, and contain <30% quartz, 15-35% plagioclase, 20-50% strongly foliated biotite and/or muscovite, and up to 5% magnetite. The thicknesses of individual layers range from <1cm to ~2m, but ~30cm is typical. The semi-pelitic layers are less abundant than the psammitic layers, and generally account for ~30% of most outcrops. Individual tabular psammitic layers can be traced continuously for up to ~50m in areas of good exposure, whereas the less competent semi-pelitic layers tend to be more irregular and discontinuous. The MBG also contains rare, pale green, calc-silicate layers up to 20cm thick that typically comprise 45% quartz, 40% clinozoisite-epidote, 15% plagioclase, 2% titanite, and <1% hornblende. These layers are discontinuous and boudinaged in the psammite/semi-pelite succession.

In many locations, the base of individual psammite beds is marked by a massive, 5-10cm thick, white-grey, quartzitic layer (>80% quartz). The quartzite grades into massive to layered psammitic schist, which in turn grades into massive semi-pelitic schist. The

Figure 2.3 Field photographs of the Ming's Bight Group and granitic pegmatites. **a)** Layered psammitic and semi-pelitic MBG schist in the hinge of a large-scale, reclined, F_2 fold along the north shore of Pelee Point (note the rhythmic aspect of the layering, and the hammer in upper-central portion of photograph for scale). **b)** Primary turbiditic layering in MBG schist on the north shore of Pelee Point. The sequence youngs toward the right (northeast). **c)** An example of an anastomosing, ~1-2m thick, granitic pegmatite dyke in a south-facing cliff face in Handy Harbour (Map 1). Note the tight, recumbent F_2 folds in the MBG immediately below the large pegmatite (arrowed). **d)** Radiating sheets of muscovite and large K-feldspar crystals in the core of the ovoid pegmatite body at White Point (Map 1).

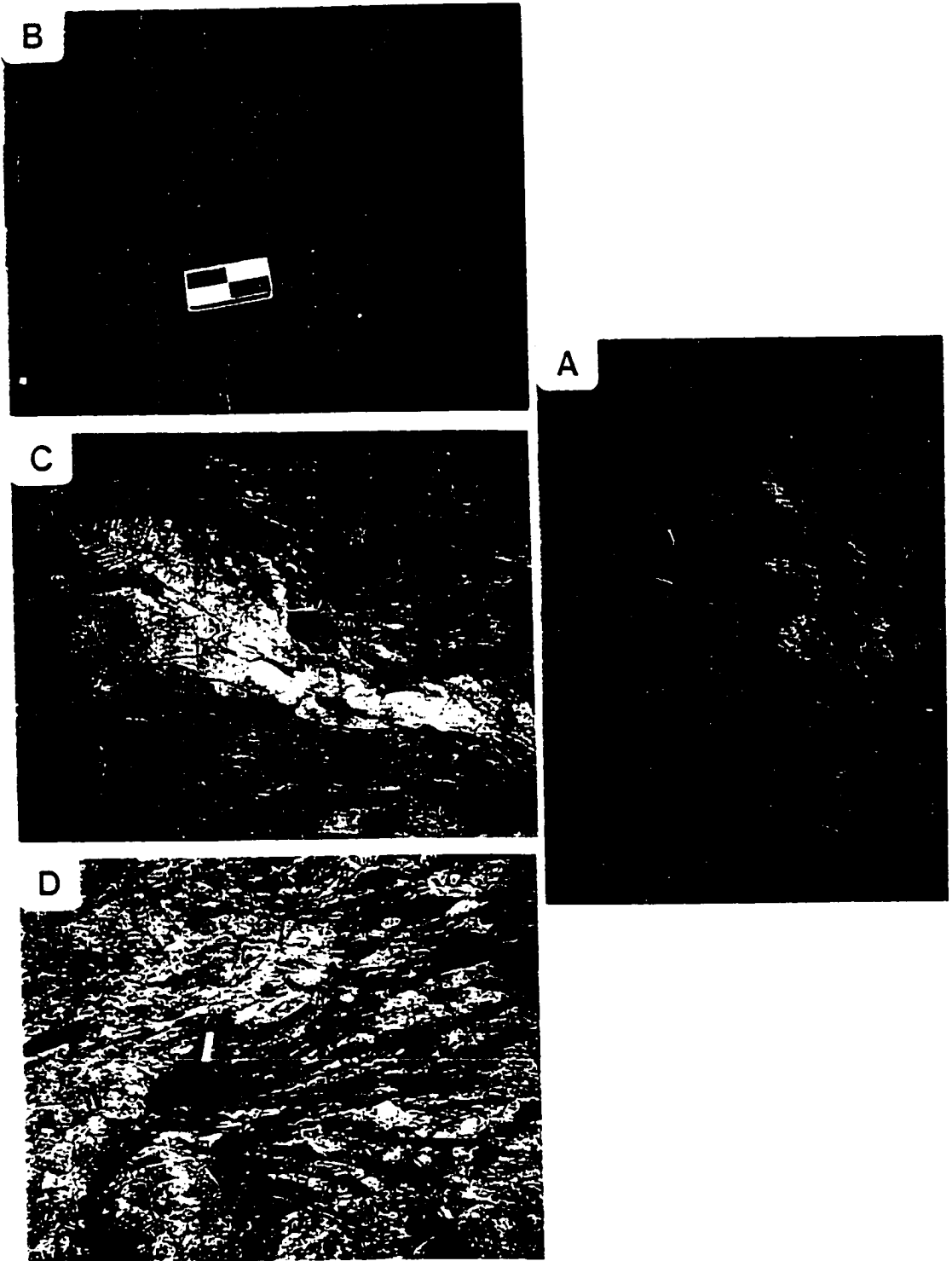


Figure 2.3

gradations are defined by a change in the colour of the rock and an associated change in the biotite, muscovite and quartz content, probably reflecting primary compositional variations (Fig. 2.3b). The contacts between individual beds are sharp, and the beds are locally rhythmically interlayered over ~10-20m thick sections. These features indicate that the protolith of the MBG probably comprised a succession of turbiditic sand, silt and mud. Detrital textures are rare in the MBG schists, although detrital apatite and zircon were noted in thin section and mineral separates.

The typical metamorphic mineral assemblage in the MBG schist consists of plagioclase + quartz + muscovite + biotite with minor garnet, kyanite, staurolite, chlorite, magnetite, rutile, ilmenite, tourmaline, and clinozoisite. This mineral assemblage is characteristic of the garnet to kyanite zones in the Barrovian zonal scheme, and is indicative of peak upper greenschist to lower amphibolite-facies metamorphism. The structure and metamorphism of the MBG are discussed in Chapters 3, 4, and 5.

Description of the MBG pegmatites

The northeastern portion of the MBG is intruded by a swarm of late-tectonic granitic pegmatite dykes (Map 1). The dykes, which range in thickness from <5cm to ~15m, can locally be traced for >500m. They typically strike northeast-southwest, dip steeply, and form tabular, very weakly-deformed bodies that cross-cut layering and deformation structures. In the area ~200m north of Red Point, the pegmatites are irregular, undeformed, and anastomose through the country rock (Fig. 2.3c, Map 1). In addition, two large ovoid pegmatite bodies are present at Red Point and White Point (Map 1). At Cape Hat, a ~1.5m thick pegmatite dyke contains a non-penetrative ductile foliation

that dips northwest; it is the only strongly deformed pegmatite observed in the study area.

The thinner pegmatite dykes (up to 2m) are typically massive, and comprise ~50% K-feldspar, ~30% quartz, ~10% plagioclase, and ~10% muscovite, with accessory garnet, apatite, columbite-tantalite, and microlite (see Section 6.3.2.1). K-feldspar crystals are coarse (1 to 30cm) and blocky in the interior of the dykes, and decrease in size and abundance towards the contacts, suggesting chilled margins and/or weak internal zoning. Plagioclase is fine- to medium-grained throughout the dykes, and may be slightly more abundant along the contacts. In a 20-40cm thick pegmatite dyke at Pelee Point, albitic plagioclase locally exhibits a fine-scale layering along the pegmatite margin. Quartz forms irregular blebs in the interior of the dykes, and muscovite is common, occurring as randomly oriented, up to 3cm, books. The thicker pegmatites (~2 to 15m) typically have massive, coarsely pegmatitic, K-feldspar-quartz-muscovite-rich cores that contain up to 70%, <30x30cm, euhedral K-feldspar crystals. The margins are fine- to coarse-grained, and comprise an albitic aplite-muscovite-K-feldspar-quartz-garnet assemblage typical of the border- or wall-zones of granitic pegmatites. The exo-contacts are typically marked by a halo, up to 30cm thick, of muscovite-rich MBG schist. At Red Point, a single, 2x3cm, pale-green, columnar-hexagonal crystal of beryl was noted within a ~15m thick pegmatite dyke. This, together with the presence of columbite-tantalite and microlite, suggests that the pegmatites are slightly enriched in beryllium, tantalum, and niobium. The dykes show no mineralogically obvious signs of 'regional' zoning over the area of the swarm.

At White Point (Map 1), a ~15x50m ovoid body of pegmatite has a well developed concentric zonation, which comprises a pegmatitic K-feldspar-quartz-muscovite core,

surrounded by a finer-grained plagioclase-muscovite-K-feldspar-quartz border zone. The core zone contains ~5-10% muscovite books up to 15cm in diameter, as well as spectacular radiating clusters of 0.5 to 2.0cm thick, up to 1m long, muscovite sheets (Fig. 2.3d). Presumably, the large ovoid pegmatites crystallized from more highly fractionated granitic melts, as suggested by the larger crystal-size and more complex internal zonation (e.g., Cerný 1991).

The mineral microlite is typically found in moderately to highly fractionated pegmatites of the rare-element class (Cerný and Ercit 1989). This, together with the relatively simple beryl-bearing mineral paragenesis and the homogeneous to concentric zoning patterns, suggests that the MBG pegmatites represent beryl-type pegmatites of the rare-element class (e.g., Cerný 1989, 1991). In general, this type of pegmatite is associated with late- to post-tectonic granite-pegmatite systems intruded into upper greenschist to lower amphibolite-facies metamorphic terranes (Cerný 1989). The pegmatite dykes only occur within the MBG, and thus have important implications for the interpretation of contact relationships and the timing of deformation.

2.3.1.2 Age and Correlation

There is a general consensus among workers on the BVP that the MBG and the Late Proterozoic to Middle Ordovician passive continental margin successions of the Fleur de Lys Supergroup are broadly correlative (e.g., Kennedy 1975; DeGrace et al. 1976; Hibbard 1983). This correlation is based on similarities in lithology, grade of metamorphism, and structural complexity. Furthermore, recent Nd-Sm isotopic studies (Fryer et al. 1992) show that both the MBG and Fleur de Lys Supergroup have strongly

negative ϵ_{Nd} values (-16, and -11, respectively), and Early Proterozoic model ages (2.4 Ga., and 2.0 Ga., respectively), indicating that both of these successions were derived from a highly evolved continental source (e.g., Laurentia). Thus, the MBG is considered to be a succession of turbiditic sediments deposited on the Laurentian passive continental margin between Late Proterozoic and Middle Ordovician time, and is thus of Humber Zone tectonostratigraphic affinity.

2.3.1.3 Contact Relations

In the Pacquet Harbour area, the MBG lies in contact to the south with the Dunamagon Granite and the PHG (Fig. 2.2). DeGrace et al. (1976) and Hibbard (1983) considered the contact between the MBG and the granite to be intrusive. This interpretation was based on the reported presence of MBG xenoliths in the granite, and the presence of cross-cutting granitic pegmatites in the MBG that were assumed to be related to the granite (DeGrace et al. 1976). However, the presence of MBG xenoliths in the granite was not confirmed in the present study, nor by the mapping of McDonald (1993). Furthermore, field relationships indicate that the granitic pegmatites in the MBG significantly post-date, and are therefore unrelated to, the Dunamagon Granite.

The controversial contact between the MBG and PHG at Pelee Point (Map 2) was interpreted by DeGrace et al. (1976) and Williams (1977) as conformable. This interpretation was apparently based on the near concordancy of layering in the MBG and PHG. However, tops indicators in the MBG (graded bedding) and PHG (cross-bedding and pillows) indicate that these units young in opposite directions on either side of the contact (see Chapter 3). Baird (1951) inferred that the contact between the MBG and

PHG is unconformable, but did not provide evidence to support this interpretation.

Hibbard (1983) suggested that the MBG-PHG contact is tectonic, and formed during obduction of Taconian ophiolite complexes. This hypothesis was based on the anomalously high strains recorded along the contact, a Middle Ordovician U-Pb zircon age for the Dunamagon Granite (Hibbard 1983; Dallmeyer and Hibbard 1984), and the presumption that the granite post-tectonically intruded the MBG-PHG contact (i.e., stitching pluton). However, recent U-Pb dating indicates an Early Silurian age for the Dunamagon Granite (Cawood and Dunning 1993). In addition, there is no evidence to support an intrusive relationship between the MBG and the granite, and structural relationships indicate that the granite is entirely pre-tectonic (see Chapter 3).

In the present study, the MBG-PHG and MBG-Dunamagon Granite contacts are both considered to be wholly tectonic. This hypothesis is based on the relationships discussed above, as well as two indirect lines of evidence. First, all lithological units to the east of the BVL except the MBG, are cut by pre-tectonic felsic dykes related to Early Silurian plutonism. Second, a distinctive suite of pre-tectonic megacrystic mafic dykes intruded all lithological units (including felsic plutons) east of the BVL (DeGrace et al. 1976; Hibbard 1983), except the MBG. These relationships indicate that the MBG and the surrounding Dunnage Zone lithologies were juxtaposed subsequent to emplacement of the Early Silurian felsic dykes and the syn- to post-Early Silurian megacrystic mafic dykes. Consequently, the MBG is probably everywhere in tectonic contact with the adjacent Dunnage Zone terranes. Zones of intense deformation developed along the MBG-Dunamagon Granite and MBG-PHG contacts support this hypothesis (see Chapter 3).

In several locations, the MBG is imbricated with discrete, fault-bounded successions of greenschist, metasediment, amphibolite, pillowed basalt, gabbro, mafic dykes, and/or granitic dykes (Fig. 2.2; Maps 4 and 7). Hibbard (1983) termed these successions the 'Pelee Point Schist' and, in accord with the interpretations of previous authors, included them as conformable members of the MBG schist (e.g., Hibbard 1983, and references therein). However, the present study illustrates that the Pelee Point Schist successions are everywhere in tectonic contact with the MBG and, in particular, only occur along the western and southern extremities of the MBG within the zones of intense deformation that mark the boundaries between the MBG and adjacent Dunnage Zone rocks (see Chapters 3 and 4; Fig. 2.2). Moreover, the Pelee Point Schist successions are lithologically and geochemically similar to the adjacent Dunnage Zone rocks (see Sections 2.3.2.3 and 2.3.6). It is therefore proposed that the Pelee Point Schist successions represent tectonic inclusions in, not conformable members of, the MBG.

2.3.2 Facquet Harbour Group

2.3.2.1 General Characteristics

The PHG outcrops in the north-central portion of the BVP, and is bounded to the west and south by the Burlington Granodiorite, to the east by the Cape Brule Porphyry, and to the north by the MBG, Dunamagon Granite, and PROC (Figs. 1.2 and 2.2). The PHG comprises a succession of variably deformed and metamorphosed mafic and felsic volcanic and volcanoclastic rocks, and hosts the Rambler volcanogenic massive sulphide deposits (e.g., Tuach and Kennedy 1978; Hibbard 1983; Fig. 2.2).

The deformation and metamorphism of the PHG is gradational from intensely

deformed, upper greenschist to amphibolite facies rocks in the north, to weakly deformed, lower greenschist facies rocks in the south (e.g., Tuach and Kennedy 1978; Hibbard 1983). In the Pacquet Harbour and Ming's Bight areas, the finite strain recorded in the PHG is heterogeneous. In most locations, massive to finely layered amphibolitic mylonite with a penetrative planar and linear fabric predominates. The local preservation of clastic or porphyritic textures within these rocks provides evidence of the protoliths. The mylonites are locally juxtaposed over short distances with weakly deformed rocks. This, together with small-scale examples of extreme transposition, indicate that the original stratigraphy of the PHG has been highly disrupted. In general however, the PHG succession in the Pacquet Harbour area strikes northeast, dips shallowly to steeply southeast, and youngs to the south. In the Ming's Bight area, the PHG succession strikes north-south, dips steeply, and lacks indicators of younging direction. The metamorphic mineral assemblage in the northern portions of the PHG generally consists of hornblende + plagioclase + biotite + epidote + quartz, with minor actinolite, chlorite, garnet, titanite, clinozoisite, and ilmenite. This assemblage is consistent with lower to middle amphibolite facies peak metamorphism.

In the Pacquet Harbour and Ming's Bight areas, the PHG comprises a succession of interleaved massive and pillowed basalt, exhalite, gabbro, mafic volcanic breccia, mafic and felsic volcanoclastic rocks, and rare felsic volcanic rocks, that have been cut by numerous pre-tectonic mafic dykes and/or sills. The basalts are typically dark green-black, massive, and recrystallized to a fine-grained hornblende-plagioclase-biotite-epidote-quartz mineral assemblage. Primary features within the basalt include amygdules, and locally well

preserved pillows up to 2m in diameter (Fig. 2.4a). The pillows locally have amygdule-rich cores, and fine-grained epidote-rich selvages. The basaltic flows in the PHG comprise both tholeiitic and boninitic compositional types (Gale 1971, 1973; Hibbard 1983; Swinden et al. 1989); the tholeiitic basalts are most abundant in the northern portions of the PHG, whereas the boninites dominate to the south (Hibbard 1983). The basalts are associated with discontinuous, up to 50cm thick, lenses of a purple-grey, massive to layered, highly siliceous lithology. These lenses probably represent exhalite deposits, as they locally contain bornite-chalcopyrite-pyrite-magnetite mineralization, and are associated with the Ming massive sulphide deposit (Tuach and Kennedy 1978; Fig. 2.2). The gabbro forms massive, green-grey, weakly foliated, <20m thick bodies that are recrystallized to a fine- to coarse-grained, equigranular, hornblende-plagioclase-epidote assemblage with an intergranular texture (Fig. 2.4b). The gabbroic bodies typically retain a porphyritic texture defined by <2cm, subhedral, plagioclase phenocrysts. Pegmatitic gabbro outcrops in the footwall of the Scrape Fault along the Ming's Bight Road. The gabbro is most abundant within successions of pillowed basalt, suggesting a synvolcanic association. This interpretation is supported by the tholeiitic chemical composition of at least some of the gabbro bodies (Gale 1971, 1973; Hibbard 1983).

Mafic volcanic breccia units are widespread to the northeast and southwest of the town of Woodstock (Fig. 2.2; Map 3). These rocks contain up to 80% very angular to rounded, equant to irregular, up to 40cm, blocks of gabbro and massive to amygdaloidal basalt. The blocks are poorly sorted, and are surrounded by a matrix of <2cm mafic volcanic fragments (Fig. 2.4c). The volcanic breccia units range up to at least 10m thick

Figure 2.4 Field photographs of the Pacquet Harbour Group. a) Weakly deformed pillows in PHG mafic volcanic rocks at Pelee Point. b) Coarse-grained, weakly-deformed gabbro within the PHG mafic volcanic sequence at Pelee Point (scale bar is 16cm long). c) Mafic volcanic breccia in a sequence of clastic rocks exposed in roadcuts north of Mill Pond (Map 3). Note the variable degree of clast roundness, and the <1cm, black, equant pyroxene pseudomorphs in the matrix and clasts. d) Trough cross-bedding in interbedded sandstone-siltstone sequence (younging toward the southeast; same outcrop as Fig. 2.4c). e) Outcrop of strongly deformed felsic volcanic rock in the PHG ~6km northeast of the Rambler main mine (Fig. 2.2). Note the pronounced L_1 stretching lineation defined by deformed lapilli. f) An example of a distinctive plagioclase-porphyritic mafic dyke in the PHG from the southern shore of Pacquet Harbour.

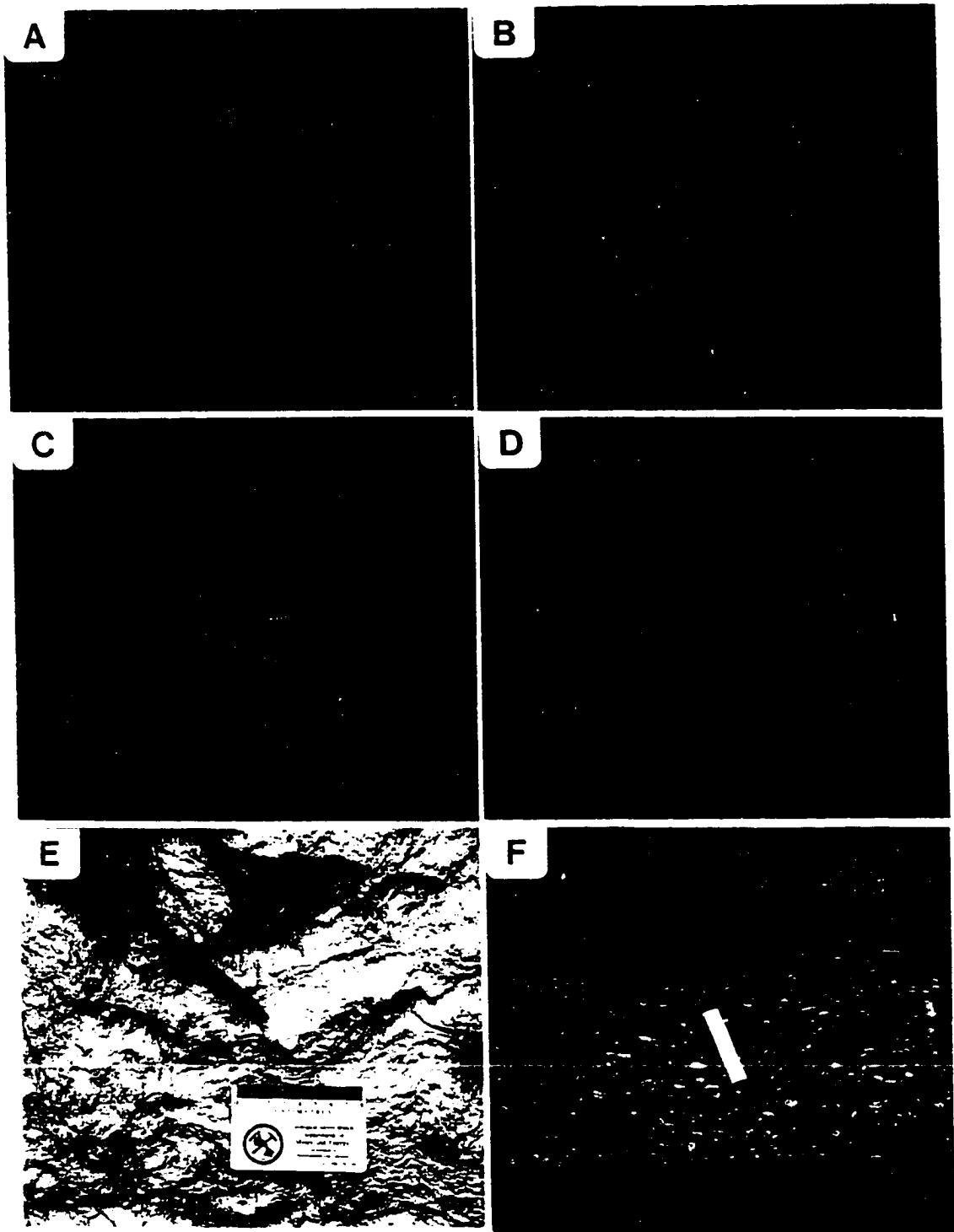


Figure 2.4

(limit of exposure), and are locally interlayered with thinly bedded successions of dark grey-green, fine- to medium-grained, mafic volcanic sandstone and mudstone which may reflect epiclastic reworking of the mafic volcanic rocks. These rocks locally exhibit graded bedding, load casts, cross bedding, and trough cross bedding (Fig. 2.4d). The matrix of the volcanic breccia, and (more rarely) discrete layers within the sandstone-mudstone succession, contain up to 30% black-green, euhedral to subhedral, equant, <1cm hornblende crystals. These crystals also occur within gabbroic and basaltic clasts in the mafic volcanic breccia, and in a few gabbroic intrusions in the PHG. In areas of less intense recrystallization, these crystals are locally cored by relict grains of pyroxene, indicating that they represent hornblende pseudomorphs after primary pyroxene phenocrysts.

In the area to the west of the Dunamagon Granite, layered felsic volcanoclastic rocks are abundant (Fig. 2.2; Map 4). These rocks are white to grey, fine- to medium-grained, and consist of thinly layered, siliceous, volcanic sandstone and mudstone which are apparently interlayered, or laterally continuous, with a succession of felsic volcanic breccia and tuffaceous rocks that outcrops further to the south in the PHG (Figs. 2.2 and 2.4e). Locally, the volcanoclastic rocks superficially resemble the layered psammites and semi-pelites of the MBG. However, in contrast to the MBG, the felsic volcanoclastic rocks are generally much more thinly or poorly bedded, have very simple metamorphic mineral assemblages and textures, and are intruded by numerous mafic and granitic dykes. In the Pacquet Harbour area, the felsic volcanic rocks are white to grey, siliceous, and contain less than 10%, 0.5 to 2.0mm diameter quartz 'eyes', and subhedral plagioclase crystals, in

a fine-grained quartz-plagioclase-sericite matrix. These rocks form discrete units up to 2m thick within the mafic volcanic rocks along Woodstock Road, and probably represent horizons of felsic tuff or lapilli tuff.

Mafic dykes cut all lithologies in the PHG and are typically fine-grained and massive with a diabasic texture, and locally well-defined chilled margins. Distinctive megacrystic mafic dykes were noted in numerous locations in the Pacquet Harbour area. These dykes are <1.5m wide, and contain <20%, euhedral to subhedral, <15cm, white-grey plagioclase phenocrysts (An_{56-60}) in a fine- to medium-grained amphibolitic matrix (Fig. 2.4f). The size and abundance of the phenocrysts decrease toward the contacts of the dykes, suggesting chilled margins. In the Pacquet Harbour area, granitic dykes within the PHG tend to be very strongly deformed and recrystallized. The dykes are <5m thick, pink to grey, and consist of very fine- to coarse-grained, equigranular (granoblastic-polygonal) K-feldspar, quartz, and plagioclase, with foliated biotite and muscovite. In the area south of Ming's Bight, the granitic dykes tend to be less deformed and exhibit mineral assemblages and phaneritic textures typical of the Dunamagon Granite and Burlington Granodiorite (e.g., Tuach and Kennedy 1978).

With regard to the depositional environment of the PHG, the association of pillowed basalts, geochemically similar gabbro (Gale 1973; Hibbard 1983), and exhalative horizons indicates a marine depositional environment and a proximal volcanic source. The angular basalt and gabbro clasts in the mafic volcanic breccia, and the detrital pyroxene crystals in the thinly bedded, locally trough cross-bedded volcanic sandstone-mudstone successions, are consistent with a proximal depositional setting, most probably on the

flank of the associated volcanic centre. The presence of felsic volcanic and volcanoclastic rocks points toward a bimodal volcanic setting, possibly in the vicinity of an island arc. This hypothesis is supported by the geochemical characteristics of the PHG pillowed basalts (Section 2.3.2.3).

2.3.2.2 Age and Correlation

The PHG is considered to be correlative with the Betts Cove and Point Rouse ophiolites and their associated cover sequences, which are collectively of Dunnage Zone tectonostratigraphic affinity (Hibbard 1983). This correlation is based on the lithological characteristics of the cover sequences overlying the PROC (e.g., Norman and Strong 1975; Kidd et al. 1978) and the Betts Cove ophiolite (i.e., the Snooks Arm Group: Upadhyay 1973; Jenner and Fryer 1980; Hibbard 1983). In addition, the boninitic and tholeiitic basaltic flows in the PHG are geochemically similar to mafic flows in both the Betts Cove and Point Rouse ophiolites (e.g., Gale 1973; Norman and Strong 1975; Kidd et al. 1978; Jenner and Fryer 1980; Hibbard 1983; Swinden et al. 1989; Fyffe and Swinden 1991), which indicate deposition on oceanic crust in a rifted-arc to back-arc tectonic environment (e.g., Gale 1973; Jenner and Fryer 1980; Hibbard 1983; Swinden et al. 1989; Fyffe and Swinden 1991).

Southwest of the Rambler mine, a halo of hornfels is developed in lower greenschist facies PHG rocks immediately adjacent to the Burlington Granodiorite (432 ± 2 Ma.; U-Pb zircon and titanite; Cawood and Dunning 1993), thereby providing an Early Silurian younger age limit for volcanism and sedimentation in the PHG. The older age limit is based on the correlation of the PHG with the Early Ordovician cover sequences of

the Point Rousse and Betts Cove ophiolites.

2.3.2.3 Contact Relations

The PHG is intruded by the Dunamagon Granite, the Cape Brule Porphyry, the Burlington Granodiorite, and a host of granitic dykes associated with these plutons. The contacts between the PHG and felsic plutons are typically strongly deformed. To the north, the PHG is structurally overlain by the Point Rousse ophiolite along the northeast-dipping Scrape Fault (e.g., Hibbard 1983; Kirkwood and Dubé 1992), and lies in tectonic contact with the MBG along the Pelee Point Shear Zone (see Chapter 3; Fig. 2.2).

Hibbard (1983), in an attempt to explain apparent 'divergent structural trends' between the apparently isolated block of mafic volcanic rocks at Pelee Point and the PHG mafic volcanic rocks on the southern shore of Pacquet Harbour, suggested that the mafic volcanic rocks at Pelee Point represent a conformable member of the MBG (i.e., the Pelee Point Schist). However, the mafic volcanic rocks at Pelee Point are lithologically identical to the PHG rocks on the south shore of Pacquet Harbour and, as shown in Chapter 3, the apparent divergent structural trends result from large-scale folding in the Pacquet Harbour area (Map 2). Therefore, there appears to be no justification on lithological or structural grounds for separating the mafic volcanic rocks at Pelee Point from the PHG.

2.3.3 Dunamagon Granite

2.3.3.1 General Characteristics

The Dunamagon Granite (Baird 1951) is an elliptical, ~5km wide by ~10km long, biotite granite pluton that crops out in the area between Ming's Bight and Pacquet Harbour (Fig. 2.2). The pluton trends east-west and is bounded to the north by the MBG,

and to the south by the PHG.

The Dunamagon Granite is massive, pink to grey, fine- to coarse-grained, and contains ~50% K-feldspar, 30% quartz, 15% plagioclase, and 5% biotite with trace amounts of titanite, allanite, epidote, magnetite, and apatite (McDonald 1993). The K-feldspar occurs as <1.5cm, euhedral to subhedral, phenocrysts which define the porphyritic texture that characterizes much of the granite. The plagioclase and quartz commonly form medium- to coarse-grained, equigranular, recrystallized grains with a locally well developed granoblastic-polygonal texture. Mafic bodies (see below) within the granite contain a medium- to coarse-grained hornblende-plagioclase-biotite-quartz-epidote mineral assemblage which, taken together with the granoblastic-polygonal textures in the granite, is consistent with amphibolite facies metamorphic recrystallization of the granite. The granite is cut by numerous quartz veins and <1m thick, pink to grey, massive, aplite dykes. The contacts between the aplite dykes and the granite are generally sharp and planar. The aplite dykes typically have steep dips, and widely variable strikes. The granite contains <1%, dark black to grey, amphibolite xenoliths, and rare, light grey, fine-grained, massive, biotite schist xenoliths.

The Dunamagon Granite contains numerous elongate bodies of dark black to green mafic rock which deserve special note. In some outcrops the mafic bodies clearly represent mafic dykes which intruded the granite. The dykes are 0.5 to 2.0m wide, >10m long (limit of exposure), and locally contain <5%, <2cm, euhedral, plagioclase phenocrysts that decrease in size and abundance towards the contacts, suggesting chilled margins. The dykes have planar, parallel contacts, and locally contain angular xenoliths of the granite.

In other outcrops however, the nature of the mafic bodies is more ambiguous.

Figure 2.5a illustrates a good example of an ambiguous mafic body in the Dunamagon Granite. This mafic body is ~40cm wide, outcrops for ~2m, and has relatively sharp, planar, parallel contacts suggesting a mafic dyke within the granite. In addition, the mafic body locally contains irregular inclusions of granitic material that appear to be granitic xenoliths, and are thus consistent with an intrusive relationship with the granite. However, in two locations along the lower contact, angular slabs of mafic rock have apparently been caught in the process of spalling off the mafic body into the adjacent granite (Fig. 2.5a). In addition, the granite immediately adjacent to the mafic body locally has a 1-3cm wide, light grey-white halo which lacks K-feldspar phenocrysts, and appears to be of a finer grain-size overall, suggesting a chilled margin. These features are consistent with a relatively competent, cool, mafic body within a granitic magma (i.e., a mafic xenolith).

However, along the upper contact of the above mafic body (Fig. 2.5a; arrowed), a narrow septum of mafic rock extends into the granite, and a bulbous 'pillow' of granite extends into the mafic rock. This feature points toward a co-magmatic relationship between the mafic rock and the granite. Towards the northwest, this mafic body can be traced into a ~3m thick zone in which narrow, irregular, wispy bodies of mafic rock and granite are intermingled (Fig. 2.5b). The contacts between the mafic rock and the granite tend to be irregular, with septa and pillows of granite extending into the mafic rock, and vice versa. The granite locally has a well developed, fine-grained halo that may represent a chilled margin or, alternatively, a narrow zone of anatexis related to intrusion of the mafic material. The mafic rock contains numerous inclusions of granite. Locally, the granite

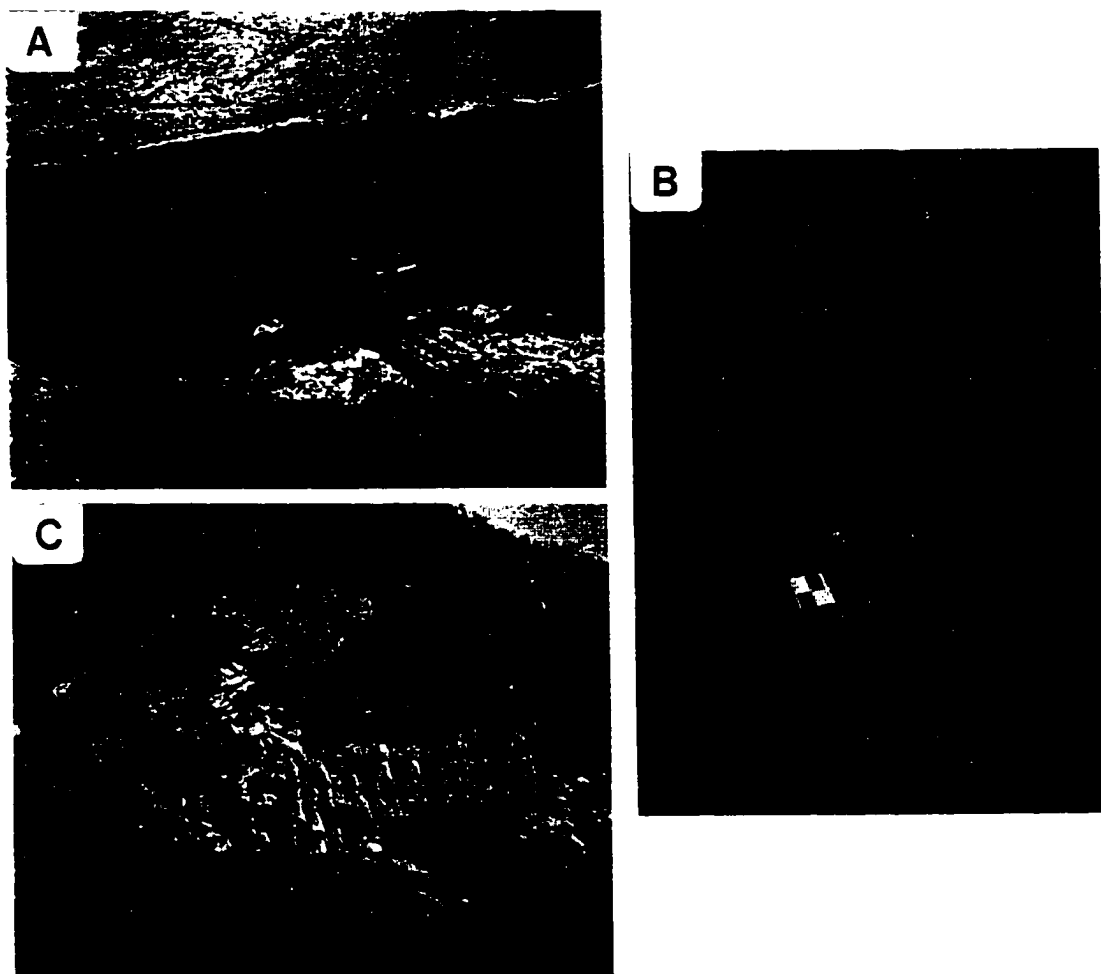


Figure 2.5 Field photographs of the Dunamagon Granite. **a)** An example of an ambiguous mafic body in the Dunamagon Granite. Note: the straight, parallel contacts; the two angular slabs of mafic material along the lower contact apparently caught in the process of spalling off into the granite; the finer grain size of the granite adjacent to the mafic body; the inclusion of granite within the mafic body; and the lobe of granite extending into the mafic body along the upper contact (arrowed). Photo taken near the eastern tip of the Dunamagon Granite in Pacquet Harbour. **b)** An example of syn-magmatic relationships between mafic material and the Dunamagon Granite (note that the mafic body in Fig. 2.5a is visible in the background; see text for discussion). **c)** A ~2m thick, strongly deformed dyke of Dunamagon Granite in PHG rocks at Pelee Point. The dyke is folded by an asymmetric F_2 fold that plunges shallowly southeast.

contains a prominent gneissic banding (syn-magmatic?) which has been folded together with narrow wisps of the mafic material. Taken together, the relationships between the mafic rock and the granite in this outcrop appear to be consistent with co-magmatic mafic and granitic melts, and point toward a more complex magmatic history for the granite than has been previously recognized.

2.3.3.2 Age and Correlation

Cawood and Dunning (1993) obtained a U-Pb (zircon) date of 429 ± 4 Ma from the Dunamagon Granite, which is interpreted as the age of intrusion of the pluton. This date is ~ 30 Ma younger than the previously accepted age of the granite (ca. 460 Ma; U-Pb zircon; Hibbard 1983), and is similar to the dates obtained from the other large felsic intrusions on the BVP (Cawood and Dunning 1993; Cawood et al. 1994). Thus, the Dunamagon Granite is probably related to the Late Ordovician - Early Silurian felsic magmatic complex which underlies much of the eastern BVP. The granitic pegmatites intruding the MBG north of Pacquet Harbour clearly post-date, and are therefore unrelated to, this magmatic activity.

2.3.3.3 Contact Relations

The Dunamagon Granite lies in tectonically modified intrusive contact with the PHG to the south. This hypothesis is supported by the abundance of mafic volcanic xenoliths in the granite, and the presence of granite dykes in the PHG (Fig. 2.5c). To the north, the granite lies in wholly tectonic contact with the MBG (see Section 2.2.3). This interpretation may be supported by the ϵ_{Nd} value of 0 obtained from the Dunamagon

Granite, which may indicate that it could not have incorporated significant amounts of MBG (Fryer et al. 1992).

2.3.4 Cape Brule Porphyry

2.3.4.1 General Characteristics

The Cape Brule Porphyry (Baird 1951) is a large quartz-feldspar porphyry pluton which crops out over a ~20 x 25km, roughly diamond-shaped area between Pacquet Harbour in the north and Green Bay in the south (Fig. 1.2). The porphyry is bounded to the west by the PHG and Burlington Granodiorite, to the southeast by the Betts Cove ophiolite, and to the northeast by Cape St. John Group.

In the thesis area, the Cape Brule Porphyry is typically white to pink to light grey, and medium- to coarse-grained. It consists of 20-25%, <5mm, subhedral, equant, quartz phenocrysts, and 10-30%, <5mm, euhedral to anhedral, pink to white, feldspar (K-feldspar and plagioclase) phenocrysts in fine-grained quartz, feldspar, sericite and/or biotite, matrix. A distinctive feature of the porphyry is the presence of 1-2%, <1mm, subhedral to anhedral, magnetite crystals. The porphyry is typically massive, but also locally contains a faint to pronounced layering which is defined by subtle changes in the proportion of phenocrysts. Hibbard (1983) suggested that some of these layered rocks are extrusive.

DeGrace et al. (1976) separated the porphyry into an early fine-grained phase and a later coarse-grained phase, which are separated by gradational and/or intrusive contacts. In the thesis area, the coarse-grained porphyry appears to predominate; however, near the PHG contact on the south shore of Pacquet Harbour, the porphyry contains a ~4m wide zone of very fine-grained, aplitic quartz porphyry with 2-3%, <1mm, subhedral quartz

phenocrysts. This zone probably represents a body (dyke or xenolith?) of fine-grained Cape Brule Porphyry, and looks very similar to quartz porphyry dykes that intrude PHG pillowed basalts and gabbro at Pelee Point.

Xenoliths are common in the Cape Brule Porphyry (1-2%) and can be separated into three lithological types: 1) fine-grained, green to grey, chloritic, mafic material; 2) fine-grained, white to grey, quartzo-feldspathic material very similar to the matrix of the porphyry (i.e., autoliths); and 3) purple to bright-green, ultramafic rock that has been altered to serpentine and fuchsite. The xenoliths rarely exceed 20cm in maximum dimension, and are concentrated near the contacts of the porphyry. Enclaves of ultramafic rock up to ~1 km in maximum dimension occur within the central portions of the porphyry (Hibbard 1983), and have been interpreted as roof pendants (DeGrace et al. 1976), although they may simply be very large xenoliths.

The porphyry contains a locally penetrative fabric defined by elongate quartz grains, foliated fine-grained sericite and/or biotite, and flattened xenoliths. The fabric results from intense strain along the northeast-trending intrusive PHG-Cape Brule Porphyry contact, and appears to decrease in intensity to the south away from the northwestern contact of the porphyry (Map 3). The northern portions of the porphyry lack textures indicative of high-temperature recrystallization, and xenoliths in the porphyry contain peak greenschist-facies metamorphic mineral assemblages. These features contrast strongly with the Dunamagon Granite, and indicate that the northeast-trending contact of the porphyry corresponds with a sharp break in the metamorphic field gradient, as discussed in detail in Chapters 3, 5, and 7.

2.3.4.2 Age and Correlation

The intrusion of the Cape Brule Porphyry is interpreted to be broadly synchronous with the Early Silurian emplacement of the King's Point and Topsails intrusive complexes, and deposition of the MicMac Lake Group, Springdale Group, and Cape St. John Group, within the high-level, epicontinental caldera complex and volcanic field in western Newfoundland (e.g., Hibbard 1983; Coyle and Strong 1987; Dunning et al. 1990; Fryer et al. 1992).

2.3.4.3 Contact Relations

The Cape Brule Porphyry intrudes the Betts Cove ophiolite, and the Burlington Granodiorite (e.g., DeGrace et al. 1976; Hibbard 1983; Fig. 1.2). In addition, the southeast-trending segment of the contact between the PHG and the porphyry is wholly intrusive, as indicated by abundant quartz-porphyry dykes in the PHG, and the presence of a well preserved, weakly deformed, intrusion breccia comprising angular xenoliths of PHG lithologies in a quartz- and feldspar-porphyritic matrix. In contrast, the northeast-trending segment of the PHG-Cape Brule Porphyry contact has been extensively deformed, and is characterized by a wide zone of mylonite developed within both the PHG and Cape Brule Porphyry (Figs. 1.2 and 2.2, Map 3). The contact between the Cape St. John Group and the Cape Brule Porphyry is typically intrusive. However, in places the quartz-feldspar porphyry apparently grades into extrusive felsic volcanic rocks of the Cape St. John Group (DeGrace et al. 1976). These relationships are compatible with the high-level caldera-complex setting proposed for the Cape St. John Group and Cape Brule Porphyry (e.g., Coyle and Strong 1987).

2.3.5 Point Rouse Ophiolite Complex

2.3.5.1 General Characteristics

The PROC is a disrupted ophiolite sequence which outcrops on the Point Rouse peninsula between Ming's Bight and Baie Verte (Norman and Strong 1975; Kidd et al. 1978; Hibbard 1983; Fig. 1.2). The PROC is bounded to the south by the PHG and the Burlington Granodiorite, to the east by the MBG, and to the west is probably continuous with the Advocate ophiolite complex which lies in contact to the west with the Fleur de Lys Supergroup (Norman and Strong 1975).

The ophiolite consists of a sequence of ultramafic rocks, gabbro, sheeted dykes, and pillowed basalts, with a mafic volcanic-volcaniclastic and metasediment cover sequence (Fig. 2.2). The ultramafic rocks outcrop at the northern tip of the Point Rouse peninsula, and at the southern end of Ming's Bight, and bound a large-scale synclinal fold which has been overturned to the southeast (Church and Stevens 1971; Kennedy 1973). The upper limb of the fold contains an essentially complete overturned ophiolite sequence, whereas the lower limb contains only a partial upright sequence (Norman and Strong 1975; Kidd et al. 1978; Fig. 2.2). The syncline has been pervasively cut by a coeval series of south-verging thrust faults, and a complex array of later strike-slip and dip-slip faults, which account for the disruption of the ophiolite sequence (Fig. 2.2). The metamorphic mineral assemblage in the PROC consists of actinolite + plagioclase (An_{10-15}) + clinozoisite/epidote + biotite + chlorite, consistent with lower to middle greenschist facies metamorphism (Norman and Strong 1975; Kidd et al. 1978), although upper greenschist to amphibolite facies rocks with a hornblende-plagioclase-biotite-quartz-epidote-titanite

assemblage are locally exposed in the structurally lowest sections of the ophiolite.

The ultramafic rocks consist mainly of harzburgite, with minor lherzolite and dunite (Norman and Strong 1975; Kidd et al. 1978). Typically, these rocks weather reddish-brown to light green and are extensively serpentized. In addition, large areas of ultramafic rock altered to talc-carbonate-fuchsite occur at the south end of Ming's Bight, and appear to be associated with zones of intense shearing. Stratigraphically upward, the ultramafic successions lie in contact with light green to grey, fine- to very coarse-grained, equigranular gabbro which locally contains well preserved cumulate layering. The gabbro is transitional into a sheeted dyke complex comprising dark green-grey, fine- to medium-grained diabase which occurs as a complex series of subvertical dykes up to 2m thick with abundant chilled margins and complex cross-cutting relationships. A thick section of pillowed basalt caps the plutonic section of the ophiolite. These rocks are dark green to grey, fine-grained, amygdaloidal, and contain well preserved pillows up to 1m in diameter. The pillow interstices contain abundant quartz-carbonate-epidote veins, as well as angular fragments of fine-grained (quenched) basalt. The pillowed basalt sections contain numerous <2m thick, ~2 to 30m long, purple-black, jasper layers which contain very fine internal laminations, and probably represent primary, interpillow exhalite or chert.

The PROC is conformably overlain by an ophiolitic cover sequence of pillowed basalts and clastic rocks. The clastic rocks were mapped by Norman and Strong (1975) as agglomerates, crystal-lithic tuff, water-lain tuff and tuffaceous breccia. However, the type section of the clastic succession south of Big Head (Kidd et al. 1978) was examined in the present study (Map 9) and, although these rocks do contain a significant component of

volcanic detritus, they are more appropriately classified as the products of epiclastic reworking of ophiolitic and volcanic rocks (e.g., Kidd et al. 1978). The following description refers to the ~350m thick type section of the clastic rocks south of Big Head.

The epiclastic rocks consist of interlayered boulder to pebble conglomerate, fine- to coarse-grained greywacke, and fine- to very fine-grained mudstones. Graded bedding and load structures indicate that these rocks are mainly overturned. The mudstones are pale yellow-brown, very fine-grained, laminated and siliceous, and are interlayered with dark-grey, graded, fine- to coarse-grained greywacke layers (Fig. 2.6a). The layering most commonly comprises <5cm thick rhythmically alternating mudstone and greywacke beds and/or laminae, although greywacke beds up to 2m thick were noted locally. The greywacke-mudstone layers locally contain a slight mottling which, in places, grades into ~10-20cm thick layers with pervasive mottling (Fig. 2.6a). In many locations the mottled layers are bounded above and/or below by un-mottled thinly layered sediments, and the contacts between these layers are locally very sharp. These features suggest that the mottling is a primary feature of the rock, possibly related to bioturbation or dewatering of the unconsolidated epiclastic sediments. The mudstone-greywacke successions contain conformable, <30cm thick, layers of pebble conglomerate that contain ~20%, very angular to rounded, locally tabular, rip-up clasts of laminated mudstone in a fine- to coarse-grained greywacke matrix (Fig. 2.6a).

On a larger scale, the greywacke-mudstone successions are interlayered with 1-1.5m thick conglomerate, and rare volcanic breccia, layers. The conglomerate typically contains ~20-50%, subrounded to angular, up to 50x15cm, poorly sorted clasts supported

Figure 2.6 Field photographs of the PROC cover sequence south of Big Head on the western shore of Ming's Bight (Map 9). **a)** Thinly bedded pebble conglomerate, greywacke, and mudstone. Note the pronounced mottling, particularly in the layer beneath the lens cap. **b)** An example of a ~1m thick layer of pebble to boulder conglomerate within a sequence of thinly-bedded greywacke and mudstone. **c)** Volcanic breccia comprising angular to subrounded clasts of gabbro, and pyroxene-phyric mafic and intermediate volcanic material. Note the abundance of coarse pyroxene crystals. **d)** Photomicrograph of a 0.5cm diameter detrital pyroxene crystal showing a pyroxene core (p; arrowed) surrounded by an actinolite rim (a).

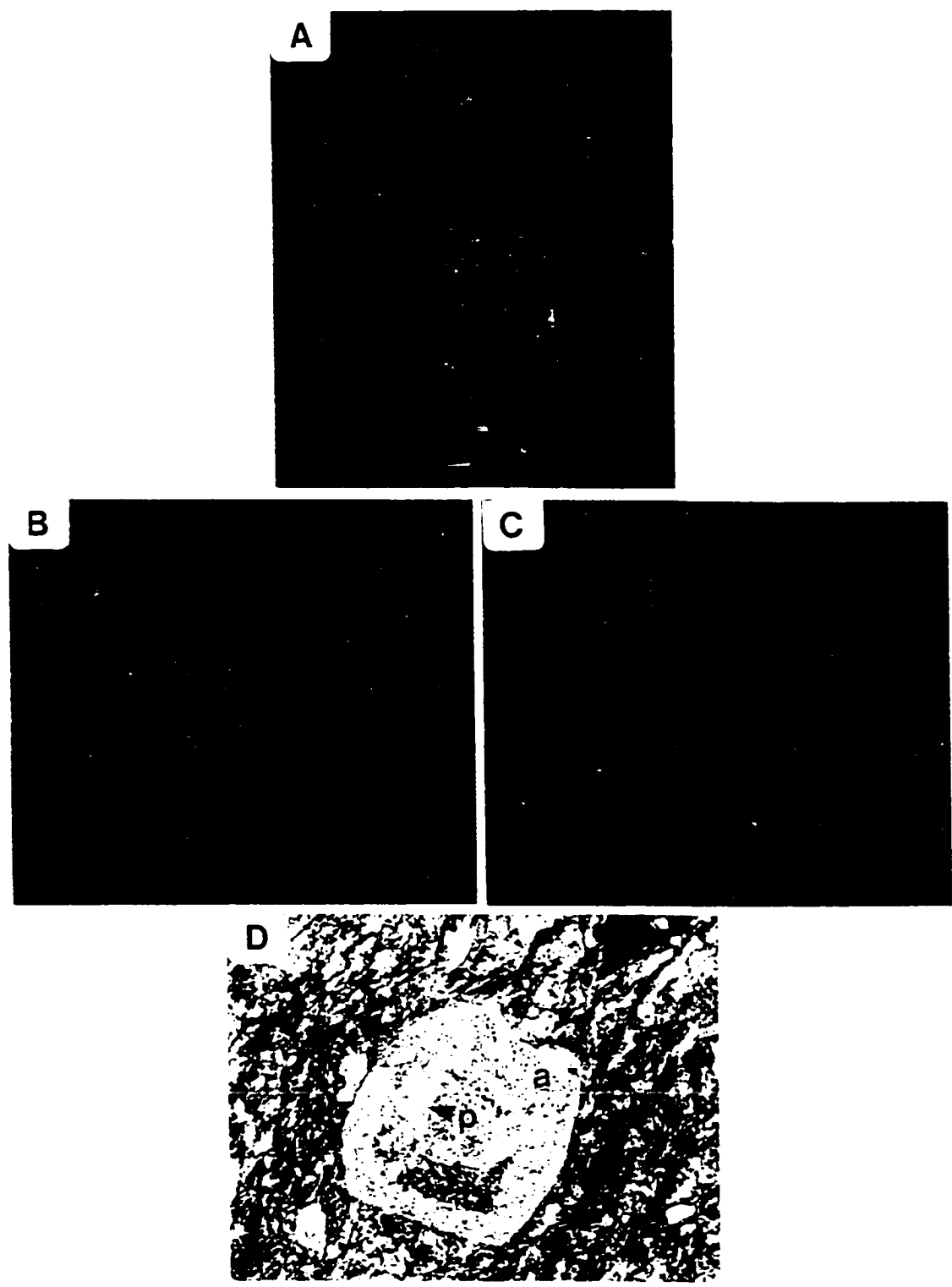


Figure 2.6

in a fine- to coarse-grained greywacke matrix (Fig. 2.6b). The clasts comprise medium- to coarse-grained greywacke and pale yellow-brown siltstone, with subordinate mafic volcanic rock. The volcanic breccia layers are exposed in several locations north of the Barry-Cunningham adit (Map 9), and comprise poorly sorted, angular to subrounded clasts up to 15cm in diameter in a volcanic sandstone matrix. The clasts include equigranular gabbro, pyroxene-phyric mafic volcanic rock, and plagioclase- and pyroxene-phyric, vesicular to pumaceous, andesitic rock. The matrix contains up to 10% dark green-black, euhedral (hexagonal) to subhedral to rounded crystals, that also occur as phenocrysts in the volcanic clasts (Fig. 2.6c). The crystals range in size up to 1.5cm, and commonly have black, massive rims, surrounding a green, recessively-weathered core. In thin section, these crystals contain core of pyroxene, surrounded by an altered rim of actinolite (Fig. 2.6d). These rocks are similar to the volcanic breccia units in the PHG.

Discrete layers within the clastic section also locally contain pale brown, angular to very angular, vesicular clasts and shards of aphanitic, siliceous material that may be felsic pyroclastic fragments. The very angular shape of these clasts may indicate a proximal felsic volcanic source.

The pillowed basalts of the cover sequence are well exposed in a ~200m thick section north of the Barry-Cunningham adit (Map 9), and are interpreted by Kidd et al. (1978) to continue for ~2km to the south as a thick unseparated succession of strongly deformed greenschists derived from pillowed basalt and minor pillow breccia, hyaloclastite, and mafic volcanoclastic rocks (Fig. 2.2). The pillowed basalts conformably overlie the epiclastic rocks, and are overturned to the south. Two thick pyroxene- and

plagioclase-porphyratic diabase sills intrude these rocks (Kidd et al. 1978). In general, this section is quite similar lithologically to PHG rocks exposed in the Pacquet Harbour area, as noted by Norman and Strong (1975).

Several mafic dykes were noted within the cover sequence. These dykes are generally ~1 m wide, dark brown to grey, and comprise a fine- to medium-grained, diabasic-textured matrix that locally surrounds <5%, <1 cm, euhedral plagioclase phenocrysts which are concentrated in the central portions of the dykes.

Norman and Strong (1975) and Kidd et al. (1978) examined the geochemistry of the pillowed lavas and all plutonic portions of the PROC, and showed that the pillowed basalt, sheeted dykes, and gabbro have tholeiitic bulk compositions, with ocean-ridge or ocean-floor basalt geochemical affinities. In addition, pillowed basalt from the eastern portion of the ophiolite locally has boninitic compositions (Kidd et al. 1978), akin to at least some of the PHG pillowed basalts. Ramezani (1992) examined the geochemistry of synvolcanic gabbro sills and volcanic-volcaniclastic rocks of the ophiolitic cover sequence, and proposed that their geochemical attributes reflect a transition from mid-ocean ridge/oceanic-island volcanism to island-arc volcanism, respectively.

2.3.5.2 Age and Correlation

As stated previously, the PROC is correlated with the PHG, Snooks Arm Group and the Betts Cove ophiolite, and was probably deposited in an oceanic island, rifted arc or back-arc basin tectonic environment (Norman and Strong 1975; Kidd et al. 1978; Jenner and Fryer 1980; Hibbard 1983; Dunning and Krogh 1985; Ramezani 1992; Williams 1992). Ramezani (1992) obtained a U-Pb zircon date of $483 \pm 1/2$ Ma from a

synvolcanic gabbro sill which intruded the cover sequence of the PROC, consistent with an Early Ordovician age for the PROC and the regional correlations.

2.3.5.3 Contact Relations

To the east, the PROC is imbricated with the MBG along a series of shear zones and faults that post-date intrusion of the Dunamagon Granite (Fig. 2.2, Maps 4 and 7). To the south, the PROC is thrust over the PHG and Burlington Granodiorite along the Scrape Fault (e.g., Kidd et al. 1978; Hibbard 1983; Kirkwood and Dubé 1992; Fig. 2.2). The PROC is probably, at least in part, continuous with the strongly deformed Advocate ophiolite complex to the west (Norman and Strong 1975). The Advocate complex is imbricated with the Fleur de Lys Supergroup along a series of ductile shear zones that dip steeply, strike northeast, and collectively mark the trace of the BVL (Bursnall 1975; Williams and St. Julien 1982; Goodwin and Williams 1996).

2.3.6 Eastern Shore of Ming's Bight

2.3.6.1 Background

Coastal exposures along the eastern shore of Ming's Bight contain several fault-bounded, lithologically distinct sections of rock that can be separated on the basis of lithology into: 1) MBG schist; 2) PROC serpentized ultramafic rock; and 3) successions of metasedimentary rock and greenschist which are cut by numerous gabbro, diabase, and granitic intrusions, and interleaved with units of strongly deformed amphibolite (Fig. 2.2). Kidd et al. (1978) and Hibbard (1983), on the basis of regional magnetic data, showed that the section of serpentized ultramafic rock is laterally continuous with the ultramafic rocks at the south end of Ming's Bight, and is therefore correlative with the PROC. The

rest of the rocks along the eastern shore of Ming's Bight have traditionally been included in the MBG (e.g., Watson 1947; Baird 1951; Kennedy 1975; DeGrace et al. 1976; Kidd et al. 1978; Hibbard 1983), in spite of their markedly different lithological characteristics. An alternative interpretation is presented below, which invokes the presence of fault-bounded sections of PROC cover sequence rocks on the eastern shore of Ming's Bight. This hypothesis is supported by the geology of these successions, the geochemical signature of the mafic intrusions, and the regional magnetic data.

2.3.6.2 General Characteristics

Ming's Bight Group

The MBG crops out in several ~1 km wide fault-bounded sections, and numerous <200m-thick fault slivers, along the eastern shore of Ming's Bight (Maps 4 and 7). These rocks consist of light to dark grey-brown, monotonously interlayered, psammitic and semi-pelitic schist that is strongly deformed and records peak upper greenschist facies metamorphism (see Section 2.2.1). In the field, the MBG (Fig. 2.7a) has several attributes that readily distinguish it from PROC rocks, including: 1) prominent psammite/semi-pelite layering; 2) nearly ubiquitous subhedral albite porphyroblasts; and 3) lithologic homogeneity (in particular, the absence of mafic or granitic intrusions).

PROC ultramafic rocks

The ultramafic rocks crop out in a ~1 km wide fault-bounded section near Deep Cove on the eastern shore of Ming's Bight (Map 4). These rocks consist of rusty-brown to green-weathering serpentized harzburgites that are cut by several diabase dykes up to 10m thick (Kidd et al. 1978).

Figure 2.7 Field photographs of the sequences exposed on the eastern shore of Ming's Bight. **a)** Typical MBG schist at Grappling Point (Map 7). Note the psammite and semi-pelite layering, plagioclase porphyroblasts, and the refolding of an isoclinal (F_2) fold by open (F_4) folds that plunge shallowly southeast. **b)** Thinly bedded greywacke-siltstone at Barker's Point (Map 7). Graded bedding and load structures indicate that these rocks are upright and young to the southeast. **c)** Pebble conglomerate grading eastward (to the right) into thinly bedded greywacke-siltstone at Barker's Point. **d)** Thinly bedded greenschist (crystal tuff) with distinct pyroxene crystals in the greenschist sequence south of Deep Cove (Map 4; ruler is 16cm long). **e)** Strongly foliated amphibolite (right) grading into equigranular metagabbro (left). Photo taken within the sequence of amphibolite ~150m north of Caplin Cove (Map 8). **f)** Boudinaged granitic dykes cutting thinly layered siltstone and mudstone at Barker's Point. **g)** A massive mafic dyke cutting bedded sedimentary rocks south of Barker's Point. Note the truncation of granitic dykes in the country rock by the mafic dyke.

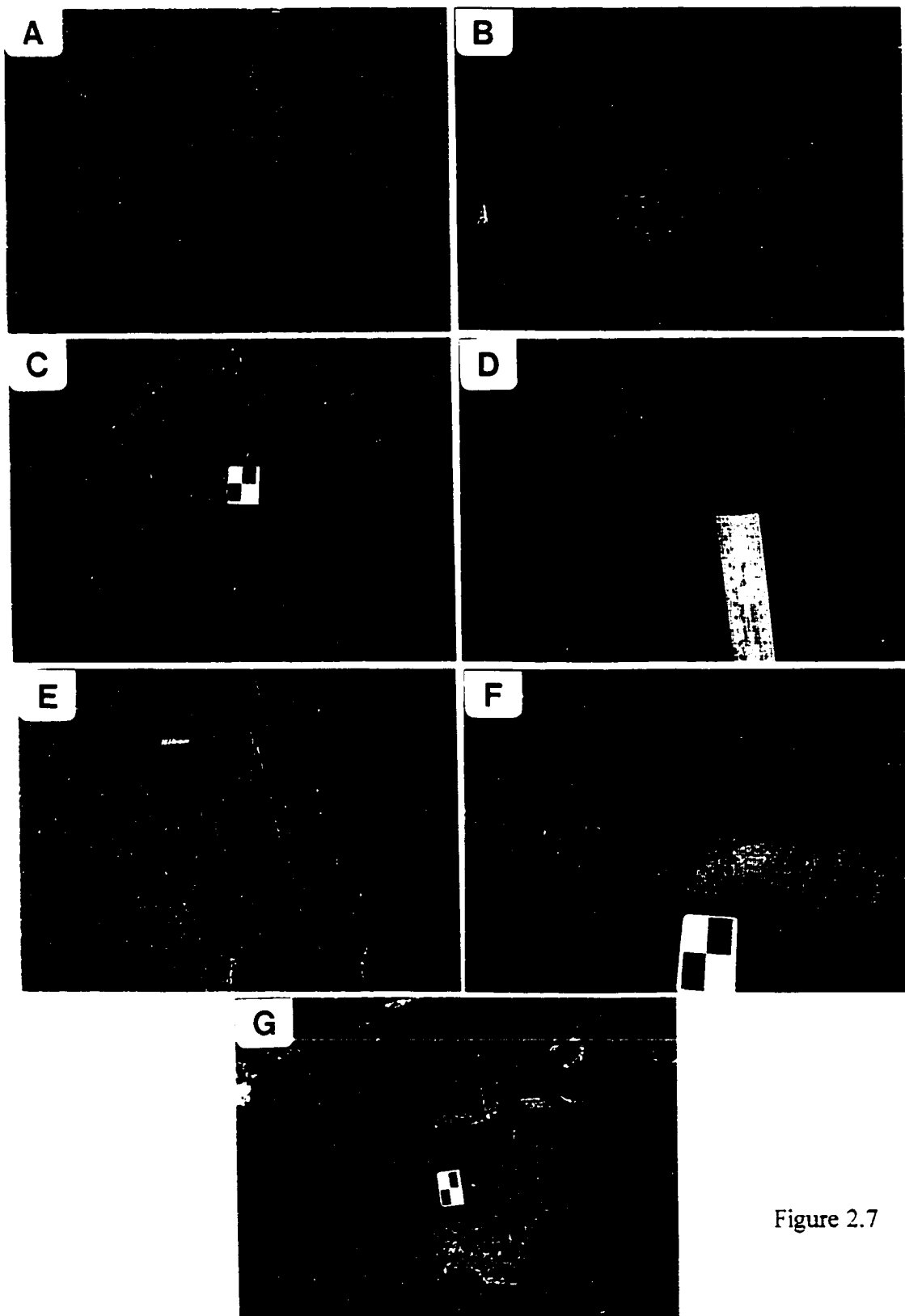


Figure 2.7

PROC cover sequence

The PROC cover sequence on the eastern shore of Ming's Bight comprises metasedimentary rocks, greenschist, and amphibolite disposed in a series of structural blocks bounded by brittle-ductile faults or ductile shear zones up to 20m wide. Typically, the interiors of these blocks are strongly deformed and record peak greenschist facies metamorphism, with the exception of the amphibolites that record intense ductile deformation associated with peak amphibolite facies metamorphism.

Metasedimentary rocks - The metasedimentary rocks have a highly variable character, ranging from fine-grained laminated black slate, to successions of thinly-bedded greywacke-siltstone, to layers of pebble to boulder conglomerate. Graded bedding and load structures indicate that these rocks are primarily upright and south- or east-younging, and locally overturned to the north. Metamorphic mineral assemblages in these rocks consist of biotite, muscovite, and chlorite with rare actinolite, and indicate greenschist facies metamorphism. The metasediments are best exposed in the area of Barker's Point and Long Point, and the following description mainly refers to these areas (Map 7).

Interlayered greywacke and siltstone are the dominant lithologies in the metasedimentary succession, although thick sections (>300m) of monotonous siltstone/argillite locally dominate, as in the Jimmy's Cove and Caplin Cove areas (Map 7). The siltstone is dark to light grey-brown, very fine- to fine-grained, finely layered to laminated, and contains biotite (\pm white mica and chlorite) which imparts a phyllitic cleavage to the rocks. The greywacke is light grey-brown, fine- to very coarse-grained, and contains angular to subrounded clasts of quartz and siliceous to chloritic lithic

material. The greywacke layers range in thickness from <5cm to ~1m, and commonly grade upwards into siltstone (Fig. 2.7b). The pebble to boulder conglomerate forms concordant layers up to 2m thick which are well exposed at Barker's Point. These layers contain <50%, angular to rounded, pebble to boulder-sized clasts supported in a fine- to coarse-grained greywacke matrix. These layers typically grade upwards into adjacent greywacke-siltstone successions (Fig. 2.7c). Clast types include crystalline quartz, greywacke-siltstone, greenschist, mafic volcanic, quartz porphyritic felsic volcanic, and rare carbonate. Locally, the conglomerate contains ~50%, up to 10x40cm, tabular clasts of siltstone which were apparently ripped up from the immediately underlying layers.

The sedimentological attributes of these rocks indicate deposition in fairly deep water, possibly on a distal flank of a mafic/felsic volcanic centre. These rocks are quite similar to epiclastic rocks of the PROC cover sequence (e.g., Kidd 1977; Kidd et al. 1978; Section 2.6.1), which supports the proposed correlation of these successions.

Greenschist - The greenschist units outcrop in two locations near Ming's Tickle (Map 8), and at the northern contact of the serpentinized ultramafic rocks. In zones of intense deformation, the greenschist forms units of strongly foliated chloritic schist with abundant boudinaged quartz veins. Typically, however, the greenschist is light to dark green-grey weathering, layered to massive, and consists of fine- to medium-grained plagioclase, quartz, chlorite, biotite, epidote, and hornblende, with trace amounts of titanite, muscovite, pyrite and carbonate. The hornblende forms scattered <1cm, euhedral, acicular, crystals which account for <30% of the rock. The plagioclase forms coarse-grained, rounded to euhedral, detrital crystals (<5%), or fine- to medium-grained,

equigranular, recrystallized grains in the matrix. The distinctive feature of the greenschist is the local presence of up to 50%, <1mm to 1cm, black to green, euhedral (hexagonal-equant) to anhedral hornblende pseudomorphs after pyroxene (Fig. 2.7d). These crystals are generally scattered throughout the greenschist, but are locally concentrated in a series of crystal-rich layers up to 40cm thick. The crystals are randomly distributed within the layers, and lack any indication of size grading.

The presence of detrital plagioclase and pyroxene crystals within the greenschist indicates proximal deposition, possibly as a thick succession of volcanoclastic rocks with thin horizons of pyroxene-crystal tuff on the flank of a nearby volcanic centre. Very similar pyroxene-bearing volcanoclastic rocks were mapped by Kidd (1977) and Kidd et al. (1978) in the cover sequence of the PROC. In several locations, the greenschist is interlayered with thin layers of greywacke and fine-grained siliceous metasediments, possibly indicating a conformable relationship between the greenschist and metasedimentary rocks.

Amphibolite - Amphibolite crops out in two locations in the Ming's Tickle area (Map 8). The amphibolites are typically black to green, massive to finely layered, and contain 30-60%, euhedral to subhedral, acicular to equant, black to green hornblende porphyroblasts in a fine- to coarse-grained, equigranular to granoblastic-polygonal matrix of plagioclase and quartz with trace amounts of fine-grained biotite, titanite, epidote, ilmenite, apatite, chlorite, pyrite and zircon. Typically, the amphibolites contain a penetrative ductile fabric defined by foliated and lineated hornblende porphyroblasts (Fig. 2.7e). The foliation is parallel to a weak to prominent layering defined by variations in grain size and the abundance of hornblende. Where massive, the amphibolite has a relict

equigranular ophitic texture defined by randomly oriented hornblende crystals and aggregates of plagioclase and/or quartz. In both locations near Ming's Tickle, strongly deformed, layered amphibolites apparently grade into more massive, equigranular, gabbroic-looking amphibolite, possibly indicating that the layering formed through intense deformation of gabbro (Fig. 2.7e).

The ductile fabrics and amphibolite facies mineral assemblages in these rocks indicate intense deformation at relatively high temperature. The only similar rocks in the area occur in the northern part of the PHG. Thus, the sections of amphibolite exposed on the eastern shore of Ming's Bight are interpreted as tectonic inclusions which were derived from this area, and imbricated with the metaclastic rocks during late structural reworking (see Chapters 4, 5, and 6).

Intrusions - Mafic and granitic intrusive rocks are widespread in the metasedimentary successions, and are less common in the greenschist. The granitic rock forms numerous dyke-like bodies that range in thickness from <10cm to ~50m (Fig. 2.7f). These rocks weather orange-pink to grey-white, are fine- to medium-grained, and generally consist of 50-60% K-feldspar, 30-50% quartz (often as distinctly blue phenocrysts), 5-10% plagioclase, <5% biotite ± muscovite. The K-feldspar locally occurs as <1cm, euhedral phenocrysts which define a porphyritic texture. Sharp, though subtle, compositional changes are locally visible in outcrop, indicating that the larger granitic bodies may be composite. The granite contains ~5% angular xenoliths up to 2m in diameter of the adjacent country rock. Significantly, the country rock adjacent to the granitic intrusions does not contain any evidence of contact metamorphic effects, and the

granite is locally chilled adjacent to small (<20cm) xenoliths. These features indicate that the granite was probably intruded at a very high structural level, and must have cooled very rapidly after emplacement.

The mafic intrusions in these successions are highly variable in terms of composition, texture and relative age. Gabbro forms several <5m thick dykes and sills in the greenschist and metasediments, and a ~30m thick, fault-bounded body in the metasediments north of Caplin Cove (Map 8). The gabbro is dark to light green-grey, coarse-grained, equigranular, and massive, with an ophitic texture defined by ~60% elongate to equant clusters of fine-grained, green-black hornblende, and ~40% euhedral to anhedral plagioclase crystals. In many locations, the plagioclase is recrystallized into clusters of fine- to medium-grained granoblastic-polygonal grains that pseudomorph the primary plagioclase phenocrysts. Diabase occurs in numerous dykes up to 2m thick that are typically dark rusty-brown to green-grey, with a fine- to medium-grained diabasic texture, and locally well developed chilled margins (Fig. 2.7g). The dykes locally have a porphyritic texture defined by up to 15% <7x5cm, euhedral to subhedral, randomly oriented, plagioclase phenocrysts. In several locations diabase dykes with chilled margins are completely contained within earlier diabase dykes. In addition, evidence exists for emplacement of diabase dykes prior, and subsequent, to intrusion of the granitic dykes. These observations indicate that the emplacement of the diabase dykes most probably involved multiple intrusive events.

Geochemistry of gabbro - Two gabbro intrusions from the eastern shore of Ming's Bight were sampled for whole-rock geochemistry. Sample 93-79 was collected from a 4m

thick gabbro dyke which cuts metasedimentary rocks ~400m south of Caplin Cove (Map 7), and has a tholeiitic bulk chemical composition and a trace-element geochemical signature consistent with enriched mid-ocean ridge basalts (Fig. 2.8). Sample 92-204 was collected from the large body of gabbro ~100m north of Caplin Cove (Map 8), and has a tholeiitic bulk chemical composition, with a trace-element geochemical signature which is transitional between island arc and mid-ocean ridge basalts (Fig. 2.8).

Aside from the obvious paleotectonic implications, the most significant aspect of these results is that the gabbro samples from the eastern shore of Ming's Bight have two distinctive geochemical signatures which are essentially identical to the two geochemical types of gabbro documented by Ramezani (1992) in the cover sequence of the PROC (Fig. 2.8). In particular, samples 93-79 and 92-204 are geochemically correlative with the 'MGAB' (main Stog'er Tight) and 'LFTG' (low Fe-Ti) gabbro suites, respectively, defined by Ramezani (1992). Though not conclusive, these data indicate a geochemical correlation between gabbroic rocks on the eastern shore of Ming's Bight and gabbro sills in the PROC cover sequence, and support the correlation of these sequences.

2.3.6.3 Age and Correlation

Mattinson (1977) obtained a U-Pb zircon date of 435 ± 15 Ma from the largest granitic body on the eastern shore of Ming's Bight, which may provide an Early Silurian younger age limit for these rocks (Fig. 2.2). In addition, based on their similar lithological and geochemical characteristics, these successions are correlated with the PROC cover sequence, thereby indicating an Early Ordovician depositional age.

Figure 2.8 Trace and rare-earth element geochemical characteristics of gabbro from the eastern shore of Ming's Bight as compared to syn-volcanic gabbro sills in the PROC cover sequence. Major elements and the trace elements Cr, Zr, and Ba were determined by inductively coupled plasma-optical emission spectrophotometry (ICP-OES) in the Newfoundland Department of Mines and Energy analytical laboratory. Rare-earth elements and the remaining trace elements were determined by inductively coupled plasma-mass spectrometry (ICP-MS) at Memorial University of Newfoundland. Analytical methods are described by Jenner et al. (1990), and the average primitive-mantle elemental concentrations used as normalizing values are from G.A. Jenner (pers. comm., 1995; refer to Ramezani 1992). Solid circle, sample SA-93-79; open circle, sample SA-92-204; solid squares, MGAB samples from Ramezani (1992); open squares, LFTG samples from Ramezani (1992). Note the marked similarity in geochemistry between sample 93-79 and the MGAB samples, and sample 92-204 and the LFTG samples. These data support a geochemical correlation between gabbro on the eastern shore of Ming's Bight and gabbro sills in the PROC cover sequence.

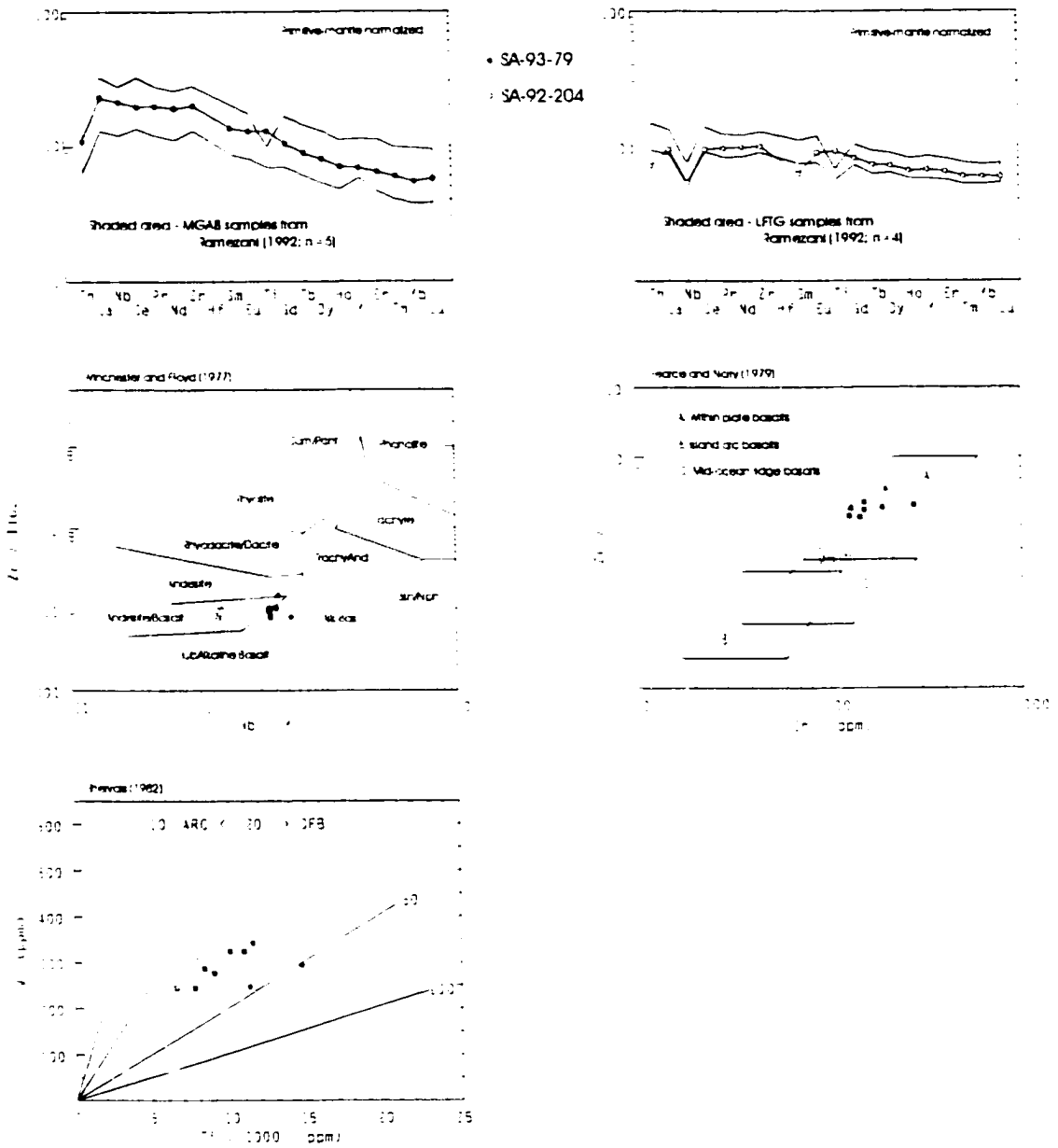


Figure 2.8

2.3.6.4 Contact Relations

The successions exposed on the eastern shore of Ming's Bight are everywhere in fault contact with the adjacent MBG schist, and are probably laterally continuous with the main body of the PROC under Ming's Bight (Fig. 2.2).

2.4 CONCLUSIONS

The above interpretation of the geology of the Ming's Bight - Pacquet Harbour area is completely compatible with regional relationships, and provides a relatively simple and coherent tectonostratigraphic framework. The thesis area is separated into three lithotectonic elements that reflect the regional-scale tectonic evolution of the BVP: 1) Late Proterozoic to Early Ordovician rifted margin sediments of Laurentian affinity (i.e., MBG); 2) Early Ordovician ophiolitic, back-arc and/or island arc assemblages of Dunnage Zone affinity (i.e., PHG, PROC, and the successions on the eastern shore of Ming's Bight); and 3) Early Silurian high-level, epicontinental felsic intrusive suites (i.e., Dunamagon Granite, Cape Brule Porphyry, and, probably, the granitic intrusions on the eastern shore of Ming's Bight).

Because all the lithotectonic elements are present in a relatively small area, the Ming's Bight - Pacquet Harbour area is an ideal location to examine and test models for the tectonic evolution of the BVP. The structural, metamorphic, and geochronologic attributes of this area are addressed in Chapters 3 and 4, 5, and 6, respectively.

Chapter 3 Structural Geology - Pacquet Harbour area

3.1 INTRODUCTION - CHAPTERS 3 AND 4

Structural geology is a key component in any comprehensive study of the tectonic evolution of an orogenic belt. The structural geology of a region represents the framework, without which the metamorphic textures, geochronologic constraints, and pressure - temperature determinations cannot easily be incorporated in a regional tectonic context. On the BVP a wealth of metamorphic, geochronologic, and structural data exist, but incorporation of these data into a coherent model for the tectonic evolution of the BVP is hampered by the lack of a regional structural framework.

In simple terms, the structural framework of the western Newfoundland Appalachians is currently viewed in terms of three pulses of deformation: 1) west-directed compressional deformation associated with the development of a fold and thrust belt and burial of the Laurentian margin during the Middle Ordovician Taconian orogeny (e.g., Williams 1979; Cawood et al. 1995); 2) a climactic phase of Early to Late Silurian sinistral transpressional deformation (e.g., Currie and Piasecki 1989; Lin et al. 1994; Dubé et al. 1996) associated with oblique convergence of Laurentia and Gondwana (e.g., Dunning et al. 1990; O'Brien et al. 1991; Cawood et al. 1994, 1995; Lin et al. 1994); and 3) a protracted phase of distributed latest Silurian to Devonian, west-directed thrusting (Cawood and Williams 1988; Stockmal and Waldron 1990; Waldron and Stockmal 1991, 1994) and transpressional to transtensional deformation associated with continued, though dextral, oblique convergence (e.g., Kusky et al. 1987; Ferrill and Thomas 1988; Currie

and Piasecki 1989; Stockmal et al. 1990; Malo et al. 1992; LaFrance and Williams 1992; Dunning et al. 1993; O'Brien et al. 1993; Hibbard 1994; Holdsworth 1994; Dubé et al. 1996; Dubé and Lauzière 1996). This deformation may have continued into the Carboniferous, as indicated by the development of Carboniferous sedimentary basins in a bulk transtensional regime (e.g., Bradley 1982; Hyde et al. 1988; Langdon and Hall 1994; Lynch and Tremblay 1994; Lynch 1996; Lynch and Giles 1996).

On the BVP, recent detailed structural (Kirkwood and Dubé 1992; Dubé et al. 1993; Goodwin and Williams 1993; McDonald 1993; Bélanger et al. 1996; Goodwin and Williams 1996) and metamorphic studies (Jamieson and Vernon 1987; Jamieson 1990; Jamieson and O'Beirne-Ryan 1991), together with regional-scale geochronologic (Dallmeyer and Hibbard 1984; Cawood and Dunning 1993; Cawood et al. 1994, 1995) and structural studies (Piasecki 1988; Goodwin and Williams 1990; Piasecki et al. 1990; Piasecki 1995) indicate that the regional structural framework outlined above may be broadly applicable to the BVP.

Chapters 3 and 4 document the structural geology of two key areas bounding the controversial MBG on the BVP. These data are used to reconstruct the deformation history of the MBG, which includes: 1) Silurian to earliest Devonian sinistral transpressional deformation; and 2) Early Devonian to Carboniferous dextral transpressional to transtensional deformation. This deformation history is fully compatible with the regional structural framework for the Newfoundland Appalachians outlined above, and reconciles the many peculiar geological features of the BVP, including the anomalous tectonostratigraphic setting of the MBG.

3.1.1 Structural setting and previous work

The structural geology of various portions of the BVP has been examined in detailed studies (Coates 1970; Gale 1971; de Wit 1972, 1974; Kidd 1974; Bursnall 1975; Tuach 1976; Tuach and Kennedy 1978; Kirkwood and Dubé 1992; Dubé et al. 1993; Goodwin and Williams 1993; McDonald 1993; Bélanger et al. 1996; Goodwin and Williams 1996), or on a more regional scale (Baird 1951; Church 1969; Kennedy 1973, 1975; Bursnall and de Wit 1975; DeGrace et al. 1976; de Wit 1980; Hibbard 1982, 1983; Piasecki 1988; Goodwin and Williams 1990; Piasecki et al. 1990; Piasecki 1995). In the interest of brevity, the structural geology of BVP is here summarized in terms of structures west of, within, and east of, the BVL. Traditionally, deformation to the west and east of the BVL was attributed to Taconian and 'Acadian' tectonism, respectively (Hibbard 1983); however, recently published U-Pb dates indicate that this model is an oversimplification (Cawood et al. 1994, 1995).

West of the BVL, post-Early Ordovician deformation structures in the East Pond Metamorphic Suite and Fleur de Lys Supergroup are separated, on the basis of overprinting relationships, into three generations (early, D_E ; main, D_M ; late, D_L ; de Wit 1972; Bursnall and de Wit 1975; Hibbard 1983). The D_E structures are significantly less pervasive than the D_M structures and are spatially associated with a series of early high strain zones. These zones typically contain tectonic inclusions of ophiolitic rocks (Bursnall 1975; Williams 1977), and are probably attributable, at least in part, to Middle Ordovician westward transport of the Taconian allochthons (Bursnall and de Wit 1975; Williams 1977; Hibbard 1983). D_E structures are transposed by the regional D_M fabric, which is

axial planar to upright, tight to isoclinal folds that plunge north and south (de Wit 1972, 1980; Bursnall 1975; Bursnall and de Wit 1975), including the regional-scale antiforms defined by the East Pond Metamorphic Suite (de Wit 1972; Hibbard 1983; Fig. 1.2). The D_M foliation strikes northeast, dips steeply, and parallels a series of anastomosing ductile shear zones that transect the Fleur de Lys Supergroup, and separate it from the East Pond Metamorphic Suite (de Wit 1980; Hibbard 1983; Piasecki 1988). Kinematic indicators in these shear zones were examined by Piasecki (1988, 1995) and Piasecki et al. (1990), who presented ambiguous and, in some instances, conflicting evidence for sinistral and dextral transcurrent shearing, as well as north- and south-directed thrusting. D_M structures were attributed to Middle Ordovician orogenesis by Hibbard (1983); however, it has recently been demonstrated that D_M is contemporaneous with an Early Silurian amphibolite facies metamorphic peak in the Fleur de Lys Supergroup (Jamieson and Vernon 1987; Cawood et al. 1994). Towards the BVL, the D_M fabric is progressively overprinted by D_L fabrics that gradationally intensify eastward from a spaced crenulation cleavage to a penetrative mylonitic foliation, and are attributed to post-Early Silurian shearing along the BVL (e.g., Bursnall and de Wit 1975; Hibbard 1983; Piasecki 1988; Cawood et al. 1994).

The structural geology of the BVL has been examined by several authors (Kidd 1974; Bursnall 1975; Hibbard 1982, 1983; Piasecki 1988, 1995; Goodwin and Williams 1990, 1993, 1996; Bélanger et al. 1996). However, as noted in Chapter 2, relatively little is known about the structural development of this major tectonic boundary. In general, the BVL contains spatially and temporally heterogeneous planar fabrics that dip steeply, record variable amounts of finite strain, and range from spaced crenulation cleavages to

penetrative mylonitic foliations. These fabrics contain subhorizontal to subvertical stretching lineations, and formed in metamorphic conditions ranging from middle amphibolite to lower greenschist facies. In the Baie Verte area, up to five generations of planar ductile fabrics have been recognized (Bursnall 1975), whereas portions of the Flat Water Pond and MicMac Lake Groups contain only a local mylonitic S_1 foliation, and more widespread S_2 crenulation cleavage (Kidd 1974; Bélanger et al. 1996). In addition, a complex series of brittle-ductile faults, termed the Baie Verte Road fault system (Kidd 1974; Hibbard 1983), overprints the earlier fabrics, and records the latest increments of movement along the BVL.

Traditionally, the structural evolution of the BVL was thought to include early west-directed thrusting during the Taconian orogeny, and later heterogeneous reactivation during the 'Acadian' and/or Alleghanian orogeny (Bursnall 1975; Bursnall and de Wit 1975; Williams 1977; Hibbard 1983). However, recent studies suggest a significantly more complex and protracted structural history (e.g., Piasecki 1988, 1995; Goodwin and Williams 1990, 1996; Piasecki et al. 1990; Bélanger et al. 1996). In the present study, structural and geochronologic data from the Ming's Bight area (Chapters 4 and 6) provide important new insights into the structural history of the BVL.

East of the BVL, deformation structures record a general transition from rocks strongly deformed at amphibolite facies in the north, to rocks with a single, locally bedding-parallel, cleavage formed in lower greenschist facies in the south (Hibbard 1983; Fig. 3.1). These deformation structures overprint, and thus post-date, Early Silurian felsic plutons (DeGrace et al. 1976; Hibbard 1983). The structural geology in portions of the

Figure 3.1 Simplified geology of the thesis area illustrating the locations of Maps 1, 3, 4, 7, and 9 (refer to these maps for the location of Maps 2, 5, 6, 8, and Cross sections 1 to 7). The distribution of upper greenschist to middle amphibolite facies rocks is shown (after Hibbard 1982, 1983). The large foliation symbols schematically illustrate the change in orientation of the main fabrics in the area around the Rambler camp. The 'D₁-D₂' adjacent to the foliation symbol northwest of the Rambler camp denotes that this fabric was assigned to D₁ by Gale (1971), and to D₂ by Tuach (1976) and Tuach and Kennedy (1978). The 'D₂' adjacent to the foliation symbol northeast of the Rambler camp denotes that this fabric was assigned to D₂ by all of these authors (see Section 4.1.2.2). The structural geology of the Pacquet Harbour and Ming's Bight areas is described in detail in Chapters 3 and 4, respectively.

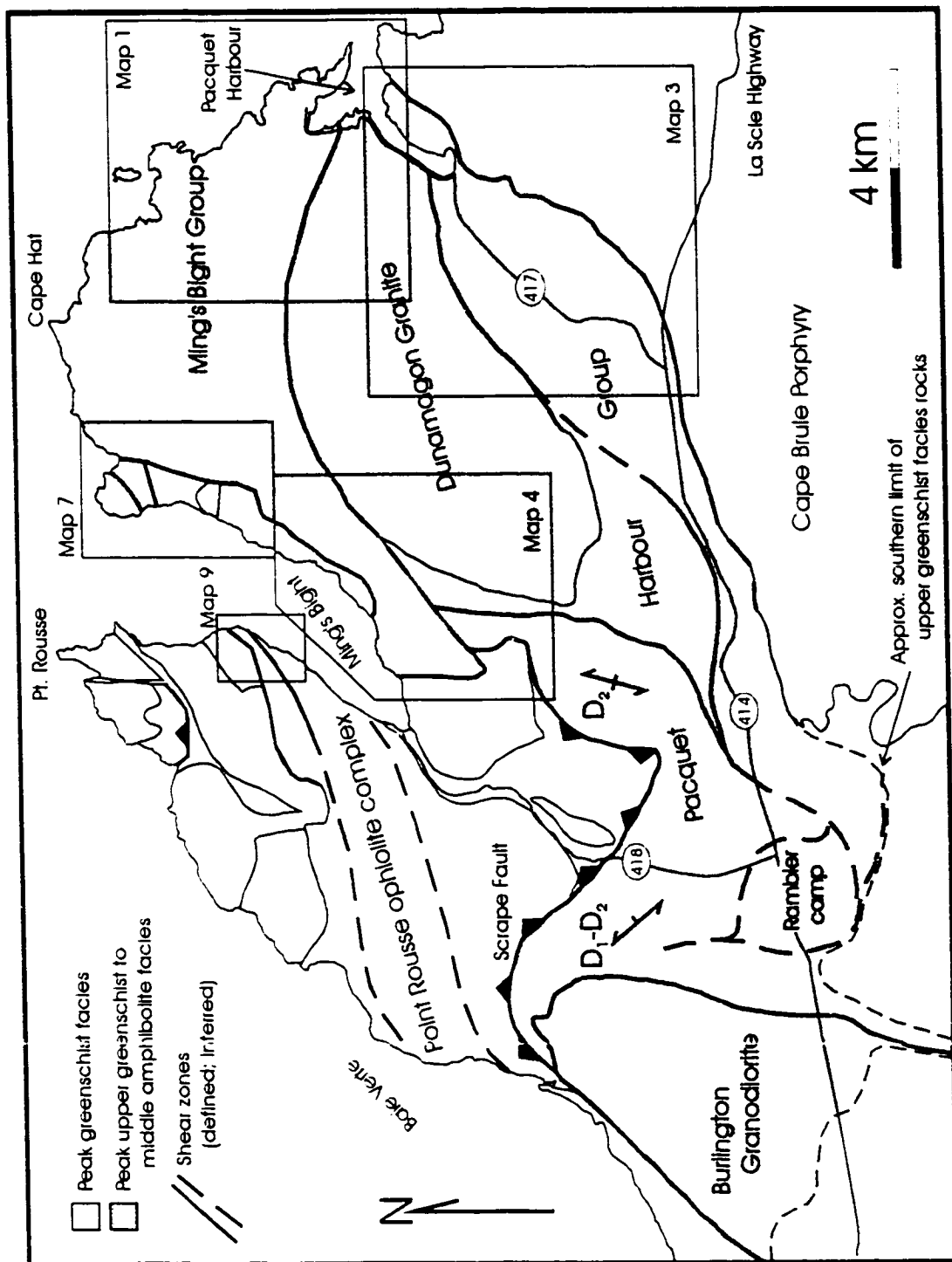


Figure 3.1

northern area has been examined previously (Church 1969; Coates 1970; Gale 1971; Kennedy 1975; DeGrace et al. 1976; Tuach 1976), and Hibbard (1983) summarized this work, recognizing a deformation sequence comprising three generations of structure (early, D_E ; main, D_M ; late, D_L). D_E structures are poorly preserved and comprise a weak bedding-parallel S_E foliation and/or L-S fabric that is axial planar to small-scale, tight to isoclinal, F_E folds. The S_E fabric was folded into a series of large, upright, tight to isoclinal F_M folds that plunge shallowly northeast. The most prominent examples of these folds are the major synclines that pass through the central portions of the Cape St. John Group and PROC (DeGrace et al. 1976; Hibbard 1983; Fig. 2.2). F_M folds are associated with an axial planar S_M fabric which typically contains a prolate shape fabric, which may indicate constrictional D_M strains. D_M structures formed in greenschist to amphibolite facies, and were overprinted by D_L structures, attributed by DeGrace et al. (1976) to inhomogeneous vertical shortening. In the north, metre scale reclined F_L folds are prominent and are associated with a subhorizontal S_L crenulation cleavage. South of the La Scie highway (Fig. 3.1), the amplitude and wavelength of the F_L folds decrease, and the S_L fabric diminishes. This change in intensity of D_L structures is associated with a change in syn- D_L metamorphism from amphibolite facies in the north, to greenschist facies in the south (Hibbard 1983).

On the basis of the foregoing descriptions, a marked similarity in style, apparent timing, and syn-deformation metamorphic grade of D_M structures west and east of the BVL is apparent, and in the present study these structures are collectively interpreted to record progressive transpressional deformation. Perhaps significantly, Hibbard (1983)

attributed D_M - D_L deformation to "...northward strike-slip movement of the (Dunnage Zone) along the north trending segment of the Baie Verte Line...and southerly overthrusting of rocks from the north due to uplift of the Fleur de Lys Supergroup". This model is modified and further developed below.

3.1.2 Methodology and terminology

The structural geology of the MBG and adjacent Dunnage Zone lithologies has been examined in detail, with particular emphasis on documenting the structural evolution of the deformation zones that bound the MBG, and everywhere separate it from the adjacent Dunnage Zone terranes. A preliminary examination of these zones revealed a marked spatial variation in character, kinematics, and apparent timing. Consequently, the zones are separated into three adjoining map areas of contrasting structural character: Pacquet Harbour; Ming's Bight; and the PROC (Fig. 3.1). The structural geology of each of these map areas is described in detail.

The standard method of distinguishing structures of different generations involves grouping structures according to their style, patterns of orientation, and overprinting relationships with metamorphic minerals and/or other structures (Williams 1985). In coastal exposures, where outcrop is relatively continuous, overprinting relations allowed confident determination of the deformation sequence. However, the relative lack of exposure away from the coast (particularly in the Ming's Bight area) required correlation of structures mainly on the basis of style and orientation. Further complications for correlating structures arise when one considers that: 1) multiple generations of structures can form during progressive deformation; and 2) subsequent deformation may reactivate

earlier structures, resulting in composite structures. In areas where progressive deformation and/or reactivation are thought to be a factor, particular attention was paid to the interrelationships between kinematic indicators, associated mineral textures and assemblages, and overprinting relations.

In this thesis D_1 , D_2 , D_3 , etc. refer to successive sets of deformation structures that are distinguished by overprinting relationships, grade of metamorphism, and U-Pb and $^{40}\text{Ar}/^{39}\text{Ar}$ geochronologic constraints (see Chapter 6). These symbols are used to distinguish deformation phases that are chronologically distinct, or that represent separate increments of a progressive deformation (e.g., Tobisch and Paterson 1988). No general correlation of D_1 structures (for example) from spatially separate areas is implied, unless specifically stated. This also applies for the annotations F_1 , F_2 , F_3 , etc. which refer to successive generations of folding; S_1 , S_2 , S_3 , etc. which refer to successive generations of planar fabric; and L_1 , L_2 , L_3 , etc. which refer to successive generations of linear fabric.

This thesis makes considerable use of kinematic indicators in order to deduce the sense of movement in ductile shear zones. In all cases, the kinematic indicators described in this study are interpreted in the context of the generally accepted review of shear-sense criteria presented by Hanmer and Passchier (1991). As noted by these authors however, "...the accumulating evidence strongly suggests that natural deformations commonly represent significant deviations from the idealized simple models...", and "...the nature of the flow at the scale at which geologists make their observations may strongly deviate from the type of flow at the bulk scale". Indeed, several authors have recently noted that the common assumption of a monoclinic symmetry, wherein the stretching lineation and

the poles to the S- and C-surfaces plot in a great circle girdle, may not be valid for the analysis of most shear zones (e.g., Passchier 1995; Lin et al. 1997). In particular, these authors have described transpressional and transtensional shear zones in which stretching lineations from the adjacent wall rock do not plot in the same great circle girdle, and thus indicate a bulk triclinic symmetry. These observations have several potential implications for the interpretation of shear-sense indicators since, for example, the stretching lineation need not indicate the bulk displacement direction in shear zones with a triclinic symmetry (Lin et al. 1997). Thus, shear-sense indicators and stretching lineations observed on a local scale may have no direct relationship to the bulk sense of movement of the shear zone.

Although the present author acknowledges that potential problems exist in the interpretation of shear-sense criteria in triclinic shear systems, it should be noted that triclinic shear systems in general are incompletely understood, with much of the currently published research of a preliminary nature, and several significant problems exist. For example, domains of stretching lineations that plunge steeply and shallowly within a single shear zone are commonly cited as evidence of a triclinic symmetry; however, it is rarely possible to demonstrate conclusively within a single shear zone that the variously-plunging lineations developed contemporaneously during a single phase of deformation (e.g., Goodwin and Williams 1996). In the present study, the sense of movement inferred from kinematic indicators is in all cases contemplated with consideration of the following. First, is there evidence, such as variably plunging stretching lineations or sense of shear indicators developed on planes oblique to the stretching lineation, to suggest non-coaxial flow types other than simple shear (e.g., Passchier 1995)? Second, due to such factors as

inhomogeneous boundary conditions and rheological heterogeneities, the flow characteristics of regional-scale shear systems will be strongly dependent on the location and scale of observation. Thus, the sense of movement inferred from kinematic indicators in a relatively small portion of a regional shear system (e.g., the BVL) should be considered in context with the flow characteristics on a regional scale. Third, the sense of movement inferred for a given shear zone should be compatible with constraints provided by regional stratigraphic and thermochronologic data.

3.2 PACQUET HARBOUR AREA - INTRODUCTION

3.2.1 Background

Structural relationships between the MBG and adjacent units in the Pacquet Harbour area have figured prominently in many interpretations of the tectonostratigraphy and tectonic evolution of the BVP. For example, several authors inferred Late Proterozoic to Early Ordovician ages for the PHG, Cape Brule Porphyry, and Cape St. John Group, and correlated these units with the Fleur de Lys Supergroup, on the basis of structural similarities between the MBG and PHG in Pacquet Harbour (e.g., Church 1969; Coates 1970; Dewey and Bird 1971; Kennedy 1975). In addition, Hibbard (1982, 1983) used structural 'trends' in the MBG, PHG, and Dunamagon Granite to define the eastern extension of the BVL, and the location of the Baie Verte Flexure.

However, despite the importance that has previously been assigned to structures in the Pacquet Harbour area, no detailed structural descriptions have been published, and there is no information available concerning their regional significance. Therefore, one of the major goals of the present study is to document the structural geology of the Pacquet

Harbour area in detail, and develop a comprehensive model for the structural and kinematic evolution.

3.2.2 Previous structural studies

The structural geology of portions of the Pacquet Harbour area has been described in two unpublished theses. Coates (1970) described the deformation and metamorphism in the northern portions of the PHG, Cape Brule Porphyry, and Cape St. John Group, and proposed a structural history comprising three deformation phases. In this history, D_1 structures include a penetrative L-S fabric which is axial planar to rare, tight to isoclinal F_1 folds, and nearly parallel to primary layering in the PHG and Cape St. John Group. The S_1 fabric is folded by recumbent to upright folds that plunge southeast, and are associated with a regional subhorizontal to subvertical, axial planar L-S fabric. Coates assigned these structures to D_2 , and defined a large-scale, recumbent F_2 fold structure that plunges shallowly southeast. Coates provided evidence for hornblende growth syn- to post- D_1 , and pre-, syn-, and post- D_2 , and suggested that both D_1 and D_2 were associated with upper greenschist to lower amphibolite facies metamorphism. Coates also noted that the D_1 - D_2 structures are less complex and non-penetrative, and the grade of metamorphism decreases, to the south away from the Pacquet Harbour area. Locally developed crenulations and open folds of the S_2 fabric were ascribed to D_3 .

Hibbard (1983) correlated Coates' D_1 and D_2 - D_3 deformation with the D_M and D_L regional deformation, respectively. The deformation history of Coates (1970) is broadly similar to that documented in the present study. However, recent advances in the analysis of deformation mechanisms and kinematic indicators have facilitated a more detailed

understanding of the various generations of structure.

The second detailed study in the area was performed by McDonald (1993) on the structural geology of the Dunamagon Granite. In this study, McDonald documented two increments of deformation related to north-directed movement of the granite over the MBG: an early, high-temperature increment associated with peak amphibolite facies metamorphism, and a late, relatively low-temperature increment associated with greenschist to prehnite-pumpellyite facies metamorphism. The contact between the granite and PHG was interpreted as intrusive, and that between the granite and MBG was considered to be wholly tectonic, or a tectonically modified intrusive contact. The results of this study are partly consistent with those of the present study; however, the north-directed movement of the Dunamagon Granite over the MBG could not be confirmed, and an alternative interpretation is presented in Section 3.3.6.

The only other detailed structural and metamorphic studies in the Pacquet Harbour area were conducted in the vicinity of the Rambler massive sulphide deposits (Gale 1971; Tuach 1976; Fig. 2.2), and are discussed with the structural description of the Ming's Bight map area in Chapter 4.

3.3 DETAILED STRUCTURAL ANALYSIS

Detailed analysis of deformation structures and overprinting relationships in the Pacquet Harbour area reveals three phases of ductile deformation (i.e., D_1 , D_2 , D_3 ; refer to Table 3.1; Maps 1, 2, and 3; Cross-sections 1, and 2; and Fig. 3.2). D_1 structures are well developed in the Early Silurian Dunamagon Granite (Cawood and Dunning 1993), indicating that most, if not all, deformation in this area post-dates the Early Silurian.

Table 3.1 Deformation structures - Pacquet Harbour area

	Late brittle faulting		
D ₃ deformation *pre- to syn-360 Ma *post-380 Ma	Bkj Brook Shear Zone F ₃ folds Rare; open to tight; east to southeast-plunging	S ₃ - L ₃ fabrics Semi-penetrative foliation in BBSZ; moderately south-dipping; rare southeast-plunging stretching and mineral lineation	Southeast-directed extensional shearing associated with exhumation of the MBG
D ₂ deformation *pre-360 Ma *syn-380 Ma *post-429 Ma	"Regional" deformation F ₂ folds Open to isoclinal; southeast- plunging; cylindrical to tubular; mainly southwest-verging; axes parallel to extension direction	S ₂ - L ₂ fabrics Penetrative mylonitic foliation to spaced crenulation fabric; shallowly southeast-dipping; axial planar to F ₂ ; prominent mineral and stretching lineation	Southeast-directed extensional shearing associated with exhumation of the MBG
D ₁ deformation *pre-385 Ma *post-429 Ma	Pelee Point Shear Zone F ₁ folds Tight to isoclinal; intrafolial; rootless; sheath folds	S ₁ - L ₁ fabrics Penetrative mylonitic foliation in PPSZ; weak fabric external to PPSZ; Group 1 shear zones in DG; local stretching lineation	Sinistral-reverse oblique-slip shearing associated with subsidence of the MBG

Note: double-solid and single-dashed horizontal lines denote separate and progressive deformations, respectively

* Time constraints (see Chapter 6)

Figure 3.2 Lower hemisphere, equal area projections of structural data in the Pacquet Harbour area. Planar structural elements are plotted as poles. Abbreviations in the top row refer to the general location of the structural measurements, and generally progress from north to south across the Pacquet Harbour area: MBG, Ming's Bight Group north of Pacquet Harbour; PP, Pelee Point; BBSZ, Big Brook shear zone; DG, Dunamagon granite; SSPH, south shore of Pacquet Harbour; WR, Woodstock Road; LSH, La Scie Highway (see Maps 1, 2, and 3). L_2 includes both mineral (hornblende) and stretching lineations. S_1 in the Dunamagon Granite corresponds to 'Group 1' structures, whereas S_2 - L_2 correspond to 'Group 2' structures (see Section 3.3.6). The plot of S_2 in the Dunamagon Granite includes measurements taken from McDonald (1993). S_1 at Pelee Point includes measurements from the MBG and PHG to the north and south of the PPSZ, respectively.

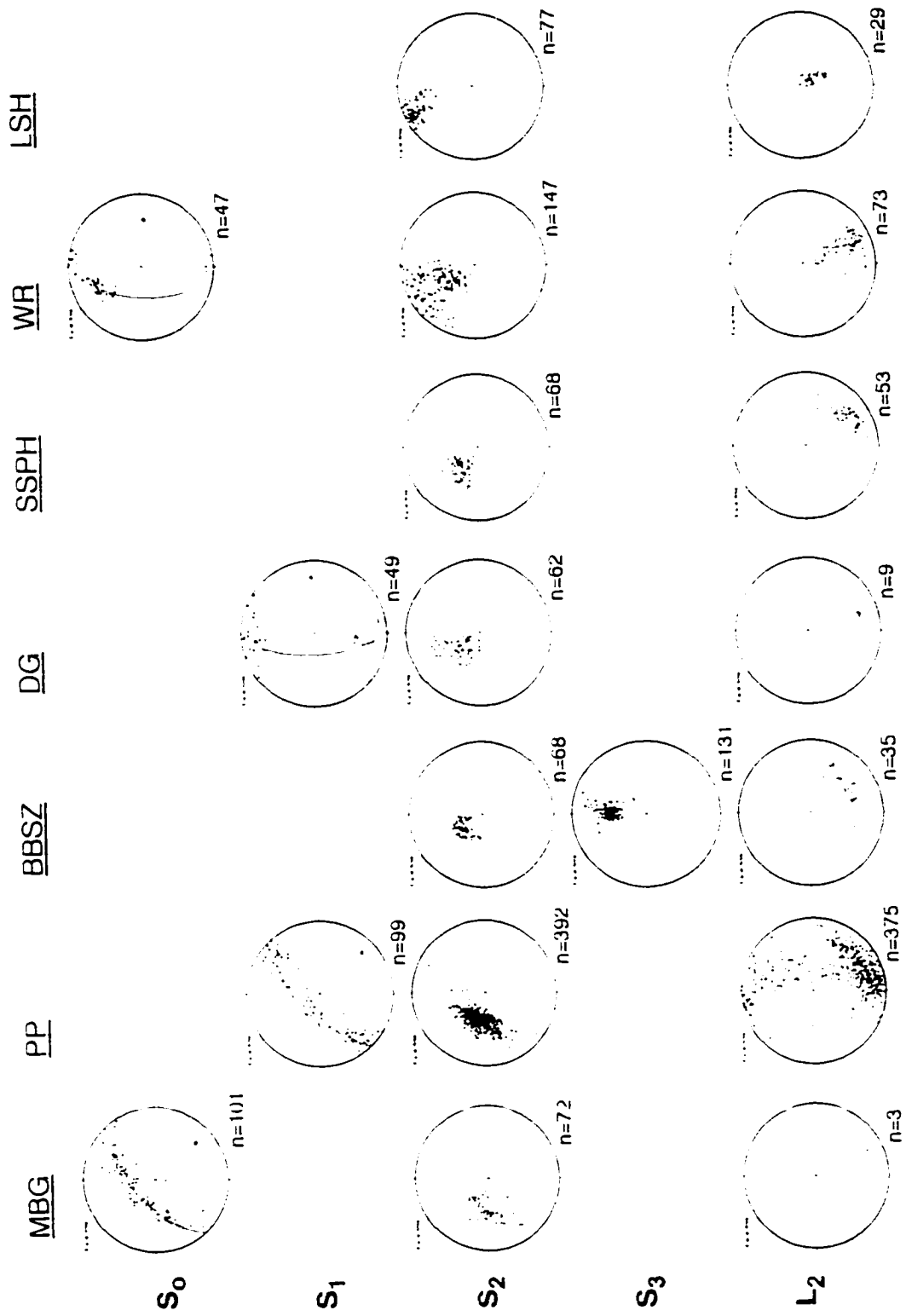


Figure 3.2

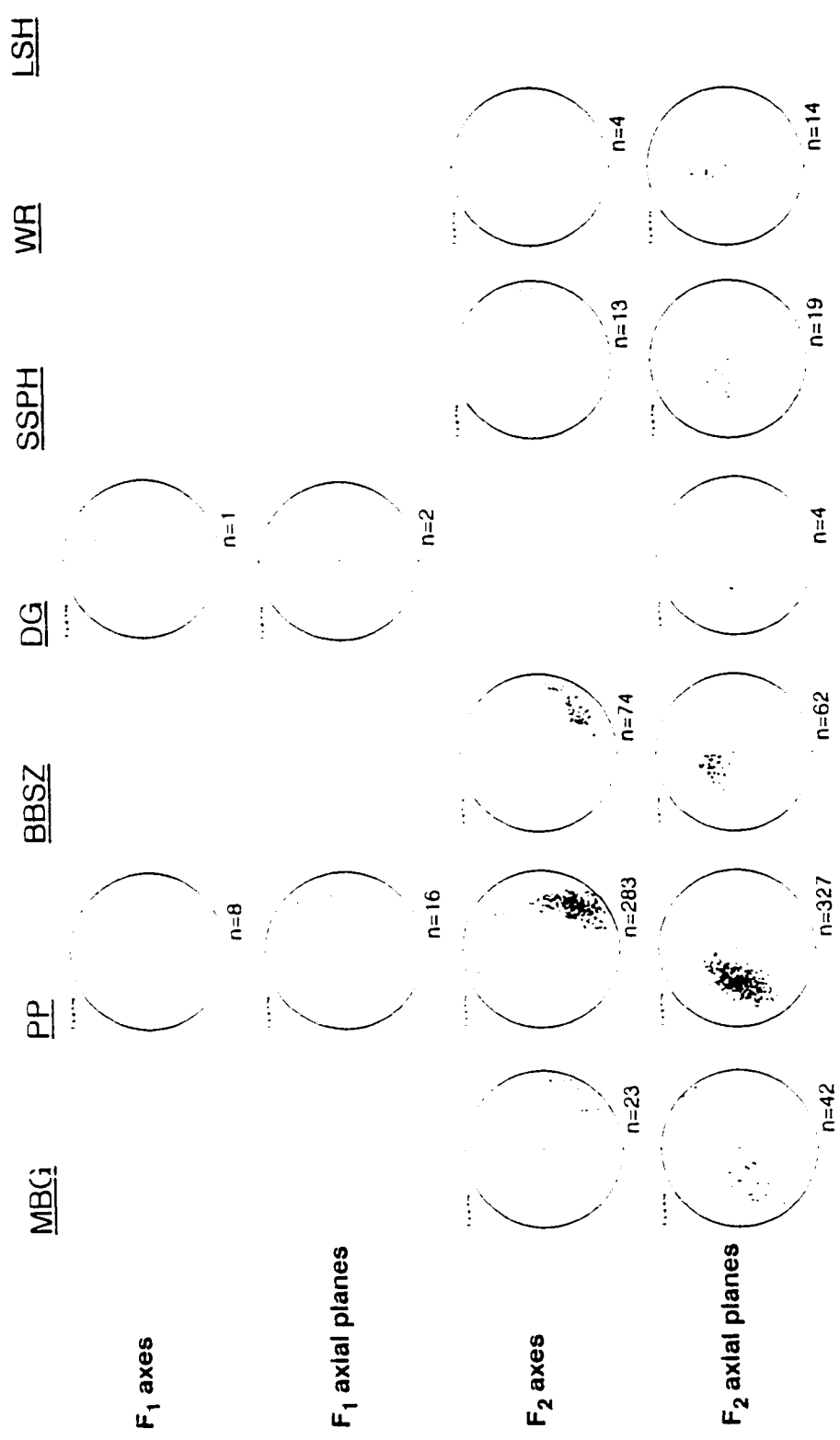


Figure 3.2

3.3.1 Primary Structures

In structural analysis, younging directions derived from primary structures are particularly useful for inferring the sequence of deformation. In Pacquet Harbour, most primary structures have been obscured by intense deformation, and this has contributed significantly to the controversy surrounding the MBG-PHG contact. One of the goals of the present study was to examine the rocks in the Pacquet Harbour area with an eye for primary structures and potential younging criteria. As a result of this work, primary structures have been documented in both the PHG and MBG, and provide an important constraint on the nature of the controversial PHG-MBG contact.

In the MBG, younging criteria include consistent gradations from psammitic to semi-pelitic schist, coupled with the presence of sharp contacts between the psammitic and semi-pelitic layers (see Section 2.3.1.1; Fig. 2.3b). These younging criteria are commonly preserved north of Pelee Point, and indicate that the MBG is mainly upward facing on the S_2 foliation that dips shallowly southeast.

In the PHG, well preserved trough cross beds and graded bedding in metasediments (Fig. 2.4d) indicate that the bedding is downward facing on S_2 . Abrupt changes in younging direction are locally observed within the metasediments, indicating the presence of isoclinal folds, possibly related to structural overturning during D_1 . In the PHG at Pelee Point, pillow basalts are common (Fig. 2.4a) and consistently face downward on S_2 .

The interpretation of the facing direction data is complicated by the limited data set. However, the available data indicate that the PHG is mainly downward-facing on S_2 ,

whereas the MBG is mainly upward-facing on S_2 . This change in facing direction is particularly obvious at Pelee Point, where PHG basalts and MBG metasediments young in opposite directions on the same limb of a large F_2 fold (Map 2; Cross section 1). Though not conclusive, these data cast doubt on the suggestion that the MBG-PHG contact is conformable in this location (e.g., Hibbard 1983, and references therein).

3.3.2 D_1 deformation - the Pelee Point Shear Zone

Structures related to D_1 deformation are pervasive within a ~200m thick ductile shear zone which is well exposed at Pelee Point in Pacquet Harbour (the Pelee Point shear zone; PPSZ; Map 2). The shear zone is located at the contact between the MBG and the PHG, and contains interleaved tectonic inclusions of PHG and MBG lithologies. Within the PPSZ, discrete zones of anomalously high strain separate zones predominantly comprised of MBG mica schist from zones predominantly comprised of PHG amphibolite. Thus, the general features of the PPSZ are consistent with a ductile shear zone associated with juxtaposition of the MBG and PHG. The entire PPSZ is folded by large, reclined F_2 folds that plunge southeast (Map 2; Cross-section 1), resulting in substantial reorientation of D_1 structures (Fig. 3.2).

Within the PPSZ, the S_1 foliation is penetrative and defined by fine- to medium-grained hornblende and biotite in PHG amphibolite, and muscovite and biotite in MBG schist. This foliation is parallel to a pronounced tectonic layering defined by highly elongate, interleaved, tectonic inclusions of MBG schist and PHG amphibolite (Fig. 3.3a). The PPSZ contains two discrete zones of anomalously high strain up to 5m thick. These zones parallel the S_1 foliation and tectonic layering, and contain a particularly intense S_1

Figure 3.3 Field photographs of D_1 and D_2 structures in the PPSZ, MBG, and PHG. **a)** Tectonic layering comprising PHG amphibolite (black) and MBG schist (grey) in the PPSZ at Pelee Point. There are two generations of pre- F_2 fold in this outcrop. The earlier folds are generally tight, intrafolial, asymmetric, and exhibit opposite vergence and highly variable plunge over short distances (arrowed). The later folds are gentle, symmetric, and plunge steeply south. **b)** F_1 sheath fold in MBG schist at Pelee Point. **c)** Typical F_2 folds that plunge southeast and verge southwest in MBG schist at Pelee Point. The axial planar S_2 gradationally changes orientation toward the horizontal with increased fold tightness (towards the right). **d)** Rootless, asymmetric F_2 folds (arrowed) defined by calc-silicate layers in MBG schist at the mouth of Big Brook in Pacquet Harbour (Map 2; notebook in upper right corner for scale). These folds verge in opposite directions, plunge southeast, and are wrapped around by S_2 . **e)** Penetrative L>S fabric in high-strain MBG schist north of Pacquet. **f)** Asymmetrically transposed layering in D_2 mylonitic amphibolites that dip east on the south shore of Pacquet Harbour. L_2 in this outcrop is oriented $\sim 70^\circ$ from the northeast-plunging line of intersection between the transposition planes and S_2 . This relationship, coupled with the sense of asymmetry, is consistent with dextral-normal oblique-slip shear. Quarter folds associated with the inclusion in the upper central portion of the photograph (arrowed) also indicate dextral-normal oblique-slip shear (Hanmer and Passchier 1991).

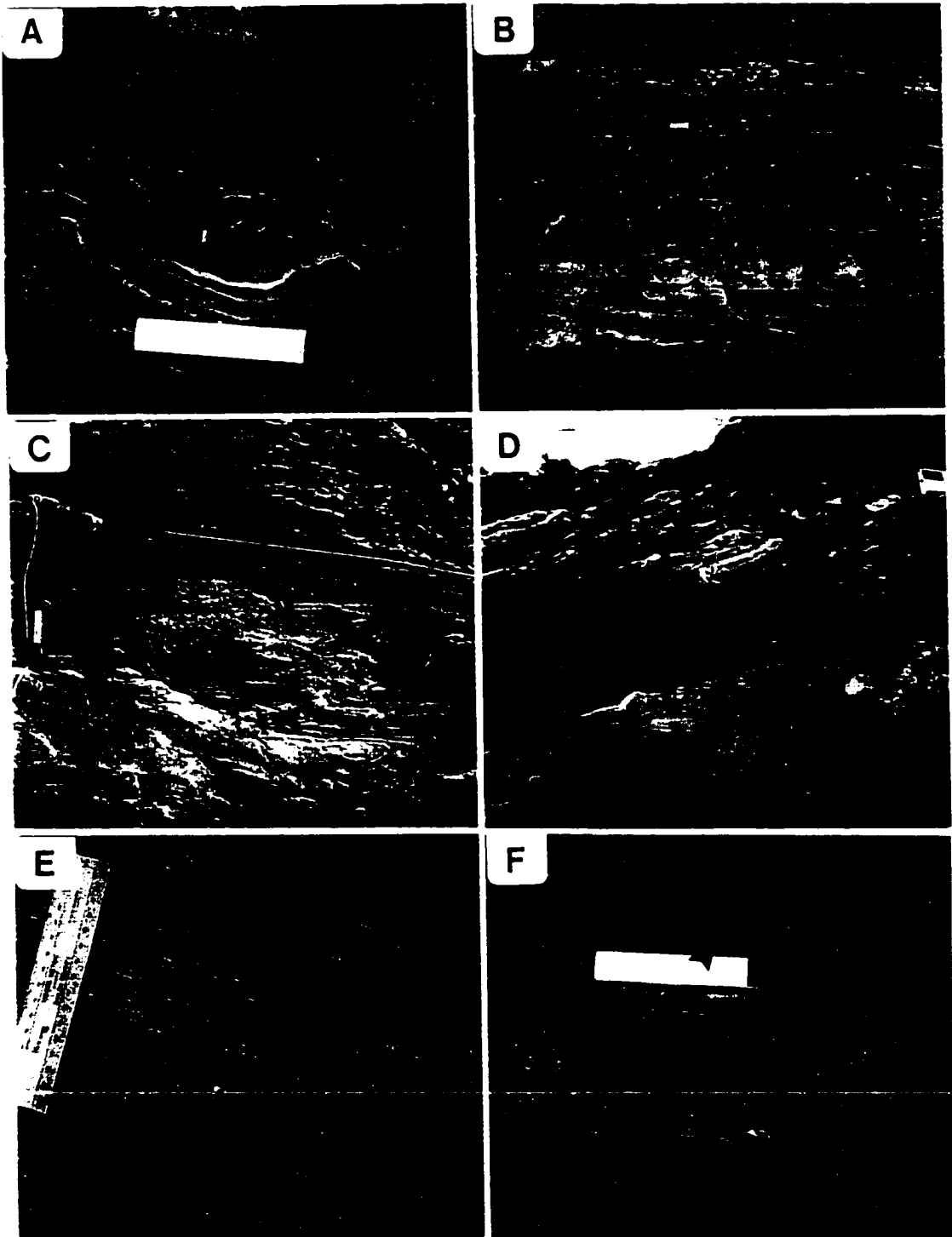


Figure 3.3

fabric that is axial planar to rootless, isoclinal folds. In general, these zones have a more homogeneous, equigranular texture and are finer-grained than the surrounding rock.

Within these zones, the individual hornblende and biotite grains that define S_1 are generally idioblastic and only weakly strained, and quartz and plagioclase form a medium- to coarse-grained, granoblastic polygonal texture. These features may be explained in two ways: 1) extensive syntectonic recrystallization during D_1 ; or 2) recrystallization during D_2 .

Porphyroblast-matrix microstructural relationships indicate that garnet and hornblende porphyroblasts in the PPSZ grew during D_2 deformation and peak amphibolite facies metamorphism (see Section 5.2.1.1). Significantly, these porphyroblasts contain very fine-grained inclusions, and the included mineral assemblages lack minerals indicative of medium- to high-temperature metamorphism. These observations suggest that the high-strain zones within the PPSZ were not metamorphosed at high temperature prior to D_2 , and lend support to the latter hypothesis.

The S_1 fabric is axial planar to small-scale, tight to isoclinal, asymmetric F_1 folds (Fig. 3.3a). F_1 fold hinges are curvilinear, plunge shallowly northwest and southeast, and define a weak girdle on a stereographic plot (Fig. 3.2). Sheath-like F_1 folds are common within the higher-strain zones in the PPSZ (Fig. 3.3b). In horizontal outcrop surfaces, F_1 folds mainly have a sinistral sense of vergence, and are commonly rootless and intrafolial.

The northern margin of the PPSZ is bounded by a very distinctive ~20-30m thick unit of rusty-brown biotite schist (Map 2) that contains 5-20% recrystallized quartz pods or boudins that range up to 20cm long and evenly distributed in a fine- to medium-grained biotite schist matrix. The biotite schist unit lacks the prominent layering of the MBG, but

local discontinuous layers of massive psammitic schist suggest that it represents strongly disrupted MBG. The biotite schist contains a prominent fabric which is defined by foliated biotite and a preferred orientation of elongate quartz pods. This fabric is parallel to S_1 in the PPSZ, and the contact between the biotite schist and coherent MBG is marked by a narrow high strain zone with local outcrops of high-strain rocks that are identical in appearance and structural character to those in the core of the PPSZ. Thus, the field relationships are consistent with disruption of the MBG to form the biotite schist unit during D_1 . The abundant quartz pods in this unit can be explained in two ways: 1) subsolidus segregation of quartz during amphibolite facies metamorphism (e.g., Sawyer and Robin 1986); or 2) ductile shearing of a brittle stockwork of quartz veins associated with an early increment of D_1 . However, if the quartz pods formed as segregations during amphibolite facies metamorphism they should be more widely distributed (particularly in the adjacent MBG schists). Therefore, the second hypothesis is tentatively accepted as the mode of formation of the quartz pods.

In the MBG north of the PPSZ, S_1 is defined by a penetrative, fine-grained, biotite-muscovite foliation that is parallel to primary layering, and is particularly obvious in the hinge regions of F_2 folds. This foliation is axial planar to rare, tight to isoclinal F_1 folds of the primary layering and layer-parallel quartz veins. In the PHG south of the PPSZ, S_1 is preserved as a crenulated hornblende-biotite foliation between S_2 crenulation planes, and as an early foliation in the hinges of F_2 folds. The S_1 fabric is also particularly well preserved in strongly deformed, 1-4m thick, granitic dykes which intruded the PHG prior to D_1 (e.g., Fig. 2.5c). In these dykes, S_1 is pervasive and parallel to the sharp contacts,

and is variably defined by a penetrative biotite and muscovite foliation, pronounced gneissosity, highly attenuated layers of strongly foliated amphibolite, and a locally well developed augen texture. The dykes and internal S_1 fabric are folded by F_2 folds. In mafic metasediments north of Mill Pond (Map 3), bedding and bedding-parallel quartz veins are folded by F_1 folds. These folds are tight to isoclinal, and are associated with a weak axial planar S_1 fabric which is transected by S_2 . In these rocks, abrupt changes in younging direction may indicate that there are larger isoclinal F_1 folds in the PHG.

Because of extensive amphibolite facies D_2 deformation and recrystallization, the sense of movement of the PPSZ cannot be conclusively determined. In the PPSZ, microscopic and macroscopic kinematic indicators associated with D_1 have been either obliterated by, or rendered indistinguishable from, structures associated with D_2 . Consequently, indirect methods must be used to infer the possible movement sense and tectonic significance of D_1 deformation.

Several observations indicate that D_1 may have initiated at a relatively shallow crustal level. First, abundant quartz pods in the biotite schist along the northern margin of the PPSZ may be consistent with an early stockwork of quartz-filled brittle fractures. Second, pre- and syn- D_2 porphyroblasts lack included mineral assemblages indicative of high temperature metamorphic conditions, which may indicate that these rocks were not metamorphosed above greenschist facies prior to at least the middle stages of the D_1 . Third, probable D_1 structures within the Dunamagon Granite comprise a heterogeneous series of discrete shear zones anastomosing around low-strain domains (e.g., McDonald 1993; see Section 3.3.6). This structural style is generally associated with relatively low

temperature deformation in pre-tectonic granitic plutons (i.e., sub-amphibolite facies; Gapais 1989).

While not conclusive, these observations are consistent with initiation of the PPSZ at a relatively shallow crustal level. Furthermore, since the early stages of D_2 were associated with lower to middle amphibolite facies metamorphism, the Pacquet Harbour area (and PPSZ) must have been buried to significant depths (>15 km) prior to the onset of D_2 . These observations provide indirect evidence that D_1 was associated with a bulk compressional tectonic regime, resulting in structural burial of the Pacquet Harbour area, and the juxtaposition of the MBG and PHG. This hypothesis is further developed below.

3.3.3 D_2 deformation

In the Pacquet Harbour area, D_2 deformation structures include a 'regionally' pervasive S_2 foliation, L_2 lineation, and reclined F_2 folds (Fig. 3.2), that are associated with development of a prominent ductile shear zone that dips southeast and parallels the northern contact of the Cape Brule Porphyry (Map 3).

The MBG, PHG, Dunamagon Granite and Cape Brule Porphyry each contain a distinctive set of D_2 structures, and this is interpreted to reflect fundamental differences in the accommodation of D_2 strain. For example, the MBG appears to have accommodated D_2 strain primarily through folding at various scales (e.g., Map 2), whereas D_2 strain in the PHG was accommodated through development of penetrative L-S and L>S fabrics at various scales, with subordinate folding. These differences undoubtedly reflect the presence of a pronounced primary anisotropy in the MBG (i.e., bedding), and the relative lack of primary anisotropy in the PHG (e.g., Lister and Williams 1983; Fletcher and

Bartley 1994). Moreover, the geology of the Pacquet Harbour area is dominated by two large felsic plutons (Dunamagon Granite and Cape Brule Porphyry) which represented significant heterogeneities in the deforming rock mass. These heterogeneities could have resulted in variable patterns of finite strain at outcrop scale (e.g., Paterson and Tobisch 1988; Lagarde et al. 1990). In light of this, D_2 structures in the MBG, PHG, and Cape Brule Porphyry are discussed separately below, and D_2 structures in the Dunamagon Granite are discussed in Section 3.3.6.

3.3.3.1 Ming's Bight Group

In the MBG, the S_2 foliation is defined by a preferred orientation of biotite and muscovite, and can generally be characterized as a differentiated crenulation cleavage formed through transposition of S_1 . In psammitic layers, S_2 is typically defined by narrow mica-rich domains that anastomose around discontinuous domains of medium- to coarse-grained quartz and feldspar which are characterized by a pronounced granoblastic polygonal texture and crystallographic preferred orientation, consistent with fairly high temperature conditions during D_2 . In several locations, S_2 is continuous into sigmoidal inclusion trails in garnet and staurolite porphyroblasts, suggesting syntectonic growth and amphibolite facies metamorphism during D_2 (e.g., Bell et al. 1986; Jamieson and Vernon 1987; Johnson and Vernon 1995). In semi-pelitic layers, S_2 is penetrative and defined by medium- to coarse-grained, foliated biotite and muscovite, with subordinate, elongate, quartz and plagioclase grains. The heterogeneous development of S_2 , coupled with refraction of S_2 through the layering in the MBG, can locally be misinterpreted as multiple generations of planar fabrics, rather than the product of one progressive deformation

phase (e.g., Williams 1985; Tobisch and Paterson 1988). In the hinges of large F_2 folds, S_2 forms a crenulation cleavage at a high angle to S_1 and the MBG layering. In the limbs of these folds, S_2 is generally penetrative, and is nearly parallel to S_1 and layering. The orientation of S_2 in the MBG gradually changes from a shallow east-northeast dip near Handy Harbour to a shallow southeast dip in Pacquet Harbour (Map 1; Cross section 2). This change is ascribed to large-scale rotation of S_2 during D_3 (see Section 3.3.4.2).

The S_2 crenulation fabric is axial planar to F_2 folds that are pervasive in the MBG, and that fold the psammitic and semi-pelitic layering, layer-parallel quartz veins, and S_1 . F_2 folds occur on all scales, with wavelengths varying from $<1\text{cm}$ up to $>500\text{m}$ (Map 2; Cross-section 1). These folds are typically open to tight, reclined, and consistently plunge shallowly to the southeast (Fig. 3.3c and 3.3d). In the hinges of large F_2 folds, parasitic F_2 folds are open to tight, symmetrical, and have a parallel to similar style, whereas parasitic F_2 folds on the limbs are tight to isoclinal, asymmetric, and have a similar style. Rootless and intrafolial F_2 folds are common on the limbs of the large F_2 folds (Fig. 3.3d). The vergence of the minor F_2 folds varies according to the location of individual folds within the larger F_2 fold structures; however, southwest-verging folds clearly predominate towards the southeast (Fig. 3.3c).

In the MBG, S_2 contains a rare L_2 lineation defined by a preferred orientation of biotite and muscovite grains, and elongate lozenges of equigranular, recrystallized quartz and feldspar. The L_2 lineation plunges to the southeast, and is parallel to F_2 fold axes. In several locations, the hinges of F_2 folds contain, and are parallel to, a pronounced rodding of axial planar quartz veins. About 0.5 km northeast of Pacquet, a penetrative $L \geq S$ fabric

is preserved within a discrete zone of anomalously high strain on the limb of a large reclined F_2 fold. Semi-pelitic layers in this zone contain a penetrative biotite-muscovite foliation that is continuous with S_2 outside the zone. In contrast, psammitic layers contain a penetrative $L \geq S$ fabric defined by a preferred orientation of distinct plagioclase-rich and quartz-rich domains (Fig. 3.3e). The plagioclase-rich domains form slightly flattened prolate ellipsoids (axial ratios typically $X=10 : Y=3 : Z=1$). In thin section, the plagioclase-rich domains consist of medium-grained, equant, equigranular, plagioclase grains with smooth curving to polygonal grain boundaries, and a strong crystallographic preferred orientation. Quartz occurs in elongate, <2 mm thick domains that anastomose around the plagioclase-rich domains. In these domains, quartz is medium-grained, and forms inequigranular, irregular grains with sutured to irregular-smooth curving grain boundaries. A fine-grained muscovite \pm biotite foliation anastomoses around the plagioclase and quartz domains. The linear and planar fabric elements within the high strain zone are concordant with S_2 and L_2 , respectively, outside the high strain zone.

In general, there appears to be a complete gradation between structures in the high strain zone and D_2 structures external to the zone; no overprinting relationships were observed. These observations suggest that all of these fabrics formed during D_2 , and indicate that significant strain gradients existed within the MBG during D_2 deformation.

3.3.3.2 Pacquet Harbour Group

In the PHG, D_2 structures are heterogeneous in orientation and intensity. For example, the orientation of S_2 gradually changes from shallowly east-dipping to steeply south-southeast-dipping from northeast to southwest across the PHG (Fig. 3.2; Map 3).

Furthermore, finite D_2 strain was most intense along the margins of the Silurian plutons, and was less intense in the interior of the PHG (Cross-section 2). In order to address this heterogeneity, D_2 structures are described from northeast (Peleé Point) to southwest (La Scie Highway) across the PHG.

At Peleé Point and along the south shore of Pacquet Harbour, the PHG consists mainly of mylonitic amphibolites. Their protoliths included mafic intrusive, extrusive, and sedimentary rocks. The S_2 foliation in these rocks is penetrative, dips shallowly northeast to southeast, and defined by aligned hornblende and biotite porphyroblasts. S_2 is typically parallel to a pronounced mylonitic banding which probably formed through intense transposition of an early, possibly primary, layering (Fig. 3.3f). In thin section, hornblende is fine- to coarse-grained, subhedral and poikiloblastic. The matrix consists of fine- to coarse-grained equigranular quartz and plagioclase. Typically, individual mineral grains in these rocks are not significantly strained, consistent with relatively high temperature conditions (and complete recovery) during deformation. In several locations, S_2 is continuous into sigmoidal inclusion trails in garnet and hornblende porphyroblasts, suggesting syntectonic growth and amphibolite facies metamorphism during D_2 (see Section 5.2.1.1). Locally, the porphyroblasts are randomly oriented within and across S_2 , suggesting late- to post- D_2 hornblende growth. Sense of shear indicators, including asymmetrically transposed layering (Fig. 3.3f) and δ -porphyroclasts, indicate a component of south-side-down shear parallel to S_2 - L_2 .

The S_2 fabric contains a pervasive L_2 mineral and stretching lineation that consistently plunges shallowly to the southeast (Fig. 3.2). In many locations the linear

fabric is penetrative and the rocks approach pure L-tectonites (e.g., Coates 1970). The L_2 mineral lineation is defined by the preferred orientation of hornblende porphyroblasts, whereas the L_2 stretching lineation is defined by elliptical aggregates of fine- to coarse-grained epidote and plagioclase, that probably represent recrystallized primary plagioclase phenocrysts. In coastal exposures near the Cape Brule Porphyry-PHG contact, the stretching lineation is defined by clasts of gabbro and basalt in volcanic breccia layers. In addition, hornblende pseudomorphs after pyroxene within these layers have been stretched and recrystallized, to form elliptical masses of fine-grained lineated hornblende (Fig. 3.4a). At Pelee Point, clasts in metaconglomerate locally have aspect ratios of X:Y 3-10:1 and Y:Z <4:1, consistent with constrictional or plane finite D_2 strains. Near the northern contact of the Cape Brule Porphyry, S_2 anastomoses around large (<10 x 20 m) elliptical pods of massive to weakly deformed pillowed basalt and/or gabbro. These pods are elongate parallel to L_2 in the plane of S_2 , and are thus interpreted as 'mega-augen' (e.g., Park et al. 1994) associated with heterogeneous mylonitization of gabbro and basalt during D_2 shear.

In many locations, the mineral and stretching lineations are folded around the hinge of F_2 folds, resulting in a great circle distribution on a stereographic projection, and consistent with an L_1 designation; however, this folded lineation is herein interpreted as L_2 (Fig. 3.2). This interpretation is justified on the basis of the following: 1) the folded lineation is typically defined by coarse-grained, idioblastic, hornblende porphyroblasts, suggesting development during amphibolite facies metamorphism, and thus D_2 deformation; 2) porphyroblast-matrix microstructural relationships within individual F_2

Figure 3.4 Field photographs of D_2 structures in the PHG. a) L_2 lineation in strongly deformed mafic volcanic breccia on the south shore of Pacquet Harbour. Lineation is defined by stretched pyroxene pseudomorphs and mafic clasts, and lineated hornblende porphyroblasts. b) F_2 tubular fold that plunges southeast in amphibolite at Pelee Point. c) South-verging asymmetric folds and quartz-filled tension gashes in bedded PHG metasedimentary rocks in roadcuts north of Mill Pond (facing west; Map 3). Several examples of north-verging folds in quartz veins are arrowed. See text for discussion. d) Discrete anastomosed shear zones and a subhorizontal tension gash filled with subvertical plagioclase and hornblende fibers in metagabbro on the Woodstock Road (X-Z section). The sense of rotation of the tension gash, as indicated by the slight deflection of the S_2 foliation (see text for discussion), and the slight fabric obliquity (upper right corner) are consistent with south-side-down shear. e) Photomicrograph of a σ -porphyroblast (1.5mm long) in PHG mylonite adjacent to the northern contact of the Cape Brule Porphyry at the Woodstock Road - La Scie highway junction (X-Z section; top side to the right; equates to south-side-down shear). f) Photomicrograph of an S-C-C' fabric in PHG mylonite adjacent to the northern contact of the Cape Brule Porphyry. The shear bands (C'-fabric) are defined by foliated biotite and hornblende, and are oriented $\sim 10-15^\circ$ clockwise from the long edge of the photo. The C-fabric is oriented parallel to the long edge of the photo. The σ -porphyroblast (1.0mm long) and the sense of fabric asymmetry indicate top side to the right, which equates to south-side-down shear (X-Z section).

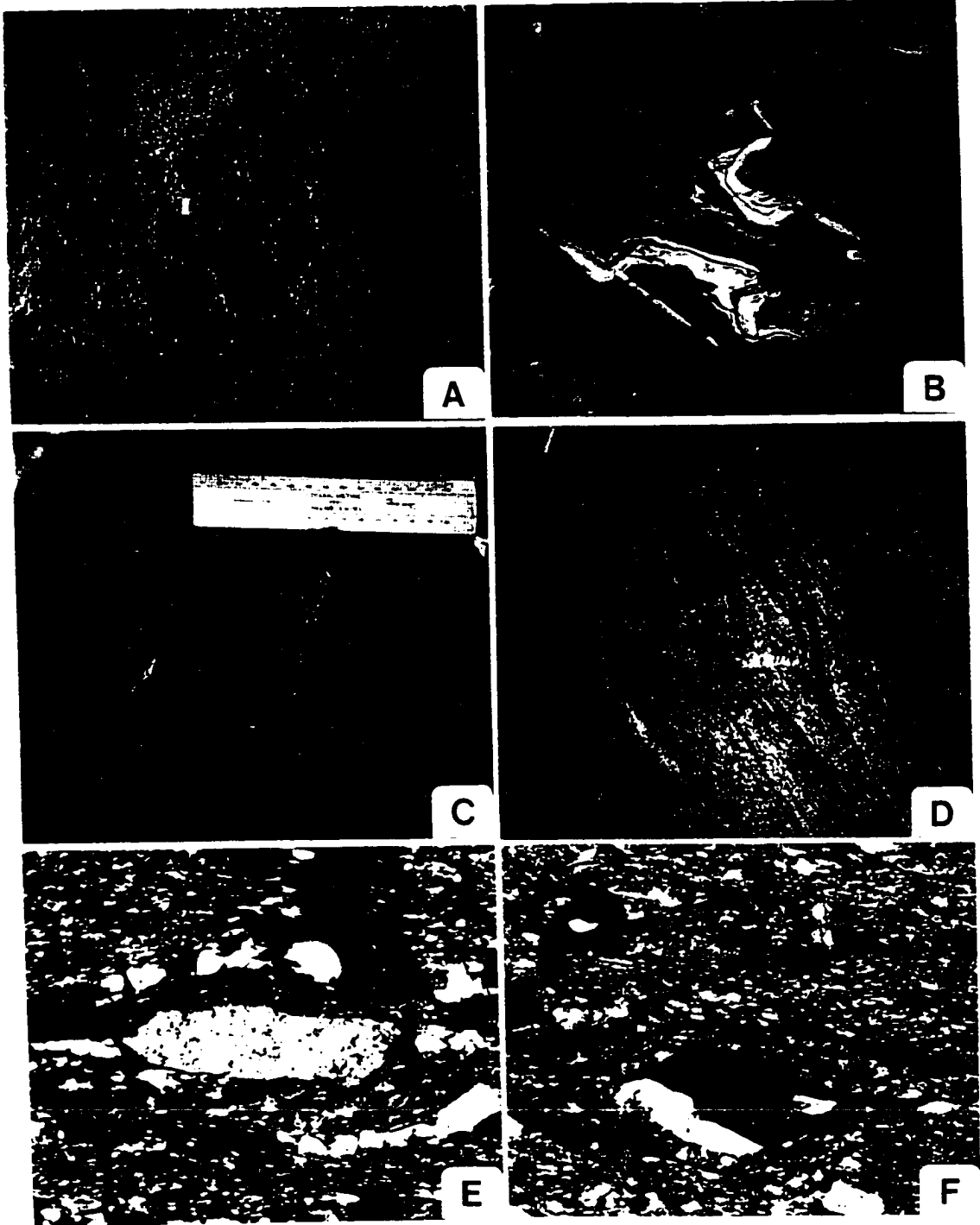


Figure 3.4

folds indicate that lineated hornblende porphyroblasts are synkinematic with respect to F_2 (see Section 5.2.1.1); and 3) angular relationships between the folded lineation and F_2 axes are consistent with progressive development of the lineation during F_2 folding (e.g., Ghosh and Sengupta 1987; see below). These observations collectively indicate that the folded lineation is a L_2 that developed, and was folded, during progressive D_2 deformation.

Pelee Point is located in the axial region of a large F_2 fold (Map 2; Cross-section 1). In this area, S_2 is axial planar to open to isoclinal F_2 folds which fold quartz veins, compositional layering, granitic dykes, and a locally penetrative S_1 fabric. F_2 folds are reclined, plunge shallowly east to southeast, and are symmetrical or verge southwest. Along the limbs of F_2 folds, S_1 is transected at a low angle and/or reactivated by S_2 (Fig. 3.3c). Along the south shore of Pacquet Harbour, F_2 folds consistently verge southwest, and are commonly rootless and intrafolial. The axes of F_2 folds are generally parallel to, or trend slightly counterclockwise (plan view) from, L_2 . In many locations, particularly in the area of the PPSZ, F_2 fold hinges are prominently curvilinear, and define curvilinear, sheath, and tubular folds (Skjernaa 1989; Fig. 3.4b). The bisectors of sheath and tubular folds are subparallel to L_2 .

In recent years, folds with axes subparallel to a contemporaneous stretching lineation in ductile shear zones have been the focus of extensive research (e.g., Berthé and Brun 1980; Cobbold and Quinquis 1980; Ridley 1986; Ghosh and Sengupta 1987; Malavieille 1987; Ridley and Casey 1989; Holdsworth 1990; Mawer and Williams 1991; Mies 1991; Chauvet and Séranne 1994; Culshaw et al. 1994; Fletcher and Bartley 1994; Mancktelow and Pavlis 1994; Grujic and Mancktelow 1995). Two mechanisms have been

proposed to explain these folds: 1) fold axis rotation toward the stretching lineation during progressive shear; or 2) fold initiation with axes subparallel to the stretching lineation.

The first mechanism involves initial nucleation of fold axes at a high angle to the stretching lineation (which is generally assumed to approximate the X-axis of the bulk strain ellipsoid, and to indicate the finite transport direction), and rotation of the hinge line toward the transport direction during progressive non-coaxial shear (e.g., Berthé and Brun 1980; Cobbold and Quinquis 1980; Ghosh and Sengupta 1987; Malavieille 1987; Mies 1991). In the case of F_2 folds in the Pacquet Harbour area, several observations support this folding mechanism. First, F_2 axes are commonly curvilinear, and sheath folds are abundant, consistent with differential rotation of the F_2 axes toward the transport direction (the mean orientation of the L_2 mineral and stretching lineation in the Pacquet Harbour area is interpreted to approximate the transport direction). Second, F_2 axes define a partial great-circle distribution in S_2 (Fig. 3.2), consistent with progressive development and differential rotation of the F_2 axes toward the transport direction. Third, in cases where F_2 hinges contain a folded lineation, the angle between the fold axis and folded lineation decreases as the orientation of the fold axis approaches the transport direction (Fig. 3.5a). This relationship is consistent with initiation of the F_2 axes at a high angle to the transport direction, followed by progressive rotation of the fold axis (Ghosh and Sengupta 1987). Indeed, in several locations in Pacquet Harbour the hinges of isoclinal F_2 folds with axes subparallel to the transport direction contain two hornblende lineations: an early, folded lineation which is highly oblique to the fold axis, and a later, non-folded lineation which is subparallel to the fold axis.

Figure 3.5 Schematic sketches of D_2 - D_3 structures, and a graph of the angular relationship between F_2 axes and L_2 in the Pacquet Harbour area. See text for detailed discussions. The instantaneous stretching axes inferred from the orientation and kinematics of the structures are shown in Figures 3.5b and 3.5c. a) Graph of the measured angle between the folded L_2 and the associated F_2 axis vs. trend of the fold axis. This graph illustrates that the angle between the folded lineation and the associated fold axis decreases as the fold axis approaches the mean trend of the stretching lineation (i.e., 150°), consistent with progressive rotation of the axes toward the finite stretching direction during non-coaxial shear. Open triangle indicates the angular relationship between the mean L_2 stretching lineation and mean F_2 axis at Pelee Point. b) Simplified sketch illustrating the inferred progressive development (1 to 3) of tension gashes, F_2 folds, and S_2 in bedded metasedimentary rocks north of Mill Pond (Fig. 3.4c; refer to text for detailed discussion). Dark grey tension gashes, Type 2 veins; Light grey tension gashes; Type 3 veins. c) Simplified sketch illustrating the possible structural significance of tension gashes in metagabbro units within PHG amphibolite on Woodstock Road (Fig. 3.4d; refer to text for detailed discussion). The upper and lower tension gashes schematically illustrate the early and late increments, respectively, in the progressive development of the structures in Figure 3.4d. d) Simplified sketch of S_1 - S_2 - S_3 fabric relationships in the BBSZ. Note the similarity between the BBSZ fabric geometry and that associated with a single episode of progressive non-coaxial shear and folding (inset diagram; after Ghosh and Sengupta 1987).

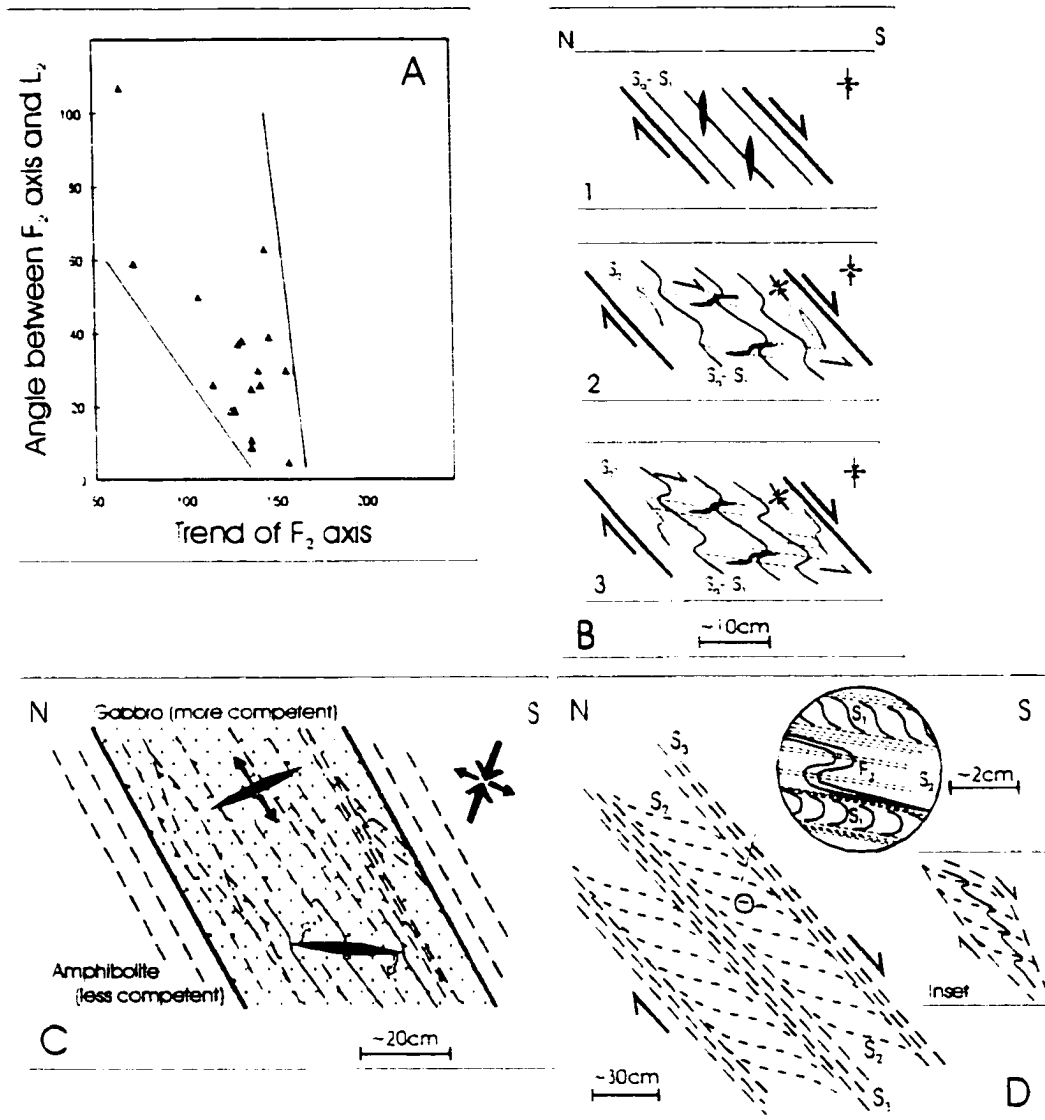


Figure 3.5

The first folding mechanism predicts that F_2 folds would have been continuously forming and progressively rotating toward parallelism with the transport direction (Berthe and Brun 1980; Cobbold and Quinquis 1980). Since rotation of the fold axes would necessarily have involved large strains and progressive tightening of the folds, only tight to isoclinal folds with axial planes at a low angle to the shear plane should have axes subparallel to the transport direction. The presence in the Pacquet Harbour area of upright, open F_2 folds with axes subparallel to the transport direction is therefore inconsistent with this mechanism. It is, however, consistent with the second folding mechanism which predicts that upright, open folds with axes at a low angle to the transport direction can originate during non-coaxial shear in a ductile shear zone that contains a pronounced planar anisotropy. This mechanism requires either a component of wrench shear in the slip plane (due to shear strain rate gradients normal to the transport direction; e.g., Coward and Potts 1983; Ridley 1986; Ridley and Casey 1989; Holdsworth 1990), or shortening parallel to the Y-axis of the shear zone in a constrictional strain regime (Fletcher and Bartley 1994). In Pacquet Harbour, open F_2 folds are typically found in fold trains with fold axes consistently subparallel to the transport direction. Within individual fold trains, fold profiles grade from gentle to isoclinal with an associated change in axial plane orientation from upright to reclined, respectively (i.e., rotation toward the S_2 plane; Fig. 3.3c). Thus, assuming that the gentle-upright folds represent an early increment in the development of the folds, these relationships indicate that F_2 folds nucleated with axes subparallel to the transport direction. As deformation progressed, the inter-limb angle decreased and the axial planes rotated toward the shear plane, but the F_2 axes did not

rotate significantly.

Thus, the available evidence indicates that both folding mechanisms are probably applicable to F_2 folding in the Pacquet Harbour area. Interestingly, several authors have noted that folds with axes subparallel to the transport direction are particularly common in low-angle extensional shear zones (e.g., Chauvet and Séranne 1994; Culshaw et al. 1994; Manktelow and Pavlis 1994), such as those bounding metamorphic core complexes (e.g., Malavieille 1987; Fletcher and Bartley 1994; Grujic and Manktelow 1995). The possible significance of this relationship is discussed in Chapter 7.

In exposures of metasediment northwest of Mill Pond (Map 3), steeply dipping bedding and a parallel S_1 fabric are transposed by a S_2 fabric that dips moderately southeast. The S_2 fabric is penetrative to spaced, and is defined by fine-grained foliated hornblende and biotite. This fabric contains a southeast-plunging L_2 mineral lineation defined by aligned fine-grained hornblende, and is axial planar to gentle to tight, reclined F_2 folds that plunge east and verge south. The short limbs of the F_2 folds are locally transected by narrow, normal sense, shear zones parallel to S_2 . The well preserved bedding in these outcrops indicates a significant, apparently gradational, decrease in the intensity of finite D_2 strain between the south shore of Pacquet Harbour and Mill Pond.

Within one of the metasediment outcrops near Mill Pond, there is a particularly interesting structural relationship between layering (S_0 - S_1) that dips moderately south, a S_2 fabric that dips shallowly south, F_2 folds, and a series of narrow, <15 cm long, quartz veins (Fig. 3.4c). Three types of quartz vein are distinguished in this outcrop. *Type 1* veins are parallel to S_0 , and folded by south-verging F_2 folds. These veins were probably

emplaced along the layering prior to F_2 folding, and are not considered further here. *Type 2* veins are subparallel to the axial planes of south-verging F_2 folds, and are commonly folded by north-verging folds. These veins only occur in the axial regions of F_2 folds, and transect the immediately adjacent layering at an angle of $\sim 45^\circ$ (clockwise; looking east). The amplitude of the F_2 folds associated with *Type 2* veins commonly decreases toward the lateral tips of the veins, suggesting that the amplification of the F_2 folds is directly related to the presence of the veins. *Type 3* veins have a sigmoidal tension gash morphology, and cross-cut S_2 at an angle of $\sim 35^\circ$ (clockwise; looking east). These veins are folded by trains of south-verging F_2 folds (Fig. 3.4c; lower left corner).

The structures and structural relations described above are attributed to progressive non-coaxial shearing during D_2 deformation (Fig. 3.5b). In this model, the *Type 2* veins are viewed as early tension gashes that formed during south-side-down shear parallel to layering (Fig. 3.5b, panel 1). This interpretation is consistent with the $\sim 45^\circ$ angle between the *Type 2* veins and the immediately adjacent layers. Once formed, the tension gashes probably acted as heterogeneities within the non-coaxial flow regime, causing perturbation of the flow, localized conversion of the shear-induced vorticity into spin, and folding of the layering (e.g., Lister and Williams 1983). This interpretation accounts for the association of *Type 2* veins with F_2 folds, as well as the vergence and change in amplitude of the F_2 folds (e.g., Hudleston 1989). The tension gashes would have initially formed with long axes in the shortening field of the instantaneous strain ellipsoid, and thus the *Type 2* veins would have been folded by south-verging F_2 folds. However, the sense of asymmetry of these folds would have changed as a consequence of the rotation of

the *Type 2* veins during the progressive non-coaxial deformation (Hanmer and Passchier 1991). Therefore, the north-verging folds are only developed in the *Type 2* veins (Fig. 3.5b, panel 2). As D_2 deformation progressed, the S_2 fabric intensified, and may have accommodated an increasing proportion of the non-coaxial strain. The *Type 3* veins probably formed as tension gashes during non-coaxial shear along the intensified S_2 in the later stages of deformation (Fig. 3.5b, panel 2). This would explain the angular relationship between the *Type 3* veins and the S_2 fabric. The *Type 3* veins are folded by south-verging F_2 folds (Fig. 3.5b, panel 3), indicating that the long axes were oriented in the shortening field of the instantaneous strain ellipsoid associated with the development of the F_2 folds. Presumably, had D_2 deformation continued, *Type 3* tension gashes would have also rotated, and would have developed the same characteristics as the *Type 2* veins.

The relationship between the *Type 2* and *3* quartz veins, S_2 foliation, and F_2 folds indicates that these structures formed during progressive, non-coaxial, south-side-down shear (Fig. 3.5b). This model is consistent with other kinematic indicators associated with S_2 in the Pacquet Harbour area, and may explain the common association of axial planar quartz veins and F_2 folds in the Pacquet Harbour area.

Approximately 2 km southwest of the metasedimentary outcrops, a ~30m thick unit of medium- to coarse-grained, equigranular metagabbro contains several interesting deformation structures. In the metagabbro, the primary igneous texture is locally transposed into a series of narrow (<10 cm thick) shear zones which dip moderately southeast and anastomose around low-strain domains (Fig. 3.4d). The shear zones contain a penetrative foliation and down-dip lineation defined by aligned hornblende

porphyroblasts. The shear fabrics are parallel to penetrative S_2 - L_2 fabrics in the adjacent amphibolite country rock, and are attributed to distributed D_2 shear in the (presumably) more competent metagabbro. Within low-strain domains in the metagabbro, a weak fabric is locally preserved which is oriented $<15^\circ$ (counterclockwise; looking east) from the shear zone fabric. The overall geometry and sense of obliquity of these fabrics are consistent with progressive, normal-sense, non-coaxial shear in the metagabbro (e.g., Ramsay 1980; Poulsen and Robert 1989; Hanmer and Passchier 1991).

The fabrics in the metagabbro are cross-cut by numerous <20 cm long, <4 cm wide, sub-horizontal fractures which have a tension gash morphology (Fig. 3.4d). The fractures are filled with hornblende and albite fibres that are generally straight, subvertical, and perpendicular to the margins of the fractures. In some examples, the fibres extend inward from the wall-rock and meet along a centrally located suture parallel to the margins of the fractures. This fibre morphology typifies syntaxial fibre veins, and the overall morphology of the veins indicates that they formed as extensional fractures. The fibres formed in the stability field of hornblende and albite, consistent with development of the veins during relatively high temperature (D_2) deformation. The veins are typically planar and undeformed. This could be attributed to lower finite D_2 strain in the metagabbro, or may indicate that the veins formed late- D_2 . Locally, the veins are spatially associated with gentle, south-verging folds of the shear fabric in the metagabbro (Fig. 3.4d). The amplitude of the folds decreases towards the lateral tips of the veins, indicating that the folding is related to the presence of the veins (Hudleston 1989). Within the folds, the folded shear fabric is orthogonal to the margins of the veins. These relationships indicate

that the fractures initially formed perpendicular to the shear fabric, and the fractures and the fabric were subsequently rotated, resulting in the passive development of the folds (Fig. 3.5c). The sense of rotation (based on the asymmetry of the folds) is consistent with normal-sense non-coaxial shear.

Since the extensional fractures are only developed in the metagabbro, they probably result from strength difference between the metagabbro and the surrounding amphibolite (e.g., Lister and Williams 1983; Robert et al. 1994); this is common where competent layers within a less competent host-rock undergo bulk non-coaxial strain (e.g., Robert et al. 1994; Fig. 3.5c). The opening vector of extensional veins (as defined by the fibres and offset features in the wall-rock) corresponds to the local direction of incremental elongation in the rocks. Thus, the geometry of the extensional veins in the metagabbro, prior to rotation and the development of the folds, indicates an incremental elongation direction that plunges moderately south, parallel to the direction of elongation indicated by L_2 in the country rock.

From this outcrop south towards the Cape Brule Porphyry contact along Woodstock Road, S_2 and L_2 in the PHG become progressively more steeply south-dipping and southeast-plunging, respectively (Map 3; Fig. 3.2). These fabrics also become more intense to the south, and at the Cape Brule Porphyry contact a 100-200m thick shear zone is developed in the PHG amphibolites. Within the shear zone, the amphibolites contain a pervasive and penetrative S_2 fabric defined by foliated biotite and hornblende porphyroblasts, recrystallized quartz-rich bands, and a pronounced compositional banding. The S_2 fabric dips steeply south and contains a L_2 mineral lineation that plunges steeply

south, and is defined by a preferred orientation of hornblende porphyroblasts. In thin section these rocks display typical mylonitic textures, including a groundmass of very fine-grained, recrystallized quartz and plagioclase, elongate recrystallized quartz bands, fine-grained quartz ribbons, and abundant plagioclase porphyroclasts up to 1 mm in diameter (Fig. 3.4e). Evidence of F_2 folding is rare in these rocks. In one location however, a quartz vein is folded by an isoclinal, apparently rootless fold that plunges steeply south. S_2 is axial planar to this fold, suggesting that the folding is related to D_2 deformation. These rocks lack the granoblastic polygonal texture that characterizes the PHG amphibolites further north in Pacquet Harbour, and no garnet was observed, which may indicate somewhat lower temperature conditions during D_2 deformation in this location. In some locations, hornblende porphyroblasts are spectacularly developed, and are randomly oriented within, and across, the S_2 plane, consistent with local late- to post- D_2 hornblende growth.

The banding in these rocks is defined by changes in mineral content (quartz-plagioclase rich vs. hornblende-biotite rich), probably produced by mineral segregation during mylonitization. Commonly, discrete layers parallel to S_2 contain a non-penetrative fabric which dips slightly more steeply south than S_2 . These oblique fabrics are defined by foliated biotite and lineated hornblende porphyroblasts, and seem to be preferentially developed in the more mafic layers (hornblende-biotite rich), possibly indicating a compositional and/or mechanical control (e.g., Hanmer 1979). Within the domains of oblique fabric, the trend of the lineation is parallel to the trend of L_2 , and perpendicular to the line of intersection between the oblique- and S_2 -fabrics. In thin section, the oblique fabric is similar to S_2 in both microstructure and mineral assemblage, but is defined by

closely-spaced asymmetrical shear bands (e.g., Platt and Vissers 1980; Denis and Secor 1987, 1990; Hanmer and Passchier 1991). The sense of asymmetry of the shear bands, together with σ -type plagioclase porphyroclasts in both the S_2 and oblique fabric domains, are consistent with normal sense non-coaxial shear parallel to S_2 (Figs. 3.4e and 3.4f). Based on these relationships, the shear zone at the northern contact of the Cape Brule Porphyry is interpreted to have accommodated normal sense, non-coaxial D_2 shear.

3.3.3.3 Cape Brule Porphyry

Along its northern margin, the Cape Brule Porphyry contains a non-penetrative planar fabric that is concordant with S_2 in the adjacent PHG (Map 3), and that dies out over ~300m toward the south. This fabric is typically defined by <1cm thick zones of fine-grained recrystallized quartz and foliated white mica and biotite which anastomose around subhedral K-feldspar and quartz phenocrysts. Locally, the fabric is also defined by elongate recrystallized quartz ribbons and quartz stringers, and/or discontinuous wisps of fine-grained magnetite. The concentration of magnetite along the fabric may indicate that pressure solution occurred along these surfaces. In thin section, quartz-filled strain shadows on feldspar porphyroclasts range from symmetric to asymmetric, with both normal and reverse senses of shear, and no consistent overprinting relationships. Xenoliths within the porphyry are typically elongate in the plane of the fabric and define a prominent stretching lineation which is parallel to L_2 in the adjacent PHG mylonites. The stretched xenoliths form oblate ellipsoids (axial ratios: $X/Y \sim 3-6$; $Y/Z \sim 5-15$), which indicate flattening strains (see also Coates 1970).

The planar and linear fabrics in the Cape Brule Porphyry are attributed to D_2 on

the basis of their parallelism with D_2 fabrics in the PHG. Indeed, on a larger scale, a prominent array of air-photo lineaments is visible in the porphyry, and field mapping indicates that the trend of these lineaments is concordant to the trend of the planar fabric in the porphyry (Map 3). The trend of these airphoto lineaments gradually changes along the northern contact of the porphyry, from east-trending at the La Scie highway, to northeast-trending at Pacquet Harbour, and reflects a gradational change in the orientation of the planar fabric in the porphyry. This change exactly mimics the change in orientation of S_2 in the PHG, and provides further evidence for the correlation of S_2 in the PHG and the planar fabric in the Cape Brule Porphyry.

Across the PHG-Cape Brule Porphyry contact near the La Scie highway, there is a marked change from penetrative, non-coaxial fabrics formed in amphibolite facies in the PHG, to non-penetrative fabrics with ambiguous kinematic indicators formed in greenschist facies in the porphyry. This change is interpreted as reflecting the higher structural position of the porphyry with respect to extensional D_2 deformation, as well as the higher competence of the porphyry compared to the PHG.

3.3.4 D_3 deformation - the Big Brook Shear Zone

The D_3 structures are pervasive within a ~300m thick ductile shear zone developed along Big Brook at the northern contact of the Dunamagon Granite (the Big Brook shear zone; BBSZ; Map 2), and are only sparsely developed elsewhere in Pacquet Harbour.

The BBSZ transposes the PPSZ and structures related to the D_2 deformation phase (Map 2; Cross-section 1), and consequently records a complex sequence of fabric development, transposition, folding, and metamorphic mineral growth associated with

three phases of deformation. In order to correctly interpret the structural geology of the BBSZ, it is therefore important to understand the characteristics of the pre- D_3 structures preserved within the BBSZ.

3.3.4.1 D_1 - D_2 structures in the BBSZ

In the BBSZ, D_1 structures are locally preserved in discontinuous units of PPSZ high strain rocks that are readily distinguished on the basis of the distinctive tectonic interleaving of MBG schist and PHG amphibolite. Outside these high strain rocks, D_1 structures are most commonly observed as a penetrative, layer-parallel fabric that has been folded by trains of open to isoclinal, reclined F_2 folds that plunge shallowly southeast and primarily verge southwest (Fig. 3.5d). In some cases, there is a progressive change from open-recumbent to tight-reclined folds within a single train of F_2 folds, and the long fold limbs are locally transposed into an axial planar S_2 crenulation fabric that dips shallowly southeast. The S_2 fabric ranges from a differentiated crenulation to a penetrative foliation, and all stages in the progressive development of the S_2 crenulation cleavage are found in the BBSZ (e.g., Bell and Rubenach 1983). S_2 locally contains a biotite and hornblende lineation that plunges southeast. The short F_2 fold limbs are commonly preserved between S_2 planes as narrow domains of crenulated S_1 fabric with a south-verging, sigmoidal geometry, which superficially resembles an asymmetric S-C fabric (Fig. 3.5d).

The D_1 - D_2 fabrics and folds are commonly preserved within discrete domains that parallel, and are wrapped around by, zones of penetrative S_3 foliation (Fig. 3.5d). The resulting structural geometry is very similar to the shear zone fabrics described by Ghosh and Sengupta (1987), Bell and Johnson (1992), and Osmundsen and Andersen (1994). In

particular, the sense of asymmetry of the F_2 folds, as well as the relationship between fold tightness and axial plane orientation, are consistent with rotation of the fold axial planes with progressive tightening of the folds during normal sense non-coaxial shear (e.g., Ghosh and Sengupta 1987; Hanmer and Passchier 1991; Fig. 3.5d). These D_1 - D_2 structures could easily be mistaken for D_3 structures formed during synchronous transposition and drag-folding within discrete zones of progressive, normal sense, non-coaxial shear in the BBSZ (e.g., Ghosh and Sengupta 1987; Osmundsen and Andersen 1994). However, regardless of the intensity of the adjacent S_3 foliation, the geometrical relationships of the S_1 - S_2 - F_2 structures remain indistinguishable from that external to the BBSZ, although there is a slight change in orientation of the S_2 fabric (Fig. 3.2; see below). This indicates that the geometry is independent of, and therefore unrelated to, D_3 deformation. This interpretation is further supported by microstructural relationships, which indicate that garnet porphyroblasts in the BBSZ are everywhere syn- F_2 , but pre- S_3 (see Section 5.2.1.1). The S_1 - S_2 - S_3 fabric geometry in the BBSZ is therefore attributed to three overprinted deformations (e.g., Bell and Johnson 1992).

3.3.4.2 D_3 structures in the BBSZ

D_1 - D_2 structures are transposed by an S_3 foliation in the BBSZ that dips moderately to steeply south, and is defined by a preferred orientation of biotite and chlorite (Figs. 3.2, 3.5d, and 3.6a), consistent with greenschist facies metamorphic conditions during D_3 . In some locations S_3 is penetrative, mylonitic, and developed within 1-15m thick zones, whereas in other locations it forms discrete, widely spaced, extensional crenulation cleavage planes (e.g., Platt and Vissers 1980) which transect S_2 (Fig. 3.6b).

Figure 3.6 Structural relationships in the BBSZ and Dunamagon Granite in the Pacquet Harbour area. **a)** F_2 fold hinge and axial planar S_2 transected by non-penetrative S_3 (arrowed) in the BBSZ ~1 km west of Pacquet Harbour. The sense of asymmetry indicates south-side-down shear. **b)** Axial planar S_2 transposed by discrete, spaced, extensional crenulation cleavage planes (Platt and Vissers 1980) in the BBSZ in Pacquet Harbour. **c)** A Group 1 shear zone that dips moderately northwest in the Dunamagon Granite in Pacquet Harbour. Sense of shear indicators, and a stretching lineation that plunges northeast, indicate sinistral-reverse oblique-slip shear. **d)** A Group 2 shear zone that dips shallowly southeast in the Dunamagon Granite in Pacquet Harbour. Note the pronounced augen texture which defines a prominent stretching lineation that plunges southeast in the foliation plane. **e)** Hand sample obtained from the previous outcrop and cut parallel to the X-Z plane of the finite strain ellipsoid. The large (1.0cm) feldspar σ -porphyroclast indicates south-side-down shear.

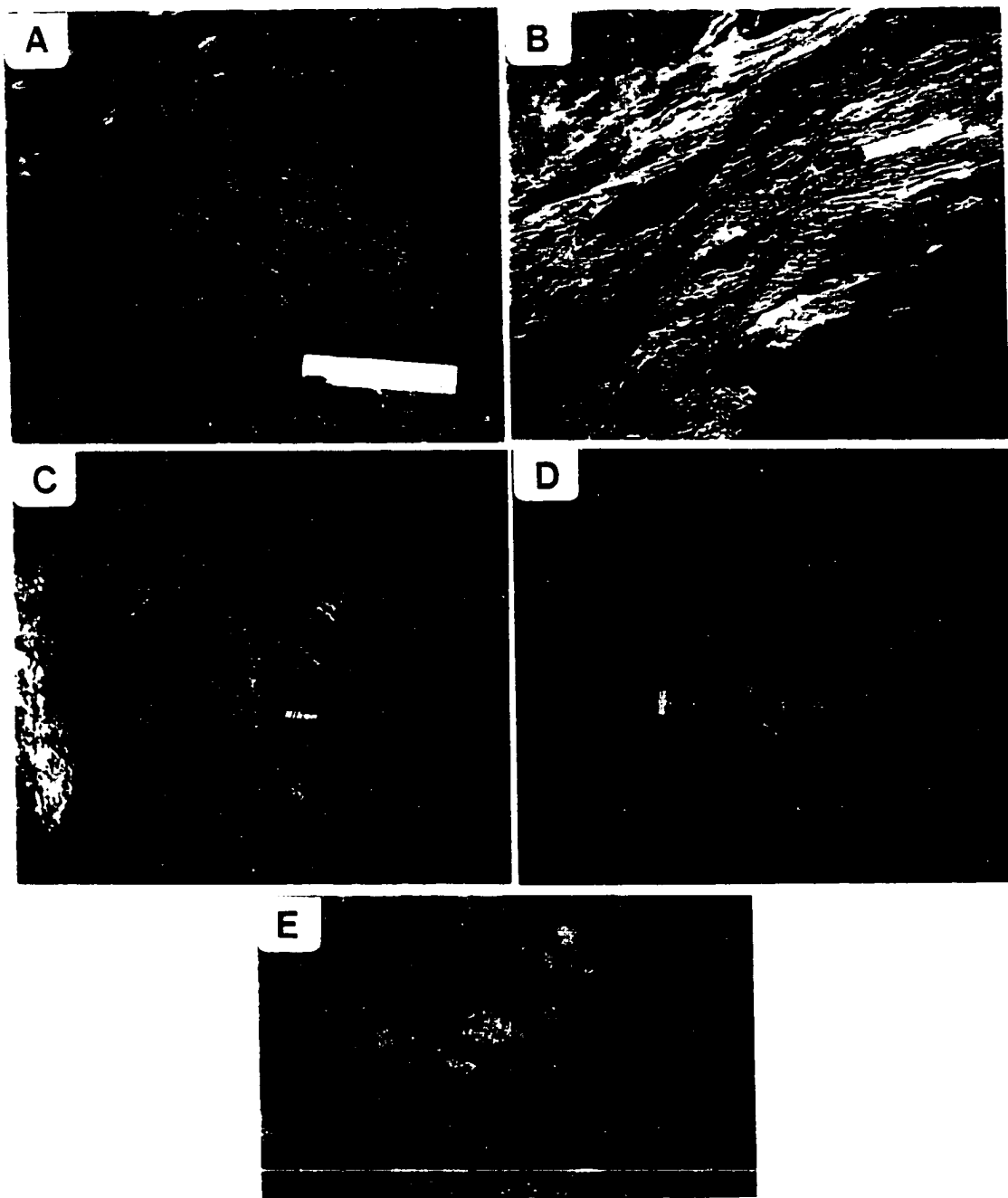


Figure 3.6

Shear bands are common within the pervasive S_3 and, together with the sense of asymmetry indicated by drag-folding of S_1 - S_2 fabrics along the transposition planes, consistently indicate normal shearing (south-side-down). S_3 contains a rare southeast-plunging mineral lineation defined by a preferred orientation of biotite. Only two examples of F_3 folds were noted. These folds are tight to isoclinal, south-verging, and are associated with an axial planar S_3 , which clearly transposes S_2 .

In general, S_3 intensifies to the south, and is penetrative immediately adjacent to the northern contact of the Dunamagon Granite. A weak fabric defined by foliated biotite is locally developed in the granite, and dissipates to the south over ~4-5m. This fabric dips moderately south, and is probably associated with D_3 deformation. The change in the intensity of S_3 toward the northern contact of the granite is associated with a gradual change in orientation of the S_2 fabric from shallowly east-dipping north of the BBSZ, to moderately southeast-dipping within the BBSZ (Map 2). In the present study, this change in orientation is attributed to passive rotation of S_2 during D_3 deformation along the BBSZ. This interpretation is supported by the complementary change in the orientation of S_2 with the changing intensity of S_3 , and the consistent geometry of the S_1 - S_2 - F_2 structures internal and external to the BBSZ. The sense of rotation of S_2 agrees with the south-side-down shear recorded by D_3 structures.

As a consequence of this rotation, S_1 is locally concordant to S_3 in the BBSZ. In order to distinguish these fabrics in areas where D_2 structures are not developed, three criteria were employed: 1) S_3 is typically defined by foliated biotite and/or chlorite, whereas S_1 is, at least locally, defined by foliated and lineated hornblende; 2) S_1 is

overgrown by randomly-oriented hornblende porphyroblasts; and 3) garnet porphyroblasts in the BBSZ consistently overgrow S_1 , but are everywhere wrapped-around by S_3 .

D_3 structures are coaxial with, and record the same sense of movement as, D_2 structures, and are therefore interpreted as a late increment of extensional deformation in the Pacquet Harbour area (see Chapter 6).

3.3.5 Late Faulting

In Pacquet Harbour, a series of late faults cuts PHG amphibolites. These faults are typically less than 0.5m wide, dip steeply north or south, and are associated with a prominent set of parallel joints. The faults are usually associated with brecciation of the host rock, consistent with relatively low temperature deformation. Slickenlines in the fault planes primarily indicate strike-slip movement. Offset and dragging of markers in the wall rocks indicate both dextral and sinistral movements, typically associated with <2m displacements. In one location, the late joints and faults are associated with en-echelon tension gashes that cross-cut S_2 - L_2 in PHG amphibolite. The tension gashes are subvertical, east-west striking, and locally contain quartz growth-fibres perpendicular to the margins. The en-echelon fractures consistently indicate sinistral movement along the associated strike-slip faults.

3.3.6 Dunamagon Granite

The structural geology of the Dunamagon Granite is critical to understanding the character, timing, and significance of deformation in the Pacquet Harbour area. However, establishing a deformation sequence for the granite is made difficult by the heterogeneity of the structures, and the apparent lack of overprinting relationships. In general, the

deformation sequence apparently involves a phase of syn-magmatic deformation (see Section 2.3.3.1) and at least one phase of solid-state deformation (excluding the local S_3 fabric at the northern contact of the granite which, for reasons that will become apparent below, is considered to post-date the solid-state deformation structures throughout the remainder of the granite). The lack of overprinting relations could be taken as evidence for the synchronicity of all solid-state structures. However, in the present study, these deformation structures are separated into two groups on the basis of their orientation, style, and apparent sense of shear.

3.3.6.1 Group 1 structures

Group 1 structures comprise a series of shear zones that strike east and west, dip moderately to steeply north and south, and range in thickness from <1cm to ~3 m. The shear zones are mutually subparallel, but anastomose at various scales around zones and lozenges of less deformed massive granite. The poles to the shear zones define a partial great-circle girdle (Fig. 3.2; plotted as 'S₁'). In the field, the shear zones are defined by zones of grain size reduction, an increased abundance of fine-grained foliated biotite (imparts a darker grey colour to the granite), and prominent K-feldspar porphyroclasts. The thinner shear zones (≤ 10 cm) are most common, and characteristically have a weak fabric that anastomoses around coarse K-feldspar porphyroclasts. The thicker shear zones (≥ 50 cm) are less common, but are characterized by a penetrative, mylonitic fabric that contains finer-grained K-feldspar porphyroclasts (Fig. 3.6c). Locally, numerous thin shear zones are concentrated within 1 to 10m thick zones in the granite. Within these zones, the thin shear zones are spaced, and anastomose around lozenges of undeformed granite up to

50cm thick.

In thin section, the fabric in the shear zones consists of fine-grained aligned biotite, and a parallel compositional layering defined by quartz and feldspar domains. The quartz occurs as fine- to medium-grained, equigranular, recrystallized grains which are concentrated in elongate foliation-parallel wisps. The plagioclase is fine- to coarse-grained, equigranular, and locally recrystallized to a granoblastic-polygonal texture. The K-feldspar forms <0.5cm, equant, subhedral porphyroclasts. Undulose extinction and subgrains within the crystals are consistent with ductile deformation at relatively high temperature (i.e., upper greenschist facies; Gapais 1989). Strain shadows on the K-feldspar crystals are filled with equigranular quartz and plagioclase.

The planar fabrics in the shear zones generally lack a linear fabric element and kinematic indicators (McDonald 1993). In one location however, a shear zone that dips moderately north contains a weak, northeast-plunging stretching lineation defined by elongate recrystallized quartz-rich tails on K-feldspar porphyroclasts. Kinematic indicators in this shear zone, including asymmetric (σ) tails on the K-feldspar porphyroclasts, a weak asymmetric foliation, and possible imbricated porphyroclasts indicate a component of sinistral-reverse shear (north-over-south).

In many locations, aplite dykes within the granite are deflected distances of ~30-40cm parallel to the shear zones. In these locations the aplite dykes are locally folded, boudinaged, and contain a planar fabric which is parallel to the shear zone fabric. The sense of offset, as indicated by offset and dragging of the aplite dykes, is predominantly sinistral. The apparent displacement, as indicated by offset aplite dykes, is generally <1m.

On the basis of width, continuity of shearing, and microstructure, McDonald (1993) separated the shear zones in the granite into 'wide' and 'narrow' types, and concluded that these shear zones were associated with ductile and brittle deformation, respectively. The ductile deformation was thought to pre-date the brittle deformation. In the present study however, the narrow vs. wide terminology is not adopted for the following reasons. 1) The narrow and wide shear zones contain similar, primarily ductile, microstructures, and generally lack microstructures indicative of brittle deformation. Indeed, the deflection, folding, and boudinage of aplite dykes that are cut by the narrow shear zones clearly indicates that these zones are associated with a significant amount of ductile deformation. 2) The narrow and wide shear zones have similar orientations, and both record mainly sinistral displacement. 3) Overprinting relationships between the narrow and wide shear zones were not observed in the present study, nor by McDonald (1993). This may indicate that these structures formed during one phase of deformation.

In general, the characteristics of Group 1 structures in the granite are typical of heterogeneous shearing of granitic rocks at upper greenschist-facies metamorphic conditions (e.g., Gapais et al. 1987; Gapais 1989).

3.3.6.2 Group 2 structures

Group 2 structures comprise a planar fabric that strikes northeast and dips shallowly southeast and stretching lineation that plunges southeast (Fig. 3.2; plotted as S_2 and L_2), and are variably developed throughout the granite (McDonald 1993). Typically, the planar fabric is defined by weakly foliated biotite and elongate wisps of quartz. In many locations however, particularly in the easternmost exposures of the granite, the

planar fabric is penetrative and defined by foliated biotite and elongate quartz stringers anastomosed around K-feldspar phenocrysts, resulting in a pronounced augen texture (Fig. 3.6d). In these zones, the planar fabric contains a lineation defined by a preferred orientation of stretched K-feldspar phenocrysts. The stretching lineation consistently plunges to the southeast in the plane of the foliation.

In the area of the augen-textured zones, the granite contains numerous <30cm (maximum dimension) xenoliths. These xenoliths are typically elongate, and the trend of the elongation in sub-horizontal outcrop surfaces is consistently towards the southeast. Locally, the lineated xenoliths weather in relief, allowing essentially complete measurement of their orientation and axial ratios (e.g., X, 15cm; Y, 5.5cm; Z, 3cm; prolate ellipsoid). The measured orientation of the lineated xenoliths is parallel to the stretching lineation that plunges shallowly southeast in the augen-textured granite.

In thin section, the fabric in these rocks consists of foliated biotite, quartz-rich zones, and rare quartz plates that wrap around K-feldspar phenocrysts. The quartz is medium- to coarse-grained, and typically forms sutured, elongate to irregular grains that are concentrated in narrow zones parallel to the foliation. These may represent recrystallized quartz ribbons. The plagioclase is medium- to coarse-grained, and is locally recrystallized to an equigranular or granoblastic-polygonal texture. The K-feldspar phenocrysts are <1cm, equant, subhedral, and contain undulose extinction, subgrains, and recrystallized quartz-filled fractures. The margins of these crystals are locally sutured, and associated with myrmekitic intergrowths of plagioclase and quartz. The phenocrysts typically have recrystallized quartz-filled strain shadows. The strain shadows are locally

asymmetrical (σ -porphyroclasts), and are consistent with south-side-down shear parallel to the foliation and lineation (Fig. 3.6e). The microstructures within the augen-textured granite are consistent with non-coaxial deformation under amphibolite facies metamorphic conditions (e.g., Gapais 1989). This inference is also consistent with the amphibolite facies mineral assemblages in mafic xenoliths and dykes in the granite (McDonald 1993).

Group 2 structures in the granite have the same orientation and style (high temperature L-S tectonite), and record the same sense of shear, as D_2 structures in the adjacent MBG and PHG, and are therefore correlated with D_2 . This correlation requires that Group 2 structures are broadly contemporaneous with peak amphibolite facies metamorphism and F_2 folding.

3.3.6.3 Relative chronology of Group 1 and 2 structures

As noted above, Group 1 and Group 2 structures in the Dunamagon Granite are markedly different in terms of their orientation, style, and apparent sense of shear. These structures are attributed to two separate phases of deformation. The microstructural similarity of Group 1 and 2 structures indicates that they probably formed under broadly similar metamorphic conditions (e.g., Gapais 1989), although Group 1 structures may have been associated with somewhat lower temperatures, and were recrystallized during subsequent high-temperature metamorphism. This hypothesis is based on the strongly recrystallized, equigranular, quartz and plagioclase grains in Group 1 shear zones.

The lack of overprinting relations makes determination of the deformation sequence difficult. However, two indirect lines of evidence indicate that Group 2 structures are younger. 1) In one location, the fabric in a Group 1 shear zone is folded by

open to tight, symmetrical, reclined folds that plunge east. The orientation of these folds is similar to typical F_2 folds in the Pacquet Harbour area, and these structures are therefore tentatively correlated (Fig. 3.2). If so, Group 1 structures must pre-date Group 2 structures. 2) In another location, a particularly well developed zone of Group 2 augen-textured granite is directly along strike from numerous Group 1 shear zones, yet, the Group 1 shear zones do not cut across the Group 2 structures. Overprinting relationships between these structures were not observed; however, these relationships may indicate that Group 2 structures are later than, and completely transpose, Group 1 structures.

The Group 1 shear zone with a reverse-sinistral sense of movement contains a <1.5m thick, >30m long (limit of outcrop) slice of strongly deformed biotite schist which resembles typical MBG schist. The biotite schist contains a penetrative foliation that is parallel to the mylonitic fabric in the sheared granite, possibly indicating that these rocks were deformed synchronously during development of the shear zone. The presence of a slice of apparent MBG schist within the shear zone may indicate that the Dunamagon Granite and MBG were juxtaposed during development of Group 1 shear zones. Furthermore, the timing relationships of structures in the granite may indicate that Group 1 structures are associated with D_1 , and development of the PPSZ. If the reverse-sinistral sense of shear within the shear zone is representative of Group 1 structures in the granite, Group 1 structures and D_1 deformation may have been associated with south-directed overthrusting of the granite and PHG by the MBG. This inference is particularly important in light of structural relationships in the Ming's Bight map area (see Section 4.4).

3.3.7 Quartz veins and pegmatite dykes

The structural geology of vein systems is an important, and often overlooked, aspect of detailed structural analysis in complexly deformed areas. Vein systems provide constraints on: 1) the relative, and more rarely, absolute, timing of deformation structures; 2) deformation mechanisms; 3) ambient stress conditions in a progressively-deforming rock mass; and 4) sense of shear. The abundant quartz veins and granitic pegmatite dykes in the Pacquet Harbour area have been examined in detail, and provide important structural information.

3.3.7.1 Quartz veins - general characteristics and timing

An important first step in the structural analysis of quartz vein systems is to separate the veins into different morphologic types and/or generations. Typically, this is accomplished by examining the mineral assemblages and textures within the veins, the geometrical arrangement and structural sites of the veins, and the geometric and overprinting relationships between the veins and other structures. However, in the Pacquet Harbour area, quartz veins consist mainly of massive quartz, with <5% carbonate, plagioclase, chlorite, and/or tourmaline. In addition, textures indicative of the vein-forming mechanism (i.e., mineral fibres) are generally lacking, probably due to recrystallization of the mineral phases, or to very rapid opening of the original fracture (i.e., the rate of mineral precipitation is much less than the rate of separation of the fracture walls; Barker 1990). Thus, in the present study the quartz veins were separated into four distinct groups on the basis of morphology, orientation, and relationship to other structures. The relative age of the different vein groups is established in relation to D_2 structures, largely because

these are the most widespread in the study area.

Group 1 veins include all veins that clearly pre-date D_2 . These veins are generally boudinaged in the plane of S_0 - S_1 , and folded by F_1 and F_2 folds. In MBG schist, these veins are typically associated with black, tourmaline-rich haloes. Undoubtedly, the Group 1 veins include more than one generation and type, but intense D_2 deformation and recrystallization preclude unambiguous separation of these veins in the field.

Group 2 veins cut S_0 - S_1 in the MBG and PHG, but are generally subparallel to, and boudinaged in, the S_2 plane. These veins are generally 5-10cm thick, 0.2 to 1.0m long, and consist of massive, recrystallized quartz. The Group 2 veins are subparallel to the axial planes of F_2 folds, but in some cases the lateral tips of the veins are folded by F_2 . In many locations, Group 2 veins form en-echelon sets of tension gashes in the S_0 plane. Within the sets, individual veins consistently occur at a moderate to high angle to S_0 , suggesting that the veins formed as extensional fractures during shear parallel to S_0 (e.g., the Type 2 veins in Fig. 3.5b). The Group 2 veins are interpreted to be syn- D_2 .

Group 3 veins are conspicuous in the Pacquet Harbour area. These veins cut S_1 and S_2 in the MBG and PHG, and are typically planar, 0.2 to 2.0m long, 1 to 10cm wide, undeformed, and dip shallowly (oriented significantly oblique to S_2 ; Fig. 3.7a). The Group 3 veins consist of massive, recrystallized quartz, and have a distinct tension gash morphology (Fig. 3.8a) although they do not occur in en-echelon sets. These veins are common in both the MBG and PHG, but were not noted in the BBSZ. This may indicate that these veins were destroyed during D_3 shear, and thus post-date D_2 , but pre-date D_3 .

Three mechanisms may be invoked to explain the morphology, orientation, and

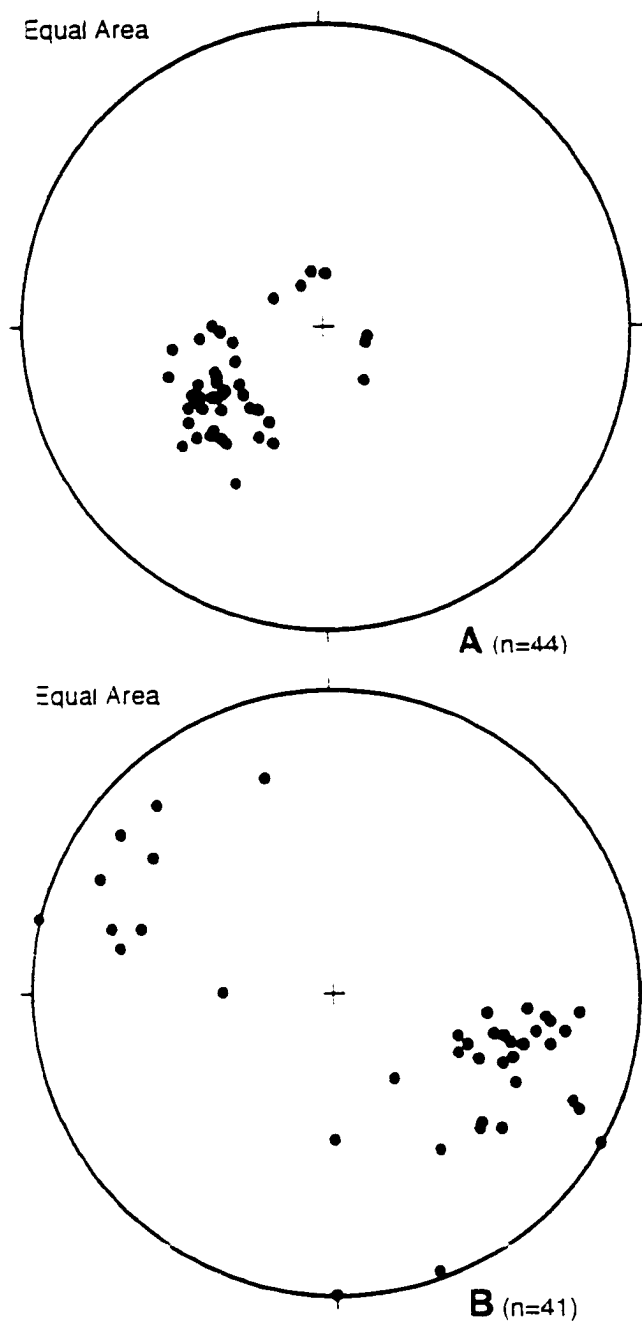


Figure 3.7 Lower hemisphere, equal area projections of the orientation of quartz veins and granitic pegmatites in the Pacquet Harbour area. a) Poles to tension gashes at Pelee Point and north of Pacquet Harbour. b) Poles to granitic pegmatite dykes in the MBG north of Pacquet Harbour.

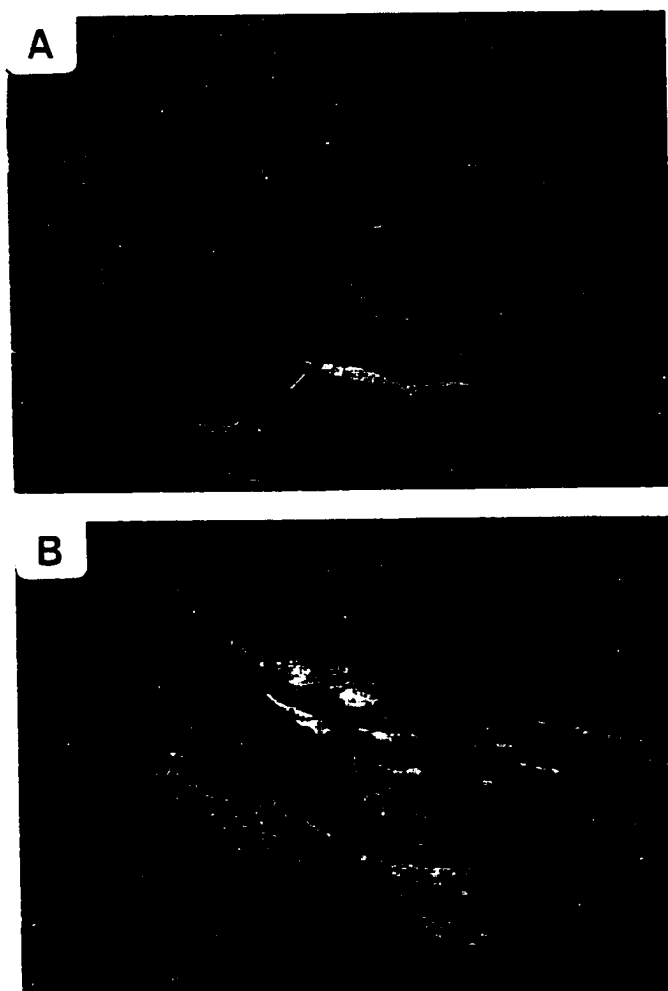


Figure 3.8 Field photographs of quartz veins and granitic pegmatites in the Pacquet Harbour area. a) Examples of quartz-filled tension gashes that dip shallowly in layered, weakly deformed MBG schist ~700m north of Pacquet. b) Granitic pegmatite dykes (<2m thick) in the shallowly southeast-dipping S_2 plane at Cape Corbin (Fig. 2.2). The pegmatites are exposed in approximately south- and east-facing subvertical cliff faces in the left and right portions of the photograph, respectively.

field relationships of the Group 3 veins. First, the veins may have formed due to filling of tension fractures formed during a late phase of horizontal compression. This mechanism would be consistent with the shallow dip of the veins (perpendicular to subvertical extension direction in a compressional regime), but is inconsistent with the lack of late compressional structures in the Pacquet Harbour area. Second, the veins may have formed as tension fractures during non-coaxial shear parallel to S_2 . In this model, the tension gashes would have rotated into their present orientation during progressive shear. However, this mechanism seems unlikely due to the lack of en-echelon tension gash sets, the undeformed nature of most of the Group 3 veins, and, in some cases, the relatively undeformed nature of the host rocks (Fig. 3.8a). Third, Coney (1980) and Reynolds and Lister (1987) proposed that these types of veins may form due to rapid unroofing during extensional deformation. In this mechanism, rapid unroofing would result in a corresponding rapid decrease in the lithostatic load (i.e., the vertical compressive stress). Under conditions where the deviatoric stress is less than the tensile strength of the rock, the fluid pressure may locally, and temporarily, exceed the lithostatic load ($P_{\text{fluid}} > P_{\text{load}}$), allowing the subhorizontal extension fractures to form, and these fractures would have then been filled with the vein material (e.g., Coney 1980; Reynolds and Lister 1987). This mechanism appears to be consistent with the relative timing of the Group 3 veins with respect to extensional deformation in the Pacquet Harbour area.

Group 4 veins cut all structures in the Pacquet Harbour area (including S_3 in the BBSZ). These veins are essentially undeformed, tabular, and consist of massive granular quartz. The Group 4 veins consistently strike west and dip steeply, and therefore may

represent a single generation that formed very late in the structural evolution of the Pacquet Harbour area. In one location on Pelee Point, a Group 4 vein can be traced continuously into the extreme tip of a narrow pegmatite dyke. Thus, these veins may be related in some way to the pegmatites in the MBG, or they may simply be exploiting pre-existing planes of weakness in the rock.

3.3.7.2 Pegmatites - general characteristics and timing

In the Pacquet Harbour area, the MBG is intruded by a suite of granitic pegmatites, which are assumed to represent one phase of intrusion (see Section 2.3.1.1). The pegmatites typically form <500m long, <15m thick, planar dykes that dip steeply to moderately to the northwest and southeast (Fig. 3.7b). In the immediate vicinity of Pacquet Harbour, the dykes mainly dip steeply northwest, and are nearly orthogonal to L_2 . These dykes are everywhere late- to post-tectonic with respect to D_2 (Fig. 2.3c). Pegmatite dykes nearest to the BBSZ locally contain a fabric which is continuous with S_3 in the adjacent country-rock, and is thus ascribed to D_3 deformation. In these pegmatites, the S_3 fabric is non-penetrative, and is defined by discrete planes of fine- to coarse-grained, foliated muscovite that anastomose around K-feldspar and plagioclase phenocrysts. This relationship indicates that intrusion of the pegmatites occurred prior to, or during, D_3 . This interpretation is supported by microstructures observed in feldspar phenocrysts in the pegmatites (i.e., brittle fractures, undulose extinction, relatively strain-free subgrains, and warped twin-planes) which are consistent with weak deformation at upper greenschist facies temperatures (ca. 400-500° C; Gapais 1989).

The apparent late- D_2 to syn- D_3 relative timing suggest that pegmatite intrusion

may have occurred during a relatively 'quiescent' interval between D_2 and D_3 . The nearly orthogonal angular relationship between many of the pegmatite dykes and the L_2 - L_3 stretching lineations may provide further support for this hypothesis (see below).

3.3.7.3 Structural significance - pegmatites and Group 3 & 4 veins

The general structural characteristics of the granitic pegmatite dykes and Group 3 and 4 quartz veins in the Pacquet Harbour area are quite similar to the vein systems described by Coney (1980) and Reynolds and Lister (1987) in low angle detachment zones associated with Cordilleran metamorphic core complexes. Rocks in the footwall of these detachment zones contain syn to late-mylonitic, extensional fractures that are perpendicular to the subhorizontal extension direction. These fractures include extensional veins (tension gashes), as well as planar quartz veins and igneous dykes. Within the footwall rocks, local subhorizontal, late-mylonitic, extension fractures may indicate that the deviatoric stress was low enough that the fluid pressures intermittently exceeded the lithostatic load during rapid unroofing (Coney 1980; Reynolds and Lister 1987).

In light of the above observations, and the late- D_2 to syn- D_3 apparent timing of intrusion, several aspects of the pegmatites and the Group 3 and 4 quartz veins are intriguing. 1) Granitic pegmatites and Group 3 quartz veins are only found north of Pacquet Harbour, in the footwall of the extensional shear zone at the northern contact of the Cape Brule Porphyry. 2) The Group 3 quartz veins may provide evidence that the fluid pressure locally, and temporarily, exceeded the lithostatic load during rapid unroofing, allowing fracturing perpendicular to the vertical compressive stress. The pegmatites that dip shallowly at Cape Corbin north of Handy Harbour (Map 1) may also be an example of

this process (Fig. 3.8b; refer to Chapter 7 for a detailed explanation of the chocolate-tablet boudinage of these pegmatites). 3) Granitic pegmatites in the MBG are typically subvertical, and oriented perpendicular to the L_2 - L_3 stretching and mineral lineation. Insofar as the emplacement of dykes provides an 'instantaneous' sample of the ambient stress conditions at the time of intrusion (e.g., Reynolds and Lister 1987), the predominance of subvertical pegmatites oriented perpendicular to L_2 - L_3 is consistent with intrusion in an extensional D_2 - D_3 stress regime (i.e., subvertical σ_1 , subhorizontal σ_3).

Collectively, these relationships may be consistent with emplacement of the granitic pegmatites, and the Group 3 and 4 quartz veins, into extensional fractures associated with an intratectonic stage of extensional D_2 - D_3 deformation in the Pacquet Harbour area. The significance of this interpretation is discussed in detail in Chapter 7.

3.4 CONCLUSIONS - PACQUET HARBOUR AREA

(1) The PPSZ is characterized by penetrative, ductile, D_1 structures, and is interpreted as the locus of D_1 strain in the Pacquet Harbour area. Field relationships indicate that the PPSZ may have initiated at a relatively shallow crustal level during initial juxtaposition of weakly deformed, low-grade, MBG and PHG rocks. Correlative Group 1 shear zones that dip north in the Dunamagon Granite locally record reverse-sinistral oblique-slip, consistent with south-directed overthrusting of the granite and PHG by the MBG during D_1 . Since the early stages of D_2 were associated with lower to middle amphibolite facies metamorphism, the Pacquet Harbour area (and PPSZ) must have been buried to significant depth (>18 km) prior to the onset of D_2 . This observation provides further evidence that D_1 was associated with a bulk compressional tectonic regime.

(2) D_2 deformation involved a complex sequence of fabric development, folding, syn-tectonic porphyroblast growth and, in the later stages, pegmatite intrusion, which is attributed to progressive bulk non-coaxial strain in an extensional stress regime. Accordingly, D_2 structures record normal-sense, southeast-directed, non-coaxial shear within a thick structural zone that dips moderately southeast, and initiated during peak amphibolite facies metamorphism. This deformation is associated with rapid post-metamorphic cooling (e.g., Dallmeyer and Hibbard 1984; see Chapter 6) and exhumation of the Pacquet Harbour area.

(3) D_3 structures are nearly coaxial with D_2 structures, and record normal-sense, southeast-directed, non-coaxial shear in the BBSZ. The BBSZ is probably associated with waning strain and metamorphism in the latest stages of extensional deformation in the Pacquet Harbour area. This interpretation is supported by the greenschist-facies metamorphic mineral assemblages in the BBSZ, $^{40}\text{Ar}/^{39}\text{Ar}$ data (see Chapter 6), and may well be reflected in the geometrical relationship of the BBSZ to S_2 , which resembles that of a discrete, large-scale, late-stage, asymmetric shear band (Cross section 1).

(4) Structures attributed to D_1 in the present study are correlated with D_1 of Coates (1970) and the regional D_M of Hibbard (1983), whereas D_2 structures are correlated with D_2 of Coates (1970) and the regional D_L of Hibbard (1983). These correlations are based on comparisons of the style, syn-deformational metamorphic grade, orientation, and overprinting relationships (refer to Sections 3.1.2 and 3.2.2). The regional significance of these deformation events is further discussed in Section 4.4.

Chapter 4 Structural Geology - Ming's Bight area

4.1 MING'S BIGHT AREA - INTRODUCTION

4.1.1 Background

The structural geology of the Ming's Bight area has been described in regional-scale studies by Hibbard and Gagnon (1980), Bursnall and Hibbard (1980), and Hibbard (1983). In addition, there have been several detailed structural studies of the PHG south of Ming's Bight (Gale 1971; Tuach 1976; Tuach and Kennedy 1978), the PROC west of Ming's Bight (Norman and Strong 1975; Kidd 1977; Kidd et al. 1978), and of the structurally controlled gold deposits in the PROC (Kirkwood and Dubé 1992; Ramezani 1992; Dubé et al. 1993; Patey and Wilton 1993; Fig. 1.2). However, the structural geology to the east, and immediate south, of Ming's Bight has never been documented in detail (Fig. 3.1). This omission is particularly crucial since exposures in these areas record the tectonic interaction of the MBG, PHG, PROC, and the Dunamagon Granite, and are thus invaluable in any attempt at regional correlation of structures.

One of the major goals in the present study is to document the structural geology of the previously unmapped areas to the east and south of Ming's Bight, and to incorporate these data into a comprehensive structural model for the Ming's Bight area. The structural model presented in this chapter incorporates the results of the previous structural studies, as summarized below.

4.1.2 Previous structural studies

4.1.2.1 Point Rouse Ophiolite Complex

The PROC has been the focus of a number of structural studies. Norman and Strong (1975) noted that the PROC is characterized by a penetrative S_1 foliation that dips moderately northwest, and is defined by foliated actinolite and chlorite. This foliation contains a pervasive L_1 mineral and stretching lineation that plunges north. These authors attributed the S_1 - L_1 fabrics to inhomogeneous deformation related to the early stages of Early Ordovician ophiolite emplacement. They further suggested that the ophiolite was disrupted by thrust faults of unspecified age, and folded into a large syncline in the Middle Devonian (Church and Stevens 1971; Kennedy 1973). In contrast, Kidd (1977) and Kidd et al. (1978) demonstrated that the large syncline, S_1 - L_1 fabrics, and thrust faults formed synchronously during south-directed overthrusting of the PHG by the PROC. These authors attributed this overthrusting to the Middle Devonian closure of an Ordovician oceanic marginal basin, and concluded that there was no evidence for deformation of the PROC prior to Early Devonian time. It was further suggested that structures in adjacent units (i.e., Fleur de Lys Supergroup, MBG, PHG, Dunamagon Granite, and Burlington Granodiorite) formed prior to the Early Ordovician, and thus entirely pre-dated the Middle Devonian deformation. Kidd et al. (1978) also described a pervasive set of late faults that consistently downthrow the rocks of the PROC to the west and/or north, and attributed these faults to "...a relaxation of the convergent motion and a fall-back of the rocks into the steeply-dipping pinched zone from which they had just been expelled". These faults are discussed in Section 4.2.7.

Except for the inferred timing, the structural data of Kidd (1977) and Kidd et al. (1978) are broadly consistent with the results of recent investigations of the structural geology of mesothermal gold mineralization in the PROC. In general, these studies have concluded that the S_1 - L_1 fabrics are contemporaneous with intense, ductile, north over south-directed thrusting, greenschist facies metamorphism, and the development of gold-bearing hydrothermal vein systems (e.g., Kirkwood and Dubé 1992; Ramezani 1992; Dubé et al. 1993; Patey and Wilton 1993). Kirkwood and Dubé (1992) divided the ductile thrust faults in the PROC into three different 'orders' of structure. In this scheme, the thrust faults associated with S_1 - L_1 fabrics in the PROC are interpreted to be third-order structures associated with north over south-directed thrusting along the first-order Scrape Fault (Fig. 3.1). These interpretations are consistent with those of Kidd (1977) and Kidd et al. (1978). However, Ramezani (1992) demonstrated (through U-Pb dating of hydrothermal zircon) that the system of syn-thrusting hydrothermal veins formed during Late Silurian time (420 ± 5 Ma), and concluded that thrust-related deformation is of broadly similar age. In the present study, D_1 deformation in the PROC, and the south-directed overthrusting of the PHG by the PROC along the Scrape Fault, are considered to have occurred in late-Early to Late Silurian time.

4.1.2.2 Pacquet Harbour Group

PHG rocks in the footwall of the Scrape Fault should record evidence for Silurian thrusting. Gale (1971), Tuach (1976), and Tuach and Kennedy (1978) examined the structural geology of the PHG in the vicinity of the Rambler massive sulphide deposits, and concluded that the deformation history involved three main phases of deformation.

However, there is an important discrepancy in the structural descriptions presented by these authors which, in the opinion of this author, provides a key to the structural framework of the entire Ming's Bight area. The salient points of these studies are outlined below, followed by a discussion of the resulting discrepancy.

The following description of the structural geology of the PHG is simplified from Gale (1971). D_1 produced a S_1 foliation that dips northeast and contains a pervasive L_1 mineral and stretching lineation that plunges northeast. These fabrics are regionally developed northwest of the Rambler camp, and the Rambler massive sulphide orebodies are lineated parallel to L_1 . Axial ratio measurements of the stretched objects indicate constrictional strains. D_1 was synchronous with the upper greenschist facies metamorphic peak, and the syn- D_1 grade of metamorphism increases from south to north across the PHG. D_2 produced a vertical crenulation cleavage northeast of the Rambler camp that dips east to southeast, and is axial planar to tight to isoclinal, upright F_2 folds. The F_2 axes plunge shallowly northeast and are coaxial with L_1 . D_3 produced a crenulation cleavage that dips shallowly south, and is axial planar to open, recumbent F_3 folds.

The following description is simplified from Tuach (1976) and Tuach and Kennedy (1978). D_1 produced a layer-parallel S_1 foliation that is preserved in the hinges of F_2 folds and between S_2 crenulation planes. S_2 is the main planar fabric around the Rambler camp. On a regional scale, the orientation of S_2 gradually changes from moderately northeast-dipping to the northwest of the Rambler camp, to steeply east- and west-dipping to the northeast of the Rambler camp (Fig. 3.1). In strongly deformed lithologies, S_2 contains a very prominent L_2 mineral and stretching lineation that plunges northeast, and the Rambler

massive sulphide bodies are lineated parallel to L_2 . Axial ratios indicate constrictional D_2 strain, and the intensity of the strain apparently increases from south to north across the PHG. L_2 is coaxial with tight to isoclinal, upright, locally intrafolial F_2 folds. D_2 is interpreted to be synchronous with lower amphibolite facies peak metamorphism. D_3 produced a crenulation cleavage that dips shallowly northeast, and is axial planar to open, recumbent F_3 folds that plunge northeast.

Although the structures recognized by these authors are essentially the same, the main discrepancy arising from their structural descriptions is that the moderately northeast-dipping, constrictional, high temperature fabric northwest of the Rambler camp was assigned to D_1 by Gale (1971), and to D_2 by Tuach (1976) and Tuach and Kennedy (1978). The latter interpretation requires a large-scale change in orientation of the D_2 fabric from west to east across the Rambler area, which Tuach and Kennedy (1978) attributed to a large, upright fold in the central portions of the PHG (Fig. 3.1). However, this interpretation does not fully address the coaxiality and constrictional character of D_1 and D_2 structures, and their apparent synchronicity with the upper greenschist to lower amphibolite facies metamorphic peak in the PHG. Thus, an alternative interpretation is proposed below wherein the D_2 fabric of Tuach (1976) and Tuach and Kennedy (1978) was not simply folded, but formed concurrently with the D_1 - D_2 fabrics of Gale (1976) during amphibolite facies metamorphism in a thrust/wrench-shear system (e.g., Coward and Potts 1983).

This interpretation is further developed in the following structural descriptions, based on mapping conducted by the author in the Ming's Bight area and, in particular,

along the southern and eastern shores of Ming's Bight (Fig. 3.1). In the present study, the Ming's Bight area is considered to represent the eastern margin of the wide deformation zone that marks the trace of the BVL. Therefore, the conclusions reached in this section have important implications for the structural evolution of the BVL.

4.2 DETAILED STRUCTURAL ANALYSIS

Detailed structural analysis of the areas to the east and south of Ming's Bight revealed five phases of ductile deformation (D_1 , D_2 , D_3 , D_4 , D_5 ; Table 4.1; Maps 4 to 9; Cross sections 3 to 7; and Fig. 4.1). D_1 structures are well developed in the Burlington Granodiorite (432 ± 2 Ma; U-Pb zircon; Cawood and Dunning 1993), indicating that most, if not all, deformation in the Ming's Bight area post-dates the earliest Silurian. The structural geology and deformation history of the PROC to the west of Ming's Bight, based on mapping conducted by the author, is described separately in Section 4.2.6.

4.2.1 D_1 deformation

D_1 deformation structures are pervasive in the northwestern portions of the PHG and along the northeastern contact of the Burlington Granodiorite, and correspond to D_1 of Gale (1971) and, partly, D_2 of Tuach (1976) and Tuach and Kennedy (1978). In the PHG, the regional S_1 fabric varies from a penetrative mylonitic foliation to a spaced cleavage, and dips moderately to the northeast or north (Fig. 4.1), although northeast of the Rambler camp the orientation is quite variable due to extensive F_3 folding. In PHG mafic volcanic rocks, S_1 is defined by foliated hornblende and biotite porphyroblasts. The hornblende porphyroblasts are fine- to very coarse-grained, acicular-idioblastic, and are relatively strain-free, suggesting either high temperature deformation, or subsequent

Table 4.1 Deformation structures - Ming's Blight area

D ₅ deformation * syn-380 to 388 Ma	Northwest- and southwest-dipping dextral-normal oblique-slip shear zones F ₅ folds light to isoclinal; sheath folds; assoc. with late shear zones S ₅ - L ₅ fabrics Mylonitic foliation; mineral and stretching lineation in late shear zones	Linked southwest- and northwest-directed extensional shear
D ₄ deformation * pre- to syn-390 Ma * post-420 Ma	Northwest-dipping dextral oblique-slip shear zones F ₄ folds Open to close; reclined; shallowly west-plunging; large-scale fold structures S ₄ - L ₄ fabrics Mylonitic to spaced crenulation fabric; shallowly west-dipping; axial planar to F ₄ ; local mineral and stretching lineation	Progressive dextral transpressional to transpressional oblique-slip shear
D ₃ deformation * pre-390 Ma * post-420 Ma	South-dipping extensional shear zones F ₃ folds Gentle to tight; recumbent; shallowly south-plunging S ₃ - L ₃ fabrics Spaced crenulation cleavage; axial planar to F ₃ ; rare mineral lineation	South-directed extensional shear marking the onset of exhumation of the MBG
D ₂ deformation * pre-405 Ma * syn-420 Ma * post-430 Ma	Sinistral transpression in west-dipping lateral ramp F ₂ folds Open to isoclinal; upright; shallowly south-plunging; rootless; sheath folds S ₂ - L ₂ fabrics Mylonitic to spaced crenulation fabric; steeply-dipping; subhorizontal mineral and stretching lineation	Silurian sinistral transpressional shear
D ₁ deformation * pre-405 Ma * syn-420 Ma * post-430 Ma	Sinistral-reverse oblique-slip shear in north-dipping frontal ramp F ₁ folds light to isoclinal; inirtalocal; north-plunging; sheath folds S ₁ - L ₁ fabrics Penetrative mylonitic foliation; northwest- to northeast-dipping; penetrative stretching lineation	Silurian sinistral transpressional shear

Note: double-solid and single-dashed lines denote separate and progressive deformation, respectively.

* Time constraints (see Chapter 6)

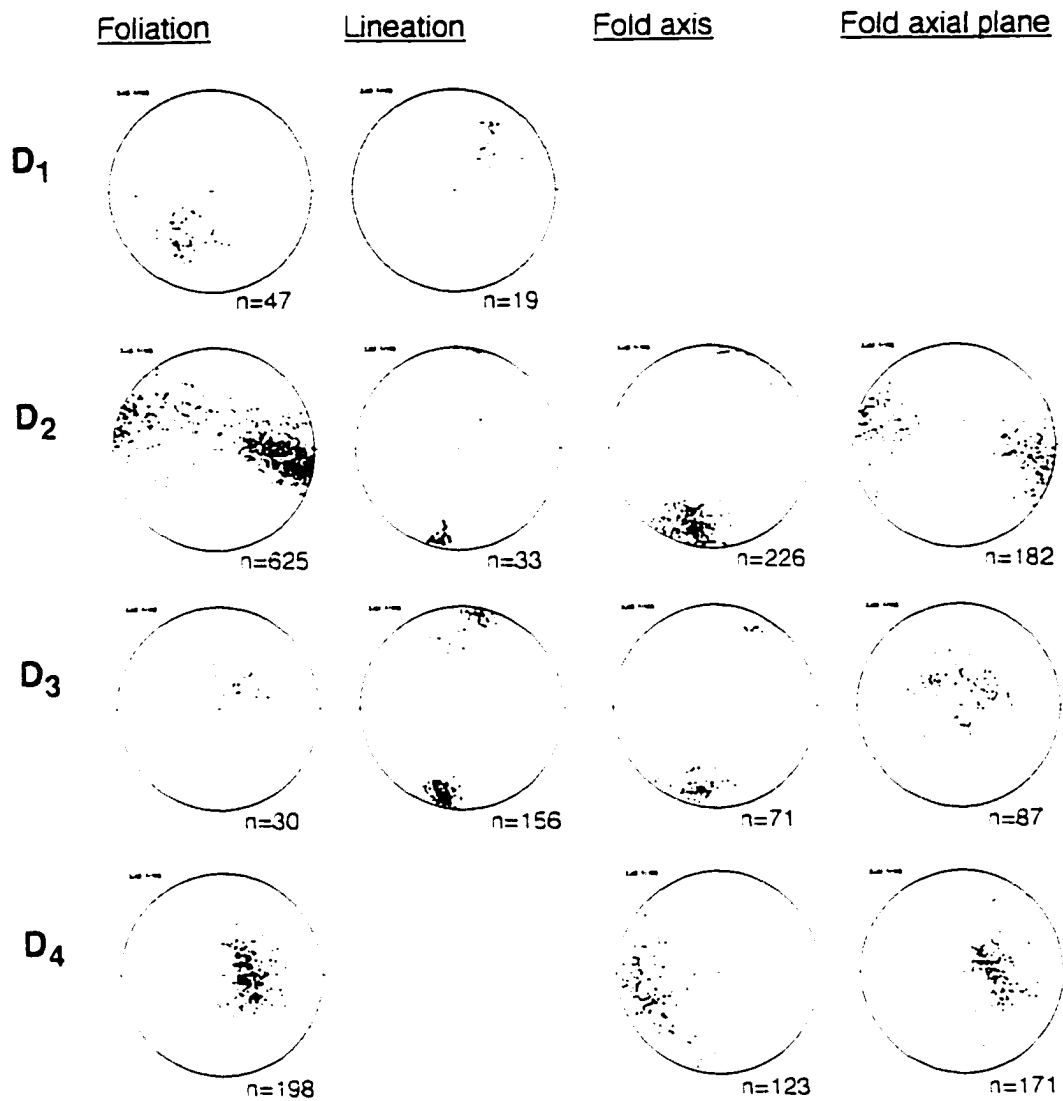


Figure 4.1 Lower hemisphere, equal area projections of structural data in the Ming's Bight area. Planar structural elements are plotted as poles. Structural measurements were obtained in the area northwest of the Rambler camp (D₁), immediately south of Ming's Bight (D₂-D₃), and in the area north of the granitic intrusions on the eastern shore of Ming's Bight (D₄). This distribution reflects the lack of post-D₁ structures in the area northwest of the Rambler camp, and rare preservation of pre-D₄ structures north of the granitic intrusions. Plot of S₂ includes some measurements of S₁ south of Ming's Bight, and L₃ is the intersection lineation between S₃ and S₁-S₂. L₁ and L₂ include both mineral (hornblende) and stretching lineations.

recrystallization. In many locations, S_1 is parallel to a pronounced banding defined by alternating hornblende-biotite and plagioclase-quartz-rich domains, consistent with metamorphic segregation and relatively high-temperature deformation (Tuach 1976; Tuach and Kennedy 1978). This banding is particularly well developed in D_1 shear zones, and is interpreted to reflect high finite strains (i.e., mylonitic banding). In felsic volcanic rocks, S_1 is defined by foliated biotite, muscovite, and prominent recrystallized quartz-plagioclase ribbons, and is parallel to mylonitic banding defined by alternating plagioclase-muscovite and quartz-rich domains. In the Burlington Granodiorite, S_1 is defined by a non-penetrative biotite foliation, and a preferred orientation of elongate feldspar augen.

In general, the mylonitic S_1 in the PHG is more prominent in the north, where it is developed within discrete, <100m thick shear zones which are separated by less deformed rock. The most prominent D_1 shear zone is the Scrape Fault (i.e., first order shear of Kirkwood and Dubé 1992), which separates the PROC and PHG (Fig. 3.1, 4.2a). Other significant D_1 shear zones are located in the PHG above the north-striking contact of the Burlington Granodiorite (Fig. 3.1), and along the northwest margin of the felsic volcanic succession northeast of the Rambler camp (Figs. 2.2 and 3.1).

The S_1 foliation contains a very prominent L_1 mineral and stretching lineation that plunges moderately to the north and northeast in S_1 (Fig. 4.1). L_1 is particularly pervasive in D_1 shear zones (Fig. 4.2b), although it is regionally developed in the northern portion of the PHG, as evident from the extreme lineation of the Rambler massive sulphide deposits (Gale 1971; Tuach 1976; Tuach and Kennedy 1978). The mineral lineation is primarily defined by acicular hornblende porphyroblasts, and to a lesser extent by lineated biotite,

Figure 4.2 Field photographs of D_1 and D_2 structures in the Ming's Bight area. **a)** Example of D_1 mylonitic amphibolite exposed in the footwall of the Scrape Fault on Ming's Bight Road. The asymmetric quartz pod in the centre of the photograph illustrates the non-coaxiality of the flow, but is ambiguous with regard to shear sense. **b)** L_1 stretching lineation that plunges steeply north in the D_1 shear zone along the northern margin of the felsic volcanic succession ~6km northeast of the Rambler camp. **c)** Upright, tight to isoclinal F_2 folds that plunge shallowly south, and the axial planar S_2 in MBG schist along the south shore of Ming's Bight. **d)** S_2 fabric wrapped around asymmetric hornblende "fish" in mylonitic amphibolite east of Deep Cove (hornblende fish is 1.5mm long; S_2 parallels the long edge of the photo). **e)** Shallowly south-plunging L_2 stretching lineation defined by stretched clasts (arrowed) in felsic volcanic rocks exposed on the Logging Road south of Ming's Bight (Map 4). **f)** Photograph (facing east) illustrating: i) the penetrative, subvertical S_2 fabric that strikes north in PROC metasedimentary rocks south of Barkers Point (Map 7); ii) an asymmetrically boudinaged subvertical granite dyke; and iii) a truncated and drag-folded subvertical mafic dyke (truncation plane indicated by the dashed line). Sinistral transcurrent shear is indicated by the sense of asymmetry of the granite boudin, and the drag-folding and off-set of the mafic dyke (~15m of left-lateral displacement).

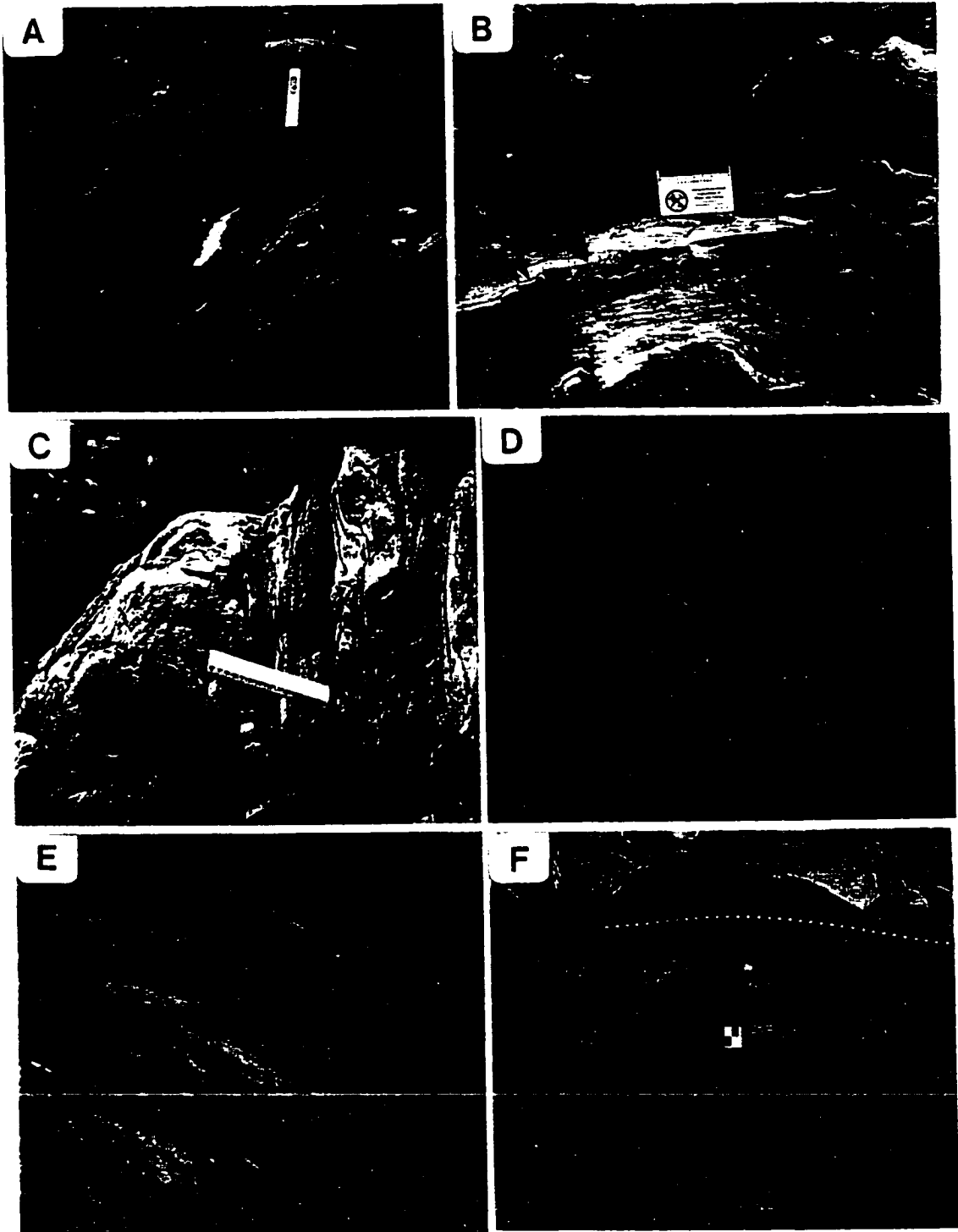


Figure 4.2

chlorite, and muscovite. The L_1 stretching lineation is defined by stretched pillows, amygdules, and clasts in mafic volcanic rocks, by stretched lapilli, blocks, and bombs in felsic pyroclastic rocks (Fig. 2.4e), and by stretched feldspar phenocrysts in the Burlington Granodiorite. Axial ratios of the stretched objects typically define strongly prolate ellipsoids, consistent with constrictional finite D_1 strain (Gale 1971; Tuach 1976).

S_1 is axial planar to tight to isoclinal, reclined F_1 folds that plunge shallowly north. These folds are rare in the northwestern portions of the PHG, probably due to the relative lack of primary strength anisotropies (i.e., bedding). However, F_1 folds were observed in the mylonitic banding in D_1 shear zones. These folds are isoclinal and intrafolial, with fold axes coaxial with L_1 . These F_1 folds have a consistent S-sense of asymmetry (looking down-plunge). In one location ~2 km east of the Ming Mine, rootless and sheath F_1 folds were noted in the D_1 shear zone at the northern margin of the felsic volcanic succession.

Kinematic indicators associated with S_1 , including en-echelon sigmoidal quartz-filled tension gashes, offset quartz veins, and asymmetric shear-modified boudins (e.g., Hanmer and Passchier 1991), are consistent with reverse non-coaxial shear parallel to S_1 - L_1 . The orientation, style, and sense of shear of D_1 structures in the PHG are essentially identical to D_1 structures in the PROC (e.g., Norman and Strong 1975; Kidd 1977; Kidd et al. 1978; Kirkwood and Dubé 1992; Dubé et al. 1993), and these structures are therefore correlated. This correlation implies that D_1 structures in both the northwestern portion of the PHG and the PROC formed during south-directed tectonic transport of the PROC over the PHG along the Scrape Fault.

To the northeast towards the Dunamagon Granite, D_1 structures are transected by

D₂ structures. The D₁ shear zone along the northern margin of the felsic volcanic succession can be traced continuously northward from the La Scie highway to the area immediately west of the Dunamagon Granite (Figs. 2.2 and 3.1). Near the La Scie highway, this shear zone dips steeply north and contains a down-dip L₁ stretching lineation (Fig. 4.2b). To the northeast, the shear zone becomes steeply northwest-dipping, and the mylonitic S₁ is folded by upright F₂ folds that plunge steeply north. Further to the northeast, S₁ is typically observed in the hinges of tight to isoclinal F₂ folds and between S₂ crenulation planes in zones of non-penetrative D₂ strain. Locally, S₁ is also preserved in pre to syn-D₂ albite and garnet porphyroblasts as inclusion trails that are typically highly oblique to the matrix S₂.

Further north, the PROC metasedimentary rocks on the eastern shore of Ming's Bight contain a bedding-parallel fabric defined by a fine-grained foliated chlorite-biotite ± white mica that probably represents S₁. This foliation was observed in thin sections of the thinly bedded black slates north of Long Point and the greywacke-siltstone successions at Jimmy's Cove (Map 7), and is transposed into S₂ in these locations. In these locations, S₁ is axial planar to tight to isoclinal F₁ folds. These folds are commonly intrafolial, and have wavelengths about ~5 to 20cm. In Actinolite Bay (Map 5), F₁ folds are particularly well developed within a <10cm thick cotecule layer (e.g., Cross-section 4). These folds are isoclinal, and coaxially refolded by isoclinal F₂ folds. F₁ folds are also common in the MBG, and are recognized as faint, isoclinal fold closures that are coaxially re-folded in the hinges of F₂ folds. In the Ming's Tickle area (Map 7), the presence of D₁ structures can only locally be inferred, for example, in structurally complex amphibolite succession to the

north of Caplin Cove which apparently contains a large, isoclinally refolded, isoclinal fold that is interpreted to record F_1 - F_2 interference folding (Map 8; Cross section 7).

4.2.2 D_2 deformation

D_2 structures are well developed in the north-central portions of the PHG, where they correspond to D_2 of Gale (1971), Tuach (1976), and Tuach and Kennedy (1978). To the immediate southeast and south of Ming's Bight, D_2 structures are regionally developed, but are particularly pervasive in the area immediately west of the Dunamagon Granite (Fig. 3.1: Maps 4, 5, and 6). Further northeast along the eastern shore of Ming's Bight, D_2 structures have been extensively overprinted by later structures, and locally occur within discrete blocks of structurally complex amphibolite in D_4 - D_5 shear zones. D_2 structures were not noted in the PROC west of Ming's Bight.

On the south shore of Ming's Bight, the MBG, PHG, and PROC are imbricated along a series of shear zones that dip moderately to steeply west and are parallel to the regional S_2 fabric. Shear zones exposed in Actinolite Bay, White Cow Bay, and Carbonate Cove comprise tectonic inclusions of MBG schist, actinolite-talc schist (altered ultramafic rock), coticule, and carbonate-biotite schist in a matrix of PHG and/or PROC greenschist and amphibolite (Map 5; Cross sections 3 and 4). The tectonic inclusions and matrix in these zones, and the margins of the shear zones, contain mutually parallel D_2 structures, consistent with development of the shear zones during D_2 .

In general, the S_2 foliation dips moderately to steeply west, although the orientation is quite variable due to F_3 folding (Fig. 4.1). S_2 is pervasive in the MBG and PHG, and is heterogeneously developed along the western margin of the Dunamagon

Granite and in the eastern-most exposures of PROC ultramafic rocks. In the MBG, S_2 varies from a penetrative mylonitic foliation to a spaced crenulation cleavage (Fig. 4.2c). This fabric is defined by fine- to coarse-grained foliated biotite and muscovite, and is generally parallel to the subvertical layering in the MBG. In places, the mica is segregated into foliation-parallel domains that alternate with quartz and plagioclase-rich domains. In two locations, S_2 is continuous with sigmoidal inclusion trails in garnet porphyroblasts, suggesting syntectonic garnet growth and (at least) upper greenschist facies metamorphism during D_2 . In the PHG, S_2 is defined by foliated biotite and white mica in metasedimentary and felsic volcanic rocks. In mafic volcanic rocks, S_2 is defined by foliated biotite, actinolite, and hornblende, although S_2 in the northernmost portions of the PHG is typically defined by foliated and lineated hornblende porphyroblasts. In these rocks the oriented hornblende forms relatively strain-free euhedral, acicular, poikiloblastic porphyroblasts. In one sample, coarse-grained hornblende porphyroblasts form prominent amphibole-fish (e.g., Lister and Snoke 1984) which indicate a component of sinistral strike-slip shear parallel to the lineation (Fig. 4.2d). Hornblende is locally concentrated into foliation-parallel domains that alternate with domains of medium- to coarse-grained, equigranular to granoblastic-polygonal plagioclase \pm quartz. The plagioclase grains have a slight crystallographic preferred orientation and weak undulose extinction. These microstructures are consistent with amphibolite facies metamorphism during D_2 . A particularly intense mylonitic S_2 occurs in PHG amphibolites in the footwall of the shear zone separating the PROC and PHG near Ming's South Brook (Map 6). This foliation contains a L_2 hornblende lineation that plunges shallowly south. Asymmetric shear bands

transect the foliation at a low angle, and suggest a component of sinistral strike-slip shear parallel to S_2 .

In the Dunamagon Granite, S_2 is heterogeneously developed, and is defined by fine-grained, aligned biotite anastomosing around K-feldspar phenocrysts. Xenoliths in the granite contain a planar fabric that is parallel to the long axes of the xenoliths, and parallel to S_2 in the host granite. Granitic dykes within the PHG contain a S_2 fabric defined by anastomosing domains of quartz ribbons, foliated muscovite and biotite, and grain-size reduction. These domains wrap around K-feldspar phenocrysts with brittle fractures, undulose extinction, warped twin-planes, well-developed subgrains, and mortar-textures along the margins, indicating deformation under upper greenschist facies conditions (e.g., Gapais 1989). In PROC ultramafic rocks, S_2 is defined by fine-grained foliated chlorite, talc, fuchsite, and serpentine, and contains a rare L_2 mineral (talc) lineation that plunges shallowly south. S_2 is penetrative along the margins of the ultramafic rocks, and is parallel to the regional S_2 . In the interior of the ultramafic bodies S_2 is penetrative in discrete, up to 2m thick shear zones that dip shallowly to steeply west, and is locally axial planar to tight to isoclinal folds of an early (S_1) serpentine-talc fabric. Further to the north in PROC metasedimentary rocks on the eastern shore of Ming's Bight, S_2 is north-south-striking, subvertical, and varies from a spaced crenulation fabric, to a penetrative, layer-parallel foliation defined by fine-grained foliated biotite, white mica, and chlorite.

S_2 commonly contains a prominent L_2 linear fabric that plunges shallowly south (Fig. 4.1), and is variably defined by a mineral, intersection, and/or stretching lineation. The L_2 mineral lineation is defined by a preferred orientation of acicular hornblende

porphyroblasts in PHG amphibolites, and a rare biotite lineation in PHG metasediments and MBG schist. The L_2 intersection lineation is defined by the line of intersection of S_2 and S_1 , and is well developed in layered MBG schist. The L_2 stretching lineation is defined by quartz-filled strain shadows on pyrite cubes in fine-grained amphibolites on the south shore of Ming's Bight, and by stretched clasts in the PHG metasediments on the logging road (Fig. 4.2e). The clasts form prolate ellipsoids with axial ratios of 5-10:1:1 (X:Y:Z), and are thus consistent with constrictional finite strains in these rocks. Thin granitic dykes cutting the metasediments contain elongate quartz rods that are subparallel to L_2 .

S_2 is axial planar to open to isoclinal, upright F_2 folds that are very well developed in the MBG and PHG, and to a lesser extent in the PROC metasedimentary rocks on the eastern shore of Ming's Bight (Fig. 4.1, 4.2c). F_2 folds occur on various scales, with wavelengths and amplitudes varying up to ~20m. F_2 folds fold primary layering, layer-parallel quartz veins, granitic dykes, and S_1 . In areas of non-penetrative S_2 , F_2 folds tend to be open to tight, and locally symmetrical. In areas where the mylonitic S_2 is developed, F_2 folds tend to be tight to isoclinal, and strongly asymmetrical, with highly variable fold vergence over short distances. In zones of particularly high strain, isoclinal F_2 folds are rootless and intrafolial in S_2 . In general, the axes of the F_2 folds plunge shallowly to the south and are subparallel to L_2 (Fig. 4.1). The orientations of the fold axes define a partial girdle (Fig. 4.1), and in places F_2 axes are slightly curvilinear in S_2 . Sheath-like F_2 folds with hinges that plunge shallowly south were noted in three locations.

Outcrops of bedded PHG metasediments near the logging road (Map 4) contain a heterogeneous set of D_2 structures that provide some important insights into the

mechanism of F_2 folding. In one outcrop, the primary layering and parallel S_1 fabric are cut by a spaced S_2 that dips steeply west and is axial planar to gentle to tight, upright F_2 folds that plunge steeply. These folds commonly have a sinistral sense of asymmetry (i.e., S-folds), and the layering is locally offset in a sinistral sense along S_2 . The intersection lineation between S_2 and the primary layering plunges steeply to the south. In an adjacent outcrop, however, the layering and S_1 fabric are strongly transposed into a penetrative S_2 foliation that is axial planar to tight to isoclinal, upright F_2 folds that plunge moderately south. The limbs of the F_2 folds are locally completely transposed into S_2 , and axes of these folds are subparallel to the shallowly south-plunging L_2 stretching lineation. The structural relationships in these two outcrops suggest that the F_2 fold axes initially plunged steeply south, but rotated in S_2 toward L_2 during progressive tightening of the folds. This hypothesis is consistent with the local preservation of non-cylindrical and sheath F_2 folds (e.g., Cobbold and Quinquis 1980).

If this folding model were generally correct for the F_2 folds, steeply plunging folds would have been continuously forming, and progressively rotating toward the transport direction (as inferred from the mean orientation of the L_2 stretching lineation) during D_2 (e.g., Cobbold and Quinquis 1980). Thus, one would expect to see numerous steeply plunging F_2 folds, sheath-like F_2 folds, and F_2 axes that define a great circle distribution. Furthermore, one would expect to see only tight to isoclinal folds with axes subparallel to L_2 , since rotation of the axes toward the transport direction would have involved relatively large strains, and progressive tightening of the folds during rotation (Skjernaa 1989). However, in the area south of Ming's Bight, steeply plunging and sheath-like F_2 folds are

scarce, and open F_2 folds with axes subparallel to the stretching lineation are common. These relationships indicate that F_2 folding probably involved both hinge-line rotation, and fold initiation with axes nearly parallel to the transport direction. In general, the latter folding mechanism is thought to involve initial nucleation of upright, open folds with axes at a low angle to the transport direction during non-coaxial shear in a ductile shear zone that contains a pronounced planar anisotropy. This mechanism requires either a component of wrench shear in the slip plane (due to shear strain rate gradients normal to the transport direction; e.g., Coward and Potts 1983; Ridley 1986; Ridley and Casey 1989; Holdsworth 1990), or shortening parallel to the Y-axis of the shear zone in a constrictional strain regime (Fletcher and Bartley 1994). As demonstrated below, this mechanism of folding appears to be compatible with the style of D_2 deformation.

In the area south of Ming's Bight, kinematic indicators associated with S_2 , including mica and hornblende fish, σ -porphyroclasts, oblique asymmetric boudin trains (Fig. 4.2f; Hanmer and Passchier 1991), and asymmetric fabrics, indicate a sinistral component of non-coaxial shear parallel to S_2 - L_2 . In several locations on the southern shore of Ming's Bight, syn- S_2 albite porphyroblasts with sigmoidal S_1 that are continuous into the matrix S_2 have σ -type strain shadows in X-Z sections that indicate sinistral strike-slip shear. In several locations, quartz veins and granitic dykes have undergone 'chocolate-tablet' boudinage in S_2 , suggesting a component of shortening perpendicular to S_2 , and possibly indicating that D_2 deformation included a component of coaxial strain. In one outcrop ~100m east of Birchy Cove (Map 5), a ~10cm thick quartz vein is chocolate-tablet boudinaged in S_2 , and two of the boudins are asymmetrically pulled-apart (Fig. 4.3a;

Figure 4.3 Photographs of D_2 and D_3 structures and syn- D_1 - D_2 porphyroblasts along the south shore of Ming's Bight. **a)** Boudinaged and asymmetrically pulled-apart quartz vein in S_2 that dips moderately west. Note the tight to isoclinal, east-vergent F_2 folds that plunge shallowly, and the boudinaged psammite layer. **b)** Photomicrograph of S_1 - S_e relationships in thin section SA-93-44a, which is oriented perpendicular to L_1 - L_2 . S_1 and S_2 parallel the long and short edges of the photograph, respectively. Note the curvature of the inclusion trails at the immediate margins of the porphyroblasts (see text for a detailed description; large garnet is ~ 0.8 mm in diameter). **c)** Photomicrograph of S_1 - S_e relationships in thin section SA-93-44c, which is oriented parallel to $L_{1,2}$. S_1 parallels the long edge of the photograph. Note the curvature of the inclusion trails at the immediate margins of the porphyroblasts (see text for a detailed description; large garnet is ~ 1.0 mm in diameter). **d)** Recumbent F_3 crenulations, and spaced S_3 crenulation cleavage in PROC metasedimentary rocks at Deep Cove (facing south). **e)** Upright, isoclinal F_2 fold coaxially refolded by recumbent, open F_3 folds in MBG schist on the south shore of Ming's Bight (facing south).

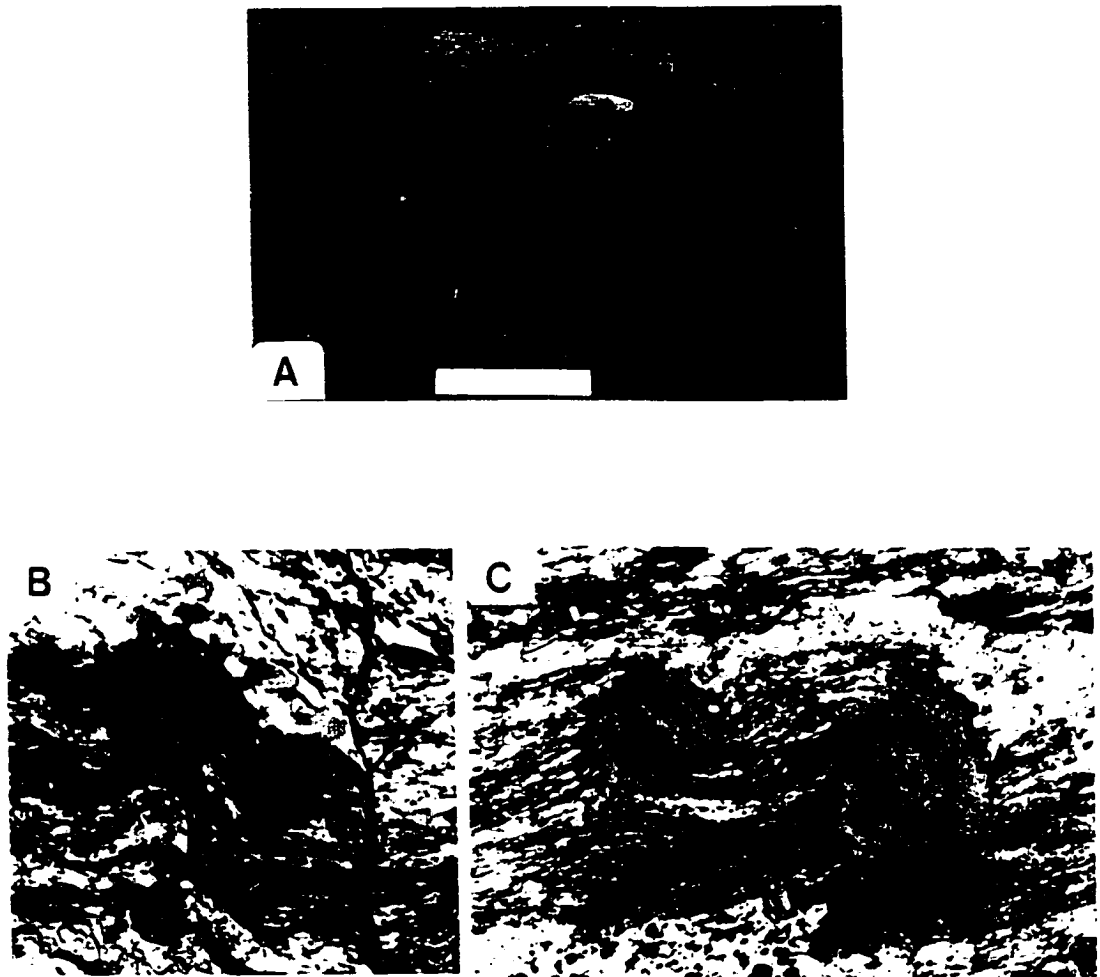


Figure 4.3



Hanmer 1986; Hanmer and Passchier 1991). In the X-Z plane of the finite strain ellipsoid, the sense of asymmetry indicates a component of sinistral non-coaxial shear (Hanmer 1986; Hanmer and Passchier 1991). If the boudinage and shear occurred synchronously, this structure provides evidence for extension parallel to the X- and Y-axes of the finite strain ellipsoid, and contemporaneous sinistral shear parallel to S_2 . Thus, based on the definition of transpression presented by Sanderson and Marchini (1984: "...a wrench or transcurrent shear that includes components of shortening perpendicular to the shear plane, and stretching perpendicular to the shear direction in the shear plane"), these D_2 structures indicate sinistral transpressional shear. This hypothesis is further supported by the overall style of D_2 structures in the area to the south of Ming's Bight (e.g., Sanderson and Marchini 1984; Holdsworth and Strachan 1991; Holdsworth 1994), and by the microstructural observations presented below.

Relative timing and sense of shear of D_1 and D_2 structures - microstructural evidence

Detailed microstructural analysis of porphyroblast inclusion trails can potentially provide important constraints on the relative timing of deformation structures and the sense of shear (e.g., Jamieson and Vernon 1987; Vernon 1989; Johnson 1990, 1992; Bell and Johnson 1992; Aerden 1994, 1995; Johnson and Bell 1996). The microstructural characteristics of an oriented sample (SA-93-44) of garnet porphyroblastic MBG schist were therefore examined in detail. This sample was taken from an outcrop of MBG schist just south of the town of South Brook and ~100m to the east of the shear zone that separates MBG schist and PROC ultramafic rocks (Map 4).

The sample (Fig. 4.4) was collected from the hinge of a metre-scale, tight, upright

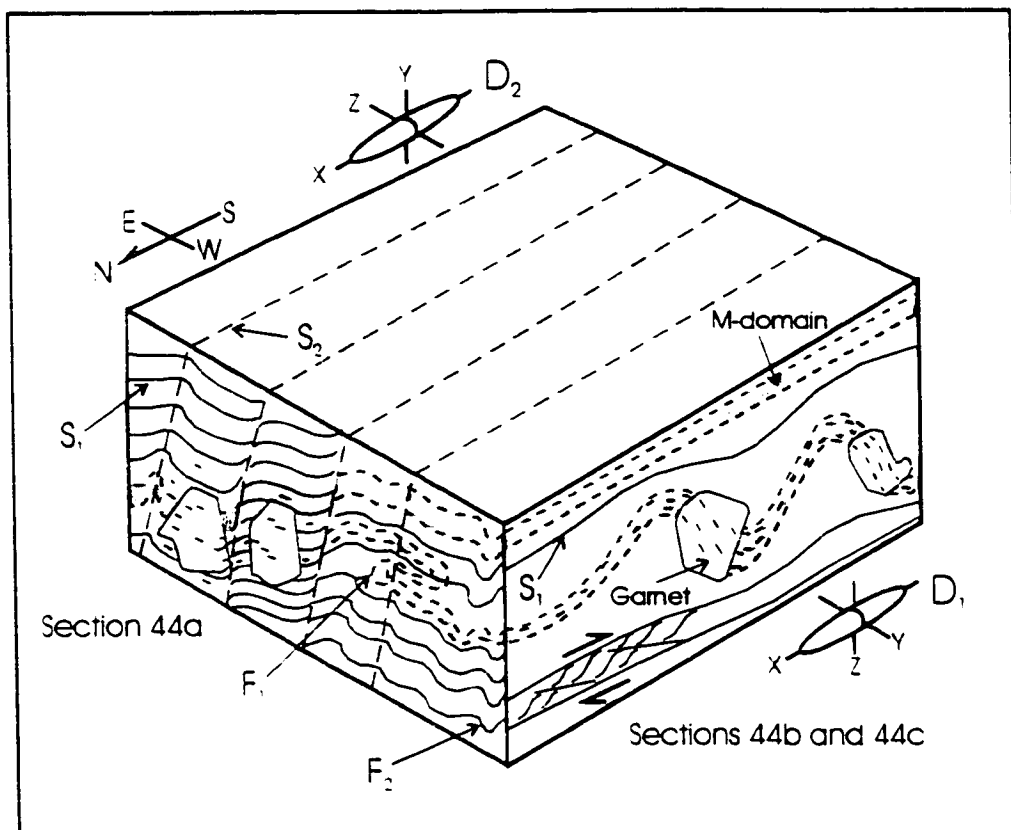


Figure 4.4 Schematic, composite sketch illustrating S_1 - S_2 relationships and fabric geometries in garnet porphyroblastic MBG schist south of South Brook town. Curved S_1 provide evidence for synchronous shear parallel to S_1 and S_2 . The D_1 and D_2 strain ellipses are idealized, and are meant to illustrate the coaxiality of D_1 - D_2 structures. See text for detailed discussion.

F_2 fold that plunges shallowly south. The F_2 fold is associated with a subvertical, north-striking, axial planar S_2 crenulation cleavage defined by foliated biotite and muscovite. S_2 cuts a subhorizontal S_1 fabric defined by domains of fine-grained, foliated muscovite, biotite, and opaque mineral grains, alternating with domains of very fine- to medium-grained quartz and plagioclase. The line of intersection of the orthogonal S_1 - S_2 fabrics defines a L_{1-2} intersection lineation that plunges shallowly south. S_1 is axial planar to tight, intrafolial, asymmetric F_1 microfolds. In addition, both S_1 and S_2 are folded by open, recumbent F_3 crenulations that plunge shallowly south. Thus, D_1 , D_2 and D_3 structures are well developed in sample SA-93-44, and three subvertical thin sections were cut in order to facilitate the microstructural analysis. Section 44a is perpendicular to L_{1-2} (i.e., parallel to the Y-Z plane of the D_2 finite strain ellipsoid), whereas sections 44b and 44c are parallel to L_{1-2} (i.e., parallel to the X-Y plane of the D_2 finite strain ellipsoid), and were cut with the intention of examining D_1 structures in the relative absence of D_2 structures.

Section SA-93-44a - In section 44a, quartz and plagioclase form equant to slightly tabular grains with undulose extinction, and angular to polygonal to slightly sutured grain boundaries. Garnet porphyroblasts preferentially overgrew S_1 mica-rich domains and are <1mm in diameter, idioblastic, and contain trails of tabular opaque inclusions (S_1) which are continuous with the external S_1 . In several locations, S_1 is curvilinear, and continuous into domains of crenulated S_1 and/or the S_2 crenulation fabric (Fig. 4.3b). In addition, garnet porphyroblasts with straight to curved S_1 subparallel to S_1 are locally completely enclosed within oblique S_2 fabric domains. Collectively, these relationships indicate garnet growth in the early stages of the crenulation of S_1 by S_2 . The sense of transposition of S_1

along S_2 crenulation planes consistently indicates west-side-up shear, consistent with an oblique-shear folding mechanism for the mesoscopic F_2 fold.

Sections SA-93-44b and 44c - In contrast to the generally equant shape of quartz grains in section 44a, highly elongate quartz ribbons are abundant in sections 44b and c, and indicate a quartz-grain lineation. Quartz ribbons are parallel or slightly oblique (see below) to S_1 , and are interpreted as an L_1 quartz lineation which parallels the north-south trending, subhorizontal L_{1-2} noted in outcrop and hand sample. Kinematic indicators, including abundant shear bands, mica fish, C-S fabrics, and domains of asymmetrical quartz ribbons oriented slightly oblique to S_1 , consistently indicate top-side to the south sense of shear along S_1 . In addition, the S_1 fabric and mica-rich domains are folded into trains of open, locally intrafolial, south-verging, asymmetrical microfolds to which the oblique quartz-ribbon fabric is axial planar. These folds are interpreted as drag-folds formed through rotation of S_1 during progressive non-coaxial shear parallel to S_1 (e.g., Lister and Snoke 1984). The microfolds are only developed in association with garnet porphyroblasts that are invariably located on the short (south) limb of the microfolds. These porphyroblasts have straight to south-verging sigmoidal S_1 that are continuous into the folded S_1 on the short limbs of the folds, and are consistently oriented $\sim 10-65^\circ$ clockwise (looking east) to the unfolded S_1 (Fig. 4.3c and 4.4). Thus, the S_1 - S_e relationships and kinematic indicators strongly suggest synkinematic growth of the garnet during folding and rotation of S_1 in south-directed non-coaxial shear parallel to S_1 .

To summarize, the garnet porphyroblasts in section 44a apparently grew syn- D_2 , whereas those in sections 44b and 44c apparently grew syn- D_1 (Fig. 4.4). One method of

reconciling the apparently conflicting timing relationships would be to argue that the microfolds in 44b and 44c represent oblique sections through F_2 crenulations, and the sigmoidal inclusion trails in garnet simply result from passive syn- S_2 overgrowth of these crenulations. However, this hypothesis is unlikely for the following reasons: 1) the thin sections were cut parallel to the F_2 crenulation axes; 2) the microfolds, unlike the F_2 crenulations, are locally intrafolial in S_1 ; 3) the F_2 crenulations have a variable sense of asymmetry, but the garnet porphyroblasts in sections 44b and 44c always have the same sense of S_1 asymmetry, and are always located on the south limb of consistently south-verging microfolds; and 4) the sense of rotation indicated by sigmoidal S_1 , rotated (folded) S_1 , and the kinematic indicators is mutually consistent.

The microstructures in sample SA-93-44 are interpreted to result from growth of the garnet porphyroblasts (i.e., peak metamorphism in this area) during south-directed shear parallel to S_1 (D_1) and upright folding and cleavage development (D_2). Thus, D_1 - D_2 structures in this location apparently evolved synchronously. On a larger scale, these relationships may indicate that D_1 - D_2 involved synchronous non-coaxial shear along two orthogonal, subvertical and subhorizontal, shear planes, and is thus by definition a wrench-shear. The significance of these observations is discussed in Section 4.3.

4.2.3 D_3 deformation

Structures associated with D_3 deformation comprise an S_3 fabric, F_3 folds, L_3 intersection lineation, and possible D_3 shear zones (Fig. 4.1). These structures are heterogeneously developed in the areas immediately south and east of Ming's Bight, but are particularly abundant in the north-central portions of the PHG, where they correspond

to D_3 of Gale (1971), Tuach (1976), and Tuach and Kennedy (1978). In general, S_3 is a crenulation fabric (Fig. 4.3d) that dips shallowly southwest to southeast, and is defined by fine-grained foliated biotite and/or muscovite, consistent with syn-deformational greenschist facies metamorphism. Locally, S_3 comprises a penetrative foliation in MBG and PROC rocks in the Deep Cove area, and in the PHG west of the Dunamagon Granite.

S_3 is axial planar to open, recumbent to reclined F_3 folds that plunge shallowly south and north (Fig. 4.3e). F_3 folds are typically symmetrical, and account for the great-circle distribution of the poles to S_1 and S_2 in Figure 4.1. Large F_3 folds with >20m wavelengths and amplitudes occur in the Deep Cove - Jimmy Cove area, and are locally associated with a prominent crenulation cleavage (Map 4; Fig. 4.3d). The geometry of these folds is identical to F_3 folds described by Gale (1971) and Tuach (1976). In many locations, particularly in the MBG, F_3 folds are only developed as a gentle crenulation of S_1 - S_2 fabrics. These F_3 folds are associated with a very prominent L_3 intersection lineation resulting from the intersection of S_1 - S_2 with recumbent F_3 crenulations and the axial planar S_3 (Fig. 4.1). The F_3 folds and L_3 intersection lineation are particularly prominent in the hangingwall of the D_2 shear zone in Actinolite Bay (Cross section 4). F_3 folds are mostly coaxial with F_2 folds; however, in some locations F_3 axes are slightly discordant to F_2 axes, and in one location the L_3 intersection lineation plunges shallowly to the north, and overprints the L_2 intersection lineation that plunges shallowly south.

Regionally, D_3 deformation is probably associated with shallowly south-dipping shear zones that post-date D_2 structures, but pre-date faults associated with D_4 . One of these shear zones is well exposed in MBG schist along the south shore of Ming's Bight

(Map 5). This shear zone is 2-4 m thick, and comprises disrupted layers of massive psammite in a matrix of semi-pelitic schist. The matrix contains an anastomosing foliation that dips moderately south, and a down-dip slickenline and chlorite lineation. In thin section, the foliation is defined by sutured quartz ribbons, and fine-grained biotite and muscovite, and is locally transected by zones of fine-grained cataclasite. A narrow quartz vein in the shear zone is offset by a series of steeply south-dipping, en-echelon, brittle-ductile shear fractures, and the tips of the quartz vein are drag-folded along both margins of the shear zone. All of these features indicate normal-sense shear. The hangingwall and footwall contacts of the shear zone are sharp, and the shear zone fabric is not developed in the adjacent MBG schists. The shear zone cuts layering and D_1 - D_2 structures in the MBG, and is not folded. In one location, a ~20 cm thick planar quartz vein cross-cuts F_2 folds in the MBG schist and is truncated by the shear zone, evincing the temporally distinct nature of the shear zone and D_2 deformation. To the west, the shear zone is truncated, and offset, by a dextral-normal oblique-slip fault that dips moderately northwest, and is ascribed to D_4 . The post- D_2 , pre- D_4 relative age of the shear zone is consistent with south-directed normal shearing during D_3 .

A structurally similar shear zone is exposed ~3 km south of Ming's Bight along Ming's South Brook (Map 6). In this location, the shear zone is defined by a ~10-15m thick zone of penetratively foliated talc-serpentine-carbonate schist in altered PROC ultramafic rocks. The foliation in this shear zone dips shallowly to the southwest and southeast, and contains a mineral lineation that plunges south. Asymmetric shear bands associated with these fabrics consistently indicate south-side-down shear. In the footwall

and hangingwall of the shear zone, a penetrative S_2 foliation that dips steeply west is transposed over ~5m into the shallowly south-dipping shear zone fabric (Map 6). The S_2 foliation is associated with the shear zone that dips steeply west and bounds the eastern contact of the PROC ultramafic rocks. This shear zone contains asymmetric shear bands and a shallowly-plunging hornblende lineation that indicate high-temperature, sinistral transcurrent shear. In one location, S_2 in the footwall of the shear zone that dips south is folded by a series of open to tight, recumbent F_3 folds that plunge shallowly south. The axial planes of these folds are parallel to the foliation in the south-dipping shear zone, which may indicate that these structures are coeval.

The field relationships described above indicate that D_3 deformation may have involved south-directed, normal-sense shear which, coupled with the orientation of the S_3 crenulation cleavage and recumbent F_3 folds, suggests a bulk extensional D_3 stress regime, as inferred by DeGrace et al. (1976). Significantly, S_3 in MBG schist east of Deep Cove (Maps 4 and 7) transposes S_2 , and can be traced, apparently continuously, into south-dipping extensional fabrics along the northern contact of the Dunamagon Granite (i.e., Pacquet Harbour S_2 - S_3). These relationships suggest that D_3 in the Ming's Bight area may have been diachronous with extensional deformation in the Pacquet Harbour area. The extensional shear zone in the area of Map 6 is inferred to continue northeastward (Map 4), and merge with the shear zone along the northern contact of the Dunamagon Granite. Toward the west, the trace of this shear zone is indeterminate.

4.2.4 D_4 deformation

D_4 structures are heterogeneously developed along the southern shore of Ming's

Bight, but become pervasive north of the small granitic intrusions on the eastern shore of Ming's Bight (Maps 5 and 7). They comprise an S_4 foliation, rare L_4 mineral and stretching lineation, and F_4 folds, which are spatially associated with a series of D_4 ductile to brittle-ductile shear zones. The main D_4 shear zone is exposed in Grand Toss Cove (the Grand Toss Cove shear zone; GTCSZ), and can be traced continuously southward to Deep Cove where it defines the southeastern margin of the PROC rocks (Map 4). This west-dipping shear zone represents the locus of D_4 strain in the Ming's Bight area, and separates MBG schist in the footwall from PROC lithologies in the hangingwall.

The GTCSZ is associated with a prominent system of topographic lineaments that anastomose around >200m long lozenges of MBG schist (Fig. 4.5a). In the field, these lineaments coincide with a system of <200m thick brittle-ductile shear zones that define the main GTCSZ as well as a series of associated splay-shears, the most prominent of which is exposed in Caplin Cove (Map 7). The GTCSZ is best exposed in MBG schists along the western shore of Grand Toss Cove. In this location, the shear zone is 200-300m thick, and is characterized by a series of <10m thick mylonite zones that are preferentially developed in semi-pelitic schist and anastomose around disrupted pods of relatively massive psammite. The mylonite contains a shallowly west-dipping, S_4 foliation (Fig. 4.6) defined by fine- to coarse-grained foliated muscovite and biotite, and elongate, sutured quartz ribbons. The biotite and muscovite locally form prominent asymmetric mica-fish. The foliation is anastomosed around medium- to coarse-grained, equigranular, recrystallized quartz-plagioclase lozenges, and large, subhedral, poikiloblastic plagioclase porphyroblasts. S-C fabrics, shear-bands, mica fish, and offset quartz veins consistently

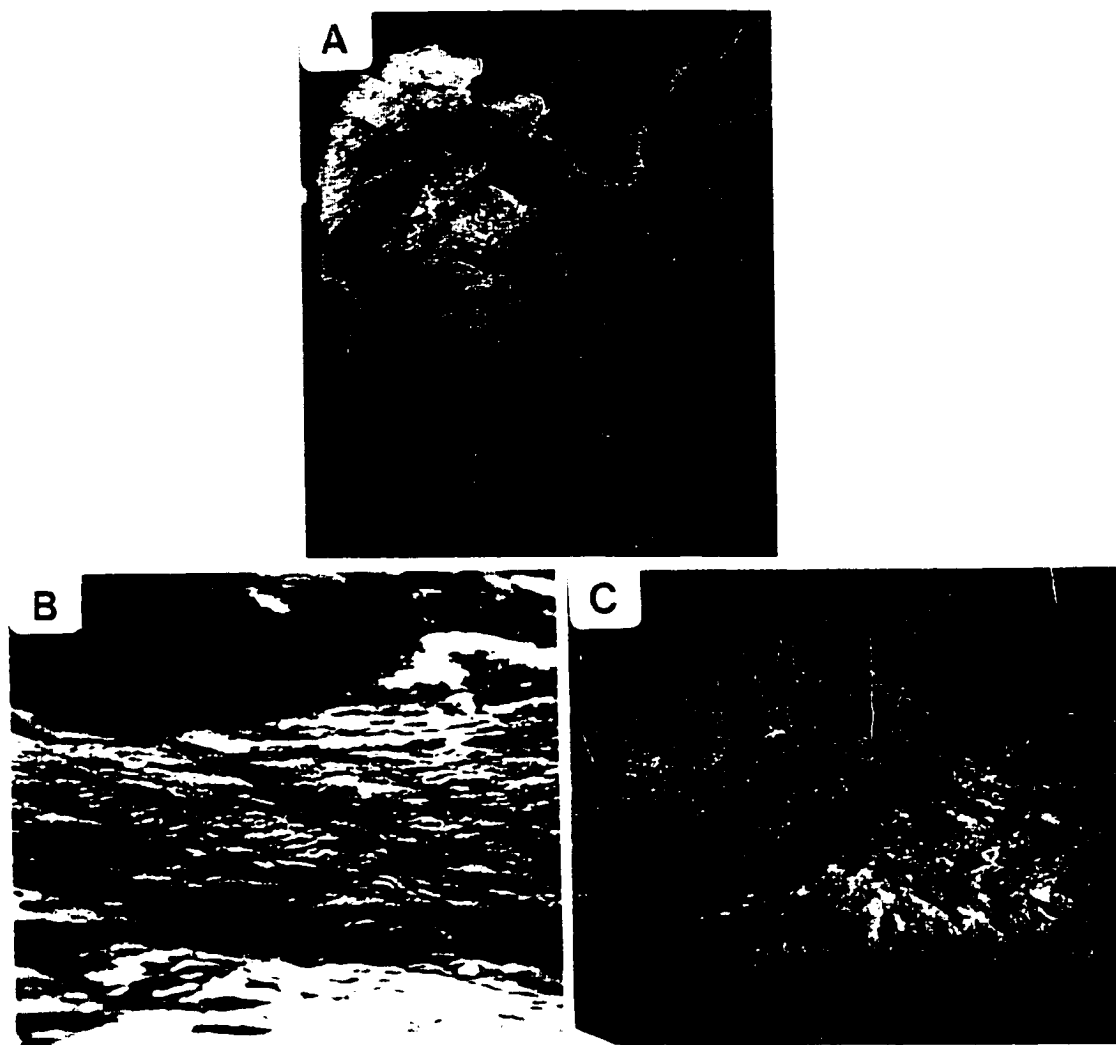


Figure 4.5 Photographs of D_4 structures in the Grappling Point area (Map 7). a) Airphotograph illustrating the anastomosed series of topographic lineaments which correspond to D_4 and D_5 shear zones in the field. GTCSZ is marked by the prominent series of lineaments trending southward from Grand Toss Cove (arrowed). b) S-C mylonite and shear bands in the GTCSZ in Grand Toss Cove (facing west; dextral shear). c) Reclined, asymmetric F_4 folds (on right) that plunge shallowly west cut by a D_5 shear zone (on left) that dips northwest. Outcrop is located south of Ming's Tickle in Ming's Bight (facing east; Map 8; outcrop height is ~4-5m).

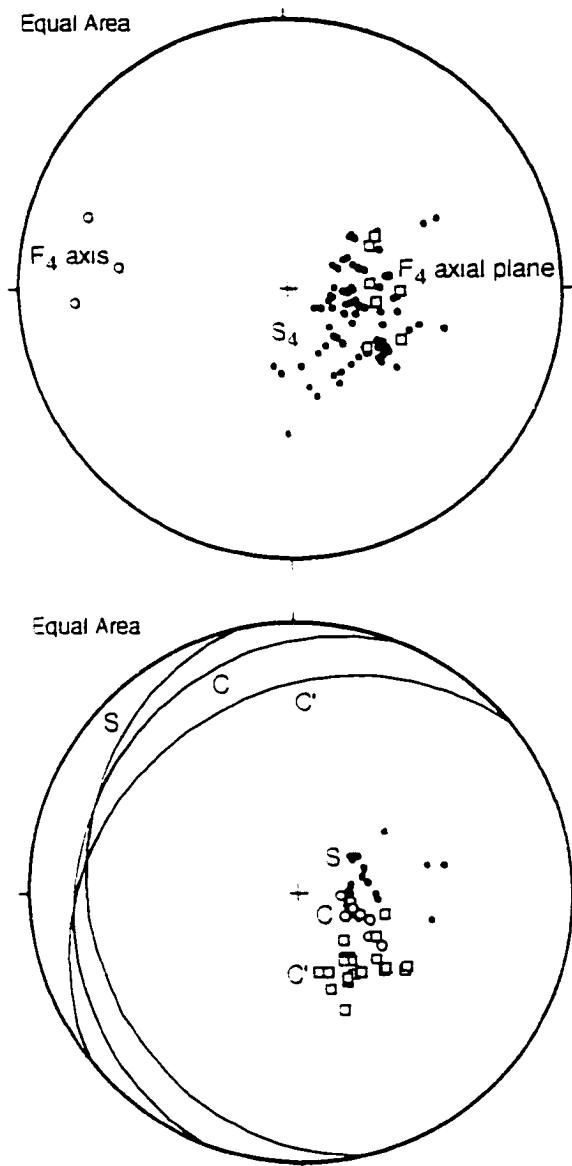


Figure 4.6 Lower hemisphere, equal area projections of structural data from the GTCSZ in Grand Toss Cove. Planar structural elements are plotted as poles. F₄ axial planes, n=7; F₄ axes, n=3; S₄ (mylonitic foliation), n=78; C-planes, n=10; S-planes, n=19; C'-planes (shear bands), n=21. Note that the line of intersection of the C-, S-, and C'-planes plunges shallowly west, subparallel to the F₄ axes.

indicate a dextral sense of shear (Figs. 4.5b and 4.6). The intersection lineation between the S, C, and C' planes plunges shallowly to the west, suggesting strike-slip shear along the shallowly west-dipping mylonite (Fig. 4.6). Rarely, a lineation defined by biotite and muscovite plunges shallowly to the southwest, consistent with a slight component of dextral-reverse oblique-slip shear. Local brittle-ductile shear fractures associated with the mylonite consistently indicate dextral-normal oblique-slip shear. These features may indicate that the movement vector of the GTCSZ progressively evolved from dextral-reverse to dextral-normal.

The mylonitic S_4 is axial planar to open to isoclinal, reclined F_4 folds that plunge shallowly west and verge predominantly north (Fig. 4.6). The folds are most common in the massive, weakly foliated, psammite layers, and tend to have somewhat more open profiles than F_4 folds within the semi-pelitic layers. Typically, the S-planes of the S-C mylonites are parallel to the F_4 axial planes, and F_4 hinge lines are oriented subparallel to the S-C-C' intersection lineation (Fig. 4.6). F_4 hinges are also locally curvilinear in S_4 . In one location, the hinge of an F_4 fold has been offset in a dextral sense parallel to the axial planar S_4 . These features are compatible with folding during shear in the GTCSZ.

In Deep Cove and Jimmy's Cove Brook, the GTCSZ contains veins, stringers, and up to ~20m thick (limit of outcrop) zones of maroon-grey, fine-grained, massive cataclasite and ultracataclasite, which may indicate either: 1) contemporaneous ductile and brittle D_4 deformation in the GTCSZ, reflecting factors like transient changes in strain rate or fluid pressure (e.g., Sibson 1977; Handy 1989; Hanmer 1989; Hadizadeh et al. 1991); 2) a progressive evolution from ductile to brittle D_4 deformation; or 3) reactivation during

later (D_5) deformation.

On a 'regional' scale, S_4 is typically developed as a spaced crenulation cleavage. In the MBG, this cleavage is defined by foliated, fine- to coarse-grained biotite and muscovite, that anastomose around large albite porphyroblasts. This foliation is axial planar to open to isoclinal, reclined F_4 folds that plunge shallowly west (Fig. 4.1; Fig. 4.5c). These folds are regionally pervasive in MBG schist, and in units of greenschist and amphibolite between Grappling Point and Caplin Cove. In the area around Ming's Tickle and Grappling Point, metre-scale F_4 folds have open, symmetrical, profiles, suggesting the presence of a large-scale F_4 fold hinge in this area. In contrast, the large unit of MBG schist that outcrops between Ming's Tickle and Caplin Cove contains metre-scale, tight to isoclinal, south-verging F_4 folds, suggesting a large-scale F_4 fold limb (Map 8; Fig. 4.5c).

D_4 structures become less abundant towards the south, and along the south shore of Ming's Bight probable D_4 structures form discrete brittle-ductile shear zones and faults that transect pre- D_4 structures. Some of these shear zones may be more appropriately ascribed to the D_5 deformation episode. However, the F_4 folds are generally not developed along the south shore of Ming's Bight, and therefore the timing relationships between the shear zones and F_4 folds could not be unambiguously determined. The orientation and sense of movement of these shear zones are more consistent with D_3 shear zones, and these structures are therefore correlated. Two examples of these shear zones are described below.

(1) In several locations, there is evidence to suggest that D_2 structures were locally reactivated by D_4 shear zones. For example, D_1 - D_2 - D_3 structures in the D_2 shear zone in

Actinolite Bay are transposed by a ~10m thick shear zone comprising quartz-veined chlorite-actinolite schist (Map 5; Cross-section 4). The shear zone contains a penetrative fabric that dips moderately west, and is defined by foliated chlorite, actinolite, and elongate pods and stringers of quartz. The fabric is axial planar to inclined, tight to isoclinal folds that plunge shallowly west and are found only within the shear zone. The fabric in the axial region of the fold is cut by a series of dextral-normal shear fractures that dip moderately northwest and contain a slickenline lineation that plunges northeast. These structural relations may indicate synchronous folding and dextral-normal shearing. The structural association of folds that plunge shallowly west, west-dipping foliation, and dextral-normal oblique-slip shearing is typical of D_4 shear zones.

(2) An array of brittle-ductile shear zones and faults occurs in MBG schist along the south shore of Ming's Bight; a good example is exposed along the western shore of Birchy Cove (Map 5). In this location, D_2 - D_3 structures in the MBG are cross-cut by a ~50cm thick shear zone that dips shallowly northwest. Ductile structures within the shear zone comprise an oblique shear-fabric, S-C fabrics, and shear bands, which collectively indicate dextral-normal oblique-slip shear. The ductile fabrics contain a chlorite and slickenline lineation that plunges shallowly northeast, and locally contain zones and/or lozenges of brecciated MBG schist. In these zones, ductile microstructures in quartz and plagioclase, including undulose extinction and highly sutured grain boundaries, are cross-cut by fine-grained zones of cataclasite. The shear zone is associated with brittle-ductile R, X', and X shear-fractures (e.g., Swanson 1988) which have various senses of movement, depending on their orientation with respect to the main shear zone.

Collectively, D_4 deformation structures are interpreted to record a progressive transition from dextral strike-slip and/or dextral-reverse oblique-slip, ductile shear to dextral-normal oblique-slip, brittle-ductile shear.

4.2.5 D_5 deformation

D_5 structures comprise a series of shear zones that are well exposed along the coast between Caplin Cove and Ming's Tickle, and diminish to the south (Map 8). These shear zones contain penetrative mylonitic S_5 foliations, L_5 mineral and stretching lineations, and F_5 folds which are associated with progressive ductile shear, and are only developed within the D_5 shear zones. The shear zones are separated on the basis of orientation into northerly- and southerly-dipping sets, which are described separately below.

4.2.5.1 Northerly-dipping D_5 shear zones

Two northerly-dipping D_5 shear zones are developed approximately 300m south of Ming's Tickle (Maps 7 and 8; Cross-section 6a; Fig. 4.7). The northern shear zone juxtaposes MBG schist in the hangingwall against MBG schist in the footwall, whereas the southern shear zone juxtaposes greenschist and amphibolite of PROC affinity in the hangingwall against MBG schist in the footwall. Each of these shear zones is approximately 15-20m thick, and comprises a series of discrete, northwest-dipping, high strain zones that anastomose around lower-strain blocks of MBG schist. These shear zones are associated with extensive chloritization and quartz veining. The salient structural features and overprinting relationships are well exposed in the northernmost shear zone (the Northern Ming's Tickle Shear Zone; NMTSZ; Map 8), and the following description

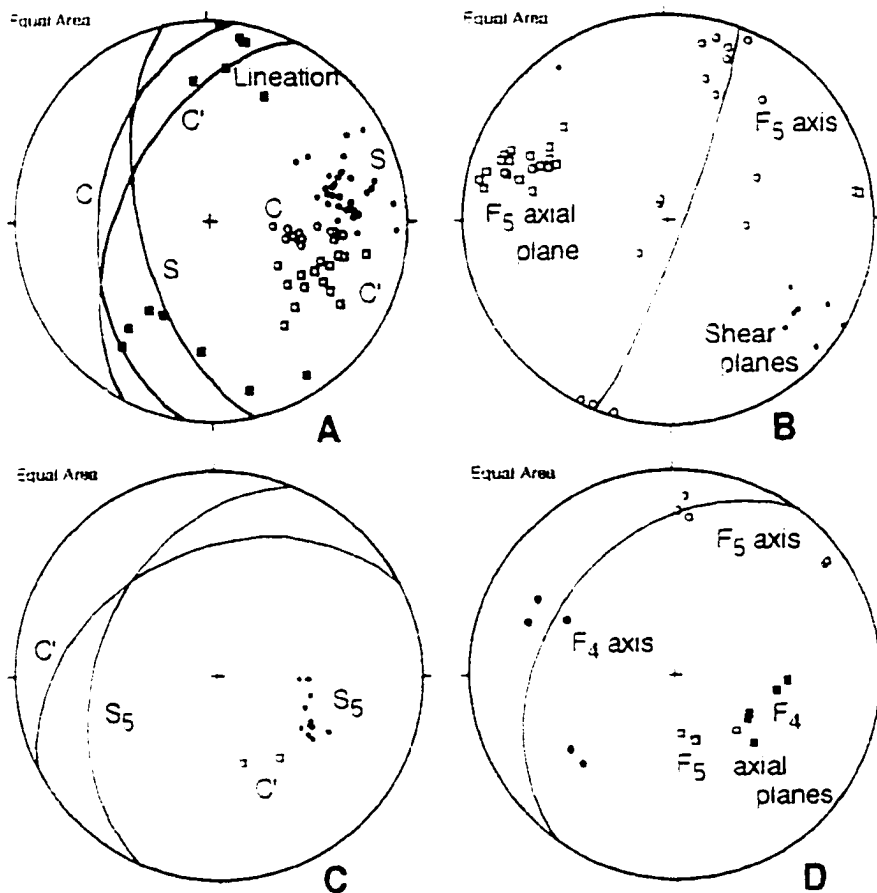


Figure 4.7 Lower hemisphere, equal area projections of structural data from northerly-dipping D_5 shear zones south of Ming's Tickle (Map 8; Cross section 6a). Planar structural elements are plotted as poles. a) and b) Structural data from the NMTSZ. C-planes, $n=14$; S-planes, $n=32$; C'-planes (shear bands), $n=16$; L_5 , $n=14$; F_5 axial planes, $n=22$; F_5 axes, $n=16$; discrete shear planes in hangingwall, $n=8$. c) and d) Structural data from the southern northerly-dipping D_5 shear zone. Mylonitic foliation, $n=11$; C'-planes (shear bands), $n=2$; F_5 axial planes, $n=3$; F_5 axes, $n=5$; F_4 axial planes in footwall, $n=5$; F_4 axes in footwall, $n=5$.

is based mainly on this shear zone.

Hangingwall Mylonite - The hangingwall of the NMTSZ contains a ~5-10m thick unit of mylonitized MBG schist. The mylonite lies in sharp contact with the structurally underlying altered chlorite schist in the NMTSZ, and grades structurally upward into typical, layered MBG schist. In the immediate hangingwall of the chlorite schist, the mylonitic fabric is penetrative, markedly planar, dips moderately northwest, and is defined by foliated fine- to medium-grained biotite and muscovite, wispy compositional layering, and boudinaged quartz veins. The 'planar' mylonite is ~1m thick, and grades structurally upward into strongly folded mylonites. In these rocks, the mylonitic fabric is folded by numerous open to moderately tight, upright folds with a consistent Z-sense of asymmetry (looking northeast). These folds decrease in abundance structurally upward into the MBG schist, and are only well developed in the hangingwall mylonites. These relationships suggest that the folding is related to the mylonitization. The folds have upright axial planes that dip steeply southeast, and are consistently oriented ~10-45° counterclockwise from the mylonitic foliation (looking northeast; Fig. 4.7b). In some locations a spaced, axial planar crenulation fabric is associated with the folds. The folds are developed in trains, and individual folds within the trains have similarly oriented axial planes, but radically variable hinge-line orientations that define a partial great circle girdle (Fig. 4.7b). No overprinting relationships were observed between individual folds, suggesting that the folds are the product of a single deformation. These folds are locally associated with asymmetric, shear-modified boudins of mylonite, which indicate a reverse shear along the mylonitic fabric (Hanmer and Passchier 1991), consistent with the sense of fold asymmetry, and the

angular relation between the fold axial planes and mylonitic fabric. Euhedral pyrite crystals without strain shadows and cross-cutting quartz veins indicate that the mylonite pre-dates the alteration that accompanied shearing in the interior of the NMTSZ.

To the north of the NMTSZ, the upright folds with variable plunges gradually diminish over ~50m, and the reclined F_4 folds that plunge west become prominent. The F_4 folds do not occur within the mylonite or the chlorite schists in the NMTSZ, and do not re-fold the upright folds associated with the mylonite zone. These relationships confirm the relative timing of D_4 and the D_5 shear zones, and indicate that the hangingwall mylonite probably formed in an early increment of shear in the NMTSZ (Cross-section 6a).

Interior chlorite schist - The interior of the NMTSZ contains highly altered chlorite schist. The alteration assemblage comprises fine- to medium-grained chlorite, carbonate, quartz, biotite, titanite, rutile, pyrite, white mica, and apatite. The protolith of the chlorite schist was probably the MBG, as indicated by the presence of numerous chloritized blocks of MBG schist, and detrital zircon grains in mineral separates. The chlorite schist also contains two <1x2m blocks of highly altered mafic volcanic rock. Since no mafic volcanic rock was noted in the MBG, these blocks probably represent 'exotic' fragments that were incorporated in the NMTSZ during D_5 shear, suggesting that the NMTSZ transects the PROC further to the west (see Section 4.2.6.2).

The chlorite schist contains abundant quartz veins (Fig. 4.8a). In higher-strain zones, the quartz veins are narrow, wispy, and contain thin slivers of foliated wall-rock. These veins parallel the penetrative foliation in the chlorite schist, commonly have striated surfaces, and are interpreted as fault-fill veins formed during shear in the high-strain zones

(e.g., Robert et al. 1994). In lower-strain portions of the NMTSZ, quartz veins are massive, billowy, and contain numerous randomly oriented blocks of chlorite schist and MBG schist. These veins are subparallel to the fabric in the NMTSZ, and are interpreted as breccia veins (e.g., Robert et al. 1994).

Two zones of particularly high strain in the chlorite schist are separated by a ~5m thick block of relatively low-strain MBG schist. The high strain zones are 1-2m thick, and are characterized by a penetrative chlorite foliation that dips moderately northwest. The foliation contains asymmetric S-C-C' fabrics that indicate dextral strike-slip shear (Figs. 4.7a and 4.8a). The foliation also contains a chlorite lineation that plunges shallowly northeast and southwest (Fig. 4.7a), and a slickenline/chlorite lineation is developed on the surfaces of the fault-fill veins. These lineations indicate that the dextral strike-slip shearing was accompanied by components of normal and reverse oblique-slip. No systematic overprinting relationships were noted between the lineations; however, the presence of pre-alteration mylonite with evidence for reverse movement in the hangingwall indicates that dextral-reverse shear probably pre-dated dextral-normal shear.

At the contact between the hangingwall mylonite and one of the high-strain chlorite schist zones, tabular 'rafts' of foliated, quartz-veined MBG mylonite occur within the chlorite schist. The chlorite schist surrounding the rafts contains up to 25% rutile and titanite porphyroblasts. These porphyroblasts range in size up to 1x2cm, and are euhedral to anhedral, elongate, and generally randomly oriented. In some locations, there is a clear transition from unaltered MBG mylonite with a penetrative planar fabric, to slightly chloritized mylonite with rare, fine-grained rutile-titanite, to strongly chloritized mylonite

Figure 4.8 Field photographs of D_5 structures in the Ming's Tickle area, and extensional structures in the PROC on the western shore of Ming's Bight south of Big Head. **a)** Example of a narrow zone of chloritic schist in the NMTSZ (facing northeast). Note the prominent asymmetric shear bands (dextral), fault-fill veins (left), and breccia veins (right). **b)** Photomicrograph (X-Z section) of a quartz-ribbon mylonite in MBG schist in the footwall of the middle southerly-dipping D_5 shear zone (Map 8). Shear bands and biotite fish indicate dextral (south-side-down) non-coaxial shear (long edge of the photo is ~ 0.5 mm). **c)** Zone of S-C mylonite in the northern southerly-dipping D_5 shear zone (photo taken subparallel to X-Z plane; dextral-normal oblique-slip shear). **d)** F_5 sheath fold developed in the footwall of the NMTSZ. **e)** Asymmetric fabric indicating north-side-down shear within a D_2 shear zone in the PROC south of Big Head. **f)** Example of a D_3 shear zone that dips steeply north in the PROC near Point Rousse. North-side-down shear is indicated by the 'dragged' S_1 fabric, the obliquity of the fault-fill veins, and the prominent shear band in the lower-central portion of the shear zone (arrowed).

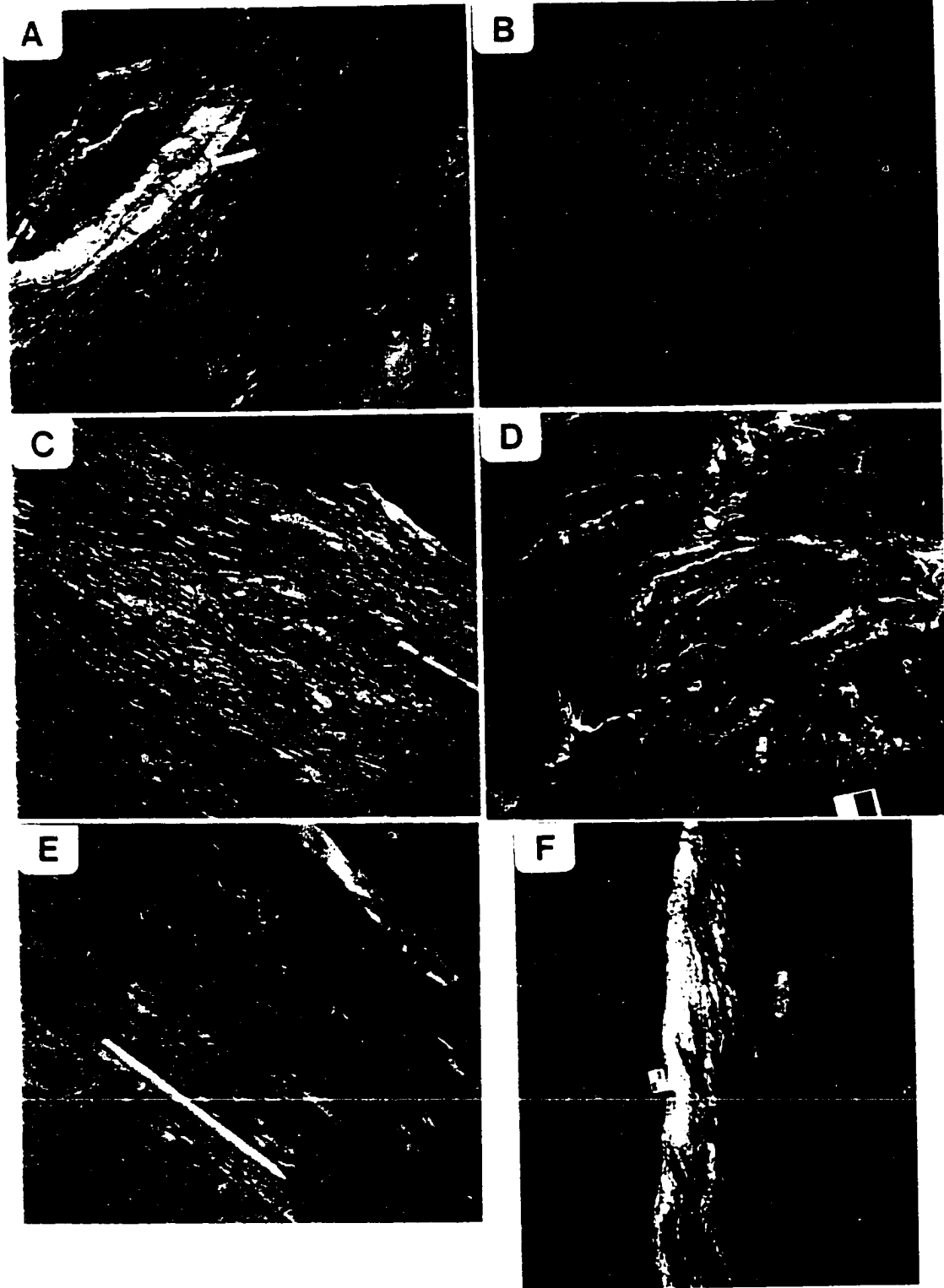


Figure 4.8

with abundant coarse-grained rutile-titanite, to chlorite schist with a weak fabric and abundant, coarse-grained rutile-titanite. These features suggest that growth of the titanite and rutile in the hangingwall mylonite occurred during the alteration that accompanied non-coaxial shear and development of the chlorite schist. Thus, the growth of these porphyroblasts is inferred to be closely bracketed by the dextral-reverse and dextral-normal non-coaxial shear in the NMTSZ (e.g., Gower 1993). U-Pb dates of 380-388 Ma from rutile and titanite (see Chapter 6) are interpreted to constrain the time of shearing.

Footwall MBG schist - In the footwall of both northerly-dipping D_5 shear zones there is a gradual change in the structural character of the MBG schists. Approximately 10m structurally below the footwall, the MBG schists are well layered, and folded by open to tight, reclined south-verging F_4 folds that plunge west (Figs. 4.5c and 4.7d). However, structurally upward into the footwall of the D_5 shear zones, the MBG layering becomes indistinct, and an anastomosing, moderately northwest-dipping foliation defined by white mica, chlorite, and boudinaged quartz veins becomes prominent. In addition, F_4 fold axes progressively rotate, and in the immediate footwall of the shear zone the folds verge north, plunge northeast, and have curvilinear fold axes. Sheath folds are common in these locations (Fig. 4.8d). The sheath fold culminations mainly plunge to the northeast, and are strikingly similar to the tubular fold culminations modeled by Skjernaa (1989). In the footwall of both shear zones, MBG schist is cross-cut by late, steeply northwest-dipping, brittle-ductile, dextral-normal oblique-slip faults, consistent with a progression from ductile to brittle shear.

On a large scale, D_5 shear zones transect F_4 folds, and are thus ascribed to a later

deformation phase (Fig. 4.5c). However, the northerly-dipping D_5 shear zones also apparently merge with the GTCSZ in Grand Toss Cove (Map 7; Fig. 4.5a). Furthermore, one of these shear zones apparently records a transition from dextral-reverse to dextral-normal oblique-slip shear and brittle-ductile faulting. These relationships are compatible with D_5 shearing during, or in a later increment of, a progressive D_4 - D_5 deformation.

4.2.5.2 Southerly-dipping D_5 shear zones

Three southerly-dipping shear zones are developed between Ming's Tickle and Caplin Cove (Map 8; Cross-sections 6a and 6b; Fig. 4.9). The northern and middle shear zones juxtapose MBG schist in the footwall against greenschist and amphibolite in the hangingwall, whereas the southern shear zone juxtaposes greenschist and amphibolite in the footwall against metasediments and metagabbro in the hangingwall. These shear zones range in thickness from ~5m to ~15m, and have similar structural characteristics.

Footwall Mylonites - The footwalls of the southerly-dipping D_5 shear zones contain 1-5m thick units of mylonite. In the footwall of the northern and middle shear zones, layered MBG schist containing well-developed F_4 folds is clearly transposed into a mylonitic fabric defined by foliated muscovite and biotite, and quartz ribbons (Fig. 4.8b). Plagioclase within this mylonite occurs as anhedral, equant porphyroclasts, and elongate sutured ribbons. Shear bands and mica fish within the mylonite indicate dextral-normal oblique-slip shear (Fig. 4.8b).

In the footwall of the southern shear zone, pyroxene pseudomorph-bearing greenschist is transposed into a ~3m thick zone of penetratively foliated and lineated amphibolite. The transition from greenschist to amphibolite occurs over ~2m, and the

Figure 4.9 Lower hemisphere, equal area projections of structural data from southerly-dipping D_5 shear zones south of Ming's Tickle (Map 8; Cross sections 6a and 6b). Planar structural elements are plotted as poles. Fold axes and fold axial planes are plotted as circles and squares, respectively in 4.9b and 4.9e. **a)** and **b)** Structural data from the northern southerly-dipping D_5 shear zone. C-planes, $n=15$; S-planes, $n=7$; C'-planes (shear bands), $n=4$; L_5 , $n=18$; F_5 axial planes, $n=5$; F_5 axes, $n=8$; F_4 axial planes in hangingwall, $n=5$; F_4 axes in hangingwall, $n=4$. **c)** Structural data from the middle southerly-dipping D_5 shear zone. C-planes, $n=4$; S-planes, $n=6$; C'-planes (shear bands), $n=4$; L_5 , $n=9$. **d)** and **e)** Structural data from the southern southerly-dipping D_5 shear zone. C-planes, $n=6$; S-planes, $n=9$; C'-planes (shear bands), $n=2$; L_5 , $n=2$; F_5 axial planes, $n=2$; F_5 axes, $n=2$; S_5 mylonitic foliation, $n=28$; F_4 axial planes in hangingwall, $n=11$; F_4 axes in hangingwall, $n=9$.

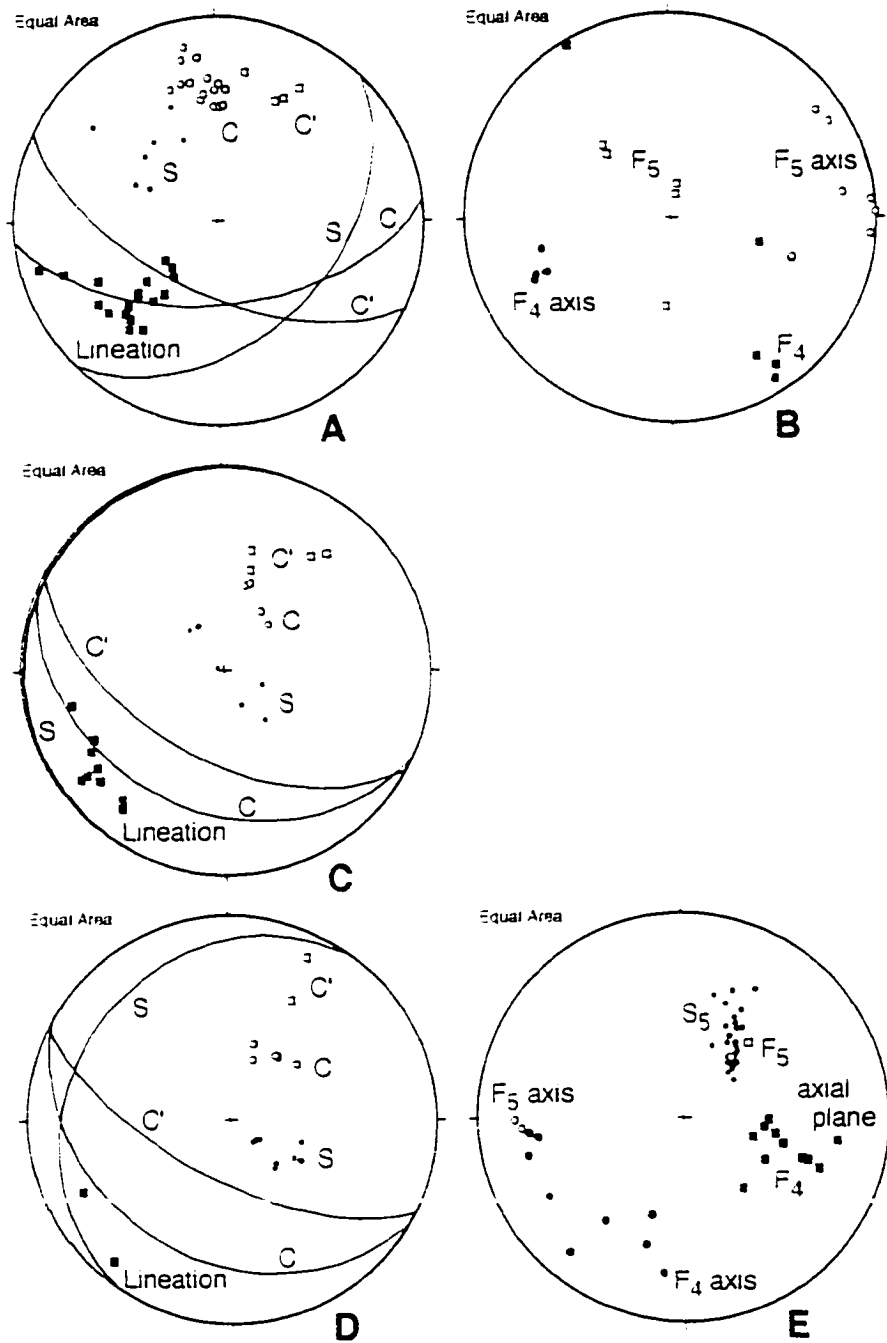


Figure 4.9

amphibolite contains rare shear boudins of pyroxene greenschist, indicating that the amphibolite probably formed through shear-related recrystallization of the greenschist. The amphibolite is dark grey-black, and contains up to 35%, fine- to coarse-grained, euhedral, acicular hornblende porphyroblasts in a very fine-grained, granular, quartz and plagioclase matrix with a strong crystallographic preferred orientation. The penetrative foliation and lineation, coupled with the crystallographic preferred orientation in the matrix, are consistent with high strains. However, the hornblende porphyroblasts within the amphibolite do not appear to be significantly strained, and lack strain shadows. These features may indicate that recrystallization of hornblende occurred during, and subsequent to, shearing. This hypothesis is supported by the local random orientation of hornblende within, and across, the foliation plane. The amphibolite contains a prominent mylonitic layering that dips southwest and is parallel to the penetrative hornblende foliation and shallowly west-plunging lineation. The layering within the amphibolite is folded by open to tight, inclined F_3 folds that plunge shallowly west and verge downward. The axial planes of these folds are parallel to the foliation in the amphibolite, and the axes nearly parallel the hornblende lineation (Fig. 4.9e).

Interior S-C mylonites - The footwall mylonites lie in sharp to gradational contact with structurally overlying S-C mylonites that characterize the southerly-dipping shear zones (Figs. 4.8c, 4.9a, 4.9c, 4.9d). The S-C mylonites mainly occur within greenschist and amphibolite in the interior of the shear zones. In these rocks the mylonitic fabric comprises anastomosed S, C and C' planes (shear bands) which are defined by foliated biotite, hornblende, and elongate, sutured quartz ribbons. The S-C fabrics contain a

chlorite and hornblende mineral lineation that plunges southwest, as well as a rare stretching lineation defined by quartz-filled strain shadows on pyroxene pseudomorphs. In the northern shear zone, hornblende porphyroblasts are lineated in both the C- and S-planes. In many locations, hornblende porphyroblasts are randomly oriented within and across the S-C fabrics, suggesting that hornblende growth outlasted shearing. The orientation of the lineation and the sense of asymmetry of the S-C fabrics are consistent with dextral-normal oblique-slip shear in the D_5 shear zones.

The S-planes in the S-C mylonites are axial planar to asymmetric microfolds in thin section and mesofolds in outcrop (Fig. 4.9b), and are thus structurally similar to the S-C mylonites described by Berthé et al. (1979), White et al. (1980), and Lister and Snoke (1984). The vergence of these folds is consistent with the sense of shear recorded by the S-C fabrics, and the fold axes are locally subparallel to the intersection lineation of the S, C, and C' planes (Fig. 4.9b and 4.9e). These features are compatible with development of these folds during the dextral-normal shear in the D_5 shear zones (F_5 folding).

On the basis of mineral assemblage and fabric intensity, the S-C fabric in the middle shear zone can be separated into four distinct structural zones. In the footwall, the S-C fabrics are pervasively developed in quartz-ribbon and mica-fish mylonites derived from MBG schist (Zone 1; Fig. 4.8b). Structurally upward, these mylonites lie in sharp contact with a <1m thick unit of chlorite schist that contains pervasive S-C fabrics (Zone 2), and the chlorite schist grades structurally upward into a ~3-4m thick unit of hornblende mylonite (Zone 3). The hornblende mylonite contains pervasive, small-scale S-C fabrics, and grades structurally upwards into moderately well-foliated greenschists with a large-

scale, non-penetrative S-C fabric (Zone 4; Cross section 6b). The transition in S-C fabric geometry and intensity from Zone 3 to 4 is similar to that documented by Berthé et al. (1979), and is consistent with an increasing strain gradient towards the core of the shear zone. Furthermore, the transition from chlorite schist to amphibolite in the shear zone is consistent with progressive shearing from upper greenschist to lower greenschist facies metamorphic conditions (e.g., Lin 1995).

The hornblende mylonites in the middle shear zone contain a concordant, ~10m long, <1m thick unit of dark grey-black, coarse-grained metagabbro. In the interior, the metagabbro is only slightly deformed, and preserves a weak ophitic texture defined by randomly oriented, recrystallized, lath-shaped plagioclase phenocrysts, and ~20% coarse-grained, subhedral, randomly oriented, poikiloblastic hornblende. The metagabbro is wrapped around by, and apparently gradational with, dark green-black, fine-grained, Zone 3 hornblende mylonites. Shear bands and σ -type plagioclase porphyroclasts in the mylonite indicate a normal sense of shear, and the contacts of the metagabbro are offset and back-rotated by large-scale shear bands which also indicate normal shear. The apparent gradational contacts between the mylonite and the metagabbro indicate that, at least locally, the hornblende mylonite formed through intense deformation of the metagabbro. The plagioclase porphyroclasts in the mylonite may represent primary plagioclase phenocrysts derived from the metagabbro. These relationships are significant, since $^{40}\text{Ar}/^{39}\text{Ar}$ dating of hornblende of both the metagabbro and mylonite place some important constraints on the timing of D_5 deformation in the Ming's Bight area (see Chapter 6).

Hangingwall - The hangingwalls of the southerly-dipping shear zones comprise

moderately well-foliated greenschists, metasediments, and/or metagabbro. In the immediate hangingwall, the foliation in these rocks is parallel to S_5 fabrics in the shear zones. However, further upward in the hangingwall the foliation gradually changes orientation, and is locally axial planar to, or folded by, reclined F_4 folds that plunge west. Thus, the foliation in the hangingwall, at least locally, represents a pre to syn- S_4 fabric which was transposed into S_5 during the deformation that produced the shear zones.

In general, rocks in the hangingwalls of the southerly-dipping shear zones are significantly less deformed than rocks in the footwalls. In the southern shear zone for example, the hangingwall contains bedded metasediments. The bedding in these rocks is parallel to the shear zone, and pebble conglomerate layers contain well preserved graded bedding which indicates that the metasediments young to the southwest. The presence of lower strain rocks in the hangingwall can probably be attributed to the extensional character of the D_5 shear zones, since the hangingwalls of extensional shear zones generally contain rocks from relatively higher structural levels.

4.2.6 Point Rousse Ophiolite Complex

In order to facilitate a direct comparison of the structural geology of the eastern and western shores of Ming's Bight, the structural geology of the PROC was examined in the area south of Big Head (Map 9; Fig. 4.10). This area comprises clastic rocks and pillowed basalts of the PROC cover sequence, and was selected for structural analysis for two reasons: 1) the clastic rocks and pillowed basalts are well exposed and allow confident determination of younging directions; and 2) the bedding in the clastic rocks represents a major anisotropy, and consequently structures such as folds and shear zones

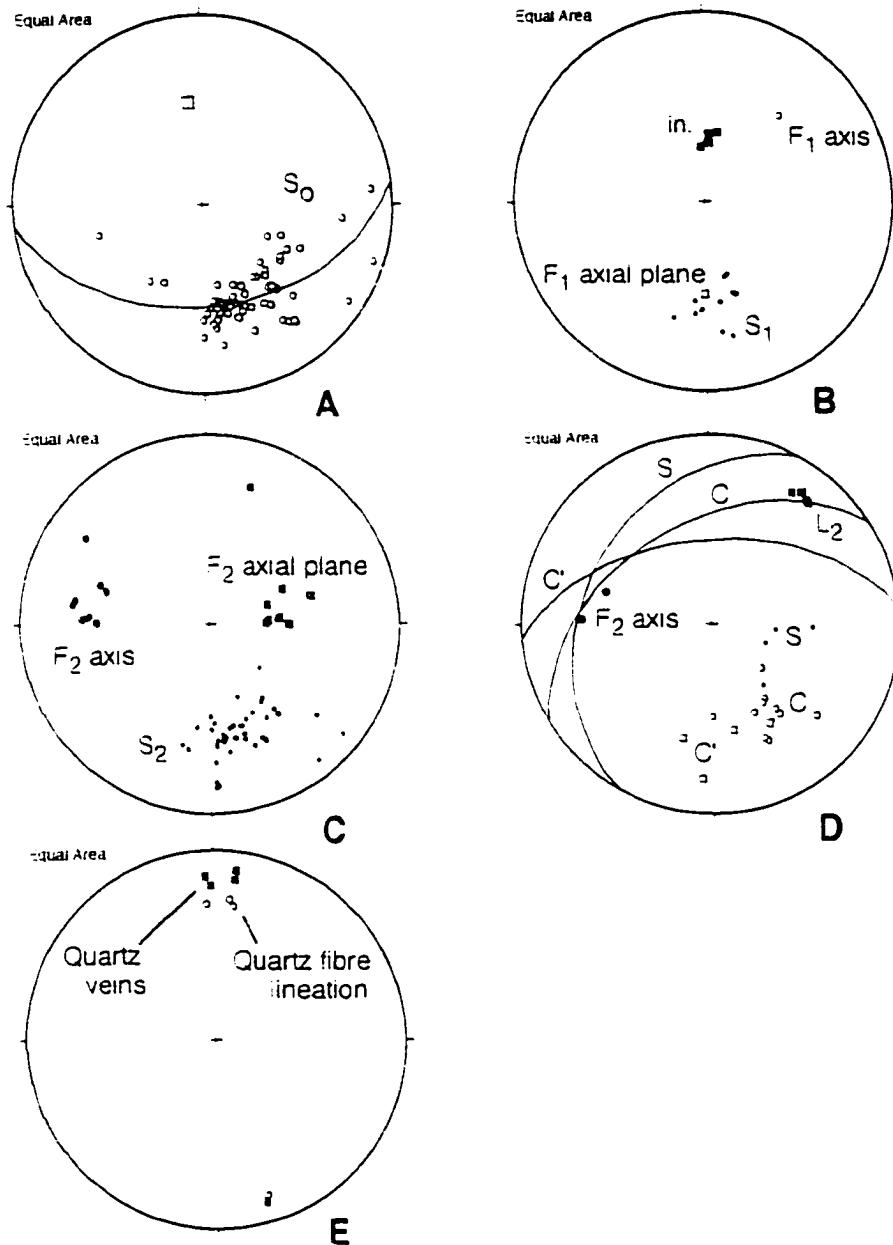


Figure 4.10 Lower hemisphere, equal area projections of structural data from the PROC south of Big Head (Map 9). Planar structural elements plotted as poles. a) S_0 , $n=65$. Note the weak girdle. b) S_1 , $n=12$; F_1 axial plane, $n=1$; F_1 axis, $n=1$; L_1 (lin.; includes stretching and S_0 - S_1 intersection lineation), $n=6$. c) Structural data from several D_2 shear zones. S_2 , $n=40$; F_2 axial planes, $n=8$; F_2 axes, $n=8$. d) Structural data from the D_2 shear zone ~100m south of Big Head. C-planes, $n=10$; S-planes, $n=5$; C'-planes, $n=4$; L_2 , $n=4$; F_2 axes, $n=2$. e) Poles to quartz-fibre veins ($n=5$) and the quartz-fibre lineation ($n=4$) associated with dextral-normal, brittle-ductile faults north of the Barry-Cunningham adit.

are better developed in these rocks than in the more isotropic intrusive and extrusive rocks of the ophiolite suite. The structural analysis of the cover sequence revealed three phases of ductile deformation (D_1 , D_2 , D_3).

4.2.6.1 D_1 deformation

D_1 structures are pervasive within the PROC cover sequence, and comprise an S_1 foliation, L_1 mineral and stretching lineation, and F_1 folds. S_1 is generally penetrative, dips moderately north, and is defined by foliated chlorite, biotite and actinolite. S_1 is almost concordant with the overturned bedding in the clastic rocks (Figs. 4.10a and 4.10b), and is penetratively developed along the contacts between the main lithological units in the ophiolite sequence, and in several ~10-20m thick high-strain zones which probably represent second or third-order D_1 shear zones (e.g., Kirkwood and Dubé 1992). The foliation contains a L_1 chlorite mineral lineation that plunges north, as well as a parallel L_1 stretching lineation. The stretching lineation is locally defined by stretched volcanic clasts within the coarse-grained clastic layers, and Kirkwood and Dubé (1992) described a penetrative grain-shape L_1 lineation (L-tectonite) in mylonitized gabbro sills. These features, and the pronounced elongation of volcanic clasts in S_1 ($X:Y > 4:1$), are consistent with high finite D_1 strains. S_1 is axial planar to rare tight to isoclinal, west-verging F_1 folds with axes subparallel to L_1 . In the folded sections, the S_0 - S_1 intersection lineation also plunges north, parallel to L_1 (Fig. 4.10b). The sense of asymmetry of the F_1 folds, coupled with the overturned bedding, indicates that the lithological succession in this area is located on the upper limb of the large, reclined F_1 syncline defined by Kidd et al. (1978).

D_1 structures are attributed to ductile, south-directed, reverse shear (e.g., Kidd et

al. 1978; Kirkwood and Dubé 1992; Dubé et al. 1993). In most locations, the pitch of L_1 in S_1 is consistent with a significant component of sinistral oblique-slip shear (e.g., Kirkwood and Dubé 1992; Dubé et al. 1993). This relationship has important regional implications, which are discussed in Chapter 7. On the basis of orientation, style, and sense of movement, D_1 structures in the PROC are correlated with D_1 in the PHG.

4.2.6.2 D_2 deformation

D_2 structures in the PROC comprise an S_2 foliation, L_2 lineation, and F_2 folds which are spatially associated with discrete shear zones that reactivated D_1 structures (Map 9). S_2 is defined by fine-grained chlorite and biotite, and is generally subparallel to S_1 (Fig. 4.10c), although in some locations S_1 is clearly transected by a slightly more southwest-striking S_2 . S_2 is only penetrative in discrete shear zones that transect S_1 at low angles. These are associated with abundant kinematic indicators, including S-C fabrics, asymmetric shear bands, offset quartz veins, asymmetric boudinage of quartz veins, and dragging of S_1 , that consistently indicate north-side down shear along S_2 (Fig. 4.8e). The S_2 foliation contains a chlorite and slickenline L_2 lineation which pitches moderately to the northeast in the plane of the foliation. The lineation, coupled with the kinematic indicators, is compatible with dextral-normal oblique-slip shear during reactivation and transposition of S_1 . F_2 folds are open to tight, reclined, plunge shallowly to the west, and are spatially associated with zones of D_2 -related dextral-normal shear (Fig. 4.10c). These folds fold S_0 - S_1 , have <0.5m amplitudes, and locally have an open, box-fold morphology. The orientation and style of these folds are very similar to F_2 folds described by Kirkwood and Dubé (1992), and these structures are therefore correlated. Broad, north-northeast

trending, open F_3 folds described by Kirkwood and Dubé (1992) were not observed in the present study, possibly owing to limited along-strike exposure in the coastal sections.

A particularly good example of a D_2 shear zone that dips northwest is well exposed ~100m south of Big Head (BHSZ; Map 9; Fig. 4.10d). This shear zone is developed along the contact between pillowed basalt in the hangingwall and clastic rocks in the footwall. The S_2 fabric transects S_1 in the pillowed basalts, and contains a chlorite lineation that plunges northeast. Asymmetric fabrics (S-C-C') indicate dextral-normal oblique-slip shear (Fig. 4.10d). The orientation, sense of movement, style of deformation, and syndeformational metamorphic grade (greenschist facies) of this shear zone are very similar to those in the NMTSZ on the eastern shore of Ming's Bight. Moreover, the NMTSZ is directly on strike from the shear zone at Big Head (Map 7; Map 9; Fig. 3.1), and contains blocks of mafic volcanic rock of possible PROC affinity. On the basis of these relationships, the BHSZ and NMTSZ are interpreted to represent segments of the same shear zone. This interpretation requires that D_2 in the PROC is correlative with D_2 on the eastern shore of Ming's Bight.

4.2.6.3 D_3 deformation

D_3 structures in the PROC are spatially associated with D_2 shear zones, and are interpreted as the latest increment in a progressive D_2 - D_3 deformation phase. D_3 structures are separated into two basic types. The first type comprises a series of steeply north-dipping ductile shear zones that transect D_1 - D_2 structures, and are associated with 1-2m thick zones of quartz veined chlorite-carbonate-pyrite schist. These shear zones contain a penetrative S_3 chlorite foliation that dips steeply north, and a down-dip chlorite and

slickenline lineation. Dragging of S_1 - S_2 fabrics along the margins of the shear zones, together with S-C fabrics and shear bands, indicate north-side-down shear. In one location, a D_3 shear zone contains abundant fault-fill quartz veins that are parallel to S_3 , but slightly oblique (counterclockwise; looking west) to the margins of the shear zone (Fig. 4.8f). The sense of obliquity of the fault-fill veins to the margins of the shear zone indicates north-side-down shear (e.g., Robert et al. 1994).

The second type of D_3 structure comprises a series of narrow, late, brittle-ductile, dextral-normal oblique-slip faults. These faults transect D_2 structures within D_2 shear zones, and are locally well developed in the pillowed basalts just north of the Barry-Cunningham adit. In this location the late faults are spatially associated with a series of quartz veins that dip steeply south, and contain quartz fibres that plunge shallowly north (Fig. 4.10e). The opening vector of these veins is consistent with a subhorizontal extension direction during D_3 deformation.

The D_3 structures probably represent the steeply dipping faults attributed by Kidd et al. (1978) to "...a relaxation of the convergent motion and a 'fall-back' of the rocks into the steeply-dipping pinched zone from which they had just been expelled". These structures are further discussed below.

4.2.7 Kinematic analysis of D_2 , D_4 , and D_5 shear zones and faults

4.2.7.1 Introduction

Fault-slip analysis and kinematic analysis of fault-slip data are useful tools in the study of brittle-ductile fault systems in the shallow, sub-greenschist facies regions of orogenic systems. These methods can provide important insights into paleostress and

strain, and can be useful for establishing the kinematics and tectonic significance of small to regional-scale fault systems (e.g., Malavieille 1987; Marrett and Allmendinger 1990; Angelier 1994; Duebendorfer and Simpson 1994; Teyssier et al. 1995). Recently, several authors have proposed that these methods may also be applicable to ductile shear zones, provided strain magnitudes are small, and are thus potentially useful for studies in the deeper, lower greenschist facies regions of orogenic systems (e.g., Cobbold et al. 1991; Srivastava et al. 1995).

In the present study, a kinematic analysis of fault-slip data (Marrett and Allmendinger 1990) is applied to the D₃, D₄ and D₅ shear zones and faults (hereinafter collectively referred to as faults) in the Ming's Bight area in order to constrain the principal directions of shortening and extension for the fault population, and to evaluate the hypothesis that they record increments of a progressive deformation which accomplished bulk, north-south directed, subhorizontal extension.

4.2.7.2 Assumptions

The application of fault-slip analyses to a system of faults requires five basic assumptions (e.g., Angelier 1994; Srivastava et al. 1995): 1) all the faults must have formed synchronously, under a homogeneous stress regime; 2) the direction of maximum shear stress resolved onto the plane of each fault must be parallel to the lineation that defines the slip direction; 3) the faults must not have been re-oriented subsequent to their development; 4) the strain magnitude must be small; and 5) the sampled faults must be representative of the entire fault population.

In most fault systems these assumptions are difficult to justify adequately.

Consequently, the standard method of addressing these assumptions in the literature is through empirical observation and somewhat circular reasoning (Angelier 1994). In this method, the validity of the initial assumptions is temporarily assumed, the analysis is performed, and internally consistent results are taken to confirm the validity of the initial assumptions. Alternatively, authors might appeal to similarities in orientation, style, apparent metamorphic grade, and/or sense of movement in order to demonstrate the homogeneity of a measured population of faults, or might suggest that the analysis represents a valid 'first-order approximation' of a complex fault system. Several authors have noted that the assumptions generally hold for most fault populations, possibly reflecting a fundamental characteristic of the faulting process (e.g., Marret and Allmendinger 1990; Angelier 1994).

With respect to shear zones, justification is significantly more complicated. In particular, shear zones typically record intense ductile strains over protracted time intervals, and the early deformation history of a shear zone may be completely obliterated during subsequent shearing. In these situations, the assumption of a small strain magnitude may be invalid, and that of a homogeneous stress regime is untestable. In addition, shear zones typically show a certain degree of scatter in the orientation of mineral and stretching lineations. In many shear zones, lineations are produced during one or more shearing episodes, and are not necessarily coincident with the direction of shear (e.g., Ridley 1986; Lin and Williams 1992). Thus, the assumption that the measured lineation defines the shear direction may not be valid in all situations. Despite these limitations, several authors have recently proposed that fault-slip analyses of shear zones can provide useful

information on paleostress, state of strain, and kinematics (e.g., Cobbold et al. 1991; Srivastava et al. 1995), provided bulk strain magnitudes are small.

4.2.7.3 Kinematic analysis - Ming's Bight area

In the present study, the D_3 , D_4 and D_5 faults in the Ming's Bight area are analyzed using a modified version of the fault kinematic analysis method of Marrett and Allmendinger (1990), and the assumptions are addressed through empirical observation.

The analysis is based on 32 separate faults (12 ductile shear zones; 20 brittle-ductile faults) and 40 measurements from these faults (12 from ductile shear zones; 28 from brittle-ductile faults). Each measurement includes a mean orientation of the fault plane, the mean orientation of the lineation, and the sense of shear. On the basis of similar syn-deformational metamorphic mineral assemblages these faults are inferred to be broadly contemporaneous (Assumption 1). The individual faults and measurements included in the analysis were selected on the basis of reliability of the sense of shear criteria (asymmetric fabrics, offset markers, drag-folding), and the presence of a consistently oriented lineation (i.e., uniform slip-direction; Assumption 2). Offset markers adjacent to the faults typically show <2m separations, suggesting small strain magnitudes (Assumption 4), although this assumption may or may not hold for the 12 ductile shear zones. No attempt was made to separate measurements on the basis of geographic location or orientation, or to weight the data toward a particular population, and the data set is considered to be representative of the faults in the Ming's Bight area (Assumption 5).

The first step in the kinematic analysis involved plotting the poles to the entire measured population of faults in Ming's Bight, including those for which the slip-direction

and sense of movement could not be determined. The poles define a partial girdle (Fig. 4.11a), consistent with development of the faults under the same bulk stress regime (Assumption 1), and the pole to the great circle defined by the girdle approximates the intermediate principal stress axis (e.g., Swanson 1988; Kirkwood and Malo 1993; Fig. 4.11b). Figure 4.11c illustrates the orientation, slip direction, and sense of shear for each of the analyzed faults, and the shortening and extension axes are plotted in Figure 4.11d. These axes simply represent an alternative representation of the original data, as they lie within the plane that contains the normal to the shear plane and the slip-direction, and are oriented at an angle of 45° to the slip direction and shear plane normal. The shortening and extension axes are distinguished using the sense of shear on the shear plane (Marrett and Allmendinger 1990). Contoured plots of these data (Figs. 4.11e and 4.11f), indicate that the principal shortening axis plunges $\sim 75^\circ$ to the east-northeast, and the principal extension axis plunges $\sim 5^\circ$ to the south. Moreover, the intermediate principal axis, as indicated by the intersection of the extension and compression field-boundaries in the 'fault plane solution' (Fig. 4.11d), plunges $\sim 10^\circ$ to the west, subparallel to that derived from the symmetry plane of the entire population (Fig. 4.11b). The relative consistency of the data from the entire fault population is considered to support the validity of the initial assumptions (e.g., Marrett and Allmendinger 1990; Angeiler 1994).

4.2.7.4 Discussion

As noted above, the assumptions required for a rigorous kinematic analysis of a given fault system cannot be justified adequately in most instances. However, the results presented above indicate that the shortening and extension axes for D_3 , D_4 and D_5 faults in

Figure 4.11 Lower hemisphere, equal area projections of the results of the fault kinematic analysis in the Ming's Bight area. **a)** Poles to all measured faults in the Ming's Bight area. **b)** Contoured plot of the previous data (2σ contour interval) illustrating the great circle distribution (i.e., symmetry plane; e.g., Swanson 1988), and the intermediate principal stress axis (pole to the symmetry plane; shaded square). **c)** Plot of the orientation, slip direction, and sense of shear for each of the analyzed faults. The analysis includes 11 measurements from 11 faults in the Ming's Tickle area (Map 8), 11 measurements from 10 faults in the PROC (Map 9), and 18 measurements from 11 faults to the south of Ming's Bight (Maps 4 and 5). The arrow indicates the movement of the hangingwall. This plot clearly illustrates the predominance in the analyzed population of dextral-normal oblique-slip faults that dip northwest and north. In the field, faults that dip south or southwest tend to contain ambiguous kinematic indicators. Consequently, few were acceptable for analysis. **d)** Plot of the shortening (solid circles) and extension (open squares) axes for each of the measurements (Marrett and Allmendinger 1990; see text for discussion). Solid squares indicate the principal (i.e., mean) shortening (P) and extension (T) axes. **e)** and **f)** Contoured plots of the shortening and extension axes, respectively (2σ contour interval), illustrating bulk, north-south directed, subhorizontal extension associated with the brittle-ductile faults in the Ming's Bight area.

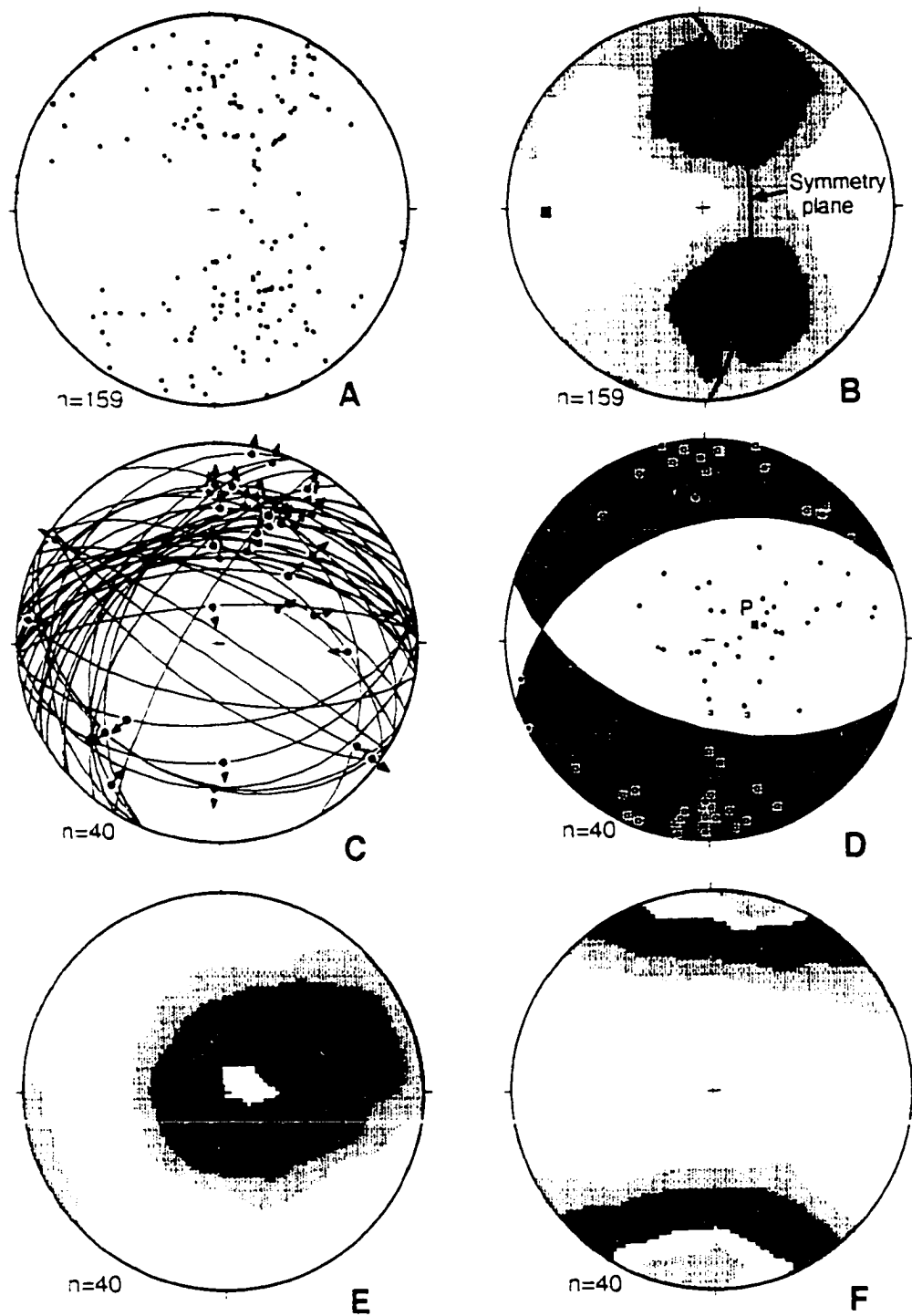


Figure 4.11

the Ming's Bight area display a significant degree of homogeneity.

Marrett and Allmendinger (1990) and Cobbold et al. (1991) propose that this type of analysis most likely provides an estimate of the state of bulk strain in a fault system, provided bulk strain magnitudes are small. In the present study, the orientation of the principal extension axis for the fault population is considered to provide an estimate on the orientation of the X-axis of a bulk strain ellipsoid, and the D₃-D₄-D₅ faults are inferred to have collectively accommodated progressive, bulk, north-south directed, subhorizontal extension. As discussed in Chapter 7, this interpretation is compatible with the overall geometry of D₃-D₄-D₅ structures in Ming's Bight, and the orientation of the stretching lineation in the Pacquet Harbour area which is considered to be coeval with these structures (refer to Chapters 6 and 7 for further discussion).

4.3 CONCLUSIONS - MING'S BIGHT AREA

(1) D₁ structures are well developed in the PROC and the northern portions of the PHG, and are associated with lower greenschist to lower amphibolite facies metamorphism depending on structural level. D₁ structures record non-coaxial, reverse shear within a series of moderately northeast-dipping ductile shear zones, the most prominent of which is the Scrape Fault. These shear zones formed during south-directed over-thrusting of the PHG by the PROC.

(2) D₂ structures are pervasive in the area immediately to the west of the Dunamagon Granite, and are associated with lower amphibolite facies metamorphism. The D₂ structures record sinistral, transpressional shear associated with imbrication of the PHG, MBG, and PROC along a series of ductile shear zones that dip steeply west.

(3) Several structural relationships indicate that D_1 and D_2 structures in the Ming's Bight area evolved synchronously: i) metamorphic mineral assemblages and microstructural relationships indicate that D_1 and D_2 structures are synchronous with the metamorphic peak in the PHG; ii) D_1 and D_2 fabrics are coaxial, and apparently record constrictional finite strains (Gale 1971; Tuach 1976); and iii) microstructural analysis suggests that garnet porphyroblasts are syn-tectonic with respect to south-directed shear along S_1 and transpressional shear along S_2 (see Section 4.3.2.3).

The style, sense of movement, spatial distribution, and relative timing of D_1 and D_2 structures in the Ming's Bight area are interpreted to reflect deformation within the frontal and lateral ramps (Coward and Potts 1983) of a combined thrust/wrench shear system that formed through large-scale partitioning (Tobisch and Paterson 1988) of a single progressive deformation phase. In this model, D_1 is ascribed to progressive reverse shear within the frontal ramp, whereas D_2 is ascribed to progressive transpressional wrench shear in the lateral ramp developed to the south of Ming's Bight (Fig. 4.12). The large-scale fold proposed by Tuach and Kennedy (1978) in the PHG is viewed as the lateral tip of the frontal ramp (Fig. 3.1). Indeed, along the inferred axial trace of this fold northeast of the Rambler camp, D_1 shear zones are folded by open, upright, asymmetric F_2 folds that become progressively more pervasive, tight, and shallowly-plunging towards the northeast. This structural setting is similar to the frontal to lateral ramp transition zones described by Coward and Potts (1983), Ridley (1986), and Ridley and Casey (1989).

This model reconciles the structural observations of Gale (1971), Tuach (1976), Kidd et al. (1978), Tuach and Kennedy (1978), Kirkwood and Dubé (1992), and Dubé et

al. (1993), as well as many of the key structural and metamorphic features of the Ming's Bight area, including: 1) the sense of movement along the Scrape Fault, and the relationship between the Scrape Fault and D_1 structures in both the PHG and PROC; 2) the significance and sense of movement of D_2 shear zones south of Ming's Bight; and 3) the increase in the intensity of deformation and grade of metamorphism structurally upwards in the footwall of the Scrape Fault (i.e., possible inverted metamorphic sequence; see Chapter 5).

(4) D_3 structures are best developed in the northern portions of the PHG, and are associated with greenschist facies metamorphism. D_3 structures comprise crenulation fabrics that dip shallowly, recumbent folds, and a series of south-dipping extensional shear zones, which are compatible with 'regional' sub-vertical shortening (e.g., DeGrace et al. 1976). These structures are probably associated with the earliest increment of extensional deformation in the Ming's Bight area, and may be synchronous with extension in the Pacquet Harbour area.

(5) D_4 structures comprise a series of shear zones that dip shallowly west, and generally separate MBG schist in the footwall from PROC rocks in the hangingwall. These shear zones formed under greenschist facies metamorphic conditions, and apparently record a progressive transition from ductile dextral transpressional shear to brittle-ductile dextral transtensional shear, probably in the middle increments of extensional deformation in the Ming's Bight area.

(6) D_5 structures comprise a series of northerly- and southerly-dipping, brittle-ductile shear zones that record dextral-normal oblique-slip shear under greenschist facies

metamorphic conditions. D_5 structures are only observed within D_5 shear zones, and the distributed character of this deformation suggests that it is associated with waning strain in the latest increments of extensional deformation in the Ming's Bight area.

(7) Structures attributed to D_1 and D_2 in the present study are correlated with the regional D_E - D_M of Hibbard (1983), whereas D_3 is correlated with the regional D_L of Hibbard (1983). These correlations are based on comparisons of the style, syn-deformation metamorphic grade, orientation, and overprinting relationships of the structures (see Section 3.1.3). D_4 and D_5 structures have not been previously described, but are also considered broadly correlative with the D_L of Hibbard (1983). The D_4 GTCSZ and D_5 NMTSZ record an apparently progressive transition from dextral transpression to dextral transtension. The phase of dextral transpression in the Ming's Bight area may have been contemporaneous with the partitioned dextral transpressional shear described by Goodwin and Williams (1996) in Marble Cove, Baie Verte.

4.4 DISCUSSION - CHAPTERS 3 AND 4

4.4.1 *Timing of deformation*

In the Pacquet Harbour area, the relative and absolute timing of deformation are fairly well constrained by field relationships and previously published U-Pb and $^{40}\text{Ar}/^{39}\text{Ar}$ geochronology. D_1 compressional deformation probably occurred between Early Silurian and early-Middle Devonian time, after intrusion of the Dunamagon Granite (ca. 429 Ma; U-Pb zircon; Cawood and Dunning 1993), but prior to the amphibolite facies metamorphic peak in the Pacquet Harbour area (ca. 385 Ma; U-Pb titanite; G.R. Dunning 1995, pers. comm.). D_2 extensional deformation occurred between Early Silurian and

Early Carboniferous time, after intrusion of the Dunamagon Granite, and prior to regional cooling below the biotite closure temperature (ca. 350 Ma; $^{40}\text{Ar}/^{39}\text{Ar}$; Dallmeyer 1977; Dallmeyer and Hibbard 1984). The early stages of D_2 coincided with peak amphibolite facies metamorphism in the Pacquet Harbour area (ca. 385 Ma). Thus, D_2 probably occurred in Middle to Late Devonian time. D_3 extensional deformation occurred sometime after the metamorphic peak in Pacquet Harbour, and is therefore post-Middle Devonian.

In the Ming's Bight area, the relative timing of deformation is well constrained by field relationships. However, in contrast to the Pacquet Harbour area, the paucity of previously published U-Pb and $^{40}\text{Ar}/^{39}\text{Ar}$ geochronology leads to a relative lack of absolute time constraints. D_1 - D_2 deformation in the combined thrust/wrench shear system post-dates intrusion of the Burlington Granodiorite (ca. 432 Ma; U-Pb zircon; Cawood and Dunning 1993), and is inferred to be synchronous with hydrothermal mineralization and syn- D_1 quartz veins (Kirkwood and Dubé 1992) in the PROC (ca. 420 Ma; U-Pb zircon; Ramezani 1992). The younger age limit for D_1 - D_2 , and the absolute timing of D_3 , D_4 , and D_5 are unconstrained, except that they all probably pre-date regional cooling through the biotite closure temperature in Early Carboniferous time (ca. 345 Ma; $^{40}\text{Ar}/^{39}\text{Ar}$; Dallmeyer and Hibbard 1984).

Further constraints on the timing of deformation are provided by new U-Pb and $^{40}\text{Ar}/^{39}\text{Ar}$ dates presented in Chapter 6.

4.4.2 Correlation of deformation - Ming's Bight and Pacquet Harbour areas

Table 4.2 provides a comparison and correlation of deformation in the Ming's Bight and Pacquet Harbour areas (refer to Tables 3.1 and 4.1). Based on the style and

Table 4.2 Correlation and regional significance of deformation - Pacquet Harbour and Ming's Bight

Pacquet Harbour	Ming's Bight	Regional significance (see Chapter 7)
<p>D₂ deformation</p> <p>Southeast-directed extensional shear</p> <p>* pre- to syn-360 Ma</p> <p>* post-380 Ma</p>	<p>D₂ deformation</p> <p>Linked southwest- and northwest-directed extensional shear</p> <p>* syn-380 to 388 Ma</p>	<p>Exhumation of the MBG during Devonian regional dextral transcurent shear, and northwest-southeast-directed divergent extension</p>
<p>D₃ deformation</p> <p>Southeast-directed extensional shear</p> <p>* pre-360 Ma</p> <p>* syn-380 Ma</p> <p>* post-430 Ma</p>	<p>D₄ deformation</p> <p>Progressive dextral transpressional to oblique-slip shear</p> <p>* pre- to syn-390 Ma</p> <p>* post-420 Ma</p> <p>D₃ deformation</p> <p>South-directed extensional shear</p> <p>* pre-390 Ma</p> <p>* post-420 Ma</p>	
<p>D₁ deformation</p> <p>Sinistral-reverse oblique-slip shear</p> <p>* pre-385 Ma</p> <p>* post-430 Ma</p>	<p>D₂ deformation</p> <p>Sinistral transpressional shear</p> <p>* pre-405 Ma</p> <p>* syn-420 Ma</p> <p>* post-430 Ma</p> <p>D₁ deformation</p> <p>Sinistral-reverse oblique-slip shear</p> <p>* pre-405 Ma</p> <p>* syn-420 Ma</p> <p>* post-430 Ma</p>	<p>Exhumation of the Fleur de Lys Supergroup and subsidence of the MBG during Silurian regional sinistral transpression</p>

Note: double solid horizontal lines separate kinematically and temporally distinct deformations

* Time constraints (see Chapter 6)

sense of movement of the deformation structures, and the timing constraints presented above, the deformation in the thesis area is attributed to regionally significant phases of Early Silurian to early-Early Devonian sinistral transpressional deformation, and Early Devonian to Early Carboniferous dextral transtensional deformation. In this model, D_1 in the PROC and Pacquet Harbour map area, and D_1 - D_2 in the Ming's Bight map area are attributed to the transpressional deformation (Fig. 4.12), whereas the transtensional deformation is recorded by D_2 - D_3 in the PROC and Pacquet Harbour map area, and D_3 - D_4 - D_5 in the Ming's Bight map area (Fig. 4.13). This hypothesis is further developed in Chapters 5 and 6, and is discussed in detail in Chapter 7.

Figure 4.12 Simplified geological and structural map of the thesis area (see Fig. 2.2 for a legend of lithological units) illustrating the location and sense of movement of structures attributed to Silurian compressional deformation, as well as the lateral/frontal ramp geometry of Silurian structures between the Burlington Granodiorite and Dunamagon Granite. Note the L_1 stretching lineation that plunges moderately to the north-northeast in the frontal ramp, and the L_2 stretching lineation that plunges shallowly south in the lateral ramp. Inset illustrates the inferred regional kinematic framework, which is consistent with Silurian sinistral transpression (see Chapter 7).

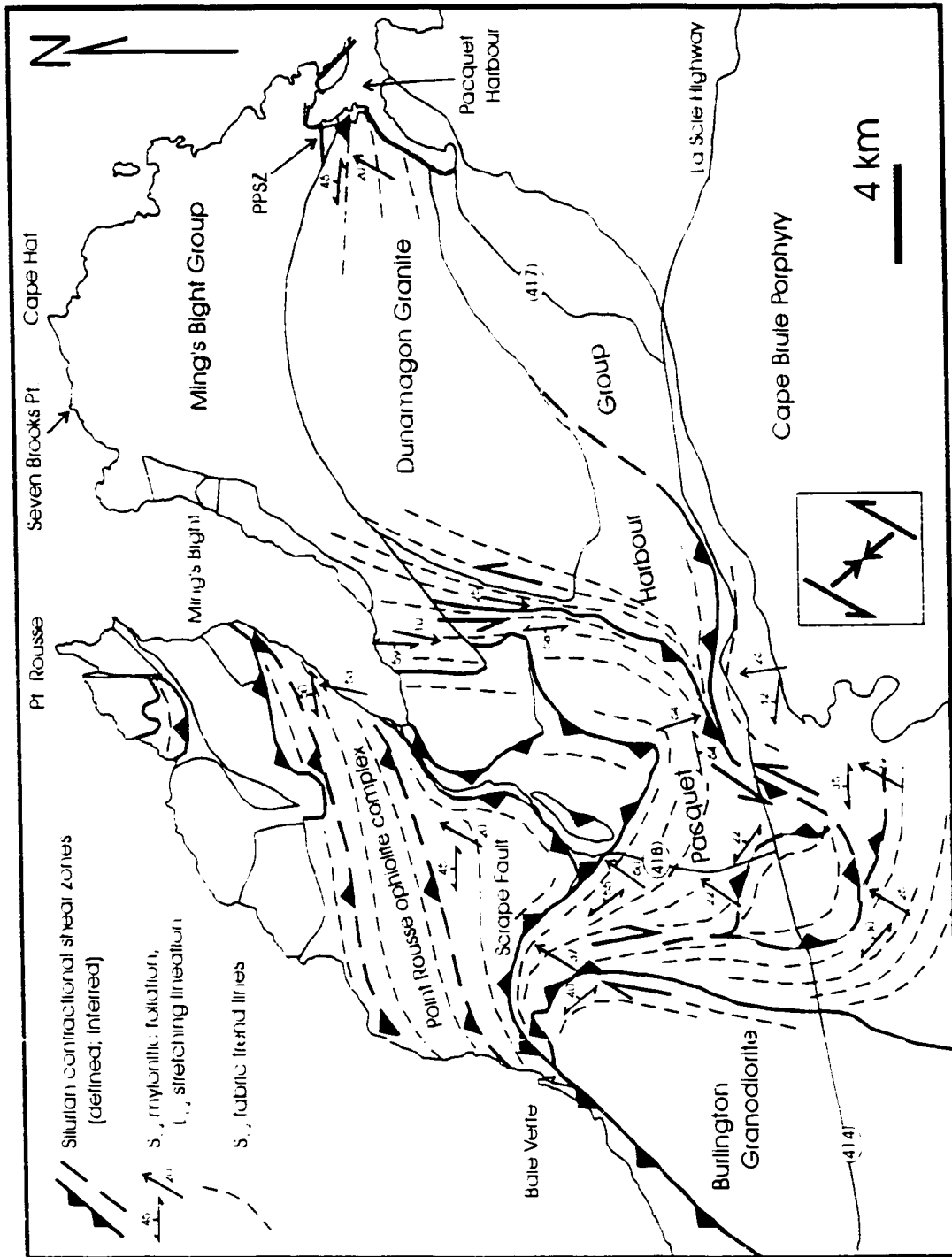


Figure 4.12

Figure 4.13 Simplified geological and structural map of the thesis area (see Fig. 2.2 for a legend of lithological units) illustrating the location and sense of movement of structures attributed to Devonian extensional deformation. The heavy double-ended arrows denote the extension directions inferred from the L_2 stretching lineation and extended structures in the Pacquet Harbour area, and the analysis of brittle-ductile faults and shear zones in the Ming's Bight area. Measurements of the subhorizontal foliation in the Cape Corbin area are plotted as poles in the lower hemisphere, equal area projection in the upper right corner (see Chapter 7). Note the overall domal geometry of Devonian structures in the MBG. Inset illustrates the inferred regional kinematic framework, which is consistent with Devonian dextral transtension (see Chapter 7).

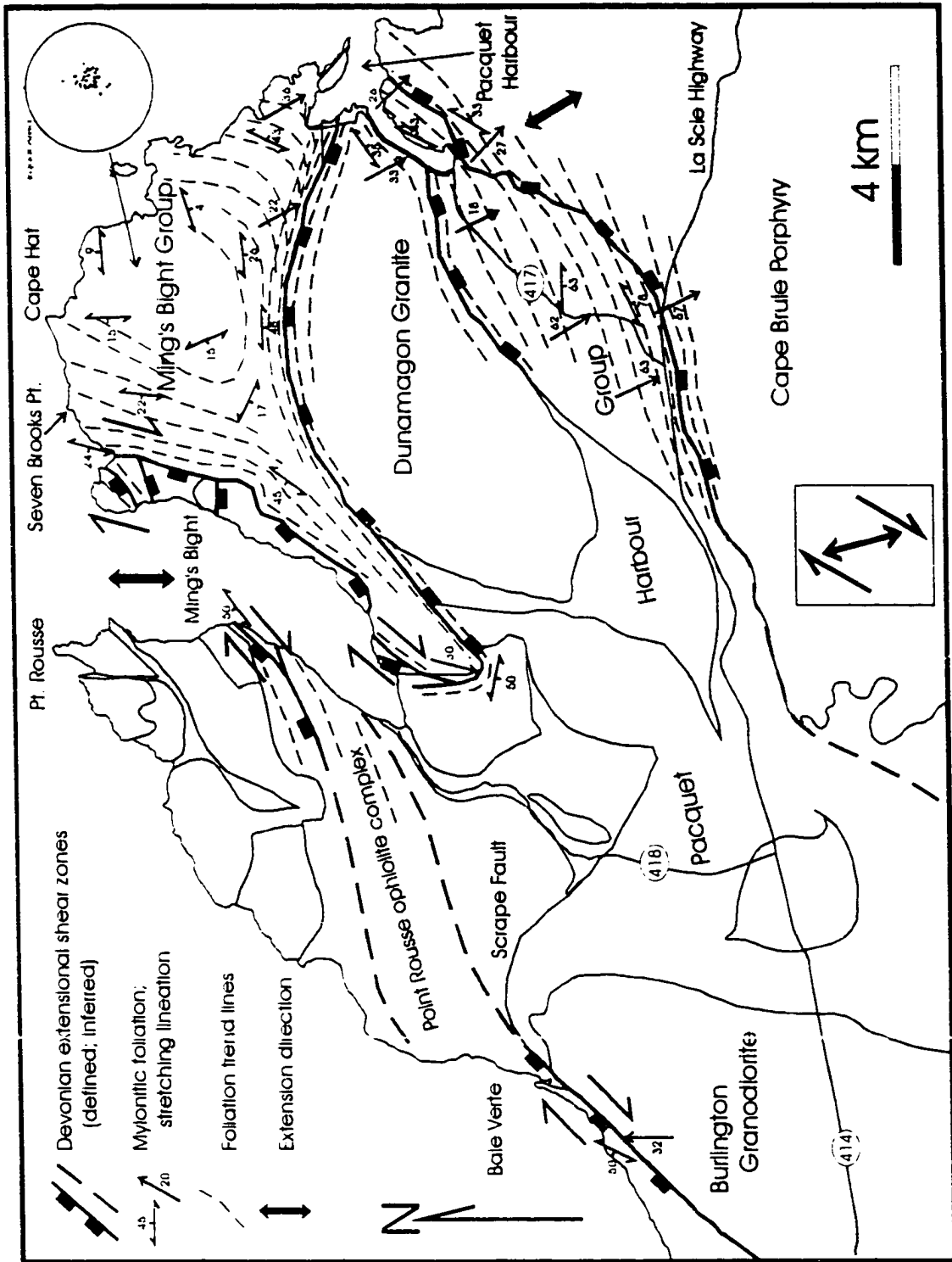


Figure 4.13

Chapter 5 Metamorphic Petrology and Thermobarometry

5.1 INTRODUCTION

5.1.1 Background

Establishing the tectonic evolution of a region requires careful consideration of the metamorphic characteristics of the constituent lithologies. Metamorphic mineral assemblages and textures provide important constraints on the relative timing of deformation, and can be used semi-quantitatively to assess changes in P-T conditions. In addition, P-T estimates derived from thermobarometry can be used to construct quantitative P-T paths which, in conjunction with $^{40}\text{Ar}/^{39}\text{Ar}$ and U-Pb thermochronology, can be used to deduce P-T-t paths (e.g., Hodges 1991). Collectively, these data provide valuable information on the tectonothermal evolution of a region, which is essential in constructing and testing tectonic models (e.g., Thompson and England 1984; Selverstone 1985; Jamieson 1991).

On the BVP, the metamorphic characteristics of rocks west of the BVL have been examined in considerable detail, and the P-T-t path is well constrained by quantitative thermobarometry and $^{40}\text{Ar}/^{39}\text{Ar}$ and U-Pb geochronology. However, the metamorphic characteristics of high-grade metamorphic rocks east of the BVL have only been qualitatively addressed in two local-scale studies, and no attempt has been made to quantitatively assess the peak P-T conditions.

In light of the new structural framework outlined in the previous chapters, the metamorphic characteristics of the thesis area have been examined in detail. The purpose

of the present chapter is: 1) to describe in detail the metamorphic mineral assemblages, textures, and deformation relations in the thesis area; and 2) to present the results of a quantitative thermobarometric analysis of peak-metamorphic mineral assemblages which, in conjunction with $^{40}\text{Ar}/^{39}\text{Ar}$ and U-Pb thermochronology (Chapter 6), are used to constrain general P-T-t paths for the MBG.

5.1.2 Regional metamorphic setting and previous work

In simple terms, the BVP encompasses two tectono-metamorphic terranes: those rocks west of the BVL, which underwent burial to >20km depth prior to the Early Silurian, and those rocks east of the BVL which, in the northern areas, locally underwent burial to >15km depth subsequent to the Early Silurian. The BVL itself comprises a complex series of lower greenschist to amphibolite facies rocks with highly variable metamorphic mineral assemblages and textures, that are locally juxtaposed over short distances along and across strike (e.g., Bursnall 1975; Hibbard 1983). The metamorphic evolution of these rocks probably reflects the protracted greenschist to amphibolite facies deformation history of the BVL, as well as an 'inherited' metamorphic history contained within large slices of tectonically juxtaposed rock. The best example of this is the imbricated amphibolite and lower greenschist facies rocks in the Advocate - Point Rouse ophiolite complex (Bursnall 1975; Sections 2.3.5 and 2.3.6, this study).

The metamorphic evolution west of the BVL has been examined in detail (e.g., de Wit 1972; Bursnall 1975; Kennedy 1975; Jamieson and Vernon 1987; Jamieson 1990; Vance and O'Nions 1990; Jamieson and O'Bierne-Ryan 1991), and is conveniently summarized in relation to the deformation history. D_E structures are typically associated

with greenschist facies metamorphic mineral assemblages, likely reflecting regional burial of the Laurentian margin during Taconian orogenesis. The localized emplacement of relatively hot ophiolite may be indicated by local amphibolite facies mineral assemblages along D_E ductile shear zones (Bursnall 1975; Hibbard 1983). D_M structures in the Fleur de Lys Supergroup are associated with synkinematic growth of garnet, plagioclase, and staurolite porphyroblasts during peak amphibolite facies metamorphism (de Wit 1972; Hibbard 1983; Jamieson and Vernon 1987). Jamieson (1990) examined syn- D_M metamorphic mineral assemblages in the East Pond Metamorphic Suite and Fleur de Lys Supergroup, and proposed a two stage history involving an early phase of high pressure - low temperature metamorphism (East Pond Metamorphic Suite, >10-12 kbar, 450-500°C; Fleur de Lys Supergroup, 7-8.5 kbar, ~450°C), locally producing eclogitic assemblages in mafic dykes of the East Pond Metamorphic Suite, and a later phase of lower pressure - higher temperature metamorphism (East Pond Metamorphic Suite, >7-9 kbar, 700-750°C; Fleur de Lys Supergroup, 6.5 kbar, 550-600°C). These results were interpreted in terms of burial of the Laurentian margin during the Taconian orogeny and subsequent thermal relaxation (Jamieson 1990), and are consistent with a typical P-T path resulting from overthrusting (e.g., Thompson and England 1984; Jamieson 1991). This model is broadly consistent with Sm-Nd and Rb-Sr dates of ca. 445 Ma (Vance and O'Nions 1990) from syn- D_M garnet porphyroblasts, and a U-Pb monazite date of ca. 430 Ma (Cawood et al. 1994) from syn- D_M migmatite. Widespread retrogression of the peak-metamorphic assemblages to greenschist facies occurred during D_L , particularly adjacent to the BVL.

East of the BVL, the metamorphic evolution of the northern, higher-grade, area

(Fig. 5.1) was examined in detail by Coates (1970) and Tuach (1976), with contributions from Gale (1971), Kennedy (1975), and Hibbard (1983). Coates (1970) examined the structure and metamorphism in the Pacquet Harbour area, and concluded that both D_M and D_L were associated with (peak) greenschist to amphibolite facies metamorphic conditions. In contrast, Tuach (1976) concluded that peak amphibolite facies metamorphism in the Rambler area occurred during D_M , with a greenschist facies overprint associated with D_L . Both authors noted that the grade of metamorphism decreases toward the south into lower greenschist facies rocks (Coates 1970; Tuach 1976; Fig. 5.1); however, neither author presented a model to explain the discrepancies in apparent timing and distribution of metamorphism.

Based on the structural constraints provided in Chapters 3 and 4, and an examination of the relative timing of mineral growth, recrystallization, and deformation, the metamorphism of the MBG and surrounding units is interpreted as reflecting two spatially and temporally distinct metamorphic peaks: one in Late Silurian to early-Early Devonian time associated with compressional deformation in the Ming's Bight area, and one in late-Early to early-Middle Devonian time associated with the early stages of extensional deformation in the Pacquet Harbour area.

5.2 MINERAL GROWTH, RECRYSTALLIZATION, AND DEFORMATION

5.2.1 *Pacquet Harbour area*

In the Pacquet Harbour area, microstructural relationships between porphyroblasts, inclusion trails (S_i), and matrix fabrics (S_e) allow for a reliable determination of the evolutionary sequence of metamorphic mineral assemblages and

Figure 5.1 Simplified geology of the thesis area showing the distribution of greenschist and upper greenschist to amphibolite facies metamorphic rocks. Note that the amphibolite facies rocks occur in the immediate footwalls of the Scrape Fault and the major extensional shear zones that bound the MBG.

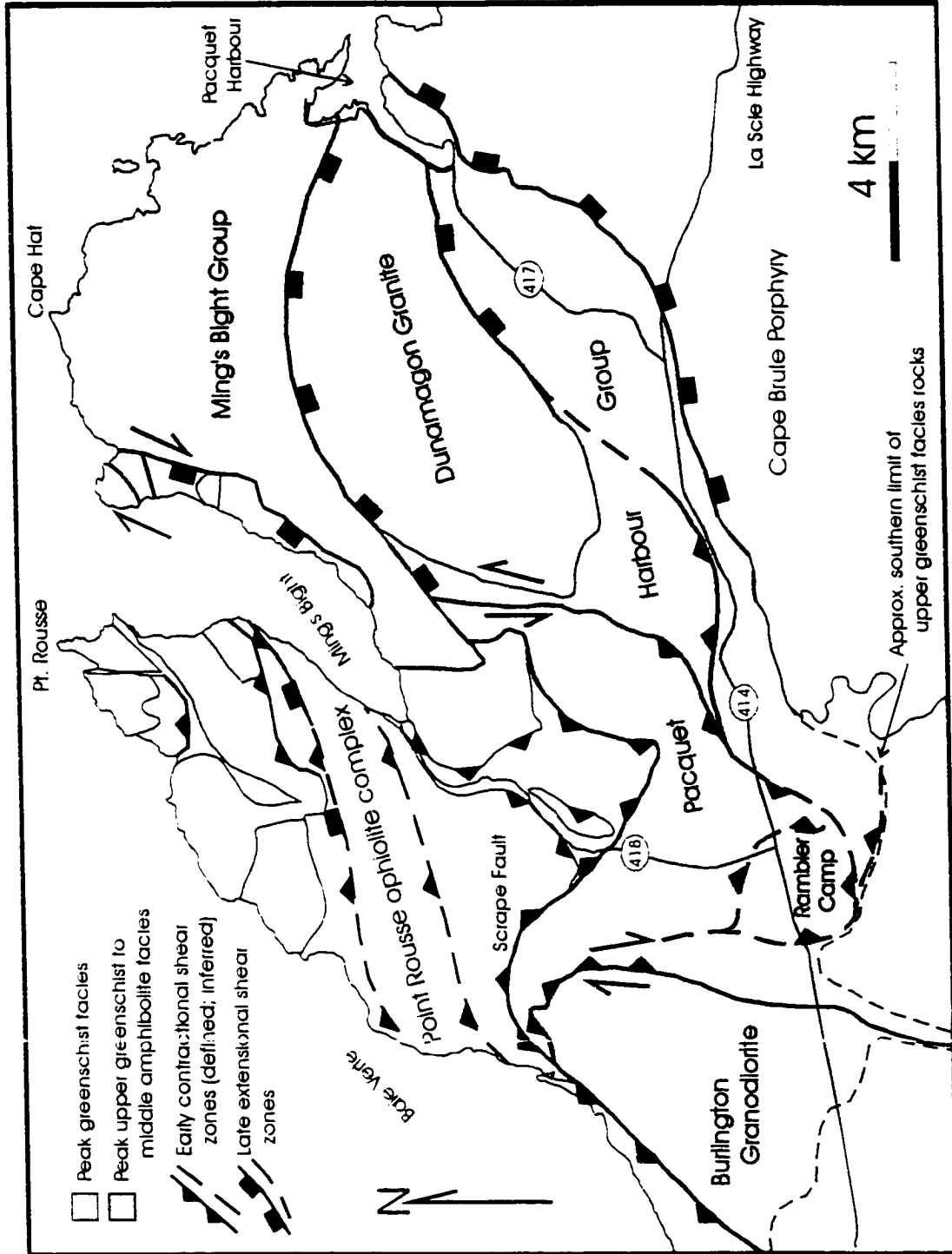


Figure 5.1

textures (e.g., Vernon 1977). In particular, metamorphic mineral assemblages can be conveniently categorized as “pre-peak”, “peak”, or “post-peak”, which correspond temporally to D_1 , D_2 and D_3 , respectively. Prior to describing these assemblages, the porphyroblast-matrix (S_1 - S_e) microstructural relationships of garnet, hornblende, and staurolite porphyroblasts are described, since these provide the basis for the proposed sequence of metamorphic mineral growth.

5.2.1.1 Microstructural relationships

In order to analyze the S_1 - S_e relationships, approximately 30 oriented samples of porphyroblastic rock were collected from the MBG and PHG in widely spaced locations throughout the Pacquet Harbour area. All of the samples had one approximately north-south oriented, subvertical thin section cut perpendicular to the dominant mesoscopic foliation (generally S_2) and approximately parallel to the L_2 lineation (i.e., X-Z section). Twelve samples had an additional thin section cut perpendicular to the mesoscopic lineation (i.e., Y-Z section), and three samples had a third thin section cut parallel to the mesoscopic foliation (i.e., X-Y section). The microstructural descriptions provided below refer mainly to X-Z sections, unless otherwise stated.

Staurolite S_1 - S_e relationships

Staurolite occurs in MBG pelitic schist in two locations in the BBSZ (Map 2). The staurolite porphyroblasts are up to 3cm in maximum dimension, idioblastic to xenoblastic, equant to columnar, and are typically located in quartz-plagioclase-rich domains in the differentiated S_2 crenulation fabric (Bell and Rubenach 1983; Fig. 5.2a). These porphyroblasts are highly poikiloblastic, and contain S_1 defined by fine-grained, elongate

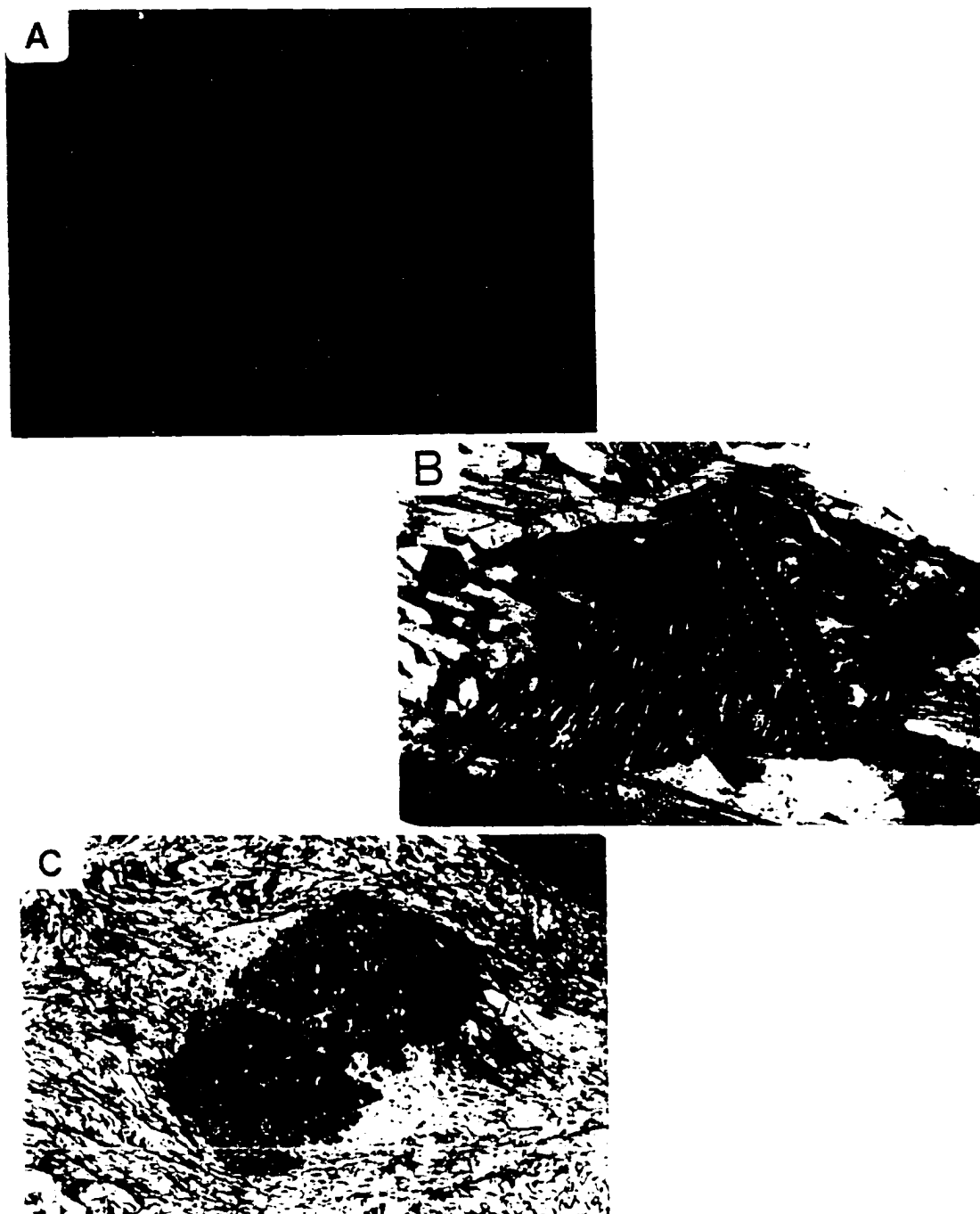


Figure 5.2 Photomicrographs of staurolite and garnet porphyroblasts in the Pacquet Harbour area. See text for details. a) Staurolite porphyroblasts (~0.5cm long) from MBG schist in the BBSZ ~1.5km west of Pacquet Harbour (X-Z section). b) Staurolite porphyroblast (~3.5mm long) that apparently overgrew a differentiated S₁-S₂ crenulation fabric. S₂ plane is marked by the dashed line (X-Z section; same outcrop as above). c) Garnet porphyroblast (~7mm wide) from MBG schist in the BBSZ ~2km west of Pacquet Harbour. r. garnet rims; cz. core zone. (X-Z section).

quartz, plagioclase, and opaque-mineral inclusions. The S_1 are curved to sigmoidal, completely randomly oriented with respect to S_2 , and are generally not continuous into the matrix fabrics (Fig. 5.2a), although in one porphyroblast S_1 appears to be continuous into the crenulated S_1 preserved between S_2 crenulation planes. In another porphyroblast, S_1 defines open microfolds which are transected by an axial planar S_1 crenulation fabric (Fig. 5.2b), consistent with growth of the staurolite over an early stage of S_2 .

S_1 in the staurolite porphyroblasts commonly has an asymmetric, sigmoidal, geometry. In the X-Z sections (looking east), the sigmoidal S_1 always has a Z-sense of asymmetry (e.g., Figs. 5.2a and 5.3a). In contrast, sigmoidal S_1 in Y-Z sections (looking north) always has an S-sense of asymmetry. This pattern of vergence is identical to that illustrated by the F_2 crenulations that plunge southeast and verge southwest; therefore, the S_1 asymmetry is interpreted to reflect growth of the staurolite porphyroblasts over an early stage of the asymmetric F_2 crenulations (Fig. 5.3a). The random orientation of S_1 with respect to S_2 likely results from rotation of the staurolite porphyroblasts about an axis lying in S_2 , since it is difficult to reconcile with passive growth over the crenulations combined with non-rotation (e.g., Passchier et al. 1992).

Hornblende S_1 - S_2 relationships

Hornblende is the most widespread porphyroblastic phase in the Pacquet Harbour area. The mesoscopic structural relationships of these porphyroblasts are variable, and locally consistent with pre-, syn- or post- D_2 growth. The following discussion refers to those porphyroblasts that apparently grew syn- D_2 .

The hornblende porphyroblasts are typically idioblastic to subidioblastic, acicular

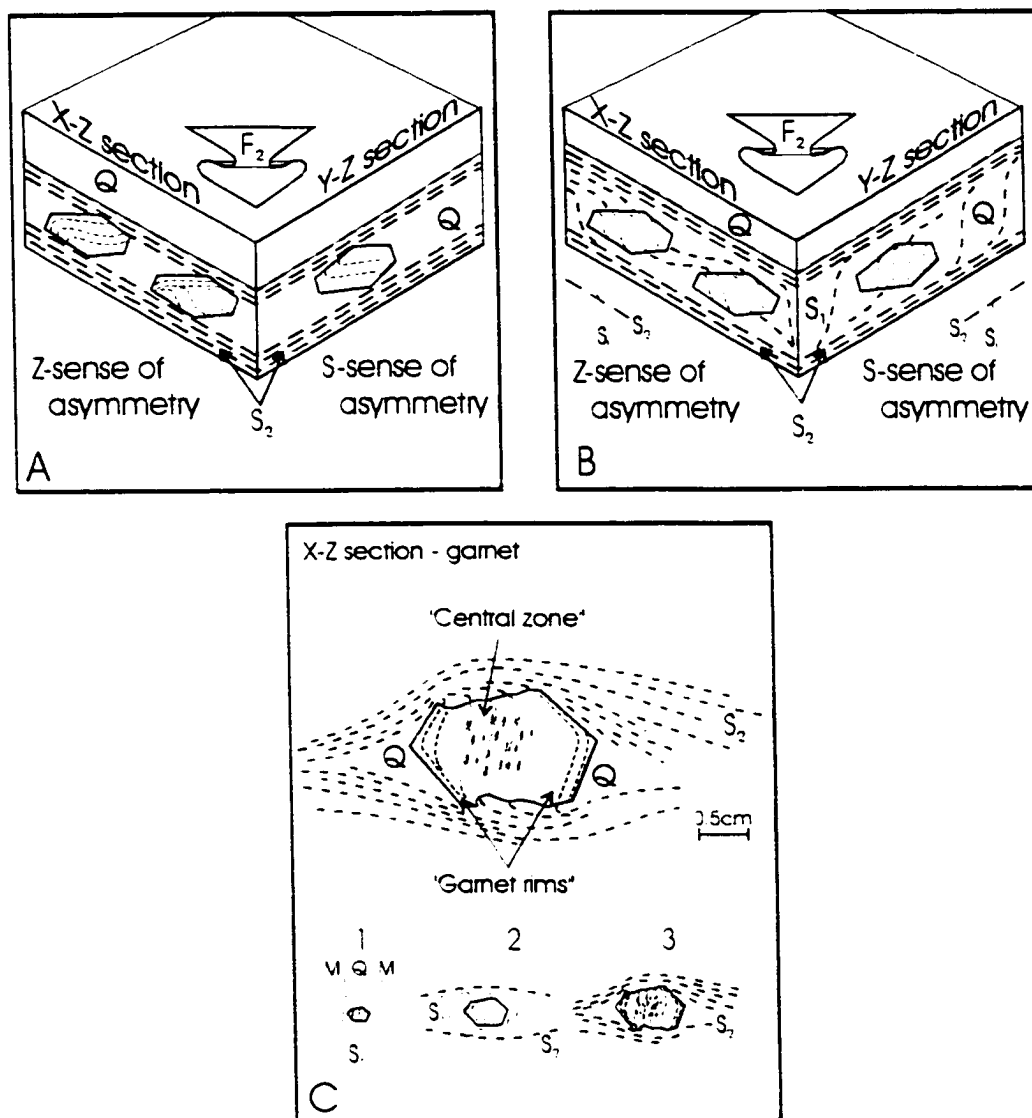


Figure 5.3 Schematic, composite sketches of S₁-S₄ relationships in the Pacquet Harbour area. In all diagrams, 'Q' refers to quartz-rich domains in the matrix. See text for a detailed description. a) Staurolite porphyroblasts. b) Hornblende and garnet porphyroblasts. c) Detailed sketch of S₁-S₄ relationships in a single garnet porphyroblast from the MBG schist in the BBSZ ~2km west of Pacquet Harbour (see Fig. 5.2c), and a schematic model illustrating the development of the S₁-S₄ geometry.

to equant, and up to 5cm in maximum dimension. The porphyroblasts are variably poikiloblastic, and commonly contain well developed S_1 defined by elongate, fine- to medium-grained, quartz, plagioclase, clinozoisite-epidote, and/or ilmenite inclusions. The S_1 vary from straight to sigmoidal, parallel to highly oblique to the matrix S_2 , and exhibit varying degrees of continuity with matrix fabrics. In most examples, S_1 is oblique to S_2 and concordant with, and laterally continuous into, domains of crenulated S_1 . These relationships indicate that the oblique S_1 represents S_1 overgrown early in the development of S_2 (e.g., Jamieson and Vernon 1987; Johnson and Vernon 1995). In X-Z sections (looking east), S_1 is consistently oriented clockwise to S_2 , and sigmoidal S_1 always have a Z-sense of asymmetry (Fig. 5.3b). In Y-Z sections (looking north), S_1 is consistently oriented counterclockwise to S_2 , and sigmoidal S_1 always have an S-sense of asymmetry. These microstructural relationships indicate that the hornblende porphyroblasts with sigmoidal S_1 syntectonically overgrew S_2 crenulations during D_2 (Fig. 5.3b).

Garnet S_1 - S_2 relationships

Garnet is common in the immediate area of the PPSZ, within both the PHG amphibolites and MBG schists. Unlike hornblende, the mesoscopic and microscopic structural relationships of the garnet porphyroblasts are remarkably consistent throughout the Pacquet Harbour area, and these porphyroblasts are thus attributed to a single, relatively short-lived, growth event.

The garnet porphyroblasts range up to ~2cm in diameter, and are idioblastic to sub-idioblastic to highly embayed, and generally equant. The porphyroblasts are variably poikiloblastic, and commonly contain spectacular S_1 defined by elongate, fine- to medium-

grained, quartz, plagioclase, rutile, and/or ilmenite inclusions (Fig. 5.2c).

Internal relationships (X-Z sections) - In many garnet porphyroblasts, a highly poikiloblastic zone comprising fine- to medium-grained quartz and plagioclase inclusions transects the centre of the porphyroblast (Figs. 5.2c and 5.3c). The central zone contains relatively straight S_1 that have a slight sigmoidal geometry at their lateral tips. At the margins of the porphyroblast, the central zone is associated with highly irregular garnet grain boundaries that are bounded by quartz-rich domains in the matrix.

The central zone is bounded by two symmetrically disposed garnet rims that contain very fine-grained rutile and ilmenite inclusions. The semi-massive rims contain S_1 which parallel the porphyroblast margins and curve through $\sim 90^\circ$ (Fig. 5.3c). In contrast to the central zone, the rims generally have well developed external crystal faces that are partly bounded by biotite-rich domains in the matrix. S_1 in both the central zone and the rims are continuous into the matrix S_1 - S_2 crenulation fabric (Fig. 5.3c).

The internal relationships outlined above are consistent with growth of the garnet porphyroblasts over pre-existing S_1 -parallel quartz-domains, and progressive transposition (i.e., rotation) of the domains relative to the garnet porphyroblast during development of the S_2 crenulation fabric (Fig. 5.3c). In this model, the continually growing garnet porphyroblast in the quartz-domain impinges on the adjacent mica-domains in a somewhat later increment of transposition, resulting in the inclusion-poor euhedral rims, and S_1 that record a larger relative change in the orientation of the matrix fabric (e.g., Bell et al. 1986; Fig. 5.3c). In X-Y sections, and sections cut subparallel to the mesoscopic crenulation axis, S_1 are straight to slightly curved, consistent with overgrowth of relatively concentric

crenulations that plunge southeast (Fig. 5.4). Because the garnet porphyroblasts lack closed S_1 loops in Y-Z sections (e.g., Johnson 1993a) growth must have occurred during a brief hiatus in the crenulation event, or growth must have been very rapid relative to the development of the crenulations (Johnson 1993a). The generally high abundance of inclusions, and the consistency of the S_1 - S_e relationships, support the latter hypothesis.

External relationships (X-Z sections) - S_1 in garnet porphyroblasts ranges from straight to curved, but most commonly has a pronounced sigmoidal geometry collectively defined by the 'central' and 'rim' S_1 . Several important microstructural relationships exist between the S_1 and S_e : 1) In X-Z and Y-Z sections, the central S_1 tend to be parallel to, and continuous into, crenulated S_1 domains in the matrix which mimic the sigmoidal geometry and sense of asymmetry of S_1 (Fig. 5.3b and 5.4). 2) The rim and, to a lesser extent, central S_1 are generally continuous into the matrix S_2 (Fig. 5.4). 3) In most samples, the central S_1 are mutually parallel in all garnet porphyroblasts. In these samples, S_1 is parallel to the crenulated S_1 , but highly oblique to S_2 (Fig. 5.4). 4) In X-Z sections (looking east), sigmoidal S_1 in the garnet porphyroblasts always have a Z-sense of asymmetry, and are generally oriented ~ 60 - 90° clockwise from S_2 (Fig. 5.4). 5) In Y-Z sections (looking north), sigmoidal S_1 have a S-sense of asymmetry, and are generally oriented $\sim 60^\circ$ counterclockwise from S_2 . 6) In X-Y sections, S_1 are straight to slightly curved, and concordant to the mesoscopic and microscopic F_2 crenulation axes (Fig. 5.4). 7) Locally, garnet porphyroblasts with sigmoidal S_1 that are discontinuous with S_e are wrapped-around by S_2 .

Collectively, these relationships indicate syn-kinematic garnet growth over the S_2

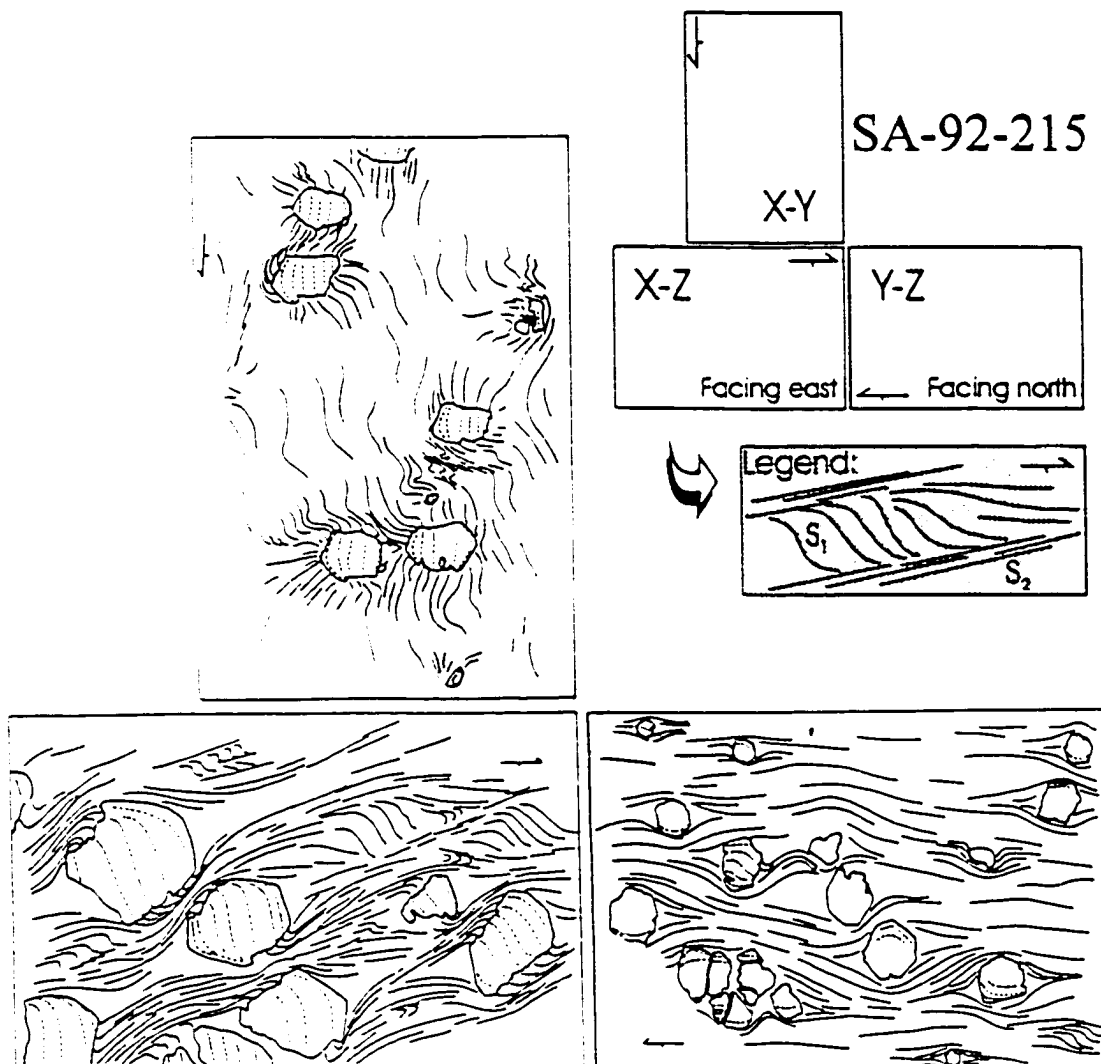


Figure 5.4 Line drawings of S_1 - S_2 relationships in three orthogonal large-format thin sections (7.5cm x 5.0cm) from a representative sample of garnet porphyroblastic MBG schist from the BBSZ ~2km west of Pacquet Harbour. X-Y section (upper left), X-Z section (lower left), and Y-Z section (lower right; see inset). Solid lines, S_2 ; dashed lines, S_1 . The X-Y and Y-Z sections are oriented subparallel to the F_2 crenulation axes, as indicated by the relative lack of sigmoidal S_1 in these sections. See text for detailed discussion.

crenulation fabric in the early stages of D_2 (e.g., Bell 1985; Bell et al. 1986; Jamieson and Vernon 1987; Johnson and Vernon 1995; Fig. 5.3c). Throughout the Pacquet Harbour area, the crenulated S_1 domains in the matrix and S_1 in garnet have a relatively consistent orientation with respect to S_2 . This includes garnet porphyroblasts that are wrapped-around by S_2 or S_3 , and have sigmoidal S_1 that are discontinuous with S_e . These relationships indicate that the garnet porphyroblasts behaved in an *essentially irrotational* manner with respect to S_2 during D_2 deformation (e.g., Bell 1985; Bell et al. 1986, 1992; Steinhardt 1989; Johnson 1990, 1993b; Vernon et al. 1993). The term 'essentially irrotational' is used in this case to acknowledge the fact that there is a locally significant variation in the angular relation between S_1 and S_2 (i.e., 10 to 110°), and that the three-dimensional orientation of most S_1 is poorly constrained (e.g., Passchier et al. 1992). However, microstructures traditionally considered to be indicative of porphyroblast rotation, such as true spiral S_1 (e.g., Rosenfeld 1970; Powell and Vernon 1979; Schoneveld 1979) and widely varying orientations of S_1 relative to S_e (e.g., Passchier et al. 1992; Vernon et al. 1993), are lacking in the examined garnet samples.

5.2.1.2 Pre-peak metamorphic assemblages

As noted in Chapter 3, porphyroblasts associated with peak metamorphism contain fine-grained included mineral assemblages, consistent with a relatively uncomplicated, low-temperature, prograde metamorphic history. In the PHG, hornblende and garnet porphyroblasts contain plagioclase (An_{32-47}), quartz, orthoclase, clinozoisite, chlorite, ilmenite, titanite and apatite inclusions, with rare biotite, whereas plagioclase porphyroblasts contain clinozoisite and biotite inclusions. In the MBG, inclusions in garnet

porphyroblasts comprise plagioclase (An_{33-49}), quartz, orthoclase, ilmenite, chlorite, apatite, and rare biotite, muscovite and rutile, whereas those in staurolite porphyroblasts comprise quartz, plagioclase (An_{33-40}), rutile, pyrite, and rare garnet. The garnet inclusions in staurolite locally contain sigmoidal inclusion trails indicative of syn- S_2 growth. Plagioclase porphyroblasts in the MBG contain quartz, orthoclase, clinozoisite, biotite, muscovite, and ilmenite inclusions, and hornblende porphyroblasts in MBG calc-silicate contain plagioclase (An_{88-93}), quartz, clinozoisite, pyrite, and rare garnet inclusions.

Further evidence of the pre-peak metamorphic mineral assemblage is found within the crenulated domains of S_1 between S_2 crenulation planes. In these domains, S_1 is typically defined by fine-grained biotite, muscovite, and ilmenite in the MBG, and biotite, amphibole, and ilmenite in the PHG. In the Dunamagon Granite, an early fabric defined by aligned biotite, epidote, and titanite is overgrown by hornblende porphyroblasts and transected by S_2 (McDonald 1993). Despite the possibility of mimetic syn- D_2 mineral growth in S_1 , these relationships indicate that amphibole growth at least locally preceded the peak metamorphism, as suggested by Coates (1970).

The pre-peak metamorphic mineral assemblage in the PHG likely comprised plagioclase + biotite + clinozoisite + quartz + chlorite + ilmenite \pm amphibole, whereas that in the MBG likely comprised plagioclase + quartz + biotite + chlorite + clinozoisite + muscovite + ilmenite + rutile. Collectively, these mineral assemblages are consistent with greenschist facies metamorphic conditions during D_1 .

5.2.1.3 Peak metamorphic assemblages

In the PHG, the peak metamorphic mineral assemblage consists of hornblende +

plagioclase (An_{28-42}) + biotite (1.2-2.6% TiO_2) + quartz + epidote-clinozoisite \pm garnet (X_{alm} 0.54-0.66; X_{gro} 0.19-0.27; X_{pyr} 0.06-0.08; X_{spe} 0.07-0.12), with accessory ilmenite, apatite and titanite. This assemblage is consistent with peak metamorphism in the epidote amphibolite facies. Hornblende is pervasive in the PHG, typically forming very coarse-grained (up to 5cm), syn-tectonic (syn- D_2), idioblastic and poikiloblastic porphyroblasts. The hornblende also forms fine- to coarse-grained euhedral to subhedral, inclusion-free grains in the matrix. Throughout the Pacquet Harbour area, hornblende in the PHG ranges from ferroan pargasite to ferroan pargasitic hornblende, and ferro-tschermakite to tschermakite to tschermakititic hornblende to magnesio-hornblende to actinolite, although no compositional zoning was noted within individual hornblende crystals, and individual samples only exhibit subsets of the range presented above. The hornblende is typically associated with fine- to coarse-grained euhedral biotite, and these minerals collectively define S_2 in most locations.

Plagioclase most commonly forms equant-angular to granoblastic-polygonal, locally strain-free grains in the matrix, although it also locally forms <5mm, sub-idioblastic, syntectonic porphyroblasts (An_{34-41}). In rare cases, these porphyroblasts are weakly zoned from relatively Ca-rich rims (An_{41}) to Na-rich cores (An_{35}). The matrix plagioclase is associated with fine- to coarse-grained, granoblastic polygonal quartz in S_2 -parallel microlithons that alternate with the hornblende-biotite microlithons. Garnet forms <1cm, idioblastic to highly embayed, syn-tectonic porphyroblasts with complex inclusion trails (see Section 5.2.1.1), and only occurs in the immediate vicinity of the PPSZ.

Textures in these rocks are consistent with well equilibrated peak-metamorphic

mineral assemblages (Fig. 5.5a). Chemical zonation profiles reveal that the cores of garnet porphyroblasts locally contain remnants of typical prograde growth-zoning patterns, whereas the outer regions exhibit reverse diffusion-zoning (e.g., Tracy 1982; Fig. 5.6a). In addition, several garnet porphyroblasts from the same outcrop as those in Figure 5.6a are associated with nearly flat chemical zonation profiles which are inferred to result from high-temperature volume diffusion during the middle stages of D_2 , implying temperatures in excess of 600°C (Woodsworth 1977; Yardley 1977; Fig. 5.6b).

In the MBG, the peak metamorphic mineral assemblage consists of plagioclase (An_{28-48}) + biotite (0.6-3.3% TiO_2) + muscovite (Si:Al = 7.2:1) + quartz \pm garnet (X_{alm} 0.60-0.72; X_{gro} 0.08-0.15; X_{pyr} 0.09-0.18; X_{spe} 0.05-0.12), staurolite, and kyanite, with accessory clinozoisite, tourmaline, magnetite, ilmenite, titanite, and rutile. This mineral assemblage is consistent with metamorphism in the upper greenschist to upper amphibolite facies. Plagioclase is a pervasive porphyroblastic phase in the MBG, typically forming <1.5cm, sub-idioblastic syntectonic porphyroblasts (An_{26-33}). In many locations, these porphyroblasts have a distinctive spongy appearance due to abundant rounded quartz inclusions. These porphyroblasts preserve S_1 as fine-grained, straight to sigmoidal inclusion trails. In several locations, sigmoidal S_1 is continuous into crenulated domains of S_1 in the matrix, consistent with plagioclase growth during development of S_2 . These porphyroblasts are wrapped around by S_2 and/or S_3 , and generally only have a slight undulose extinction. No chemical zonation was noted, although any zonation present would likely be very slight, based on the restricted compositional range illustrated by these porphyroblasts. Plagioclase also forms irregular to equant to granoblastic grains in the

Figure 5.5 Textures and mineral assemblages in MBG schist and PHG amphibolite in the Pacquet Harbour and Ming's Bight areas. **a)** Well equilibrated granoblastic polygonal texture in PHG amphibolite at Pelee Point (field of view is ~2mm wide). **b)** Staurolite-kyanite-garnet-biotite mineral assemblage in MBG schist in the BBSZ. Note the included garnet in staurolite, and the tabular kyanite porphyroblast oriented parallel to S_2 at the lower edge of the photo (field of view is ~6mm wide). **c)** Post-tectonic clinozoisite (euhedral, high relief) and biotite (large, dark) porphyroblasts which overgrew S_2 in PHG mylonite near the La Scie Highway - Woodstock Road junction (field of view is ~4mm wide). **d)** Syn- S_2 albite (light grey, highly poikiloblastic porphyroblast in the centre of the photo) in MBG schist on the south shore of Ming's Bight ~200m east of Actinolite Bay (Map 5; field of view is ~3mm wide). **e)** Garnet-staurolite-biotite MBG schist at Seven Brooks Point. The early (S_2) fabric, which trends from upper right to lower left, is transected by an S_4 shear band (field of view is ~7mm wide). **f)** Asymmetric fabric defined by fine-grained hornblende crystals in mylonite within the southerly-dipping D_5 shear zone ~150m north of Caplin Cove (Map 8; field of view is 3mm wide).

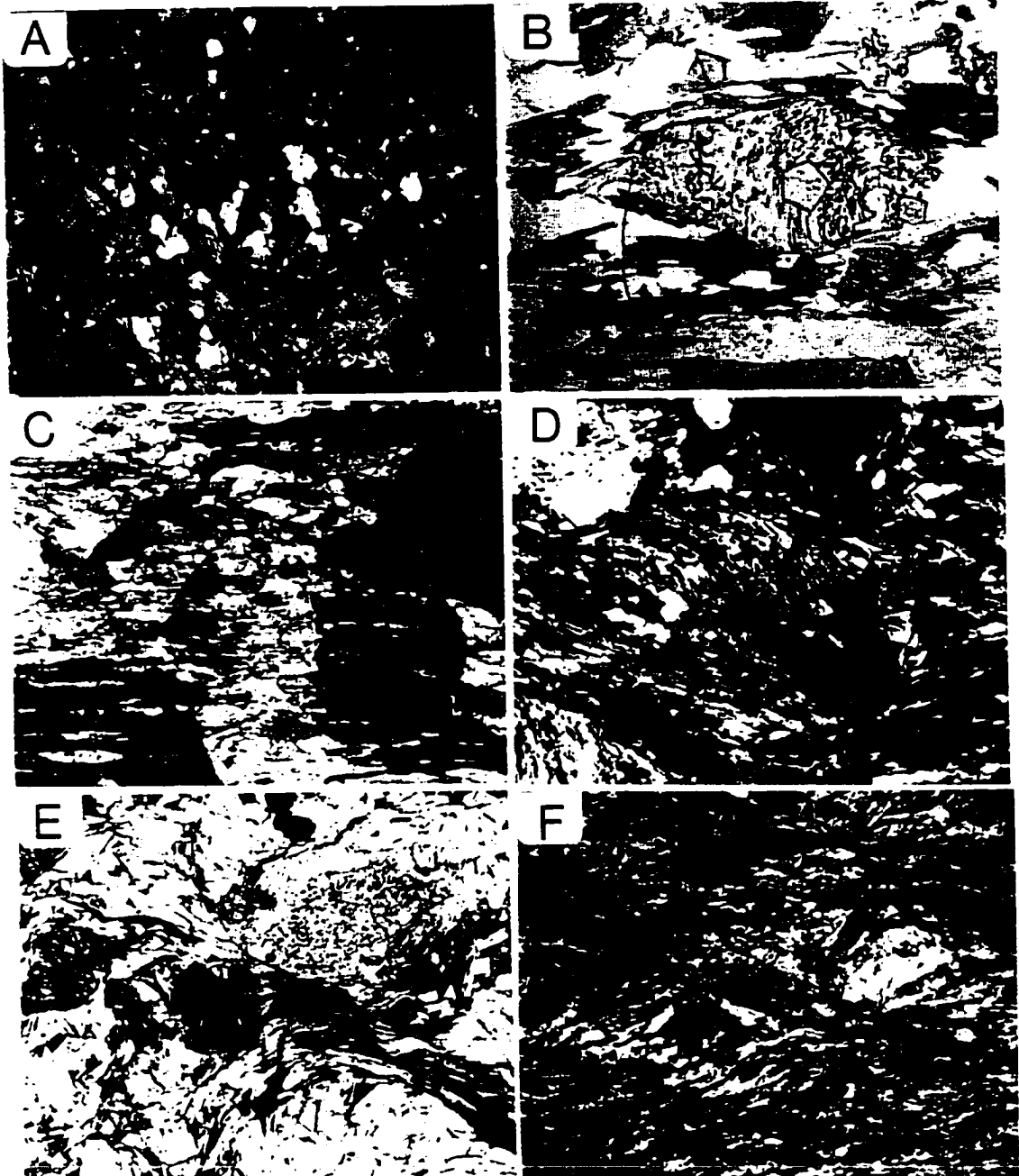


Figure 5.5

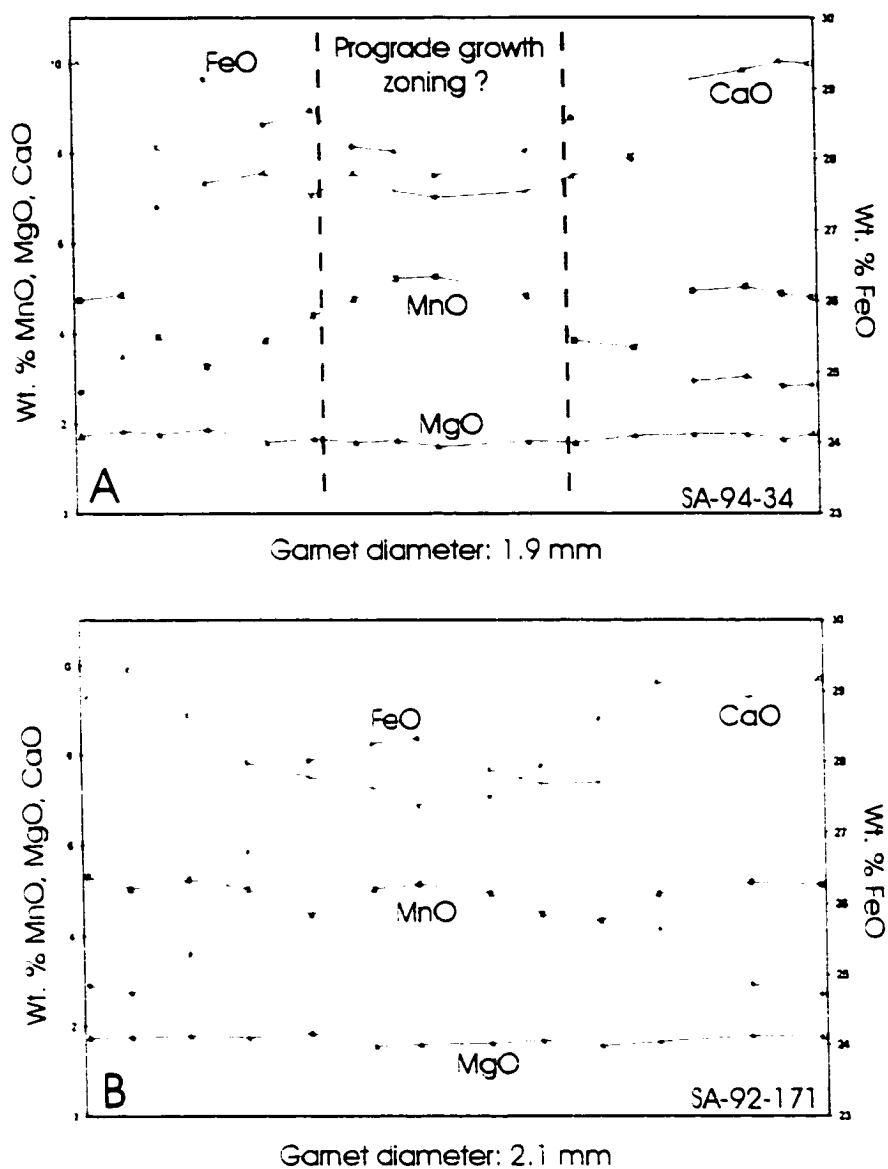


Figure 5.6 Compositional variations across idioblastic, syn-D₁, garnet porphyroblasts from PHG amphibolite at Pelee Point. The horizontal axis of the profiles represents the full diameter of the garnet porphyroblasts. In order to increase the probability of obtaining true core compositions, the profiles were constructed from those garnet porphyroblasts with the largest diameter in thin section. a) Zoning profile illustrating the possible remnants of prograde growth zoning in the core (note the partial 'bell-shaped' MnO profile), with reverse diffusion zoning in the rim. b) Garnet porphyroblast from the same outcrop as the previous garnet, but with a nearly homogeneous MnO profile, possibly indicating volume diffusion.

matrix (An_{26-43}), which generally have sutured to angular to polygonal grain-boundaries, respectively, and are closely associated with texturally similar quartz. Orthoclase was only noted as inclusions in garnet porphyroblasts.

The garnet forms <2.0cm diameter, idioblastic to sub-idioblastic, syntectonic porphyroblasts, which are most abundant adjacent to the PPSZ, but occur sporadically throughout the MBG. The garnet porphyroblasts typically have inclusion-rich cores, and symmetrical inclusion-poor rims, which are interpreted to reflect progressive overgrowth of Q- and M-domains, respectively (Fig. 5.3c). In one location, a highly poikiloblastic plagioclase porphyroblast is included within a large garnet porphyroblast, indicating that plagioclase growth may have slightly preceded that of garnet. In places, garnet porphyroblasts are associated with a reaction halo depleted in biotite, suggesting garnet growth at the expense of biotite. Chemical zonation profiles from garnet porphyroblasts in the MBG reveal very well developed prograde growth zoning patterns, with only very thin (<0.5mm) margins of reverse zoning (e.g., Tracy 1982; Fig. 5.7a), or relatively homogeneous patterns (Fig. 5.7b), possibly indicative of volume diffusion. No evidence was found in the zoning profiles for more than one phase of garnet growth.

Muscovite and biotite typically form fine- to coarse-grained, idioblastic crystals in the matrix, and collectively define S_2 . In many locations, the phyllosilicates occur in S_2 -parallel M-domains that alternate with Q-domains of granular quartz and plagioclase. Paragonite and margarite were not noted in thin section, or discovered with the microprobe, in any sample from the thesis area. The muscovite and biotite are conspicuously absent and abundant, respectively, in the immediate area of the staurolite-

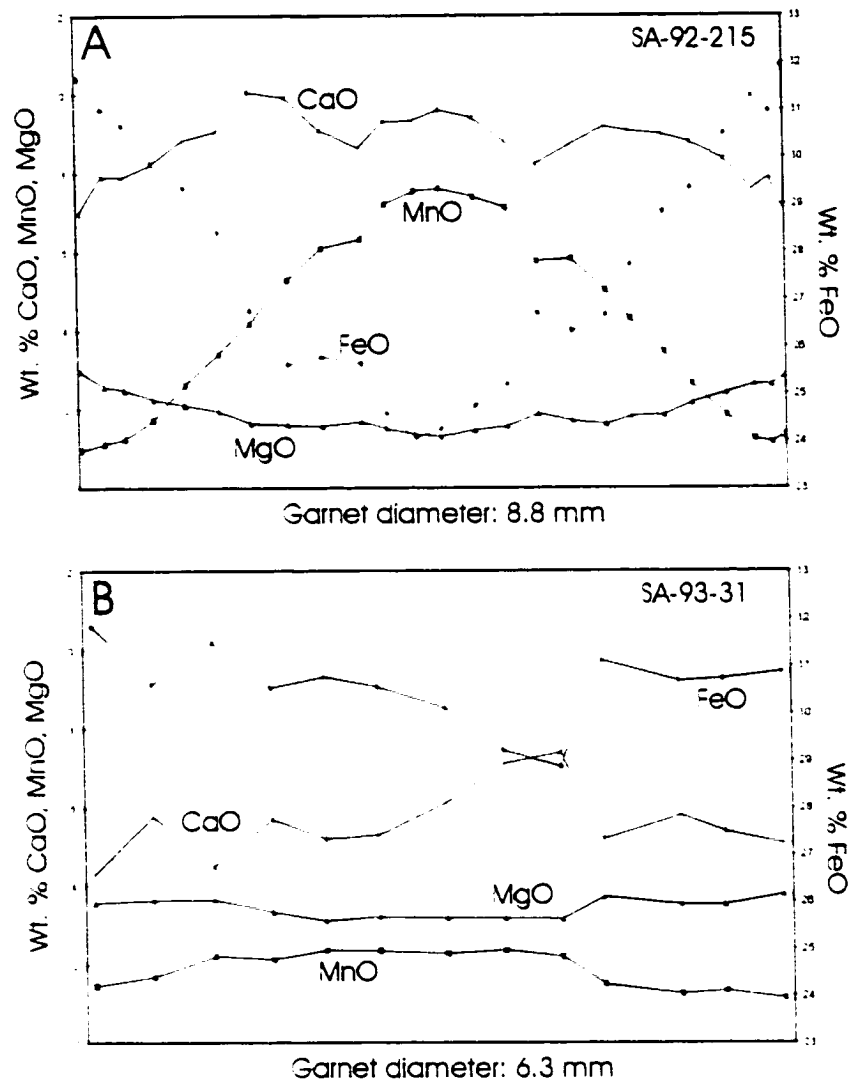
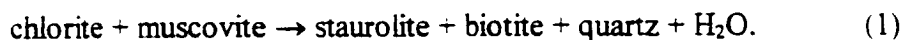


Figure 5.7 Compositional variations across large, subhedral, syn- D_2 , garnet porphyroblasts from MBG schist in the BBSZ at Pacquet Harbour. The horizontal axis of the profiles represents the full diameter of the garnet porphyroblasts. In order to increase the probability of obtaining true core compositions, the profiles were constructed from those garnet porphyroblasts with the largest diameter in thin section. a) Well preserved prograde growth zoning pattern, with only slight reverse diffusion zoning in the rim. b) Profile illustrating nearly homogeneous MnO contents. Compare with a).

bearing schist, possibly indicating that muscovite was consumed in a prograde reaction of the type:

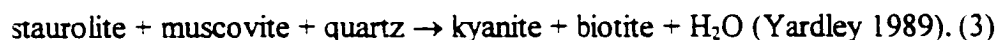


In the BBSZ, muscovite locally occurs in the hinges of F_2 folds as <5mm, idioblastic, randomly oriented porphyroblasts with coarse-grained inclusions of quartz and plagioclase. These porphyroblasts are wrapped around by the axial planar S_2 , have only a weak undulose extinction, and are thus interpreted to reflect syn- to late- S_2 growth of the muscovite in a relatively 'strain-free' environment within the F_2 fold hinges. The muscovite porphyroblasts are not associated with staurolite.

Staurolite was noted in two locations in the immediate hangingwall of the PPSZ, and typically forms <3.0cm idioblastic to anhedral and highly embayed porphyroblasts. In several thin sections, garnet forms euhedral inclusions in staurolite, suggesting that the staurolite-in reaction did not involve consumption of garnet (Fig. 5.5b). Given the absence of chloritoid in these rocks, it seems likely that staurolite formed by reaction (1) above. In both locations in the PPSZ, staurolite is associated with the only kyanite in the MBG. The kyanite forms <5cm idioblastic to anhedral, tabular porphyroblasts in the staurolite schist (Fig. 5.5b), as well as in quartz veins. In samples with minor kyanite (<1%), the staurolite forms coarse-grained, generally idioblastic, porphyroblasts. In contrast, samples with more abundant kyanite (~5%) tend to contain finer-grained, idioblastic to xenoblastic, matrix staurolite which is only locally porphyroblastic. This relationship, together with the coincidence of staurolite and kyanite, may indicate kyanite-in reactions of the type:



and/or



These reactions also account for the absence of muscovite, and abundance of biotite in the staurolite schist.

The presence of the staurolite-kyanite paragenesis in only two places in the MBG may be explained in two ways. 1) The development of a local, and unique, metamorphic environment, possibly related to a distinctive rock or fluid composition (e.g., Lang 1991). For example, the localized occurrence of kyanite as coarse crystals in quartz veins may be consistent with the local presence of a high-temperature metamorphic fluid phase (e.g., Kerrick 1988). 2) The staurolite-kyanite schist may represent tectonic inclusions transported from a different (i.e., lower) structural level of the MBG during D_2 or D_3 . Support for this hypothesis may be found in the apparently 'exotic' slivers of (PHG?) amphibolite which were noted in both these locations.

Calc-silicate boudins and layers in the MBG contain a peak metamorphic mineral assemblage of magnesio-hornblende + clinozoisite + plagioclase (An_{87-93}) + garnet (X_{alm} 0.32-0.39; X_{gro} 0.31-0.43; X_{pyr} 0.04-0.07; X_{spe} 0.16-0.22) + quartz + titanite \pm pyrite. This mineral assemblage is equivalent to the staurolite-kyanite pelite zone, and is therefore consistent with metamorphism in the amphibolite facies (Kennedy 1949). Within this lithology, garnet forms <1 mm, euhedral, relatively inclusion-free crystals. Hornblende and clinozoisite form up to 5 cm, acicular, subidioblastic, porphyroblasts, which tend to contain abundant anorthite, quartz, and garnet inclusions. In several domains, matrix hornblende,

garnet, plagioclase, quartz, and clinozoisite form an apparently well-equilibrated, medium-grained, granoblastic-polygonal texture.

In the Dunamagon Granite, metamorphic mineral assemblages diagnostic of the peak metamorphic conditions are only present within mafic dykes and xenoliths. In these rocks, the mineral assemblage consists of hornblende + biotite + plagioclase + epidote + quartz, and is consistent with peak metamorphism of the Dunamagon Granite in the epidote amphibolite facies (McDonald 1993).

Towards the south, the syn-D₂ metamorphic grade decreases in an apparently gradational manner structurally upward through the PHG. In the area of the La Scie Highway-Woodstock Road junction, mineral assemblages in PHG mafic volcanic rocks comprise actinolite-hornblende + plagioclase (An₂₈₋₃₂) + biotite + quartz + clinozoisite + ilmenite, and lack garnet. In these rocks, the amphibole forms <5cm long, acicular, idioblastic porphyroblasts that, together with fine-grained biotite, define S₁-L₂. The plagioclase and quartz form very fine- to medium-grained, anhedral grains with sutured to angular grain boundaries. In the Cape Brule Porphyry, xenoliths flattened in the S₂ plane contain fine-grained chlorite-biotite-rich mineral assemblages. Collectively, these assemblages are consistent with peak greenschist facies metamorphism in these locations.

5.2.1.4 Post-peak metamorphic assemblages

In most samples from the Pacquet Harbour area, the peak metamorphic mineral assemblage and textures appear to be quite pristine, and there is little evidence for post-peak mineral growth and recrystallization aside from slight sericitization of plagioclase and garnet, and chloritization of amphibole and biotite. Syn-D₂ hornblende, biotite, and

plagioclase porphyroblasts were not significantly deformed subsequent to D_2 , and lack obvious examples of retrograde overgrowth and/or re-equilibration (i.e., reaction textures, compositional zonation, etc.). In some cases, mesoscopic D_2 deformation structures are associated with 'unstable' microstructures (e.g., highly sutured quartz ribbons), that would have readily recrystallized to a lower surface-energy state during any significant metamorphism and/or deformation subsequent to D_2 . These relationships are collectively interpreted to reflect rapid post-metamorphic cooling of the Pacquet Harbour area.

Hornblende in the PHG locally forms randomly oriented, idioblastic porphyroblasts that overgrow S_2 , and thus may be attributable to post-peak metamorphic mineral growth. In the southern portions of the PHG near the La Scie Highway-Woodstock Road junction, the mylonitic S_2 is locally overgrown by randomly-oriented hornblende, biotite, clinozoisite, and plagioclase (An_{50-55}) porphyroblasts (Fig. 5.5c). These porphyroblasts are idioblastic, contain straight inclusion trails that are continuous into the matrix S_2 , and have a weak undulose extinction. These features are consistent with late to post-kinematic porphyroblast growth with respect to S_2 , and these porphyroblasts may therefore represent a post-peak metamorphic mineral assemblage in the PHG.

In the Pacquet Harbour area, post-peak metamorphic mineral assemblages are best-developed in the BBSZ. In this shear zone, the peak-metamorphic (D_2) fabric is transected by the S_3 foliation defined by biotite and chlorite. In addition, large randomly oriented, weakly deformed, biotite porphyroblasts commonly overgrow S_2 . McDonald (1993) noted deformed prehnite in a leucocratic layer in mylonitic amphibolite that is transected by the BBSZ near the northern contact of the Dunamagon Granite. In the

present study, the deformed prehnite is interpreted to record the latest (D_3) increment of deformation and metamorphism in the Pacquet Harbour area (i.e., $<350^\circ\text{C}$).

Staurolite porphyroblasts in the BBSZ are locally pseudomorphed by fibrous sericite (the inclusion trails are locally well preserved), and coarse-grained radiating clusters (bow-ties) of idioblastic chlorite overgrow S_3 . Garnet is also locally replaced by chlorite and sericite. In many locations, chlorite is interleaved with S_3 biotite, and occurs along fractures in syn- D_2 garnet porphyroblasts. These minerals are interpreted to reflect the latest phase of retrograde metamorphism during post-peak cooling.

5.2.2 Ming's Bight area

In the Ming's Bight area, the immediate structural footwall of the frontal and lateral ramps was subjected to peak lower amphibolite facies metamorphism during D_1 - D_2 , and the metamorphic grade apparently decreased structurally downward through the PHG, and possibly upward from the Scrape Fault through the PROC (e.g., Gale 1971; Hibbard 1983). This relatively simple metamorphic architecture has been significantly complicated by protracted D_3 , D_4 , and D_5 deformation, which juxtaposed rocks previously metamorphosed and deformed in the lower greenschist to lower amphibolite facies along a series of shear zones and faults associated with greenschist facies metamorphism. Thus, metamorphic mineral assemblages and textures associated with spatially and temporally heterogeneous deformation and metamorphism are juxtaposed over short distances in the Ming's Bight area. In order to simplify this complex distribution, the metamorphic mineral assemblages are described with reference to the deformation sequence.

5.2.2.1 D₁ metamorphic assemblages

In the PROC in the hangingwall of the Scrape Fault, syn-D₁ metamorphic mineral assemblages in mafic volcanic and meta-clastic rocks comprise actinolite + albite + chlorite + clinozoisite-epidote ± biotite, quartz, calcite, and titanite (Kidd 1974; Kidd et al. 1978; Hibbard 1983). This assemblage indicates lower greenschist facies metamorphism, and there is no evidence to support significant or widespread overprinting of this assemblage subsequent to D₁.

In PHG rocks in the immediate footwall of the Scrape Fault, syn-D₁ metamorphic mineral assemblages in the mafic volcanic and volcanoclastic rocks comprise hornblende + plagioclase + epidote-clinozoisite + biotite + quartz ± garnet, with accessory titanite, ilmenite, and pyrite. This assemblage indicates upper greenschist to lower amphibolite facies metamorphism (Gale 1971; Tuach 1976). The hornblende forms idioblastic to xenoblastic porphyroblasts that are oriented parallel to S₁ and define the L₁ mineral lineation. Gale (1971) noted that these fabrics are locally randomly overgrown by hornblende and actinolite porphyroblasts, suggesting amphibole growth in a strain-free environment subsequent to D₁. In the present study, this relationship is interpreted to reflect late- to post-D₁, but pre-D₃, amphibole growth and recrystallization in the deepest levels of the south-verging thrust-stack. This interpretation is partly supported by the fact that amphibole growth in this area pre-dates D₃, except for local recrystallized actinolite in the axial planes of F₃ folds (Tuach 1976). This interpretation may also be compatible with ⁴⁰Ar/³⁹Ar data, which imply a considerable time-span between the onset of D₁, and regional cooling through the hornblende closure temperature (~30 Ma; see Chapter 6).

Further south in the area of the Rambler mine, Gale (1971) noted that the amphibole is predominantly actinolitic, and chlorite and biotite are more abundant, indicating greenschist facies metamorphism in these locations.

In the MBG and PHG, S_1 is preserved as inclusion trails in syn- D_2 (locally syn- D_1 - D_2 ; Section 4.2.2) porphyroblasts. This relationship indicates that the early stages of D_1 were probably associated with increasing P-T conditions, with the metamorphic peak achieved in a later increment of D_1 - D_2 . The inclusion trails in plagioclase porphyroblasts comprise fine-grained quartz, biotite, muscovite, orthoclase, rutile, and ilmenite, and garnet porphyroblasts contain inclusions of plagioclase, quartz, biotite, muscovite, rutile, and ilmenite. These included assemblages indicate greenschist facies metamorphism.

Further north in the area between Jimmy's Cove and Caplin Cove, S_1 is defined by fine-grained chlorite, biotite, sericite, and ilmenite in meta-clastic rocks. In addition, syn- D_2 staurolite, garnet, and plagioclase porphyroblasts at Seven Brooks Point contain S_1 as trails of quartz, plagioclase, rutile, and ilmenite inclusions. Collectively, these assemblages are consistent with greenschist facies metamorphic conditions during development of S_1 .

5.2.2.2 D_2 metamorphic assemblages

Syn- D_2 metamorphic assemblages in the MBG comprise plagioclase (An_{0-50}) + quartz + biotite (1.0-2.2% TiO_2) + muscovite (Si:Al = 7.1-8.3:1) \pm garnet (X_{alm} 0.66-0.71; X_{gro} 0.09-0.13; X_{pyr} 0.12-0.14; X_{spe} 0.05-0.08), staurolite, and chlorite, with accessory epidote-clinozoisite, tourmaline, apatite, ilmenite, titanite, magnetite, and rutile. This mineralogy suggests peak metamorphic conditions in the upper greenschist to lower amphibolite facies.

Plagioclase is the most abundant porphyroblastic phase in the MBG, forming widespread <1.5cm diameter, sub-idioblastic porphyroblasts that are variably poikiloblastic, and commonly contain straight to curved to sigmoidal inclusion trails that are oriented at a high angle to S_2 . The sigmoidal S_1 are locally continuous into S_2 and are interpreted as reflecting syntectonic overgrowth of S_1 in the early stages of crenulation by S_2 (e.g., Bell et al. 1986; Jamieson and Vernon 1987; Fig. 5.5d). The syntectonic plagioclase porphyroblasts have compositions ranging from An_{42-48} at Seven Brooks Point, to An_{0-5} along the south shore of Ming's Bight and at Grappling Point. The coexistence of plagioclase with garnet and staurolite porphyroblasts at Seven Brooks Point may indicate that calcic plagioclase is related to slightly higher peak-metamorphic P-T conditions in this location. This hypothesis is compatible with the location of Seven Brooks Point in the structural footwall of the D_4 GTCSZ (i.e., a lower structural level of the MBG). In the matrix, plagioclase is closely associated with quartz, and both phases form fine- to medium-grained, equant grains with angular to slightly sutured grain boundaries. Quartz also commonly forms elongate, sutured, quartz ribbons with a strong crystallographic preferred orientation.

Garnet in the MBG forms <0.5cm, idioblastic porphyroblasts in several locations immediately east of Ming's South Brook in the footwall of the D_2 transpressional shear zone that separates the MBG from the PROC (Map 4). Garnet was not noted elsewhere in the Ming's Bight area, aside from outcrops at Seven Brooks Point. Microstructural relationships indicate that these porphyroblasts grew during the early stages of D_2 (e.g., Section 4.2.2; Figs. 4.3b, 4.3c, and 4.4). Biotite and muscovite form fine- to coarse-

grained, euhedral, foliated crystals in the matrix that are concentrated into S_2 -parallel mica-rich domains that alternate with quartz-plagioclase-rich domains. Biotite and muscovite also locally form fine-grained mica fish in domains of S_2 -parallel quartz-ribbons.

Outcrops of MBG schist at Seven Brooks Point contain abundant staurolite, garnet, and plagioclase porphyroblasts which are generally <1 cm in the maximum dimension, sub-idioblastic, and highly poikiloblastic with well developed inclusion trails. Locally, well preserved S_1 - S_e relationships indicate that these porphyroblasts syntectonically overgrew the late stages of a differentiated S_2 crenulation fabric prior to development of an asymmetric, shallowly northwest-dipping, S_4 shear-band foliation associated with the GTCSZ (Fig. 5.5e).

In the PHG, syn- D_2 metamorphic mineral assemblages are variable and depend on the lithology and structural setting. In felsic volcanoclastic rocks the assemblage consists of plagioclase + quartz + biotite + muscovite + chlorite \pm garnet, and clinozoisite, with accessory ilmenite and tourmaline. In these rocks, S_2 is locally defined by domains of fine-grained euhedral biotite and muscovite, alternating with domains rich in fine- to medium-grained, equigranular plagioclase and clinozoisite. In mafic volcanic rocks, the assemblage comprises actinolite-hornblende + plagioclase + biotite + chlorite + epidote-clinozoisite + quartz \pm garnet, with accessory carbonate, ilmenite, and titanite. In the northernmost exposures of the PHG near the southern shore of Ming's Bight, the mafic volcanic rocks locally contain well equilibrated, granoblastic-polygonal textures. In these locations, the hornblende forms coarse-grained, idioblastic to subidioblastic porphyroblasts which define L_2 , and locally form prominent amphibole-fish (Fig. 4.2d). In addition, granoblastic

plagioclase in the matrix comprises albite (An_{3-7}) and oligoclase (An_{15-24}), consistent with plagioclase compositions on either side of the peristerite gap, and thus upper greenschist to lower amphibolite facies metamorphic conditions (e.g., Crawford 1966; Barker 1990).

In Actinolite Bay and White Cow Bay (Map 5), mafic volcanic rocks typically contain actinolite-hornblende + plagioclase + quartz + biotite + chlorite \pm carbonate, epidote-clinozoisite, titanite, rutile, and pyrite. In these rocks, amphibole forms finer-grained, acicular to fibrous crystals, and quartz and plagioclase only locally have a granoblastic-polygonal texture. In several locations, these rocks contain abundant <0.5 cm diameter, sub-idioblastic albite porphyroblasts. These porphyroblasts contain sigmoidal S_1 which are continuous into the matrix S_2 , and locally have well-developed σ -type strain shadows which, together with asymmetric shear bands in the matrix, are consistent with sinistral transcurrent shear along S_2 . These relationships are consistent with syn- D_2 porphyroblastesis, and upper greenschist facies metamorphic conditions.

Coticules in Actinolite Bay contain a well equilibrated granoblastic assemblage comprising $\sim 50\%$ spessartine-rich garnet (X_{alm} 0.52-0.58; X_{spe} 0.22-0.33; X_{gro} 0.09-0.22; X_{pyr} 0.02-0.04), with $\sim 20\%$ amphibole (tschermakitic hornblende and cummingtonite-anthophyllite), $\sim 20\%$ quartz, 5% magnetite, and $<1\%$ biotite.

In PROC rocks between Deep Cove and Caplin Cove (Maps 4 and 7), the metamorphic assemblage that defines S_2 comprises very fine- to fine-grained plagioclase + quartz + biotite + chlorite + sericite \pm actinolite, carbonate, titanite, and epidote-clinozoisite. These mineral assemblages may indicate greenschist facies metamorphism during D_2 in these locations. In contrast, the block of structurally complex amphibolite to

the north of Caplin Cove (Map 8) contains pre-D₃ coarse-grained, idioblastic, tschermakitic hornblende porphyroblasts, matrix oligoclase (An₂₀), and anhedral, poikiloblastic garnet, consistent with (at least) upper greenschist facies metamorphic conditions. The anomalously high pre-D₃ metamorphic grade within this block supports the hypothesis that it was transported from a lower structural level, possibly during a later increment of compressional deformation, or during extensional exhumation.

5.2.2.3 D₃ metamorphic assemblages

D₃ was not associated with widespread growth or recrystallization of metamorphic minerals. In places where D₃ structures are developed (primarily in the northern portions of the PHG and along the south shore of Ming's Bight), S₃ is defined by fine- to medium-grained biotite + chlorite ± actinolite in PHG mafic lithologies, and biotite + muscovite ± chlorite in PHG felsic lithologies and the MBG. Along the contact between the MBG and PROC in Ming's South Brook (Map 4), the mylonitic S₂, as defined by a differentiated crenulation fabric and trails of fine-grained titanite and ilmenite, is locally overgrown by medium- to coarse-grained, foliated to decussate biotite and chlorite which may be related to metamorphism during D₃. In addition, the block of structurally complex amphibolite north of Caplin Cove contains weakly strained hornblende porphyroblasts that overgrew open F₃ crenulations, and are preferentially oriented parallel to the axial planes of these crenulations, consistent with hornblende growth during D₃. Because the 'regional' syn-D₃ mineral assemblage lacks hornblende, the presence of apparent syn-D₃ hornblende porphyroblasts in this location may indicate that D₃ structures initiated in the waning stages of high-grade (i.e., D₁-D₂) metamorphism, and are thus locally associated with a

higher-temperature mineral assemblage. This hypothesis is further developed in Section 6.4. Collectively, syn- D_3 mineral assemblages are consistent with lower to upper greenschist facies metamorphism.

5.2.2.4 D_4 metamorphic assemblages

F_4 folds in MBG schist are commonly associated with an axial planar S_4 foliation defined by muscovite and biotite, and this is the typical metamorphic mineral assemblage which can clearly be ascribed to D_4 . In addition, deformation in the GTCSZ resulted in extensive recrystallization of biotite, muscovite, and quartz. In the shear zone, quartz forms elongate ribbons with sutured grain boundaries, undulose extinction, and a locally well developed crystallographic preferred orientation. Muscovite and biotite form fine- to coarse-grained idioblastic foliated grains, as well as mica fish. This fabric wraps around subhedral plagioclase porphyroblasts with undulose extinction, subgrains, and S_1 which are highly oblique to, and discontinuous with, S_4 . These features are consistent with greenschist facies metamorphic conditions during D_4 .

5.2.2.5 D_5 metamorphic assemblages

The metamorphic mineral assemblage in D_5 shear zones varies with lithology. In PROC greenschist, the assemblage typically comprises actinolite-hornblende + plagioclase (Al_{13-28}) + quartz + chlorite + biotite \pm carbonate, with accessory titanite, epidote-clinozoisite, and pyrite. Amphibole forms <5mm, acicular, idioblastic to sub-idioblastic porphyroblasts of tschermakitic hornblende, or fine- to medium-grained, acicular, subhedral to fibrous grains of actinolic hornblende or actinolite. These crystals, together with fine-grained chlorite and biotite, typically define the mylonitic fabric (Fig. 5.5f), but

also form <1 mm, subhedral, porphyroclasts. In several locations, idioblastic amphibole crystals with a slight undulose extinction and no strain shadows overgrow S_5 , consistent with late to post- D_5 growth. Chlorite locally occurs in fibrous, decussate masses, which apparently replaced amphibole subsequent to D_5 shearing. Quartz and plagioclase form very fine- to fine-grained, equigranular grains in the matrix with a locally well developed crystallographic preferred orientation. Quartz locally forms prominent ribbons.

In MBG schist, the syn- D_5 assemblage comprises quartz + plagioclase + biotite + chlorite \pm muscovite and carbonate. S_5 in these rocks is defined by very well developed sutured quartz and plagioclase ribbons, biotite fish, and foliated biotite and chlorite (Fig. 4.9b). Collectively, these mineral assemblages are consistent with shear during upper greenschist facies metamorphism.

5.3 THERMOBAROMETRY

5.3.1 *Rationale, sample selection, and approach*

The thermobarometric analysis in the present study was undertaken with the goal of establishing the peak P-T conditions achieved in the MBG and northern portions of the PHG. However, several factors collectively served to hinder this analysis: 1) mineral assemblages amenable to thermobarometry mainly occur in the Pacquet Harbour area; 2) important thermobarometers involving aluminosilicate, such as garnet- Al_2SiO_5 -quartz-plagioclase (GASP; Ghent 1976) and garnet- Al_2SiO_5 -rutile-ilmenite-quartz (GRAIL; Bohlen et al. 1983), proved unreliable due to extensive retrograde alteration of kyanite-bearing mineral assemblages in the BBSZ; 3) garnet is relatively rare in the MBG and PHG, and very rarely contains inclusion suites amenable to thermobarometry; 4) in the few

locations adjacent to the PPSZ where garnet is abundant in the MBG, the mineral assemblage lacks muscovite, and thus the thermobarometer garnet-biotite-muscovite-plagioclase (Ghent and Stout 1981) is not applicable; 5) chemical zoning profiles from garnet porphyroblasts typically display zoning anomalies, reverse diffusional zoning, and/or the effects of volume diffusion, and thus the selection of garnet compositions for thermobarometric analysis is highly subjective; and 6) the garnet-muscovite-biotite-plagioclase thermobarometer, which could be applied to several samples from the MBG, comprises only two independent equilibria, leading to difficulties in assessing the validity of P-T estimates obtained from this assemblage (Berman 1991).

In light of the above limitations, only two samples were eventually selected for thermobarometry. The samples (92-171, 93-34) were collected from PHG amphibolite at Pelee Point, and contain a texturally well-equilibrated (e.g., Vernon 1977) mineral assemblage comprising hornblende + plagioclase + biotite + quartz + garnet + epidote-clinzoisite + ilmenite + titanite, which represents the peak metamorphic mineral assemblage in the PHG, as described in Section 5.2.1.3. Aside from the very minor alteration of plagioclase and garnet to sericite, and biotite to chlorite, these samples contain no obvious retrograde mineral phases.

Mineral compositions were obtained using the automated JEOL 733 Superprobe at Dalhousie University. Operating conditions were: 40 second counting time; ~15 nA beam current; 15kv accelerating voltage; and 1 μ m beam diameter. Reduction of the raw data was done using the ZAF data reduction program. One polished thin section was cut from each sample, and the compositional data were collected from at least two domains in each

section. The domains were selected on the basis of mineral assemblage, and textural and spatial relationships between the mineral phases. The rims of mineral grains were analyzed at points of mutual contact. In addition, core and rim compositions were obtained and compared, and any grains illustrating compositional zonation were further examined with core to rim probe traverses. Significant chemical zonation was only noted in garnet and, in rare cases, plagioclase (sample 92-171). The compositional variation of single mineral phases within each sample is very slight. However, the analyses used in the thermobarometric calculations in the present study were not averaged. As is typical in thermobarometric analyses, P-T conditions were calculated either from porphyroblast core-inclusion suite compositions, or from porphyroblast rim and/or well equilibrated matrix suite compositions. In all cases, data from separate domains in the thin section were treated separately, and could thus be used as an internal check on the consistency of the P-T determinations.

All of the thermobarometric calculations were performed using the TWQ method of Berman (1991). In this method, all possible equilibria for a given mineral assemblage are calculated using an internally consistent thermodynamic database for end-member mineral compositions (Berman 1988, 1990), and solution properties for non end-member compositions. The results are plotted as a series of univariant curves in P-T space. If the thermodynamic and compositional data are correct, and all of the phases in the given mineral assemblage mutually equilibrated at the same P-T conditions, the univariant curves should all intersect at a single point in P-T space. In the ideal case, equilibria displaced from the intersection point indicate a poorly equilibrated mineral assemblage. In this

manner, the TWQ method can be used to provide an assessment of the equilibrium state of a given sample which comprises phases for which the thermodynamic properties are reasonably well known (Berman 1991). In practice however, "offending" equilibria may be due to any one of: incorrect thermodynamic data, inaccurate compositional data, and/or disequilibrium in the mineral assemblage.

The calculations were performed using the solution models of Fuhrman and Lindsley (1988) for plagioclase, Berman (1990) for garnet, McMullin et al. (1991) for biotite, and Mader (1993; written communication; modified from Mader and Berman 1992) for amphibole. All other minerals were treated as pure phases.

In thermobarometric analyses using TWQ, it is generally considered preferable to obtain a P-T estimate from the intersection of three or more independently calibrated equilibria, since this provides an 'internal' assessment of the consistency of the thermobarometric results. However, the validity of a TWQ P-T estimate can also be weighed against: i) the standard deviation of the average pressure and temperature indicated by all intersections within a single sample (i.e., less than $\pm 40^\circ\text{C}$ and ± 0.5 kbar; Berman 1991); ii) the consistency of the P-T results among different domains within a single sample, and among different samples that are thought to have had a similar metamorphic history; and iii) qualitative or semi-quantitative estimates of P-T conditions. Taking into account errors in electron microprobe analyses, thermodynamic data, and solution models, the uncertainty in the absolute position of the intersections in P-T space is likely about $\pm 50^\circ\text{C}$ and ± 1 kbar (e.g., Essene 1989).

5.3.2 *P-T results*

5.3.2.1 TWQ calculations

Based on the apparent textural equilibrium between garnet, hornblende, plagioclase, and biotite, P-T estimates were calculated from the component system albite-anorthite-annite-phlogopite-pyrope-almandine-grossular-ferropargasite-pargasite-ferrotremolite-tremolite-ferrotschermakite-tschermakite-quartz. This system allowed the application of at least four independent reactions to each P-T calculation.

The P-T calculations were performed on mineral compositions obtained from: 1) the rims of porphyroblasts and texturally well equilibrated matrix phases within single domains; 2) included assemblages in garnet porphyroblasts; 3) domains of texturally well equilibrated matrix phases; and 4) porphyroblast cores that exhibit compelling textural evidence for synchronous growth (i.e., S_1 - S_6 relationships) within a single domain. In each of these domains, P-T estimates were calculated using various subsets of the mineral assemblage listed above, and various estimates for the activity of H_2O .

Unfortunately, all but one of the calculations yielded poor quality, highly-scattered intersections. Sample 92-171 yielded one relatively good P-T estimate of 9.6 kbar and 610° C from analyses of the rims of plagioclase and garnet porphyroblasts, biotite included in the rim of the plagioclase porphyroblast, and matrix amphibole adjacent to the plagioclase porphyroblast. However, this calculation was performed with an assumed $a_{H_2O} = 0$, which is almost certainly not reasonable for these samples. Subsequent calculations performed using the same mineral compositions and assumed $a_{H_2O} = 0.5$ and 1.0 yielded a greater degree of scatter in the intersections, although most remained within

the range of 9-10 kbar and 550-650° C. Thus, given the uncertainty associated with this P-T estimate, and the lack of reproducibility, the TWQ results are not considered to be acceptable in the present study.

The poor results of the TWQ analysis of samples 92-171 and 94-34 may be due to any combination of the following factors: 1) the reliability of the thermodynamic data, particularly that of annite (e.g., Berman 1991); 2) the reliability of the solution models, particularly amphibole; 3) the accuracy of the compositional data obtained from the microprobe; and 4) the analyzed phases may not have last equilibrated at the same pressure and temperature, possibly reflecting lack of equilibration during peak metamorphism or differential retrograde re-equilibration. Given the evidence for retrograde diffusional zoning and possible volume diffusion in the garnet porphyroblasts (Section 5.2.1.3), and the associated difficulty in selecting 'significant' garnet compositions, this last option seems likely in the present case.

5.3.2.2 Semi-quantitative estimates of P-T conditions

In the absence of acceptable quantitative P-T results, an estimate of the peak P-T conditions in the Pacquet Harbour area can be made on the basis of several semi-quantitative P-T indicators, including the following. 1) Textural relationships indicate that the crystallization of kyanite in the MBG may have involved the consumption of staurolite. According to the petrogenetic grid of Spear and Cheney (1989) for pelitic schists in the KFMASH system, this reaction requires P-T conditions in excess of ~600°C and 6 kbar. 2) Chemical zoning profiles from garnet porphyroblasts in both the MBG and PHG in Pacquet Harbour are consistent with chemical homogenization through volume diffusion,

indicating temperatures in excess of 600°C (Woodsworth 1977; Yardley 1977). 3)

Dunning (1995, pers. comm.) and Cawood et al. (1995) reported the presence of reset or 'disturbed' titanite in the Dunamagon Granite, indicating temperatures of about 600°C (e.g., Tucker et al. 1987; Heaman and Parrish 1991; Mezger et al. 1991). 4) Mineral parageneses within both the MBG and PHG are consistent with metamorphism in the middle to upper amphibolite facies, and thus P-T conditions around ~600° C and 6-7 kbar (e.g., Yardley 1989).

Collectively, these constraints are consistent with peak metamorphism at temperatures of $\geq 600^\circ$ C, and pressures in excess of 6 kbar in the Pacquet Harbour area. Given that a melt phase would likely be associated with temperatures marginally greater than 650-700° C (H₂O-present) in pelitic rocks (e.g., Thompson 1982), the temperature estimate of 600° C is reasonable for peak metamorphism in the Pacquet Harbour area. However, the estimation of peak pressures is significantly impeded by the relative lack of temperature-independent equilibria (i.e., geobarometers) in the amphibolite facies. The estimate of 6 kbar is tentatively accepted as a minimum.

In the Ming's Bight area, there are considerably fewer constraints on peak P-T conditions although, based on the relative absence of garnet in PHG amphibolite and kyanite in MBG schist, this area doubtlessly records significantly lower peak P-T conditions than the Pacquet Harbour area. In the Ming's Bight area, the mineral parageneses in both the MBG and PHG are consistent with peak upper greenschist to lower amphibolite facies metamorphism, and thus temperature and pressure conditions in the range of 500° C and 3-5 kbar (Yardley 1989). This interpretation is supported by

published petrogenetic grids, which indicate that temperatures between 450-500° C are required for the garnet and staurolite-in reactions in pelitic schists (e.g., Spear and Cheney 1989; Yardley 1989). The peak pressure conditions in the Ming's Bight area are more difficult to establish. The lack of andalusite or cordierite-bearing assemblages in the MBG might be taken to indicate pressures in excess of 3 kbar. However, these phases could simply have been consumed in later prograde or retrograde reactions, or have failed to stabilize in the first place, due (for example) to the possible lack of true pelite in the MBG, or an Fe-rich bulk composition of the protolith. Yardley (1989) noted that the presence of garnet in meta-basites indicates medium- to high-pressure metamorphic conditions. The scarcity of garnet in the PHG amphibolites, particularly in the footwall of the Scrape Fault, may thus indicate relatively low-pressure metamorphic conditions (i.e., ≤ 5 kbar). Collectively, these constraints are consistent with peak P-T conditions in the range $\sim 500^\circ$ C and 3-5 kbar in the Ming's Bight area.

5.4 DISCUSSION

5.4.1 Generalized P-T paths of the MBG in Pacquet Harbour and Ming's Bight

Establishing P-T paths for the MBG in Pacquet Harbour and Ming's Bight is hindered by the lack of quantitative P-T estimates. However, several inferences on the overall shape, and location in P-T space, of the P-T paths can be made based on the semi-quantitative P-T estimates, and petrographic observations (e.g., Selverstone 1985; Jamieson 1991). In addition, several aspects of the deformation history can provide important insights into the overall shape of the P-T path, as discussed by Thompson and England (1984) and Chamberlain and Karabinos (1987). Thus, the deformation history,

together with P-T and petrographic data, are used to provide general constraints on the P-T paths followed by the MBG.

The P-T paths presented in this section represent the simplest possible paths that are consistent with all the data. The temperature constraints on these paths may be reasonably accurate. However, the pressure estimates are poorly constrained, and thus there is potential for a significant shift of the overall position of the paths relative to the P-axis of the P-T diagram.

The P-T path for the MBG in the Pacquet Harbour area is inferred to be similar to the typical P-T path produced through thickening and exhumation (e.g., Thompson and England 1984; Fig. 5.8a). In the MBG, fine-grained and mineralogically simple included assemblages in syn-D₂, peak-metamorphic porphyroblasts are consistent with relatively low-grade (greenschist facies) metamorphism prior to D₂. The growth of peak-metamorphic mineral assemblages early during D₂ suggests that the Pacquet Harbour area must have undergone significant burial (to >20 km) during, or subsequent to, D₁. Based on the regional characteristics of D₁ structures, this burial is inferred to have occurred during south-directed thrusting. Thus, early increments of the P-T path for these rocks may have involved a phase of nearly isothermal compression, as is typical in P-T paths associated with thrusting and/or thickening (e.g., Thompson and England 1984; Jamieson 1991). A phase of thermal relaxation and heating (Thompson and England 1984) may have occurred in the latest stages of D₁ burial and/or the earliest stages of D₂. Based on the extensional character of D₂ structures, thermal relaxation and heating were probably followed by a phase of nearly isothermal decompression associated with exhumation of the

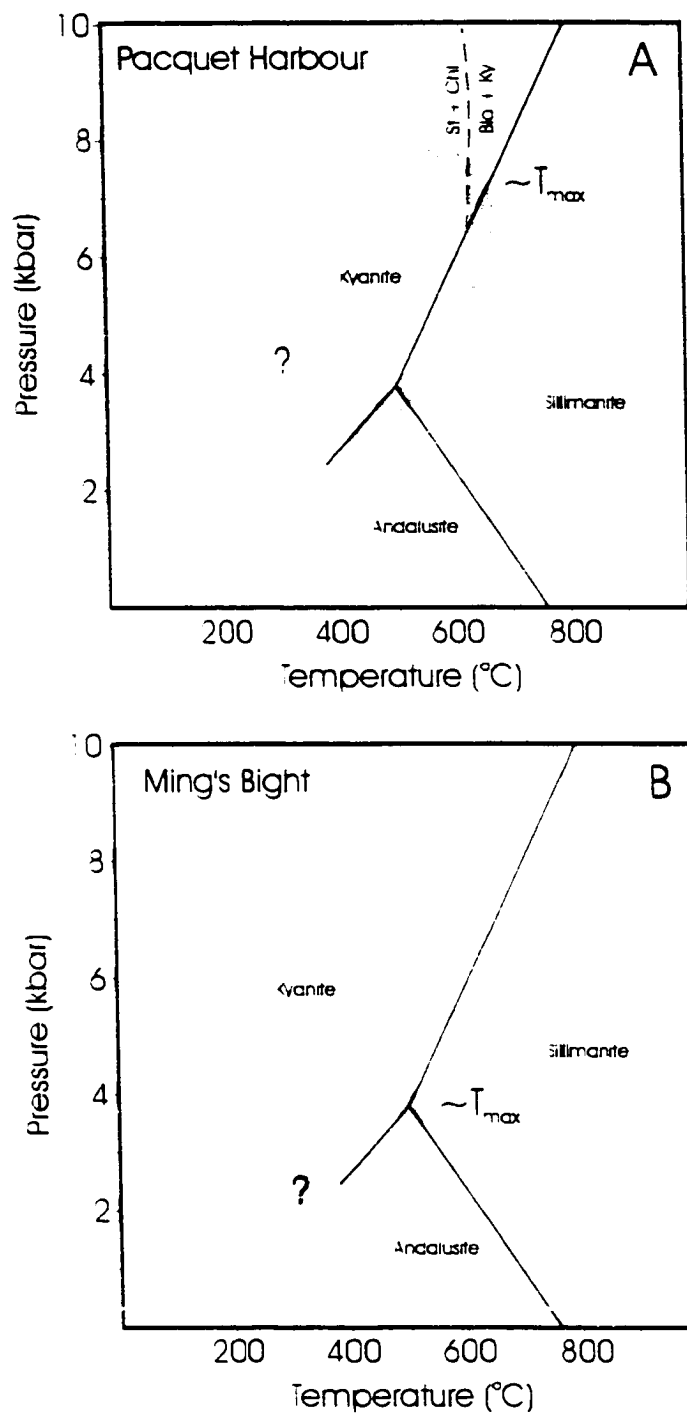


Figure 5.8 Schematic, generalized, P-T paths for the Ming's Bight Group, incorporating constraints provided by semi-quantitative thermobarometry and deformation history. Aluminosilicate phase boundaries after Holdaway (1971). Staurolite + chlorite \rightarrow kyanite + biotite equilibria after Spear and Cheney (1989). See text for detailed discussion. a) P-T path for the MBG in Pacquet Harbour. b) P-T path for the MBG in Ming's Bight.

high-grade rocks (e.g., Thompson and England 1984). Furthermore, $^{40}\text{Ar}/^{39}\text{Ar}$ evidence for rapid cooling through the hornblende and muscovite closure temperatures (e.g., Dallmeyer and Hibbard 1984; Cawood et al. 1995; see Chapter 6), indicates that isothermal decompression was followed by continued late- D_2 and/or syn- D_3 cooling, presumably in association with a more gradual rate of decompression (e.g., Thompson and England 1984; Jamieson 1991).

In the Ming's Bight area, a P-T path of similar shape to that in the Pacquet Harbour area is proposed on the basis of the general similarity in deformation and metamorphic histories (Fig. 5.8b). However, this P-T path must encompass a much smaller range of pressures and temperatures, and be shifted towards lower pressure and temperature overall, reflecting the lower peak-metamorphic grade in the Ming's Bight area. $^{40}\text{Ar}/^{39}\text{Ar}$ data indicate that the Ming's Bight area also underwent rapid cooling through the muscovite, and possibly hornblende, closure temperatures, consistent with a late phase of rapid exhumation.

5.4.2 Metamorphic gradient - Ming's Bight

The metamorphic sequence in the northwestern portion of the PHG is characterized by an apparently gradational change structurally downward from rocks recording intense finite D_1 strain and amphibolite facies metamorphism in the north, to rocks recording weak finite D_1 strain and greenschist facies metamorphism in the south (Gale 1971) (Fig. 5.1). This gradation occurs over a distance of ~5-6 km, and appears to be consistent with an inverted metamorphic sequence (e.g., Jamieson et al. 1996). The apparent relationship between intensity of finite D_1 strain and metamorphic grade implies

either: 1) the presence of a local heat-source that is directly related to the deformation: for example, shear-heating during thrusting, or heat transfer between hot hangingwall rocks and cooler footwall rocks; and/or 2) syn- to post- D_1 structural juxtaposition of low and high grade rocks (cf. Jamieson et al. 1996).

$^{40}\text{Ar}/^{39}\text{Ar}$ data from the northern portions of the PHG in the Ming's Bight area indicate that the amphibolite facies rocks may have cooled through the hornblende closure temperature (ca. 500°C) $\sim 20\text{-}30$ My after the onset of south-directed reverse shear and amphibolite facies metamorphism (see Chapter 6). Given that a small-scale thermal anomaly associated with, for example, heat transfer between hot hangingwall and cool footwall rocks would probably relax over a period of <1 Ma (e.g., Sleep 1979; Chamberlain and Karabinos 1987), it seems unlikely that either shear heating or heat transfer could account for the considerable duration of high-grade metamorphism. Thus, the high-grade rocks must have been at considerable depth for a considerable period of time and, since the structurally underlying PHG rocks were metamorphosed only to greenschist facies during D_1 , the high-grade rocks must have been exhumed from a deeper structural level sometime after the syn- D_1 - D_2 metamorphic peak. Thus, the apparently gradational metamorphic sequence in the PHG must be transected by discrete or, more likely, distributed late- to post- D_1 structures which juxtapose the low- and high-grade rocks (e.g., Jain and Manickavasagam 1993).

5.5 CONCLUSIONS

5.5.1 *Pacquet Harbour area*

1) Pre-peak mineral assemblages are consistent with greenschist facies metamorphic conditions, possibly associated with nearly isothermal compression during D_1 , and rapid burial of the Pacquet Harbour area to at least ~20 km depth.

2) Syn-peak metamorphic assemblages in the MBG, PHG, and Dunamagon Granite are consistent with at least lower amphibolite facies metamorphic conditions ($T > 600^\circ \text{C}$ and $P > 6 \text{ kbar}$) during maximum burial of the Pacquet Harbour area in the late-Early or early-Middle Devonian (ca. 385 Ma; G.R. Dunning 1995, pers. comm.; see Chapter 6). The metamorphic peak marks the earliest increment of extensional D_2 deformation, and exhumation of the Pacquet Harbour area. The apparent lack of post-peak metamorphic recrystallization is consistent with relatively rapid exhumation. In the Cape Brule Porphyry, mineral assemblages suggest greenschist facies metamorphism during D_2 , consistent with the location of the porphyry in the structural hangingwall of the extensional D_2 shear zone in Pacquet Harbour.

3) Post-peak metamorphic assemblages record greenschist to prehnite-pumpellyite-facies metamorphism, likely during the latest increments of extensional D_2 and D_3 deformation, and exhumation of the Pacquet Harbour area.

5.5.2 *Ming's Bight area*

1) The syn- D_1 - D_2 metamorphic mineral assemblages in the MBG and PHG in the structural footwall of the thrust/wrench-shear system are consistent with upper greenschist to lower amphibolite facies metamorphism ($T \sim 500^\circ \text{C}$ and $P \sim 3 \text{ kbar}$). This

metamorphism probably occurred in Late Silurian time (ca. 420 Ma; Ramezani 1992), during regional burial of the footwall rocks to ca. 10km depth. Greenschist facies conditions prevailed during D_1 - D_2 in the southern, structurally lower, portions of the PHG, and the northern, structurally higher, portions of the PROC.

2) The syn- D_3 - D_4 - D_5 metamorphic mineral assemblages are generally consistent with greenschist facies metamorphic conditions, although assemblages indicative of upper greenschist facies metamorphism are locally preserved in D_5 shear zones. This metamorphism was associated with extensional exhumation of the Ming's Bight area subsequent to latest Silurian time.

Chapter 6 Geochronology

6.1 INTRODUCTION

6.1.1 Background

Studies concerned with the tectonic evolution of orogenic belts require well-constrained geochronologic data in order to establish the relative and absolute timing of events such as plutonism, sedimentation, deformation, and metamorphism. This is particularly true in interior portions of orogenic belts where stratigraphic and paleontologic constraints are commonly lacking. In recent years, significant insights into the tectonic evolution of the Newfoundland Appalachians have been achieved through the application of combined U-Pb and $^{40}\text{Ar}/^{39}\text{Ar}$ geochronologic studies (e.g., Dunning et al. 1990; Cawood et al. 1994, 1995; Dubé et al. 1996). This success is due in large measure to the wide range of orogenic processes which can be tightly constrained using these isotopic systems in tandem. For example, U-Pb dating of zircon, monazite, and titanite provides constraints on the age of igneous crystallization, the age and early cooling history of high-temperature metamorphic terranes, the maximum age of sedimentation, and the timing of deformation (e.g., Heaman and Parrish 1991). Furthermore, U-Pb dating of rutile and $^{40}\text{Ar}/^{39}\text{Ar}$ dating of hornblende and muscovite are particularly useful for establishing the age and cooling history of low to medium-grade metamorphic terranes, and the timing of deformation (e.g., Hanes 1991; Heaman and Parrish 1991).

This chapter presents new U-Pb and $^{40}\text{Ar}/^{39}\text{Ar}$ geochronologic data obtained from the MBG, PHG, PROC, and Dunamagon Granite. The U-Pb data constrain the age of

granitic pegmatites cutting the MBG, the timing of deformation and metamorphism in Pacquet Harbour, and the timing of extensional deformation in Ming's Bight. The $^{40}\text{Ar}/^{39}\text{Ar}$ data constrain the timing of metamorphism, post-metamorphic cooling, and deformation in both the Ming's Bight and Pacquet Harbour areas.

6.1.2 Previous geochronology

The BVP has already been the focus of a number of geochronologic studies (e.g., Mattinson 1975, 1977; Bell and Blenkinsop 1977, 1978a, 1978b; Dallmeyer 1977; Pringle 1978; Hibbard 1983; Dallmeyer and Hibbard 1984; Dunning and Krogh 1985; Vance and O'Nions 1990; Ramezani 1992; Cawood and Dunning 1993; Cawood et al. 1994). However, several of these studies (e.g., Bell and Blenkinsop 1977, 1978a; Pringle 1978; Hibbard 1983; Dallmeyer and Hibbard 1984) report the results of Rb/Sr whole-rock analyses which, in several instances, yield ages that are highly variable within single units and/or are clearly at variance with established field relationships. For example, Bell and Blenkinsop (1977, 1978a) and Pringle (1978) reported Rb/Sr whole-rock ages ranging from 325 ± 14 Ma to 520 ± 40 Ma for the Silurian Cape Brule Porphyry and Cape St. John Group. In light of these inconsistencies and, in particular, the potential for complex open-system behavior in Rb/Sr whole-rock dating, these results are not incorporated into the present study.

U-Pb analyses performed by Mattinson (1975, 1977), Hibbard (1983), and Dallmeyer and Hibbard (1984) all involved large fractions of zircon which presumably comprised mixed populations of both xenocrystic (i.e., inherited) and primary zircon. The potential for significant components of inherited U and Pb creates a considerable amount

of uncertainty regarding the geologic significance of these analyses. This problem was acknowledged by Mattinson (1977), and may well explain why he obtained U-Pb zircon ages of 486 ± 40 Ma and 488 ± 35 Ma from La Scie granite that clearly intruded the Silurian Cape St. John Group (Hibbard 1983; Fig. 1.2). In light of both the inconsistency and uncertainty, these U-Pb dates are not incorporated into the present study.

6.1.2.1 West of the BVL

In recent years, several more precise and accurate U-Pb geochronologic studies have been carried out on the BVP. Cawood and Dunning (1993) and Cawood et al. (1994) conducted a regional U-Pb geochronology study focused on establishing the timing of the main phase of orogenesis on the BVP. Identical U-Pb monazite dates of 427 ± 2 Ma from a syn-tectonic phase of the Wild Cove Pond Igneous Suite and migmatite derived from the Fleur de Lys Supergroup indicate intrusion and peak metamorphism, respectively, in the Early Silurian (Cawood and Dunning 1993; Cawood et al. 1994).

Garnet porphyroblasts from the Fleur de Lys Supergroup yielded Sm/Nd ages of 448.6 ± 2.3 Ma and 443.4 ± 7.9 Ma (Vance and O'Nions 1990), which were interpreted to reflect the time of garnet growth during prograde metamorphism. This interpretation is broadly consistent with the results of U-Pb and $^{40}\text{Ar}/^{39}\text{Ar}$ geochronologic studies in the Fleur de Lys Supergroup, as well as regional timing constraints. However, the validity of this interpretation must be weighed against the potential for open-system behavior of garnet in amphibolite facies metamorphism, and the possibility that the analyses include Sm and Nd inherited from included phases in the highly poikiloblastic garnet porphyroblasts (e.g., Heaman and Parrish 1991).

From south to north in the Fleur de Lys Supergroup, $^{40}\text{Ar}/^{39}\text{Ar}$ total-gas ages grade from 429 ± 10 to 394 ± 5 Ma for hornblende, 421 ± 15 to 398 ± 5 Ma for muscovite, and 394 ± 5 to 373 ± 5 Ma for biotite (Dallmeyer 1977; recalculated by Dallmeyer and Hibbard 1984). These ages are interpreted to record post-metamorphic cooling through ca. 500°C , 350°C , and 280°C , respectively. The general younging trend of the total-gas ages toward the north, and the brief interval between hornblende and biotite closure in each location, are interpreted to record diachronous and rapid cooling, respectively, during exhumation of the Fleur de Lys Supergroup (Dallmeyer 1977).

6.1.2.2 East of the BVL

Dunning and Krogh (1985) presented a U-Pb zircon date of $488.6^{+1.1}_{-1.8}$ Ma from gabbro of the Betts Cove ophiolite, and Ramezani (1992) presented a U-Pb zircon date of $483^{+3.2}_{-2}$ Ma from a gabbro sill in the cover sequence of the PROC. Both of these dates confirm the Tremadoc-Arenig age of the ophiolites on the BVP. In addition, zircon from the Dunamagon Granite yielded a 429 ± 4 Ma age, and zircon/titanite from the Burlington Granodiorite yielded a 432 ± 2 Ma age (Cawood and Dunning 1993). These dates support the hypothesis that most, if not all, of the felsic plutons on the BVP are associated with Early Silurian caldera complexes (e.g., Coyle and Strong 1987), and provide an older age limit on the time of deformation and high-grade metamorphism east of the BVL. In addition, Ramezani (1992) presented U-Pb zircon date of 420 ± 5 Ma for hydrothermal alteration in the shear-hosted Stog'er Tight Au deposit in the PROC. This alteration was ascribed to a late increment of D_1 deformation by Kirkwood and Dubé (1992). In the present study this U-Pb date is interpreted to constrain the timing of D_1 - D_2 deformation

and high-grade metamorphism in the Ming's Bight area.

Dallmeyer (1977) and Dallmeyer and Hibbard (1984) conducted an extensive $^{40}\text{Ar}/^{39}\text{Ar}$ study east of the BVL. Samples collected from the Burlington Granodiorite in the vicinity of the town of Burlington on Green Bay (Fig. 1.2), yielded total-gas ages ranging from 418 ± 5 to 406 ± 5 Ma for hornblende, and 414 ± 10 to 409 ± 15 Ma for biotite. The overlap (within analytical error) of the hornblende and biotite ages in this location, and lack of regional metamorphism capable of re-setting hornblende, suggest either: 1) these ages record a local thermal disturbance, possibly related to contact metamorphism during a late phase of intrusion in the Silurian King's Point Complex; or 2) these ages record rapid post-intrusion cooling (e.g., Dallmeyer and Hibbard 1984; Coyle and Strong 1987). In contrast, samples collected from the northern portions of the Burlington Granodiorite and PHG, as well as from the Dunamagon Granite and MBG, yielded total gas ages ranging from 371 ± 10 to 350 ± 5 Ma for hornblende, and 352 ± 5 to 337 ± 5 Ma for biotite. These ages were interpreted by Dallmeyer and Hibbard (1984) to reflect regional post-metamorphic cooling following Middle to Late Paleozoic (i.e., 'Acadian') tectonothermal activity associated with the Baie Verte Flexure (Hibbard 1982, 1983). The post-metamorphic cooling hypothesis is supported by Early Devonian titanite ages from the Early Silurian Dunamagon Granite (Cawood et al. 1995).

6.2 SAMPLE SELECTION AND ANALYTICAL TECHNIQUES

6.2.1 U-Pb samples

Three fresh samples each weighing ~25 kg were collected from single outcrops in the thesis area for U-Pb dating. These samples include: 1) late-tectonic granitic pegmatite

from Pelee Point in Pacquet Harbour (Map 2); 2) rutile and titanite-bearing chlorite schist from the NMTSZ in Ming's Bight (Map 8); and 3) MBG staurolite-garnet-kyanite schist from the BBSZ ~600m west of Pacquet Harbour (Map 2). The MBG sample was collected in order to obtain monazite U-Pb ages, and thus constrain the timing of peak metamorphism in the Pacquet Harbour area (e.g., Parrish 1990, Smith and Barreiro 1990). However, no monazite was recovered from this sample, and it is not included in the discussion below.

Under clean conditions, the samples were washed, and reduced to a fine powder in a jaw crusher and Bico pulverizer. The powder was passed over a Wilfley table in order to obtain a heavy and light mineral concentrate. The washed and dried heavy concentrate was sieved (70 mesh), and the minerals of interest in the fine fraction were separated using the standard combination of heavy liquids (methylene iodide and bromoform) and the Frantz isodynamic separator. The initial pass through the Frantz separator was conducted at 25° slope, 10° side-tilt, and magnetic splits were obtained at 0.25, 0.50, 1.0, and 1.7 Amps. The final Frantz pass was conducted at 25° slope, 1.7 Amps., and magnetic splits were obtained at 5°, 3°, 1°, and 0° side-tilt. Individual grains for analysis were selected by hand-picking under a binocular microscope. Rutile was picked from the final magnetic splits at 3° and 5° side tilt, and titanite was picked from the initial magnetic splits at 1.7 Amps. Microlite (see Section 6.3.2.1) was obtained from the initial magnetic split at 1.7 Amps, and the final magnetic split at 5° side-tilt. The grains for analysis were chosen on the basis of morphological characteristics, clarity, and lack of inclusions and cracks.

Under ultraclean conditions, all fractions selected for analysis were abraded,

washed with distilled nitric acid, water, and acetone, carefully weighed, spiked with a $^{205}\text{Pb}/^{235}\text{U}$ tracer solution in proportion to the sample weight, and completely dissolved over 5 days in a hydrofluoric and nitric acid mixture in sealed Savillex beakers on a hot plate. U and Pb were eluted using HBr large-column ion exchange chromatography (e.g., Krogh 1973; Corfu and Stott 1986). The samples were loaded on single outgassed Re filaments in a silica gel- H_3PO_4 mixture. The isotopic ratios of U and Pb were measured at temperatures in the range of 1400-1600° C on the Finnigan MAT 262 multi-collector mass spectrometer at Memorial University, Newfoundland.

The measured isotopic ratios were corrected for isotopic fractionation in the mass spectrometer, laboratory contamination (blank), and the $^{205}\text{Pb}/^{235}\text{U}$ spike. The correction for the isotopic composition of initial common-lead was assigned using the model of Stacey and Kramers (1975) and an estimated time of crystallization. Uncertainties in the isotopic ratios are reported at the 2σ level. The fraction descriptions, U-Pb concentrations, isotopic ratios, and ages are reported in Table 6.1.

6.2.2 $^{40}\text{Ar}/^{39}\text{Ar}$ samples

Eighteen fresh samples each weighing ~1 kg were selected from the thesis area for $^{40}\text{Ar}/^{39}\text{Ar}$ analysis. These included eight samples containing hornblende, and ten samples containing muscovite. Biotite was not included in the analysis, in order to avoid problems associated with excess-argon uptake (e.g., Hanes 1991).

The samples were reduced to the consistency of coarse sand using a hammer and small jaw crusher. Each sample was then passed through a sieve stack in order to obtain splits in the size range +20 mesh, +60 mesh, +120 mesh, and -120 mesh. Each of the splits

Table 6.1 U-Pb analytical data

Sample Fraction; description	Weight (mg)	Concentration		Measured		Corrected Atomic Ratios				Age (Ma)		
		U (ppm)	Pb rad. (ppm)	Total ^{206}Pb	common ^{204}Pb	$^{208}\text{Pb}/$ ^{206}Pb	$^{206}\text{Pb}/$ ^{238}U	$^{207}\text{Pb}/$ ^{235}U	$^{207}\text{Pb}/$ ^{206}Pb	$^{207}\text{Pb}/$ ^{235}U	$^{207}\text{Pb}/$ ^{206}Pb	
NMTSZ												
R1; clear, orange, abr	0.872	16	0.9	224	257	0.0165	0.06088 +/- 26	0.4592 +/- 32	0.05470 +/- 30	381	384	400
R2; clear, orange, abr	0.890	15	0.8	192	285	0.0078	0.06085 +/- 24	0.4541 +/- 32	0.05412 +/- 32	381	380	376
T1; clear, sl. turbid, abr	0.500	46	2.8	1729	70	0.0656	0.06245 +/- 88	0.4910 +/- 284	0.05702 +/- 298	391	406	492
T2; clear, sl. turbid, abr	0.531	51	3.0	2159	71	0.0512	0.06185 +/- 20	0.4488 +/- 74	0.05263 +/- 80	387	376	313
Pelee Point Pegmatite												
M1; clear, yellow, abr	0.242	29560	1524.5	68912	388	0.0020	0.05687 +/- 96	0.4189 +/- 72	0.05342 +/- 14	357	355	347
M2; three, clear, yellow, abr	0.005	38637	1997.8	1944	404	0.0079	0.05669 +/- 20	0.4177 +/- 20	0.05344 +/- 14	355	354	348
M3; single, clear, yellow, abr	0.004	46992	2417.9	1442	525	0.0045	0.05659 +/- 18	0.4176 +/- 18	0.05352 +/- 12	355	354	351
M4; single, clear, yellow, abr	0.004	32848	1696.6	847	512	0.0054	0.05674 +/- 24	0.4207 +/- 22	0.05378 +/- 14	356	357	362

was washed thoroughly in water to remove surface dust, and washed and dried in acetone. The splits were then examined under a binocular microscope in order to determine which contained the greatest number of grains liberated from the matrix, and the greatest number of relatively intact mineral grains. Hornblende was obtained from the +60 or +120 split, whereas muscovite was obtained from the +20, +60, or +120 splits. Hornblende samples were passed through the Frantz isodynamic separator at 20° slope, 10° side-tilt, and ~0.45 Amps in order to obtain a relatively pure hornblende concentrate. Individual hornblende grains for analysis were hand-picked under a binocular microscope on the basis of relatively intact crystal shape, lack of adhering matrix grains, apparent lack of inclusions, and lack of obvious alteration effects. Pure muscovite separates were also obtained through hand picking under a binocular microscope. The final pure mineral separates for analysis comprised ~20-60 mg of hornblende and ~5-10 mg of muscovite.

The $^{40}\text{Ar}/^{39}\text{Ar}$ analyses of hornblende and muscovite were conducted at Dalhousie University using the analytical methods described by Muecke et al. (1988). The samples were analyzed in VG3600 mass spectrometer coupled to an internal tantalum resistance furnace of the double-vacuum type. The standard used for all analyses was Hornblende MMhb-1, which has an assumed age of 520 ± 2 Ma (Samson and Alexander 1987). Uncertainties in the reported ages and plotted age spectra are at the 2σ level, and the analytical data are presented in Appendix 1.

6.2.3 Closure temperatures

The temperature at which a mineral phase effectively closes to the loss of radiogenic daughter isotopes is termed the closure temperature (T_c ; Dodson 1973). The

T_C is of fundamental importance in the interpretation of geochronologic results since, in the simplest case, the apparent age derived from a mineral reflects either: 1) the time of cooling through the closure temperature (i.e., cooling age); or 2) the time of crystallization, provided that the mineral phase crystallized at temperatures below the effective closure temperature. In the present study, the estimated closure temperatures for $^{40}\text{Ar}/^{39}\text{Ar}$ diffusion are: $530 \pm 40^\circ\text{C}$ for hornblende (Harrison 1981); $\sim 350^\circ\text{C}$ for muscovite (Purdy and Jager 1976); and $280 \pm 40^\circ\text{C}$ for biotite (Harrison et al. 1985). The estimated closure temperature for U-Pb diffusion in rutile is $400 \pm 30^\circ\text{C}$ (Mezger et al. 1989), and that in titanite is $600 \pm 30^\circ\text{C}$ (Heaman and Parrish 1991). Based on the apparently rapid cooling rates in the area (e.g., Dallmeyer and Hibbard 1984), the closure temperatures are inferred to lie near the high end of the above ranges (Dodson 1973).

6.3 RESULTS

6.3.1 $^{40}\text{Ar}/^{39}\text{Ar}$ incremental release analyses

6.3.1.1 Muscovite

In the present study, the $^{40}\text{Ar}/^{39}\text{Ar}$ age reported for each muscovite analysis is a weighted average of the apparent ages, with each apparent age weighted according the percentage of ^{39}Ar released in that heating increment. Apparent ages in the initial and/or final heating increments that were anomalously old or young, or that had anomalously high 2σ relative uncertainties, were omitted from the weighted averaging calculations. In all cases the reported age incorporates at least 88% of the total ^{39}Ar released. The analytical error associated with the apparent ages used in the weighted averaging calculations was significantly $<1\%$. Therefore, the error values (2σ) reported below were assigned

according to the error associated with the corresponding J-value (i.e., $J = 0.002055 \pm 1.0\%$ to $0.002227 \pm 0.7\%$), since this error is significantly larger than the analytical error in all cases.

Ming's Bight Group - schist

Six samples of muscovite were separated from MBG schist for $^{40}\text{Ar}/^{39}\text{Ar}$ analysis. The samples were collected near the northern (93-49), eastern (92-75, 92-184), and southwestern (92-102) exposure limits of the MBG, and along the BBSZ (92-85c, 94-5; Fig. 6.1). Five of these samples (92-75, 92-85c, 92-102, 92-184, 93-49) were collected from typical MBG schist. In these samples, muscovite comprises 5-25% of the mode, and is fine- to coarse-grained, idioblastic, and strongly foliated. In all samples, muscovite is concentrated with biotite into mica-rich domains that define the local S_2 fabric, and transect an earlier (S_1) fabric defined by fine-grained foliated muscovite and biotite. The remaining sample (94-5) was collected from the hinge of an F_2 fold in the BBSZ, and comprises coarse-grained, idioblastic, muscovite porphyroblasts, which contain numerous rounded inclusions of quartz and plagioclase. In all samples, muscovite was completely separated from closely associated and locally intergrown biotite through hand picking and, in the case of sample 92-102, the Frantz isodynamic separator.

All of these samples yielded very flat $^{40}\text{Ar}/^{39}\text{Ar}$ spectra, consistent with compositionally uniform and undisturbed muscovite (Fig. 6.2). Sample 92-75 was collected from MBG L>S tectonite ~750 m northeast of Pacquet Harbour (Map 1), and yielded an age of 363 ± 3 Ma. Muscovite from a sample of MBG garnet schist (92-184) located ~200 m northwest of the White Point pegmatite (Map 1) yielded an age of 360 ± 3

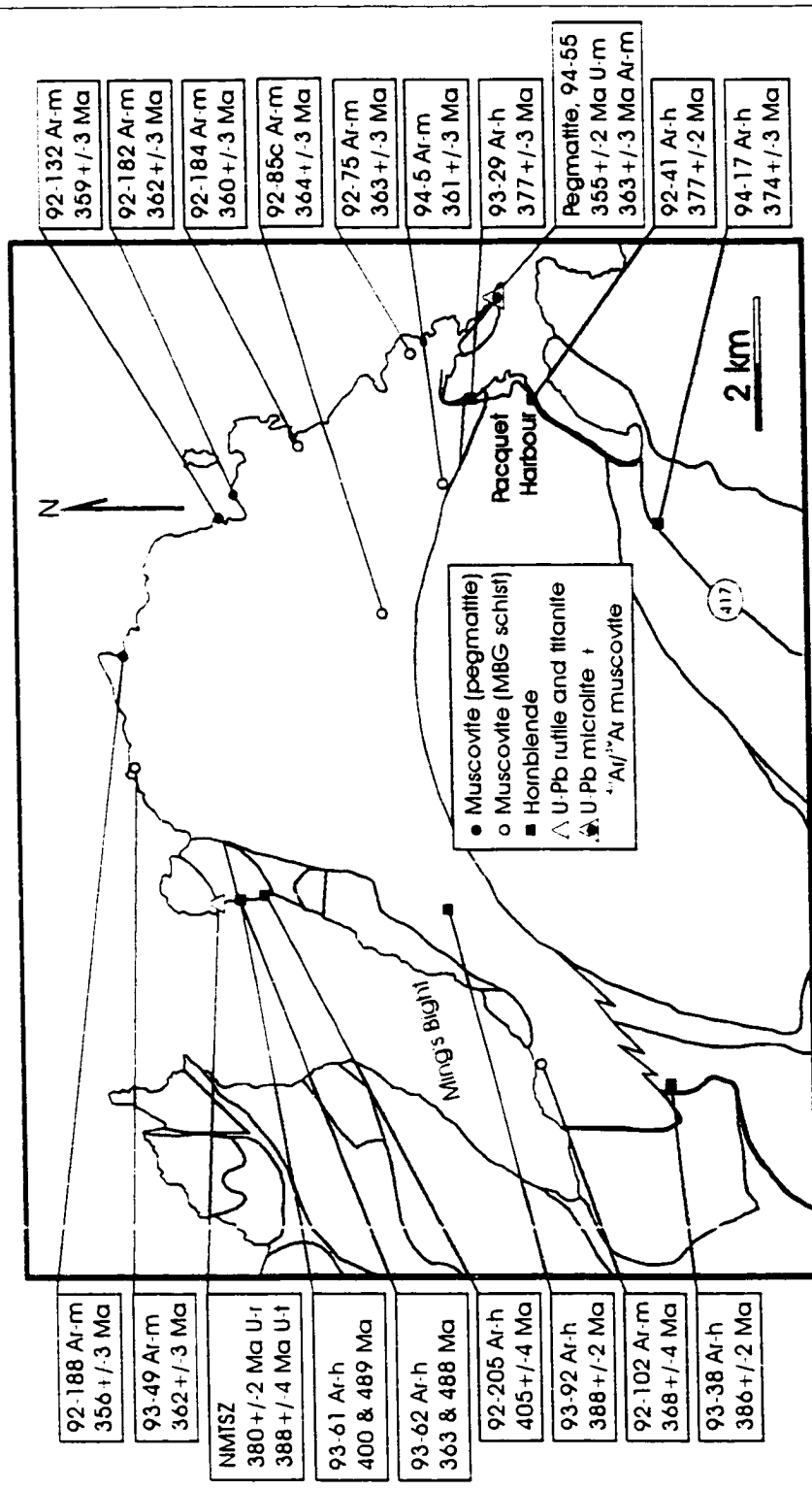


Figure 6.1 Simplified geological map of the thesis area showing the location of geochronology samples. Each box contains the sample number or name, the geochronologic technique employed, the mineral dated, and the age obtained. U-r, U-Pb rutile; U-t, U-Pb titanite; U-m, U-Pb microcline; Ar-h, $^{40}\text{Ar}/^{39}\text{Ar}$ Ar hornblende; Ar-m, $^{40}\text{Ar}/^{39}\text{Ar}$ Ar muscovite

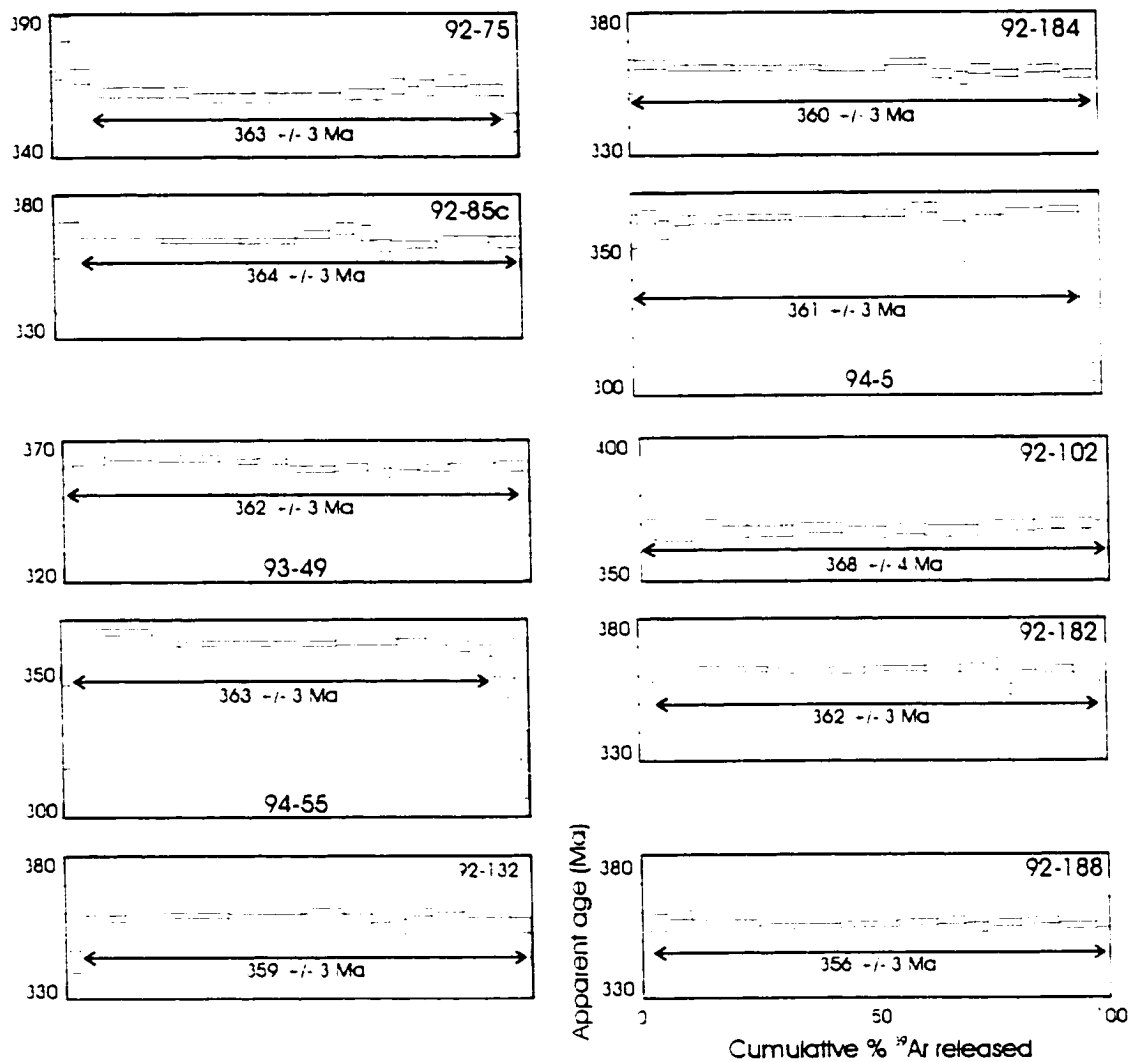


Figure 6.2 $^{40}\text{Ar}/^{39}\text{Ar}$ age spectra for muscovite samples. The half-heights of the rectangles indicate the 2σ relative (between-step) uncertainties. The age reported for each spectrum is a weighted-average age based on the fraction of gas indicated. Refer to Figure 6.1 for sample locations.

Ma. In the BBSZ ~3.5 km west of Pacquet Harbour, muscovite from MBG muscovite-biotite schist (92-85c) yielded a nearly identical spectrum with an age of 364 ± 3 Ma. In addition, the sample of porphyroblastic muscovite (94-5) collected ~1.2 km west of Pacquet Harbour in the BBSZ yielded an age of 361 ± 3 Ma. Further north at Seven Brooks Point (Fig. 6.1), muscovite from a sample of MBG staurolite-garnet schist (93-49) yielded an age of 362 ± 3 Ma. Finally, in the southwestern portion of the MBG at the southern end of Ming's Bight, muscovite from a sample of albite porphyroblastic schist located ~1 km east of Actinolite Bay (92-102; Map 5) yielded an age of 368 ± 4 Ma.

Ming's Bight Group - pegmatite

Three widely-spaced samples of pegmatite, and one sample from the muscovitized exo-contact of a pegmatite, were collected and processed for $^{40}\text{Ar}/^{39}\text{Ar}$ dating of muscovite. Samples 94-55 and 92-182 were collected from two weakly deformed (i.e., deformation structures only apparent microscopically) pegmatite dykes that cut tight to isoclinal F_2 folds at Pelee Point and the south shore of Handy Harbour, respectively (Fig. 6.1; Map 1). In these samples, the muscovite forms very coarse-grained, randomly oriented, euhedral to subhedral crystals that contain rare inclusions of quartz and opaque mineral phases. Samples 94-55 and 92-182 yielded very flat $^{40}\text{Ar}/^{39}\text{Ar}$ spectra which indicate ages of 363 ± 3 and 362 ± 3 , respectively (Fig. 6.2). In addition, sample 92-132 was collected from muscovitized MBG schist adjacent to the external contact of the cross-cutting, beryl-bearing pegmatite at Red Point (Fig. 6.1; Map 1). This sample comprised ~100% coarse-grained, randomly-oriented, muscovite books, and yielded a very flat $^{40}\text{Ar}/^{39}\text{Ar}$ spectrum which indicates an age of 359 ± 3 Ma (Fig. 6.2).

In contrast to the above samples, sample 92-188 was collected from the penetratively foliated pegmatite located in the northern most exposures of the MBG at Cape Hat (Fig. 6.1). In this sample, the muscovite occurs as strongly foliated, fine- to medium-grained, subhedral flakes and mica-fish, and yielded a very flat $^{40}\text{Ar}/^{39}\text{Ar}$ spectrum indicating an age of 356 ± 3 Ma (Fig. 6.2).

6.3.1.2 Hornblende

In the present study, the $^{40}\text{Ar}/^{39}\text{Ar}$ age reported for each hornblende analysis is a weighted average of the apparent ages, with each apparent age weighted according the percentage of ^{39}Ar released in each heating increment. In all cases, the weighted averages were calculated from at least 9 adjacent heating increments, comprising at least 77% of the total ^{39}Ar released. Initial and/or final heating increments which recorded highly anomalous apparent ages, $^{37}\text{Ar}/^{39}\text{Ar}$ ratios, and/or analytical errors, were omitted from the weighted averaging calculations. The J-values range between $0.002079 \pm 0.5\%$ and $0.002231 \pm 0.7\%$. For each sample, the 2σ absolute error reported below incorporates the analytical errors associated with the measured $^{40}\text{Ar}/^{39}\text{Ar}$ ratios, and the error associated with the J-value (J-error dominates the error calculation). Isotope correlation plots were constructed for all hornblende analyses, although these plots only yielded additional useful information in the case of sample 94-17 (see below). $^{37}\text{Ar}/^{39}\text{Ar}$ ratios calculated from microprobe-determined Ca/K ratios are plotted for comparison on the $^{37}\text{Ar}/^{39}\text{Ar}$ spectra.

Pacquet Harbour Group - amphibolite

Two samples of mylonitic amphibolite were selected from the northern portions of the PHG for $^{40}\text{Ar}/^{39}\text{Ar}$ analysis (Fig. 6.1). Sample 94-17 was collected from a sequence of

mafic volcanoclastic rocks and pillowed basalts ~1 km west of Woodstock, whereas sample 93-38 was collected from a sequence of pillowed basalt and gabbro ~2.5 km south of South Brook within the transpressional shear zone that separates the PROC and PHG. Both of these samples are mylonitic amphibolites which comprise ~40-70%, fine- to medium-grained, idioblastic to xenoblastic, equant to acicular, relatively strain-free hornblende porphyroblasts. The hornblende defines S_2 in both locations, and is lineated parallel to the regional L_2 . In both samples the hornblende is slightly intergrown with actinolite, contains rare inclusions of titanite and quartz, and is not associated with biotite.

Sample 93-38 yielded a fairly flat spectrum, consistent with a weighted average age of 386 ± 2 Ma (incorporates 96% of the total ^{39}Ar released; Fig. 6.3). However, this spectrum also records a slight gradational increase in apparent age from the lower- to higher-temperature heating increments. At lower temperatures, two heating increments, collectively comprising 26.3% of the total ^{39}Ar released, record apparent ages of 377.4 and 377.8 Ma, whereas at higher temperatures, a single heating increment comprising 25.1% of the total ^{39}Ar released records an apparent age of 393.3 Ma. Insofar as the $^{37}\text{Ar}/^{39}\text{Ar}$ ratio is reasonably consistent through these portions of the spectrum (i.e., 12.4-13.4; Fig. 6.3), this gradation is interpreted to reflect minor loss of radiogenic ^{40}Ar (Maboko et al. 1991), and therefore may be geochronologically significant.

Sample 94-17 yielded a relatively poor quality disturbed spectrum, with a weighted average age of 374 ± 3 Ma (incorporates 77% of the total ^{39}Ar released; Fig. 6.3). The spectrum records a gradational increase in apparent age from 342 Ma in a lower-temperature heating increment (13.3% of total ^{39}Ar released) to 380.6 - 383.9 Ma in three,

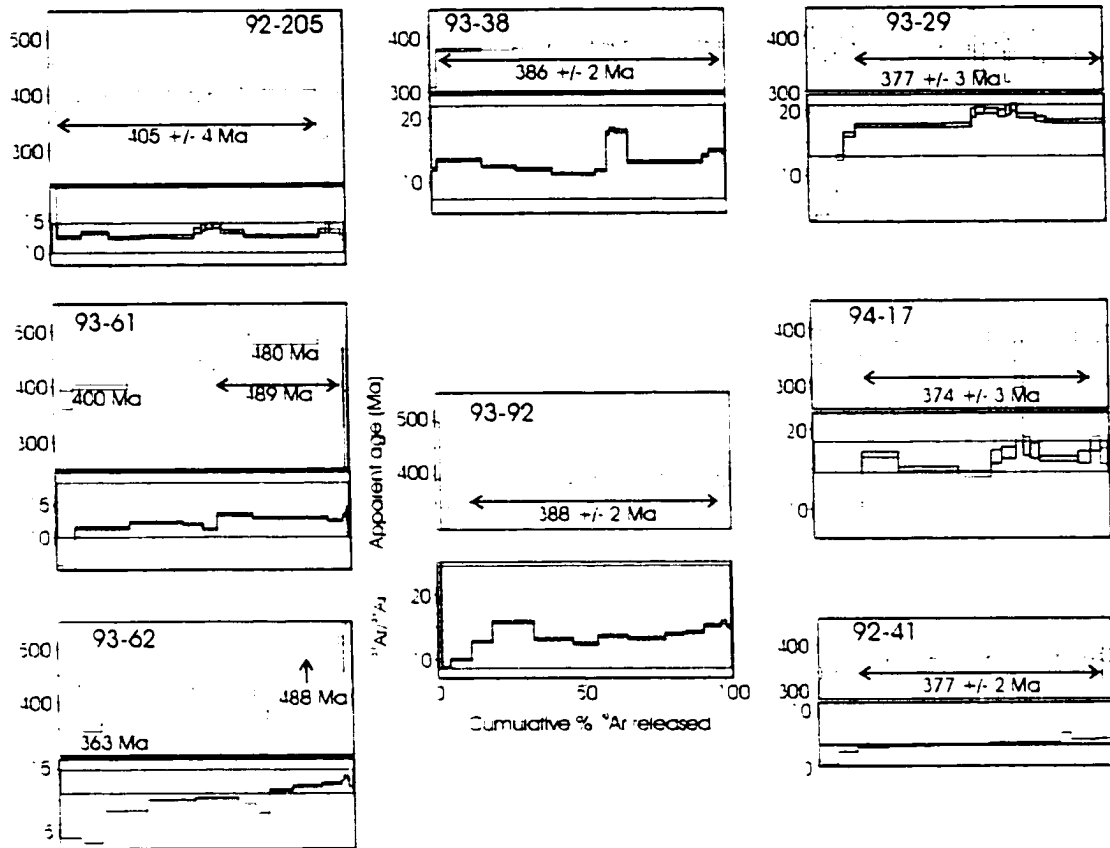


Figure 6.3 $^{40}\text{Ar}/^{39}\text{Ar}$ age spectra (upper graphs) and measured $^{37}\text{Ar}/^{39}\text{Ar}$ ratios (lower graphs) for hornblende samples. The half-heights of the rectangles indicate the 2σ relative (between-step) uncertainties. The age reported for each spectrum is a weighted-average age based on the fraction of gas indicated. $^{37}\text{Ar}/^{39}\text{Ar}$ ratios inferred from microprobe Ca/K analyses are indicated by the shaded horizontal band on the $^{37}\text{Ar}/^{39}\text{Ar}$ plots. Refer to Figure 6.1 for sample locations.

non-adjacent, higher-temperature heating increments (44.6% of total ^{39}Ar released). However, the 342 Ma apparent age is associated with an anomalously low $^{37}\text{Ar}/^{39}\text{Ar}$ ratio (10.5) as compared to the remainder of the apparent ages (16.8, average) and the microprobe determined $^{37}\text{Ar}/^{39}\text{Ar}$ ratios (Fig. 6.3). Thus, it seems likely that this apparent age reflects gas released from a less retentive contaminant phase in the hornblende (Maboko et al. 1991). The presence of actinolite intergrowths with low Ca/K ratios supports this hypothesis. The apparent ages recorded by the higher-temperature, and presumably more retentive, heating increments (i.e., those used in the weighted averaging calculation) were plotted on an isotope correlation diagram. Within the statistically-defined limits of an acceptable fit (i.e., $SUM S = 7.4$; where $SUM S$ must be <10), the apparent ages define a straight line with a tightly-constrained X-intercept value of 0.945, which corresponds to an age of 382 ± 3 Ma (Fig. 6.4). This isotope correlation age is interpreted as the geochronologically significant age for this sample.

Dunamagon Granite - mafic dyke

One sample (92-41; see McDonald 1993) of an amphibolitic mafic dyke from the eastern-most exposures of the Dunamagon Granite was collected for $^{40}\text{Ar}/^{39}\text{Ar}$ analysis (Fig. 6.1). This sample comprises ~15%, fine- to coarse-grained, idiomorphic to xenoblastic, acicular to equant, hornblende porphyroblasts which are moderately poikiloblastic (inclusions comprise quartz, plagioclase, epidote, and titanite). The hornblende porphyroblasts are commonly intergrown with biotite along the grain-margins, and great care was taken during hand-picking to avoid the intergrown grains.

Sample 92-41 yielded a fairly flat spectrum, consistent with a weighted average

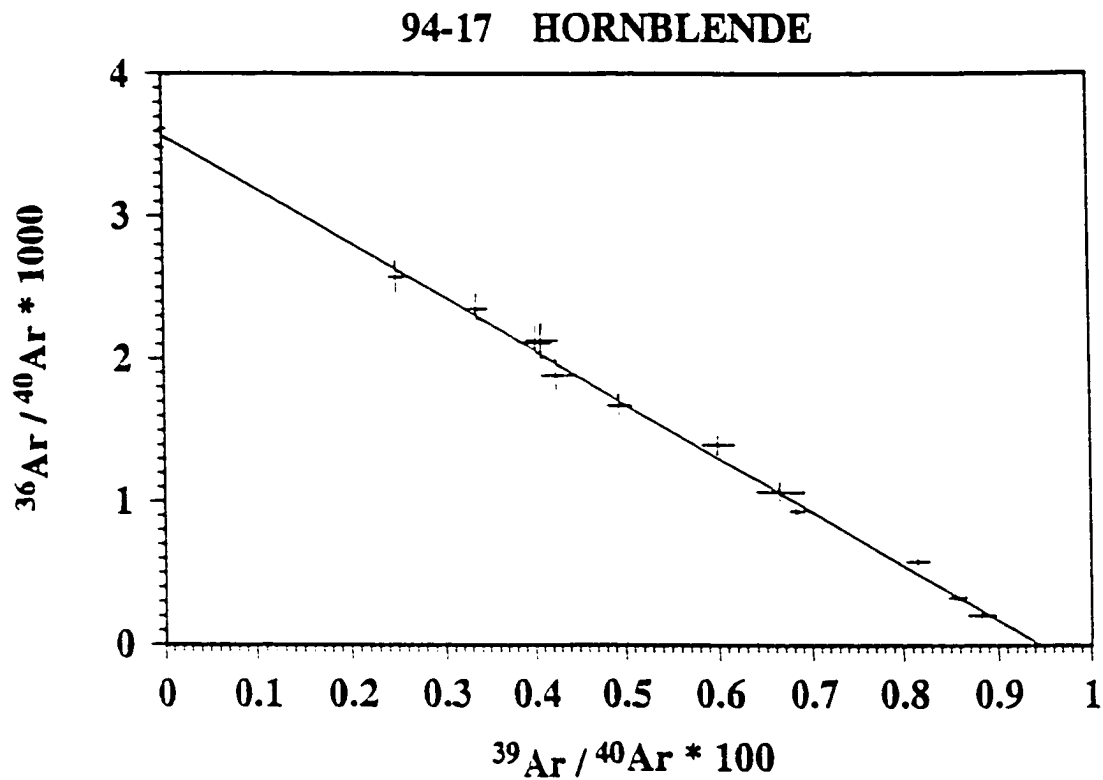


Figure 6.4 Isotope correlation plot for sample 94-17. The correlation plot includes all but the first two increments of the $^{40}\text{Ar}/^{39}\text{Ar}$ spectra, which were excluded on the basis of their anomalously low $^{37}\text{Ar}/^{39}\text{Ar}$ ratio (see Fig. 6.3).

age of 377 ± 2 Ma (incorporates 83% of the total ^{39}Ar released; Fig. 6.3). However, this spectrum also records a gradational increase in apparent age from the lower- to higher-temperature heating increments. At lower temperatures, six adjacent heating increments comprising 57.5% of the total ^{39}Ar released record apparent ages that grade with increasing temperature from 348.1 to 376.9 Ma. At higher temperatures, a single heating increment, comprising 23.8% of the total ^{39}Ar released, records an apparent age of 380 Ma. The gradational increase in apparent age is associated with a corresponding slight increase in $^{37}\text{Ar}/^{39}\text{Ar}$ ratio (0.4 to 3.7), and the first three heating increments are associated with $^{37}\text{Ar}/^{39}\text{Ar}$ ratios well below those derived from microprobe analyses of the hornblende (Fig. 6.3). These relationships indicate that the apparent age gradient records gas released from minor amounts of a contaminant phase, possibly intergrown biotite. Therefore, the weighted average age of 377 ± 2 Ma, which is weighted toward the higher temperature increments, is considered to be the geochronologically significant age of this sample.

Big Brook Shear Zone - mafic dyke

One sample (93-29) of a strongly deformed amphibolitic mafic dyke from the easternmost exposures of the BBSZ was collected for $^{40}\text{Ar}/^{39}\text{Ar}$ analysis (Fig. 6.1). This sample comprises ~75% fine- to coarse-grained, idioblastic to xenoblastic, acicular, hornblende porphyroblasts that are locally highly poikiloblastic (inclusions comprise quartz and opaque mineral grains). The hornblende varies from strongly foliated and lineated parallel to S_2 - L_2 , to completely randomly oriented. This sample contains <2% biotite, which is not intergrown with hornblende.

Sample 93-29 yielded a highly disturbed spectrum (Fig. 6.3). The initial five

heating increments, comprising 15.7% of the total ^{39}Ar released, are associated with highly variable apparent ages, and anomalously low $^{37}\text{Ar}/^{39}\text{Ar}$ ratios relative to the hornblende, suggesting the presence of a less retentive contaminant phase. The higher temperature heating increments are also associated with variable apparent ages, but have very uniform $^{37}\text{Ar}/^{39}\text{Ar}$ ratios (17.6 to 20.3), consistent with gas evolved from variably retentive, though compositionally homogeneous, hornblende. These heating increments were used to calculate a weighted average age of 377 ± 3 Ma (comprising 83% of the total ^{39}Ar released). This age is considered to be geochronologically significant, particularly in light of the mutually overlapping $^{40}\text{Ar}/^{39}\text{Ar}$ ages recorded by all three hornblende samples in the Pacquet Harbour area (i.e., samples 92-41, 93-29, and 94-17).

Eastern Shore of Ming's Bight - amphibolite

Four samples of amphibolite were collected along the eastern shore of Ming's Bight (Fig. 6.1). Samples 93-61 and 93-62 were collected from coastal exposures of a D_2 shear zone located ~200m north of Caplin Cove (Map 8), and sample 92-205 was collected from a sequence of amphibolite in the hangingwall of this shear zone (~100m north of Caplin Cove; Map 8). Further south, sample 93-92 was collected from a small inland outcrop of amphibolite that is surrounded by MBG schist ~1.0 km east of Deep Cove, and is interpreted as a tectonic inclusion emplaced into the MBG during D_2 transpressional shear (Map 4).

Sample 93-92 - In thin section, two distinct populations of hornblende are apparent in sample 93-92. The first comprises ~4-5% of the sample, and forms 0.5 to 3.0 mm, equant, idioblastic, twinned hornblende porphyroblasts which are variably

poikiloblastic (inclusions comprise quartz, plagioclase, epidote, and titanite). The second comprises ~40% of the sample, and forms <0.5 mm, acicular, euhedral to subhedral, strongly foliated hornblende crystals which are only slightly poikiloblastic. These crystals are foliated parallel to S_2 , and define a prominent L_2 mineral lineation. In X-Z sections, hornblende crystals of the first population are wrapped-around by S_2 and commonly have asymmetric quartz-filled strain shadows and fish-like shapes (e.g., Lister and Snoke 1984) that indicate sinistral transcurrent shear (Fig. 4.2d). These porphyroblasts are interpreted as having grown in the early stages of transpressional shear. The hornblende selected for $^{40}\text{Ar}/^{39}\text{Ar}$ analysis primarily comprised the first population of hornblende, and yielded a fairly flat spectrum, consistent with a weighted average age of 388 ± 2 Ma (incorporates 84 % of the total ^{39}Ar released; Fig. 6.3). The initial heating increments record gradationally increasing apparent ages, and somewhat low $^{37}\text{Ar}/^{39}\text{Ar}$ ratios, suggesting the presence of a less retentive contaminant phase in the hornblende.

Sample 92-205 - This sample was collected from a ~20m thick sequence of mylonitic amphibolite that contains mesoscopic deformation structures that record three phases of deformation prior to folding of the entire sequence by a large F_1 fold (Map 8; Cross section 7). Structures associated with the first two deformation phases comprise a penetrative mylonitic foliation, hornblende lineation, and a large isoclinally refolded isoclinal fold (hence, two deformation phases), whereas structures ascribed to the third phase comprise a spaced crenulation fabric and open folds. On the basis of the marked similarity in structural style and overprinting relationships, these structures are correlated with D_1 , D_2 , and D_3 , respectively, in the Ming's Bight area. This correlation is significant

because the sample selected for $^{40}\text{Ar}/^{39}\text{Ar}$ analysis (92-205) contains weakly-strained hornblende porphyroblasts that overgrew S_3 , and are commonly preferentially oriented parallel to the axial planes of the open F_3 crenulations. These relationships may indicate growth of the hornblende during D_3 , possibly immediately following, or in the waning stages of, amphibolite facies metamorphism associated with D_1 - D_2 (see Section 5.2.2.3).

Sample 92-205 comprises strongly recrystallized mylonitic amphibolite. In several locations in the field, a weak ophitic texture is preserved, and apparently grades into more massive metagabbro, which suggests that the mylonite formed through intense deformation of gabbro (Fig. 2.7e). The sample contains ~25% fine- to very coarse-grained, idioblastic, acicular, poikiloblastic (inclusions of quartz, plagioclase, and ilmenite) hornblende porphyroblasts. As noted above, the hornblende is locally foliated parallel to the weak S_3 fabric and/or randomly-oriented. Compelling textural or compositional evidence for more than one generation of hornblende is lacking. Indeed, the hornblende separates from sample 92-205 yielded a fairly flat spectrum, and very uniform $^{37}\text{Ar}/^{39}\text{Ar}$ ratios (12.5 to 14.1), consistent with a weighted average age of 405 ± 4 Ma (incorporates 88 % of the total ^{39}Ar released; Fig. 6.3).

Samples 93-61 and 93-62 - These samples were collected from mylonitic amphibolite in the core of a D_3 shear zone (93-62; Fig. 5.5f), and from a body of metagabbro within the mylonite (93-61). The mylonitic amphibolite comprises ~70% fine- to medium-grained, acicular to fibrous, euhedral to subhedral, strongly foliated hornblende crystals which are only slightly poikiloblastic. These crystals are foliated parallel to S_5 , and locally define a prominent L_5 mineral lineation. The mylonite contains a concordant, ~10m

long, <1 m thick body of dark grey-black, coarse-grained metagabbro. In the interior, the metagabbro is only slightly deformed, and preserves a weak ophitic texture defined by randomly oriented, recrystallized, lath-shaped, plagioclase phenocrysts that surround ~20% coarse-grained, subhedral, randomly oriented, poikiloblastic (inclusions of quartz, plagioclase, epidote, and opaque minerals) hornblende. The metagabbro is wrapped-around by, and gradational with, the penetratively foliated mylonite, and the contacts of the metagabbro are off-set and back-rotated by large-scale shear bands that are compatible with the sense of shear in the mylonite. The presence of gradational contacts between the mylonite and the metagabbro indicate that, at least locally, the mylonite may have formed through intense deformation of metagabbro. This hypothesis is supported by the presence of subhedral plagioclase porphyroclasts in the mylonite which may represent primary plagioclase phenocrysts derived from metagabbro.

Samples 93-61 and 93-62 yielded highly disturbed $^{40}\text{Ar}/^{39}\text{Ar}$ spectra (Fig. 6.3). However, by considering these spectra in conjunction with field relationships and other geochronologic data, several potentially meaningful ages can be extracted. For example, the sample of metagabbro (92-61) yielded a highly disturbed spectrum with an increasing apparent age gradient from lower to higher temperatures, but very uniform $^{37}\text{Ar}/^{39}\text{Ar}$ ratios (11.2 to 13.5), which suggests that the apparent ages are recording significant loss of radiogenic Ar from compositionally homogeneous hornblende (e.g., Hanes 1991; Maboko et al. 1991). At lower temperatures, a single heating increment comprising 18.9 % of the total ^{39}Ar released records an apparent age of 399.7 Ma, whereas at higher temperatures four adjacent heating increments, comprising 42.7 % of the total ^{39}Ar

released, record a weighted average apparent age of 489 Ma (Fig. 6.3). Both of these apparent ages are considered to be geochronologically significant, as discussed below.

The mylonite sample (93-62) yielded a strongly disturbed spectrum with an apparent age gradient increasing from 362.7 Ma to 514.2 Ma from the lower to higher heating increments, respectively (Fig. 6.3). This gradient is associated with a corresponding slight increase from 8.3 to 12.6 in the $^{37}\text{Ar}/^{39}\text{Ar}$ ratio, which may suggest the presence of a less retentive contaminant phase in the hornblende. This hypothesis is supported by the fact that only the last eight heating increments, comprising 28.4% of the total ^{39}Ar released, have $^{37}\text{Ar}/^{39}\text{Ar}$ ratios overlapping with those derived from probe analyses of the hornblende. However, given the field relationships of this sample, the age gradient might also be reasonably ascribed to Ar loss associated with deformation related recrystallization and/or alteration of the hornblende during mylonitization of the metagabbro. In this regard, it is probably significant that the two high-temperature heating increments which record the last significant release of ^{39}Ar from this sample (two steps comprising 16.5% of the total ^{39}Ar) indicate an apparent age in the range of 490-500 Ma. On the basis of the field relationships of this sample, this age gradient is considered to be geochronologically significant, as discussed below.

6.3.2 U-Pb analyses

6.3.2.1 MBG pegmatite sample - Pelee Point, Pacquet Harbour

This sample was collected from a planar, <20cm thick, granitic pegmatite dyke which can be traced for ~50m (limit of outcrop), and everywhere post-dates D_1 and D_2 folds and fabrics (Fig. 6.1; Map 2; Fig. 6.5a). In one location, the dyke is sinistrally offset

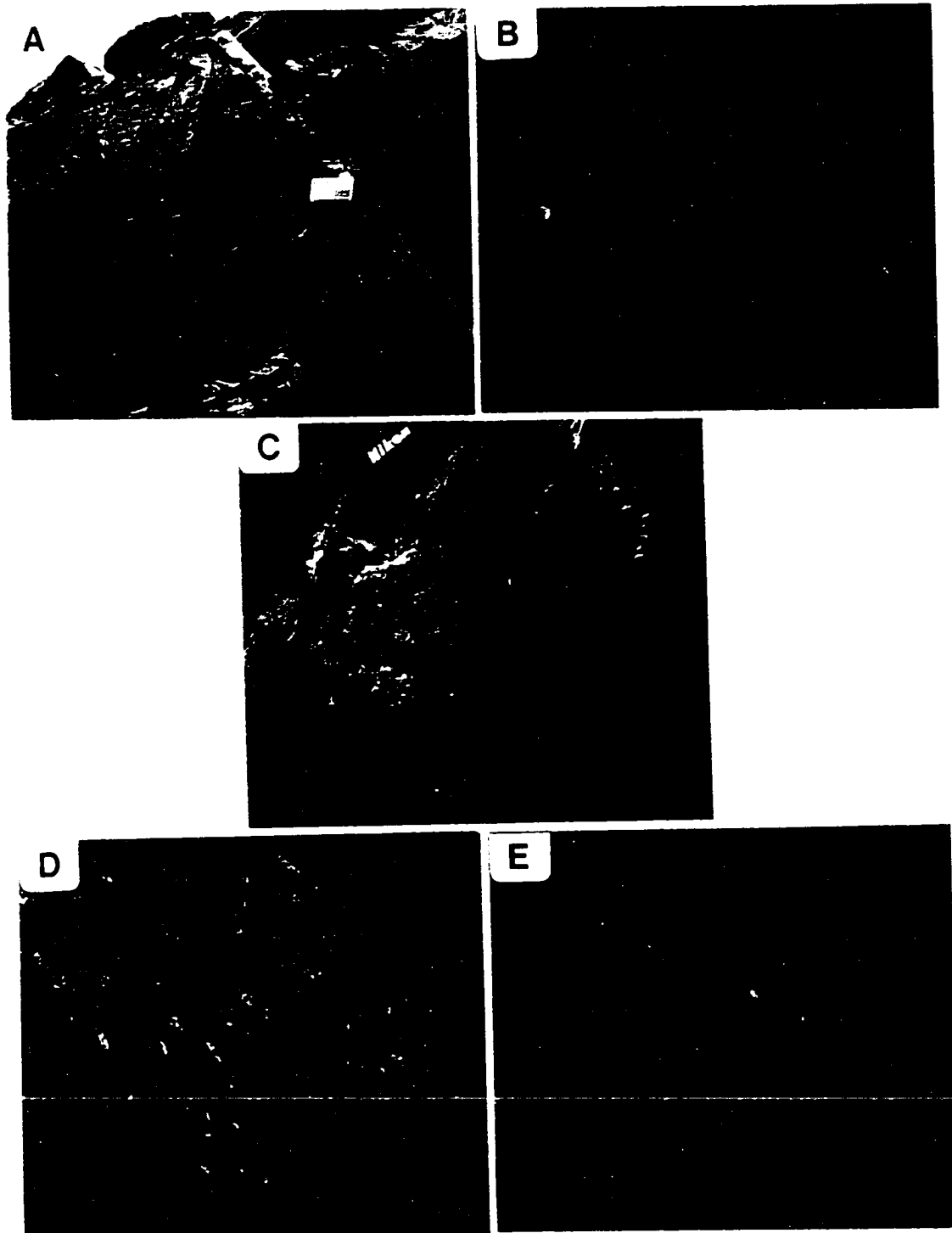


Figure 6.5 U-Pb geochronology samples (refer to Fig. 6.1 for locations). a) Post-tectonic granitic pegmatite cutting a F_2 fold (arrowed) at Pelee Point. b) Microlite from the Pelee Point pegmatite (mag. x32). c) Idioblastic rutile and titanite porphyroblasts in the NMTSZ. d) Rutile separate (mag. x20). e) Titanite separate (mag. x20).

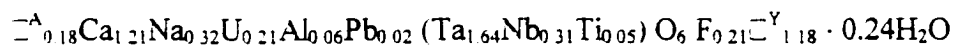
~1m by a late-stage (i.e., post-D₃) subvertical, east-striking, brittle fault which contains subhorizontal slickenlines.

Background - The pegmatite sample was processed using the standard mineral separation techniques. Zircon separates in the final Frantz magnetic splits at 1°, 3°, and 5° side-tilts typically comprise anhedral fragments, or rare octahedra, which are <1mm, white-brown, and range from slightly turbid to totally metamict. These grains contain few inclusions, but are often cracked and very soft due to extreme metamictization. No monazite or titanite was found in either the final or initial Frantz separates; however, the initial magnetic split at 1.7 Amps, and the final magnetic split at 5° side-tilt, contained numerous crystals of an unknown mineral. Given the extremely poor quality of the zircon, and lack of other datable phases, these crystals were examined in greater detail.

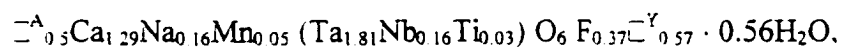
Description of unknown mineral - The unknown mineral ranges in colour from pale yellow to dark brown, and forms <1mm, euhedral octahedra or anhedral angular fragments (Fig. 6.5b). The crystals contain few inclusions, and range from clear (yellow crystals) to turbid to completely metamict (brown crystals). Individual grains are typically homogeneous in appearance, although several grains show visible concentric core-to-rim colour zoning that includes gradations from yellow to brown, and brown to yellow. Approximately 50 of these crystals were mounted in epoxy, and examined in detail with the microprobe. The ranges in values (in weight percent) are 52-79 Ta₂O₅, 1.0-12.5 Nb₂O₅, 0.0-4.3 TiO₂, 0.0-11.0 UO₃, 8.5-14.0 CaO, 0.6-3.5 Na₂O, 0.2-1.9 F, 0.0-0.8 MnO, and 0.0-0.7 Al₂O₃. Other detected elements, which are only locally measurable include <1.0 wt% FeO, ZrO₂, MgO, and PbO. Back-scattered electron images confirm that the

concentric colour zoning reflects compositional zoning, and also reveal grains that have a mottled appearance due to heterogeneous compositional variations. Microprobe analyses indicate that the brown to yellow-brown grains (or portions of grains) are U, Ti, and Nb-enriched relative to the Ta, Na, and F-enriched yellow grains. Plots of Ta₂O₅ vs. Nb₂O₅ reveal a strong linear trend, consistent with coupled substitution between Nb and Ta, and there is a distinct correlation between brown, highly metamict grains, and increased U concentrations. Inclusions are very rare, although one grain contains numerous round, dark-brown, inclusions of columbite-tantalite, possibly consistent with replacement of the columbite-tantalite (see below).

Identification of the unknown mineral - A comparison of the morphology and composition of the unknown mineral phase to those of known Ta-Nb mineral species in granitic pegmatites, indicates that the unknown mineral is the pyrochlore group mineral microlite (Hogarth 1977). The pyrochlore group minerals have the general formula A_{2-m} B₂ X₆ Y_{1-n} · pH₂O, where A = Na, Ca, U, Pb, Sr, Th, REE, Bi, Sn²⁺, Ba, Mn, Fe²⁺; B = Ta, Nb, Ti, Zr, Fe³⁺, Sn⁴⁺, W; X = O; Y = O, OH, F; m = 0 to 2; n = 0 to 1, and; p = 0 to ? (e.g., Foord 1982; Lumpkin et al. 1986). Recalculation of a U-rich and U-poor microprobe analysis on the basis of ΣB = 2.0 (H₂O estimated by difference; e.g., Lumpkin et al. 1986) reveals that the mineral phase from the Pelee Point pegmatite has formulas ranging from



[the high Y-site anion total in this analysis probably reflects an imprecise H₂O estimate] to



respectively, consistent with both the microlite general formula and compositions reported in the literature (i.e., $Ta + Nb > 2Ti$; $Ta \geq Nb$; no A-site cation other than Ca or Na accounts for >20% of total A-site cations; e.g., Hogarth 1977; Lumpkin et al. 1986).

A literature review of the typical characteristics of microlite reveals many close similarities with the microlite in the Pelee Point pegmatite, thereby supporting the identification. These characteristics are summarized below (compare with those listed in the preceding paragraphs): 1) Microlite is principally found in late- to post-tectonic, moderately to highly fractionated, granitic pegmatites of the rare-element class (e.g., Cerný 1982; Lumpkin et al. 1986; Cerný and Ercit 1989). 2) Lumpkin et al. (1986), based on an examination of microlite in the Harding pegmatite in New Mexico, reported typical compositional ranges of (wt% oxide): 60-78 Ta_2O_5 , 2.5-12 Nb_2O_5 , 0.0-3.2 TiO_2 , 0-11 UO_3 , 8-13 CaO, 2.0-5.5 Na_2O , 1.5-3.5 F, and 0.1-4.0 H_2O . However, it should be noted that highly variable compositions are possible, and reflect the extremely accommodating cubic structure of microlite (Cerný and Ercit 1989). 3) Microlite typically forms <5mm, yellow to dark brown, euhedral to anhedral crystals (Lumpkin et al. 1986), and changes in the colour of microlite from yellow to dark brown are often correlated with increasing Nb, U, and Ti content, and decreasing Ta/Nb ratio (e.g., Jahns and Ewing 1976; Lumpkin et al. 1986). 4) One of the principal substitution schemes in microlite is $Nb \leftrightarrow Ta$, and there is a positive correlation between Na and F, and a negative correlation between U and F (Lumpkin et al. 1986). 5) Microlite occurs either as a primary phase, or as a primary hydrothermal replacement product after columbite-tantalite and other minerals (e.g., Cerný and Turnock 1971; Cerný and Ercit 1989). 6) Metamictization of microlite is common due

to the presence of subordinate to substantial U contents (Cerný and Ercit 1989).

Paragenesis of microlite - Lumpkin et al. (1986) inferred, on the basis of paragenetic relationships in the Harding pegmatite, that microlite crystallized from the pegmatitic magma relatively late in the crystallization sequence, and is thus found in the core zones and subsolidus replacement units. In addition, microlite often replaces columbite-tantalite and other Ta-Nb minerals during primary hydrothermal alteration from residual magmatic fluids (Lumpkin et al. 1986; Cerný and Ercit 1989). The presence of fine-grained, rounded, inclusions of columbite-tantalite in microlite from the Pelee Point pegmatite may be consistent with this paragenesis. In addition, several grains examined in the present study exhibited concentrically decreasing Ta and Nb, coupled with increasing U, and Ti, from core to rim. Lumpkin et al. (1986) noted that this type of zoning typifies microlite found in late replacement units of the Harding pegmatite.

Results of U-Pb dating of microlite - As a result of the poor quality zircon in the Pelee Point pegmatite, microlite is the principal primary phase which is datable using the U-Pb method. Numerous <1 mm, yellow crystals of microlite with good clarity and octahedral crystal forms were selected, and abraded to round glassy beads for ~9 hours at ~1-2 psi. The abraded grains were examined at high magnification under a binocular microscope, and the best grains, lacking cracks, visible inclusions, and inhomogeneities, were selected for final analysis. Dissolution, chromatography, and analytical procedures followed those outlined above. A large, multiple-grain fraction (M1) was analyzed first, and common lead was subtracted according to the Stacey and Kramers (1975) model using an assumed age of 360 Ma. Based on the remarkably high U content of fraction M1

(Table 6.1), one three-grain fraction (M2) and two single-grain fractions (M3 and M4) were subsequently analyzed, and common lead was subtracted according to the Stacey and Kramers (1975) model for 1500 Ma, based on the following assumptions: 1) the restricted occurrence of pegmatite within only the MBG is consistent with derivation of the former through partial melting of the latter; 2) 1500 Ma is a rough approximation of the possible age of detritus in the MBG; and 3) on the basis of points 1 and 2, the 1500 Ma correction would probably provide a close approximation of the common lead in the pegmatite (G.R. Dunning 1995, pers. comm.).

The results of the microlite U-Pb analyses are presented in Table 6.1 and Figure 6.6. The four analyses contained between 46992 and 29560 ppm U, and plot between 1.61 and -2.39 % discordant, although all four mutually overlap concordia. The range of $^{206}\text{Pb}/^{238}\text{U}$ and $^{207}\text{Pb}/^{235}\text{U}$ ages is only 354 to 357, consistent with an age and uncertainty of 355 ± 2 Ma. The mutual concordancy of all four fractions clearly indicates that the analyses are not greatly affected by the age assumed for the common lead correction (i.e., the correction is negligible due to the high concentration of radiogenic Pb; Table 6.1).

6.3.2.2 Rutile-titanite bearing chlorite schist - NMTSZ, Ming's Bight

The sample selected for U-Pb analysis contained ~5-10%, <1.0cm, acicular to bladed, euhedral to subhedral rutile crystals, and ~10%, <1.0cm, subhedral, blocky titanite crystals, in a chloritic matrix (Fig. 6.5c). After mineral separation, two very large fractions of rutile and two large fractions of titanite were hand-picked. The rutile is orange-brown to deep red-brown, clear to slightly turbid, and forms angular fragments or acicular striated crystals (Fig. 6.5d). The titanite is colourless to pale purple-brown, clear to turbid,

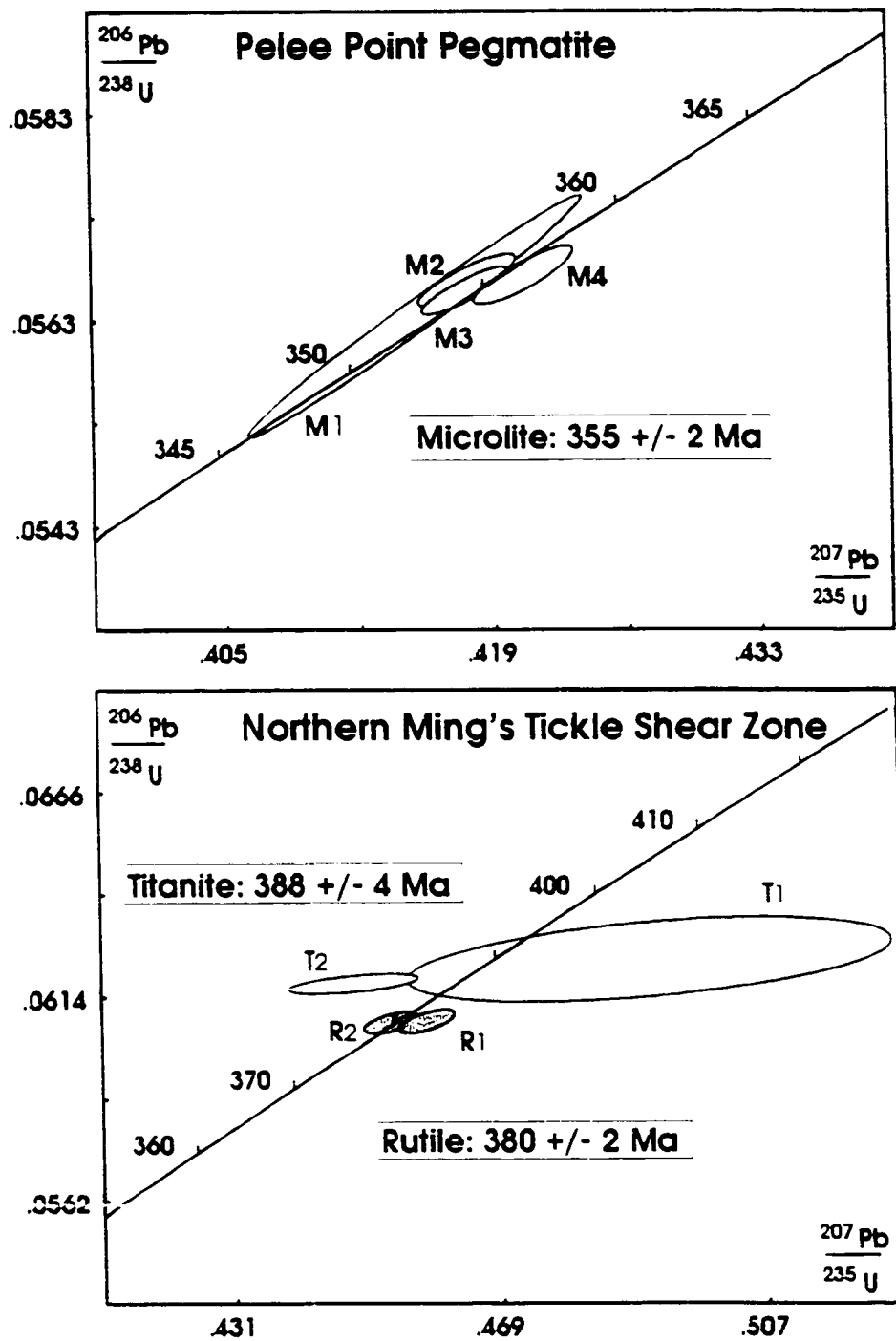


Figure 6.6 U-Pb concordia diagrams. Upper diagram - microlite from the Pelee Point pegmatite. Lower diagram - rutile and titanite from the NMTSZ.

and only forms angular fragments, probably reflecting the initial large size of the porphyroblasts (Fig. 6.5e). The rutile and titanite were abraded to a fairly uniform roundness for 3-4 hours at 2 psi, and 9-10 hours at 2-3 psi, respectively.

The results of the U-Pb analyses are presented in Table 6.1 and Figure 6.6. The two rutile fractions are mutually overlapping, with one analysis plotting on the concordia. These fractions (R1 and R2) contain 16 and 15 ppm U, respectively, and the $^{206}\text{Pb}/^{238}\text{U}$ and $^{207}\text{Pb}/^{235}\text{U}$ ages range from 380 to 384, consistent with an age and uncertainty of 380 ± 2 Ma. The two titanite fractions (T1 and T2) contained 46 and 51 ppm U, respectively, and the $^{206}\text{Pb}/^{238}\text{U}$ and $^{207}\text{Pb}/^{235}\text{U}$ ages range from 387 to 391 and 376 to 406, respectively, consistent with an age and uncertainty of 388 ± 4 Ma. The comparatively large range in $^{207}\text{Pb}/^{235}\text{U}$ ages is due to the uncertainty associated with the common lead correction, and thus the $^{206}\text{Pb}/^{238}\text{U}$ ages are taken to be the best indication of the age of the titanite, since this ratio is considerably less affected by the correction (e.g., Miller et al. 1996). The large analytical error associated with fraction T1 results from loss of the sample part way through the analysis (sample fell off the Re filament).

6.4 DISCUSSION AND CONCLUSIONS

6.4.1 *Pacquet Harbour area*

6.4.1.1 Significance of the microilite U-Pb date

There are few published reports concerning U-Pb geochronology of Ta-Nb minerals from granitic pegmatites using modern geochronologic techniques. Several studies document the results of U-Pb dating of columbite-tantalite (e.g., Romer and Wright 1992; Romer and Smeds 1994; Mauthner et al. 1995); however, there are no

reports on U-Pb dating of microlite. Consequently, the geochronological significance of the 355 ± 2 Ma U-Pb microlite date must be addressed before any conclusions can be drawn with regard to the geological significance.

Based on the fact that all four analyses mutually overlap on the concordia, it seems reasonable to assume that the microlite U-Pb date is recording a specific geologic event. In addition, since microlite is a primary phase in the Pelee Point granitic pegmatite (i.e., primary igneous or primary hydrothermal; e.g., Lumpkin et al. 1986), there are only three possible explanations for the U-Pb date: 1) the date could represent the age of initial crystallization and closure of the microlite, and thus the age of intrusion of the Pelee Point pegmatite; 2) the date could represent the age of complete resetting of the microlite during a post-intrusion thermal event; or 3) the date could represent a cooling age that records final closure of microlite subsequent to intrusion, or a post-intrusion thermal event.

Discriminating between these possibilities hinges on establishing the microlite closure temperature. However, the only information available that might help constrain the closure temperature of microlite is that provided by Lumpkin et al. (1986), who noted that microlite is stable up to conditions of ca. 500°C and 5 kbar, thereby suggesting a closure temperature for Pb diffusion in microlite of ~500°C.

Fortunately, several inferences regarding the closure temperature of microlite and the significance of the microlite U-Pb age can be made on the basis of field and microstructural relationships, and the regional $^{40}\text{Ar}/^{39}\text{Ar}$ data. In particular, field relationships indicate that the Pelee Point pegmatite is post-tectonic with respect to high-temperature D_2 deformation. Therefore, the ca. 380 Ma regional closure of hornblende

(see below) is herein considered to approximate the older age-limit of pegmatite intrusion. In addition, muscovite from the Pelee Point pegmatite (sample 94-55) yielded an $^{40}\text{Ar}/^{39}\text{Ar}$ age of 363 ± 3 Ma, thereby providing a younger age-limit of intrusion. Because the $^{40}\text{Ar}/^{39}\text{Ar}$ muscovite age is resolvably older than the U-Pb date from the same sample, a U-Pb cooling age is strongly implied.

Feldspar phenocrysts in the Pelee Point pegmatite contain microstructures (i.e., brittle fractures, undulose extinction, relatively strain-free subgrains, and bent twin-planes) that are consistent with weak deformation and recrystallization in upper greenschist facies temperature conditions (i.e., 400-500° C; Gapais 1989). Given the evidence for regional cooling below the closure temperature of muscovite (~350° C) at ca. 360 Ma (see below), the microstructural evidence indicates that the Pelee Point pegmatite must have been emplaced prior to 360 Ma, and probably soon after the closure of hornblende (e.g., ~370-375 Ma; see below). On this basis, the 355 ± 2 Ma U-Pb microlite date is most consistent with the time of microlite closure following regional metamorphism, and must therefore represent a cooling age which provides only a younger age constraint on the timing of pegmatite intrusion. Thus, although the above data are consistent with a T_C of <350° C for microlite, the U-Pb microlite date does not provide additional information of use in the present study. It is interesting to note however, that the ca. 370-375 Ma emplacement age inferred for the pegmatite is similar to U-Pb ages reported for late- to post-tectonic felsic plutons in the Avalon Zone of Newfoundland (Kerr et al. 1993), the Aspy and Mira Terranes of Cape Breton Island (Jamieson et al. 1986; Bevier et al. 1993), and the Meguma Zone of Nova Scotia (Clarke and Chatterjee 1992). This may indicate that the

late-Paleozoic, late- to post-tectonic felsic plutonism is more widespread than previously recognized in the Newfoundland Appalachians.

6.4.1.2 Overview of U-Pb and $^{40}\text{Ar}/^{39}\text{Ar}$ data

The U-Pb samples collected from the Pacquet Harbour area failed to yield additional useful results. However, the hornblende samples collected from the BBSZ (93-29), Dunamagon Granite (92-41), and PHG (94-17) in the Pacquet Harbour area yielded overlapping $^{40}\text{Ar}/^{39}\text{Ar}$ weighted-average ages of 377 ± 3 Ma, 377 ± 2 Ma, and 382 ± 3 Ma, respectively. Since the metamorphic peak in this area was associated with temperatures above the closure temperature of Ar diffusion in hornblende (ca. 530°C ; Harrison 1981), and titanite in the Dunamagon Granite records an Early Devonian age (Cawood et al. 1995), these ages are interpreted to reflect post-metamorphic cooling through the hornblende closure temperature following high-grade metamorphism. The four samples of muscovite (94-5, 92-75, 92-85c, 92-184) collected from MBG schist in the vicinity of Pacquet Harbour yielded overlapping $^{40}\text{Ar}/^{39}\text{Ar}$ weighted-average ages of 361 ± 3 Ma, 363 ± 3 Ma, 364 ± 3 Ma, and 360 ± 3 Ma, respectively. These ages are interpreted as reflecting continued post-metamorphic cooling through the muscovite closure temperature ($\sim 350^\circ\text{C}$; Purdy and Jager 1976). The nearly identical $^{40}\text{Ar}/^{39}\text{Ar}$ weighted-average ages of 363 ± 3 Ma, 362 ± 3 Ma, and 359 ± 3 Ma obtained from muscovite separated from MBG pegmatites (94-55 and 92-182) and their external contacts (92-132), respectively, are also interpreted as reflecting post-metamorphic cooling of the MBG.

6.4.1.3 Timing of deformation and metamorphism

The Middle Devonian (ca. 380 Ma) cooling ages recorded by hornblende in the Pacquet Harbour area provide a younger age limit for D_1 , and provide an estimate for the timing of D_2 and amphibolite facies metamorphism. Since peak metamorphic temperatures probably exceeded the hornblende closure temperature, these cooling ages also indicate that the onset of cooling, and presumably extensional deformation, must have occurred prior to 380 Ma. The hornblende cooling ages also provide an older age limit for D_3 and the MBG pegmatites, and confirm that the pegmatites were intruded more than 50 My after the Early Silurian Dunamagon Granite (ca. 429 Ma; Cawood and Dunning 1993).

The muscovite cooling ages in the Pacquet Harbour area cluster about the Devonian-Carboniferous boundary (360 Ma) and are interpreted to provide a general constraint on the timing of late- D_2 and/or D_3 in the Pacquet Harbour area.

6.4.2 Ming's Bight area

6.4.2.1 Overview of U-Pb and $^{40}\text{Ar}/^{39}\text{Ar}$ data

The samples of titanite and rutile collected from chlorite schist in the D_5 northern Ming's Tickle shear zone yielded precise U-Pb ages of 388 ± 4 Ma and 380 ± 2 Ma, respectively, which are interpreted to provide constraints on the timing of shearing related to D_5 deformation. The slight difference in age between the titanite and rutile fractions may indicate that the titanite is providing a crystallization age, whereas the rutile is providing a cooling age. This interpretation is consistent with the closure temperatures of these minerals (i.e., ca. 600 and 400° C, respectively; Heaman and Parrish 1991; Mezger et al. 1989), and the evidence for syn-deformational greenschist facies metamorphism (i.e.,

350-500° C; Yardley 1989) in this shear zone.

The hornblende samples collected from PHG rocks in the D₂ transpressional shear zone (93-38) and the tectonic inclusion of amphibolite in the MBG (93-92) yielded overlapping ⁴⁰Ar/³⁹Ar weighted-average ages of 386 ± 2 Ma and 388 ± 2 Ma, respectively, that can be interpreted in three ways: 1) if peak metamorphic temperatures in the Ming's Bight area were slightly below the closure temperature of hornblende, these ages may record the timing of peak amphibolite facies metamorphism; 2) if the metamorphic peak in the Ming's Bight area was associated with temperatures above the closure temperature for hornblende, the ages may record cooling through the closure temperature subsequent to the metamorphic peak; and 3) the ages might be recording hornblende growth and/or resetting during a discrete thermal event subsequent to the metamorphic peak.

On the grounds that these samples lack textural, microstructural, and compositional evidence to suggest post-D₂ growth of hornblende, and there is no evidence to suggest 'regional' post-D₂ amphibolite facies metamorphism in the Ming's Bight area, the third option is considered unlikely. Furthermore, Jamieson et al. (1998) note that the thermal peak in the footwall of overthrust regions is generally achieved ~15-20 My after the onset of convergence. In the present case, the time interval between initiation of thrusting (inferred to be ca. 420-430 Ma) and the closure of hornblende (ca. 387 Ma) is at least ca. 35 My. Therefore, the first option is also considered unlikely. Post-peak metamorphic cooling is considered the most reasonable interpretation for the hornblende ages in the Ming's Bight area.

The samples of muscovite collected from MBG schist near Actinolite Bay (92-102)

and at Seven Brooks Point (93-49) yielded overlapping $^{40}\text{Ar}/^{39}\text{Ar}$ weighted-average ages of 368 ± 4 Ma and 362 ± 3 Ma, respectively. These ages are interpreted to reflect continued post-metamorphic cooling through the muscovite closure temperature ($\sim 350^\circ\text{C}$; Purdy and Jager 1976). The weighted average $^{40}\text{Ar}/^{39}\text{Ar}$ age of 356 ± 3 Ma obtained from muscovite separated from the strongly-deformed MBG pegmatite at Cape Hat (sample 92-188) may also reflect post-metamorphic cooling of the MBG. However, it may not be coincidence that the youngest muscovite $^{40}\text{Ar}/^{39}\text{Ar}$ age was obtained from the only sample of deformed MBG pegmatite (i.e., deformation-related resetting of muscovite).

The hornblende sample obtained from amphibolite (92-205) north of Caplin Cove on the eastern shore of Ming's Bight yielded an $^{40}\text{Ar}/^{39}\text{Ar}$ weighted average age of 405 ± 4 Ma. As noted in Section 5.2.2.3, the metamorphic mineral assemblage within this block of amphibolite is consistent with at least upper greenschist-facies peak metamorphism (i.e., $>450^\circ\text{C}$; e.g., Yardley 1989). This age could be interpreted to reflect: 1) peak-metamorphic hornblende growth and closure; 2) cooling through the hornblende closure temperature following the metamorphic peak; or 3) hornblende growth and/or resetting subsequent to the metamorphic peak. Microstructural relationships in sample 92-205 are consistent with growth of the hornblende during D_3 , possibly immediately following or in the waning stages of amphibolite facies metamorphism associated with D_1 - D_2 (see Section 5.2.2.3). These relationships are consistent with any of the preceding options; however, regardless of interpretation, this age provides a younger age limit for D_1 - D_2 in the block of amphibolite, since growth of hornblende demonstrably post-dated D_1 - D_2 structures in this location. The regional significance of this interpretation is discussed below.

The samples of metagabbro (93-61) and amphibolitic mylonite (93-62) from the D₅ shear zone ~200 m north of Caplin Cove yielded highly disturbed age spectra with apparent age gradients from ~400 Ma to ~490 Ma and ~363 Ma to ~490-500 Ma, respectively. On the basis of field relationships and other ⁴⁰Ar/³⁹Ar data, the apparent ages recorded in the low-temperature increments of these age spectra are inferred to result from partial resetting of the hornblende during high-temperature metamorphism at ca. 400 Ma, and greenschist-facies mylonitization at ca. 360 Ma, respectively (see below). The apparent ages in the high-temperature increments are interpreted in the following section.

6.4.2.2 Age of the sequences on the eastern shore of Ming's Bight

The lithologic sequences exposed on the eastern shore of Ming's Bight are herein correlated with the PROC (see Section 2.3.6). In addition, gabbroic intrusions on the eastern shore of Ming's Bight are geochemically similar to, and thus correlated with, gabbro sills in the cover sequence of the PROC, from which Ramezani (1992) obtained a 483 ± 12 Ma U-Pb zircon age. This U-Pb date is similar to the ca. 490 Ma apparent ages recorded in the highest-temperature increments of the ⁴⁰Ar/³⁹Ar spectra from samples 93-61 (metagabbro) and 93-62 (mylonitized metagabbro) collected on the eastern shore of Ming's Bight. In light of this, it seems possible that the ca. 490 Ma apparent ages are recording components of primary gas (Tremadoc) released from the most retentive sites in the hornblende, and may further support the above correlations.

6.4.2.3 Timing of deformation and metamorphism

In order to correctly interpret the timing constraints provided by hornblende thermochronology in the Ming's Bight area, the field relationships and relative structural

positions of the samples must be considered. For example, hornblende sample 92-205 was collected from amphibolite facies rocks that contain penetrative D_1 - D_2 structures, and occur within a discrete, fault-bounded, structural block within a sequence of greenschist-facies rocks that contain only weak D_1 - D_2 structures. These relationships indicate that the amphibolite facies rocks must have formed at a relatively deep structural level with respect to D_1 - D_2 , and were imbricated with the greenschist facies rocks during: 1) a late increment of D_1 - D_2 compression; 2) D_3 - D_4 - D_5 extensional shear; or 3) a combination of both. Microstructural relationships between the hornblende porphyroblasts and F_3 folds in this sample are consistent with syn- to post- D_3 growth of the hornblende. Therefore, the 405 ± 4 Ma age obtained from this sample is interpreted as the younger age limit for D_1 - D_2 in this block and, based on the extensional character of D_3 , probably provides a younger age limit for D_1 - D_2 compression throughout the Ming's Bight area.

Hornblende samples 93-38 and 93-92 were collected from thick successions of amphibolite facies rock with penetrative D_2 structures, and yielded overlapping 386 ± 2 Ma and 388 ± 2 Ma hornblende cooling ages, respectively. These ages are interpreted to reflect post-metamorphic cooling following the amphibolite facies metamorphic peak in the Ming's Bight area. Furthermore, these samples were collected from rocks in the structural footwall of the major extensional structures in the Ming's Bight area. Therefore, the cooling ages are interpreted to provide a constraint on the initiation of extensional exhumation of the lowermost structural levels of the D_1 - D_2 structural pile (see below).

Overprinting relationships between D_5 structures and alteration assemblages in the northern Ming's Tickle shear zone indicate that growth of rutile and titanite

porphyroblasts took place shortly after an early increment of dextral-reverse oblique-slip shear, and prior to, or during, a later increment of dextral-normal oblique-slip shear (see Section 4.2.5.1). Since the U-Pb titanite date probably records titanite crystallization, the 388 ± 4 Ma age is interpreted to provide younger and older age-limits for dextral-reverse and dextral-normal shear, respectively, within this shear zone. The 380 ± 2 Ma rutile U-Pb date is interpreted to reflect cooling of the hangingwall through $\sim 400^\circ$ C, and to provide a general constraint on the time of D_5 extensional shear in the Ming's Bight area.

The 368 ± 4 Ma and 362 ± 3 Ma muscovite cooling ages from the southern (92-102) and northern (93-49) Ming's Bight areas, and the 356 ± 3 Ma muscovite age obtained from the deformed granitic pegmatite at Cape Hat, are taken to indicate that regional post-metamorphic cooling, greenschist facies metamorphic conditions, and extensional D_5 shear continued to latest Devonian to Early Carboniferous time.

6.4.3 Thermal history: Ming's Bight and Pacquet Harbour

Figure 6.7 illustrates the thermal history of the Ming's Bight and Pacquet Harbour areas. The various ages are plotted according to their respective estimated closure temperatures: $530 \pm 40^\circ$ C for hornblende (Harrison 1981); 350° C for muscovite (Purdy and Jager 1976; a nominal error of $\pm 20^\circ$ C was assigned); $280 \pm 40^\circ$ C for biotite (Harrison et al. 1985); $400 \pm 30^\circ$ C for rutile (Mezger et al. 1989); and $600 \pm 30^\circ$ C for titanite (Heaman and Parrish 1991).

Two temperature-time paths (T-t path) were constructed for the Ming's Bight area in order to summarize the thermal histories of two distinct pre- D_4 structural levels. In particular, the 'hangingwall' T-t path was constructed using $^{40}\text{Ar}/^{39}\text{Ar}$ data from

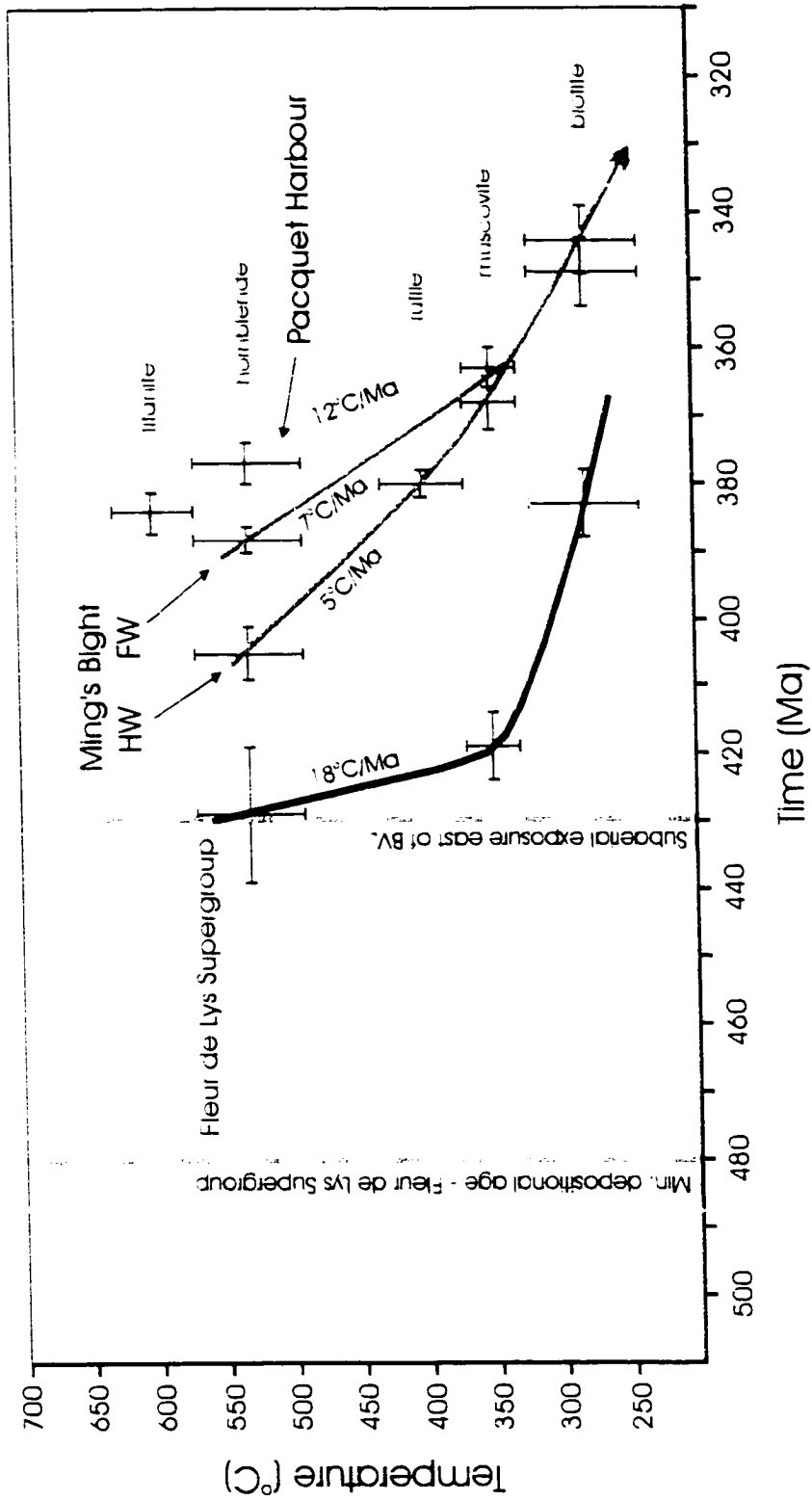


Figure 6.7 Plot of temperature-time data for the thesis area. Cooling rates calculated using the time interval between hornblende and muscovite closure are shown for each T-t path. The T-t path for the Fleur de Lys Supergroup, and the biotite ages in the Pacquet Harbour and Ming's Bight T-t paths, are from Dallmeyer (1977, recalculated in Dallmeyer and Hibbard 1984). HW, footwall of the GTCSZ. BV, hanging wall of the GTCSZ. See text for detailed discussion.

hornblende sample 92-205 and U-Pb data from rutile in the NMTSZ, since both samples are located in the structural hangingwall of the GTCSZ, and presumably represent a relatively high pre-D₄ structural level (Fig. 6.1). The 'footwall' T-t path was constructed using ⁴⁰Ar/³⁹Ar data from hornblende sample 93-92, since this sample is located in the structural footwall of the major extensional structures in the Ming's Bight area, and thus represents a relatively low pre-D₄ structural level (Fig. 6.1). The low-temperature ends of both T-t paths were constrained using ⁴⁰Ar/³⁹Ar data from muscovite samples 92-102 and 93-49, and a biotite date from the northwestern margin of the Dunamagon Granite (Dallmeyer and Hibbard 1984).

The T-t path for the Pacquet Harbour area was constructed using U-Pb data from titanite in the Dunamagon Granite (G.R. Dunning 1995, pers. comm.), and ⁴⁰Ar/³⁹Ar data from hornblende sample 93-29, muscovite sample 92-75, and a biotite sample from the BBSZ (Dallmeyer 1977; recalculated in Dallmeyer and Hibbard 1984). Insofar as these rocks record the highest metamorphic temperatures in the Ming's Bight - Pacquet Harbour area, this T-t path is interpreted to record the thermal history of the lowest pre-D₂ structural level.

The T-t path from the central portions of the Fleur de Lys Supergroup, based on ⁴⁰Ar/³⁹Ar hornblende, muscovite, and biotite data collected near Osborne's Pond and Seal Cove (Dallmeyer 1977; recalculated in Dallmeyer and Hibbard 1984), as well as thermobarometric data (Jamieson 1990), is shown for comparison (see Chapter 7).

A comparison of the T-t paths followed by the various structural levels provides several important insights into the structural and thermal evolution of the thesis area. In

particular, the closure of hornblende in the structurally highest levels may signal the latest stages of compressional deformation and/or the initiation of extensional exhumation of the structural pile at ca. 405 Ma (sample 92-205). The hornblende closure ages become progressively younger from higher to lower structural levels, as would be expected during progressive extensional exhumation of a high-grade metamorphic sequence. It may not be coincidence that the hornblende closure ages also apparently become progressively younger from northwest to southeast toward the D₂ extensional shear zone that dips southeast in Pacquet Harbour. A similar distribution of cooling ages has previously been noted in the footwall of detachment faults, and is interpreted to reflect progressive uplift and rotation of footwall rocks from beneath the detachments (e.g., Lee and Sutter 1991; Holm et al. 1992; Lee 1995).

The cooling rates in the study area, as measured by the time interval between hornblende and muscovite closure in each location, are uniformly high, consistent with relatively rapid post-metamorphic cooling. In addition, there is a marked increase in cooling rate from higher to lower structural levels, as well as from northwest to southeast across the MBG. Lee and Sutter (1991) and Lee (1995) documented a nearly identical pattern of decreasing closure ages and increasing cooling rates toward the northern Snake Range decollement in Nevada, and provided several possible explanations for the differential cooling: 1) asymmetric exhumation from beneath a detachment system that dipped moderately to steeply, and progressively rotated to a shallow dip (e.g., Lee et al. 1987); 2) asymmetric exhumation associated with a rolling hinge and isostatic rebound (e.g., Buck 1988; Wernicke and Axen 1988); 3) asymmetric exhumation coupled with a

late increment of relatively rapid movement along the detachment system; and 4) late increments of extensional deformation are preferentially accommodated by a system of younger, higher-level, normal faults during asymmetric exhumation. Although none of these hypotheses can be entirely discounted in the present case, the latter hypothesis is preferred, since the transtensional high-angle shear zones in the Ming's Bight area apparently initiated during the earliest increments of rapid cooling the Pacquet Harbour area (i.e., ca. 385 Ma). Moreover, there is little evidence to support significant brittle-ductile extensional deformation in the Pacquet Harbour area, which may indicate that late increments of the extensional deformation were preferentially accommodated along the brittle-ductile shear zones in Ming's Bight. The significance of these observations is addressed in Chapter 7.

All of the T-t paths from the thesis area converge at about the closure temperature of muscovite, and follow a single T-t path to sub-greenschist facies metamorphic conditions. This suggests that the rocks attained relative thermal equilibrium at ~360 Ma, possibly during the latest stages of extensional deformation in the thesis area.

Chapter 7 Tectonic Synthesis and Discussion

7.1 INTRODUCTION

In this chapter, the lithostratigraphic, structural, metamorphic, and geochronologic constraints detailed in the preceding chapters are incorporated into a comprehensive model for the Late Proterozoic to Early Carboniferous tectonic evolution of the MBG and thesis area. This model incorporates the revised deformation histories of the Ming's Bight and Pacquet Harbour areas, and offers a new and original framework in which to address the regional tectonic evolution of the BVP.

In Section 7.2, the tectonic model is developed with particular emphasis on comparisons with the Fleur de Lys Supergroup west of the BVL. These comparisons emphasize the distinct tectonothermal histories of the MBG and Fleur de Lys Supergroup, and place important constraints on the tectonic evolution of the BVP. The regional implications of the model are discussed in the context of the tectonic evolution of the western Newfoundland and northern Appalachians, with emphasis on evaluating the potential mechanisms for rapid post-metamorphic cooling and the recent hypotheses for 'extensional collapse' of the orogen (e.g., Cawood et al. 1995; van Staal and de Roo 1995). Section 7.3 examines the implications of this study for mesothermal vein-type gold and volcanogenic massive sulphide exploration on the BVP.

7.2 TECTONIC EVOLUTION AND REGIONAL IMPLICATIONS

7.2.1 *Late Proterozoic to Early Silurian (ca. 600–440 Ma)*

In western Newfoundland, the Late Proterozoic to Early Silurian time interval (Fig. 7.1) was associated with: 1) ca. 600 Ma rifting of Laurentia to form the Iapetus ocean margin (Stukas and Reynolds 1974; Kamo et al. 1989), and deposition of the Late Proterozoic to Middle Ordovician passive margin succession (Stevens 1970); 2) Late Cambrian initiation of an extensive island-arc system (i.e., Notre Dame Subzone; Dunning et al. 1987; Williams et al. 1988; Dec et al. 1997) above an east-dipping subduction zone proximal to the Laurentian margin (van der Pluijm et al. 1993); 3) obduction of the Taconian allochthons and destruction of the passive margin due to attempted eastward subduction of the continental margin, and arc-continent collision(s) during the Middle Ordovician Taconian orogeny (Williams 1979; Cawood et al. 1995); and 4) closure of the Iapetus ocean basin in Late Ordovician to Early Silurian time due to convergence of the Laurentian and Gondwanan continental margins (Dunning et al. 1990; Lin et al. 1994).

In the thesis area, this tectonic history is recorded, in part, by the MBG, PHG, and PROC. Siliciclastic rocks of the MBG have an ϵ_{Nd} value of -16 and model age of 2400 Ma (Fryer et al. 1992), consistent with an Archean source area, and deposition proximal to Laurentia in a continental slope or rise depositional setting in Late Proterozoic to Middle Ordovician time (e.g., Hibbard 1983; Fig. 7.1). The geochemical attributes of Early Ordovician mafic volcanic rocks in the PHG and PROC indicate deposition in a rifted-arc or back-arc basin environment in the Notre Dame island-arc system (Swinden et al. 1989; Fyffe and Swinden 1991). Biogeographic and paleomagnetic data indicate that the Notre

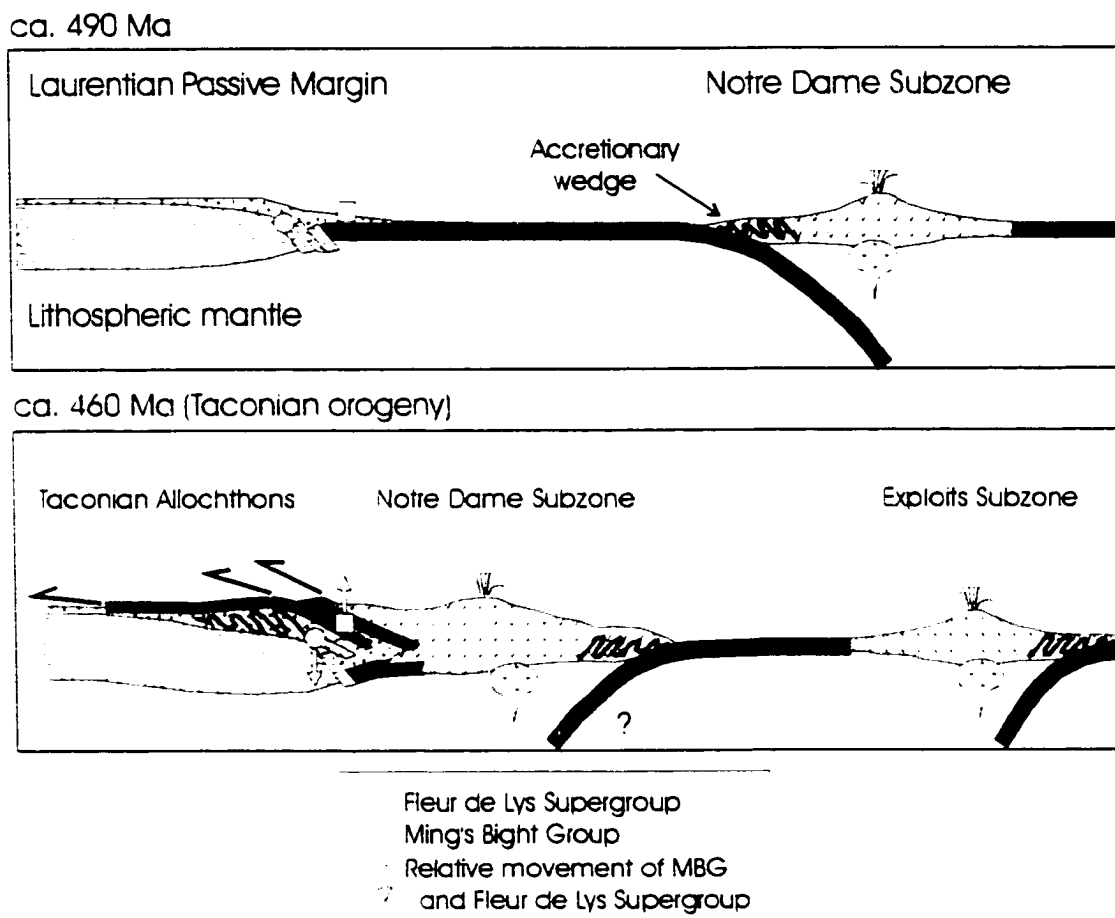


Figure 7.1 Schematic diagrams illustrating the generalized tectonic evolution of western Newfoundland in Early to Middle Ordovician time. The sections are modified after Williams (1979), van der Pluijm (1987), Cawood et al. (1995), and van Staal and de Roo (1995), and thus incorporate observations from several different segments of the northern Appalachians. See text for a detailed discussion.

Dame island-arc successions developed proximal to Laurentia (Johnson et al. 1991; Williams et al. 1992), and the absence of widespread calc-alkaline felsic plutonic rocks in the Laurentian margin is generally cited as evidence in favour of development of the island-arc system over a subduction zone that dipped east (e.g., Strong et al. 1974; van der Pluijm 1987; van Staal 1994; Cawood et al. 1995; Fig. 7.1).

Collision of the Notre Dame island-arc system and the Laurentian margin during the Taconian Orogeny resulted in extensive thin-skinned, west-vergent thrusting in western Newfoundland (Williams 1979; Cawood et al. 1995; Fig. 7.1). On the BVP, continental margin rocks of the Fleur de Lys Supergroup locally contain early (D_E) structures that verge west, and metamorphic mineral assemblages record subsidence to >25km depth prior to Early Silurian time (e.g., Jamieson 1990; Cawood et al. 1994, 1995), consistent with significant crustal thickening during Taconian orogenesis. East of the BVL however, the MBG, PHG, and PROC lack evidence for high-temperature regional metamorphism prior to late-Early Silurian time, and D_1 structures cut the Early Silurian Dunamagon Granite and Burlington Granodiorite (Cawood and Dunning 1993). These relationships suggest that the MBG, PHG, and PROC occupied a relatively high structural level of the Taconian thrust stack (Fig. 7.1), and must have remained at this level during high-grade metamorphism and regional deformation of the Fleur de Lys Supergroup in Late Ordovician to Early Silurian time (e.g., Jamieson 1990; Cawood et al. 1994, 1995).

The contrasting early tectonothermal histories of the MBG and Fleur de Lys Supergroup indicate that they were spatially separate during Taconian orogenesis. This

separation may reflect stratigraphic and/or geographic separation within the Laurentian passive margin, and/or tectonic transport in different levels of the Taconian thrust stack (Fig. 7.1). Regardless of mechanism, this observation contradicts the Baie Verte Flexure hypothesis of Hibbard (1982, 1983), which implies that the MBG and Fleur de Lys Supergroup are part of a continuous belt of Late Proterozoic to Middle Ordovician Humber Zone rocks that preserve a promontory in the rifted Laurentian margin.

It is generally accepted that during the Taconian orogeny significant portions of the Notre Dame Subzone were thrust over the Laurentian margin, and are thus allochthonous with respect to continental crust (e.g., Williams 1979; Waldron and Milne 1991; Stockmal et al. 1987; Cawood et al. 1995). This interpretation is supported by regional seismic data, which show that the western portions of the Dunnage Zone are underlain by a 'Grenvillian' lower crustal block at 10-20km depth (e.g., Keen et al. 1986; Quinlan et al. 1992). However, ϵ_{Nd} values obtained from the Early Silurian Dunamagon Granite (0), Burlington Granodiorite (+1 to +2), Cape Brule Porphyry (-3), and Cape St. John Group (-3) have been interpreted to record derivation from relatively juvenile material, with minimal contamination by older continental crust (Fryer et al. 1992). If this interpretation is correct, it seems unlikely that the eastern portion of the BVP was directly underlain by Laurentian continental crust (i.e., Humber Zone rocks) in the Early Silurian (Fryer et al. 1992). This may indicate that, at least on the BVP, the allochthonous portions of the Dunnage Zone were thrust westward over the Laurentian margin (i.e., Grenvillian lower crustal block) subsequent to Early Silurian time.

7.2.2 Early Silurian to Early Devonian (ca. 440-400 Ma)

The western and eastern portions of the BVP are characterized by markedly different tectonothermal histories in Early Silurian to late-Early Devonian time. West of the BVL, penetrative regional deformation (D_M) and peak amphibolite facies metamorphism in the Fleur de Lys Supergroup, and syn-tectonic intrusion of the Wild Cove Pond igneous suite, are constrained to the Early Silurian (e.g., Jamieson and Vernon 1987; Jamieson 1990; Cawood et al. 1994, 1995). Jamieson (1990) examined the syn- D_M metamorphic mineral assemblages in the Fleur de Lys Supergroup, and proposed a two stage history involving an early phase of high pressure - low temperature metamorphism (7-8.5 kbar, $\sim 450^\circ\text{C}$), and a later phase of lower pressure - higher temperature metamorphism (6.5 kbar, $550\text{-}600^\circ\text{C}$). These results were interpreted to reflect burial of the Laurentian margin to significant depth (ca. 25km) during the Taconian orogeny and subsequent thermal relaxation (Jamieson 1990) prior to the Early Silurian metamorphic peak (Cawood et al. 1994). In addition, the P-T data of Jamieson and O'Beirne-Ryan (1991), together with $^{40}\text{Ar}/^{39}\text{Ar}$ cooling ages from hornblende and muscovite (Dallmeyer 1977; Dallmeyer and Hibbard 1984), indicate that the Early Silurian metamorphic peak in the Fleur de Lys Supergroup was closely followed by nearly isothermal decompression, and Late Silurian to Early Devonian rapid cooling through the muscovite closure temperature (Fig. 6.7).

East of the BVL, the Early Silurian was marked by widespread felsic plutonism (e.g., Hibbard 1983; Coyle and Strong 1987; Cawood and Dunning 1993). Several field relationships indicate intrusion at shallow crustal depths: 1) granite exposed along the

eastern shore of Ming's Bight is not associated with significant contact metamorphism of the low-grade country rocks, and is locally chilled against 20-30cm diameter xenoliths; 2) the upper levels of the Cape Brule Porphyry grade into subaerial felsic volcanic rocks of the Cape St. John Group (DeGrace et al. 1976); and 3) the Silurian Cape St. John and MicMac Lake Groups were deposited unconformably over the Snooks Arm Group and Early Silurian Burlington Granodiorite, respectively (e.g., Hibbard 1983). These observations, coupled with the lack of evidence for significant deformation or metamorphism prior to the Late Silurian, further indicate that the eastern portion of the BVP occupied the highest levels of the Taconian thrust stack until Late Silurian time.

East of the BVL, penetrative regional deformation and high-grade metamorphism are, for the most part, limited to those areas north of the La Scie Highway (Neale and Kennedy 1967; Church 1969; Hibbard 1983). In these areas, the pre-tectonic Dunamagon Granite and Burlington Granodiorite are cut by Late Silurian to early-Early Devonian (405 ± 4 Ma) compressional (D_1) structures that verge southeast, and syn-tectonic metamorphic mineral assemblages are consistent with peak amphibolite facies metamorphism (ca. 500° C and 6 kbar) and subsidence to ≥ 20 km depth. The thermal peaks in the Ming's Bight and Pacquet Harbour areas are constrained to late-Early and early-Middle Devonian time, respectively, by $^{40}\text{Ar}/^{39}\text{Ar}$ cooling ages from hornblende (pre- to syn-388 Ma) and U-Pb dating of reset titanite (ca. 385 Ma; G.R. Dunning 1995, pers. comm.). These relationships indicate that, in marked contrast to those areas west of the BVL, the Silurian tectonothermal history of the northeastern portions of the BVP is characterized by pre-tectonic felsic plutonism at shallow crustal depths, compressional

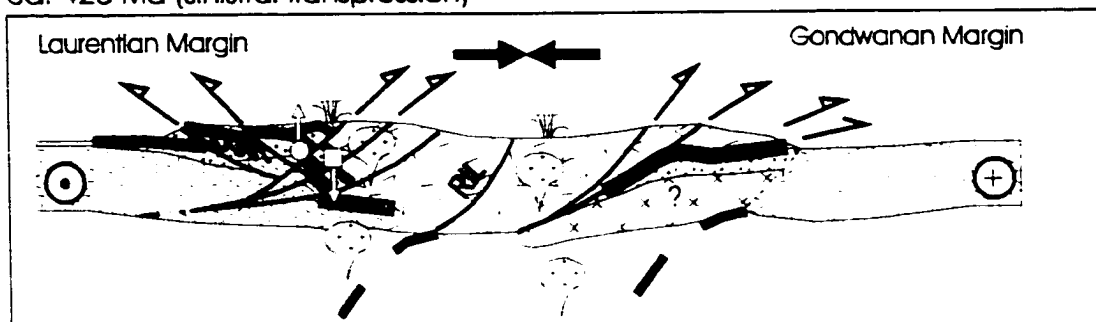
deformation associated with regional subsidence, and subsequent high-grade metamorphism in the Early to Middle Devonian.

In the following section, a regional kinematic model, based mainly on structural data collected in the present study, is developed which reconciles the contrasting tectonothermal histories of the eastern and western portions of the BVP by invoking regional Early to Late Silurian sinistral transpression.

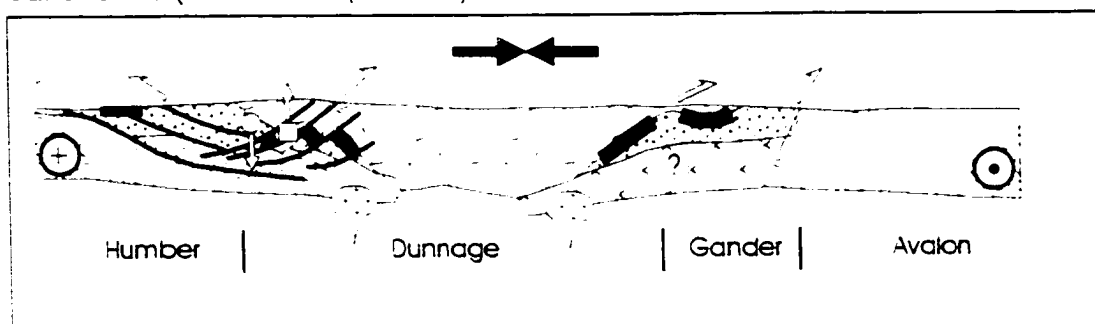
7.2.2.1 Sinistral transpression and deformation partitioning along the BVL

Recent structural studies in the Newfoundland and northern Appalachians indicate that the major tectonostratigraphic boundaries record a phase of Silurian sinistral transpression (e.g., Hanmer 1981; Currie and Piasecki 1989; Holdsworth and Strachan 1991; Soper et al. 1992; Hibbard and Hall 1993; O'Brien et al. 1993; de Roo and van Staal 1994; Hibbard 1994; Holdsworth 1994; Lin et al. 1994; Lin 1995; van Staal and de Roo 1995; Dubé et al. 1996; Lynch 1996; Fig. 7.2 and 7.3), which was locally partitioned between domains of (predominantly) sinistral strike-slip and reverse dip-slip shear (e.g., Currie and Piasecki 1989; Holdsworth and Strachan 1991; Strachan et al. 1995). On the BVP, several authors have presented evidence for significant components of reverse dip-slip (west over east) and sinistral strike-slip ductile shear along the BVL (e.g., Hibbard 1983; Piasecki 1988, 1995; Currie and Piasecki 1989; Goodwin and Williams 1990; Piasecki et al. 1990), although the relative and absolute timing of these movements is unclear. However, D_1 structures in the PROC, which is located within the BVL proper, record intense Early to Late Silurian reverse dip-slip ductile shear with a significant component of sinistral-reverse oblique-slip (e.g., Kirkwood and Dubé 1992; Ramezani

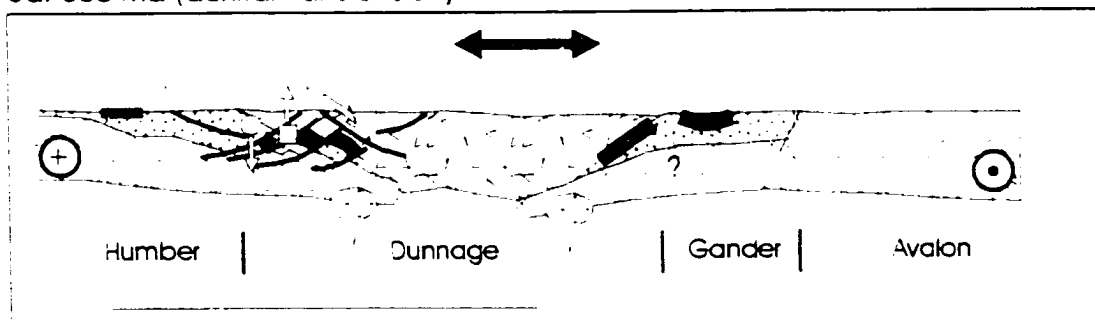
ca. 425 Ma (sinistral transpression)



ca. 390 Ma (dextral transpression)



ca. 380 Ma (dextral transtension)



Fleur de Lys Supergroup

Ming's Bight Group

Relative motion of the MBG
and Fleur de Lys Supergroup

-380 Ma Extensional fault

-390 Ma Transpressional fault

-425 Ma Transpressional shear

-470 Ma Thrust fault

Figure 7.2 Schematic diagrams illustrating the generalized tectonic evolution of the Newfoundland Appalachians in Early Silurian to Middle Devonian time. The sections are modified after Cawood and Williams (1988), Waldron and Milne (1991), Quinlan et al. (1992), and Cawood et al. (1995), and incorporate observations from several different segments of the northern Appalachians. Regional-scale movement perpendicular to the line of section is indicated by the symbols at the far ends of each diagram. The distribution of lower crustal blocks, as proposed by Keen et al. (1986), is based on Lithoprobe East reflection seismic data. RIL, Red Indian Line; ?, lower crustal block of uncertain affinity.

Figure 7.3 Correlation chart illustrating the general location, style, sense of movement, and inferred timing of regional deformation in the northern Appalachians as proposed by the indicated authors. The solid black, dark grey, and light grey boxes denote regional deformation which is kinematically compatible with sinistral transpression, dextral transpression, and dextral transtension, respectively. The vertically ruled box indicates extensional collapse as proposed by van Staal and de Roo (1995). The diagonally ruled box indicates the general time-frame provided by Elliot et al. (1991) for regional deformation in eastern Notre Dame Bay. In this area, Lafrance and Williams (1992) inferred a deformation history involving Early Silurian south-directed thrusting followed by Late Silurian folding and dextral transpression, consistent with several of the listed studies. The time scale of Harland et al. (1989) was utilized for post-Middle Devonian time, whereas that of Tucker and McKerrow (1995) was adopted for pre-Middle Devonian time.

1992; Dubé et al. 1993). In addition, Bélanger et al. (1996) presented evidence for Silurian, northwest-southeast directed, subhorizontal shortening along a segment of the BVL in the Flat Water Pond Group. This shortening direction, coupled with the predominance of fabrics within the BVL that dip moderately to steeply west-northwest (Hibbard 1983), is also compatible with sinistral-reverse oblique-slip shear in the Silurian.

On the basis of these data and regional constraints, a significant phase of Early to Late Silurian sinistral transpression along the BVL is inferred. The evidence for sinistral strike-slip and reverse dip-slip movements within the BVL, as well as the large domain of (predominantly) dip-slip reverse shear in the PROC, are consistent with local partitioning of the transpressional deformation. In the case of the PROC, this partitioning is inferred to result from the presence of the Burlington Granodiorite, which is a ~900 km² batholith of relatively isotropic and competent granodiorite in the footwall of the BVL (Fig. 1.2). This batholith is considered to represent a major rheological heterogeneity (stiff inclusion) which induced local perturbation (e.g., Lister and Williams 1983; Vilotte et al. 1984) of the transpressional strain regime within the BVL. If regional northwest-southeast-directed (present coordinates) shortening is assumed during sinistral transpression (e.g., Bélanger et al. 1996; Fig. 4.12), strain accommodation around the northwestern margin of the footwall heterogeneity should have resulted in a slight eastward deflection of structures, including the BVL, as observed in the area north of Baie Verte. In the sinistral shear regime, this deflection would produce a transpressional restraining bend (Crowell 1974) in the regional flow, which could have induced partitioning of the transpressional deformation around the north-dipping northern margin of the granodiorite into a domain

of (predominantly) reverse dip-slip shear at the present location of the PROC (Fig. 7.4).

Therefore, D_1 reverse-sinistral oblique-slip shear within the PROC is attributed to perturbation of the regional flow, strain accommodation around the granodiorite, deflection of the BVL, and development of a transpressional restraining bend.

This model is analogous to the partitioned-transpression model proposed by Cobbald et al. (1991) to explain the contemporaneous development of a fold-and-thrust belt and adjacent zone of wrench shear in the Variscan Sierras Australes of Argentina, as well as the self-indentation model proposed by Vauchez et al. (1994) to explain similar complex strain patterns developed at the termination of a stiff inclusion (craton) in the Ribeira-Aracuai belt of Brazil. It is also similar to the model proposed by Hibbard (1983) for D_M - D_L deformation east of the BVL: "...northward strike-slip movement of the (Dunnage Zone) along the north-trending segment of the Baie Verte Line...and southerly overthrusting of rocks from the north due to uplift of the Fleur de Lys Supergroup".

This model provides simple explanations for a number of the outstanding regional structural and geochronologic problems on the BVP. For example, it provides a relatively simple and well constrained regional kinematic explanation for the eastward deflection of the BVL at Baie Verte (i.e., the Baie Verte Flexure; Hibbard 1982, 1983; see Section 2.2.2.4) and, together with potential field data presented by Miller and Wiseman (1994), indicates that the BVL passes northeastward through the PROC, not eastward through Pacquet Harbour (*cf.* Hibbard 1982, 1983; Fig. 1.2 and 7.4). The model also provides a simple explanation for the rapid post-metamorphic cooling recorded in the Fleur de Lys Supergroup (i.e., rapid exhumation in the structural hangingwall of the BVL), and the

coeval subsidence of the northeastern portion of the BVL (i.e., loading associated with southeast-directed thrusting along the BVL; Fig. 7.2 and 7.4). In addition, large-scale imbrication of Humber and Dunnage successions within a regional transpressional shear system offers a straightforward explanation for the location of the MBG east of the main trace of the BVL (Fig. 7.4). Indeed, a similar imbrication of Humber and Dunnage Zone rocks is well exposed, albeit on a smaller scale, along the western shore of Baie Verte (Bursnall 1975; Bursnall and de Wit 1975; Williams 1977; Hibbard 1983). In this area, slices of Fleur de Lys Supergroup ranging from ~10cm to >1km thick are imbricated with greenschist, metagabbro, and serpentinite of the Advocate ophiolite complex. Williams (1977, 1979) interpreted these exposures as ophiolitic melange formed at the base of Taconian ophiolitic allochthons during west-directed thrusting; however, the structural attributes of the melange are equally consistent with small-scale imbrication during Silurian and/or Devonian transpressional shear. In the present study, the latter hypothesis is offered as an alternative explanation for the 'ophiolitic melange' along the BVL.

7.2.2.2 D₁-D₂ deformation in the Ming's Bight area

In the Ming's Bight area, the D₁-D₂ thrust/wrench shear system located to the south and southeast of the PROC (Fig. 4.12) is attributed to regional sinistral transpression. In particular, the component of sinistral transcurrent ductile shear along the BVL presumably resulted in relative convergence of the Burlington Granodiorite and the domain of partitioned reverse dip-slip ductile shear in the PROC (Fig. 7.4). As this shearing progressed, the leading, north-dipping tip of the granodiorite is inferred to have impinged on the domain of dip-slip shear, resulting in perturbation of the flow, and

partitioning of the non-coaxial deformation around the relatively resistant tip of the granodiorite (Fig. 7.4). Ideally, this partitioning would result in discrete domains with sinistral-reverse oblique-slip, reverse dip-slip, and dextral-reverse oblique-slip movement along the western, northern, and eastern margins of the granodiorite, respectively, analogous to (for example) the indenters described by Tapponnier et al. (1982) and Vauchez et al. (1994). Indeed, field examination of the northern and eastern margins of the granodiorite revealed zones of non-coaxial strain which contain evidence for reverse dip-slip and dextral-reverse oblique-slip, respectively (Fig. 4.12). As sinistral transpression progressed, the differential northward motion of the granodiorite relative to the domain of progressive, partitioned, reverse dip-slip shear in the PROC resulted in a 'secondary' partitioning of the deformation into zones of wrench- and thrust-shear, and produced the lateral ramp-frontal ramp-lateral ramp geometry from west to east, between the granodiorite and Dunamagon Granite (Fig. 7.4).

Within this framework, the PPSZ in the Pacquet Harbour area is considered to have had a relatively minor role as a discrete ductile shear zone that juxtaposed the MBG with the Dunamagon Granite and PHG during regional deformation related to the sinistral transpression (Figs. 4.12 and 7.4). The presence of strongly deformed dykes of Dunamagon Granite within the PPSZ precludes the possibility that it developed during Taconian deformation.

This model is completely compatible with the character, distribution, sense of movement, and timing of D_1 - D_2 structures in the Ming's Bight area. Moreover, the prolate shape of the finite D_1 - D_2 strain ellipsoid in rocks south of Ming's Bight (e.g., Gale 1971;

Tuach 1976) can be seen to result from constriction between the two symmetrically opposed lateral ramps. Significantly, all four volcanogenic massive sulphide deposits in the Rambler camp are stretched parallel to the L_1 lineation (Tuach and Kennedy 1978), and are located directly in the 'nose' of the proposed frontal ramp (Fig. 4.12). These relationships suggest remobilization of the sulphides into the nose of the frontal ramp during high-temperature constrictional deformation in the PHG, analogous to deformation-related remobilization of volcanogenic massive sulphides into structural basins produced through interference folding (e.g., van Staal and Williams 1984).

7.2.2.3 Extensional collapse in the northern Appalachians

Extensional collapse of orogens, as defined by Dewey (1988), is a somewhat nebulous term that refers to rapid regional exhumation of the middle-crustal levels of an orogen in response to extensional body forces resulting from: 1) subduction zone rollback; and/or 2) isostatically compensated uplift related to excessive elevation contrasts or 'catastrophic' convective or advective thinning of the thermal boundary conduction layer (i.e., lithospheric mantle) beneath thickened continental crust. According to Dewey (1988), extensional collapse of an orogen may be manifest as nonmarine extensional basins, rapid marine transgressions, metamorphic core complexes, rapid isobaric heating paths, prograde high-temperature metamorphism, post-tectonic granite intrusion, the preservation of high-T / low-P metamorphic rocks, isothermal pressure drops, back-arc spreading, and/or underplating of the crust by large volumes of mafic magma.

In the Newfoundland Appalachians, Silurian transpression was typically associated with regional amphibolite facies metamorphism (e.g., Dunning et al. 1990; O'Brien et al.

1991, 1993; Holdsworth 1994; Lin et al. 1994; Cawood et al. 1994, 1995; Burgess et al. 1995; Dubé and Lauzière 1996; Dubé et al. 1996). In western Newfoundland, recent thermobarometric and thermochronologic studies indicate that the amphibolite facies metamorphic peak was locally followed by isothermal decompression (Jamieson and O'Beirne-Ryan 1991) and regional rapid cooling through the muscovite closure temperature in the Late Silurian (e.g., Dallmeyer 1977; Dallmeyer and Hibbard 1984; Cawood et al. 1994; Burgess et al. 1995; Dubé et al. 1996). In light of this data, Cawood et al. (1995) presented structural evidence for subvertical shortening, localized extensional faulting, and late-stage extensional remobilization of the Taconian allochthons in western Newfoundland, and proposed that the Laurentian margin experienced extensional collapse in the latter stages of Silurian orogenesis. Cawood et al. (1995) further suggested, mainly on the basis of evidence for widespread magmatic activity across the orogen at this time, that the extensional collapse resulted from isostatically compensated uplift related to delamination of the thickened orogenic lithosphere.

In the New Brunswick Appalachians, de Roo and van Staal (1994) and van Staal and de Roo (1995) also proposed Late Silurian to Early Devonian extensional collapse. This hypothesis was based on evidence for regional low-pressure metamorphism, bimodal magmatism, and marine sedimentation, as well as the presence of recumbent, open, F_3 folds which were attributed to regional subvertical flattening (de Roo and van Staal 1994). The mechanisms proposed for extensional collapse involved subduction zone rollback, coupled with isostatically compensated uplift of the orogen due to detachment of a slab of subducted oceanic lithosphere from the continental lithosphere or delamination of the

lithospheric mantle from the continental crust.

In both of the examples presented above, Late Silurian extensional collapse of the orogen is attributed to orogen-scale mechanisms, and should therefore be manifest over large areas of the northern Appalachians. However, extensional structures of Silurian age are apparently quite rare in the northern Appalachians, since their presence has only been inferred locally (e.g., Cawood 1989, 1993; Cawood et al. 1995). Several authors have recently presented evidence for extensional structures in other segments of the Appalachian-Caledonian orogenic system (e.g., Snoke and Frost 1990; Fossen and Rykkelid 1992; Chauvet and Séranne 1994; Lynch and Tremblay 1994; Lynch 1996; Lynch and Giles 1996); however, in all cases this deformation is too young to explain rapid Late Silurian-Early Devonian cooling. In addition, although the Fleur de Lys Supergroup preserves evidence for an Early Silurian metamorphic peak (Cawood and Dunning 1993; Cawood et al. 1994), nearly isothermal decompression (Jamieson and O'Beirne-Ryan 1991), and Late Silurian rapid cooling through the muscovite $^{40}\text{Ar}/^{39}\text{Ar}$ closure temperature (Dallmeyer and Hibbard 1984), evidence for widespread extensional deformation is lacking. In particular, the open recumbent folds which Cawood et al. (1995), de Roo and van Staal (1994), and van Staal and de Roo (1995) attribute to regional subvertical shortening during extensional collapse have not been documented in the Fleur de Lys Supergroup (e.g., de Wit 1974; Bursnall and de Wit 1975; de Wit 1980; Hibbard 1983).

Based on these relationships, it seems unlikely that exhumation, decompression, and rapid cooling of high-grade metamorphic rocks in western Newfoundland result from

extensional collapse on the scale implied by van Staal and de Roo (1995) and Cawood et al. (1995). However, as demonstrated in the present study, rapid exhumation of high-grade metamorphic rocks can reasonably be ascribed to uplift in the hangingwall of the well documented east- or west-verging compressional structures related to Silurian orogenesis (e.g., Cawood et al. 1995; Fig. 7.2 and 7.4). Presumably, this compressional exhumation would have been augmented by high erosion rates and/or coeval tectonic unroofing, and could therefore fully account for the P-T-t paths of high-grade metamorphic rocks, as well as stratigraphic relationships, in western Newfoundland without appealing to orogen-scale extensional collapse.

7.2.3 Early Devonian to Early Carboniferous (ca. 400-360 Ma)

The Early Devonian to Early Carboniferous tectonic evolution of the BVP is well constrained by $^{40}\text{Ar}/^{39}\text{Ar}$ thermochronology and the T-t histories presented in Chapter 6. In Late Silurian to Early Devonian time, high-grade metamorphic rocks west of the BVL cooled rapidly through the $^{40}\text{Ar}/^{39}\text{Ar}$ muscovite closure temperature, possibly reflecting the latest stages of exhumation in the hangingwall of the BVL. This inference is supported by the 405 ± 4 Ma $^{40}\text{Ar}/^{39}\text{Ar}$ age obtained from hornblende sample 92-205 in Ming's Bight, which may indicate that the compressional deformation had ceased by early-Early Devonian time. In the Ming's Bight area, hornblende cooling ages (386 and 388 ± 2 Ma) also indicate that the amphibolite facies metamorphic peak, and thus maximum subsidence beneath the southeast-verging transpressional thrust stack, had been attained in Early Devonian time, and regional cooling had commenced by ca. 390 Ma (Fig. 6.7). In the Pacquet Harbour area, U-Pb titanite (Cawood et al. 1995) and $^{40}\text{Ar}/^{39}\text{Ar}$ hornblende (377

and 382 ± 2 Ma) cooling ages indicate a somewhat younger, late-Early Devonian, metamorphic peak, with initial cooling in the early-Middle Devonian (Fig. 6.7).

As noted in Chapter 6, the early stages of post-peak cooling in both the Ming's Bight and Pacquet Harbour areas coincided with the earliest increments of extensional deformation, and the T-t histories in these areas are markedly similar to those associated with Cordilleran detachment faults and metamorphic core complexes. In the following section, a regional kinematic model, based mainly on structural and thermochronologic data collected in the present study, is proposed that invokes regional Early Devonian to Early Carboniferous dextral transcurrent shear along the BVL, which facilitated local-scale late-orogenic extension, and metamorphic core complex development.

7.2.3.1 Early Devonian to Carboniferous dextral shear

In the northern Appalachians, regional structural and stratigraphic evidence indicates a significant phase of dextral transcurrent shear in Early Devonian to Carboniferous time, apparently resulting from regional-scale dextral-oblique convergence of Laurentia and Gondwana (e.g., Bradley 1982; Ferrill and Thomas 1988; Hyde et al. 1988; Swanson 1988; Lafrance and Williams 1992; Malo et al. 1992; Kirkwood and Malo 1993; O'Brien et al. 1993; de Roo and van Staal 1994; Hibbard 1994; Holdsworth 1994; Langdon and Hall 1994; Malo and Kirkwood 1995, van Staal and de Roo 1995; Fig. 7.2 and 7.3). Detailed structural analyses of several major Devonian shear zones indicate a transpressional style of deformation in Early to Middle Devonian time (e.g., Malo and Kirkwood 1995; Fig. 7.3), whereas thick successions of flat-lying Late Devonian to Early Carboniferous coarse clastic rocks in fault-controlled extensional basins point toward a

largely transtensional regional shear regime by Late Devonian time (e.g., Bradley 1982; Hyde et al. 1988; Fig. 7.2 and 7.3). In the present study, these relationships are taken to indicate that a regional-scale transition from dextral transpression to dextral transtension occurred in Middle Devonian time.

On the BVP, several authors have presented evidence for dextral transcurrent shear along the BVL (e.g., Piasecki 1988, 1995; Goodwin and Williams 1990, 1996; Piasecki et al. 1990). In addition, Goodwin and Williams (1996) examined the Marble Cove Slide in Baie Verte, and presented evidence for significant dextral transpressional shear of inferred Devonian age. In the present study, the early increments of dextral-reverse oblique-slip shear recorded in the northern Ming's Tickle and Grand Toss Cove shear zones in Ming's Bight are tentatively correlated with the dextral transpression in the Marble Cove Slide. Thus, the 388 ± 4 Ma U-Pb titanite age from the northern Ming's Tickle shear zone is interpreted to provide an early-Middle Devonian younger age limit for dextral transpression (Fig. 7.5). Furthermore, overprinting relationships in D_4 - D_5 shear zones in Ming's Bight record a transition from transpressional to transtensional dextral shear which probably occurred in the early-Middle Devonian (see Chapter 6).

This interpretation is supported by stratigraphic relationships on the BVP. For example, Haworth et al. (1976) mapped sea floor outcrops of flat lying Late Devonian to Early Carboniferous Anguille Group rocks (e.g., Langdon and Hall 1994; Crouse Harbour and Cape Rouge Formations; Hamblin et al. 1995) in apparent unconformable contact with MBG schist less than 5km northeast of Pacquet Harbour. In addition, flat-lying Carboniferous rocks unconformably overlie the MicMac Lake Group and King's Point

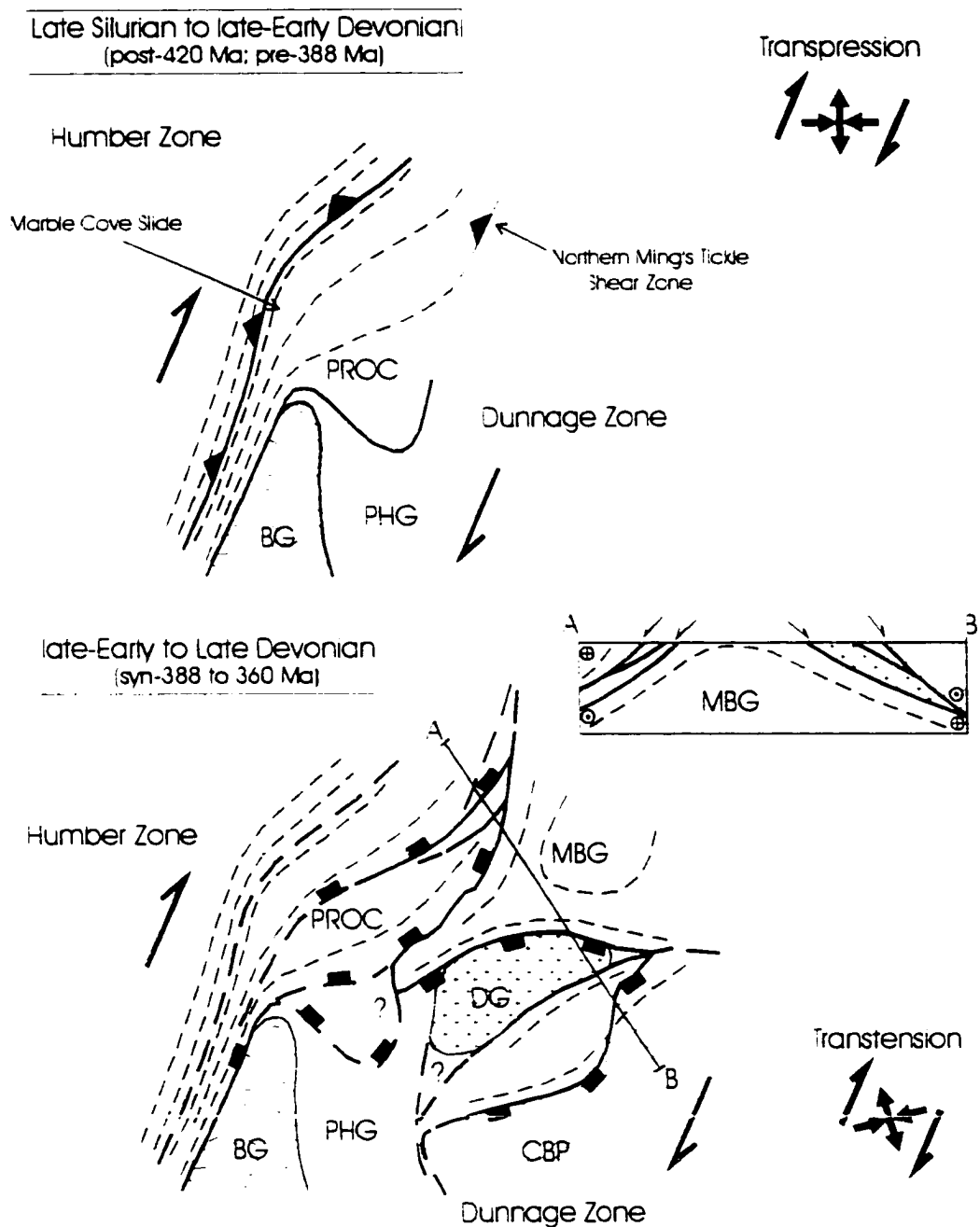


Figure 7.5 Schematic diagram illustrating the structural evolution of the north-central portion of the BVP and the MBG metamorphic core complex in Early to Late Devonian time. Light grey pattern, Humber Zone rocks; no pattern, Dunnage Zone rocks; CBP, Cape Brule Porphyry; BG, Burlington Granodiorite; DG, Dunamagon Granite. The inset diagrams illustrate regional kinematic axes inferred for each phase of deformation.

Complex near the southern extremity of the BVP (Hibbard 1983). Taken together, these successions suggest basin development, probably in a transtensional regime, by Late Devonian time (e.g., Hyde et al. 1988), and indicate that the present erosional surface of the BVP must have been largely exhumed by Early Carboniferous time. This hypothesis is supported by $^{40}\text{Ar}/^{39}\text{Ar}$ cooling ages from biotite, which indicate regional cooling below 300°C by Early Carboniferous time (Dallmeyer 1977; Dallmeyer and Hibbard 1984).

In the immediate thesis area, the early-Middle Devonian regional transition from dextral transpression to transtension, coupled with dextral transcurrent shear along the BVL, are interpreted to have reactivated the Silurian transpressional restraining bend in the PROC as a releasing bend, resulting in a localized extensional strain regime in the immediate footwall of the releasing bend (Fig. 7.5). Indeed, the kinematic analysis of extensional shear zones and faults in Ming's Bight indicates significant north-south directed subhorizontal extension, which is nearly coaxial with the extension direction inferred from coeval ductile extensional structures in the Pacquet Harbour area (Fig. 4.13). These relationships are interpreted to indicate that extensional strain within the inferred releasing bend was accommodated along the symmetrically opposed zones of extensional shear that bound the MBG (Fig. 4.13). Within these zones, extensional deformation is demonstrably coeval with exhumation of the MBG, and they are herein interpreted to define the margins of a metamorphic core complex (e.g., Davis and Coney 1979; Lister and Davis 1989; Fig. 7.5). This hypothesis is developed in detail below.

7.2.3.2 Late orogenic extension and metamorphic core complexes

In many orogenic belts, regionally pervasive structures related to early-orogenic

compression are reactivated and/or transposed by structures associated with late-orogenic extension (Dewey 1988). Commonly, this process involves the exhumation of high-grade metamorphic rocks along low-angle shear zones and detachment faults, resulting in metamorphic core complexes (Davis and Coney 1979; Wernicke 1985; Lister and Davis 1989; Malavieille 1993).

In general, metamorphic core complexes comprise a dome or arch of high-grade metamorphic rocks (lower plate) which is separated from overlying, low-grade cover rocks (upper plate) by a low-angle detachment fault (e.g., Davis and Coney 1979; Reynolds and Lister 1987; Parrish et al. 1988; Lister and Davis 1989; Wernicke 1992; Malavieille 1993). The upper plate contains a series of discrete, en-echelon to conjugate, brittle-ductile or brittle faults that record normal movement. In contrast, the structurally highest regions of the lower plate contain evidence for penetrative, ductile deformation in a noncoaxial shear zone under high P-T conditions. The shear zone is characterized by mylonitic fabrics, prominent stretching lineations, and isoclinal, recumbent folds, and commonly contains evidence for a spatial and temporal gradation from ductile to brittle deformation (e.g., Davis and Coney 1979; Reynolds and Lister 1987; Lister and Davis 1989). This gradation is thought to reflect exhumation of deforming lower plate rocks in the footwall of an extensional shear system that is progressively evolving from ductile shear zone to brittle detachment fault with decreasing depth. Core complexes bounded by a single extensional shear system are termed asymmetric, whereas those bounded by two oppositely-verging shear systems are termed symmetric (Malavieille 1993). The extension directions inferred from stretching lineations and fault-slip data in the lower and upper

plates, respectively, of the same core complex are commonly coaxial, and indicate contemporaneous ductile and brittle extensional deformation (Wernicke 1985; Malavieille 1987, 1993). Low-angle detachment faults generally coincide with sharp thermal and/or strain gradients, and the lower plate is characterized by relatively young cooling ages and high cooling rates, consistent with rapid, late-stage exhumation. The lower plate is also commonly intruded by syn- to late-mylonitic granite and granitic pegmatites. Collectively, these features are thought to record exhumation of the middle and lower continental crust from beneath the fracturing, extended upper crust during continental extension (Lister and Davis 1989).

7.2.3.3 The MBG symmetrical metamorphic core complex

Based on the characteristics outlined above, a strong similarity between the MBG and metamorphic core complexes is apparent, and in the present study the MBG is interpreted to be analogous to a symmetrical metamorphic core complex (e.g., Malavieille 1993; Hetzel et al. 1995; Fig. 4.13 and 7.5).

In particular, the MBG comprises a generally dome-shaped outcrop area of intensely deformed, amphibolite facies metamorphic rocks which are separated from relatively less deformed and metamorphosed rocks along two symmetrically opposed, contemporaneous extensional deformation zones, which coincide with gradients in extensional strain and metamorphic grade (Fig. 4.13 and 7.5). To the northwest, the MBG is separated from greenschist facies rocks of the PROC by an array of greenschist facies, dextral-normal oblique-slip (D_4 - D_5) shear zones that dip northwest and southwest. These shear zones are kinematically compatible with north-south-directed subhorizontal

extension, although they locally record an early increment of dextral transpressional shear (Maps 5, 7, 8, and 9; Cross-sections 3, 5a, 5b, 6a, and 6b; Fig. 4.13). To the southeast, the MBG is separated from greenschist facies rocks of the Cape Brule Porphyry (and Cape St. John Group further south) by a thick zone of amphibolite to greenschist facies (i.e., D_2 to D_3), dextral-normal oblique-slip, non-coaxial shear. This zone dips moderately southeast, and is particularly well developed within structurally overlying PHG rocks (Maps 1, 2, and 3; Cross sections 1 and 2; Fig. 4.13). The footwall of this extensional shear zone is intruded by subvertical pegmatite dykes, and contains a prominent stretching lineation associated with reclined folds with axes parallel to the extension direction, indicating northwest-southeast directed subhorizontal extension. Textures and mineral assemblages within the shear zone indicate that shearing continued to greenschist facies metamorphic conditions at the northern contact of the Cape Brule Porphyry, possibly reflecting the latest increments of extensional deformation along the southeast boundary of the MBG core complex.

The structural zones bounding the MBG were active from latest-Early to Late Devonian time (ca. 405 to 360 Ma), and are associated with rapid cooling through the hornblende, muscovite, and biotite closure temperatures in early-Middle Devonian to Early Carboniferous time (Dallmeyer and Hibbard 1984; see Chapter 6). $^{40}\text{Ar}/^{39}\text{Ar}$ thermochronology indicates that cooling rates increase, and hornblende closure ages decrease, toward the extensional shear zone in Pacquet Harbour (Fig. 6.7). As discussed in Chapter 6, this pattern is nearly identical to that observed in the footwalls of extensional detachments bounding Cordilleran metamorphic core complexes, and is generally

attributed to progressive asymmetric exhumation of high-grade metamorphic rocks from beneath a detachment (e.g., Lee 1995).

There is no evidence for a wide zone of brecciation and cataclastic deformation (i.e., a detachment fault) in the upper portions of the southeastern ductile shear zone. This may indicate that deformation at the present level of exposure did not continue below the brittle-ductile transition and, therefore, if a true detachment fault formed it must have been located structurally above the current level of exposure. Alternatively, low-temperature extensional deformation may have been preferentially accommodated by brittle-ductile faults along the northwestern margin of the MBG and, in particular, the zones of cataclasite in the GTCSZ (Section 4.2.4; Map 4). This inference might be supported by the distribution of $^{40}\text{Ar}/^{39}\text{Ar}$ cooling ages and rates in the MBG, as similar distributions in the Cordillera have been attributed to preferential accommodation of the late increments of extension by systems of higher-level, normal faults (e.g., Lee and Sutter 1991; Lee 1995).

Hetzel et al. (1995), in their study of symmetrical bivergent extension in the Menderes Massif of southwestern Turkey, noted that the symmetrical domains of non-coaxial, extensional shear that verge in opposite directions along the margins of a metamorphic core complex may be separated by a domain of subhorizontal fabric which contains evidence for coaxial vertical shortening. In the MBG, extensional structures that dip southeast predominate from Pacquet Harbour northwest to Handy Harbour (Map 1), whereas extensional structures that dip northwest predominate from Ming's Bight east to Cape Hat (Fig. 4.13), where several discrete, northwest-dipping, brittle-ductile shear zones with dextral kinematic indicators are exposed. Thus, if a contemporaneous domain

of coaxial vertical shortening exists, it must occur in the area between Cape Hat and Handy Harbour (i.e., in the Cape Corbin area).

Coastal exposures at Cape Corbin contain granitic pegmatite dykes (ca. 370 Ma; see Chapter 5) which exhibit chocolate-tablet boudinage in the plane of a subhorizontal fabric (correlated with Pacquet Harbour S_2 ; Fig. 3.8b). In addition, inland exposures of the MBG southwest from Cape Corbin contain a pervasive subhorizontal foliation (Fig. 4.13) that is axial planar to tight to isoclinal, recumbent folds, both of which are cut by subvertical pegmatite dykes that strike southwest. In one location, the primary layering in the MBG exhibits chocolate-tablet boudinage in a subhorizontal plane. Collectively, these structures are consistent with coaxial subvertical shortening, and indicate that Cape Corbin and the inland areas to the southwest are probably near the 'axis' of symmetrical extension in the MBG (e.g., Hetzel et al. 1995; Fig. 4.13).

The evidence for coaxial vertical shortening in the Cape Corbin area strongly supports the model for symmetrical, bivergent, extensional exhumation of the MBG in Middle to Late Devonian time (Fig. 7.5). This model is particularly compelling, since it reconciles the $^{40}\text{Ar}/^{39}\text{Ar}$ thermochronology data with regional structural and stratigraphic relationships. Several authors have presented similar models for metamorphic core complex development in localized extensional regimes associated with transcurrent faults (e.g., Snoke and Frost 1990; Wernicke 1992; Mancktelow and Pavlis 1994), although the MBG appears to be the first symmetrical metamorphic core complex documented in this type of structural setting.

7.2.3.4 Regional implications

If the above model is correct, the MBG is the first metamorphic core complex documented in the northern Appalachians. Although the exhumation of this particular metamorphic core complex appears to result from a unique structural setting on the BVP (i.e., the releasing bend), similar structural settings do exist elsewhere in the Newfoundland Appalachians. For example, in a regional regime of dextral transtension, the east-west trending portion of the Hermitage Flexure (Fig. 2.1) is favourably oriented for reactivation by Devonian extensional faults, depending on the local direction of dip. In addition, a brief examination of the western margin of the Mount Cormack Subzone by the author revealed a wide zone of penetrative extensional deformation that dips moderately west and separates high-grade rocks of the Mount Cormack Subzone from structurally overlying low-grade ophiolitic rocks of the Exploits Subzone (Fig. 1.1). Although further study is required, these observations indicate that the potential exists for additional metamorphic core complexes in the Newfoundland Appalachians.

Several authors have noted that major shear zones in the northern Appalachians record evidence for a regional-scale switch from sinistral transcurrent shear in the Silurian to dextral transcurrent shear in the Early Devonian (e.g., Soper et al. 1992; O'Brien et al. 1993; Hibbard 1994; Holdsworth 1994; de Roo and van Staal 1994; Dubé and Lauzière 1996; Dubé et al. 1996). This switch is widely inferred to reflect an orogen-scale change in the relative motion of the Laurentian and Gondwanan plates (Soper et al. 1992), resulting in a counterclockwise rotation of the regional shortening axes from north-south in the Silurian to northwest-southeast in the Early Devonian (present coordinates; e.g., Hibbard

1994; Dubé and Lauzière 1996; Dubé et al. 1996). In the present study, the regional shortening axes inferred for Siluro-Devonian deformation along the BVL apparently rotated counterclockwise from northwest-southeast in the late-Early to Late Silurian, to east-west in the Late Silurian to late-Early Devonian, to southwest-northeast in the late-Early to Late Devonian (Figs. 4.12, 4.13, 7.4, and 7.5). This change in orientation of the shortening axes fully accounts for the sequence of sinistral transpression - dextral transpression - dextral transtension recorded by structures in the BVL, and strongly suggests a progressive rotation of the kinematic axes, and thus a progressive transition between distinct phases of regional deformation on the BVP.

On the scale of the northern Appalachians, the data presented in Figure 7.5 indicate a significant overlap in the timing of kinematically distinct phases of regional deformation, and suggest that sinistral and dextral transpression, which have traditionally been attributed to separate 'Salinian' and 'Acadian' orogenies, respectively, were in fact contemporaneous on a regional scale. This interpretation, which is fully consistent with the evidence for a progressive transition between sinistral and dextral transpression on the BVP, calls into question the usefulness of the 'Salinian' and 'Acadian' terminology, since these orogenies appear to be progressive increments of a single orogenic event associated with Middle Paleozoic convergence of Laurentia and Gondwana and closure of the Iapetus ocean basin.

7.3 IMPLICATIONS FOR GOLD AND VMS EXPLORATION

7.3.1 Mesothermal gold mineralization

In western Newfoundland, gold is mainly hosted in mesothermal vein-type deposits

(Dubé 1990; Dubé et al. 1992) that are spatially associated with crustal-scale, brittle-ductile, shear zones that contain evidence for Silurian transpression (e.g., Dubé et al. 1992, 1993; Kirkwood and Dubé 1992; Bélanger et al. 1996; Dubé and Lauzière 1996). Mesothermal vein-type deposits are divisible into two main subtypes depending on the location of gold mineralization within the system (Dubé 1990). 'Quartz-vein type' deposits comprise gold-bearing fault-fill, stockwork breccia, or extensional quartz veins hosted in discrete, brittle-ductile, high strain zones that represent subsidiary structures related to major fault zones (Dubé et al. 1992). In contrast, 'altered wallrock type' deposits comprise disseminated gold mineralization in pervasively and intensely altered host rocks adjacent to quartz-carbonate vein systems that may, or may not, be related to deformation in structures subsidiary to major fault zones (Dubé et al. 1992).

On the BVP, several significant mesothermal vein-type gold deposits and showings occur along the trace of the BVL (e.g., Tuach et al. 1988; Dubé 1990; Dubé et al. 1992, 1993; Kirkwood and Dubé 1992; Patey and Wilton 1993; Bélanger et al. 1996; Fig. 1.2), making it one of the most significant and prospective gold districts in the Canadian Appalachians (e.g., Tuach et al. 1988; Dubé et al. 1992). Quartz-vein type deposits on the BVP include the Dorset, Deer Cove, and Pine Cove, as well as the Hammer Down located immediately south of the BVP (Dubé et al. 1992, Gaboury et al. 1996). The Stog'er Tight deposit is the only example of an altered wallrock type deposit on the BVP (Dubé et al. 1992; Kirkwood and Dubé 1992).

Recent structural studies of gold deposits on the BVP have established that they are spatially and genetically associated with D_1 compressional shear zones that represent

subsidiary structures to major fault zones (e.g., the BVL and Scrape Fault; Kirkwood and Dubé 1992; Dubé et al. 1993; Bélanger et al. 1996). In the present study, these structures are correlated with the phase of regional Silurian sinistral transpression. This correlation, coupled with mapping conducted in the present study, indicates that the prospective subsidiary structures are far more widespread in the Ming's Bight area than has previously been recognized (Fig. 4.12 and 7.4). Particularly prospective areas for mesothermal vein-type gold mineralization include the wide zone of transpressional shear located southeast of Ming's Bight, as well as the shear zones bounding the felsic volcanic succession in the north-central portion of the PHG (Fig. 4.12). Assessment reports indicate that very little detailed gold exploration has been conducted in these areas.

7.3.2 Volcanogenic massive sulphide mineralization

The PHG has been the focus of intensive exploration efforts since mining of the Rambler massive sulphide deposits began in the early 1960's (Tuach and Kennedy 1978). In the PHG, the majority of VMS exploration has been focused on the immediate area of the Rambler camp, and the roughly circular-shaped succession of felsic volcanic rocks that hosts the main VMS deposits. In the present study however, mapping conducted ~3km northeast of this area reveals an extensive, and previously unrecognized, succession of rocks (Fig. 2.2) comprising felsic volcanic breccia and tuff, and chloritic schist, that are nearly identical in appearance to those associated with the Rambler VMS deposits. Along the northwestern boundary, the felsic volcanic succession contains structural evidence for sinistral transpression, which is compatible with the sense of offset implied if one assumes that both felsic volcanic successions in the PHG were once contiguous. If correct, these

observations have obvious and significant implications for VMS exploration in the PHG.

It is well established that massive sulphides can experience significant remobilization during regional deformation under medium- to high-temperature metamorphic conditions (e.g., van Staal and Williams 1984). As noted in Section 7.2.2, the Rambler VMS deposits are strongly lineated parallel to the prolate L_1 - L_2 stretching lineation in the PHG, and are situated near the inferred location of the lateral tip of the thrust/wrench-shear system. Thus, although the structural attributes of the Rambler VMS deposits were not examined in detail in the present study, these observations may indicate that the Rambler sulphide deposits were remobilized into the lateral tip of the frontal ramp during intense D_1 - D_2 deformation. At the lateral tip, mylonitic fabrics produced during D_1 south-directed thrusting are folded by a series of open to tight, upright to reclined F_2 folds that plunge moderately north, and have a consistent Z-sense of asymmetry. If, for example, the hinges of these folds experienced relatively lower finite D_1 - D_2 strains as compared to the limbs, sulphides remobilized during high-temperature deformation may have preferentially migrated into the fold hinges. Alternatively, pre-existing massive sulphide bodies could have been structurally thickened in the hinges of folds of this type. These hypothesis could explain both the linear shape and structural setting of the sulphide deposits and, since the Ming Mine (Fig. 2.2) has recently been re-opened by Ming Minerals Inc., these hypotheses are submitted as possible explanations for the location and structural setting of the Rambler massive sulphide deposits that can be tested by future detailed structural analyses.

Appendix A

Table A1. $^{40}\text{Ar}/^{39}\text{Ar}$ analytical data for muscovite and hornblende

Temp. (°C)	$^{39}\text{Ar}/^{40}\text{Ar}$	$^{37}\text{Ar}/^{39}\text{Ar}$	$^{36}\text{Ar}/^{40}\text{Ar}$	^{39}Ar , % of total	Apparent age (Ma)
92-102;	J = .02055				
650	0.008311	0.01	0.000236	3.1	367.9 +/- 3.4
750	0.008834	0.00	0.000058	7.8	366 +/- 1.9
775	0.008776	0.00	0.000050	5.3	369 +/- 2.3
800	0.008795	0.00	0.000061	6.4	367.1 +/- 2
825	0.008805	0.00	0.000056	9.2	367.2 +/- 1.8
850	0.008812	0.00	0.000042	10.4	368.3 +/- 1.8
875	0.008841	0.00	0.000048	9.5	366.7 +/- 1.9
900	0.008790	0.00	0.000054	8.5	368 +/- 1.9
950	0.008794	0.00	0.000060	11.3	367.3 +/- 1.8
1000	0.008751	0.00	0.000058	12.1	369.1 +/- 1.8
1050	0.008740	0.00	0.000056	12.1	369.8 +/- 1.8
1100	0.008215	0.01	0.000219	3.1	373.6 +/- 3.1
1250	0.000588	0.11	0.000706	0.5	2368.5 +/- 115.6
1350	0.000198	0.58	0.002745	0.0	1936.4 +/- 1264.2
				Total gas age	387.4 Ma
92-75;	J = .02223				
650	0.012659	1.14	0.000626	1.1	239.5 +/- 7.1
700	0.008652	0.59	0.000286	1.1	378.4 +/- 11.1
750	0.008830	0.21	0.000160	1.7	385 +/- 4.4
800	0.009359	0.08	0.000131	4.2	368.3 +/- 2.5
850	0.009742	0.01	0.000057	21.1	362.5 +/- 1.7
900	0.009911	0.00	0.000018	32.5	360.7 +/- 1.6
925	0.009837	0.04	0.000032	9.2	361.8 +/- 1.8
950	0.009676	0.09	0.000058	4.4	364.6 +/- 2.6
975	0.009544	0.14	0.000072	3.1	367.8 +/- 3.1
1000	0.009623	0.13	0.000082	3.2	364.1 +/- 2.7
1050	0.009666	0.06	0.000042	7.0	366.6 +/- 2
1100	0.009764	0.04	0.000041	7.8	363.3 +/- 1.9
1150	0.009797	0.20	0.000145	2.5	351.9 +/- 3.3
1200	0.006233	1.18	0.001555	0.4	315.6 +/- 29.1
1300	0.006759	4.56	0.002638	0.1	125.2 +/- 80.4
				Total gas age	361.2 Ma

Temp. (°C)	³⁹ Ar/ ⁴⁰ Ar	³⁷ Ar/ ³⁹ Ar	³⁶ Ar/ ⁴⁰ Ar	³⁹ Ar, % of total	Apparent age (Ma)
92-85C;	J = .02227				
650	0.008669	0.44	0.000554	1.1	348.5 +/- 9.5
750	0.009166	0.11	0.000160	4.1	372.9 +/- 2.3
800	0.009737	0.02	0.000048	18.1	364.2 +/- .9
825	0.009797	0.02	0.000030	16.5	363.9 +/- .9
850	0.009817	0.04	0.000023	11.8	363.9 +/- 1
875	0.009722	0.06	0.000032	7.2	366.2 +/- 1.3
900	0.009631	0.10	0.000044	4.9	368.2 +/- 2
925	0.009592	0.19	0.000074	3.7	366.5 +/- 2.6
950	0.009713	0.14	0.000077	4.2	362.1 +/- 2.1
1000	0.009802	0.05	0.000042	10.0	362.5 +/- 1.2
1050	0.009765	0.04	0.000035	11.1	364.5 +/- 1.1
1100	0.009622	0.10	0.000095	5.9	363.3 +/- 1.9
1250	0.005165	1.33	0.002116	0.6	268.1 +/- 89.1
				Total gas age	363.8 Ma
93-49;	J = .02218				
650	0.009278	0.15	0.000255	2.2	357.7 +/- 3.1
750	0.009339	0.06	0.000187	7.0	362.6 +/- 1.3
775	0.009457	0.04	0.000130	9.5	364.2 +/- 1.2
800	0.009663	0.02	0.000067	15.0	363.5 +/- .9
825	0.009754	0.02	0.000046	14.4	362.4 +/- .9
850	0.009806	0.03	0.000057	10.1	359.6 +/- 1
875	0.009702	0.08	0.000085	6.9	360.3 +/- 1.1
900	0.009672	0.09	0.000115	4.8	358.3 +/- 1.5
950	0.009605	0.10	0.000113	6.1	360.8 +/- 1.4
1000	0.009667	0.07	0.000099	6.5	360.1 +/- 1.2
1050	0.009678	0.06	0.000068	9.7	362.8 +/- 1.1
1100	0.009733	0.08	0.000072	5.9	360.6 +/- 1.8
1250	0.007453	0.63	0.001094	1.0	328.6 +/- 7.7
1350	0.011650	3.80	0.004173	0.2	-84.3 +/- -30.1
				Total gas age	360.3 Ma

Temp. (°C)	$^{39}\text{Ar}/^{40}\text{Ar}$	$^{37}\text{Ar}/^{39}\text{Ar}$	$^{36}\text{Ar}/^{40}\text{Ar}$	^{39}Ar , % of total	Apparent age (Ma)
94-5;	J = .02224				
650	0.008936	0.42	0.000386	1.2	356.8 +/- 5.9
750	0.009401	0.10	0.000181	3.9	361.9 +/- 2.2
775	0.009474	0.17	0.000201	2.5	357.3 +/- 3.1
800	0.009489	0.09	0.000165	4.5	360.4 +/- 1.8
825	0.009407	0.06	0.000189	6.6	360.8 +/- 1.4
850	0.009727	0.02	0.000073	14.7	361.5 +/- 1
875	0.009828	0.02	0.000048	15.6	360.6 +/- .9
900	0.009726	0.04	0.000060	8.9	362.9 +/- 1.1
925	0.009614	0.00	0.000080	7.0	364.7 +/- 1.6
950	0.009971	0.06	0.000080	5.8	352.8 +/- 7.2
1000	0.009735	0.05	0.000077	7.4	360.8 +/- 1.3
1050	0.009783	0.03	0.000036	9.1	363.3 +/- 1
1100	0.009784	0.03	0.000028	7.7	364 +/- 1.2
1200	0.010048	0.84	0.000519	2.7	307.6 +/- 3.1
1350	0.006045	1.07	0.002093	1.5	242.6 +/- 10.6
				Total gas age	358 Ma
92-184;	J = .0222				
650	0.008993	0.28	0.000353	1.3	357.7 +/- 5.8
750	0.009046	0.07	0.000296	6.4	361.8 +/- 1.5
775	0.009718	0.03	0.000081	14.1	360.5 +/- .9
800	0.009837	0.01	0.000041	18.7	360.5 +/- .9
825	0.009868	0.03	0.000032	14.0	360.3 +/- .9
850	0.009786	0.05	0.000038	8.9	362.4 +/- 1.1
875	0.009807	0.07	0.000072	5.4	358.3 +/- 1.5
900	0.009683	0.18	0.000130	3.5	356.7 +/- 2.2
950	0.009658	0.13	0.000107	4.8	359.9 +/- 1.6
1000	0.009757	0.09	0.000089	5.7	358.3 +/- 1.3
1050	0.009769	0.07	0.000069	8.8	360 +/- 1.3
1100	0.009836	0.07	0.000065	6.7	358.1 +/- 1.3
1250	0.006932	0.73	0.000784	0.9	393.9 +/- 12.7
1350	0.012814	4.49	0.004554	0.2	-114.6 +/- -32.5
				Total gas age	359.2 Ma

Temp. (°C)	³⁹ Ar/ ⁴⁰ Ar	³⁷ Ar/ ³⁹ Ar	³⁶ Ar/ ⁴⁰ Ar	³⁹ Ar, % of total	Apparent age (Ma)
94-55	J = .02225				
650	0.007893	0.37	0.000937	1.7	332.1 +/- 14.7
750	0.009517	0.02	0.000105	17.9	365.7 +/- .9
800	0.009886	0.01	0.000021	39.3	361.5 +/- .8
825	0.009857	0.03	0.000024	13.1	362.1 +/- 1
850	0.009741	0.07	0.000037	6.2	364.8 +/- 1.4
875	0.009737	0.10	0.000055	4.4	363.1 +/- 2.2
900	0.009807	0.11	0.000058	4.7	360.4 +/- 1.8
925	0.009433	0.11	0.000198	4.7	359.1 +/- 2
950	0.009760	0.33	0.000232	1.9	344.8 +/- 5
1000	0.010030	0.43	0.000223	1.6	337.2 +/- 5
1050	0.009480	0.45	0.000210	1.4	356.3 +/- 7.1
1100	0.009892	0.77	0.000509	1.0	313.2 +/- 7
1250	0.008296	0.94	0.000927	0.8	318.5 +/- 11.9
1350	0.008836	2.03	0.002464	0.5	122.4 +/- 22.8
				Total gas age	359 Ma
92-182:	J = .02225				
650	0.001302	0.83	0.000248	0.5	1703 +/- 64.7
750	0.008411	0.16	0.000584	2.6	354.5 +/- 3
800	0.009806	0.01	0.000042	24.1	362.1 +/- .8
825	0.009905	0.02	0.000014	20.7	361.5 +/- .8
850	0.009880	0.03	0.000016	13.2	362.1 +/- .9
875	0.009844	0.04	0.000029	7.7	362.1 +/- 1.1
900	0.009776	0.08	0.000050	4.8	362.3 +/- 1.5
925	0.009641	0.18	0.000082	2.9	363.7 +/- 2
950	0.009884	0.19	0.000091	2.8	354.7 +/- 1.8
1000	0.009818	0.07	0.000056	5.2	360.3 +/- 1.3
1050	0.009826	0.07	0.000036	7.9	362 +/- 1.1
1100	0.009899	0.07	0.000044	5.9	358.8 +/- 1.3
1250	0.007298	0.85	0.001323	0.7	305 +/- 12.1
1350	0.012807	4.93	0.004583	0.2	-117.9 +/- 35.4
				Total gas age	370.3 Ma

Temp. (°C)	$^{39}\text{Ar}/^{40}\text{Ar}$	$^{37}\text{Ar}/^{39}\text{Ar}$	$^{36}\text{Ar}/^{40}\text{Ar}$	^{39}Ar , % of total	Apparent age (Ma)
92-132;	J = .02222				
650	0.003663	0.85	0.001226	0.9	585.8 +/- 23.2
750	0.009610	0.32	0.000295	2.0	343 +/- 3.8
800	0.009854	0.05	0.000062	10.0	358.1 +/- 1
825	0.009974	0.02	0.000011	21.8	359.2 +/- .8
850	0.009991	0.02	0.000011	15.7	358.5 +/- .9
875	0.009893	0.05	0.000021	9.2	360.9 +/- 1
900	0.009933	0.08	0.000036	5.8	358 +/- 1.4
925	0.009819	0.14	0.000068	3.8	358.7 +/- 1.9
950	0.009567	0.16	0.000187	3.5	355.2 +/- 2.5
1000	0.009807	0.10	0.000055	5.7	360.3 +/- 1.3
1050	0.009799	0.09	0.000072	6.6	358.9 +/- 1.4
1100	0.009849	0.06	0.000048	9.9	359.6 +/- 1.1
1250	0.008570	0.18	0.000517	4.0	355.6 +/- 2.6
1350	0.006807	2.73	0.003392	0.5	-1.6 +/- -39.1
				Total gas age	359 Ma
92-188;	J = .02202				
650	0.010647	1.11	0.000467	1.7	293.7 +/- 4.9
750	0.008481	0.08	0.000515	3.2	356.3 +/- 2.8
800	0.009614	0.06	0.000105	5.6	359 +/- 1.4
825	0.009862	0.01	0.000050	14.3	356.1 +/- .9
850	0.009958	0.01	0.000031	16.8	354.8 +/- .9
875	0.009947	0.02	0.000026	12.6	355.6 +/- .9
900	0.009915	0.03	0.000030	8.8	356.3 +/- 1
925	0.009871	0.05	0.000038	5.9	356.9 +/- 1.2
950	0.009873	0.07	0.000061	4.6	354.6 +/- 1.4
1000	0.009886	0.04	0.000041	7.1	356.1 +/- 1.1
1050	0.009887	0.04	0.000033	8.0	356.9 +/- 1.1
1100	0.009941	0.04	0.000033	7.9	355.1 +/- 1.1
1250	0.006453	0.27	0.001179	2.4	359.6 +/- 5.2
1350	0.010883	2.52	0.003488	0.4	-11.6 +/- -24.7
				Total gas age	353.5 Ma

Temp. (°C)	³⁹ Ar/ ⁴⁰ Ar	³⁷ Ar/ ³⁹ Ar	³⁶ Ar/ ⁴⁰ Ar	³⁹ Ar, % of total	Apparent age (Ma)
93-29;	J = .0223				
750	0.003543	3.55	0.001795	2.4	470.6 +/- 55
900	0.007772	4.01	0.000757	4.2	365.6 +/- 11.9
950	0.007919	7.30	0.000854	2.9	347.5 +/- 20.3
975	0.007904	12.68	0.000706	2.2	366.5 +/- 30.5
1000	0.008057	16.24	0.000368	4.0	400.9 +/- 15.3
1025	0.009278	17.63	0.000100	29.0	381.3 +/- 2.1
1050	0.009205	17.63	0.000163	9.6	377.3 +/- 3.8
1075	0.006818	19.47	0.000780	1.7	408.2 +/- 39.2
1100	0.007959	19.89	0.000682	3.0	367.1 +/- 30.6
1125	0.008359	19.76	0.000469	4.7	376.2 +/- 9.8
1150	0.007297	19.42	0.000751	2.6	387.9 +/- 18
1175	0.005798	19.96	0.001494	1.5	353.9 +/- 38.9
1200	0.005629	20.33	0.001240	2.0	407.2 +/- 37.1
1250	0.006879	19.06	0.000691	6.4	417.3 +/- 9.5
1300	0.006120	18.50	0.001518	3.3	333 +/- 17.1
1350	0.006926	18.19	0.001003	10.8	371.3 +/- 5.6
1450	0.004282	18.21	0.002022	8.7	346 +/- 12.9
				Total gas age	378.7 Ma
92-41;	J = .02091				
650	0.008807	0.70	0.000351	1.2	348.1 +/- 10.6
800	0.008760	0.35	0.000373	5.0	347.5 +/- 3.4
900	0.009328	2.27	0.000035	6.6	361.5 +/- 2.5
950	0.009160	3.02	0.000002	10.2	371.2 +/- 2
1000	0.009048	3.15	0.000005	14.7	374.7 +/- 1.9
1050	0.008959	3.36	0.000016	19.8	376.9 +/- 1.8
1100	0.008849	3.70	0.000026	23.8	380 +/- 1.8
1125	0.008714	5.18	0.000101	3.9	377.6 +/- 4
1150	0.008581	4.22	0.000130	5.5	379.9 +/- 3.2
1175	0.007498	4.21	0.000588	1.1	374.2 +/- 13.2
1200	0.007433	4.12	0.000524	1.4	384.9 +/- 10.9
1225	0.007593	4.32	0.000527	2.6	377.2 +/- 5.9
1250	0.003686	4.29	0.002063	0.6	360.9 +/- 38.7
1350	0.004402	4.29	0.001713	2.4	380 +/- 11.5
1450	0.000933	3.93	0.002870	0.4	528 +/- 93.8
				Total gas age	374.9 Ma

Temp. (°C)	$^{39}\text{Ar}/^{40}\text{Ar}$	$^{37}\text{Ar}/^{39}\text{Ar}$	$^{36}\text{Ar}/^{40}\text{Ar}$	^{39}Ar , % of total	Apparent age (Ma)
94-17;	J = .02228				
750	0.004687	7.63	0.001787	3.1	365.2 +/- 32.2
950	0.008637	10.53	0.000646	13.3	342 +/- 6.1
1000	0.008157	16.83	0.000579	11.8	368.2 +/- 6.8
1025	0.008559	14.99	0.000331	20.1	380.6 +/- 4.8
1050	0.008822	14.32	0.000207	11.5	383.9 +/- 6.7
1100	0.006643	16.48	0.001068	3.5	372.8 +/- 21.7
1125	0.005998	17.01	0.001401	5.0	355.4 +/- 17.5
1150	0.004086	20.24	0.002128	2.5	332.5 +/- 42.5
1175	0.004017	17.78	0.002108	2.4	342.5 +/- 43.8
1200	0.004246	17.25	0.001884	3.0	377.3 +/- 37.1
1250	0.006824	16.21	0.000934	13.0	382.8 +/- 7.1
1300	0.004943	16.41	0.001675	4.0	370.1 +/- 22.7
1350	0.003361	18.08	0.002354	3.2	331.6 +/- 40.6
1450	0.002494	16.49	0.002576	2.9	348.9 +/- 54
				Total gas age	367.5 Ma
93-92	J = .02085				
650	0.0028	25.10	0.002110	1.4	445.8 +/- 52.1
800	0.0067	8.66	0.001250	2.8	322.1 +/- 18.9
900	0.0093	9.92	0.000212	7.3	343.9 +/- 6.5
950	0.0085	12.68	0.000155	6.7	378.9 +/- 7
975	0.0086	15.72	0.000117	14.0	379.1 +/- 3.8
1000	0.0089	13.07	-0.000005	13.4	380.2 +/- 3.8
1050	0.0085	12.31	0.000051	8.6	390.2 +/- 5.5
1100	0.0085	13.53	0.000082	3.6	385.8 +/- 11.1
1125	0.0078	13.55	0.000278	6.3	396.1 +/- 7.7
1150	0.0079	13.15	0.000238	12.5	395.1 +/- 4.5
1175	0.0076	13.83	0.000306	6.3	399.6 +/- 8.1
1200	0.0078	14.14	0.000264	6.7	395.9 +/- 7.5
1225	0.0079	15.11	0.000312	6.0	388.8 +/- 8.5
1250	0.0070	15.67	0.000574	1.9	399.3 +/- 21
1350	0.0029	14.94	0.002241	1.4	394.1 +/- 46.7
1450	0.0011	11.47	0.003001	0.4	362.4 +/- 219.3
				Total gas age	383.9 Ma

Temp. (°C)	$^{39}\text{Ar}/^{40}\text{Ar}$	$^{37}\text{Ar}/^{39}\text{Ar}$	$^{36}\text{Ar}/^{40}\text{Ar}$	^{39}Ar , % of total	Apparent age (Ma)
93-38;	J = .02088				
800	0.003254	12.01	0.002353	2.1	324.5 +/- 16
900	0.008427	13.43	0.000233	14.8	377.4 +/- 2.1
950	0.008790	12.41	0.000094	11.5	377.8 +/- 2
975	0.008731	11.96	0.000079	12.2	381.6 +/- 2
1000	0.008634	11.17	0.000050	14.7	388.6 +/- 1.9
1025	0.008471	11.82	0.000087	4.0	391.3 +/- 3.3
1050	0.008200	17.59	0.000276	1.1	382.1 +/- 9.5
1075	0.008454	18.12	0.000203	1.8	379.6 +/- 6.2
1100	0.008409	17.83	0.000156	3.9	386.5 +/- 3.4
1150	0.008476	13.06	0.000067	25.1	393.3 +/- 1.8
1175	0.007630	14.08	0.000387	2.2	394.5 +/- 6.3
1200	0.006247	14.79	0.001003	4.6	383.9 +/- 4.8
1250	0.001312	14.47	0.002669	0.7	526.4 +/- 72
1300	0.000299	13.30	0.003238	0.1	475.2 +/- 863.6
1350	0.000215	11.54	0.002997	0.1	1353.5 +/- 641.1
1400	0.000143	3.86	0.002746	0.1	2394.6 +/- 870.5
1450	0.000058	3.41	0.002612	0.0	4009.5 +/- 958.9
				Total gas age	401.8 Ma
92-205;	J = .02231				
750	0.001931	31.41	0.002678	2.1	398.3 +/- 56.8
900	0.005948	12.46	0.001255	8.0	379.3 +/- 8.4
950	0.008059	13.18	0.000294	9.3	403.7 +/- 6.7
975	0.008264	12.43	0.000224	10.9	402.7 +/- 4.4
1000	0.008380	12.61	0.000184	10.5	402.2 +/- 3.7
1025	0.007985	12.55	0.000251	7.2	412.1 +/- 7.3
1050	0.008918	13.44	0.000255	2.4	372.6 +/- 14.7
1075	0.006565	13.96	0.000170	1.4	501.1 +/- 29
1100	0.007863	14.13	0.000539	2.1	383.1 +/- 17.8
1125	0.007147	14.16	0.000543	2.8	416.8 +/- 14.7
1150	0.007255	13.30	0.000491	7.9	418 +/- 6.5
1200	0.008091	12.61	0.000245	25.5	407.8 +/- 1.9
1250	0.008308	13.36	0.000785	2.8	335.8 +/- 16.4
1300	0.006290	15.80	0.001757	0.9	281.8 +/- 42.1
1350	0.006737	13.28	0.000917	3.6	387.3 +/- 14.9
1450	0.003068	12.32	0.001940	1.6	498.5 +/- 42.4
				Total gas age	402.8 Ma

Temp. (°C)	³⁹ Ar/ ⁴⁰ Ar	³⁷ Ar/ ³⁹ Ar	³⁶ Ar/ ⁴⁰ Ar	³⁹ Ar, % of total	Apparent age (Ma)
93-62;	J = .02082				
650	0.004431	4.09	0.001394	7.1	440.2 +/- 8.9
800	0.007476	3.20	0.000771	7.4	351.4 +/- 5.8
900	0.008368	8.30	0.000355	15.0	362.7 +/- 3.2
950	0.007483	9.97	0.000182	16.2	421.7 +/- 3
975	0.007275	10.37	0.000137	14.4	437.9 +/- 3.3
1000	0.007804	9.38	0.000087	6.2	416.9 +/- 5.1
1050	0.008497	7.91	0.000192	4.6	375.1 +/- 7.2
1100	0.006781	11.59	0.000284	8.0	447.3 +/- 5.3
1125	0.006085	12.16	0.000312	9.9	488 +/- 4.7
1150	0.005597	12.58	0.000384	6.6	514.2 +/- 6.2
1175	0.004313	13.39	0.001198	0.9	489.8 +/- 32.8
1200	0.003712	13.75	0.001420	0.5	508.4 +/- 68.2
1225	0.003339	13.77	0.001090	0.5	636.1 +/- 54.8
1250	0.003571	13.28	0.001046	0.5	610.6 +/- 66.5
1450	0.000234	12.06	0.000170	1.5	4049.3 +/- 167.4
				Total gas age	596.7 Ma
93-61;	J = .02079				
650	0.002689	5.70	0.001563	2.3	627.5 +/- 24.3
800	0.004089	4.91	0.001840	3.9	376.4 +/- 17.1
900	0.007067	11.49	0.000532	18.9	399.7 +/- 3.7
950	0.006053	12.31	0.000517	17.7	460.8 +/- 3.7
975	0.006751	11.99	0.000249	6.7	452.9 +/- 7.2
1000	0.007345	11.24	0.000202	1.7	425.9 +/- 19.8
1050	0.006724	11.22	0.000569	2.8	413 +/- 17.2
1100	0.005568	13.53	0.000499	12.1	498.6 +/- 4.7
1125	0.006034	12.99	0.000393	23.6	479.8 +/- 3.2
1150	0.005025	13.00	0.000695	2.2	512.9 +/- 22.4
1175	0.005341	12.61	0.000609	4.8	499.8 +/- 9.7
1200	0.004187	13.32	0.001712	0.8	396 +/- 69.8
1225	0.003607	13.50	0.002149	0.5	344.5 +/- 126.7
1250	0.003426	14.29	0.005127	0.1	-676.7 +/- 506.7
1450	0.002065	3.98	0.002470	1.0	437.2 +/- 46.1
				Total gas age	457.3 Ma

References

- Aerden, D.G.A.M. 1994. Kinematics of orogenic collapse in the Variscan Pyrenees deduced from microstructures in porphyroblastic rocks from Lys-Caillaouas massif. *Tectonophysics*, **238**: 139-160.
- Aerden, D.G.A.M. 1995. Porphyroblast non-rotation during crustal extension in the Variscan Lys-Caillaouas Massif, Pyrenees. *Journal of Structural Geology*, **17**: 709-725.
- Anderson, S.D. 1995. Metamorphic and structural relations between Humber and Dunnage Zone terranes, Baie Verte Peninsula, Newfoundland: post-Silurian tectonism along the Baie Verte Line. *Geological Society of America, Abstracts with Programs*, vol. 27, no. 1, p. 26.
- Angelier, J. 1994. Fault slip analysis and palaeostress reconstruction. *In Continental Deformation. Edited by P.L. Hancock*. Pergamon Press, New York, p. 53-100.
- Arnott, R.J., McKerrow, W.S., and Cocks, L.R.M. 1985. The tectonics and depositional history of the Ordovician and Silurian rocks of Notre Dame Bay, Newfoundland. *Canadian Journal of Earth Sciences*, **22**: 607-618.
- Baird, D.M. 1951. The geology of the Burlington Peninsula, Newfoundland. *Geological Survey of Canada, Paper 51-21*.
- Barker, A.J. 1990. *Introduction to Metamorphic Textures and Microstructures*. Chapman and Hall, New York.
- Bélanger, M., Dubé, B., and Malo, M. 1996. The Dorset showings: mesothermal vein-type gold occurrences associated with post-Ordovician deformation along the Baie Verte-Brompton Line, Baie Verte Peninsula, Newfoundland. *In Current Research 1996-E, Geological Survey of Canada*, p. 269-279.
- Bell, K., and Blenkinsop, J. 1977. Geochronological evidence of Hercynian activity in Newfoundland. *Nature*, **265**: 616-618.
- Bell, K., and Blenkinsop, J. 1978a. Reset Rb/Sr whole-rock systems and chemical control. *Nature*, **273**: 532-534.
- Bell, K., and Blenkinsop, J. 1978b. U-Pb ages of some crystalline rocks from the Burlington Peninsula, Newfoundland, and implications for the age of Fleur de Lys metamorphism: a discussion. *Canadian Journal of Earth Sciences*, **15**: 1208-1210.

- Bell, T.H. 1985. Deformation partitioning and porphyroblast rotation in metamorphic rocks: a radical reinterpretation. *Journal of Metamorphic Geology*, **3**: 109-118.
- Bell, T.M., and Johnson, S.E. 1992. Shear sense: a new approach that resolves conflicts between criteria in metamorphic rocks. *Journal of Metamorphic Geology*, **10**: 99-124.
- Bell, T.M., and Rubenach, M.J. 1983. Sequential porphyroblast growth and crenulation cleavage development during progressive deformation. *Tectonophysics*, **92**: 171-194.
- Bell, T.H., Rubenach, M.J., and Fleming, P.D. 1986. Porphyroblast nucleation, growth and dissolution in regional metamorphic rocks as a function of deformation partitioning during foliation development. *Journal of Metamorphic Geology*, **4**: 37-67.
- Bell, T.M., Johnson, S.E., Davis, B., Forde, A., Hayward, N., and Wilkins, C. 1992. Porphyroblast inclusion-trail orientation data: eppure non son girate! *Journal of Metamorphic Geology*, **10**: 295-307.
- Berman, R.G. 1988. Internally-consistent thermodynamic data for minerals in the system: Na₂O-K₂O-CaO-MgO-FeO-Fe₂O₃-Al₂O₃-SiO₂-TiO₂-H₂O-CO₂. *Journal of Petrology*, **29**: 445-522.
- Berman, R.G. 1990. Mixing properties of Ca-Mg-Fe-Mn garnets. *American Mineralogist*, **75**: 328-344.
- Berman, R.G. 1991. Thermobarometry using multi-equilibrium calculations: a new technique, with petrological applications. *Canadian Mineralogist*, **29**: 833-855.
- Berthé, D., and Brun, J.P. 1980. Evolution of folds during progressive shear in the South Armorican Shear Zone, France. *Journal of Structural Geology*, **2**: 127-133.
- Berthé, D., Choukroune, P., and Jegouzo, P. 1979. Orthogneiss, mylonite and non coaxial deformation of granites: the example of the South Armorican Shear Zone. *Journal of Structural Geology*, **1**: 31-42.
- Bevier, M.L., and Whalen, J.B. 1990. Tectonic significance of Silurian magmatism in the Canadian Appalachians. *Geology*, **18**: 411-414.
- Bevier, M.L., Barr, S.M., White, C.E., and MacDonald, A.S. 1993. U-Pb geochronological constraints on the volcanic evolution of the Mira (Avalon) Terrane, southeastern Cape Breton Island, Nova Scotia. *Canadian Journal of Earth Sciences*, **30**: 1-10.

- Bird, J.M., and Dewey, J.F. 1970. Lithosphere plate-continental margin tectonics and the evolution of the Appalachian orogen. *Geological Society of America Bulletin*, **81**: 1031-1060.
- Bohlen, S.R., Wall, V.J., and Boettcher, A.L. 1983. Experimental investigations and geologic applications of equilibria in the system FeO-TiO₂-Al₂O₃-SiO₂-H₂O. *American Mineralogist*, **68**: 1049-1058.
- Bosworth, W. 1985. East-directed imbrication and oblique-slip faulting in the Humber Arm Allochthon of western Newfoundland: structural and tectonic significance. *Canadian Journal of Earth Sciences*, **22**: 1351-1360.
- Bradley, D.C. 1982. Subsidence in Late Paleozoic basins in the northern Appalachians. *Tectonics*, **1**: 107-123.
- Buck, W.R. 1988. Flexural rotation of normal faults. *Tectonics*, **7**: 959-974.
- Burgess, J.L., Brown, M., Dallmeyer, R.D., and van Staal, C.R. 1995. Microstructure, metamorphism, thermochronology and P-T-t-deformation history of the Port aux Basques gneisses, south-west Newfoundland, Canada. *Journal of Metamorphic Geology*, **13**: 751-776.
- Bursnall, J.T. 1975. Stratigraphy, structure and metamorphism west of Baie Verte, Burlington Peninsula, Newfoundland. Ph.D. thesis. Cambridge University, Cambridge, England.
- Bursnall, J.T., and de Wit, M.J. 1975. Timing and development of the orthotectonic zone in the Appalachian Orogen of northwest Newfoundland. *Canadian Journal of Earth Sciences*, **12**: 1712-1722.
- Bursnall, J.T., and Hibbard, J. 1980. Fleur de Lys (12I/1) and Horse Islands (2L/4) map areas. Newfoundland Department of Mines and Energy, Mineral Development Division, Map 80-30.
- Cawood, P.A. 1989. Acadian remobilization of a Taconian ophiolite, Hare Bay allochthon, northwestern Newfoundland. *Geology*, **17**: 257-260.
- Cawood, P.A. 1993. Acadian Orogeny in west Newfoundland: definition, character, and significance. *In The Acadian Orogeny: recent studies in New England, Maritime Canada, and the autochthonous foreland. Edited by D.C. Roy and J.W. Skehan. Geological Society of America Special Paper 275, p. 135-152.*

- Cawood, P.A., and Dunning, G.R. 1993. Silurian age for movement on the Baie Verte Line: implications for accretionary tectonics in the northern Appalachians. *Geological Society of America, Abstracts with Programs*, vol. 25, no. 6, p. 422.
- Cawood, P.A., and Williams, H. 1988. Acadian basement thrusting, crustal delamination, and structural styles in and around the Humber Arm allochthon, western Newfoundland. *Geology*, **16**: 370-373.
- Cawood, P.A., Dunning, G.R., Lux, D., and van Gool, J.A.M. 1994. Timing of peak metamorphism and deformation along the Appalachian margin of Laurentia in Newfoundland: Silurian, not Ordovician. *Geology*, **22**: 399-402.
- Cawood, P.A., van Gool, J.A.M., and Dunning, G.R. 1995. Collisional tectonics along the Laurentian margin of the Newfoundland Appalachians. *In Current Perspectives in the Appalachian-Caledonian Orogen. Edited by J.P. Hibbard, C.R. van Staal, and P.A. Cawood. Geological Association of Canada, Special Paper 41, p. 283-301.*
- Cawood, P.A., van Gool, J.A.M., and Dunning, G.R. 1996. Geological development of eastern Humber and western Dunnage zones: Corner Brook - Glover Island region, Newfoundland. *Canadian Journal of Earth Sciences*, **33**: 182-198.
- Cerný, P. 1982. Anatomy and classification of granitic pegmatites. *In Granitic pegmatites in research and industry. Edited by P. Cerný. Mineralogical Association of Canada, Short Course Handbook 8, p. 1-40.*
- Cerný, P. 1989. Characteristics of pegmatite deposits of tantalum. *In Lanthanides, Tantalum and Niobium. Edited by P. Moller, P. Cerný, and F. Saupe. Springer-Verlag, Berlin, p. 195-239.*
- Cerný, P. 1991. Rare-element granitic pegmatites. Part I: anatomy and internal evolution of pegmatite deposits. *Geoscience Canada*, **18**: 49-67.
- Cerný, P., and Ercit, T.S. 1989. Mineralogy of Niobium and Tantalum: crystal chemical relationships, paragenetic aspects and their economic implications. *In Lanthanides, Tantalum and Niobium. Edited by P. Moller, P. Cerný, and F. Saupe. Springer-Verlag, Berlin, p. 27-79.*
- Cerný, P., and Turnock, A.C. 1971. Niobium-tantalum minerals from granitic pegmatites at Greer Lake, southeastern Manitoba. *Canadian Mineralogist*, **10**: 755-772.
- Chamberlain, C.P., and Karabinos, P. 1987. Influence of deformation on pressure-temperature paths of metamorphism. *Geology*, **15**: 42-44.

- Chauvet, A., and Séranne, M. 1994. Extension-parallel folding in the Scandinavian Caledonides: implications for late-orogenic processes. *Tectonophysics*, **238**: 31-54.
- Church, W.R. 1969. Metamorphic rocks of Burlington Peninsula and adjoining areas of Newfoundland and their bearing on continental drift in the North Atlantic. *In* North Atlantic Geology and Continental Drift. *Edited by* M. Kay. American Association of Petroleum Geologists, Memoir 12, p. 212-233.
- Church, W.R., and Stevens, R.K. 1971. Early Paleozoic ophiolite complexes of the Newfoundland Appalachians as mantle-oceanic crust sequences. *Journal of Geophysical Research*, **76**: 1460-1466.
- Clarke, D.B., and Chatterjee, A.K. 1992. Origin of peraluminous granites in the Meguma Zone of southern Nova Scotia: A synthesis. *Geological Association of Canada, Program with Abstracts*, **17**: A18.
- Coates, H.J. 1970. Structural and metamorphic history of the Pacquet Harbour - Grand Cove area, Burlington Peninsula, Newfoundland. M.Sc. thesis, Memorial University of Newfoundland, St. John's, Newfoundland.
- Cobbold, P.R., and Quinquis, H. 1980. Development of sheath folds in shear regimes. *Journal of Structural Geology*, **2**: 199-126.
- Cobbold, P.R., Gapais, D., and Rossello, E.A. 1991. Partitioning of transpressive motions within a sigmoidal foldbelt: the Variscan Sierras Australes, Argentina. *Journal of Structural Geology*, **13**: 743-758.
- Colman-Sadd, S.P., and Swinden, H.S. 1984. A tectonic window in central Newfoundland?. Geological evidence that the Appalachian Dunnage Zone may be allochthonous. *Canadian Journal of Earth Sciences*, **21**: 1349-1367.
- Colman-Sadd, S.P., Dunning, G.R., and Dec, T. 1992. Dunnage-Gander relationships and Ordovician orogeny in central Newfoundland: a sediment provenance and U/Pb age study. *American Journal of Science*, **292**: 317-355.
- Colman-Sadd, S.P., Hayes, J.P., and Knight, I. 1990. Geology of the island of Newfoundland. Government of Newfoundland and Labrador, Department of Mines and Energy, Geological Survey Branch, Map 90-01.
- Coney, P.J. 1980. Cordilleran metamorphic core complexes - An overview. *In* Cordilleran metamorphic core complexes. *Edited by* M.D. Crittenden, Jr., P.J. Coney, and G.H. Davis. Geological Society of America, Memoir 153, p. 7-31.

- Corfu, F., and Stott, G.M. 1986. U-Pb ages for late magmatism and regional deformation in the Shebandowan belt, Superior Province, Canada. *Canadian Journal of Earth Sciences*, **23**: 1075-1082.
- Coward, M.P., and Potts, G.J. 1983. Complex strain patterns developed at the frontal and lateral tips to shear zones and thrust zones. *Journal of Structural Geology*, **5**: 383-399.
- Coyle, M., and Strong, D.F. 1987. Geology of the Springdale Group: a newly recognized Silurian epicontinental-type caldera in Newfoundland. *Canadian Journal of Earth Sciences*, **24**: 1135-1148.
- Crawford, M.L. 1966. Composition of plagioclase and associated minerals in some schists from Vermont, USA and South Westland, New Zealand, with inferences about the peristerite solvus. *Contributions to Mineralogy and Petrology*, **13**: 269-294.
- Crowell, J.C. 1974. Origin of Late Cenozoic basins in southern California. *In* *Tectonics and sedimentation*. Edited by W.R. Dickinson. Society of Economic Paleontologists and Mineralogists, Special Publication No. 22, p. 190-204.
- Culshaw, N.G., Ketchum, J.W.F., Wodicka, N., and Wallace, P. 1994. Deep crustal ductile extension following thrusting in the southwestern Grenville Province, Ontario. *Canadian Journal of Earth Sciences*, **31**: 160-175.
- Currie, K.L., and Piasecki, M.A.J. 1989. Kinematic model for southwestern Newfoundland based upon sinistral shearing. *Geology*, **17**: 938-941.
- Dallmeyer, R.D. 1977. $^{40}\text{Ar}/^{39}\text{Ar}$ age spectra of minerals from the Fleur de Lys terrane in northwest Newfoundland: their bearing on chronology of metamorphism within the Appalachian Orthotectonic Zone. *Journal of Geology*, **85**: 89-103.
- Dallmeyer, R.D., and Hibbard, J. 1984. Geochronology of the Baie Verte Peninsula, Newfoundland: implications for the tectonic evolution of the Humber and Dunnage Zones of the Appalachian Orogen. *Journal of Geology*, **92**: 489-512.
- Davis, G.H., and Coney, P.J. 1979. Geologic development of the Cordilleran metamorphic core complexes. *Geology*, **7**: 120-124.
- Dec, T., Swinden, H.S., and Dunning, G.R. 1997. Lithostratigraphy and geochemistry of the Cottrells Cove Group, Buchans - Roberts Arm volcanic belt: new constraints for the paleotectonic setting of the Notre Dame Subzone, Newfoundland Appalachians. *Canadian Journal of Earth Sciences*, **34**: 86-103.

- DeGrace, J.R., Kean, B.F., Hsu, E., and Green, T. 1976. The geology of the Nippers Harbour map area (2E/13), Newfoundland. Newfoundland Department of Mines and Energy, Mineral Development Division, Report 76-3.
- Dennis, A.J., and Secor, D.T. 1987. A model for the development of crenulations in shear zones with applications from the Southern Appalachian Piedmont. *Journal of Structural Geology*, **9**: 809-817.
- Dennis, A.J., and Secor, D.T. 1990. On resolving shear direction in foliated rocks deformed by simple shear. *Geological Society of America Bulletin*, **102**: 1257-1267.
- de Roo, J.A., and van Staal, C.R. 1994. Transpression and extensional collapse: steep belts and flat belts in the Appalachians Central Mobile Belt, northern New Brunswick, Canada. *Geological Society of America Bulletin*, **106**: 541-552.
- Dewey, J.F. 1969. Evolution of the Caledonian / Appalachian orogen. *Nature*, **222**: 124-129.
- Dewey, J.F. 1988. Extensional collapse of orogens. *Tectonics*, **7**: 1123-1139.
- Dewey, J.F., and Bird, J.M. 1971. Origin and emplacement of the ophiolite suite: Appalachian ophiolites in Newfoundland. *Journal of Geophysical Research*, **76**: 3179-3206.
- Dewey, J.F., and Shackleton, R.M. 1984. A model for the evolution of the Grampian tract in the early Caledonides and Appalachians. *Nature*, **312**: 115-121.
- Dewey, J.F., Kennedy, M.J., and Kidd, W.S.F. 1983. A geotraverse through the Appalachians of northern Newfoundland. In *Profiles of Orogenic Belts*. Edited by N. Rast, and F.M. Delany. American Geophysical Union / Geological Society of America, Geodynamic Series, v. 10, p. 205-241.
- de Wit, M.J. 1972. The geology around Bear Cove, eastern White Bay, Newfoundland. Ph.D. thesis, Cambridge University, Cambridge, England.
- de Wit, M.J. 1974. On the origin and deformation of the Fleur de Lys metaconglomerate, Appalachian fold belt, northwest Newfoundland. *Canadian Journal of Earth Sciences*, **11**: 1168-1180.
- de Wit, M.J. 1980. Structural and metamorphic relationships of pre-Fleur de Lys and Fleur de Lys rocks of the Baie Verte Peninsula, Newfoundland. *Canadian Journal of Earth Sciences*, **17**: 1559-1575.

- Dodson, M.H. 1973. Closure temperature in cooling geochronological and petrological systems. *Contributions to Mineralogy and Petrology*, **40**: 259-274.
- Doig, R., Nance, R.D., Murphy, J.B., and Casseday, R.P. 1990. Evidence for Silurian sinistral accretion of Avalon composite terrane in Canada. *Journal of the Geological Society, London*, **147**: 927-930.
- Dubé, B. 1990. A preliminary report on contrasting structural styles of gold-only deposits in western Newfoundland. *In Current Research, Part B, Geological Survey of Canada, Paper 90-1B*, p. 77-90.
- Dubé, B., and Lauzière, K. 1996. Structural evolution of a major fault zone: the Cape Ray Fault Zone, southwestern Newfoundland, Canada. *Canadian Journal of Earth Sciences*, **33**: 199-215.
- Dubé, B., Lauzière, K., Swinden, S., and Wilson, M. 1992. Gold mineralization in western Newfoundland. Geological Association of Canada, Mineralogical Association of Canada, Joint Annual Meeting, Wolfville '92, Field Trip A-4, Guidebook.
- Dubé, B., Lauzière, K., and Poulsen, H.K. 1993. The Deer Cove deposit: an example of "thrust"-related breccia-vein type gold mineralization in the Baie Verte Peninsula, Newfoundland. *In Current Research, Part D, Geological Survey of Canada, Paper 93-1D*, p. 1-10.
- Dubé, B., Dunning, G.R., Lauzière, K., and Roddick, J.C. 1996. New insights into the Appalachian Orogen from geology and geochronology along the Cape Ray fault zone, southwest Newfoundland. *Geological Society of America Bulletin*, **108**: 101-116.
- Duebendorfer, E.M., and Simpson, D.A. 1994. Kinematics and timing of Tertiary extension in the western Lake Mead region, Nevada. *Geological Society of America Bulletin*, **106**: 1057-1073.
- Dunning, G.R., and Krogh, T.E. 1985. Geochronology of ophiolites of the Newfoundland Appalachians. *Canadian Journal of Earth Sciences*, **22**: 1659-1670.
- Dunning, G.R., Kean, B.F., Thurlow, J.G., and Swinden, H.S. 1987. Geochronology of the Buchans, Roberts Arm, and Victoria Lake groups and Mansfield Cove Complex, Newfoundland. *Canadian Journal of Earth Sciences*, **24**: 1175-1184.
- Dunning, G.R., O'Brien, S.J., Colman-Sadd, S.P., Blackwood, R.F., Dickson, W.L., O'Neill, P.P., and Krogh, T.E. 1990. Silurian Orogeny in the Newfoundland Appalachians. *Journal of Geology*, **98**: 895-913.

- Dunning, G.R., O'Brien, S.J., O'Brien, B.H., Holdsworth, R.E., and Tucker, R.D. 1993. Chronology of Pan-African, Penobscot and Salinic shear zones on the Gondwanan margin, northern Appalachians. Geological Society of America, Abstracts with Programs, vol. 25, no. 6, p. 421.
- Elliott, C.G., Dunning, G.R., and Williams, P.F. 1991. New U-Pb zircon age constraints on the timing of deformation in north-central Newfoundland and implications for early Paleozoic Appalachian orogenesis. Geological Society of America Bulletin, **103**: 125-135.
- Essene, E.J. 1989. The current status of thermobarometry in metamorphic rocks. *In* Evolution of Metamorphic Belts. Edited by J.S. Daly, R.A. Cliff, and B.W.D. Yardley. Geological Society Special Publication No. 43, p. 1-44.
- Ferrill, B.A., and Thomas, W.A. 1988. Acadian dextral transpression and synorogenic sedimentary successions in the Appalachians. *Geology*, **16**: 604-608.
- Fletcher, J.M., and Bartley, J.M. 1994. Constrictional strain in a non-coaxial shear zone: implications for fold and rock fabric development, central Mojave metamorphic core complex, California. *Journal of Structural Geology*, **16**: 555-570.
- Foord, E.E. 1982. Minerals of tin, titanium, niobium and tantalum in granitic pegmatites. *In* Granitic pegmatites in research and industry. Edited by P. Cerný. Mineralogical Association of Canada, Short Course Handbook 8, p. 187-238.
- Fossen, H., and Rykkelid, E. 1992. Postcollisional extension of the Caledonide orogen in Scandinavia: structural expressions and tectonic significance. *Geology*, **20**: 737-740.
- Fryer, B.J., Kerr, A., Jenner, G.A., and Longstaffe, F.J. 1992. Probing the crust with plutons: regional isotopic geochemistry of granitoid intrusions across insular Newfoundland. *In* Current Research, Newfoundland Department of Mines and Energy, Geological Survey Branch, Report 92-1, p. 119-139.
- Fuhrman, M.L., and Lindsley, D.H. 1988. Ternary-tetradspar modeling and thermometry. *American Mineralogist*, **73**: 201-216.
- Fyffe, L.R., and Swinden, H.S. 1991. Paleotectonic setting of Cambro-Ordovician volcanic rocks in the Canadian Appalachians. *Geoscience Canada*, **18**: 145-157.
- Gaboury, D., Dubé, B., Lafèche, M.R., and Lauzière, K. 1996. Geology of the Hammer Down mesothermal gold deposit, Newfoundland Appalachians, Canada. *Canadian Journal of Earth Sciences*, **33**: 335-350.

- Gale, G.H. 1971. An investigation of some sulphide deposits of the Rambler area, Newfoundland. Ph.D. thesis, University of Durham, England.
- Gale, G.H. 1973. Paleozoic basaltic komatiite and ocean-floor type basalts from northeastern Newfoundland. *Earth and Planetary Science Letters*, **18**: 22-28.
- Gapais, D. 1989. Shear structures within deformed granites: mechanical and thermal indicators. *Geology*, **17**: 1144-1147.
- Gapais, D., Bale, P., Choukroune, P., Cobbold, P.R., Mahjoub, Y., and Marquer, D. 1987. Bulk kinematics from shear zone patterns: some field examples. *Journal of Structural Geology*, **9**: 635-646.
- Ghent, E.D. 1976. Plagioclase-garnet- Al_2SiO_5 -quartz: a potential geobarometer-geothermometer. *American Mineralogist*, **61**: 710-714.
- Ghent, E.D., and Stout, M.Z. 1981. Geobarometry and geothermometry of plagioclase-biotite-garnet-muscovite assemblages. *Contributions to Mineralogy and Petrology*, **76**: 92-97.
- Ghosh, S.K., and Sengupta, S. 1987. Progressive development of structures in a ductile shear zone. *Journal of Structural Geology*, **9**: 277-287.
- Gill, J.B. 1981. *Orogenic andesites and plate tectonics*. Springer-Verlag, Berlin.
- Goodwin, L.B., and Williams, P.F. 1990. Strike-slip movement along the Baie Verte Line. *In* Lithoprobe East Transect Report 13, p. 75-84.
- Goodwin, L.B., and Williams, P.F. 1993. Partitioning of strike-slip and dip-slip movement within a transpressive shear zone: an example from the Appalachians. *Geological Society of America, Abstracts with Programs*, vol. 25, no. 6, p. 477.
- Goodwin, L.B., and Williams, P.F. 1996. Deformation path partitioning within a transpressive shear zone, Marble Cove, Newfoundland. *Journal of Structural Geology*, **18**: 975-990.
- Gower, C.F. 1993. Syntectonic minor intrusions or synemplacement deformation? *Canadian Journal of Earth Sciences*, **30**: 1674-1675.
- Grujic, D., and Mancktelow, N.S. 1995. Folds with axes parallel to the extension direction: an experimental study. *Journal of Structural Geology*, **17**: 279-291.

- Hadizadeh, J., Babaie, H.A., and Babaei, A. 1991. Development of interlaced mylonites, cataclasites and breccias: example from the Towaliga fault, south central Appalachians. *Journal of Structural Geology*, **13**: 63-70.
- Hamblin, A.P., Fowler, M.G., Utting, J., Hawkins, D., and Riediger, C.L. 1995. Sedimentology, palynology and source rock potential of Lower Carboniferous (Tournasian) rocks, Conche Area, Great Northern Peninsula, Newfoundland. *Bulletin of Canadian Petroleum Geology*, **43**: 1-19.
- Handy, M.R. 1989. Deformation regimes and the rheological evolution of fault zones in the lithosphere: the effects of pressure, temperature, grain size and time. *Tectonophysics*, **163**: 119-152.
- Hanes, J.A. 1991. K-Ar and $^{40}\text{Ar}/^{39}\text{Ar}$ geochronology: methods and applications. In *Applications of radiogenic isotope systems to problems in geology. Edited by L. Heaman, and J.N. Ludden. Mineralogical Association of Canada, Short Course Handbook, v. 19, p. 27-57.*
- Hanmer, S.K. 1979. The role of discrete heterogeneities and linear fabrics in the formation of crenulations. *Journal of Structural Geology*, **1**: 81-91.
- Hanmer, S. 1981. Tectonic significance of the northeastern Gander Zone, Newfoundland: an Acadian ductile shear zone. *Canadian Journal of Earth Sciences*, **18**: 120-135.
- Hanmer, S. 1986. Asymmetrical pull-aparts and foliation fish as kinematic indicators. *Journal of Structural Geology*, **8**: 111-122.
- Hanmer, S. 1989. Initiation of cataclastic flow in a mylonite zone. *Journal of Structural Geology*, **11**: 751-762.
- Hanmer, S., and Passchier, C. 1991. Shear-sense indicators: a review. Geological Survey of Canada, Paper 90-17.
- Harland, W.B., Armstrong, R.L., Cox, A.V., Craig, L.E., Smith, A.G., and Smith, D.G. 1989. A geologic time-scale 1989. Cambridge University Press, Cambridge.
- Harrison, T.M. 1981. Diffusion of ^{40}Ar in hornblende. *Contributions to Mineralogy and Petrology*, **78**: 324-331.
- Harrison, T.M., Duncan, I., and McDougall, I. 1985. Diffusion of ^{40}Ar in biotite: temperature, pressure and compositional effects. *Geochimica et Cosmochimica Acta*, **49**: 2461-2468.

- Haworth, R.T., Poole, W.H., Grant, A.C., and Sanford, B.V. 1976. Marine geoscience survey northeast of Newfoundland. *In* Geological Survey of Canada, Paper 76-1A, p. 7-15.
- Heaman, L., and Parrish, R. 1991. U-Pb geochronology of accessory minerals. *In* Applications of radiogenic isotope systems to problems in geology. *Edited by* L. Heaman, and J.N. Ludden. Mineralogical Association of Canada, Short Course Handbook, v. 19, p. 59-102.
- Hetzel, R., Passchier, C.W., Ring, U., and Dora, O.O. 1995. Bivergent extension in orogenic belts: The Menderes massif (southwestern Turkey). *Geology*, **23**: 455-458.
- Hibbard, J. 1982. Significance of the Baie Verte Flexure, Newfoundland. *Geological Society of America Bulletin*, **93**: 790-797.
- Hibbard, J. 1983. Geology of the Baie Verte Peninsula, Newfoundland. Newfoundland Department of Mines and Energy, Mineral Development Division, Memoir 2.
- Hibbard, J. 1987. Ophiolitic melange along the Baie Verte Line, Coachman's Harbour, Newfoundland. *In* Geological Society of America Centennial Field Guide-Northeastern Section, p. 457-462.
- Hibbard, J. 1994. Kinematics of Acadian deformation in the Northern and Newfoundland Appalachians. *The Journal of Geology*, **102**: 215-228.
- Hibbard, J., and Gagnon, J. 1980. Geology of the Jackson's Arm (east) and Baie Verte map areas. Newfoundland Department of Mines and Energy, Mineral Development Division, Map 80-03.
- Hibbard, J., and Hall, S. 1993. Early Acadian sinistral shear in north-central Maine, USA. *Journal of the Geological Society, London*. **150**: 815-818.
- Hodges, K.V. 1991. Pressure-temperature-time paths. *Annual Review of Earth and Planetary Sciences*, **19**: 207-236.
- Hogarth, D.D. 1977. Classification and nomenclature of the pyrochlore group. *American Mineralogist*, **62**: 403-410.
- Holdaway, M.J. 1971. Stability of andalusite and the aluminium silicate phase diagrams. *American Journal of Science*, **271**: 97-131.

- Holdsworth, R.E. 1990. Progressive deformation structures associated with ductile thrusts in the Moine Nappe, Sutherland, N. Scotland. *Journal of Structural Geology*, **12**: 443-452.
- Holdsworth, R.E. 1994. Structural evolution of the Gander-Avalon terrane boundary: a reactivated transpression zone in the NE Newfoundland Appalachians. *Journal of the Geological Society, London*, **151**: 629-646.
- Holdsworth, R.E., and Strachan, R.A. 1991. Interlinked system of ductile strike slip and thrusting formed by Caledonian sinistral transpression in northeastern Greenland. *Geology*, **19**: 510-513.
- Holm, D.K., Snow, J.K., and Lux, D.R. 1992. Thermal and barometric constraints on the intrusive and unroofing history of the Black Mountains: implications for timing, initial dip, and kinematics of detachment faulting in the Death Valley region, California. *Tectonics*, **11**: 507-???
- Hudleston, P.J. 1989. The association of folds and veins in shear zones. *Journal of Structural Geology*, **11**: 949-957.
- Hyde, R.S., Miller, H.G., Hiscott, R.N., and Wright, J.A. 1988. Basin architecture and thermal maturation in the strike-slip Deer Lake Basin, Carboniferous of Newfoundland. *Basin Research*, **1**: 85-105.
- Irvine, T.N., and Baragar, W.R.A. 1971. A guide to the chemical classification of the common volcanic rocks. *Canadian Journal of Earth Sciences*, **8**: 523-548.
- Jahns, R.H., and Ewing, R.C. 1976. The Harding mine, Taos County, New Mexico. *In* 27th Field Conference Guidebook. *Edited by* R.C. Ewing, and B.S. Kues. New Mexico Geological Society, p. 263-276.
- Jain, A.K., and Manickavasagam, R.M. 1993. Inverted metamorphism in the intracontinental ductile shear zone during Himalayan collision tectonics. *Geology*, **21**: 407-410.
- Jamieson, R.A. 1990. Metamorphism of an Early Palaeozoic continental margin, western Baie Verte Peninsula, Newfoundland. *Journal of Metamorphic Geology*, **8**: 269-288.
- Jamieson, R.A. 1991. P-T-t paths of collisional orogens. *Geologische Rundschau*, **80**: 321-332.

- Jamieson, R.A., and O'Beirne-Ryan, A.M. 1991. Decompression-induced growth of albite porphyroblasts, Fleur de Lys Supergroup, western Newfoundland. *Journal of Metamorphic Geology*, **9**: 433-439.
- Jamieson, R.A., and Vernon, R.H. 1987. Timing of porphyroblast growth in the Fleur de Lys Supergroup, Newfoundland. *Journal of Metamorphic Geology*, **5**: 273-288.
- Jamieson, R.A., van Breeman, O., Sullivan, R.W., and Currie, K.L. 1986. The age of igneous and metamorphic events in the Cape Breton Highlands, Nova Scotia. *Canadian Journal of Earth Sciences*, **23**: 1891-1901.
- Jamieson, R.A., Anderson, S.D., and McDonald, L. 1993a. Slip on the Scrape - an extensional allochthon east of the Baie Verte Line, Newfoundland. *Geological Society of America, Abstracts with Programs*, vol. 25, no. 2, p. 26.
- Jamieson, R.A., Anderson, S.D., McDonald, L., and Goodwin, L.B. 1993b. Silurian extension along the Humber-Dunnage boundary zone, Baie Verte Peninsula, Newfoundland. *Late Orogenic Extension in Mountain Belts*, Montpellier, France, Abstracts Volume, Document du BRGM 219, p. 102.
- Jamieson, R.A., Beaumont, C., Hamilton, J., and Fullsack, P. 1996. Tectonic assembly of inverted metamorphic sequences. *Geology*, **24**: 839-842.
- Jamieson, R.A., Beaumont, C., Fullsack, P., and Lee, B. 1998. Barrovian regional metamorphism: where's the heat? In *What drives metamorphism and metamorphic reactions?* Edited by P.J. Treloar and P.J. O'Brien. Geological Society, London, Special Publication 138, p. 23-51.
- Jenner, G.A., and Fryer, B.J. 1980. Geochemistry of the upper Snooks Arm Group basalts, Burlington Peninsula, Newfoundland: evidence against formation in an island arc. *Canadian Journal of Earth Sciences*, **17**: 888-900.
- Jenner, G.A., Longerich, H.P., Jackson, S.E., and Fryer, B.J. 1990. ICP-MS - a powerful tool for high precision trace element analysis in earth sciences: evidence from analysis of selected USGS reference samples. *Chemical Geology*, **83**: 133-148.
- Johnson, R.J.E., van der Pluijm, B.A., and Van der Voo, R. 1991. Paleomagnetism of the Moreton's Harbour Group, Northeastern Newfoundland Appalachians: evidence for an Early Ordovician Island arc near the Laurentian margin of Iapetus. *Journal of Geophysical Research*, **96**: 11,689-11,701.
- Johnson, S.E. 1990. Lack of porphyroblast rotation in the Otago schists, New Zealand: implications for crenulation cleavage development, folding and deformation partitioning. *Journal of Metamorphic Geology*, **8**: 13-30.

- Johnson, S.E. 1992. Sequential porphyroblast growth during progressive deformation and low-P high-T (LPHT) metamorphism, Cooma Complex, Australia: The use of microstructural analysis to better understand deformation and metamorphic histories. *Tectonophysics*, **214**: 311-339.
- Johnson, S.E. 1993a. Unravelling the spirals: a serial thin-section study and three-dimensional computer-aided reconstruction of spiral-shaped inclusion trails in garnet porphyroblasts. *Journal of Metamorphic Geology*, **11**: 621-634.
- Johnson, S.E. 1993b. Testing models for the development of spiral-shaped inclusion trails in garnet porphyroblasts: to rotate or not to rotate, that is the question. *Journal of Metamorphic Geology*, **11**: 635-659.
- Johnson, S.E., and Bell, T.H. 1996. How useful are 'millipede' and other similar porphyroblast microstructures for determining synmetamorphic deformation histories? *Journal of Metamorphic Geology*, **14**: 15-28.
- Johnson, S.E., and Vernon, R.H. 1995. Inferring the timing of porphyroblast growth in the absence of continuity between inclusion trails and matrix foliations: can it be reliably done? *Journal of Structural Geology*, **17**: 1203-1206.
- Kamo, S.L., Gower, C.F., and Krogh, T.E. 1989. Birthdate for the Iapetus Ocean? A precise U-Pb zircon and baddeleyite age for the Long Range dikes, southeast Labrador. *Geology*, **17**: 602-605.
- Karlstrom, K.E., van der Pluijm, B.A., and Williams, P.F. 1982. Structural interpretation of the eastern Notre Dame Bay area, Newfoundland: regional post-Middle Silurian thrusting and asymmetrical folding. *Canadian Journal of Earth Sciences*, **19**: 2325-2341.
- Keen, C.E., Keen, M.J., Nichols, B., Reid, I., Stockmal, G.S., Colman-Sadd, S.P., O'Brien, S.J., Miller, H., Quinlan, G., Williams, H., and Wright, J. 1986. Deep seismic reflection profile across the northern Appalachians. *Geology*, **14**: 141-145.
- Kennedy, M.J. 1973. Pre-Ordovician polyphase structure in the Burlington Peninsula of the Newfoundland Appalachians. *Nature Physical Science*, **241**: 114-116.
- Kennedy, M.J. 1975. Repetitive orogeny in the northeastern Appalachians - new plate models based upon Newfoundland examples. *Tectonophysics*, **28**: 39-87.
- Kennedy, W.Q. 1949. Zones of progressive regional metamorphism in the Moine Schists of the Western Highlands of Scotland. *Geological Magazine*, **86**: 43-56.

- Kerr, A., Dunning, G.R., and Tucker, R.D. 1993. The youngest Paleozoic plutonism of the Newfoundland Appalachians: U-Pb ages from the St. Lawrence and Francois granites. *Canadian Journal of Earth Sciences*, **30**: 2328-2333.
- Kerrick, D.M. 1988. Al₂SiO₅-bearing segregations in the Lepontine Alps, Switzerland: aluminum mobility in metapelites. *Geology*, **16**: 636-640.
- Kidd, W.S.F. 1974. The evolution of the Baie Verte lineament, Burlington Peninsula, Newfoundland. Ph.D. Thesis, Cambridge University, Cambridge, England.
- Kidd, W.S.F. 1977. The Baie Verte Lineament, Newfoundland: ophiolite complex floor and mafic volcanic fill of a small Ordovician marginal basin. *In* Island arcs, deep sea trenches, and back-arc basins. *Edited by* M. Talwani and W.C. Pitman. Maurice Ewing Series, Volume 1, p. 407-418.
- Kidd, W.S.F., Dewey, J.F., and Bird, J.M. 1978. The Ming's Bight Ophiolite Complex, Newfoundland: Appalachian oceanic crust and mantle. *Canadian Journal of Earth Sciences*, **15**: 781-804.
- Kirkwood, D., and Dubé, B. 1992. Structural control of sill-hosted gold mineralization: the Stog'er Tight gold deposit, Baie Verte Peninsula, northwestern Newfoundland. *In* Current Research, Part D, Geological Survey of Canada, Paper 92-1D, p. 211-221.
- Kirkwood, D., and Malo, M. 1993. Across-strike geometry of the Grand Pabos fault zone: evidence for Devonian dextral transpression in the Quebec Appalachians. *Canadian Journal of Earth Sciences*, **30**: 1363-1373.
- Krogh, T.E. 1973. A low-contamination method for hydrothermal decomposition of zircon and extraction of U and Pb for isotopic age determinations. *Geochimica et Cosmochimica Acta*, **37**: 485-494.
- Kusky, T.M., Kidd, W.S.F., and Bradley, D.C. 1987. Displacement history of the Northern Arm Fault, and its bearing on the post-Taconic evolution of north-central Newfoundland. *Journal of Geodynamics*, **7**: 105-133.
- Lafrance, B. 1989. Structural evolution of a transpression zone in north central Newfoundland. *Journal of Structural Geology*, **11**: 705-716.
- Lafrance, B., and Williams, P.F. 1992. Silurian deformation in eastern Notre Dame Bay, Newfoundland. *Canadian Journal of Earth Sciences*, **29**: 1899-1914.

- Lagarde, J.L., Omar, S.A., and Roddaz, B. 1990. Structural characteristics of granitic plutons emplaced during weak regional deformation: examples from late Carboniferous plutons, Morocco. *Journal of Structural Geology*, **12**: 805-821.
- Lang, H.M. 1991. Quantitative interpretation of within-outcrop variation in metamorphic assemblage in staurolite-kyanite-grade metapelites, Baltimore, Maryland. *Canadian Mineralogist*, **29**: 655-671.
- Langdon, G.S., and Hall, J. 1994. Devonian-Carboniferous tectonics and basin deformation in the Cabot Strait area, Eastern Canada. *American Association of Petroleum Geologists Bulletin*, **78**: 1748-1774.
- Lee, J. 1995. Rapid uplift and rotation of mylonitic rocks from beneath a detachment fault: insights from potassium feldspar $^{40}\text{Ar}/^{39}\text{Ar}$ thermochronology, northern Snake Range, Nevada. *Tectonics*, **14**: 54-77.
- Lee, J., and Sutter, J.F. 1991. Incremental $^{40}\text{Ar}/^{39}\text{Ar}$ thermochronology of mylonitic rocks from the northern Snake Range, Nevada. *Tectonics*, **10**: 77-100.
- Lee, J., Miller, E.L., and Sutter, J.F. 1987. Ductile strain and metamorphism in an extensional tectonic setting: a case study from the northern Snake Range, Nevada, USA. In *Continental Extensional Tectonics*. Edited by M.P. Coward, J.F. Dewey, and P.L. Hancock. Geological Society of London Special Publication 28, p. 267-298.
- Lin, S. 1995. Structural evolution and tectonic significance of the Eastern Highlands shear zone in Cape Breton Island, the Canadian Appalachians. *Canadian Journal of Earth Sciences*, **32**: 545-554.
- Lin, S., and Williams, P.F. 1992. The geometrical relationship between the stretching lineation and the movement direction of shear zones. *Journal of Structural Geology*, **14**: 491-497.
- Lin, S., van Staal, C.R., and Dubé, B. 1994. Promontory-promontory collision in the Canadian Appalachians. *Geology*, **22**: 897-900.
- Lin, S., Jiang, D., and Williams, P.F. 1997. Strain geometry of transpressional shear zones: a new model based on an example from Cape Breton Island. *Canadian Tectonics Group, Abstracts*, p. 10.
- Lister, G.S., and Davis, G.A. 1989. The origin of metamorphic core complexes and detachment faults formed during Tertiary continental extension in the northern Colorado River region, U.S.A. *Journal of Structural Geology*, **11**: 65-94.

- Lister, G.S., and Snoke, A.W. 1984. S-C Mylonites. *Journal of Structural Geology*, **6**: 617-638.
- Lister, G.S., and Williams, P.F. 1983. The partitioning of deformation in flowing rock masses. *Tectonophysics*, **92**: 1-33.
- Lumpkin, G.R., Chakoumakos, B.C., and Ewing, R.C. 1986. Mineralogy and radiation effects of microlite from the Harding pegmatite, Taos County, New Mexico. *American Mineralogist*, **71**: 569-588.
- Lynch, G. 1996. Tectonic burial, thrust emplacement, and extensional exhumation of the Cabot nappe in the Appalachian hinterland of Cape Breton Island, Canada. *Tectonics*, **15**: 94-105.
- Lynch, G., and Giles, P.S. 1996. The Ainslie Detachment: a regional flat-lying extensional fault in the Carboniferous evaporitic Maritimes Basin of Nova Scotia, Canada. *Canadian Journal of Earth Sciences*, **33**: 169-181.
- Lynch, G., and Tremblay, C. 1994. Late Devonian-Carboniferous detachment faulting and extensional tectonics in western Cape Breton Island, Nova Scotia, Canada. *Tectonophysics*, **238**: 55-69.
- Maboko, M.A.H., McDougall, I., Zeitler, P.K., and Fitz Gerald, J.D. 1991. Discordant ^{40}Ar - ^{39}Ar ages from the Musgrave Ranges, central Australia: implications for the significance of hornblende ^{40}Ar - ^{39}Ar spectra. *Chemical Geology (Isotope Geoscience Section)*, **86**: 139-160.
- Mader, U.K., and Berman, R.G. 1992. Amphibole thermobarometry: a thermodynamic approach. *In Current Research, Part E, Geological Survey of Canada, Paper 92-1E*, p. 393-400.
- Malavieille, J. 1993. Late orogenic extension in mountain belts: insights from the Basin and Range and the late Paleozoic Variscan belt. *Tectonics*, **12**: 1115-1130.
- Malavieille, J. 1987. Extensional shearing deformation and kilometer-scale "a"-type folds in a Cordilleran metamorphic core complex (Raft River Mountains, Northwestern Utah). *Tectonics*, **6**: 423-448.
- Malo, M., and Kirkwood, D. 1995. Faulting and progressive strain history of the Gaspé Peninsula in Post-Taconian time: a review. *In Current Perspectives in the Appalachian-Caledonian Orogen. Edited by J.P. Hibbard, C.R. van Staal, and P.A. Cawood. Geological Association of Canada, Special Paper 41*, p. 267-282.

- Malo, M., Kirkwood, D., De Broucker, G., and St-Julien, P. 1992. A reevaluation of the position of the Baie Verte - Brompton Line in the Quebec Appalachians: the influence of Middle Devonian strike-slip faulting in Gaspé Peninsula. *Canadian Journal of Earth Sciences*, **29**: 1265-1273.
- Mancktelow, N.S., and Pavlis, T.L. 1994. Fold-fault relationships in low-angle detachment systems. *Tectonics*, **13**: 668-685.
- Marrett, R., and Allmendinger, R.W. 1990. Kinematic analysis of fault-slip data. *Journal of Structural Geology*, **12**: 973-986.
- Mattinson, J.M. 1975. Early Paleozoic ophiolite complexes of Newfoundland: isotopic ages of zircons. *Geology*, **3**: 181-183.
- Mattinson, J.M. 1977. U-Pb ages of some crystalline rocks from the Burlington Peninsula, Newfoundland, and implications for the age of Fleur de Lys metamorphism. *Canadian Journal of Earth Sciences*, **14**: 2316-2324.
- Mauthner, M.H.F., Mortensen, J.K., Groat, L.A., and Ercit, T.S. 1995. Geochronology of the Little Nahanni pegmatite goup, Selwyn Mountains, southwestern Northwest Territories. *Canadian Journal of Earth Sciences*, **32**: 2090-2097.
- Mawer, C.K., and Williams, P.F. 1991. Progressive folding and foliation development in a sheared, coticule-bearing phyllite. *Journal of Structural Geology*, **13**: 539-555.
- McDonald, L. 1993. Structure of the Dunamagon Granite, Baie Verte Peninsula, Newfoundland. B.Sc. thesis, Dalhousie University, Halifax, Nova Scotia.
- McMullin, D.W., Berman, R.G., and Greenwood, H.J. 1991. Calibration of the SGAM thermobarometer for pelitic rocks using data from phase equilibrium experiments and natural assemblages. *Canadian Mineralogist*, **29**: 889-908.
- Mezger, K., Hanson, G.N., and Bohlen, S.R. 1989. High-precision U-Pb ages of metamorphic rutile: application to the cooling history of high-grade terranes. *Earth and Planetary Science Letters*, **96**: 106-118.
- Mezger, K., Rawnsley, C.M., Bohlen, S.R., and Hanson, G.N. 1991. U-Pb garnet, sphene, monazite, and rutile ages: implications for the duration of high-grade metamorphism and cooling histories, Adirondack Mts., New York. *Journal of Geology*, **99**: 415-428.
- Mies, J.W. 1991. Planar dispersion of folds in ductile shear zones and kinematic interpretation of fold-hinge girdles. *Journal of Structural Geology*, **13**: 281-297.

- Miller, B.V., Dunning, G.R., Barr, S.M., Raeside, R.P., Jamieson, R.A., and Reynolds, P.H. 1996. Magmatism and metamorphism in a Grenvillian fragment: U-Pb and $^{40}\text{Ar}/^{39}\text{Ar}$ ages from the Blair River Complex, northern Cape Breton Island, Nova Scotia, Canada. *Geological Society of America Bulletin*, **108**: 127-140.
- Miller, H.G., and Wiseman, R. 1994. Potential field interpretation of the Baie Verte Peninsula, Newfoundland, utilizing constraints from Lithoprobe East Seismic line 89-13. *Atlantic Geology*, **30**: 25-36.
- Miller, H.G., Kilfoil, G.J., and Peavy, S.T. 1990. An integrated geophysical interpretation of the Carboniferous Bay St. George Subbasin, Western Newfoundland. *Bulletin of Canadian Petroleum Geology*, **38**: 320-331.
- Muecke, G.K., Elias, P., and Reynolds, P.H. 1988. Hercynian/Alleghanian overprinting of an Acadian terrane: $^{40}\text{Ar}/^{39}\text{Ar}$ studies in the Meguma Zone, Nova Scotia, Canada. *Chemical Geology (Isotope Geoscience Section)*, **73**: 153-167.
- Neale, E.R.W., and Kennedy, M.J. 1967. Relationship of the Fleur de Lys Group to younger groups of the Burlington Peninsula, Newfoundland. *In Geology of the Atlantic Region. Edited by E.R.W. Neale and H. Williams. Geological Association of Canada, Special Paper 4, p. 139-169.*
- Neale, E.R.W., Kean, B.F., and Upadhyay, H.D. 1975. Post-ophiolite unconformity, Tilt Cove - Betts Cove area, Newfoundland. *Canadian Journal of Earth Sciences*, **12**: 880-886.
- Norman, R.E., and Strong, D.F. 1975. The geology and geochemistry of ophiolitic rocks exposed at Ming's Bight, Newfoundland. *Canadian Journal of Earth Sciences*, **12**: 777-797.
- O'Brien, B.H., O'Brien, S.J., and Dunning, G.R. 1991. Silurian cover, Late Precambrian-Early Ordovician basement, and the chronology of Silurian orogenesis in the Hermitage Flexure (Newfoundland Appalachians). *American Journal of Science*, **291**: 760-799.
- O'Brien, B.H., O'Brien, S.J., Dunning, G.R., and Tucker, R.D. 1993. Episodic reactivation of a Late Precambrian mylonite zone on the Gondwanan margin of the Appalachians, southern Newfoundland. *Tectonics*, **12**: 1043-1055.
- O'Brien, B.H., Swinden, H.S., Dunning, G.R., Williams, S.H., and O'Brien, F.H.C. 1997. A Peri-Gondwanan arc-back arc complex in Iapetus: Early-Mid Ordovician evolution of the Exploits Group, Newfoundland. *American Journal of Science*, **297**: 220-272.

- O'Brien, S.J., Wardle, R.J., and King, A.F. 1983. The Avalon zone: a Pan-African terrane in the Appalachian orogen in Canada. *Geological Journal*, **18**: 185-222.
- Osmundsen, P.T., and Andersen, T.B. 1994. Caledonian compressional and late-orogenic extensional deformation in the Staveneset area, Sunnfjord, western Norway. *Journal of Structural Geology*, **16**: 1385-1401.
- Owen, J.V., and Erdmer, P. 1989. Metamorphic geology and regional geothermobarometry of a Grenvillians Massif. *Precambrian Research*, **43**: 79-100.
- Park, R.G. 1989. *Foundations of Structural Geology*. Chapman and Hall, New York.
- Park, A.F., Williams, P.F., Ralser, S., and Leger, A. 1994. Geometry and kinematics of a major crustal shear zone segment in the Appalachians of southern New Brunswick. *Canadian Journal of Earth Sciences*, **31**: 1523-1535.
- Parrish, R.R. 1990. U-Pb dating of monazite and its application to geological problems. *Canadian Journal of Earth Sciences*, **27**: 1431-1450.
- Parrish, R.R., Carr, S.D., and Parkinson, D.L. 1988. Eocene extensional tectonics and geochronology of the southern Omineca Belt, British Columbia and Washington. *Tectonics*, **7**: 181-212.
- Passchier, C.W. 1995. Non-simple shear zones. Geological Society of Australia, Clare Valley Conference Abstracts, Number 40, p.136.
- Passchier, C.W., Trouw, R.A.J., Zwart, H.J., and Vissers, R.L.M. 1992. Porphyroblast rotation: eppur si muove? *Journal of Metamorphic Geology*, **10**: 283-294.
- Paterson, S.R., and Tobisch, O.T. 1988. Using pluton ages to date regional deformations: problems with commonly used criteria. *Geology*, **16**: 1108-1111.
- Patey, K.S., and Wilton, D.H.C. 1993. The Deer Cove deposit, Baie Verte Peninsula, Newfoundland, a Paleozoic mesothermal lode-gold occurrence in the northern Appalachians. *Canadian Journal of Earth Sciences*, **30**: 1532-1546.
- Pearce, J.A., and Cann, J.R. 1973. Tectonic setting of basic volcanic rocks determined using trace element analysis. *Earth and Planetary Science Letters*, **19**: 290-300.
- Pearce, J.A., and Norry, M.J. 1979. Petrogenetic implications of Ti, Zr, Y, and Nb variations in volcanic rocks. *Contributions to Mineralogy and Petrology*, **69**: 33-47.

- Piasecki, M.A.J. 1988. Strain-induced mineral growth in ductile shear zones and a preliminary study of ductile shearing in western Newfoundland. *Canadian Journal of Earth Sciences*, **25**: 2118-2129.
- Piasecki, M.A.J. 1995. Dunnage Zone boundaries and some aspects of terrane development in Newfoundland. *In Current Perspectives in the Appalachian-Caledonian Orogen. Edited by J.P. Hibbard, C.R. van Staal, and P.A. Cawood. Geological Association of Canada, Special Paper 41, p. 323-347.*
- Piasecki, M.A.J., Williams, H., and Colman-Sadd, S.P. 1990. Tectonic relationships along the Meelpaeg, Burgeo and Burlington Lithoprobe transects in Newfoundland. *In Current Research, Newfoundland Department of Mines and Energy, Geological Survey Branch, Report 90-1, p. 327-339.*
- Platt, J.P., and Vissers, R.L.M. 1980. Extensional structures in anisotropic rocks. *Journal of Structural Geology*, **2**: 397-410.
- Poulsen, K.H., and Robert, F. 1989. Shear zones and gold: practical examples from the southern Canadian Shield. *In Mineralization and Shear Zones. Edited by J.T. Bursnall. Geological Association of Canada, Short Course Notes 6, p. 239-266.*
- Powell, C.McA., and Vernon, R.H. 1979. Growth and rotation history of garnet porphyroblasts with inclusion spirals in a Karakoram schist. *Tectonophysics*, **54**: 25-43.
- Pringle, J. 1978. Rb-Sr ages of silicic igneous rocks and deformation, Burlington Peninsula, Newfoundland. *Canadian Journal of Earth Sciences*, **15**: 293-300.
- Purdy, J.W., and Jager, E. 1976. K-Ar ages on rock-forming minerals from the Central Alps. *Memoirs, Institute of Geology and Mineralogy, University of Padova*, **30**: 1-31.
- Quinlan, G.M., Hall, J., Williams, H., Wright, J.A., Colman-Sadd, S.P., O'Brien, S.J., Stockmal, G.S., and Marillier, F. 1992. Lithoprobe onshore seismic reflection transects across the Newfoundland Appalachians. *Canadian Journal of Earth Sciences*, **29**: 1865-1877.
- Ramezani, J. 1992. The geology, geochemistry and U-Pb geochronology of the Stog'er Tight gold prospect, Baie Verte Peninsula, Newfoundland. M.Sc. thesis, Memorial University of Newfoundland, St. John's, Newfoundland.
- Ramsay, J.G. 1980. Shear zone geometry: a review. *Journal of Structural Geology*, **2**: 83-99.

- Reynolds, S.J., and Lister, G.S. 1987. Structural aspects of fluid-rock interactions in detachment zones. *Geology*, **15**: 362-366.
- Ridley, J. 1986. Parallel stretching lineations and fold axes oblique to a shear displacement direction—a model and observations. *Journal of Structural Geology*, **8**: 647-653.
- Ridley, J., and Casey, M. 1989. Numerical modeling of folding in rotational strain histories: strain regimes expected in thrust belts and shear zones. *Geology*, **17**: 875-878.
- Ritcey, D., and Ramezani, J. 1993. Nature and timing of mesothermal gold mineralization in western Newfoundland. *In Atlantic Geoscience Society, 1993 Colloquium and Symposia Abstracts. Atlantic Geology*, **29**: 94-95.
- Robert, F., Poulsen, K.H., and Dubé, B. 1994. Structural analysis of lode gold deposits in deformed terranes. Geological Survey of Canada, Open File 2850.
- Romer, R.L., and Smeds, S.-A. 1994. Implications of U-Pb ages of columbite-tantalites from granitic pegmatites for the Paleoproterozoic accretion of 1.90-1.85 Ga magmatic arcs to the Baltic Shield. *Precambrian Research*, **67**: 141-158.
- Romer, R.L., and Wright, J.E. 1992. U-Pb dating of columbites: a geochronologic tool to date magmatism and ore deposits. *Geochimica et Cosmochimica Acta*, **56**: 2137-2142.
- Rosenfeld, J.L. 1970. Rotated garnets in metamorphic rocks. Geological Society of America Special Paper 129.
- Samson, S.D., and Alexander, E.C., Jr. 1987. Calibration of the interlaboratory Ar/Ar dating standard, MMhb-1. *Chemical Geology*, **66**: 27-34.
- Sanderson, D.J., and Marchini, W.R.D. 1984. Transpression. *Journal of Structural Geology*, **6**: 449-458.
- Sawyer, E.W., and Robin, P.-Y.F. 1986. The subsolidus segregation of layer-parallel quartz-feldspar veins in greenschist to upper amphibolite facies metasediments. *Journal of Metamorphic Geology*, **4**: 237-260.
- Schoneveld, C. 1979. The geometry and significance of inclusion patterns in syntectonic porphyroblasts. Ph.D. Thesis, University of Leiden.
- Selverstone, J. 1985. Petrologic constraints on imbrication, metamorphism, and uplift in the SW Tauern Window, Eastern Alps. *Tectonics*, **4**: 687-704.

- Shervais, J.W. 1982. Ti-V plots and the petrogenesis of modern and ophiolitic lavas. *Earth and Planetary Science Letters*, **59**: 101-118.
- Sibson, R.H. 1977. Fault rocks and fault mechanisms. *Journal of the Geological Society, London*, **133**: 191-213.
- Skjerve, L. 1989. Tubular folds and sheath folds: definitions and conceptual models for their development, with examples from the Grapesvare area, northern Sweden. *Journal of Structural Geology*, **11**: 689-703.
- Sleep, N.H. 1979. A thermal constraint on the duration of folding with reference to Acadian geology, New England (USA). *Journal of Geology*, **87**: 583-589.
- Smith, H.A., and Barreiro, B. 1990. Monazite U-Pb dating of staurolite grade metamorphism in pelitic schists. *Contributions to Mineralogy and Petrology*, **105**: 602-615.
- Snoke, A.W., and Frost, B.R. 1990. Exhumation of high pressure pelitic schist, Lake Murray spillway, South Carolina: evidence for crustal extension during Alleghanian strike-slip faulting. *American Journal of Science*, **290**: 853-881.
- Soper, N.J., Strachan, R.A., Holdsworth, R.E., Gayer, R.A., and Greiling, R.O. 1992. Sinistral transpression and the Silurian closure of Iapetus. *Journal of the Geological Society, London*, **149**: 871-880.
- Spear, F.S., and Cheney, J.T. 1989. A petrogenetic grid for pelitic schists in the system $\text{SiO}_2\text{-Al}_2\text{O}_3\text{-FeO-MgO-K}_2\text{O-H}_2\text{O}$. *Contributions to Mineralogy and Petrology*, **101**: 149-164.
- Srivastava, D.C., Lisle, R.J., and VanDyke, S. 1995. Shear zones as a new type of palaeostress indicator. *Journal of Structural Geology*, **17**: 663-676.
- Stacey, J.S., and Kramers, J.D. 1975. Approximation of terrestrial lead isotope evolution by a two-stage model. *Earth and Planetary Science Letters*, **26**: 207-221.
- Steinhardt, C. 1989. Lack of porphyroblast rotation in noncoaxially deformed schists from Petrel Cove, South Australia, and its implications. *Tectonophysics*, **158**: 127-140.
- Stevens, R.K. 1970. Cambro-Ordovician flysch sedimentation and tectonics in west Newfoundland and their possible bearing on a proto-Atlantic Ocean. *Geological Association of Canada, Special Paper 7*, p.165-177.

- Stockmal, G.S., and Waldron, J.W.F. 1990. Structure of the Appalachian deformation front in western Newfoundland: implications of multichannel seismic reflection data. *Geology*, **18**: 765-768.
- Stockmal, G.S., Colman-Sadd, S.P., Keen, C.E., O'Brien, S.J., and Quinlan, G. 1987. Collision along an irregular margin: a regional plate tectonic interpretation of the Canadian Appalachians. *Canadian Journal of Earth Sciences*, **24**: 1098-1107.
- Stockmal, G.S., Colman-Sadd, S.P., Keen, C.E., Marillier, F., O'Brien, S.J., and Quinlan, G.M. 1990. Deep seismic structure and plate tectonic evolution of the Canadian Appalachians. *Tectonics*, **9**: 45-62.
- Strachan, R.A., Chadwick, B., Friend, C.R.L., and Holdsworth, R.E. 1995. New perspectives on the Caledonian orogeny in northeast Greenland. *In Current Perspectives in the Appalachian-Caledonian Orogen. Edited by J.P. Hibbard, C.R. van Staal, and P.A. Cawood. Geological Association of Canada, Special Paper 41, p. 303-322.*
- Strong, D.F., Dickson, W.L., O'Driscoll, C.F., Kean, B.F., and Stevens, R.K. 1974. Geochemical evidence for eastward subduction in Newfoundland. *Nature*, **248**: 37-39.
- Stukas, V., and Reynolds, P.H. 1974. $^{40}\text{Ar}/^{39}\text{Ar}$ dating of the Long Range dikes, Newfoundland. *Earth and Planetary Science Letters*, **22**: 256-266.
- Suhr, G., and Cawood, P.A. 1993. Structural history of ophiolite obduction, Bay of Islands, Newfoundland. *Geological Society of America Bulletin*, **105**: 399-410.
- Swanson, M.T. 1988. Pseudotachylyte-bearing strike-slip duplex structures in the Fort Foster Brittle Zone, S. Maine. *Journal of Structural Geology*, **10**: 813-828.
- Swinden, H.S., Jenner, G.A., Kean, B.F., and Evans, D.T.W. 1989. Volcanic rock geochemistry as a guide for massive sulphide exploration in central Newfoundland. *In Current Research, Newfoundland Department of Mines, Geological Survey of Newfoundland, Report 89-1, p. 201-219.*
- Swinden, H.S., Jenner, G.A., Fryer, B.J., Hertogen, J., and Roddick, J.C. 1990. Petrogenesis and paleotectonic history of the Wild Bight Group, an Ordovician rifted island arc in central Newfoundland. *Contributions to Mineralogy and Petrology*, **105**: 219-241.
- Tapponnier, P., Peitzer, G., Le Dain, A.Y., Armijo, R., and Cobbold, P. 1982. Propagating extrusion tectonics in Asia: new insights from simple experiments with plasticine. *Geology*, **10**: 611-616.

- Teyssier, C., Kleinspehn, K., and Pershing, J. 1995. Analysis of fault populations in western Spitsbergen: Implications for deformation partitioning along transform margins. *Geological Society of America Bulletin*, **107**: 68-82.
- Thompson, A.B. 1982. Dehydration melting of pelitic rocks and the generation of H₂O-undersaturated granitic liquids. *American Journal of Science*, **282**: 1567-1595.
- Thompson, A.B., and England, P.C. 1984. Pressure-temperature-time paths of regional metamorphism II. Their inference and interpretation using mineral assemblages in metamorphic rocks. *Journal of Petrology*, **25**: 929-955.
- Tobisch, O.T., and Paterson, S.R. 1988. Analysis and interpretation of composite foliations in areas of progressive deformation. *Journal of Structural Geology*, **10**: 745-754.
- Tracy, R.J. 1982. Compositional zoning and inclusions in metamorphic minerals. *In* Characterization of Metamorphism through Mineral Equilibria. *Edited by* J.M. Ferry. *Reviews in Mineralogy*, **10**: 355-397.
- Tuach, J. 1976. Structural and stratigraphic setting of the Ming and other sulfide deposits in the Rambler area, Newfoundland. M.Sc. thesis, Memorial University of Newfoundland, St. John's, Newfoundland.
- Tuach, J., and Kennedy, M.J. 1978. The geologic setting of the Ming and other sulfide deposits, Consolidated Rambler Mines, northeast Newfoundland. *Economic Geology*, **73**: 192-206.
- Tuach, J., Dean, P.L., Swinden, H.S., O'Driscoll, C.F., Kean, B.F., and Evans, D.T.W. 1988. Gold mineralization in Newfoundland: A 1988 review. *In* Current Research, Newfoundland Department of Mines, Mineral Development Division, Report 88-1, p. 279-306.
- Tucker, R.D., and McKerrow, W.S. 1995. Early Paleozoic chronology: a review in light of new U-Pb zircon ages from Newfoundland and Britain. *Canadian Journal of Earth Sciences*, **32**: 368-379.
- Tucker, R.D., Raheim, A., Krogh, T.E., and Corfu, F. 1987. Uranium-lead zircon and titanite ages from the northern portion of the Western Gneiss Region, south-central Norway. *Earth and Planetary Science Letters*, **81**: 203-211.
- Upadhyay, H.D. 1973. The Bett's Cove ophiolite and related rocks of the Snooks Arm Group, Newfoundland. Ph.D. Thesis, Memorial University of Newfoundland, St. John's, Newfoundland.

- Vance, D., and O'Nions, R.K. 1990. Isotopic chronometry of zoned garnets: growth kinetics and metamorphic histories. *Earth and Planetary Science Letters*, **97**: 227-240.
- van der Pluijm, B.A. 1987. Timing and spatial distribution of deformation in the Newfoundland Appalachians: a "multi-stage collision" history. *Tectonophysics*, **135**: 15-24.
- van der Pluijm, B.A., and van Staal, C.R. 1988. Characteristics and evolution of the central mobile belt, Canadian Appalachians. *Journal of Geology*, **96**: 535-547.
- van der Pluijm, B.A., Johnson, R.J.E., and Van der Voo, R. 1993. Paleogeography, accretionary history, and tectonic scenario: a working hypothesis for the Ordovician and Silurian evolution of the northern Appalachians. *In The Acadian Orogeny: recent studies in New England, Maritime Canada, and the autochthonous foreland. Edited by D.C. Roy and J.W. Skehan. Geological Society of America Special Paper 275, p. 27-40.*
- van Staal, C.R. 1994. Brunswick subduction complex in the Canadian Appalachians: Record of the Late Ordovician to Late Silurian collision between Laurentia and the Gander margin of Avalon. *Tectonics*, **13**: 946-962.
- van Staal, C.R., and de Roo, J.A. 1995. Mid-Paleozoic tectonic evolution of the Appalachian central mobile belt in northern New Brunswick, Canada: collision, extensional collapse and dextral transpression. *In Current Perspectives in the Appalachian-Caledonian Orogen. Edited by J.P. Hibbard, C.R. van Staal, and P.A. Cawood. Geological Association of Canada, Special Paper 41, p. 367-389.*
- van Staal, C.R., and Williams, P.F. 1984. Structure, origin and concentration of the Brunswick No. 12 and No. 6 orebodies. *Economic Geology*, **79**: 1669-1692.
- Vauchez, A., Babaie, H.A., and Babaei, A. 1993. Orogen-parallel tangential motion in the Late Devonian - Early Carboniferous southern Appalachians internides. *Canadian Journal of Earth Sciences*, **30**: 1297-1305.
- Vauchez, A., Tommasi, A., and Egydio-Silva, M. 1994. Self-indentation of a heterogeneous continental lithosphere. *Geology*, **22**: 967-970.
- Vernon, R.H. 1977. Relationships between microstructures and metamorphic assemblages. *Tectonophysics*, **39**: 439-452.
- Vernon, R.H. 1989. Evidence of syndeformational contact metamorphism from porphyroblast-matrix microstructural relationships. *Tectonophysics*, **158**: 113-126.

- Vernon, R.H., Paterson, S.R., and Foster, D. 1993. Growth and deformation of porphyroblasts in the Foothills terrane, central Sierra Nevada, California: negotiating a microstructural minefield. *Journal of Metamorphic Geology*, **11**: 203-222.
- Vilotte, J.-P., Mandariaga, R., Daignieres, M., and Zienkiewicz, O. 1984. The role of a heterogeneous inclusion during continental collision. *Physics of the Earth and Planetary Interiors*, **36**: 236-259.
- Waldron, J.W.F., and Milne, J.V. 1991. Tectonic history of the central Humber Zone, western Newfoundland Appalachians: post-Taconian deformation in the Old Man's Pond area. *Canadian Journal of Earth Sciences*, **28**: 398-410.
- Waldron, J.W.F., and Stockmal, G.S. 1991. Mid-Paleozoic thrusting at the Appalachian deformation front: Port au Port Peninsula, western Newfoundland. *Canadian Journal of Earth Sciences*, **28**: 1992-2002.
- Waldron, J.W.F., and Stockmal, G.S. 1994. Structural and tectonic evolution of the Humber Zone, western Newfoundland 2. A regional model for Acadian thrust tectonics. *Tectonics*, **13**: 1498-1513.
- Watson, K.de P. 1947. Geology and mineral deposits of the Baie Verte - Ming's Bight area, Newfoundland. Geological Survey of Newfoundland, Bulletin 21.
- Wernicke, B. 1992. Cenozoic extensional tectonics of the U.S. Cordillera. *In The Cordilleran Orogen: Conterminous U.S. Edited by B.C. Burchfiel, P.W. Lipman and M.L. Zoback. The Geological Society of America, The Geology of North America, v. G-3, p. 553-581.*
- Wernicke, B. 1985. Uniform-sense normal simple shear of the continental lithosphere. *Canadian Journal of Earth Sciences*, **22**: 108-125.
- Wernicke, B., and Axen, G.J. 1988. On the role of isostasy in the evolution of normal fault systems. *Geology*, **16**: 848-851.
- White, S.H., Burrows, S.E., Carreras, J., Shaw, N.D., and Humphreys, F.J. 1980. On mylonites in ductile shear zones. *Journal of Structural Geology*, **2**: 175-187.
- Williams, H. 1964. The Appalachians in northeastern Newfoundland - a two sided symmetrical system. *American Journal of Science*, **262**: 1137-1158.
- Williams, H. 1977. Ophiolitic melange and its significance in the Fleur de Lys Supergroup, northern Appalachians. *Canadian Journal of Earth Sciences*, **14**: 987-1003.

- Williams, H. 1979. Appalachian Orogen in Canada. *Canadian Journal of Earth Sciences*, **16**: 792-807.
- Williams, H. 1993. Acadian Orogeny in Newfoundland. *In The Acadian Orogeny: recent studies in New England, Maritime Canada, and the autochthonous foreland. Edited by D.C. Roy and J.W. Skehan. Geological Society of America Special Paper 275.* p. 123-133.
- Williams, H., and Hatcher, R.D., Jr. 1982. Suspect terranes and accretionary history of the Appalachian orogen. *Geology*, **10**: 530-536.
- Williams, H., and St. Julien, P. 1982. The Baie Verte - Brompton Line: Early Paleozoic continent-ocean interface in the Canadian Appalachians. *In Major structural zones and faults in the northern Appalachians. Edited by P. St. Julien and J. Beland. Geological Association of Canada Special Paper 24.* p. 177-207.
- Williams, H., Colman-Sadd, S.P., and Swinden, H.S. 1988. Tectonic-stratigraphic subdivisions of central Newfoundland. *In Current Research, Part B, Geological Survey of Canada, Paper 88-1B.* p. 91-98.
- Williams, P.F. 1985. Multiply deformed terranes-problems of correlation. *Journal of Structural Geology*, **7**: 269-280.
- Williams, P.F., Goodwin, L.B., and LaFrance, B. 1995. Brittle faulting in the Canadian Appalachians and the interpretation of reflection seismic data. *Journal of Structural Geology*, **17**: 215-232.
- Williams, S.H. 1992. Lower Ordovician (Arenig - Llanvirn) graptolites from the Notre Dame Subzone, central Newfoundland. *Canadian Journal of Earth Sciences*, **29**: 1717-1733.
- Williams, S.H., Boyce, W.D., Colman-Sadd, S.P. 1992. A new Lower Ordovician (Arenig) faunule from the Coy Pond Complex, central Newfoundland, and a refined understanding of the closure of the Iapetus ocean. *Canadian Journal of Earth Sciences*, **29**: 2046-2057.
- Wilson, J.T. 1966. Did the Atlantic close and then re-open? *Nature*, **211**: 676-681.
- Winchester, J.A., and Floyd, P.A. 1977. Geochemical discrimination of different magma series and their differentiation products using immobile elements. *Chemical Geology*, **20**: 325-343.

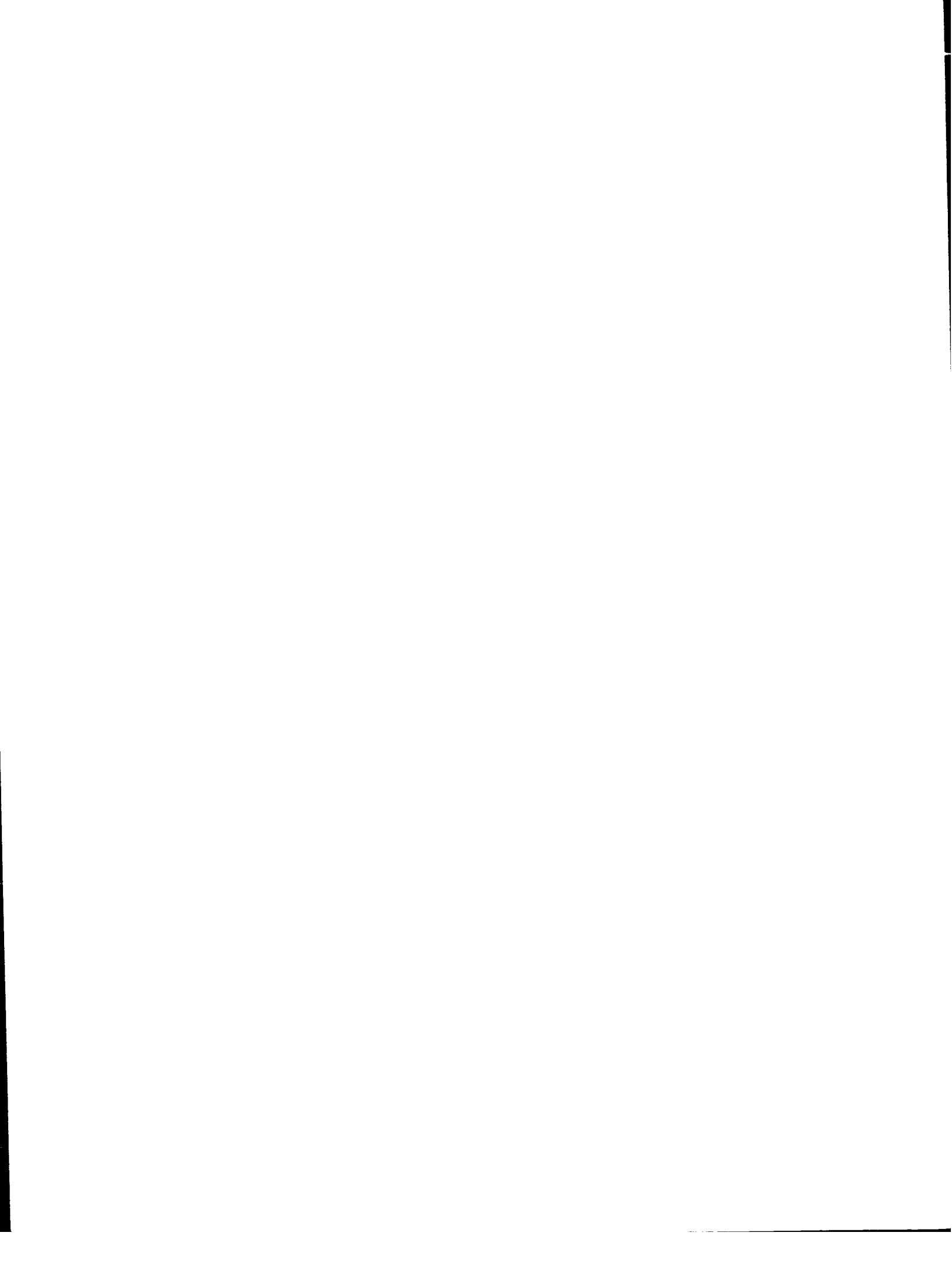
- Woodsworth, G.J. 1977. Homogenization of zoned garnets from pelitic schists. *Canadian Mineralogist*, **15**: 230-242.
- Yardley, B.W.D. 1977. An empirical study of diffusion in garnet. *American Mineralogist*, **62**: 793-800.
- Yardley, B.W.D. 1989. *An Introduction to Metamorphic Petrology*. Longman Scientific & Technical, Essex.

NOTE TO USERS

Oversize maps and charts are microfilmed in sections in the following manner:

**LEFT TO RIGHT, TOP TO BOTTOM, WITH
SMALL OVERLAPS**

UMI



Bois Island

Red Point Pegmatite

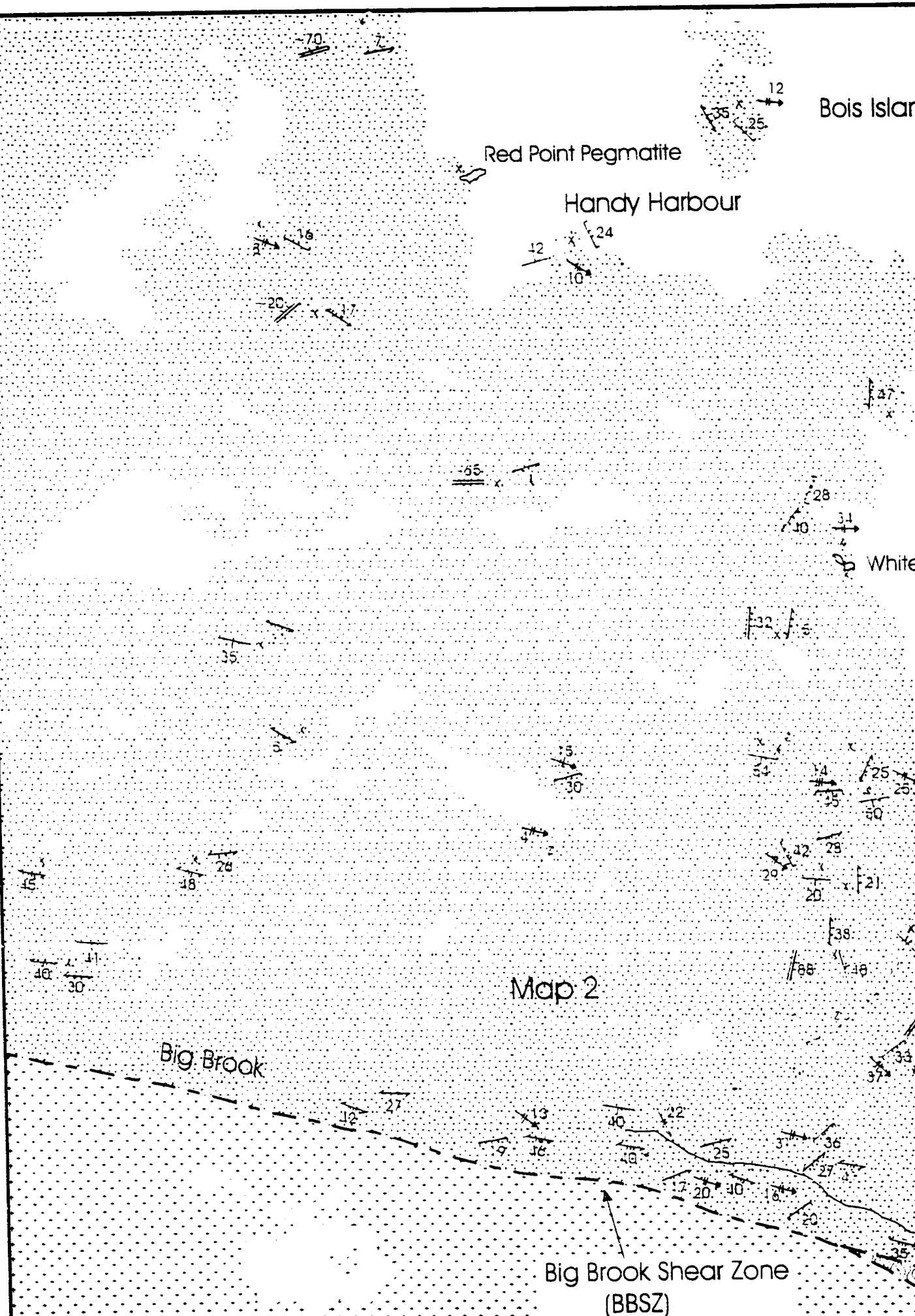
Handy Harbour

White

Map 2

Big Brook

Big Brook Shear Zone
(BBSZ)



Map 1

N

Bois Islands



White Point Pegmatite

Atlantic Ocean

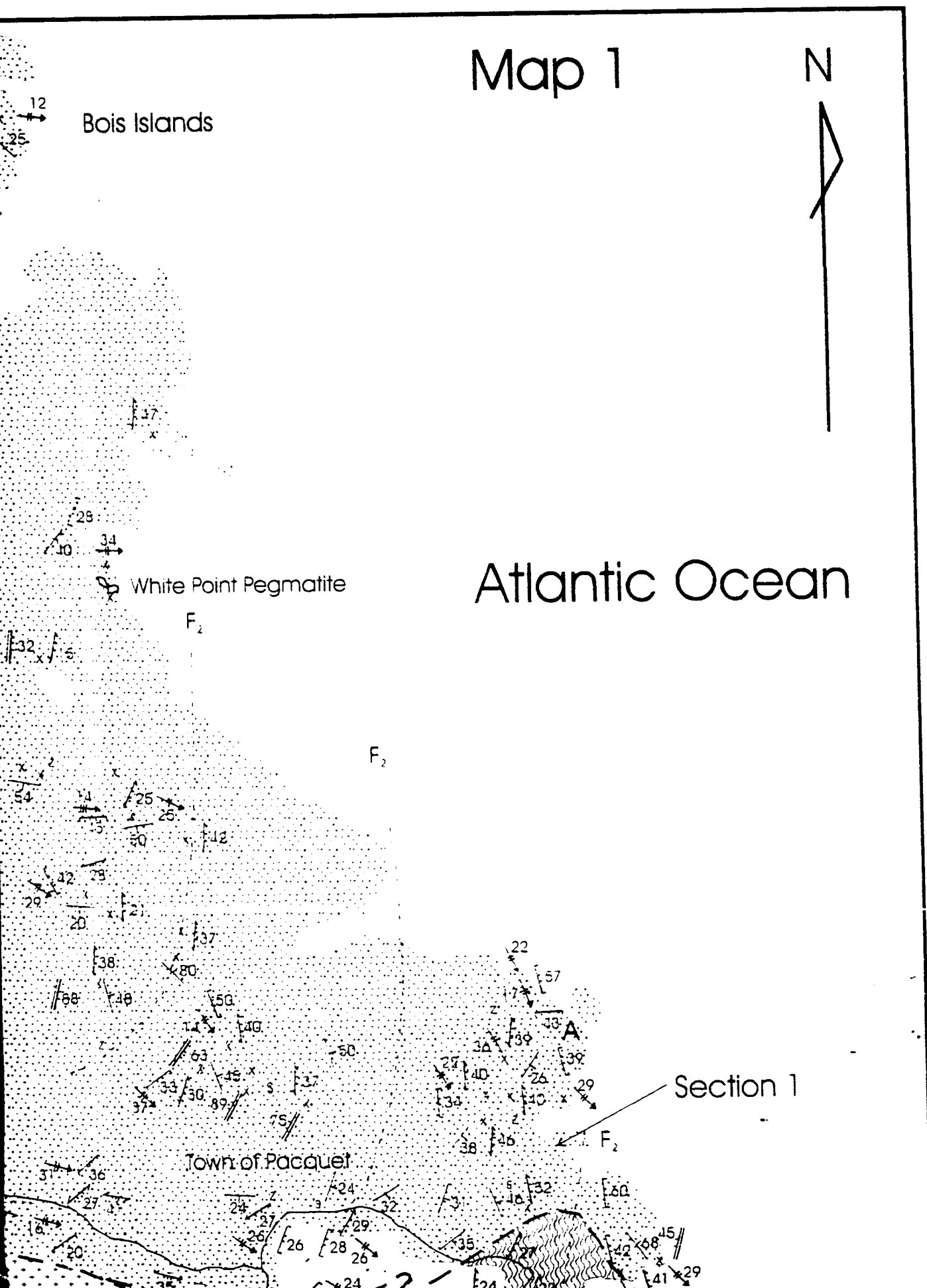
F₂

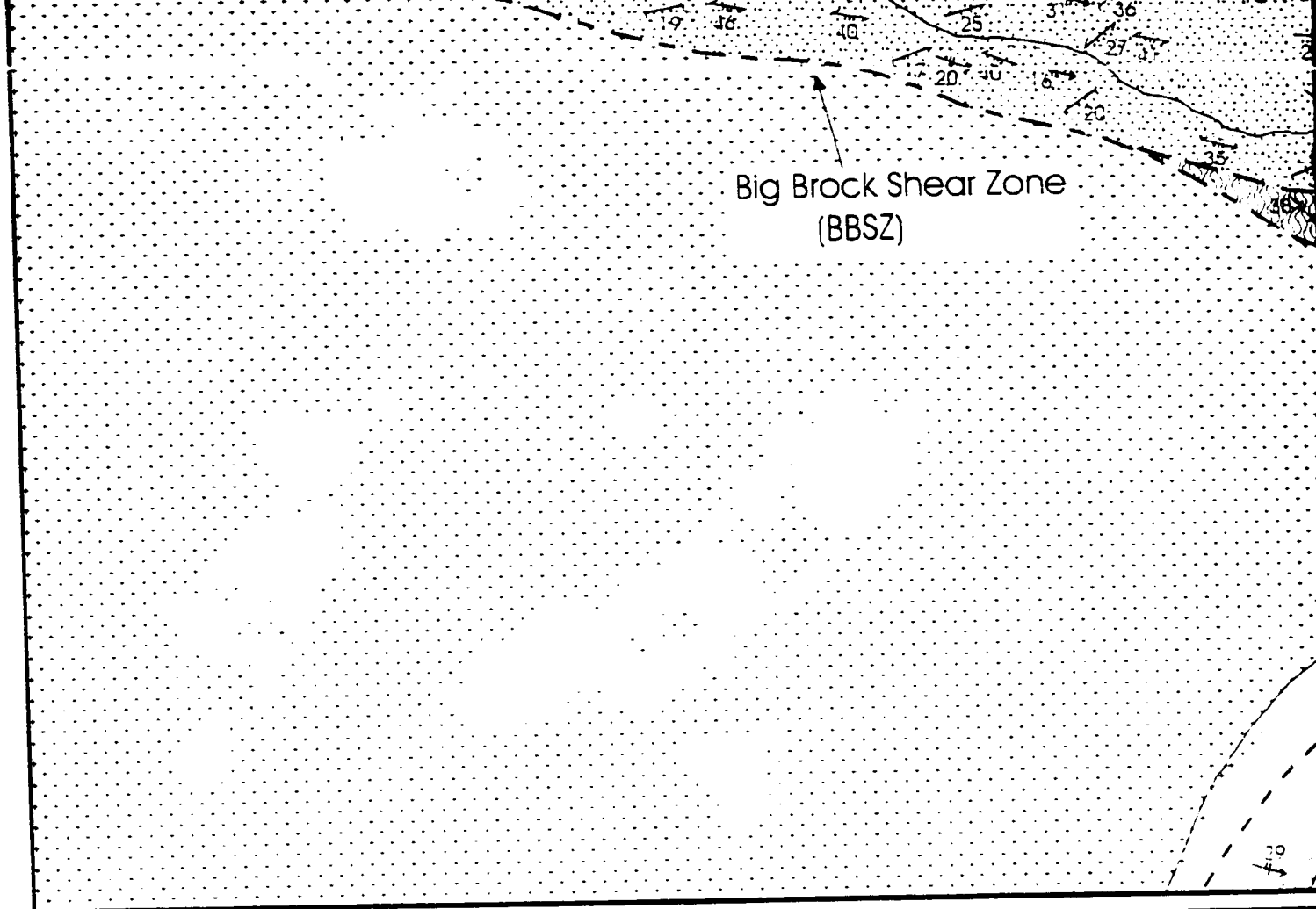
F₂

Section 1

Town of Pacquet

F₂





Pelee Point Shear Zone (PPSZ)

- strongly deformed MBG schist and PHG amphibolite

Dunamagon Granite

- minor mafic dykes

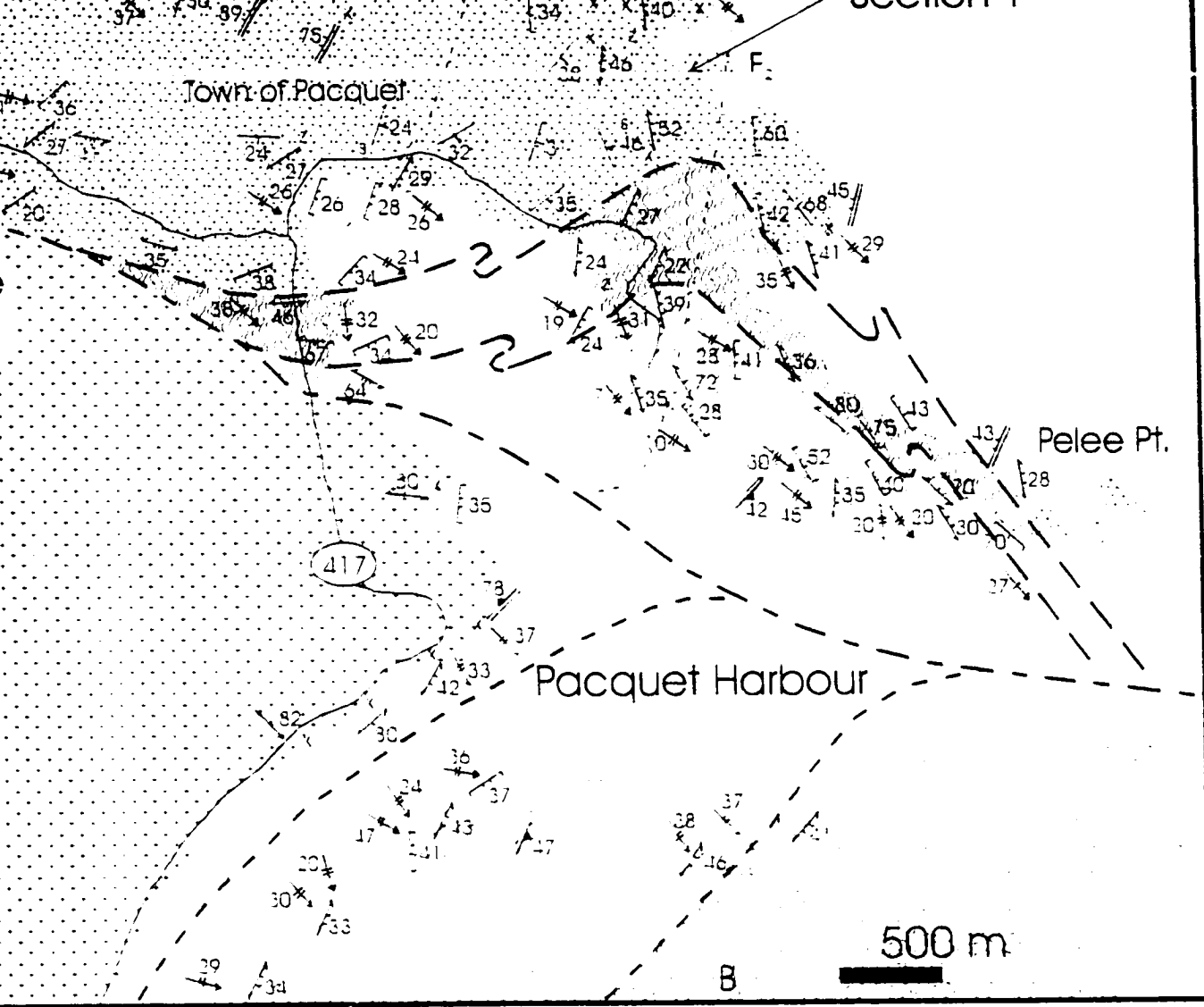
Cape Brule Porphyry

Pacquet Harbour Group

- pillowed basalt; gabbro; mafic epiclastic rocks;
minor mafic and granitic dykes



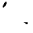





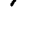

Ming's Bight Group

- psammitic and semi-pelitic schist;
minor granitic pegmatites



amphibolite

lastic rocks.

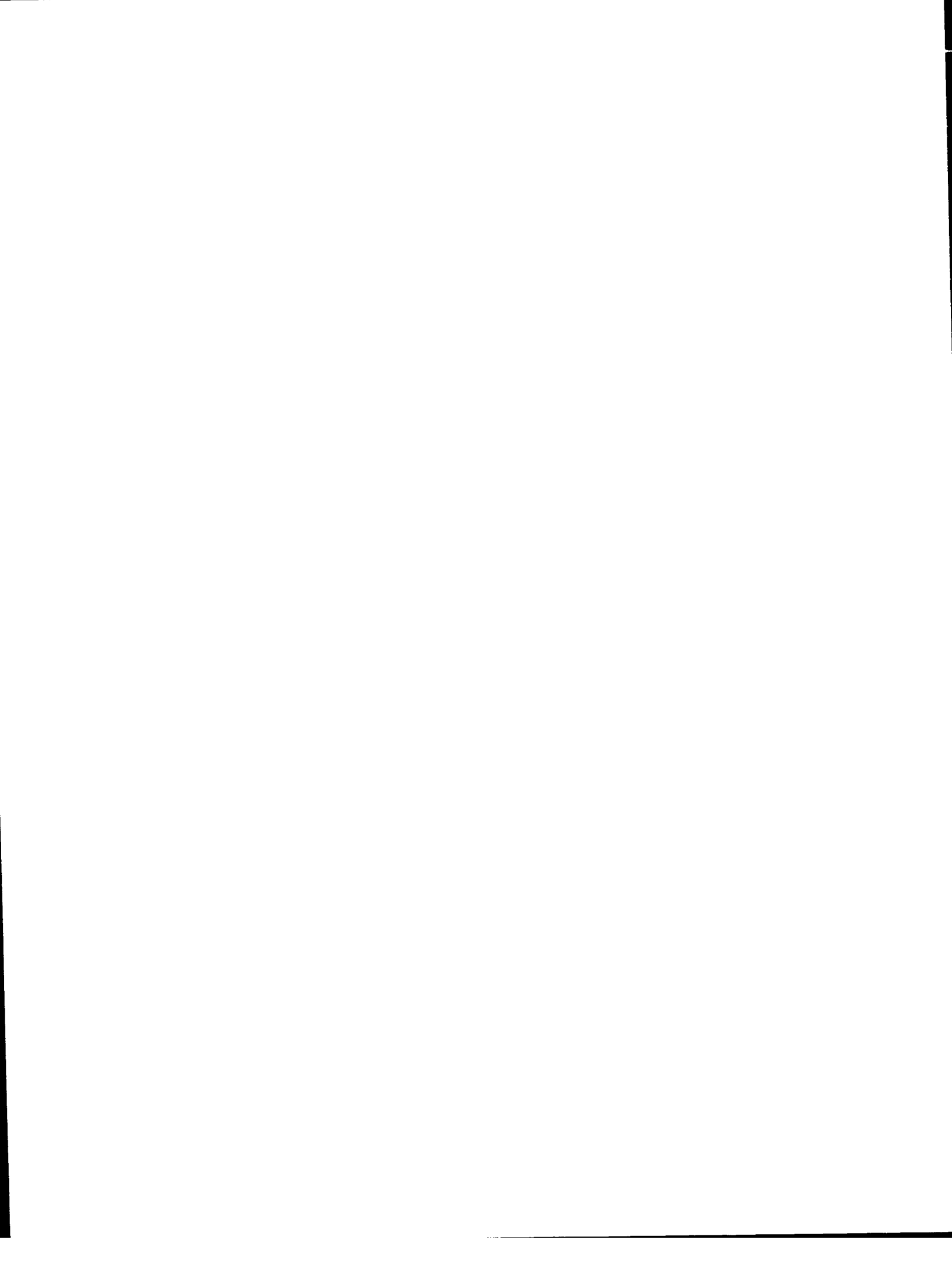
-  MBG layering
-  Foliation (S1, S2; S3)
-  Fold axial Plane (F1; F2; F3)
-  Fold axis (F1; F2; F3)
-  L2 lineation (mineral; stretching)
-  Mafic dyke
-  Granitic pegmatite
-  Station location
-  Shear zone (D1; D2; D3)
-  Approximate large-scale F2 axial plane trace

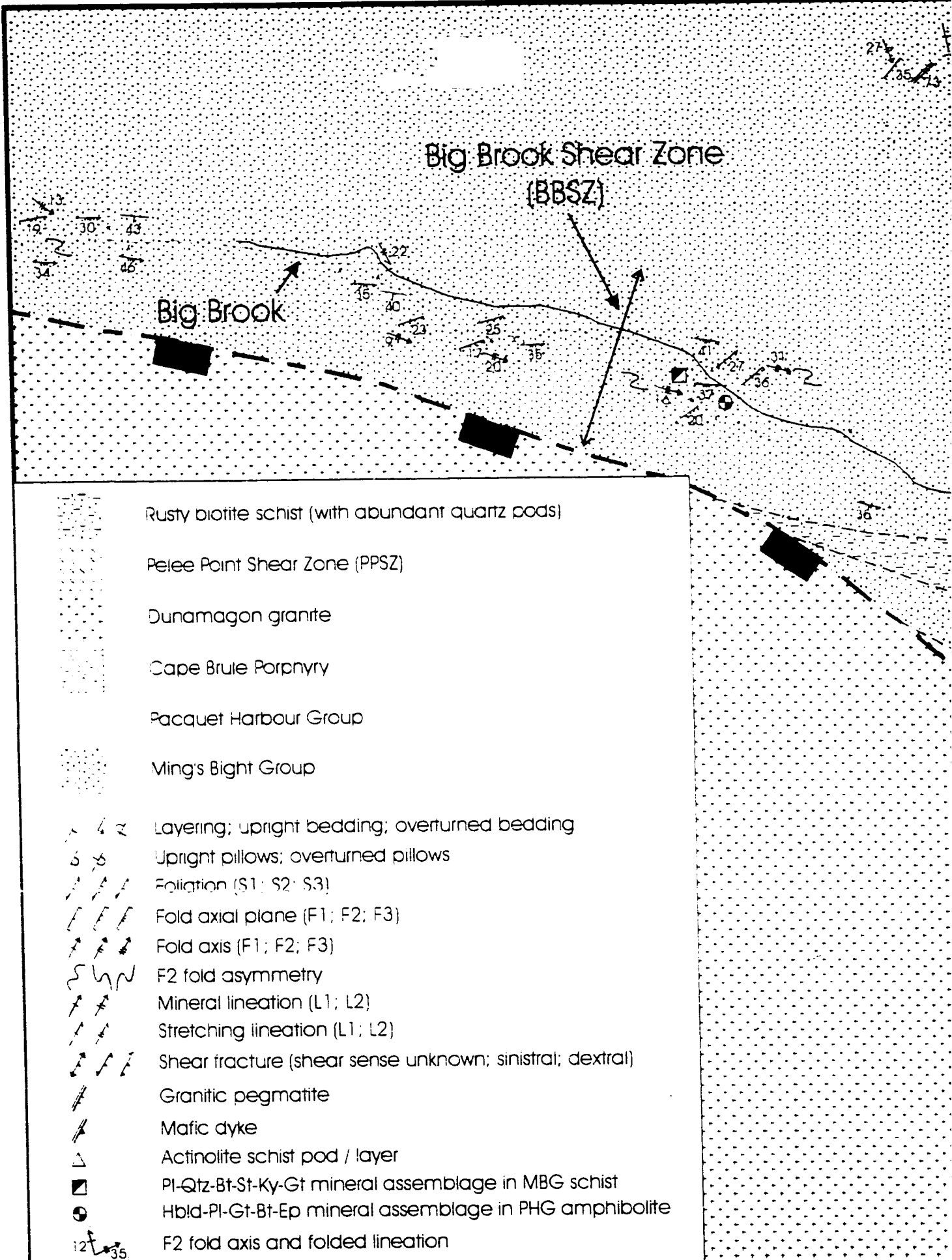
NOTE TO USERS

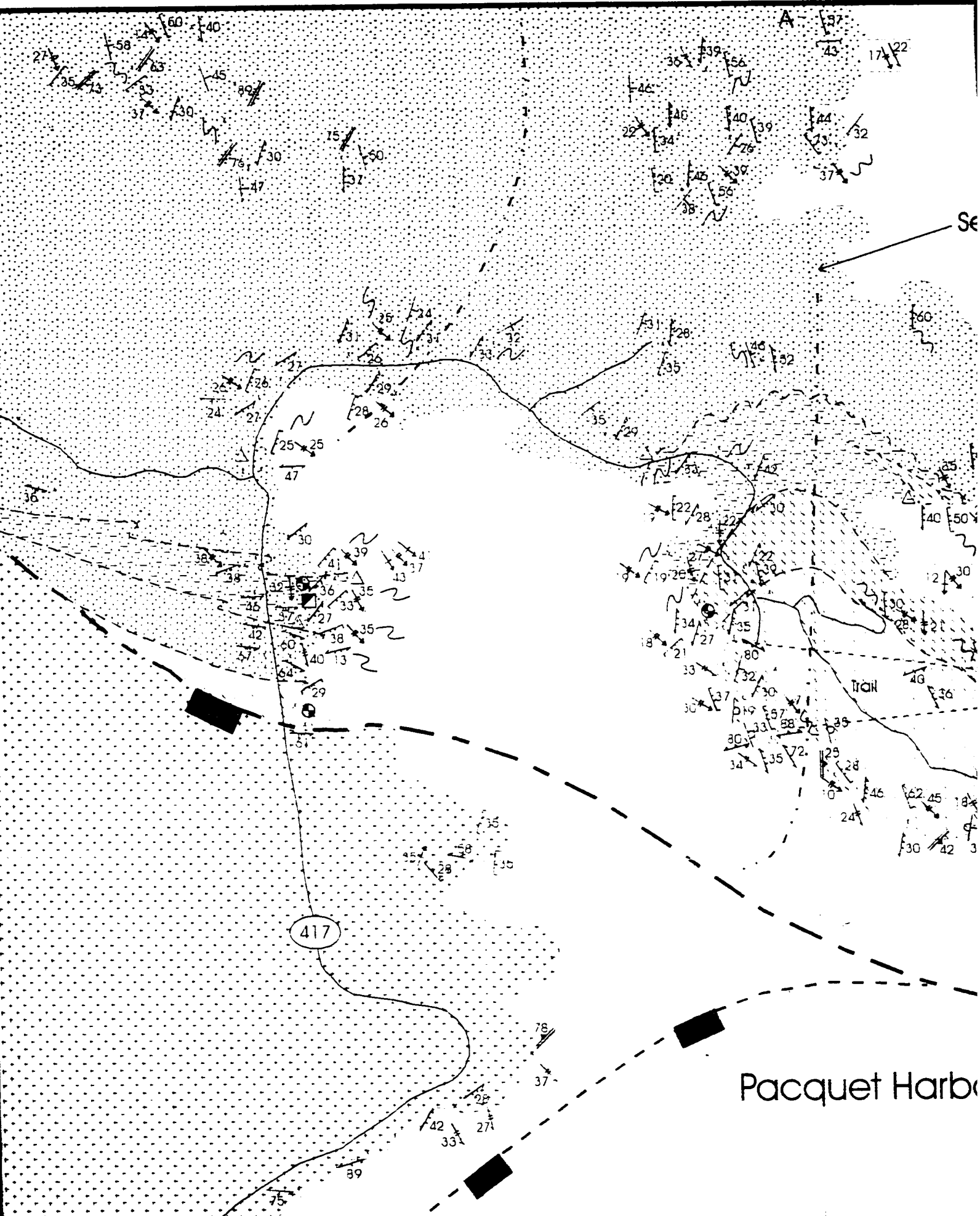
Oversize maps and charts are microfilmed in sections in the following manner:

**LEFT TO RIGHT, TOP TO BOTTOM, WITH
SMALL OVERLAPS**

UMI







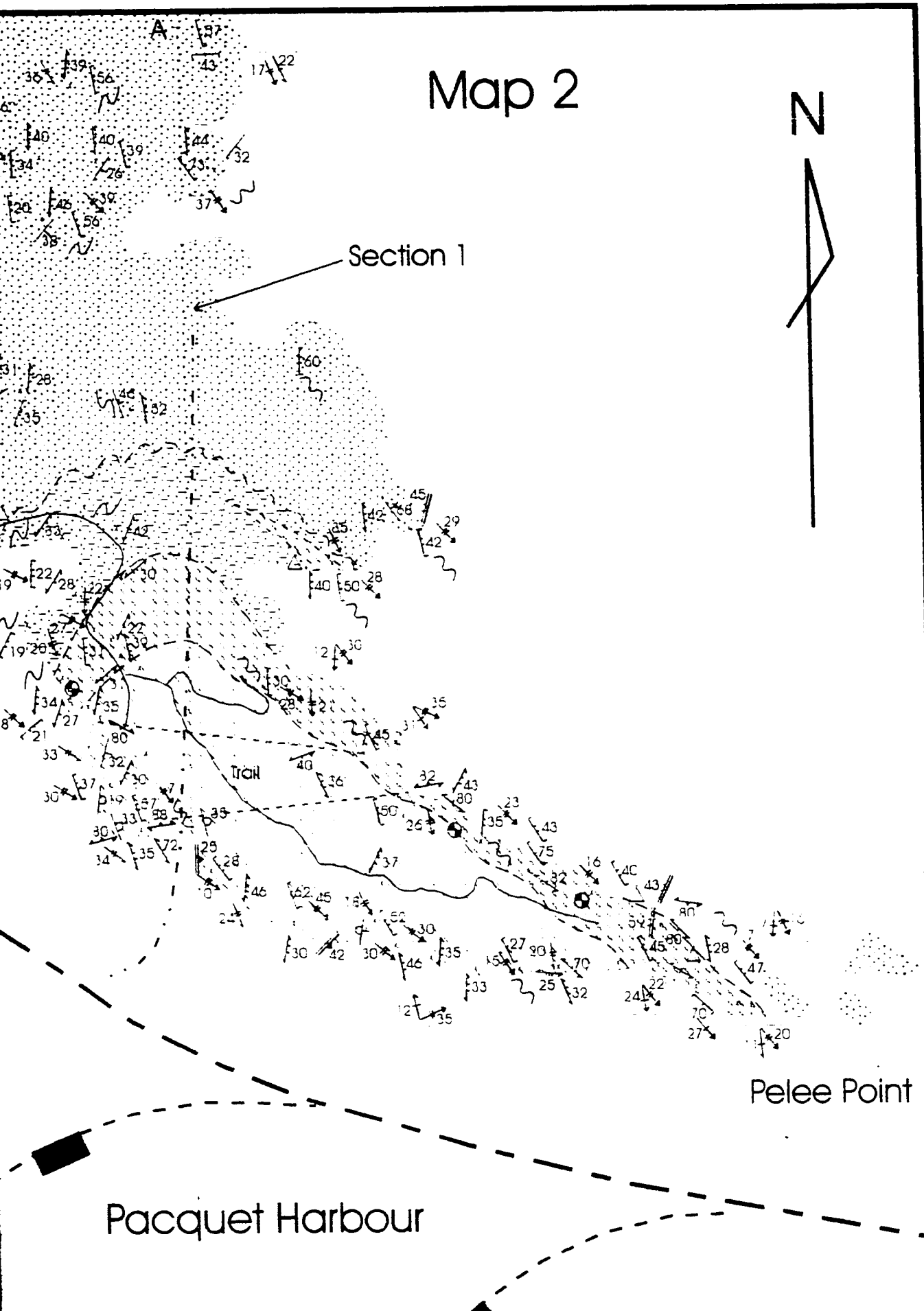
Pacquet Harbor

Map 2

N


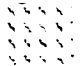






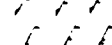

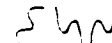
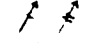






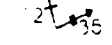

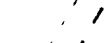



Section 1



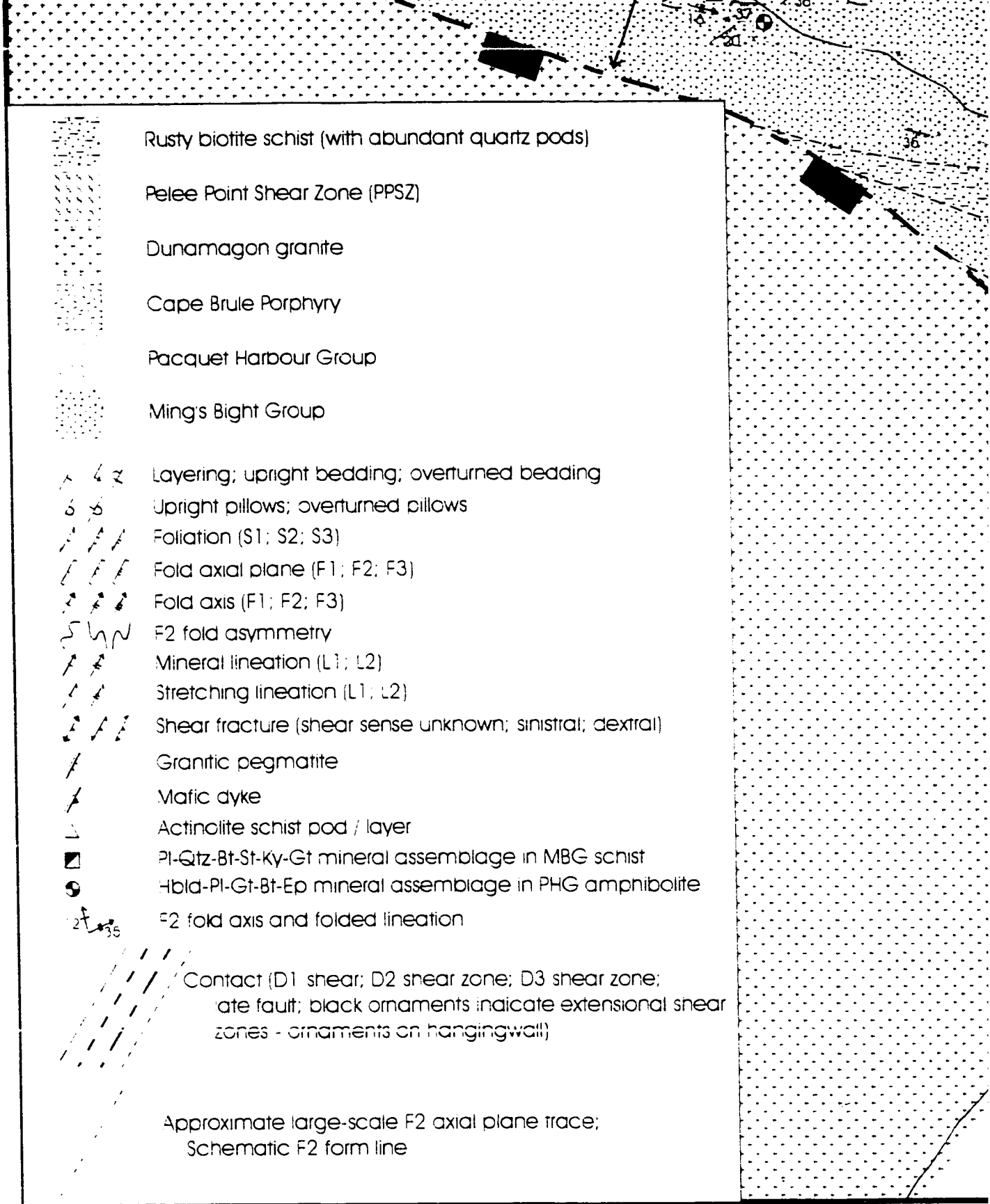
Pelee Point

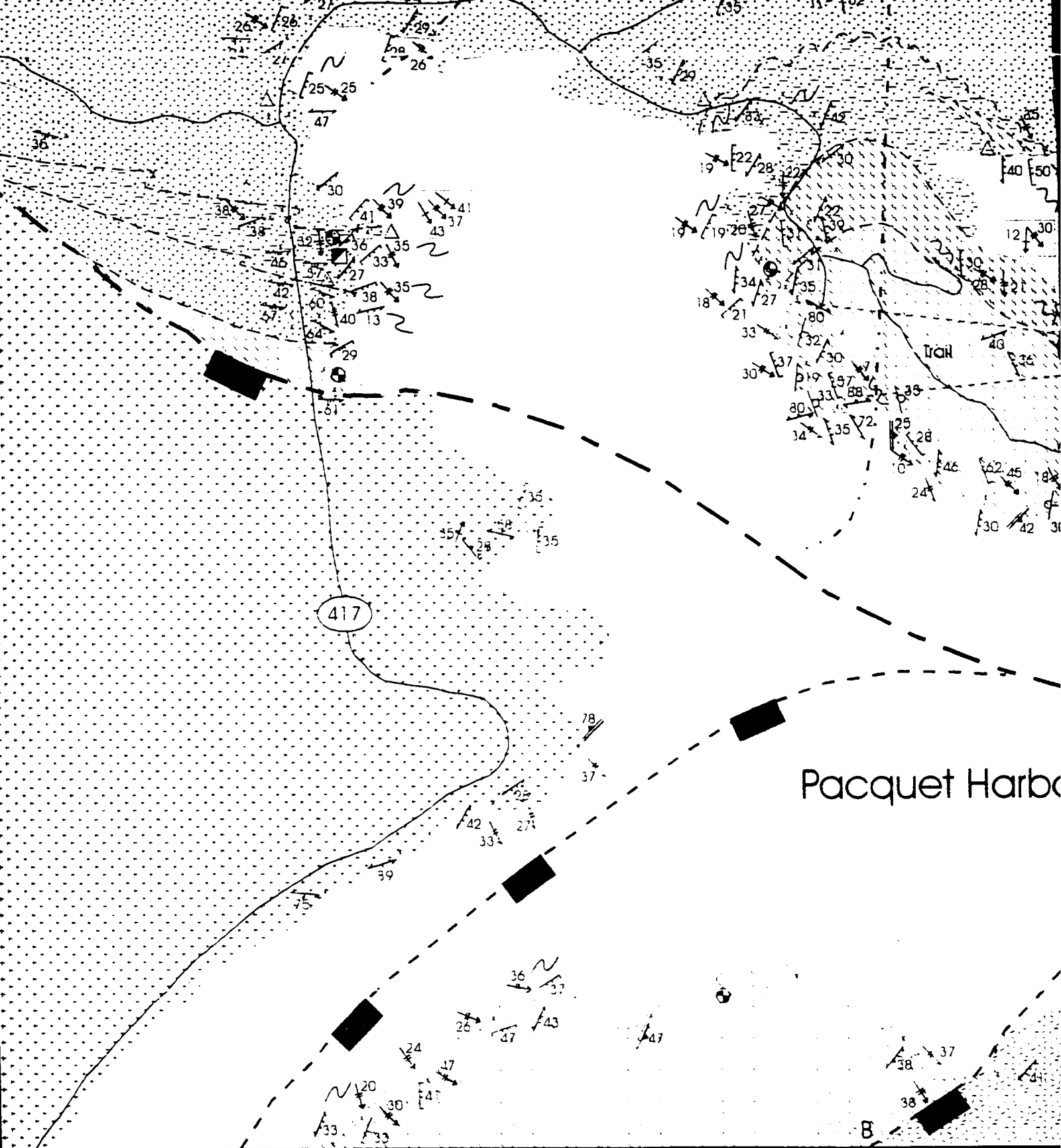
Pacquet Harbour

-  Rusty biotite schist (with abundant quartz pods)
-  Pelee Point Shear Zone (PPSZ)
-  Dunamagon granite
-  Cape Brule Porphyry
-  Pacquet Harbour Group
-  Mings Bight Group
-  Layering; upright bedding; overturned bedding
-  Upright pillows; overturned pillows
-  Foliation (S1; S2; S3)
-  Fold axial plane (F1; F2; F3)
-  Fold axis (F1; F2; F3)
-  F2 fold asymmetry
-  Mineral lineation (L1; L2)
-  Stretching lineation (L1; L2)
-  Shear fracture (shear sense unknown; sinistral; dextral)
-  Granitic pegmatite
-  Mafic dyke
-  Actinolite schist pod / layer
-  Pl-Qtz-Bt-St-Ky-Gt mineral assemblage in MBG schist
-  Hbl-d-Pl-Gt-Bt-Ep mineral assemblage in PHG amphibolite
-  F2 fold axis and folded lineation

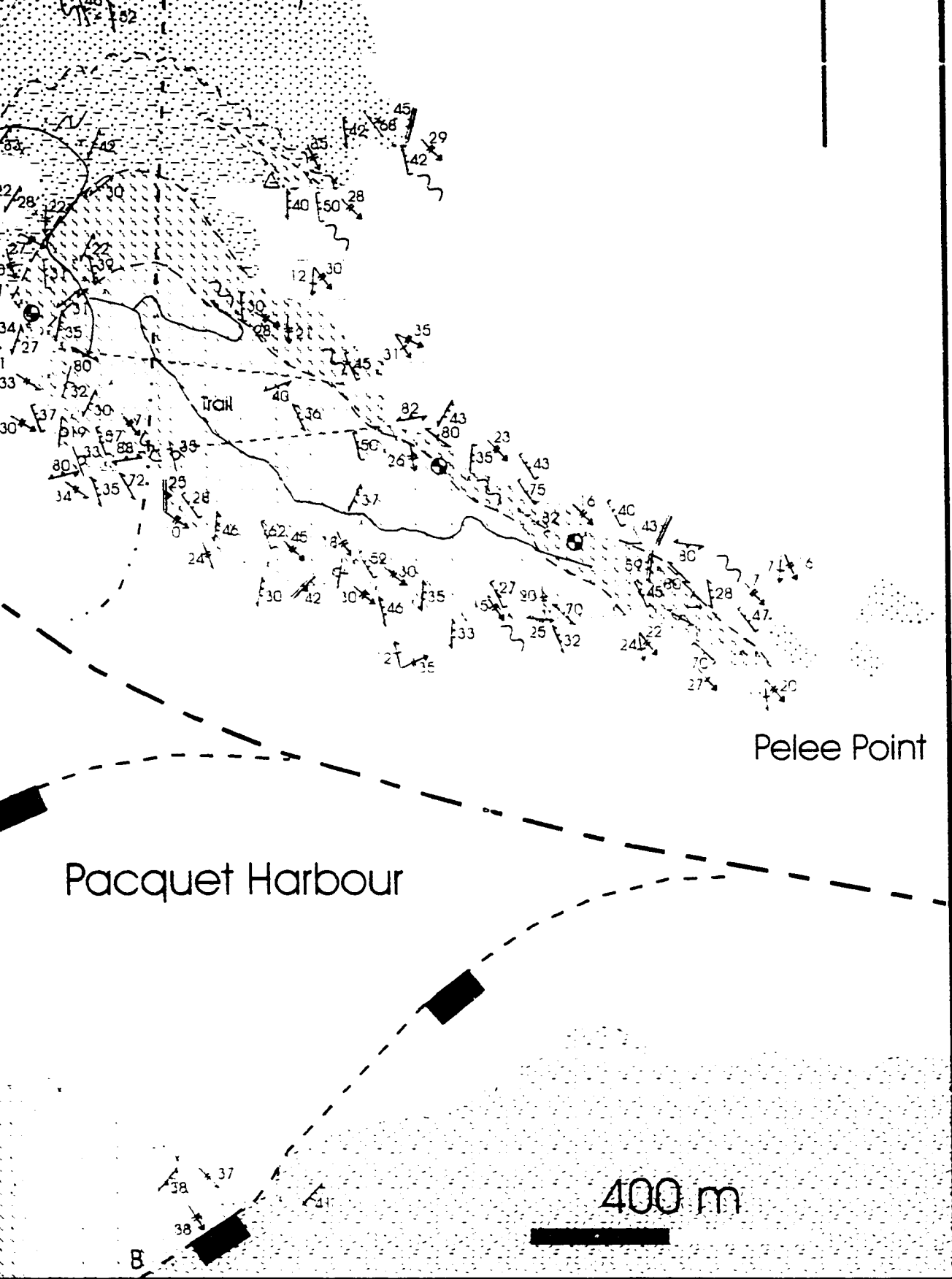
 Contact (D1 shear; D2 shear zone; D3 shear zone; late fault; black ornaments indicate extensional shear zones - ornaments on hangingwall)

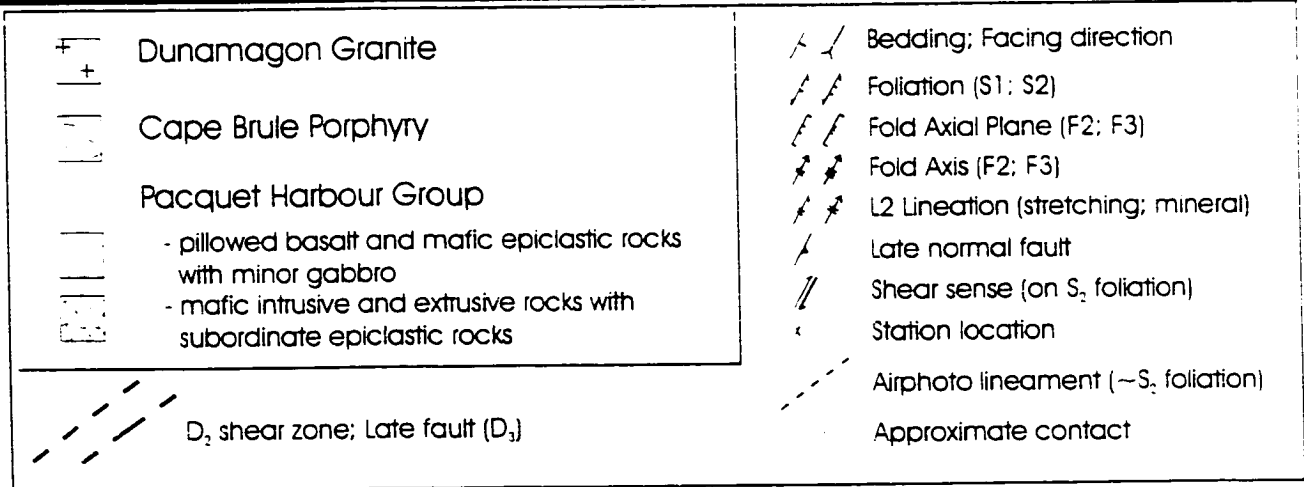
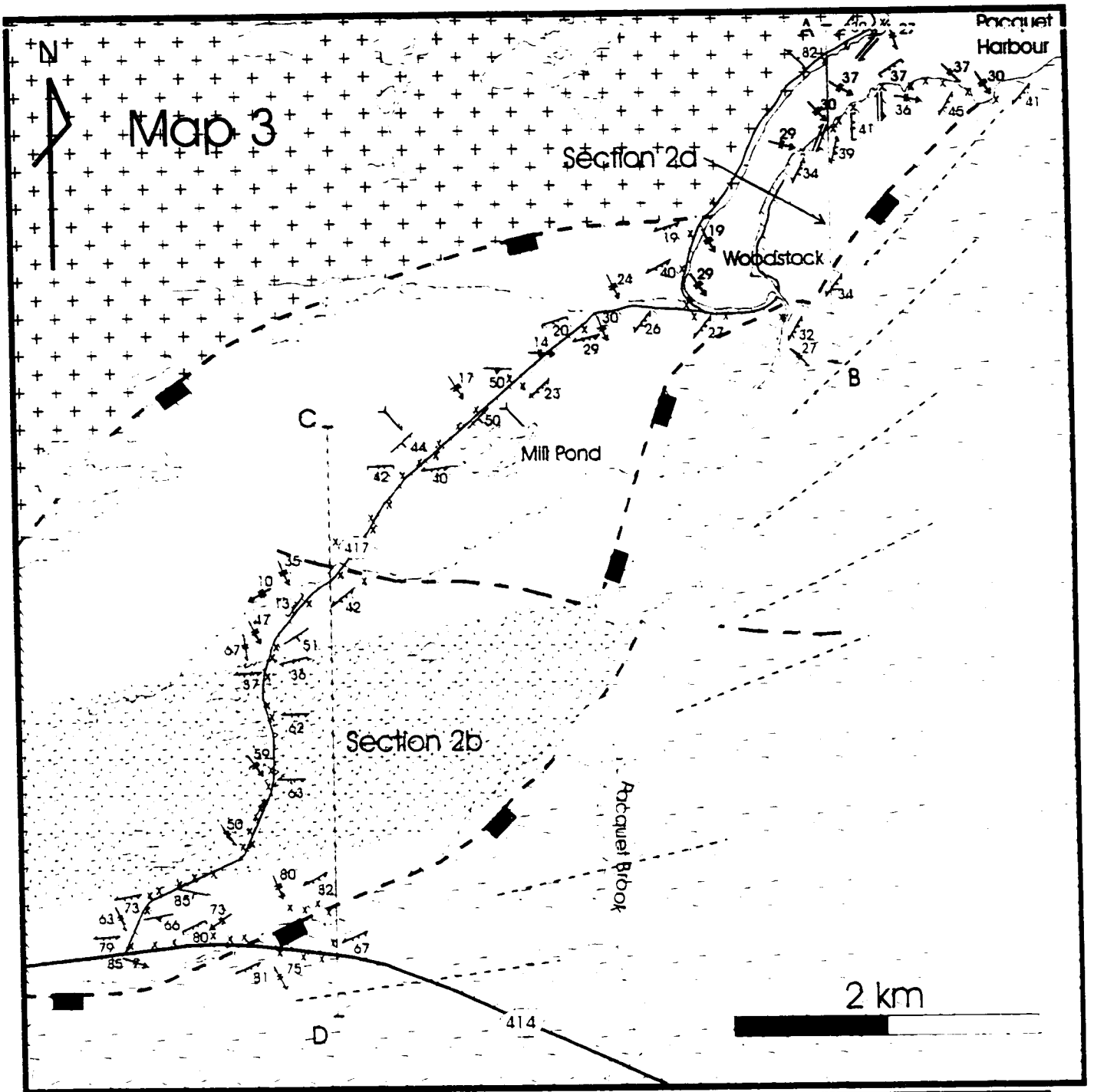
Approximate large-scale F2 axial plane trace;
Schematic F2 form line





Pacquet Harbor



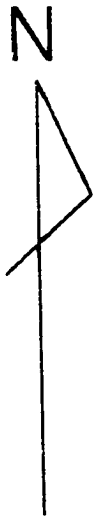


NOTE TO USERS

Oversize maps and charts are microfilmed in sections in the following manner:

**LEFT TO RIGHT, TOP TO BOTTOM, WITH
SMALL OVERLAPS**

UMI



Map 4

Ming's Bight

Map 5

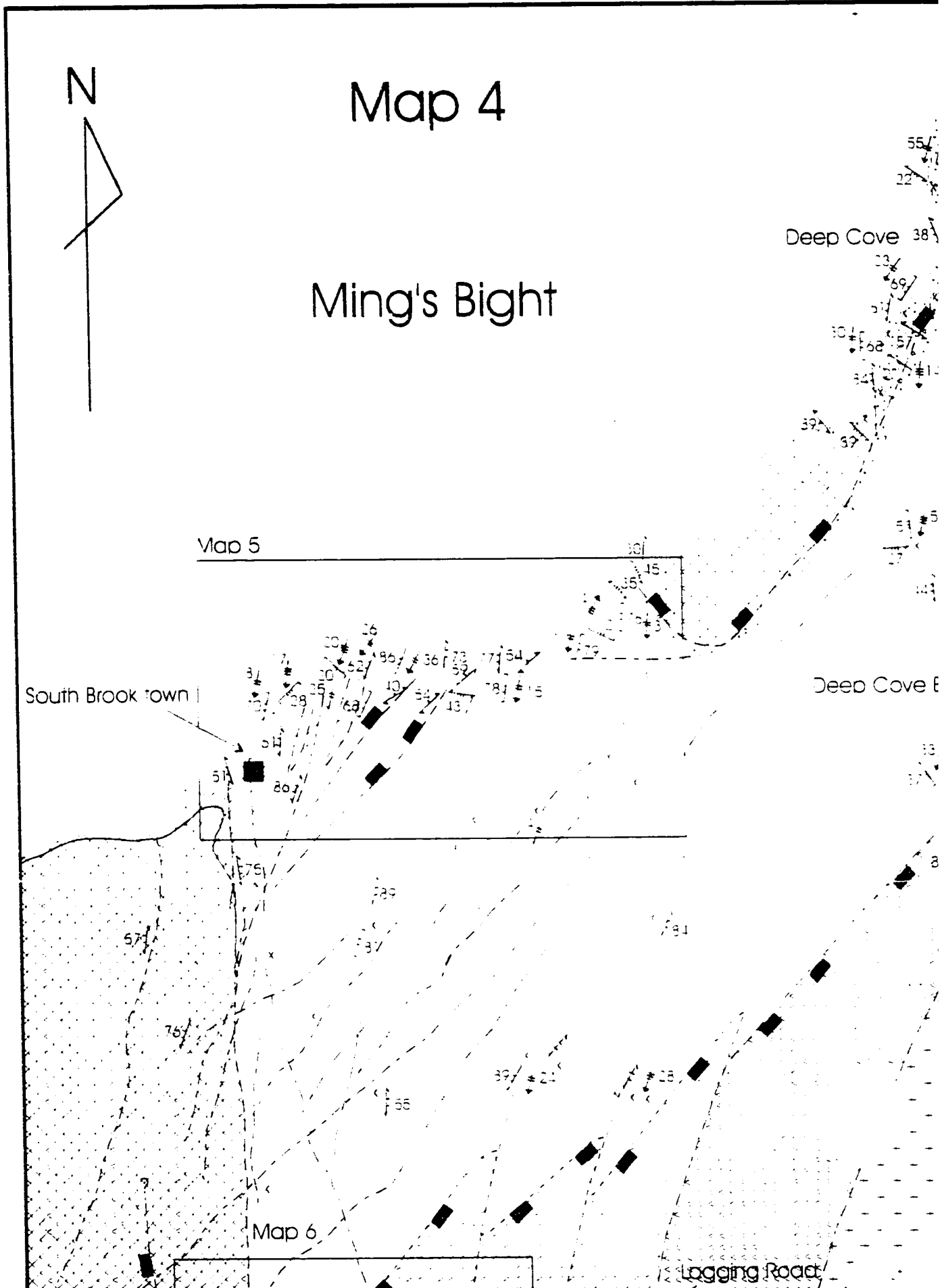
South Brook town

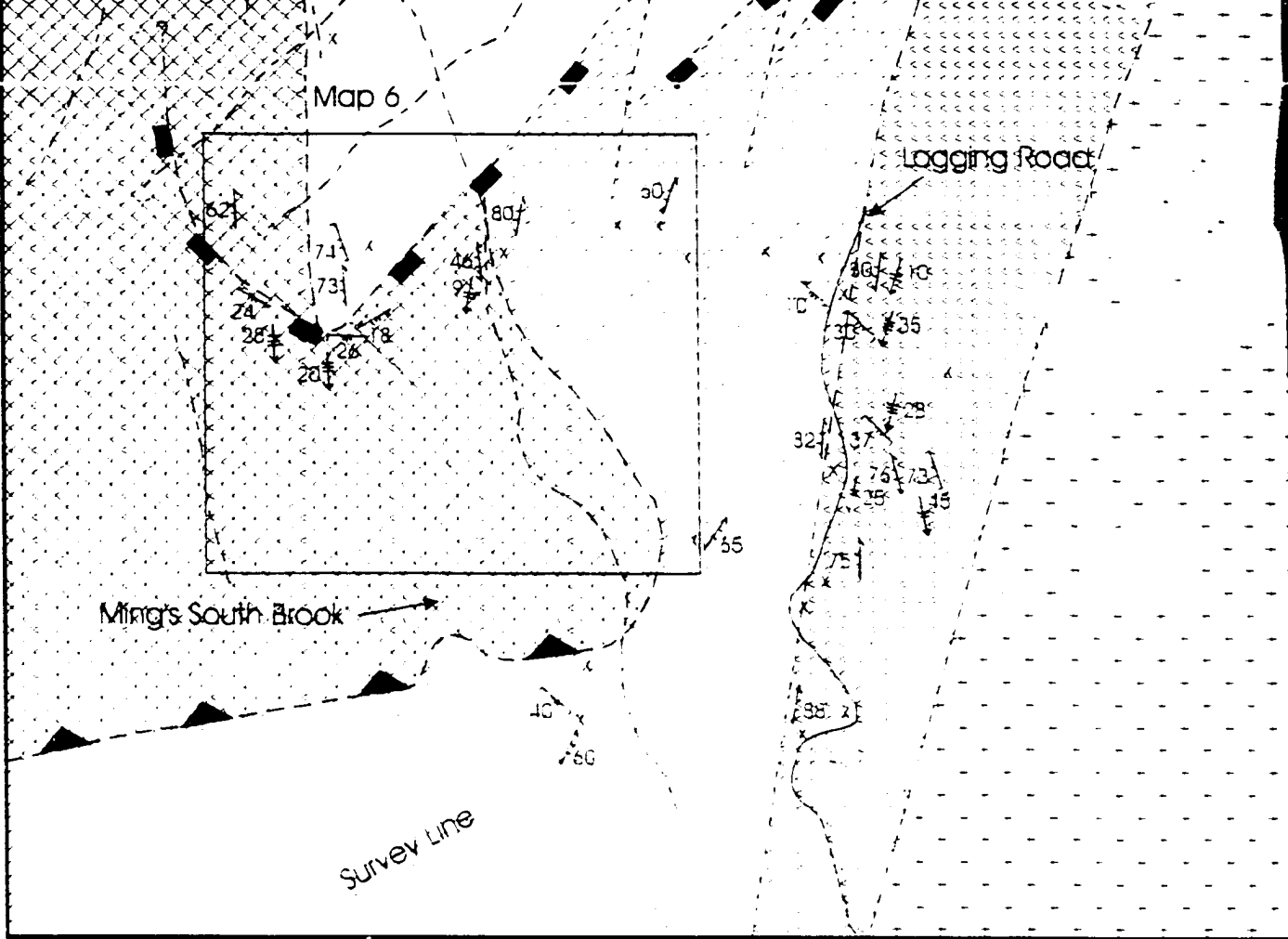
Deep Cove 38




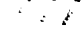
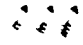

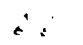





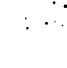
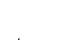


Deep Cove E

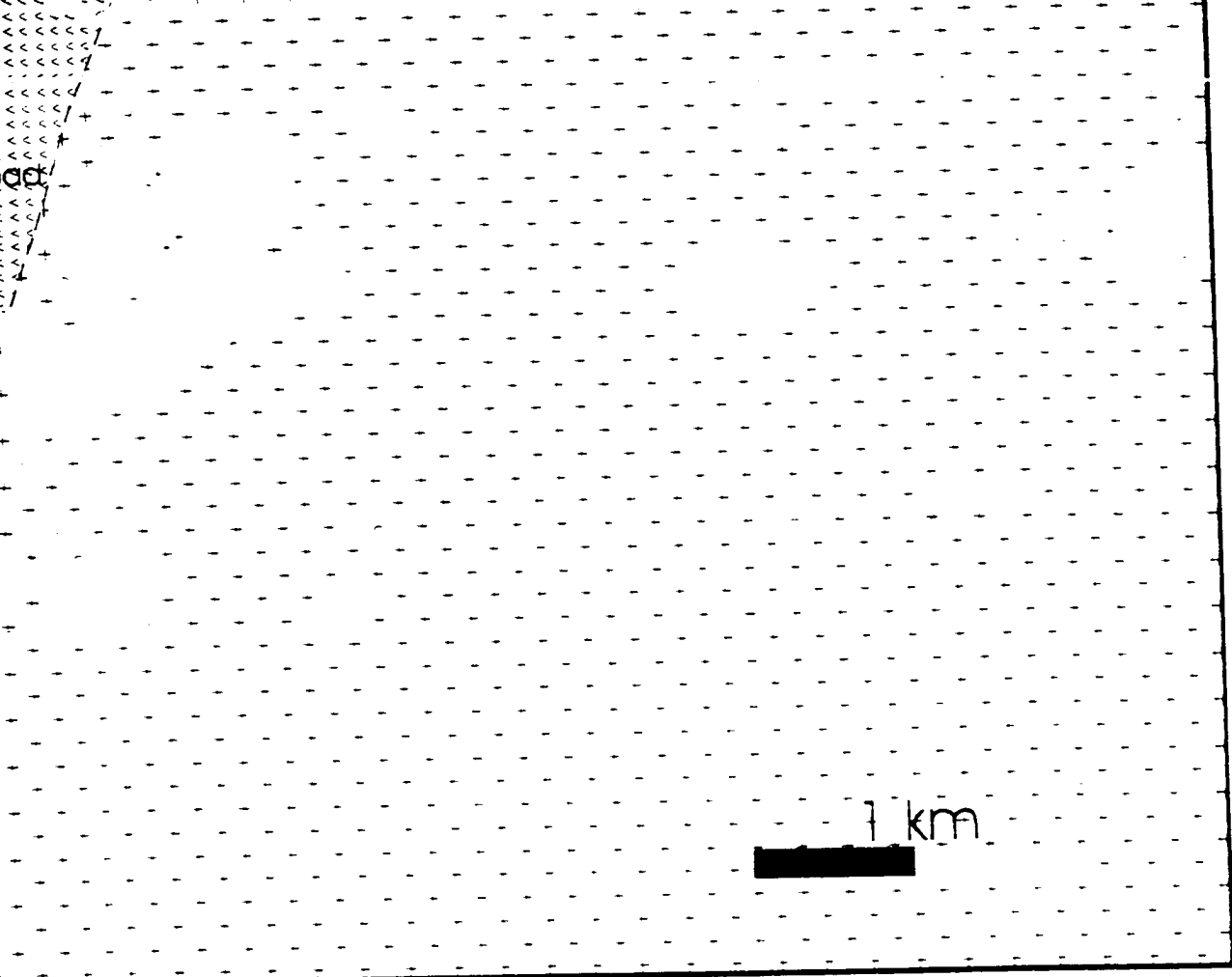
Map 6

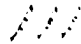
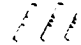






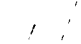

Logging Road





	Dunamagon Granite		Fold
	Pacquet Harbour Group		Fold
	- pillowed basalt; gabbro; mafic and granitic dykes		Fold
	- felsic volcanic and volcanoclastic rocks; mafic and granitic dykes		L2 Li
	Point Rouse Ophiolite		Slick
	- cover sequence: metasediments; greenschist; mafic and granitic dykes		Shear
	- ultramafic sequence: altered ultramafic rocks; gabbro		Strat
	Ming's Bight Group		Shear
	- psammitic and semi-pelitic schist		Reve
	- brecciated MBG schist		Airp



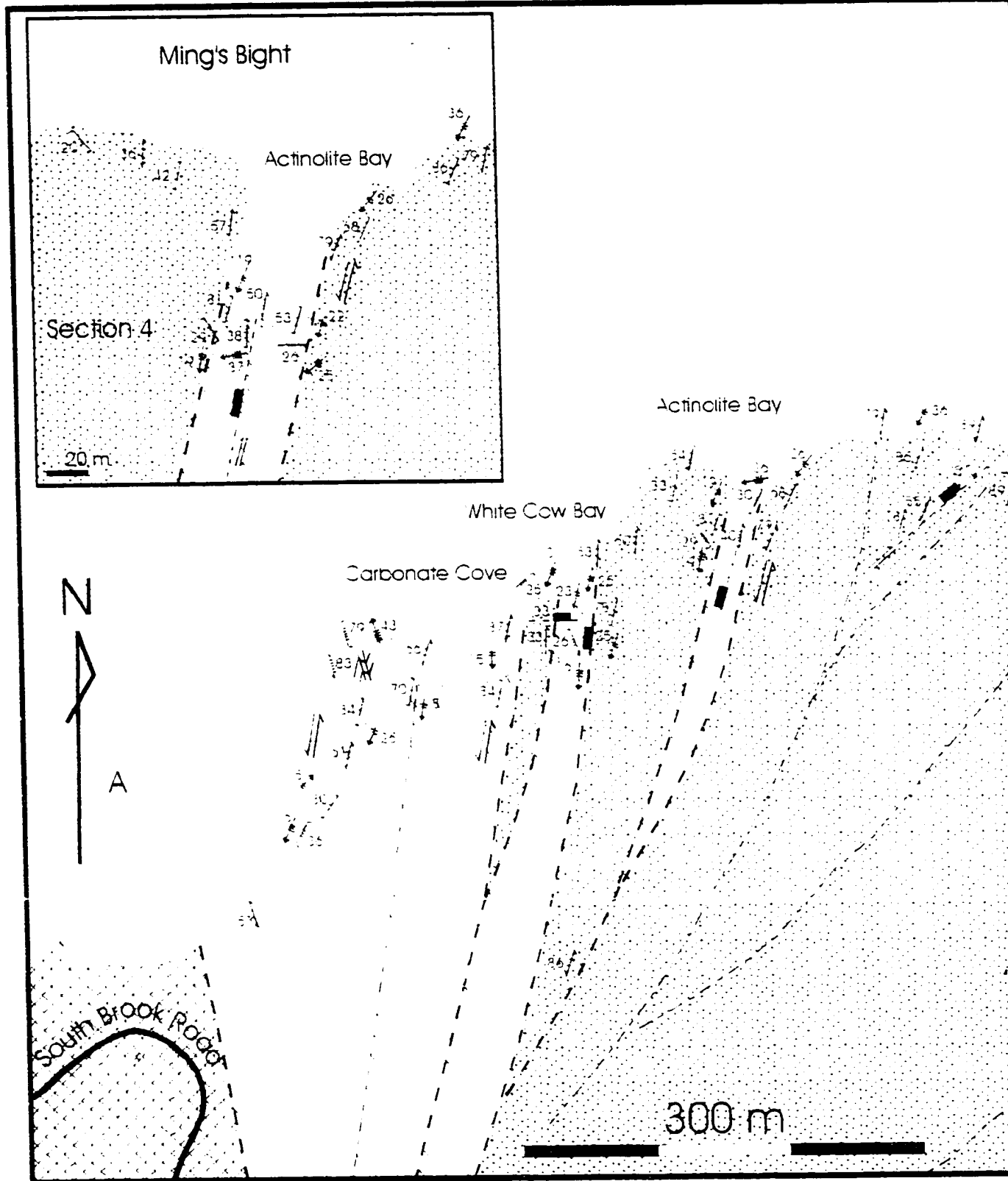
-  Foliation (S2; S3; S4)
-  Fold Axial Plane (F2; F3; F4)
-  Fold Axis (F2; F3; F4)
-  L2 Lincation (mineral; stretching)
-  Slickenside lineation
-  Shear fracture (shear sense indeterminate; dextral; sinistral)
-  Station location
-  Shear zone / fault (defined; inferred)
-  Reverse fault; normal fault (ornaments on hangingwall)
-  Airophoto lineament

NOTE TO USERS

Oversize maps and charts are microfilmed in sections in the following manner:

**LEFT TO RIGHT, TOP TO BOTTOM, WITH
SMALL OVERLAPS**

UMI

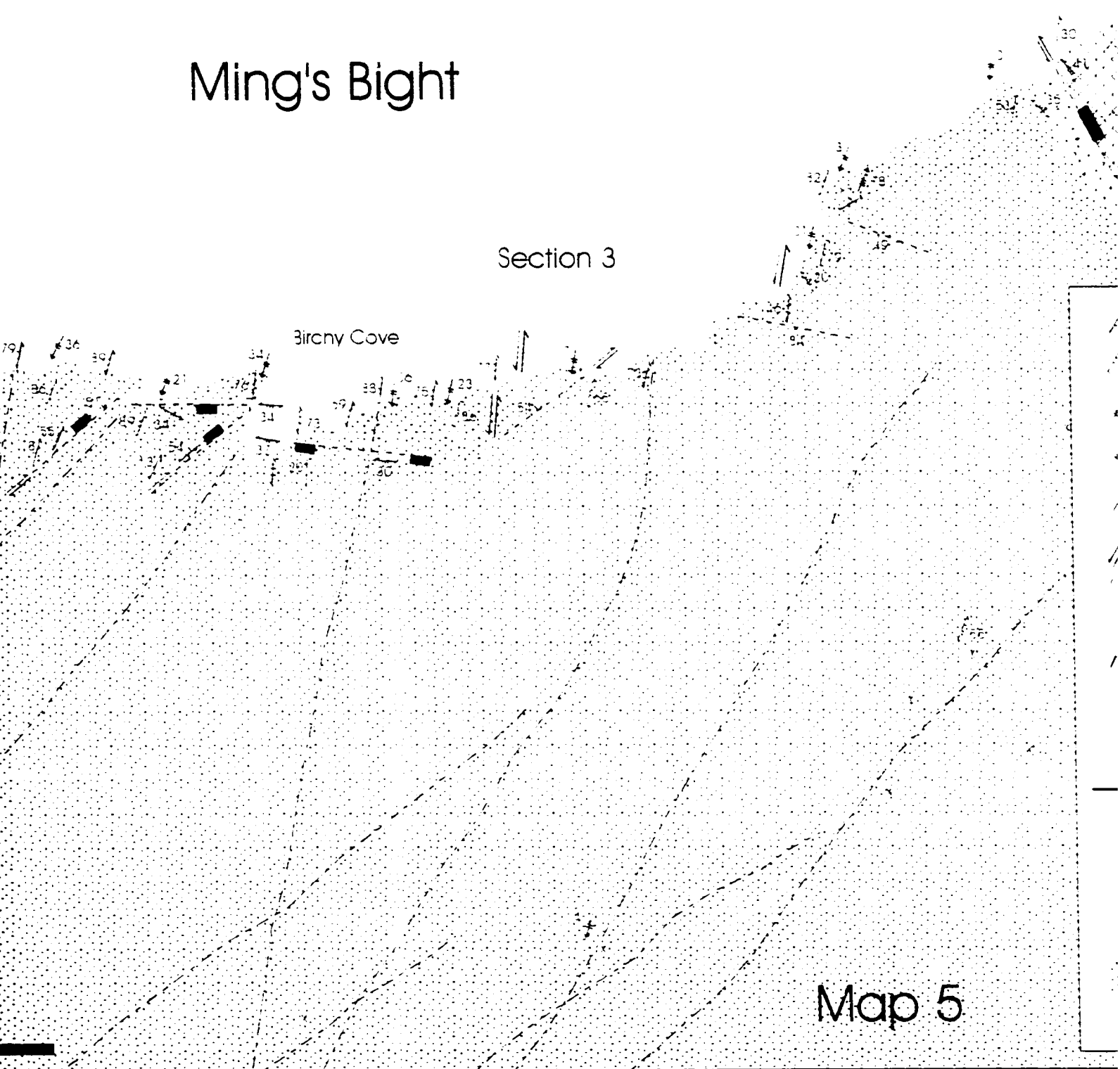


Section 3 - South shore of Ming's Bight (see Map 5 for a complete ledger)

Ming's Bight

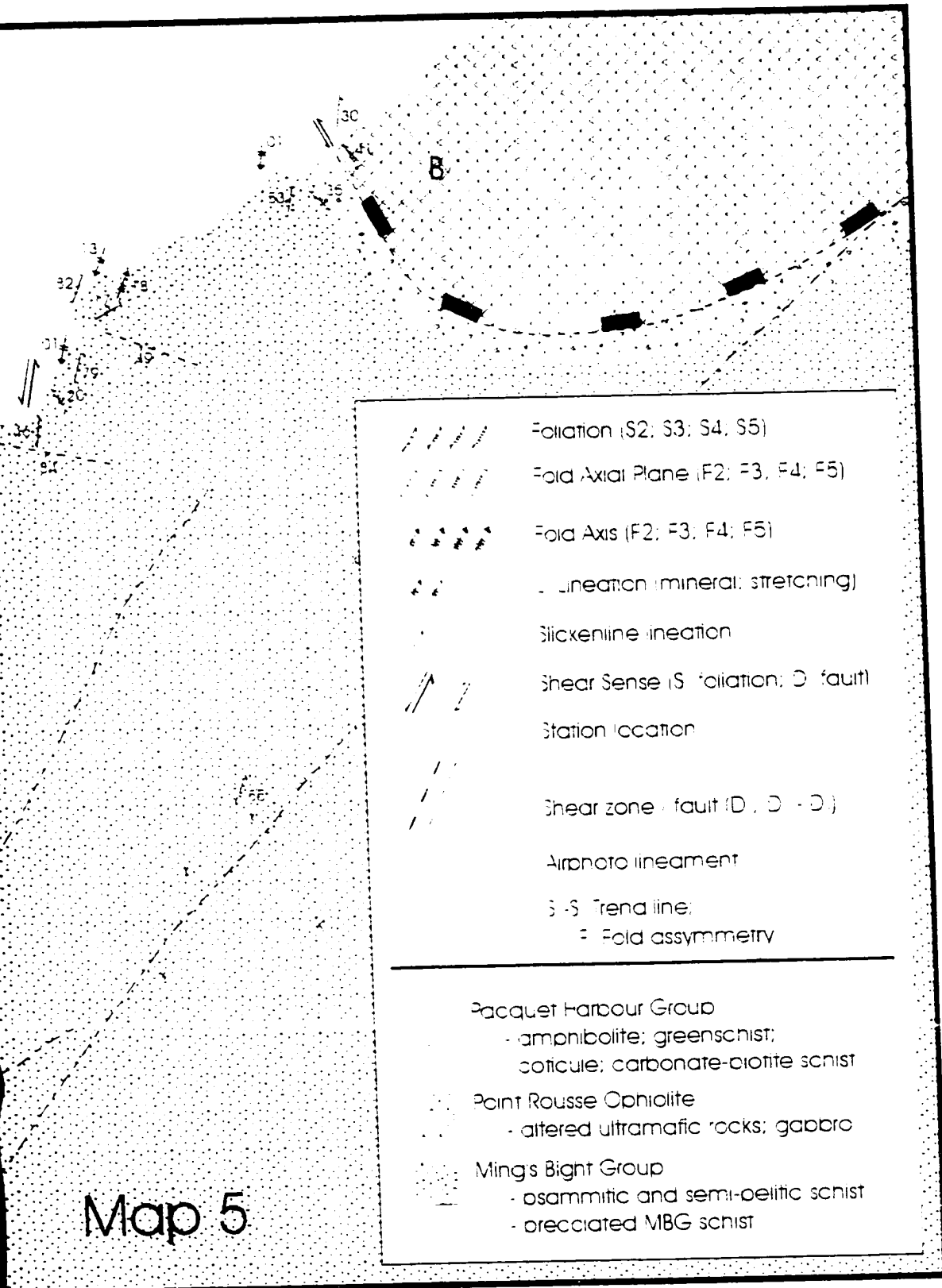
Section 3

Birchy Cove



Map 5

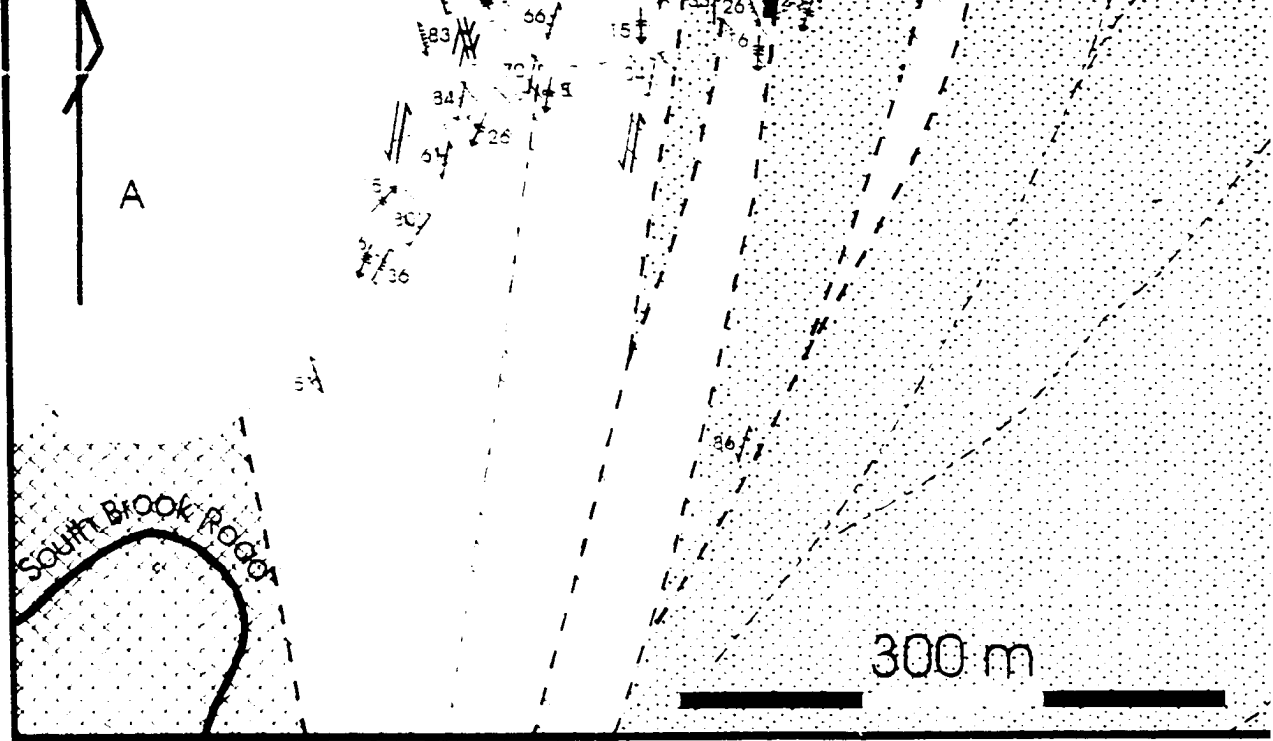
plete legend)



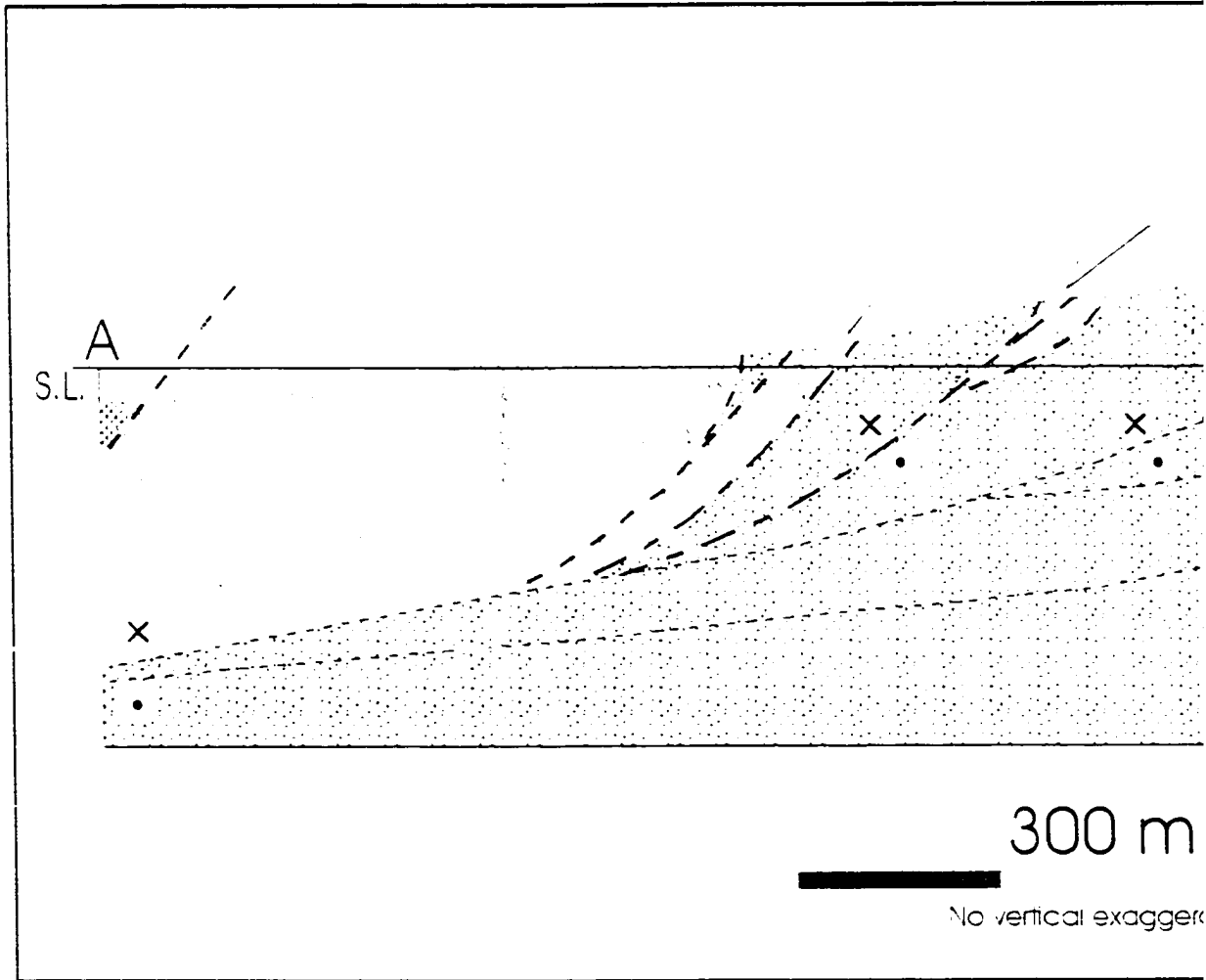
Map 5

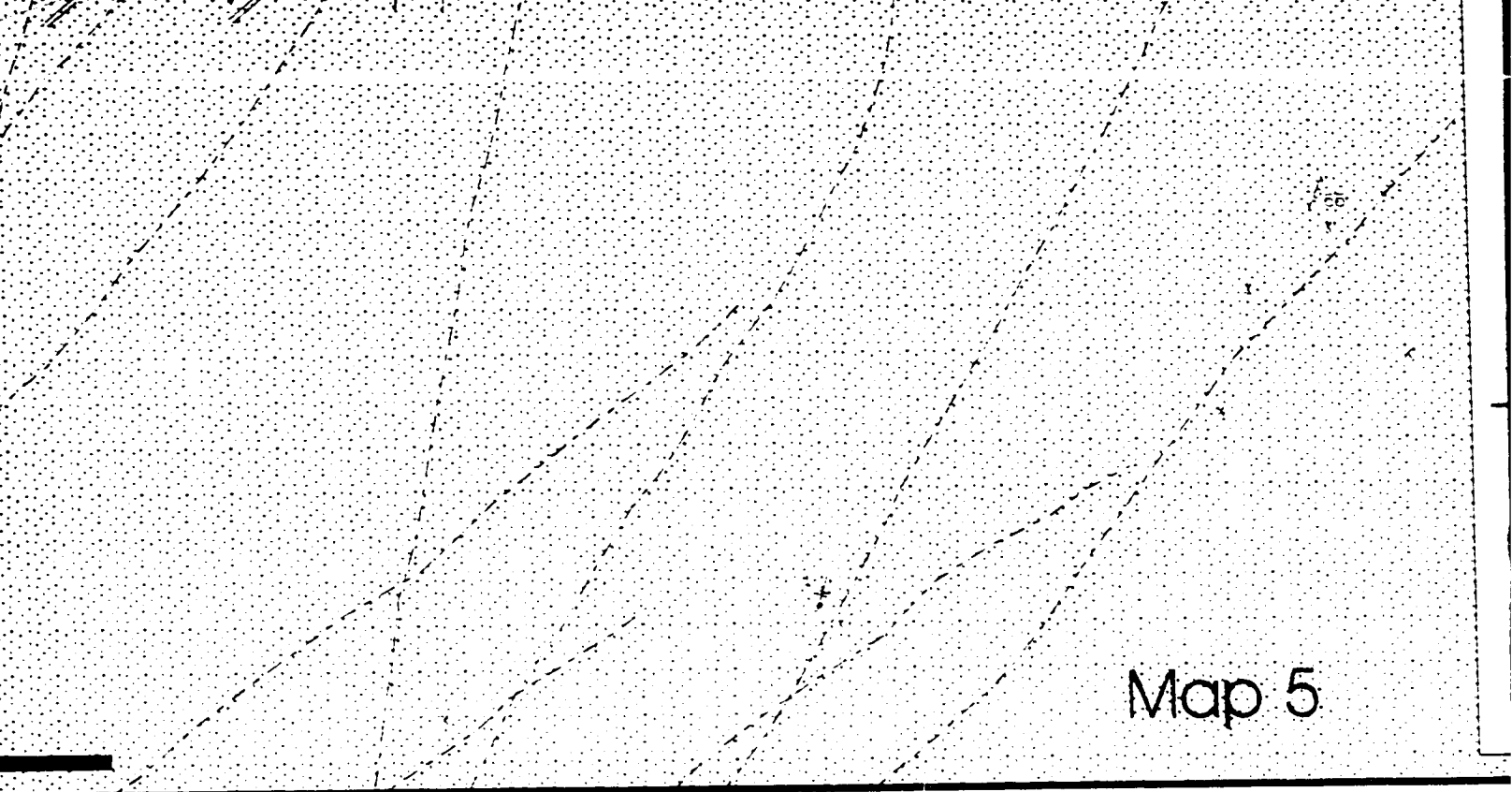
- Foliation (S2, S3, S4, S5)
- Fold Axial Plane (F2, F3, F4, F5)
- Fold Axis (F2, F3, F4, F5)
- Lineation (mineral, stretching)
- Slickenline lineation
- Shear Sense (S: foliation; D: fault)
- Station location
- Shear zone / fault (D, D - D)
- Airphoto lineament
- S-S Trend line:
- Fold asymmetry

- Pacquet Harbour Group
 - amphibolite; greenschist;
 - calcic: carbonate-biotite schist
- Point Rousse Ophiolite
 - altered ultramafic rocks; gabbro
- Mings Bight Group
 - psammitic and semi-pelitic schist
 - brecciated MBG schist

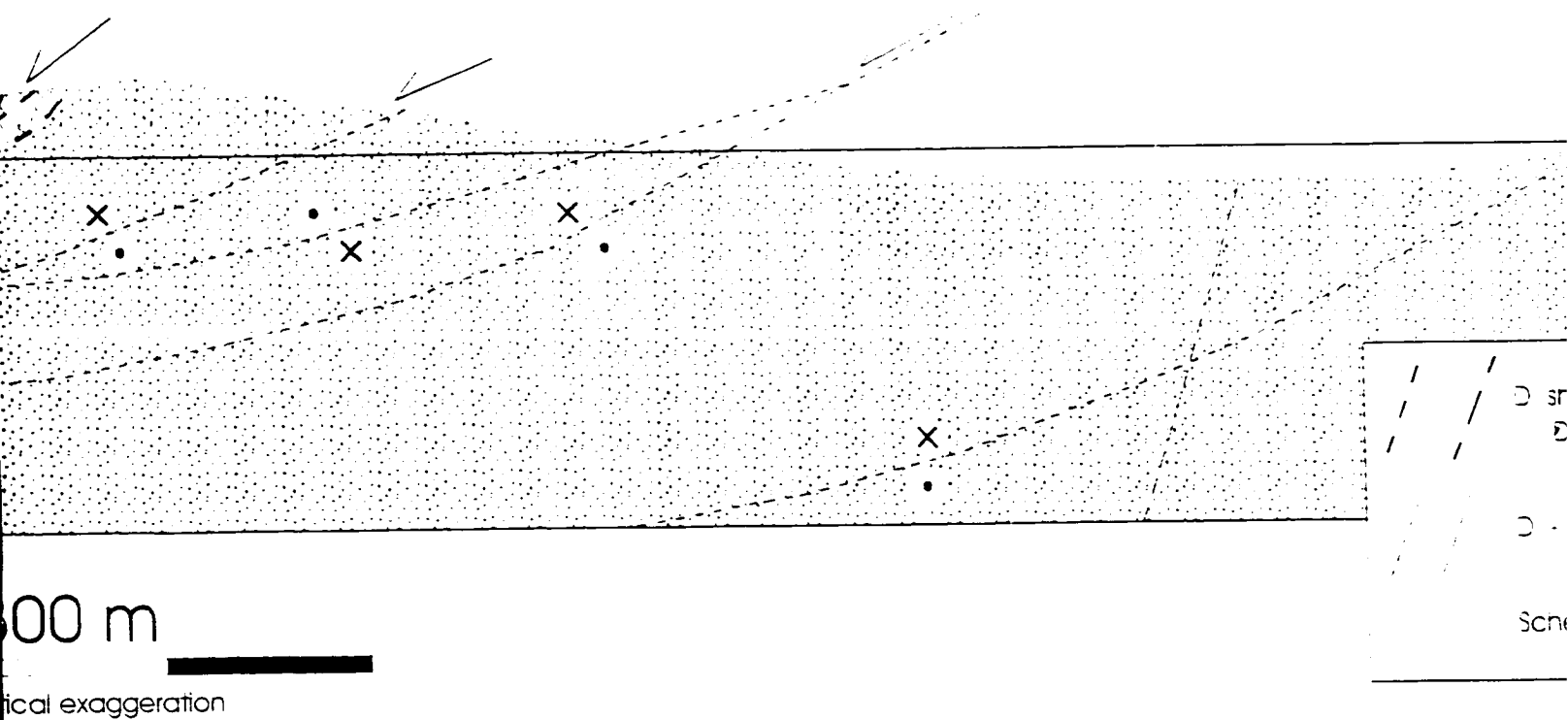


Section 3 - South shore of Ming's Bight (see Map 5 for a complete legend)





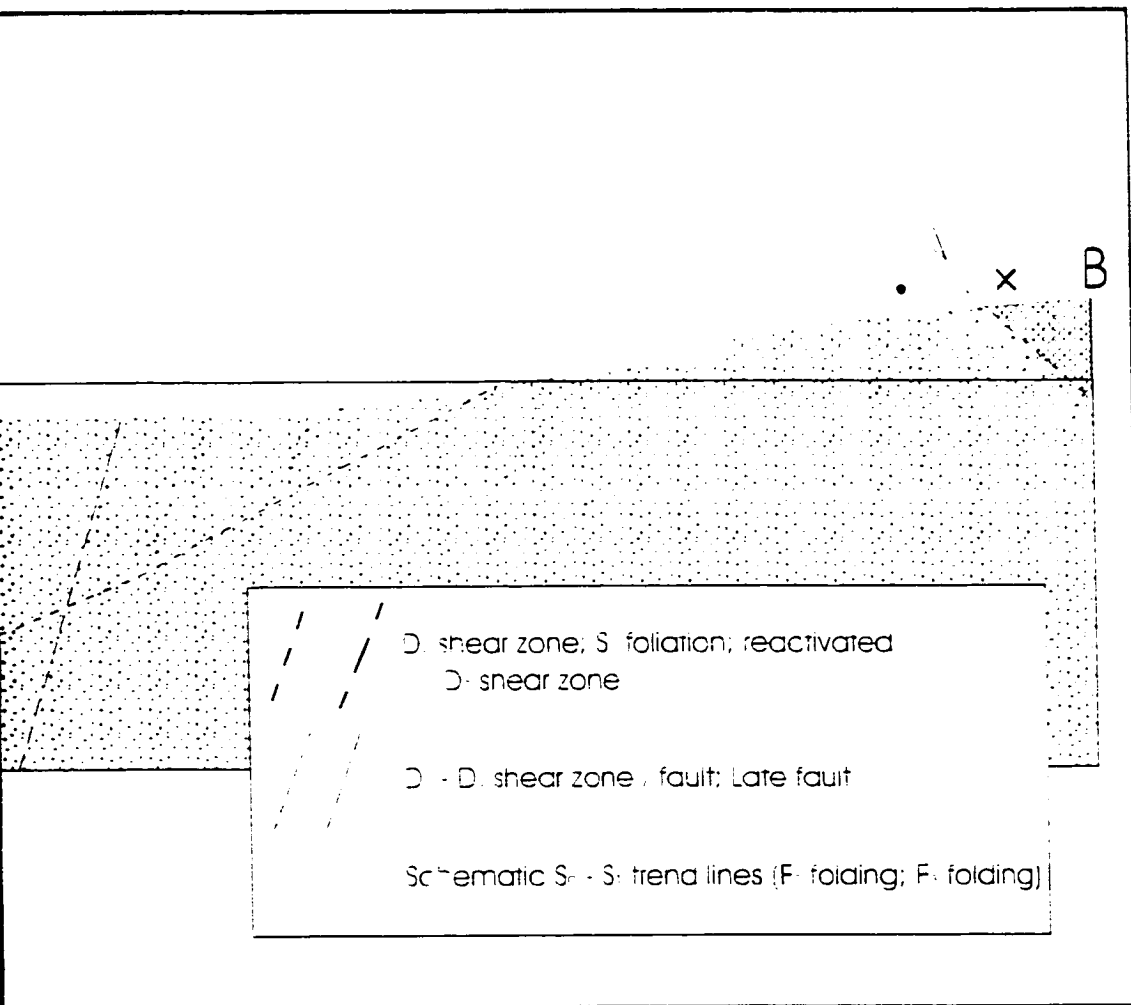
complete legend)



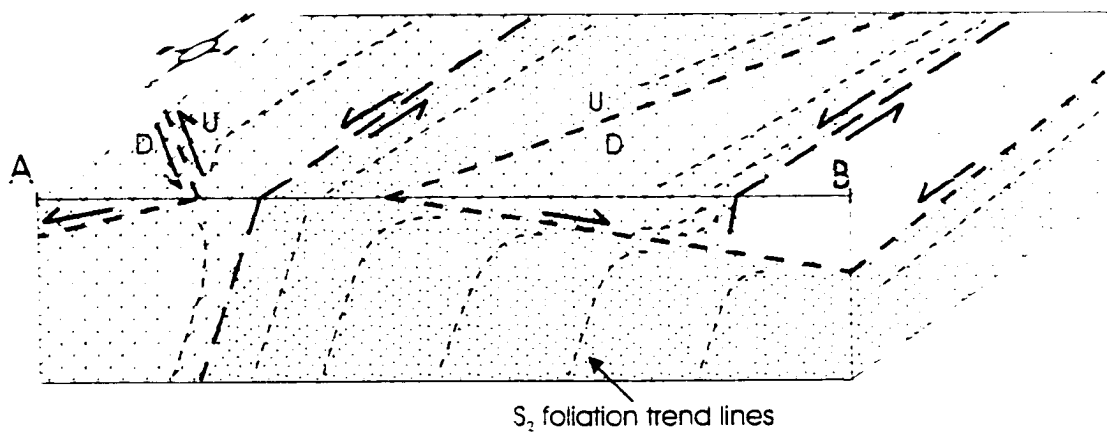
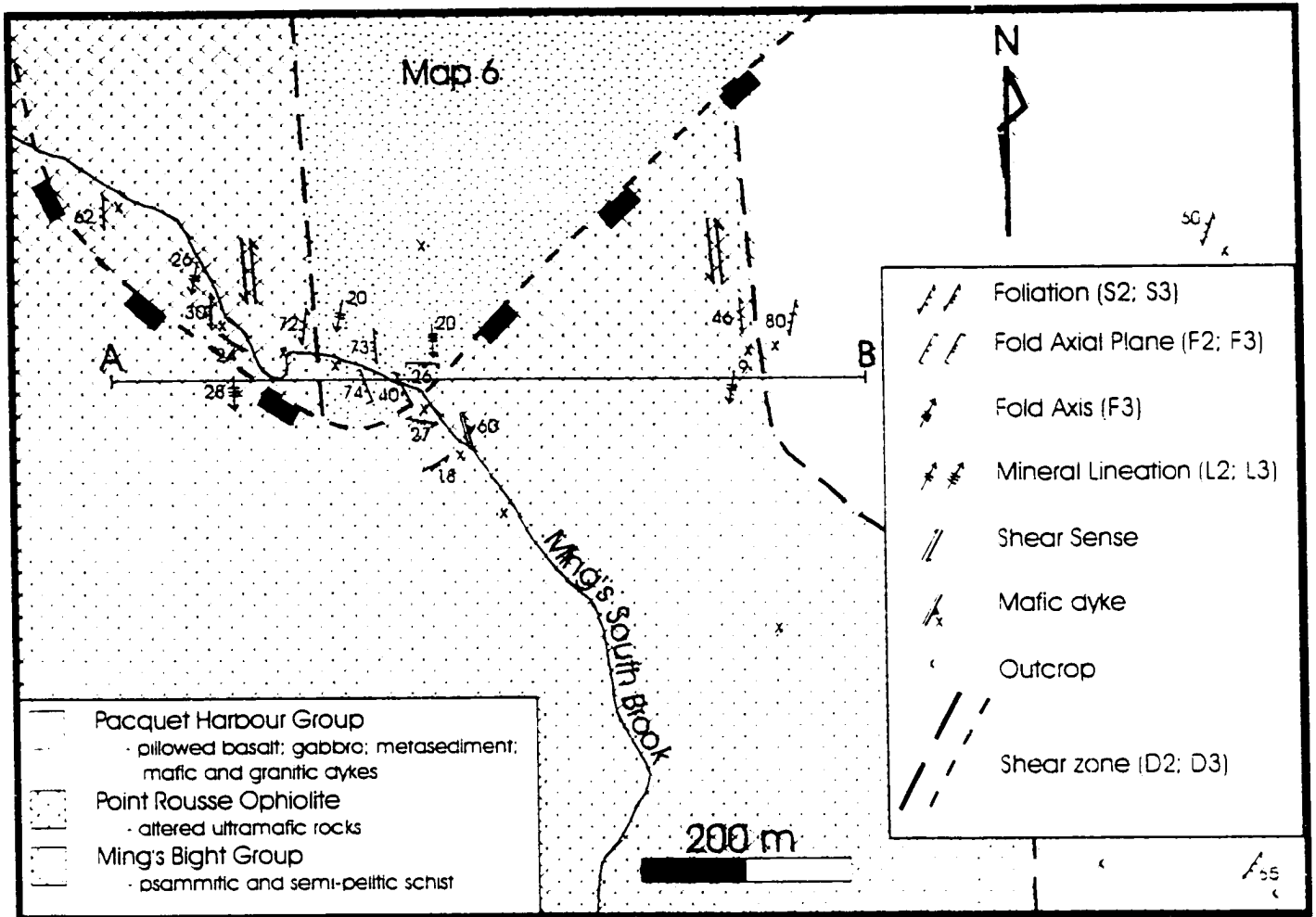
Map 5

- L. Lamination (mineral; stretching)
- Slickenside lineation
- Shear Sense (S foliation; D. fault)
- Station location
- Shear zone / fault (D ; D - D)
- Airphoto lineament
- S-S Trend line:
F Fold asymmetry

- Pacquet Harbour Group
 - amphibolite; greenschist;
 - eclogite; carbonate-biotite schist
- Point Rousse Ophiolite
 - altered ultramafic rocks; gabbro
- Mings Bight Group
 - osammitic and semi-pelitic schist
 - brecciated MBG schist



- D. shear zone; S. foliation; reactivated
- D- shear zone
- D - D. shear zone / fault; Late fault
- Schematic S - S. trend lines (F- folding; F- folding)



NOTE TO USERS

Oversize maps and charts are microfilmed in sections in the following manner:

**LEFT TO RIGHT, TOP TO BOTTOM, WITH
SMALL OVERLAPS**

UMI

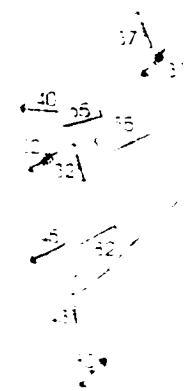
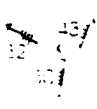


N



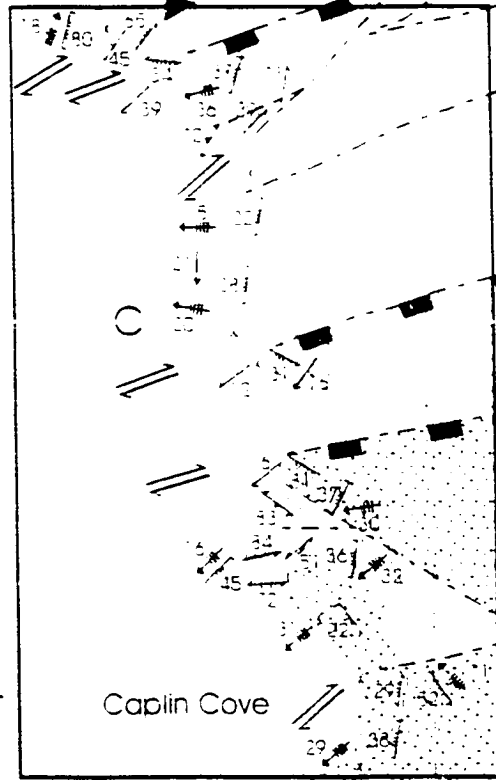
Map 7

Grappling Point A



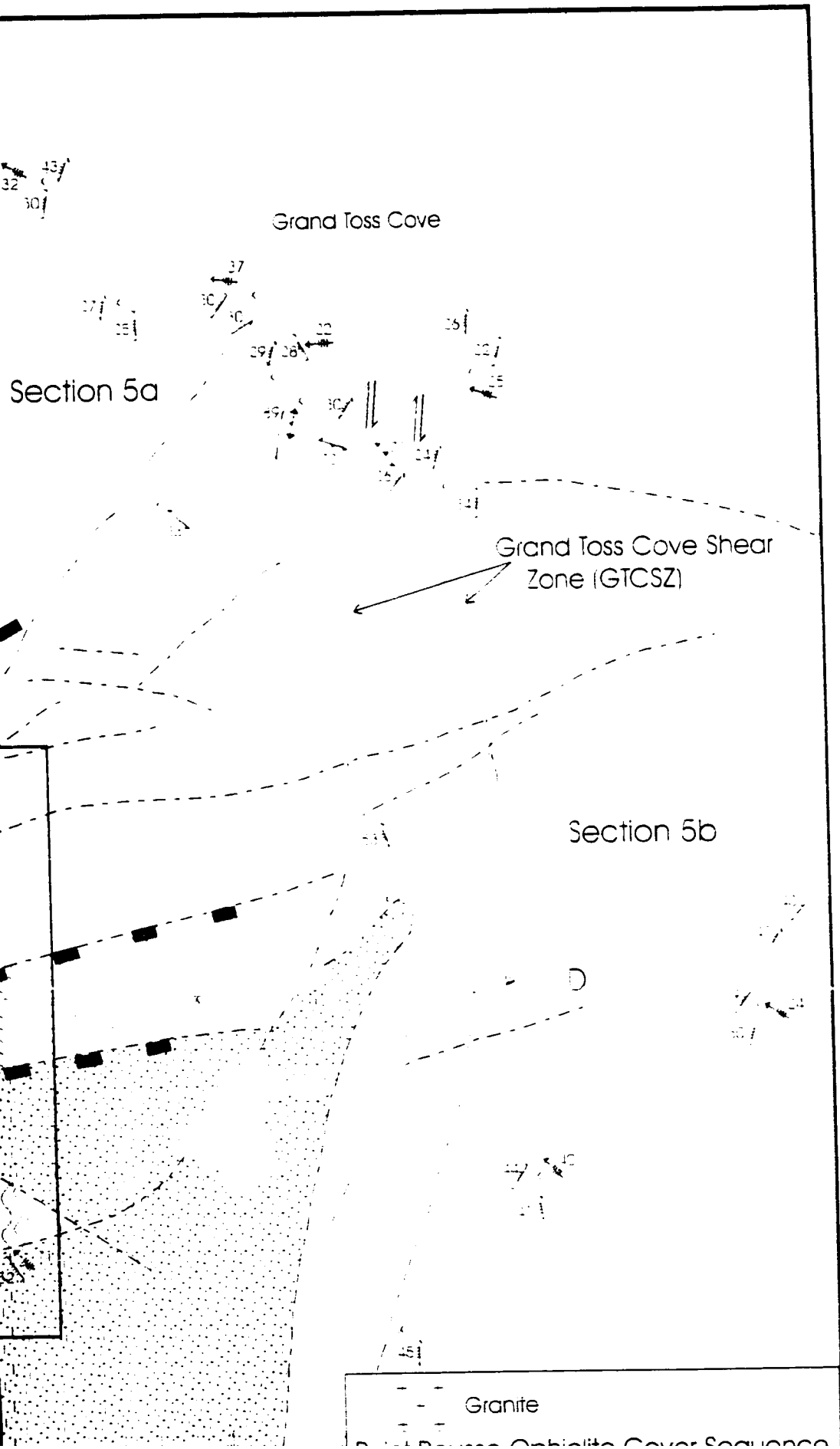
Section 5a

Mings Tickle

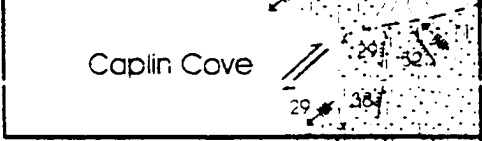


Map 8

Caplin Cove



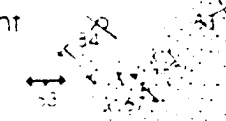
Caplin Cove



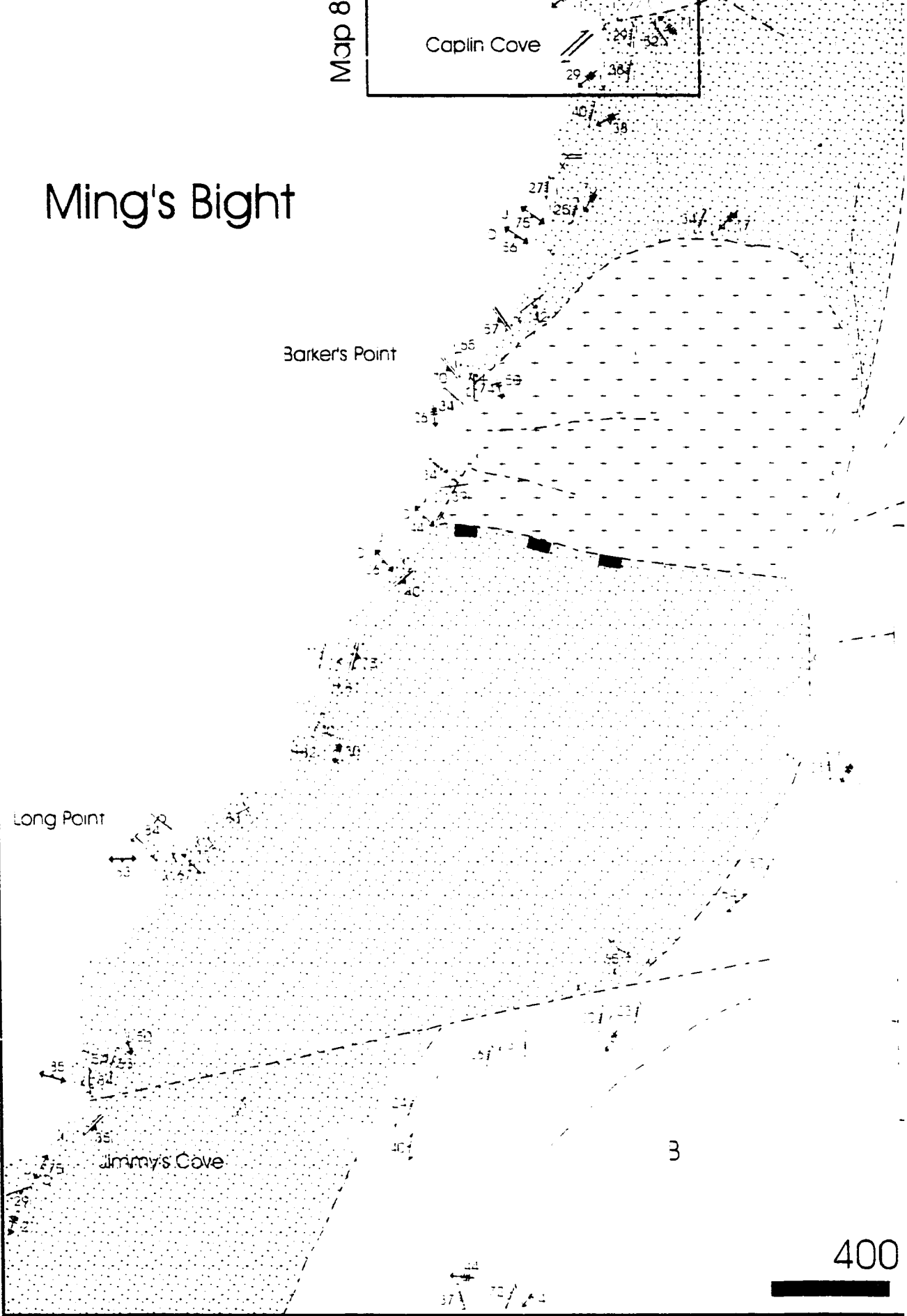
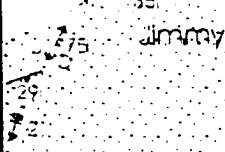
Ming's Bight

Barker's Point

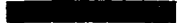
Long Point

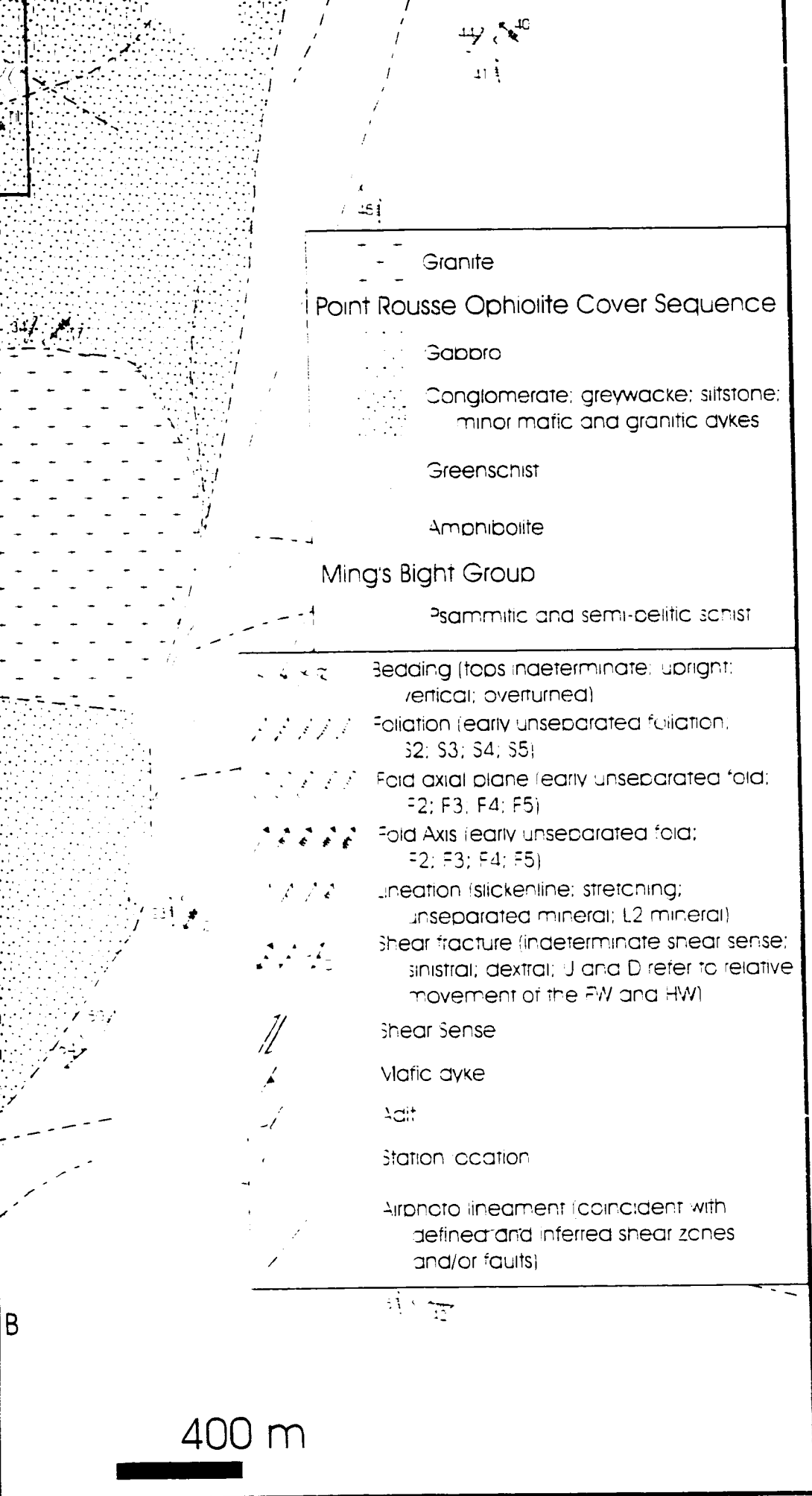


Jimmy's Cove



400





- - - Granite
 Point Rousse Ophiolite Cover Sequence
 Gabbro
 Conglomerate; greywacke; siltstone;
 minor mafic and granitic dykes
 Greenschist
 Amphibolite
 Ming's Bight Group
 Psammitic and semi-oolitic schist

Bedding (tops indeterminate; upright;
 vertical; overturned)
 Foliation (early unseparated foliation;
 S2; S3; S4; S5)
 Fold axial plane (early unseparated fold;
 F2; F3; F4; F5)
 Fold Axis (early unseparated fold;
 F2; F3; F4; F5)
 Lineation (stickline; stretching;
 unseparated mineral; L2 mineral)
 Shear fracture (indeterminate shear sense;
 sinistral; dextral; U and D refer to relative
 movement of the FW and HW)
 Shear Sense
 Mafic dyke
 Adit
 Station location
 Airphoto lineament (coincident with
 defined and inferred shear zones
 and/or faults)

400 m

B

NOTE TO USERS

Oversize maps and charts are microfilmed in sections in the following manner:

**LEFT TO RIGHT, TOP TO BOTTOM, WITH
SMALL OVERLAPS**

UMI

N



A

Northern Ming
Shear Zone

Map 8

Pole to great circle

Ming's Bight



Quartz-veined chlorite schist

Point Rouse ophiolite cover sequence

Metagabbro

Metasedimentary rocks

(conglomerate; greywacke; greenschist)

Greenschist

(contains pyroxene pseudomorphs)

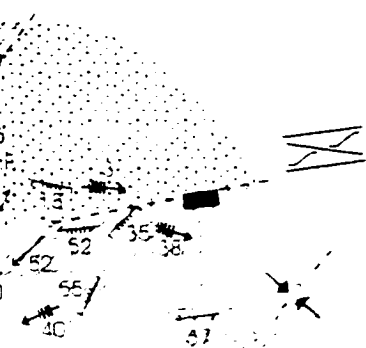
Amphibolite

Mylonitic amphibolite and metasediments

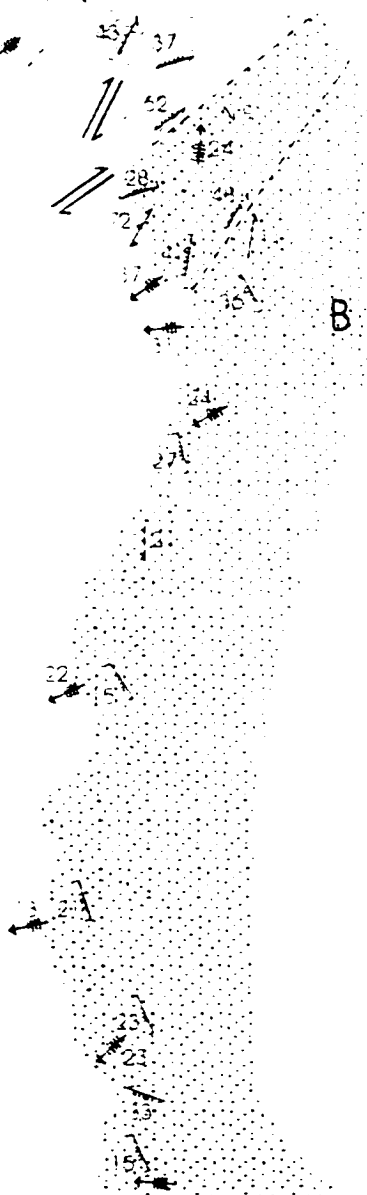
Ming's Bight Group

Layered psammitic / semi-pelitic schist

Northern Ming's Tickle
Shear Zone



at circle




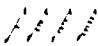
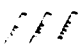



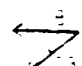



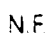


B

Section 6a

Section 6b

C

Ming's Bight

	Bedding
	Foliation (early unseparated foliation; S3, S4; S5)
	Fold Axial Plane (F3; F4; F5)
	Fold Axis (F3; F4; F5)
	Shear fracture (dextral; sinistral; shear sense indeterminate)
	Lineation (slickenline; hornblende; stretching)
	Recrystallized pyroxene crystals - mean hornblende and stretching lineation
	Shear Sense
	Asymmetric fabric
	Synform
	Non-cylindrical folding
	Quartz vein
	Shear zone / fault (black triangles and rectangles reflect reverse and normal movement of the hangingwall, respectively); Foliation / layering trend lines; Fold asymmetry

50 m



Section 6b

C

Pole to great circle

Section 7

Caplin Cove

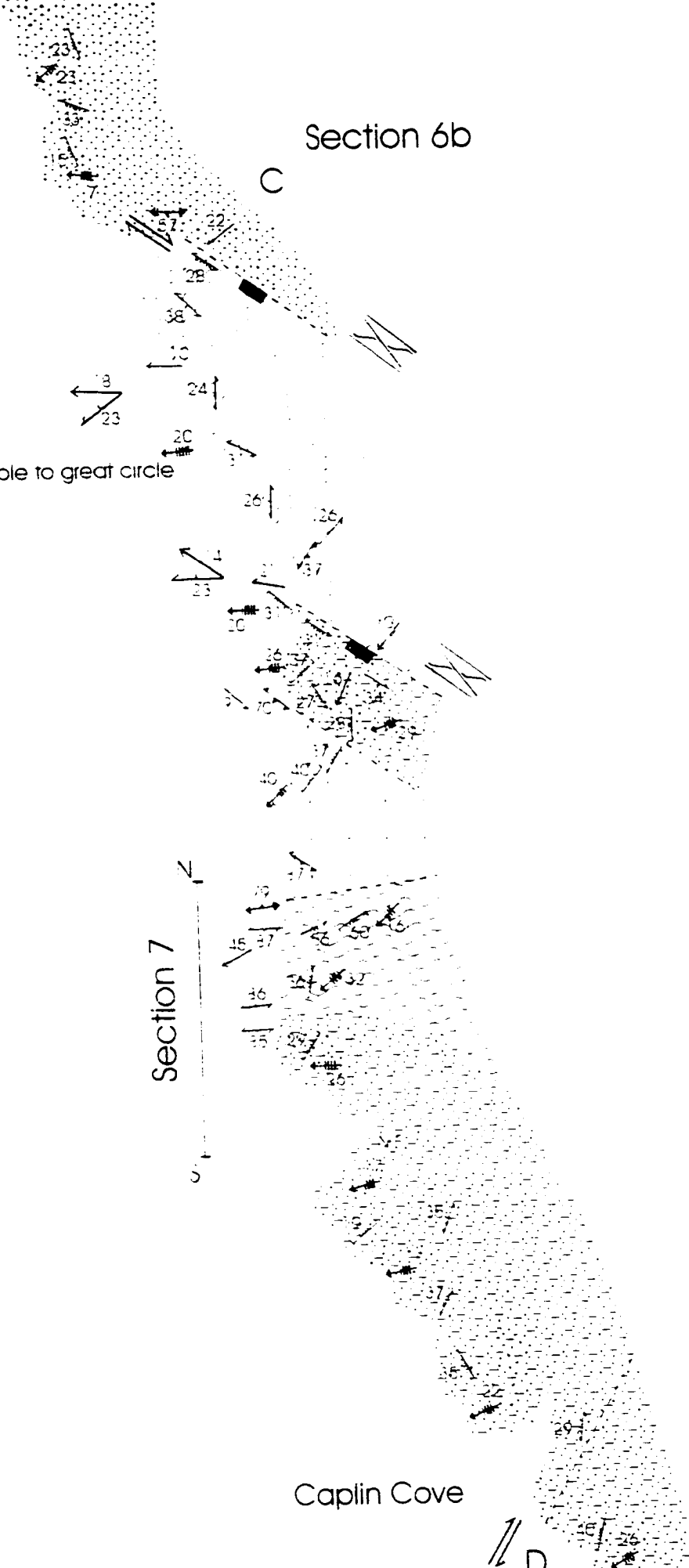
D

65]

(indeterminate)

on

angles reflect reverse
all, respectively);
metry

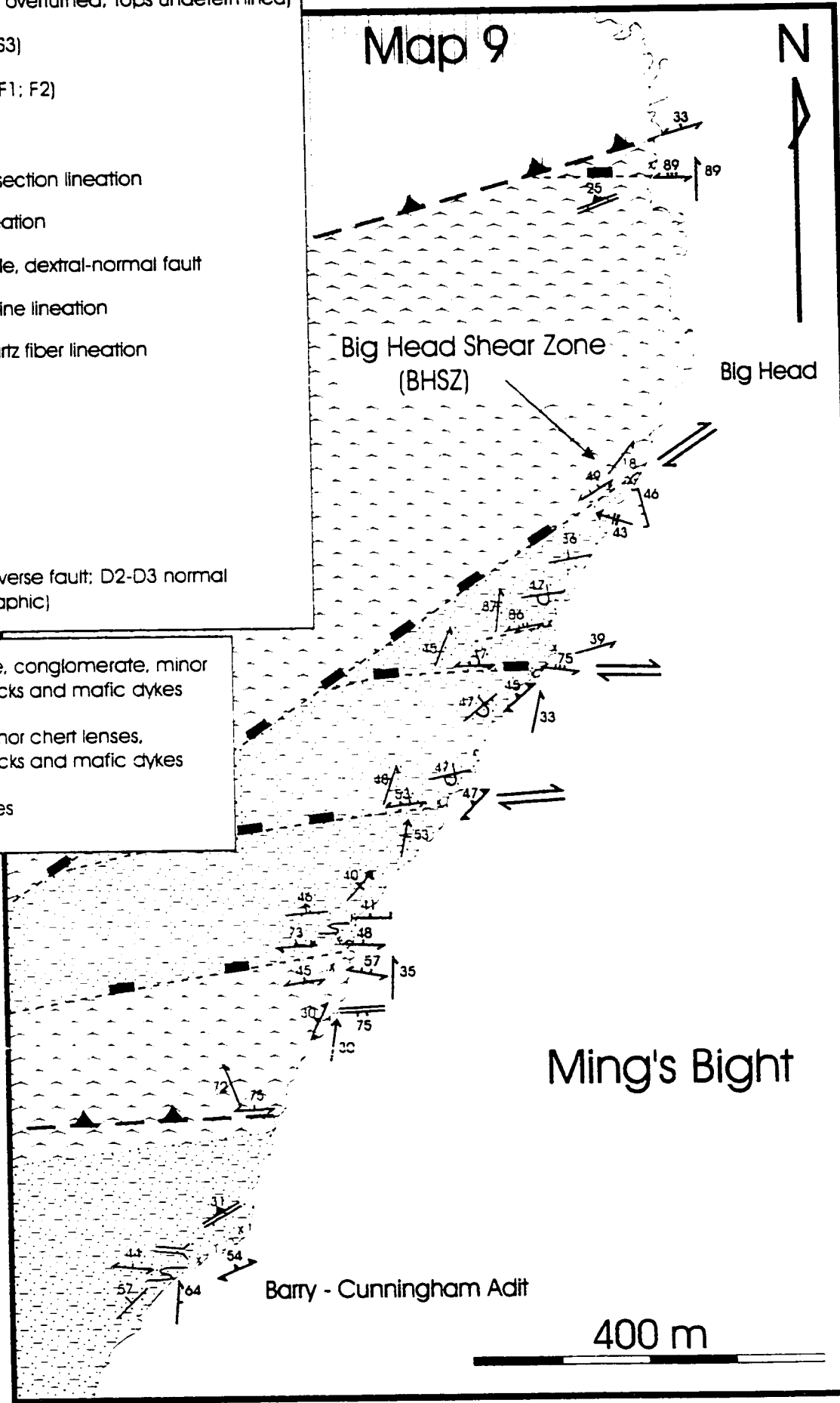


Map 9



- Bedding (upright; overturned; tops undetermined)
- Foliation (S1; S2; S3)
- Fold Axial Plane (F1; F2)
- Fold Axis (F1; F2)
- Bedding-S1 Intersection lineation
- S1 Stretching lineation
- Late, brittle-ductile, dextral-normal fault
- Chlorite / slickenline lineation
- Quartz vein: quartz fiber lineation
- Mafic dyke
- Shear Sense
- Station location
- Adit
- Contacts (D1 reverse fault; D2-D3 normal fault; stratigraphic)

- Greywacke, siltstone, conglomerate, minor volcanoclastic rocks and mafic dykes
- Pillowed basalts: minor chert lenses, volcanoclastic rocks and mafic dykes
- Sheeted mafic dykes

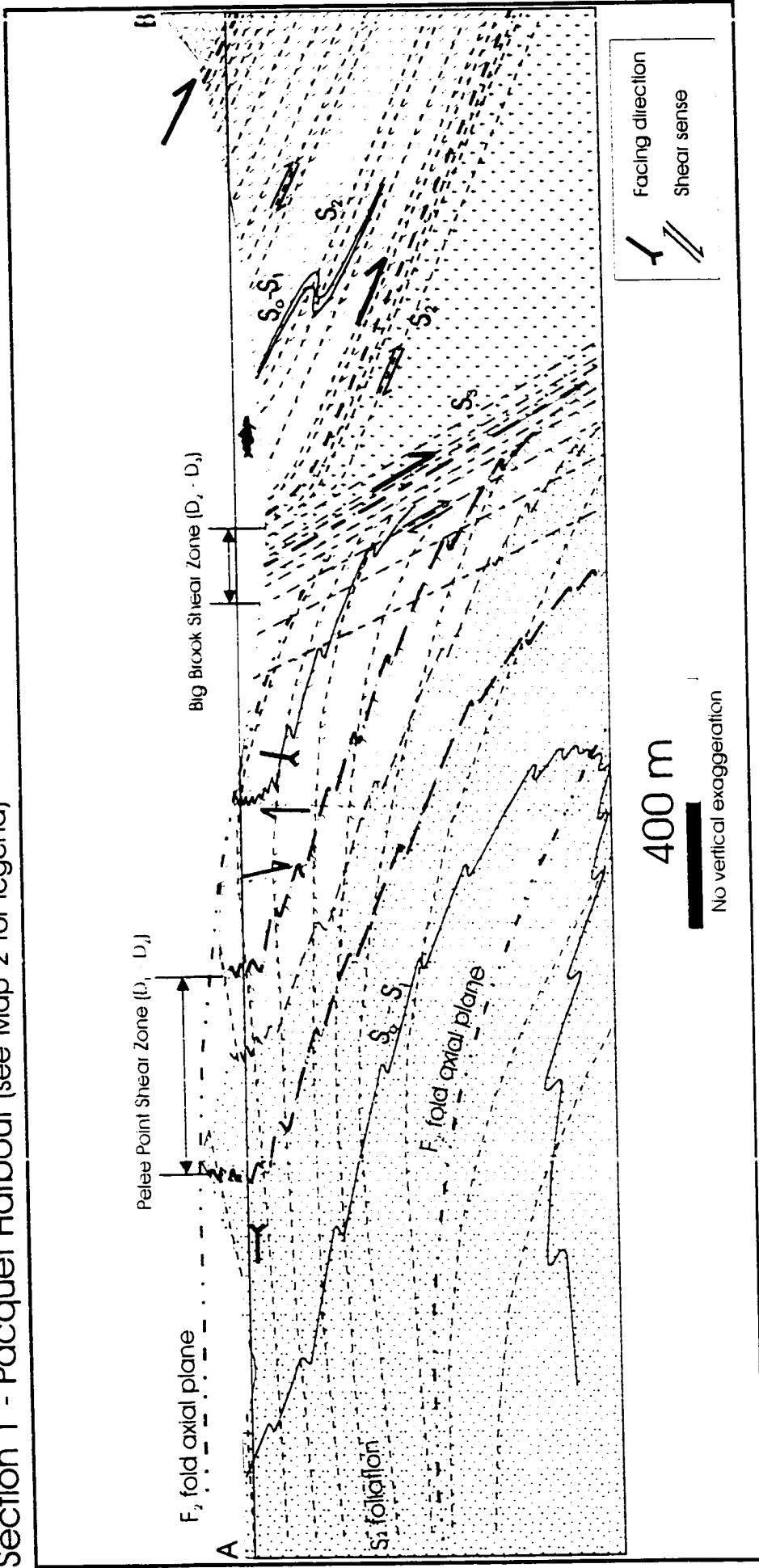


Ming's Bight

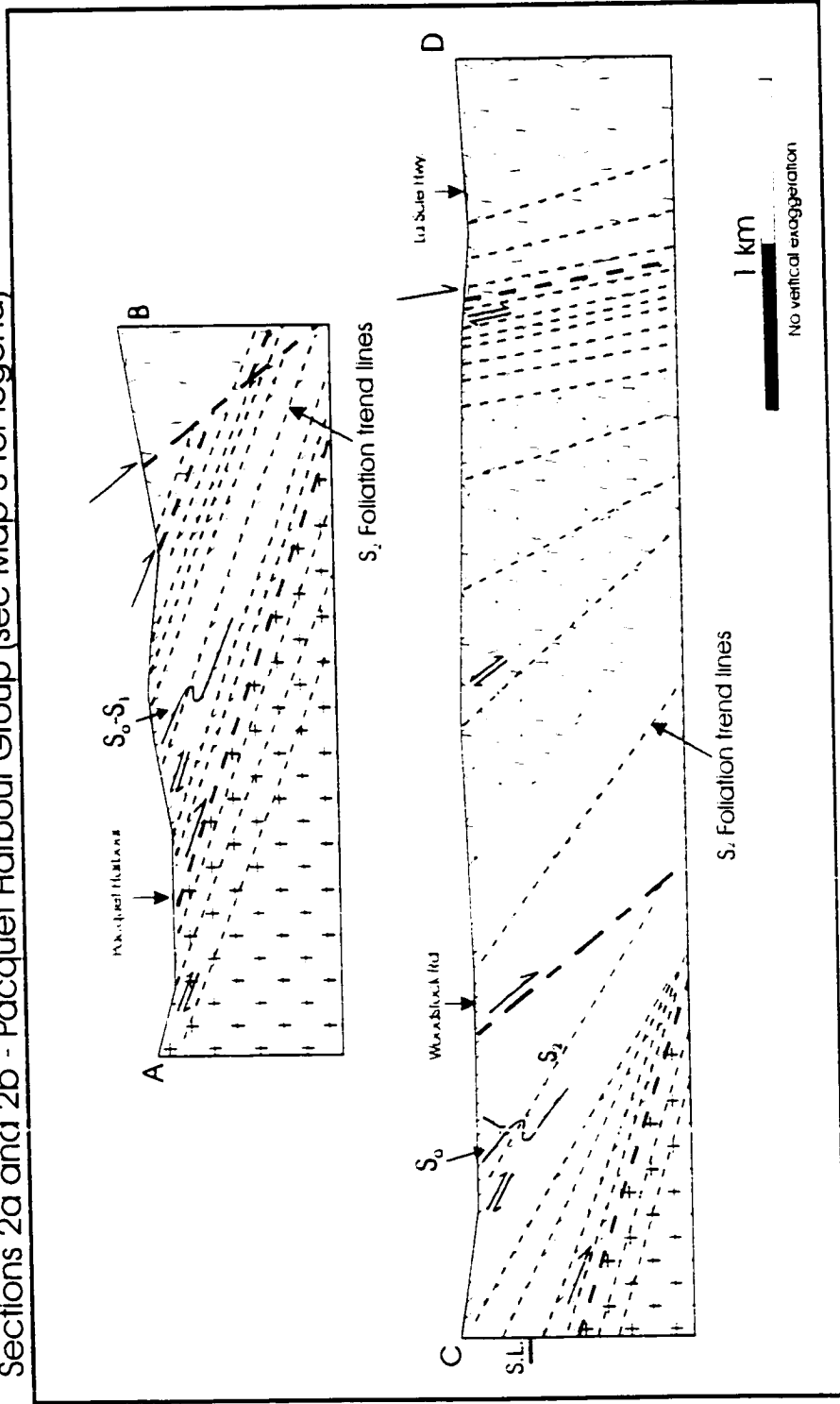
Barry - Cunningham Adit

400 m

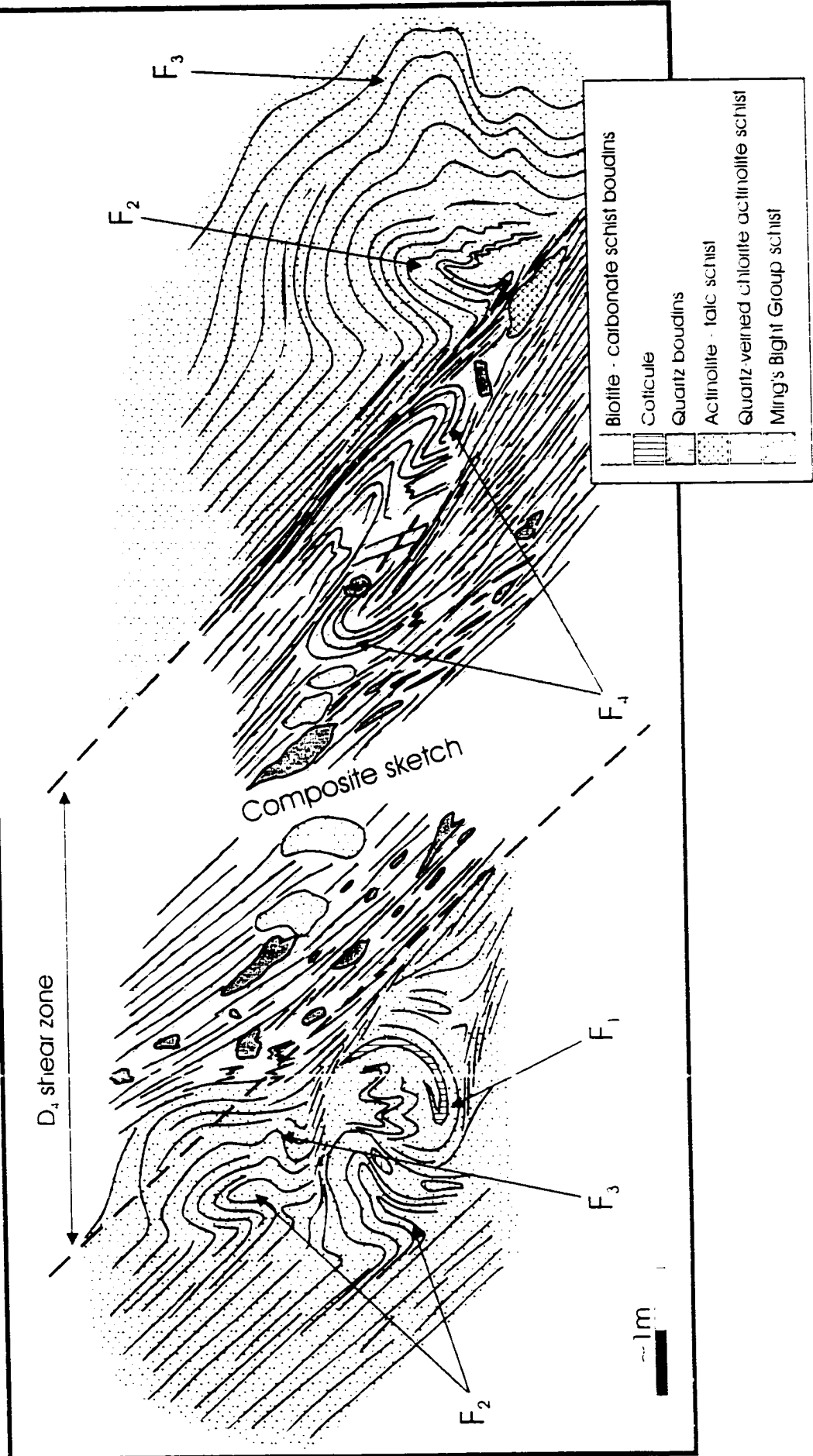
Section 1 - Pacquet Harbour (see Map 2 for legend)



Sections 2a and 2b - Pacquet Harbour Group (see Map 3 for legend)

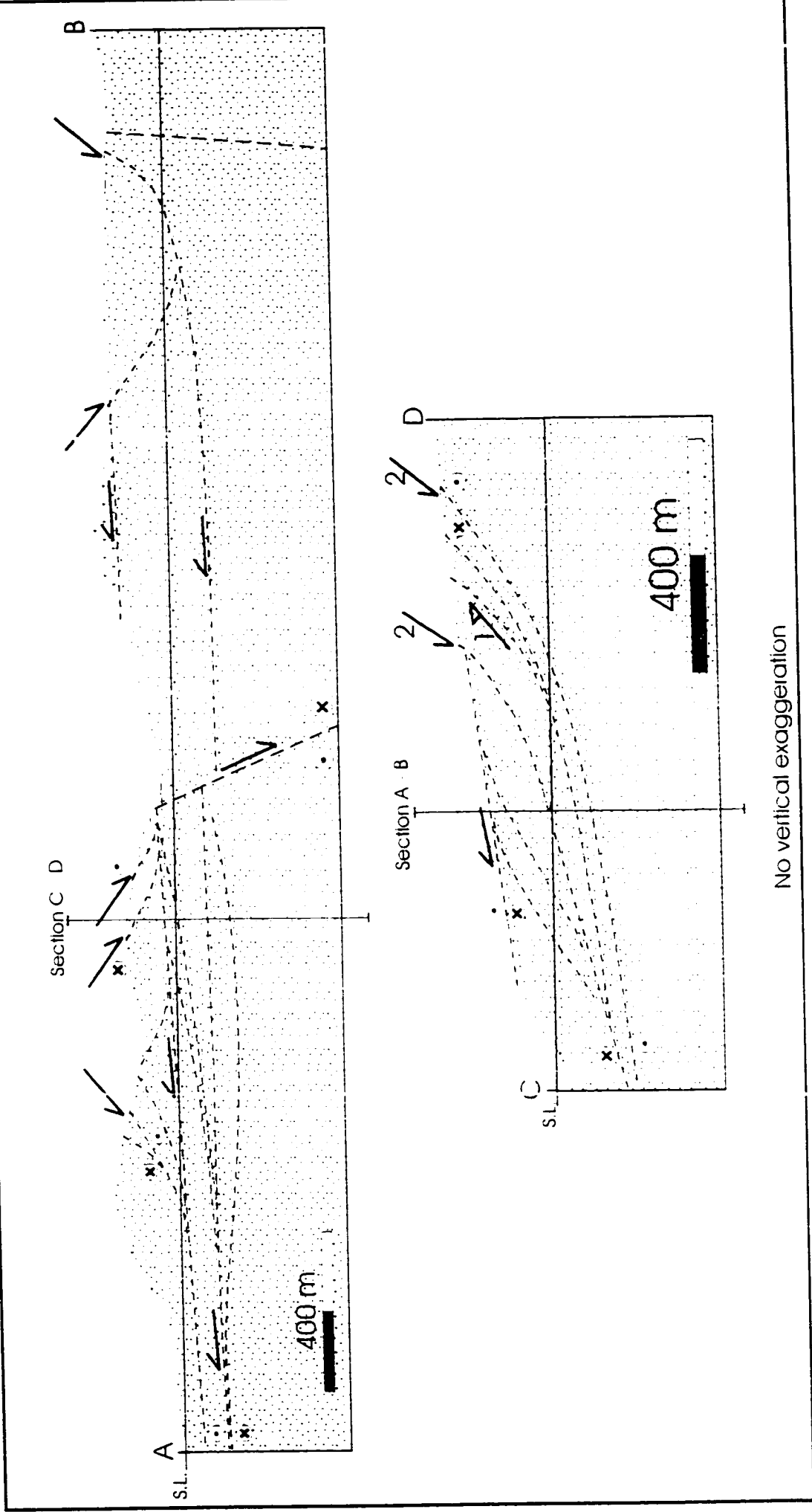


Section 4 - Actinolite Bay field sketch (vertical face; facing south)

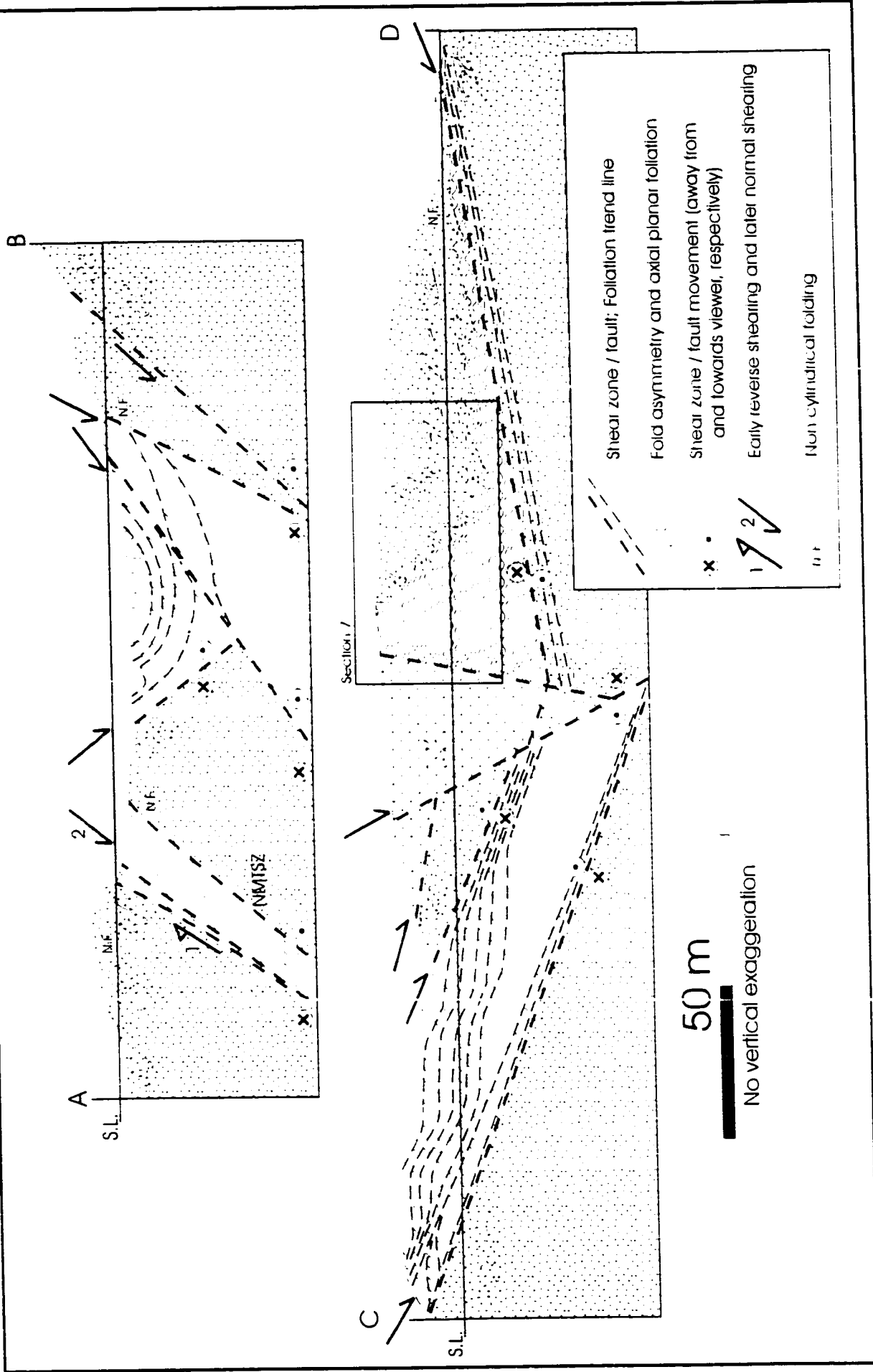


- Biotite - carbonate schist boudins
- Calcic
- Quartz boudins
- Actinolite - talc schist
- Quartz-veined chlorite actinolite schist
- Ming's Bright Group schist

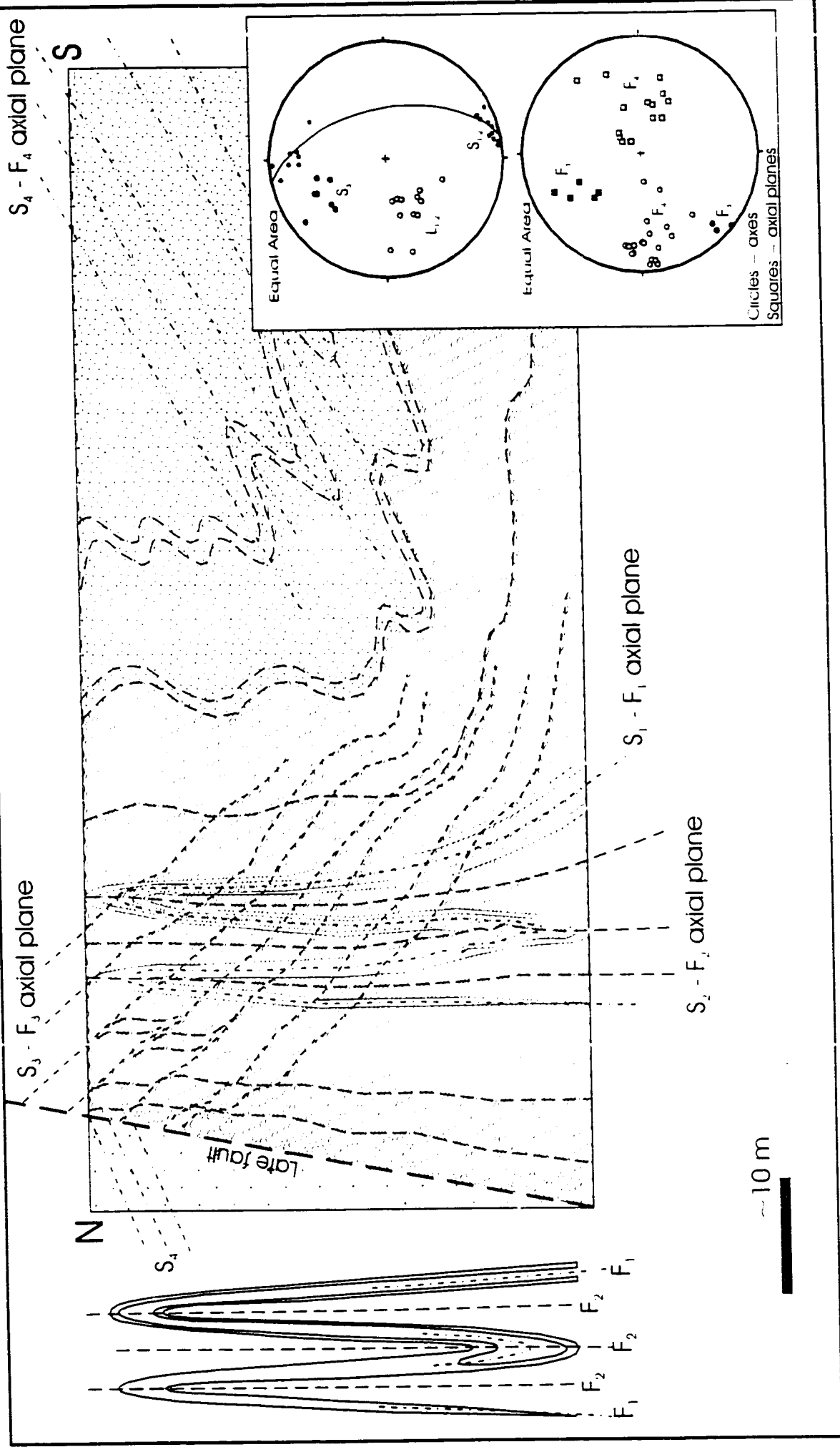
Sections 5a and 5b - Northeast shore of Ming's Bight (see Map 7 for legend)

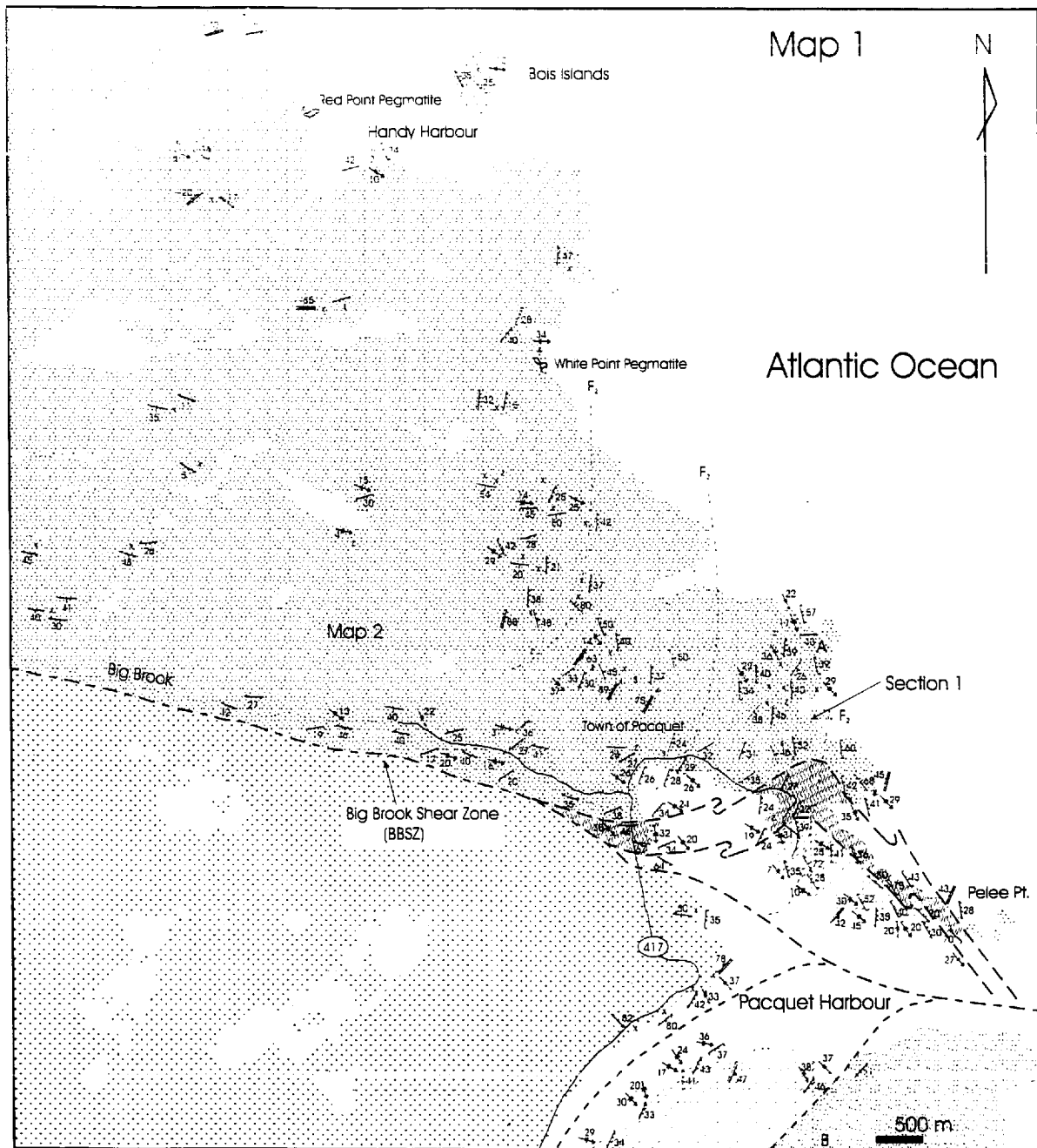


Sections 6a and 6b - Ming's Tickle to Caplin Cove (see Map 8 for legend)

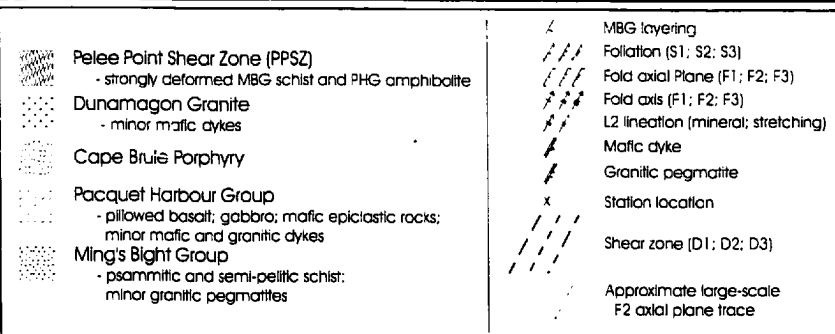


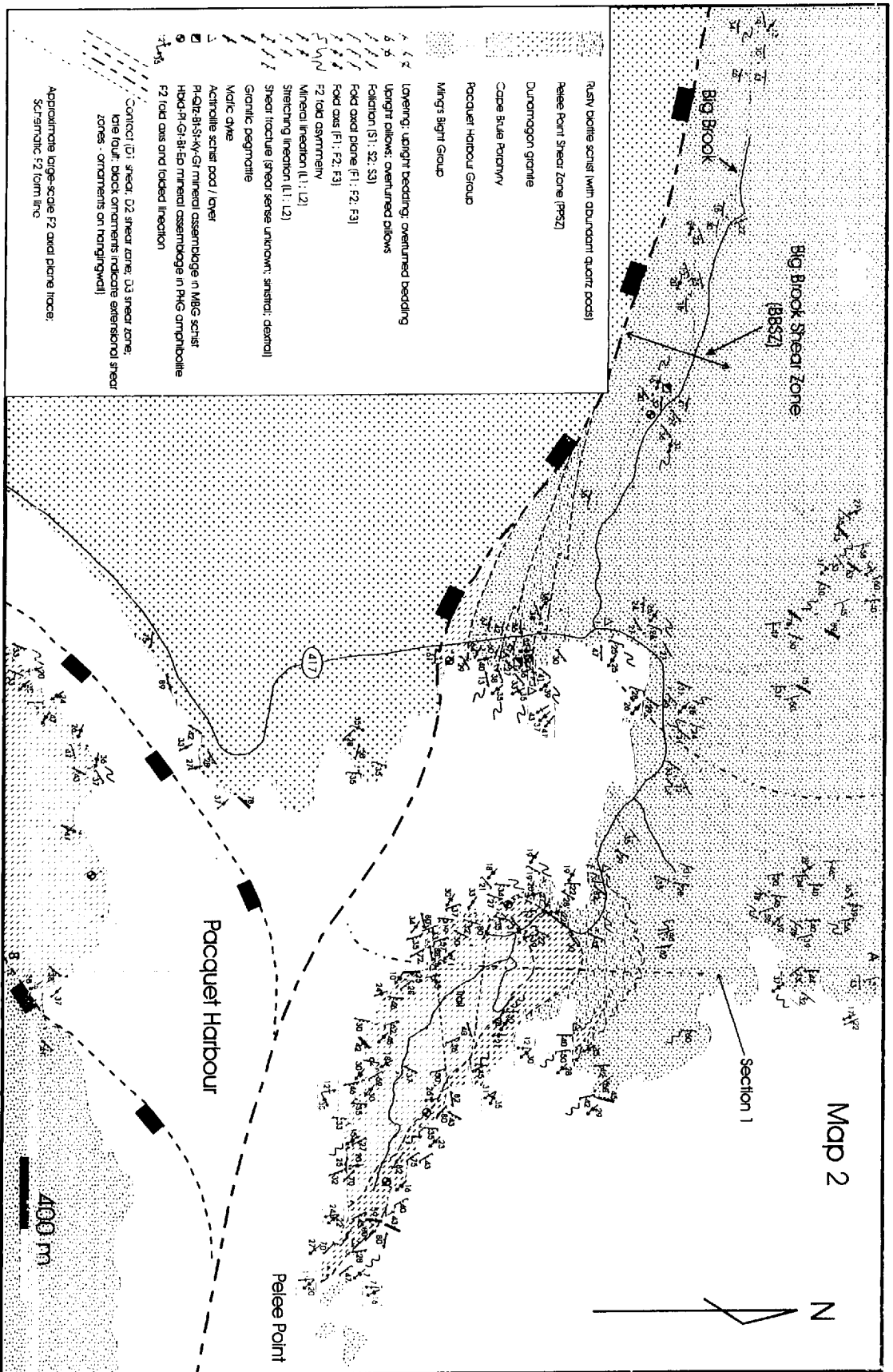
Section 7 (schematic) - Caplin Cove amphibolites (see Map 8 for legend)



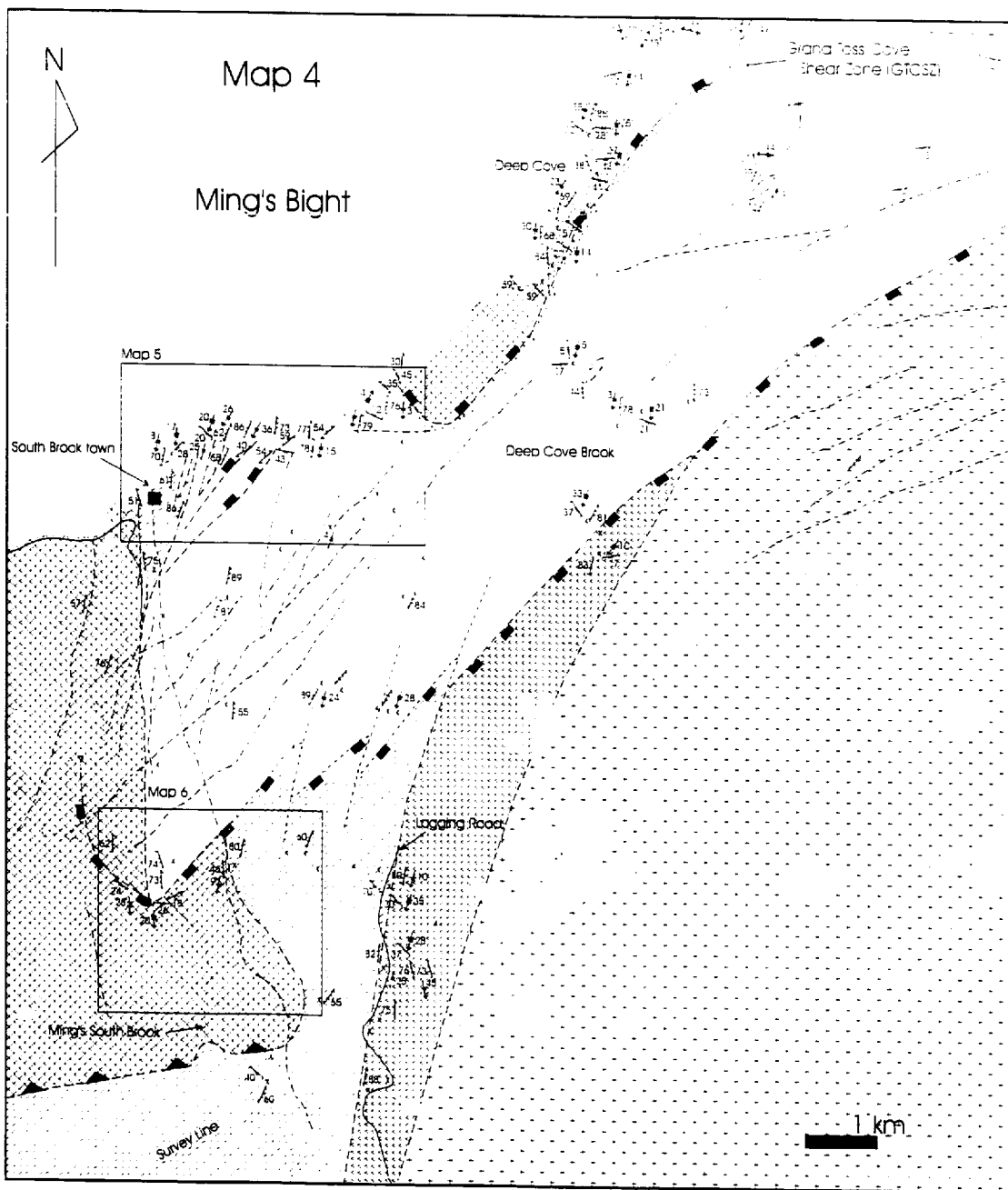


Anderson, Scott
NQ36566

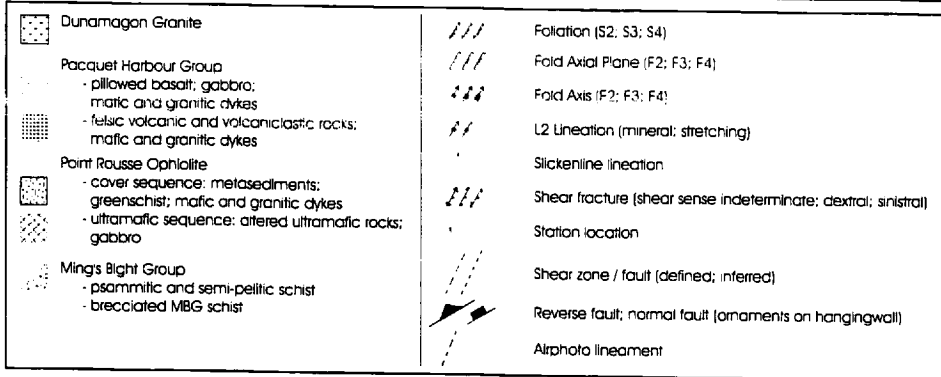


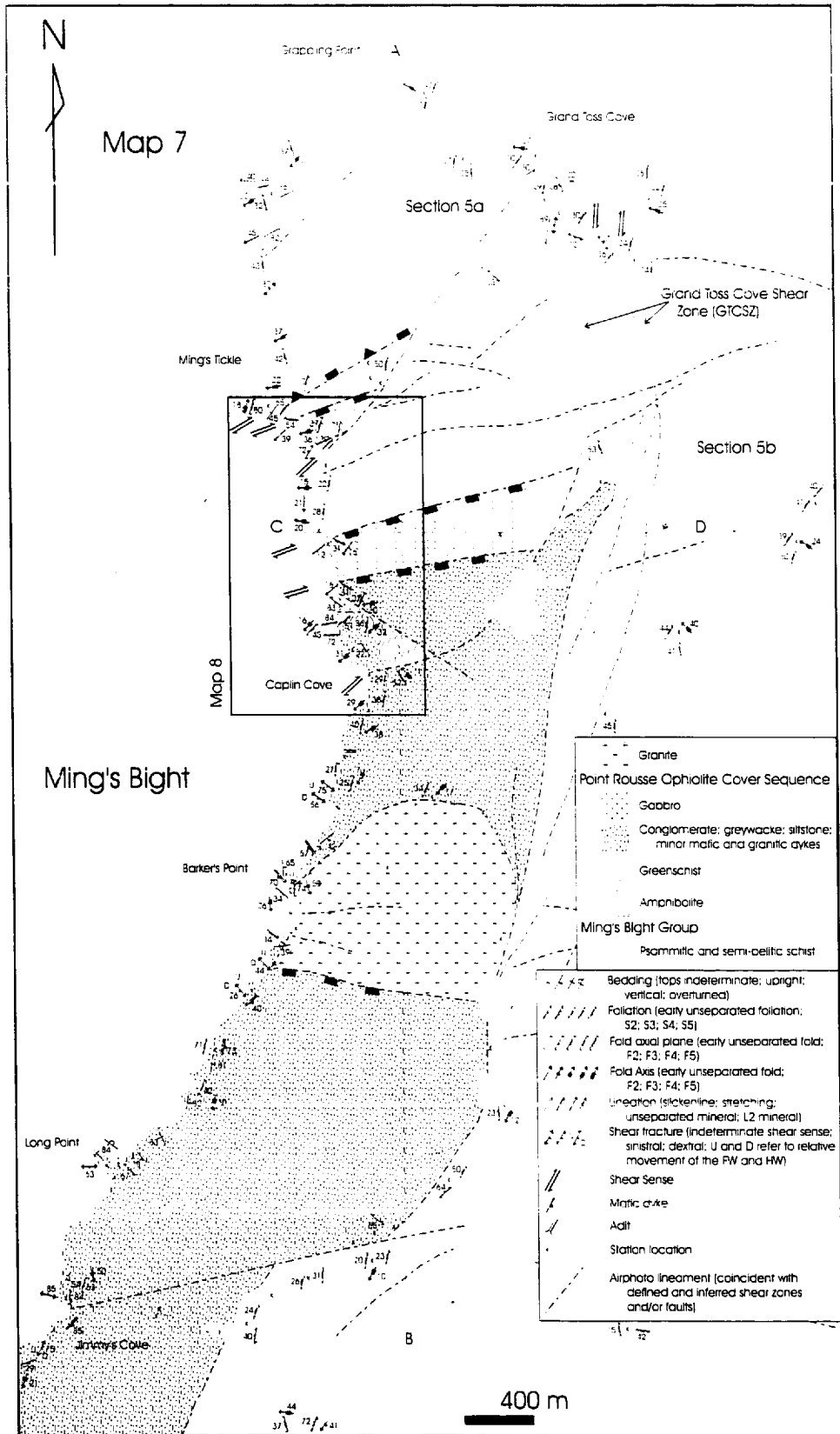


Anderson, Scott
NQ36566

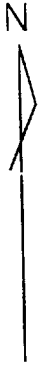


Anderson, Scott
NQ36566





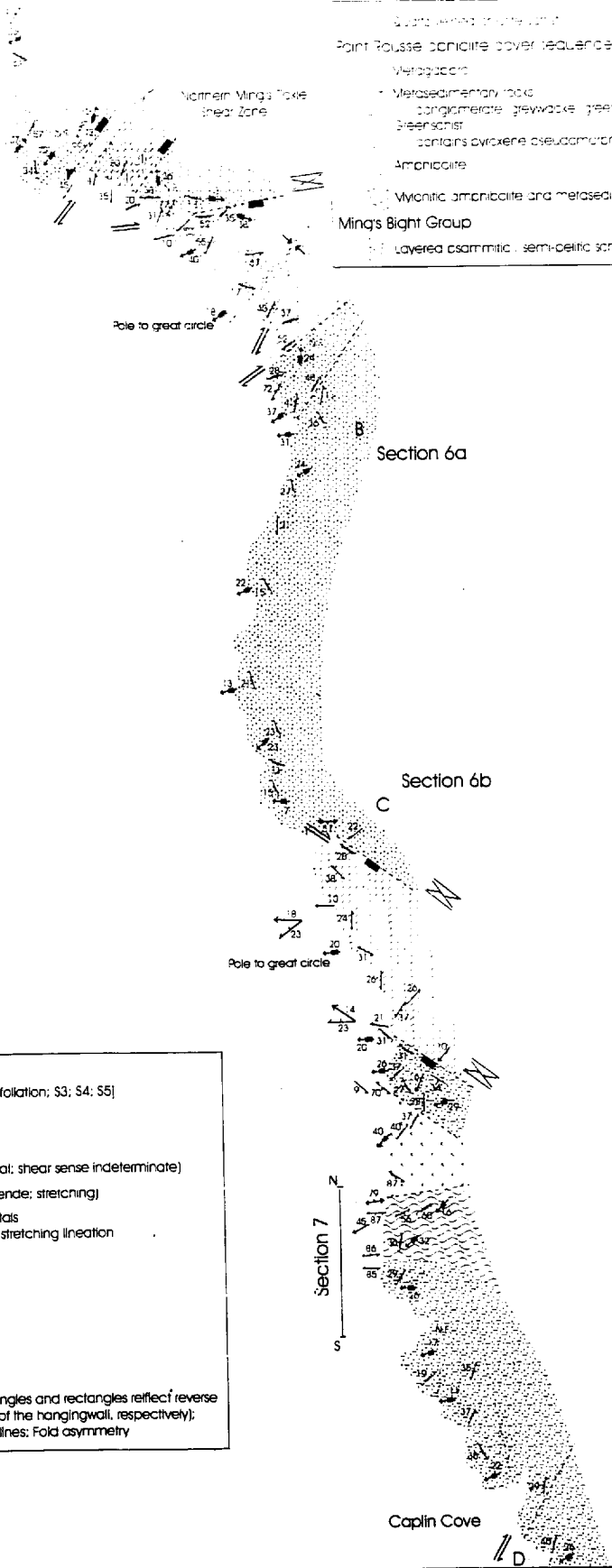
Anderson, Scott
 NQ36566



Map 8

Ming's Bight

- Quartz vein (thin line)
- Point Rousse banded cover sequence
- Metagabbro
- Metasedimentary rocks
 - conglomerate, grewacke, green schist
 - Green schist
 - contains pyroxene pseudomorphs
- Amphibolite
- Mylonitic amphibolite and metasediments
- Ming's Bight Group
 - Layered asammitic, semi-beltic schist



- | | |
|--|---|
| | Bedding |
| | Foliation (early unseparated foliation; S3; S4; S5) |
| | Fold Axial Plane (F3; F4; F5) |
| | Fold Axis (F3; F4; F5) |
| | Shear fracture (dextral; sinistral; shear sense indeterminate) |
| | Lineation (slickenline; homblende; stretching) |
| | Recrystallized pyroxene crystals
- mean homblende and stretching lineation |
| | Shear Sense |
| | Asymmetric fabric |
| | Synform |
| | Non-cylindrical folding |
| | Quartz vein |
| | Shear zone / fault (black triangles and rectangles reflect reverse and normal movement of the hangingwall, respectively);
Foliation / layering trend lines; Fold asymmetry |

50 m